

AD_____

AWARD NUMBER: W81XWH-04-1-0142

TITLE: VITAL: Vanguard Investigations of Therapeutic Approaches to Lung Cancer

PRINCIPAL INVESTIGATOR: Waun Ki Hong, M.D.
Reuben Lotan, Ph.D.
David Stewart, M.D.

CONTRACTING ORGANIZATION: The University of Texas
M.D. Anderson Cancer Center
Houston, Texas 77030

REPORT DATE: January 2006

TYPE OF REPORT: Annual

PREPARED FOR: U.S. Army Medical Research and Materiel Command
Fort Detrick, Maryland 21702-5012

DISTRIBUTION STATEMENT: Approved for Public Release;
Distribution Unlimited

The views, opinions and/or findings contained in this report are those of the author(s) and should not be construed as an official Department of the Army position, policy or decision unless so designated by other documentation.

REPORT DOCUMENTATION PAGE				Form Approved OMB No. 0704-0188	
Public reporting burden for this collection of information is estimated to average 1 hour per response, including the time for reviewing instructions, searching existing data sources, gathering and maintaining the data needed, and completing and reviewing this collection of information. Send comments regarding this burden estimate or any other aspect of this collection of information, including suggestions for reducing this burden to Department of Defense, Washington Headquarters Services, Directorate for Information Operations and Reports (0704-0188), 1215 Jefferson Davis Highway, Suite 1204, Arlington, VA 22202-4302. Respondents should be aware that notwithstanding any other provision of law, no person shall be subject to any penalty for failing to comply with a collection of information if it does not display a currently valid OMB control number. PLEASE DO NOT RETURN YOUR FORM TO THE ABOVE ADDRESS.					
1. REPORT DATE (DD-MM-YYYY) 01-01-2006		2. REPORT TYPE Annual		3. DATES COVERED (From - To) 15 Dec 2004 – 14 Dec 2005	
4. TITLE AND SUBTITLE VITAL: Vanguard Investigations of Therapeutic Approaches to Lung Cancer				5a. CONTRACT NUMBER	
				5b. GRANT NUMBER W81XWH-04-1-0142	
				5c. PROGRAM ELEMENT NUMBER	
6. AUTHOR(S) Waun Ki Hong, M.D., Reuben Lotan, Ph.D. and David Stewart, M.D. E-Mail: Whong@mdanderson.org				5d. PROJECT NUMBER	
				5e. TASK NUMBER	
				5f. WORK UNIT NUMBER	
7. PERFORMING ORGANIZATION NAME(S) AND ADDRESS(ES) The University of Texas M.D. Anderson Cancer Center Houston, Texas 77030				8. PERFORMING ORGANIZATION REPORT NUMBER	
9. SPONSORING / MONITORING AGENCY NAME(S) AND ADDRESS(ES) U.S. Army Medical Research and Materiel Command Fort Detrick, Maryland 21702-5012				10. SPONSOR/MONITOR'S ACRONYM(S)	
				11. SPONSOR/MONITOR'S REPORT NUMBER(S)	
12. DISTRIBUTION / AVAILABILITY STATEMENT Approved for Public Release; Distribution Unlimited					
13. SUPPLEMENTARY NOTES					
14. ABSTRACT The VITAL Research Program will provide a better understanding of the cellular and molecular processes that drive lung tumorigenesis so that an accurate risk model can be developed. In addition, the clinical trials that will be conducted in the VITAL Research Program will demonstrate the true rate of lung cancer recurrence and second primary tumor incidence in patients at high risk for these events and will identify the combination of biologic agents most effective in reducing these events in the high-risk population. The primary objective of the work proposed in the VITAL Research Program is development of a risk model for development of cancer recurrence and smoking-related second primary tumors based on an understanding of the biology of lung cancer development.					
15. SUBJECT TERMS lung cancer, risk model, cancer recurrence, clinical trials					
16. SECURITY CLASSIFICATION OF:			17. LIMITATION OF ABSTRACT	18. NUMBER OF PAGES	19a. NAME OF RESPONSIBLE PERSON
a. REPORT	b. ABSTRACT	c. THIS PAGE			USAMRMC
U	U	U	UU	315	19b. TELEPHONE NUMBER (include area code)

TABLE OF CONTENTS

INTRODUCTION	2
BODY	2
Project 1	2
Project 2	5
Project 3	11
Project 4	18
Project 5	22
Core B Biostatistics and Data Management	24
Core C Pathology and Specimen Procurement.....	26
Developmental Research Project 2	32
KEY RESEARCH ACCOMPLISHMENTS	37
REPORTABLE OUTCOMES.....	38
CONCLUSION.....	40
REFERENCES	41
APPENDICES	43

INTRODUCTION

Smoking-related cancers such as lung and head and neck cancers are a major cause of cancer death in the United States. About 25% of lung cancer patients are diagnosed with stage I or II disease and undergo surgery with curative intent, but the 5-year survival for the group of patients is only 30%-70%. Patients with a strong history of smoking and prior early-stage cancer are found to be at high risk for cancer recurrence or development of second primary tumors (SPTs). An effective adjuvant therapy after surgery in this group of patients is not well established yet. The survival benefit of adjuvant chemotherapy after surgery was uncertain until recent findings reported by Winton and colleagues (Winton et al., 2005). They found that adjuvant chemotherapy (vinorelbine and cisplatin) increases the 5-year survival of surgically resected non-small cell lung cancer (NSCLC) patients, resolving the debate over the benefit of adjuvant chemotherapy. Thus, better-designed clinical trials and basic studies are needed to establish the standard of care for these patients after surgery.

The program VITAL (**V**anguard Trial of Investigational Therapeutics in **A**djuvant Treatment of **L**ung Cancer) developed in 2003 leads to this direction. It aims to develop a risk assessment model for cancer recurrence and development of smoking-related SPTs based on the understanding of molecular events in pre-malignant tissues that underlie progression to malignancy in the high-risk population and identify effective agents in early prevention of these events in this group of patients. Specifically, our objectives are

- To identify biologically-based treatments for prevention of cancer recurrence and development of second primary tumors in high-risk patients
- To understand molecular events in premalignant tissues that contribute to progression or malignancy
- To develop a risk prediction model for disease recurrence and development of second primary tumors in high-risk patients by combining clinical treatment outcomes with molecular and imaging data.

PROGRESS REPORT (BODY)

Project 1: Biologic Approaches for Adjuvant Treatment of Aerodigestive Tract Cancer

(PI and co-PIs: Drs. Waun Ki Hong, Edward S. Kim, Rodolfo C. Morice, David J. Stewart)

Specific Aim 1.1 Assess the smoking-related disease-free survival in patients who are current or former smokers with a prior definitively-treated stage I/II lung or head and neck cancer.

The main objective was to open the Vanguard study at MDACC as well as the 2 other participating sites. A total of 300 patients with definitively treated stage I/II lung or head and neck cancer and at least a 20-pack-year smoking history will be enrolled in the trials. Enrolled patients will undergo baseline testing including chest x-ray, CT scan, labs, bronchoscopy, and other specimen collections (i.e., sputum, saliva, serologies). Bronchoscopies and specimen collection will be performed at baseline and at months 12, 24 and 36. White-light alone or white light and autofluorescence modalities will be used. Abnormal areas detected by bronchoscopy will also be biopsied. Histologic assessment will be performed to determine whether malignant changes will occur during the time period. If severe dysplasia, carcinoma in situ or carcinoma is discovered, patients will go for the plans outlined in the clinical protocol. Once patients have completed 3-year testing, they will be followed for additional years until the study is completed.

Update

Currently, the Vanguard trial has been activated at MDACC and Eisenhower Medical Center. Both sites are enrolling patients. The other site (Conemaugh Memorial Medical Center) has submitted the protocol through their IRB and anticipates possible activation in the first quarter 2006. The Eisenhower group has visited MDACC to familiarize themselves with the data and specimen collection procedures. The Vanguard trial was slightly delayed in its original opening due to the comprehensive review process. The approved amendment allows prior chemotherapy for surgically resected lung cancer patients that has helped enrollment. Currently, 20 patients are enrolled in the study.

Aim 2 Evaluate effects of biologic agents as adjuvant therapy on the modulation of histology and specific biomarkers in this high-risk population.

Current adjuvant chemotherapy offers some benefits in the high-risk patients, but is not a long-term preventive strategy. We plan to open several biologic adjuvant clinical trials with novel agents such as celecoxib, erlotinib, lonafarnib, and possibly others. Considerable preclinical data exist for these agents for cancer as well as normal or precancerous bronchial epithelium.

Update

The Vanguard study has been activated and is accruing patients. The first biologic adjuvant trial using celebrex has also been opened but no patients are enrolled yet. The next biologic adjuvant trial using erlotinib is now being written. The pharmaceutical company, Genentech, has agreed to supply erlotinib for this study. A letter of intent has been submitted to the company. The protocol will be completed first quarter with planned activation in the second quarter, 2006.

Aim 3 Develop a lung cancer risk model to help predict the likelihood of development utilizing imaging and biologically-based information in this high-risk population.

Patients with a history of smoking and a prior surgically resected stage I/II head and neck or lung cancer are at high risk for cancer recurrence or SPTs. There are no standard interventions which have been proven to help reduce the risk of cancer occurrence. A Gail risk model implemented in the initial management of breast cancer screening has proven useful and has helped with early detection and more stringent follow-up in the higher risk cohorts. Patients enrolled in the Vanguard trial will have aggressive post-operative follow-up with analysis including frequent serologies, bronchial specimens and CT scanning. Trends in these multiple biomarkers would be analyzed and used to develop a predictive model. Establishing a risk model will eventually help identify patients who may be at higher risk for lung cancer development and promote earlier interventions for prevention.

Update

This aim will be completed at the end of the study period.

Conclusions and Future Work

The opening of the Vanguard trial is key to the grant. Enrollment screening continues at a steady pace. Patient tissues are collected and will be distributed to support other research projects in the VITAL grant. The celecoxib biological adjuvant trial is open. We are currently writing the adjuvant erlotinib trial. We have begun new recruitment strategies for the Vanguard trial to increase patient accrual. Strategies include distributing brochures, directly contacting potential patients, increasing referrals from other disciplines, advertising the trials by website and local radio and television media, and utilizing the expertise of our Business Office to re-evaluate patient intake processes to encourage additional referrals. We are working with a representative from M. D. Anderson Physician Relations who can assist us with all the above.

We are also working through M. D. Anderson's Graduate School of Biomedical Science to recruit an intern from the UT School of Public Health to assist us to increase community and physician awareness of the Vanguard trial. We have implemented the student internship approach for a chemoprevention trial associated with a Program Project grant. We have over two years of experience with this program now and it has proven to be a positive and worthwhile endeavor which has had the desired effect on patient accrual for this study.

Project 2: Identification of Biomarkers of Response to Chemoprevention Agents in Lung Epithelium

(PI and co-PIs: Li Mao, M.D., Reuben Lotan, Ph.D., John Minna, M.D.)

We proposed to use genomic and proteomic analysis to identify changes in gene expression and proteins which correlate/associate with cancer risk in the carcinogen-damaged aerodigestive tract field and also use these signatures to monitor the response of this field to chemoprevention. We will determine modifications of these changes by chemopreventive agents in premalignant cells *in vitro* and use probes for the modified genes and proteins to analyze tissue and cellular specimens from individuals participating in the chemoprevention clinical trial.

Aim 1 Develop immortalized human bronchial epithelial cells (HBEC) using a subset of patient tissue specimens collected in Project 1 and characterize expression profiles of the HBECs using oligonucleotide microarrays.

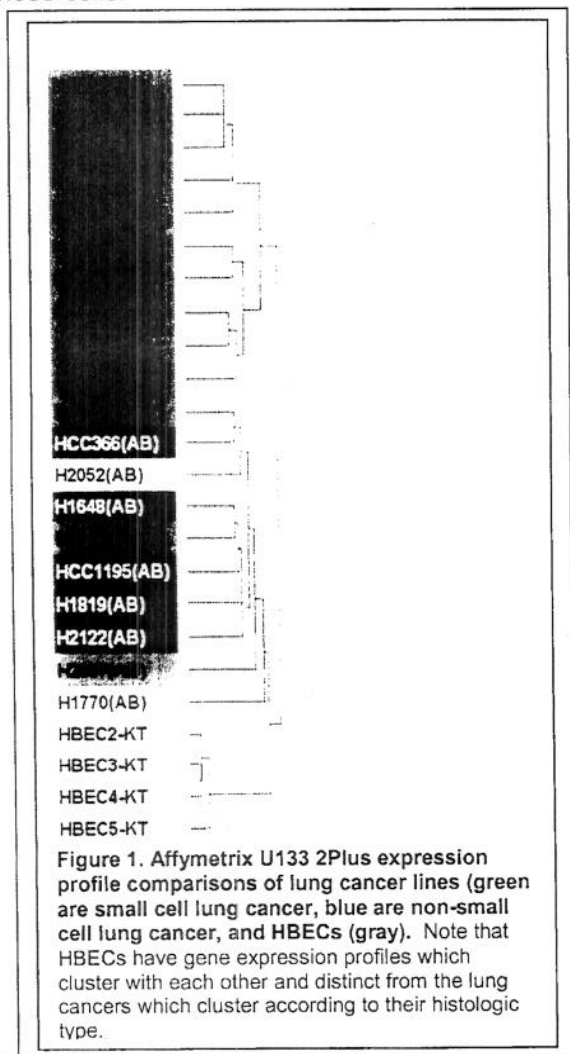
Update

Development of HBECs and characterization of their isogenic variants manipulated to progress toward malignancy

Over the past two years, we immortalized human bronchial epithelial cells with telomerase and cdk4-mediated p16 bypass using patient samples from our SPORE effort at UTSW and MDACC, and evaluated the contribution of three genetic alterations (p53 knockdown, *K-RAS*^{V12}, and mutant *EGFR*) to lung tumorigenesis using the immortalized HBECs. RNAi p53 knockdown or oncogenic *K-RAS*^{V12} resulted in enhanced anchorage-independent growth and increased saturation density of HBECs. The combination of p53 knockdown and *K-RAS*^{V12} further enhanced the tumorigenic phenotype with increased growth in soft agar and an invasive phenotype in 3-D organotypic cultures but failed to cause HBECs to form tumors in nude mice. Growth of HBECs was highly dependent on epidermal growth factor (EGF) and completely inhibited by epidermal growth factor receptor (EGFR) tyrosine kinase inhibitors (TKIs) that induced G1 arrest. Introduction of EGFR mutations E746-A750 del and L858R progressed HBECs toward malignancy as measured by soft agar growth, including EGF independent growth but failed to induce tumor formation. Mutant EGFRs were associated with higher levels of pAkt, pSTAT3 (but not pERK1/2), and increased expression of *DUSP6/MKP-3* phosphatase (an inhibitor of pERK1/2). These results indicate that: 1) the HBEC model system is a powerful new approach to assess the contribution of individual and combinations of genetic alterations to lung cancer pathogenesis; 2) a combination of four genetic alterations including hTERT overexpression, bypass of p16/RB and p53 pathways, and mutant *K-RAS*^{V12} or mutant *EGFR* is still not sufficient for human bronchial epithelial cells to completely transform to cancer, and 3) EGFR tyrosine kinase inhibitors inhibit the growth of preneoplastic HBEC cells, suggesting their potential for chemoprevention. Detailed description can be viewed in *Cancer Research* in 2006 (Sato et al., 2006).

Until now, we have developed about 30 such lines from individual patients and obtained array based CGH data and Affymetrix expression array data on about 15 of these and the rest are being completed. These arrays show that the HBECs cluster together and are distinct from lung cancers (Figure 1). Also, the isogenically manipulated HBECs (see below) altered for oncogenic changes have discrete expression profile differences. All of the HBECs have been mycoplasma tested and DNA finger printed for current and future identification. Several of these have been supplied to investigators in different components of this DOD application.

When patient samples from VITAL trials become available we will try to immortalize and study these cells.

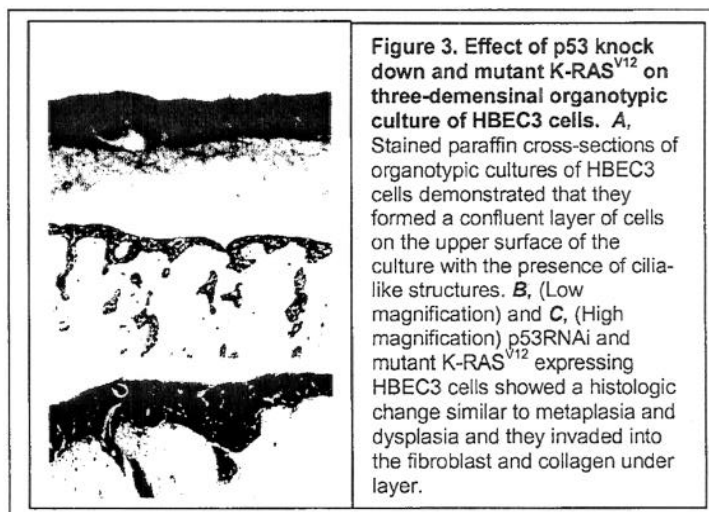


3D Organotypic Culture Differentiation of the HBECs

In the present study, we determined whether immortalized HBECs retain the ability to differentiate normally (Figure 2). HBECs were plated atop contracted collagen gels containing lung fibroblasts. This three-dimensional (3D) tissue model was cultured initially submerged, then raised to the air/liquid interface for up to 28 days. Normal differentiation was assessed by the presence of ciliated cells, goblet (mucin-producing) cells, and basal epithelial cells. Scanning electron microscopic observations revealed ciliated cells and mucin-producing cells in these 3D tissues. Histological examination revealed the presence of mucin-producing cells, and immunohistochemistry using antibodies against p63 and keratin 14 showed the presence of basal cells. These results demonstrate that immortalized HBECs retain the capacity to differentiate into each of three cell types: basal, mucin-producing, and columnar ciliated epithelial cells. Details can be reviewed in *Differentiation* (Vaughan et al., 2006)

Oncogenic manipulation leads to an invasive phenotype in a three-dimensional organotypic culture assay

To evaluate the effect of oncogenic manipulation in HBEC3s and on their ability to differentiate and to invade, we performed three-dimensional organotypic culture (Figure 3). HBEC3 cells only expressing hTERT and Cdk4 cells formed a confluent layer of cells on the upper surface of a fibroblast and collagen gel underlayer and developed both ciliated (see figure) and mucous producing cell types. In stark contrast, the cells expressing hTERT, Cdk4, K-RAS^{V12} and p53 RNAi showed histologic change similar to metaplasia/dysplasia and they invaded into the fibroblast and collagen gel similar to cancer cells invading into the submucosal layer. We conclude from these studies that p53 knockdown and K-RAS^{V12} are additive in malignant transformation leading to the development of anchorage-independent growth and the ability to invade in a three-dimensional culture system.



Aim 2 Characterize effects of the chemopreventive agents used in Project 1 on cell proliferation and apoptosis in the HBECs developed in Specific Aim 1.

Update

Last year, we reported the IC-50 and some effects of the targeted agents such as gefitinib, erlotinib, and SCH66336 on the cell lines. Not much progress for the aim this year.

Aim 3 Identify gene expression and protein signatures for lung tumorigenesis and sensitivity or resistance to chemopreventive agents used in Project 1, validate the signatures, and determine their biological importance in precancer cell models of lung cancer

Update

Last year, we characterized the CGH and gene expression profiles of HBECs, demonstrated that the oncogenically manipulated HBECs were exquisitely sensitive to EGFR inhibitors gefitinib and erlotinib, and identified gene expression signatures of sensitive and resistant lung cancers to gefitinib and erlotinib and differentially expressed proteins between NSCLC and HBEC cells.

In this period, we have focused on protein profiles of different stages of lung tumorigenesis and microRNAs (miRNAs) between NSCLC and HBEC cells.

Differential protein expression in a lung malignant progression model system

We used an *in vitro* lung carcinogenesis model consisting of normal human bronchial epithelial (NHBE) cell strain, HBE cells immortalized by SV40 T antigen (BEAS-2B), (Reddel et al., 1988) and cells derived from BEAS-2B by exposure to CSC including transformed 1198 cells and tumorigenic 1170-I cells and control immortalized cells 1799 not exposed to CSC (Klein-Szanto et al., 1992) to determine changes in protein levels in different stages of lung carcinogenesis

using a high throughput western immunoblotting technique called PowerBlot (Becton-Dickinson).

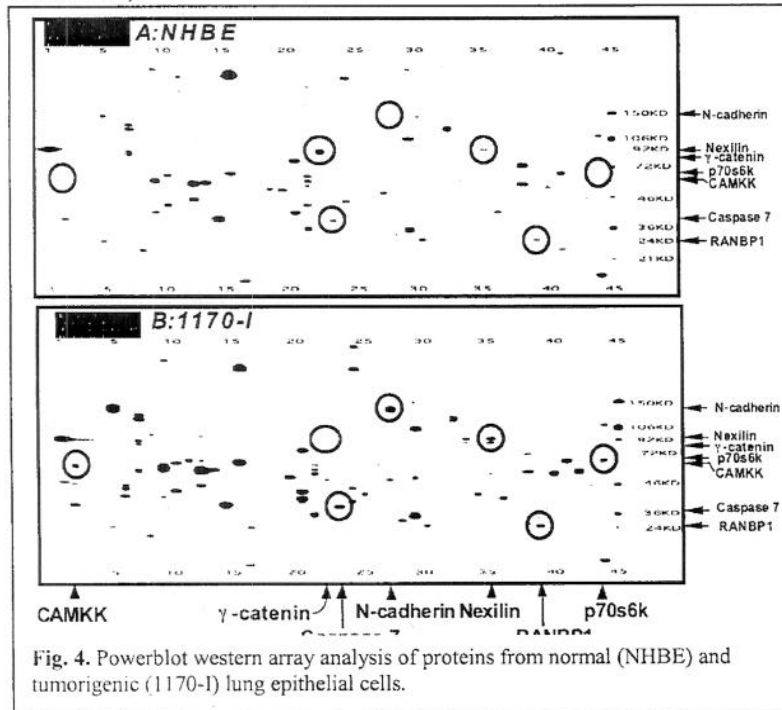


Fig. 4. Powerblot western array analysis of proteins from normal (NHBE) and tumorigenic (1170-I) lung epithelial cells.

Examples of the PowerBlot analysis of proteins in normal and tumorigenic cells are presented in Figure 4. Similar analysis using about 800 antibodies revealed that the levels of 87 proteins increased by > 2 fold and the levels of 45 proteins decreased by > 2 fold in tumorigenic 1170-I compared to normal NHBE cells. These proteins included some that are involved in DNA synthesis and DNA repair, cell cycle regulation, RNA transcription and degradation, translation, differentiation, angiogenesis, apoptosis, cell adhesion, cytoskeleton

and cell motility, and some components of the phosphatidylinositol 3-kinase signaling pathway. Conventional western blotting confirmed some of these changes. Furthermore, similar changes could be identified in immortalized HBE cells and their transformed non-tumorigenic derivatives as well as in several non-small cell lung cancer cell lines. Figure 5 shows the quantitative analyses of conventional western blotting experiments performed with the different cell lines of the in vitro carcinogenesis model.

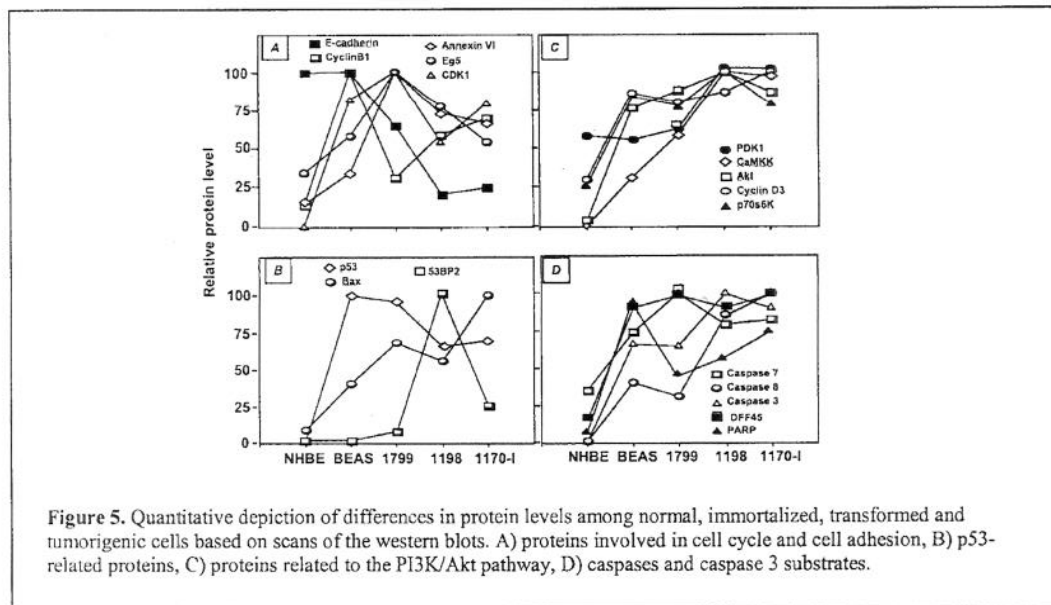


Figure 5. Quantitative depiction of differences in protein levels among normal, immortalized, transformed and tumorigenic cells based on scans of the western blots. A) proteins involved in cell cycle and cell adhesion, B) p53-related proteins, C) proteins related to the PI3K/Akt pathway, D) caspases and caspase 3 substrates.

Development of novel proteomics approach to identify protein markers different between HBEs and NSCLC

We are developing novel 2-DE-based strategies to enrich moderately abundant and low-abundance proteins in complex tissues and body fluids. One of the strategies takes advantage of the specific binding capability of certain chemicals or ions (baits) to specific protein structures to pull down a subset of cellular proteins and their binding partners before 2-DE analysis. Using this strategy, we are able to achieve enrichment of total cellular proteins by as much as 100-fold in each selection (Figure 6). More important, this strategy allows us to determine the potential functions of the proteins, which may be a result of hard to find point mutations of the corresponding genes, because changes in those functions may affect those proteins' ability to bind other proteins. A sequential use of different baits may allow enrichment and visualize more proteins with different biochemical properties.

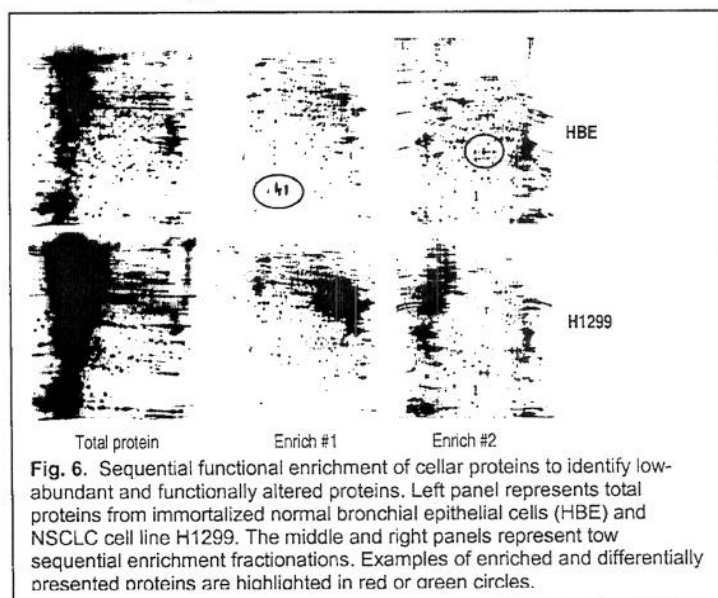


Fig. 6. Sequential functional enrichment of cellular proteins to identify low-abundant and functionally altered proteins. Left panel represents total proteins from immortalized normal bronchial epithelial cells (HBE) and NSCLC cell line H1299. The middle and right panels represent two sequential enrichment fractionations. Examples of enriched and differentially presented proteins are highlighted in red or green circles.

Differential expression of miRNAs between HBEs and NSCLC

We studied expression status of more than 200 miRNAs in five immortalized bronchial epithelial cell lines (HBE1, HBE2, HBE3, HBE4, and HBE5) and five NSCLC cell lines (H1944, H1792, H226, A549, and H1299) using a micro-fluid-based RNA microarray. We identified several miRNAs with substantial expression difference between the immortalized bronchial epithelial cells and lung cancer cells (Figure 7) suggesting a potential role of these miRNAs in lung cancer progression. Additional experiments are needed to determine the biologic roles of the miRNAs in lung tumorigenesis.

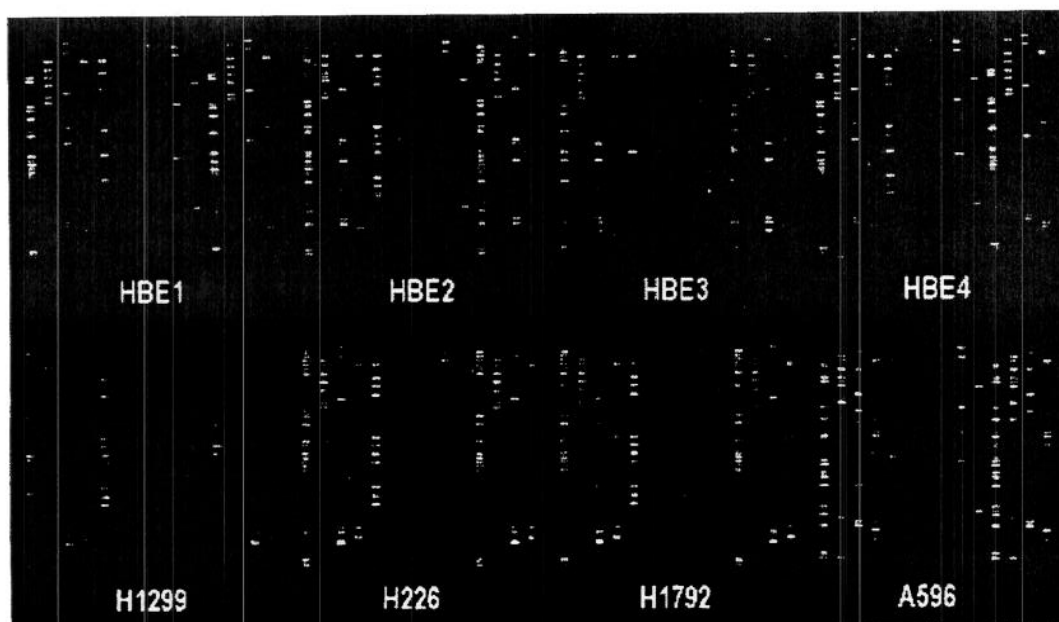


Figure 7. Expression of miRNAs in immortalized normal bronchial epithelial cells and non-small cell lung cancer cells. Circles indicate miRNAs differentially expressed between the normal and tumor cells.

Aim 4 Develop techniques to assess these molecular signatures in tissue specimens and serum obtained in Project 1 and assess the relevance of these molecular signatures as *in vivo* biomarkers using baseline and post-treatment specimens

Experiments for this aim will be initiated in the grant years 3 – 5.

Conclusion and Future Work

We can conclude that:

- 1) The isogenically manipulated HBEC system is a powerful approach to assess the contribution of individual genetic alterations to tumorigenesis of lung cancer;
- 2) The effect of p53 knockdown and K-RAS^{V12} on tumorigenesis appears to be additive and the combination of four genetic alterations, including hTERT overexpression, bypass of p16/RB and p53 pathways, and mutant K-RAS^{V12}, is not sufficient for human bronchial epithelial cells to completely transform to cancer.
- 3) EGFR tyrosine kinase inhibitors may be useful as chemopreventive drugs for lung cancer, and expression signatures for sensitivity and resistance to EGFR tyrosine kinase inhibitors are correlated with EGFR tyrosine kinase domain mutations found in lung cancers.

In the next year, we will develop HBEC lines that contain mutated EGFR found in lung cancers for testing the effect on biologic behavior and on response to chemoprevention agents. We will continue to establish new immortalized HBEC cultures when patient samples become available from the VITAL trials. We will continue to test new chemoprevention agents on the HBECs with and without oncogenic manipulation. We are proceeding with proteomic studies of the HBEC cultures.

Project 3: Premalignant Bronchial Epithelia: Molecular and Cellular Characterization of Lung Tumorigenesis

(PI and co-PIs: Walter Hittelman, Ph.D., Ja Seok Koo, Ph.D., Rodolfo C. Morice, M.D.)

Aim 1 Identify and characterize differentially expressed genes in LIFE bronchoscopy-identified abnormal areas of bronchial epithelia of enrolled subjects in VITAL trials

Previous studies show that abnormal bronchial regions have increased genetic changes compared to normal sites detected by LIFE bronchoscopy even if there are no histological differences and are at increased risk for cancer development, especially when they contain particular genetic alterations. We hypothesize that the LIFE-positive lesions represent an early-stage tumorigenesis and express genes important for tumorigenesis. We will conduct comparative gene expression analysis using LIFE-positive and LIFE-negative samples from the same patient to identify those genes.

Update

As detailed in the previous report, because of the delay of the VITAL trials and FDA approval of the Xillix OncoLIFE autofluorescence system, we focused efforts on establishing the procedures required for the Aim, such as the handling of clinical specimens and performing some microarray analysis using RNA isolated from bronchial brush specimens obtained from normal and abnormal areas, using the old version of the bronchoscopic endoscope.

LIFE Bronchoscopy

The LIFE system was finally in place on Aug 16, 2005. To date, we have performed LIFE bronchoscopies on 6 of 14 patients enrolled in the Vanguard study as described in Project 1 and the Pathology Core. We plan to select 10 qualified patients who have sites of 1) normal WL and normal LIFE; 2) normal WL and abnormal LIFE; and 3) abnormal WL and abnormal LIFE for the study. For each site, we will collect two biopsies (one for cell culture and the other for histology assessment) and two brushes (one for RNA extraction and the other for cytology examination). In addition, data of abnormalities including number, location, size, fluorescent abnormality score, and documentation of images will be recorded on all participating subjects. These clinical data will be correlated with molecular and cellular characteristics after completion of the aim.

Identification of Progressive Overexpression of Prostate Stem Cell Antigen (PSCA)

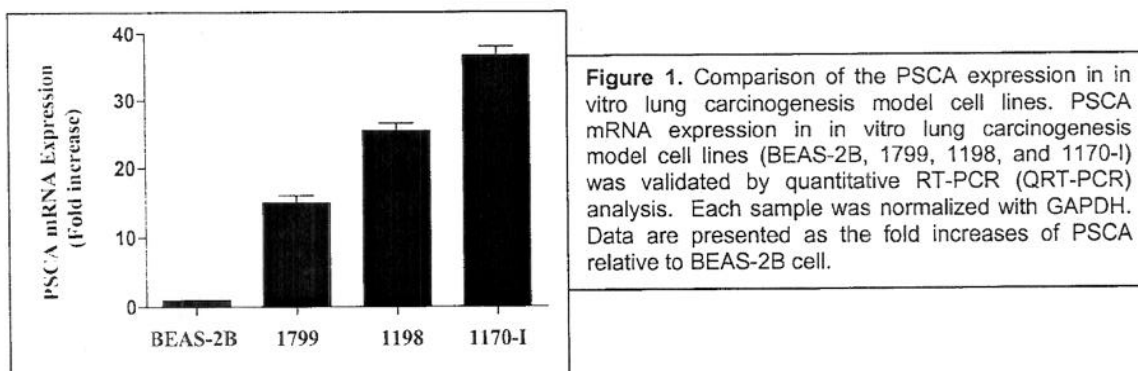
As reported last year, we conducted some microarray analysis and compared differentially expressed genes between the abnormal bronchoscopic region and normal bronchial epithelia. After verification recently, we found that prostate stem cell antigen (PSCA) is a gene differentially expressed in the abnormal bronchial region.

PSCA is a member of the Ly-61/Thy-1 family of GPI-anchored membrane proteins (Reiter, Gu et al. 1998) and highly expressed in a majority of prostate cancer cases. Increased PSCA expression is related to increased tumor stage, grade and progression of prostate cancer, and also poor prognosis (Gu, Thomas et al. 2000; Lam, Yamashiro et al. 2005). Moreover, PSCA is also highly expressed in pancreatic cancer cells, transitional cell carcinoma (Amara, Palapattu et al. 2001), and in many gastrointestinal cancers (Lukyanchuk, Friess et al. 2003). However, there is no report on the possible role and abnormal expression of PSCA in lung cancer.

To determine whether PSCA is involved in the progression of lung carcinogenesis, expression levels of PSCA mRNA were determined using RNA samples isolated from in vitro lung

carcinogenesis model cell lines that included normal immortalized (BEAS-2B and 1799), transformed (1198), and tumorigenic (1170-I) human bronchial epithelial (HBE) cells.

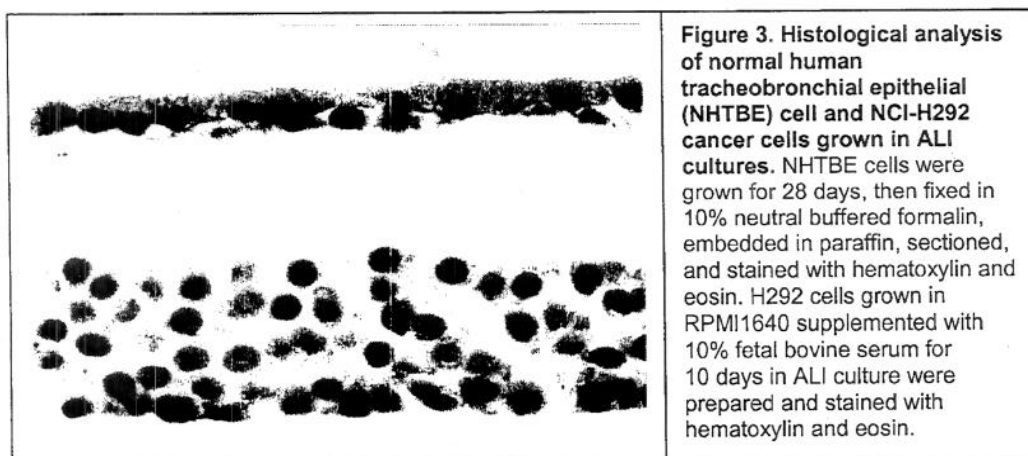
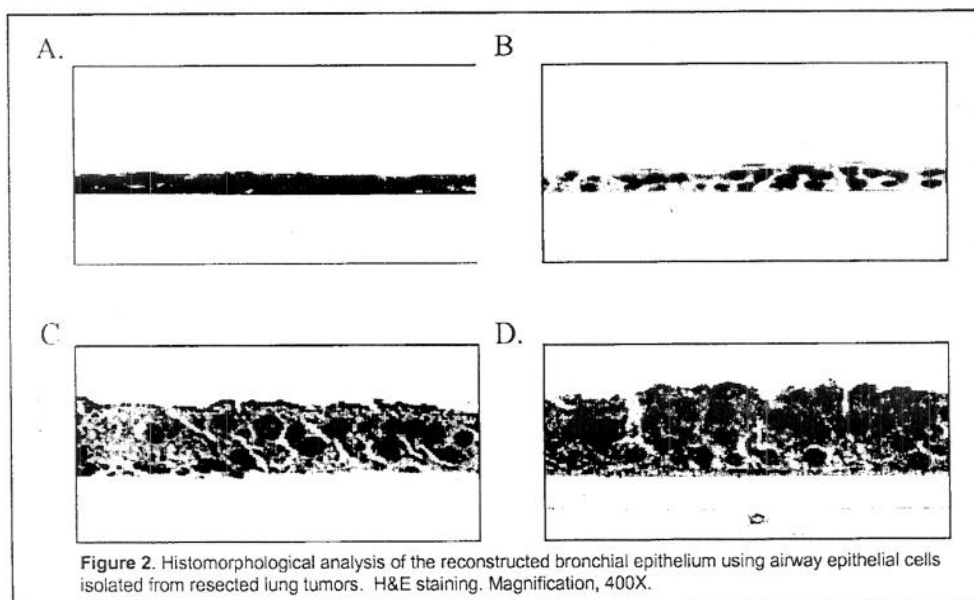
Levels of PSCA mRNA were determined by real-time PCR analysis. As shown in Figure 3, the expression of PSCA mRNA was gradually increased as carcinogenesis progressed. This preliminary result suggests that PSCA may be upregulated during multistep lung tumorigenesis. Further studies are underway to confirm this finding.



Reconstruction of bronchial epithelium of lung cancer patients in vitro

To reconstruct bronchial epithelium of lung cancer patients in vitro, we have isolated normal-appearing bronchial epithelial cells from resected lung tumor specimens and cultured them on porous membranes using an organotypic, air-liquid interface (ALI) culture method. We have so far harvested bronchial epithelial cells from 53 different cases. To characterize the in vitro reconstructed bronchial epithelium, histologic analysis was performed using sections of 28-day-old cultures. Briefly, surgically resected tissue specimens (3 mm²) containing bronchial epithelium were plated onto 60 mm dishes with BEGM media (Clonetics, San Diego, CA) containing insulin (5 µg/ml), hydrocortisone (0.072 µg/ml), transferrin (10 µg/ml), epinephrine (0.5 µg/ml), triiodothyronine (6.5 ng/ml), epidermal growth factor (0.5 ng/ml), bovine pituitary extract (1% v/v), gentamicin (50 µg/ml), amphotericin B (50 ng/ml), and retinoic acid (5 × 10⁻⁸ M). Epithelial cells were harvested by enzymatic detachment and seeded onto transwell-clear 6 well plates. The cultures were maintained in the above media for 28 days. An air-liquid interface (ALI) was created on day 7 by removing the medium overlying the cells growing on the filters. The cultures were fixed in buffered formalin solution on day 28 and histologic slide sections were prepared.

Representative histologic images of the sections are shown in Figure 2. H&E staining of the cross-sections of the cultures showed various irregular, epithelial morphologies. For example, cases A and B showed depolarized and flattened epithelium without noticeable differentiation into ciliated cells. Cases C and D showed metaplastic and mildly dysplastic multilayered epithelium with ciliated differentiation. It is noteworthy that the polarity of the epithelium was substantially compromised. However, the morphologies of bronchial epithelial cells from lung cancer patients was not as dysplastic as NCI-H292 non-small cell lung cancer cells grown by an ALI method (Figure 3).



Here, we have demonstrated that bronchial epithelial cells harvested from resected lung tumor specimens were successfully reconstructed airway epithelium *in vitro*. In a similar manner, epithelial cells isolated from LIFE abnormal lesions of the VITAL patients will be used for studies described in the subsequent aims.

Aim 2 Establish an organotypic model system that mimics *in vivo* interactions between normal, premalignant, and malignant bronchial epithelial cells in the lung by using bronchial biopsies of subjects entered in VITAL trials and immortalized bronchial epithelial cells

To better understand the molecular basis of preferential outgrowth of more advanced bronchial epithelial clones, we proposed to utilize the organotypic culture system. The organotypic culture environment mimics lung stratified epithelium, complete with basal cells, ciliated columnar cells, and mucus-producing goblet cells. Our group has extended this model system by tagging cell populations with fluorescent probes (e.g., green fluorescence protein) that allow us to carry out live cell imaging of mixed clonal populations. We aim to compare the differential growth properties in organotypic cultures of bronchial epithelial cells derived from LIFE bronchoscopy positive regions with those from negative regions

Update

As reported last year, because of the delay of Project 1 and the implementation of the new fluorescence bronchoscopy apparatus, our studies have focused on in vitro, organotypic studies using already established bronchial epithelial cell types including normal bronchial epithelial cells (NHBE), NHBE immortalized (Jerry Shay) with hTERT and cdk4 (HccBE), NHBE cells immortalized (Klein-Szanto) with Ad12/SV40 (Beas 2B), and immortalized (1799), transformed (1198), and tumorigenic (1170I) carcinogen-treated Beas2B cells. In the past year, we have obtained two new immortalized HccBE cell strains from Drs. Jerry Shay and John Minna that were derived from additional subjects who gave bronchial biopsies.

Last year we reported that NHBE cells preferentially undergo DNA synthesis and mitosis at the basal layer and HccBE cells proliferate at the basal and peribasal layers. In contrast, more advanced bronchial epithelial cells proliferate throughout the multilayer cultures (Figure 4). To determine whether immortalized bronchial epithelial cells derived from different individuals with a chronic smoking history show similar trends for the spatial location of proliferating cells, we compared the three HccBE cell strains for the spatial location of their proliferating cells using both BrdU labeling and phospho-histone 3 labeling. As shown in Figure 5, while the three cell lines differed somewhat in their overall labeling indices, most of the proliferation for the three HccBE cell strains tested occurred at the basal membrane with a fraction of the cells proliferating away from the basement membrane.

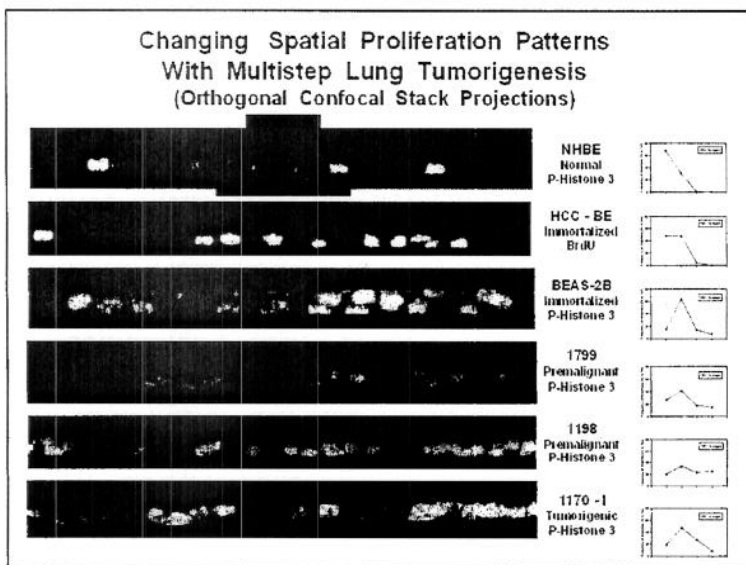
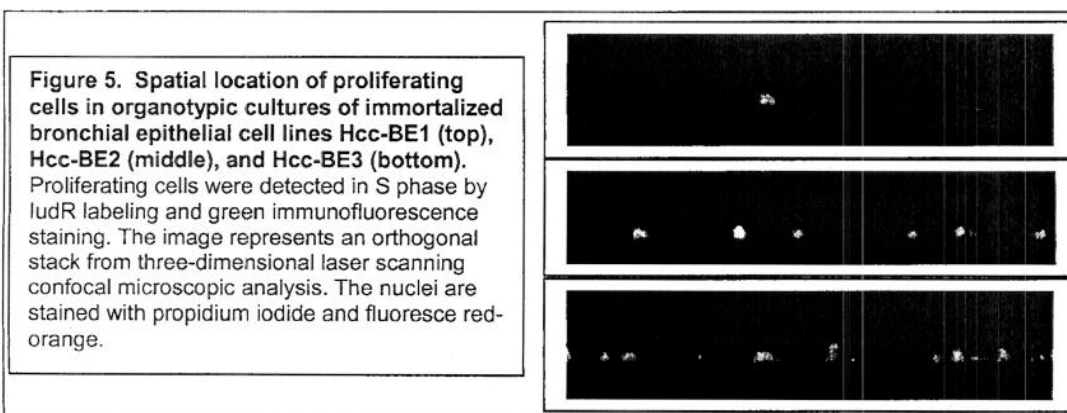


Figure 4. Spatial location of proliferating lung epithelial cells in organotypic cultures visualized by immunostaining and laser scanning confocal microscopy. Proliferating cells were detected either in S phase using BrdU immunolabeling or in mitosis with phospho-Histone H3 labeling. Note that the more advanced cells proliferated away from the basal layer.



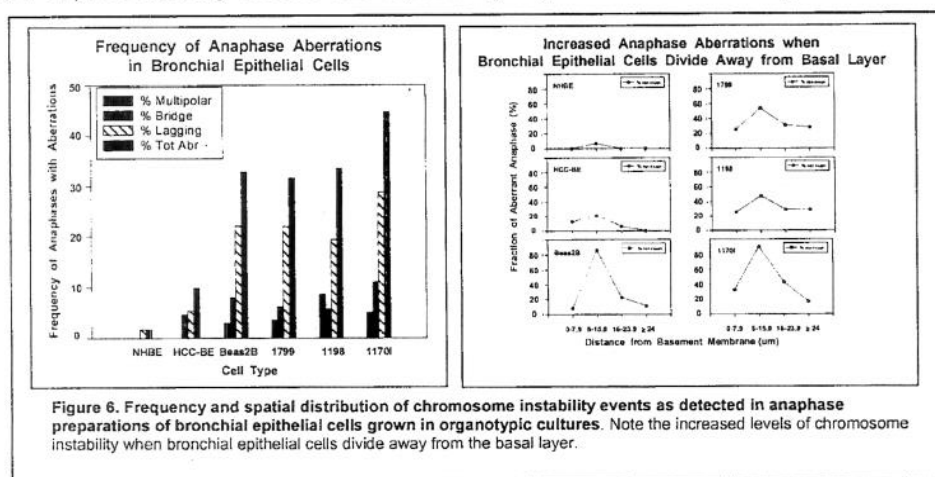
Aim 3 Determine the mechanisms of genetic instability and elucidate the signaling pathways associated with clonal outgrowth of premalignant and malignant bronchial epithelial cells using the organotypic model system

We hypothesize that years of tobacco exposure induces a chronic damage and wound healing cycle that results in the accumulation of genetic alterations in the epithelial cells that influences chromosome stability mechanisms (e.g., loss of cell cycle checkpoint and cell loss mechanisms through loss of p16 expression, p53 mutations, cyclin D1 overexpression, etc) and a poor growth environment (e.g., altered stromal signals). We will utilize the lung organotypic model to address the hypothesis using bronchial epithelial cells derived from LIFE bronchoscopically identified "abnormal" and "normal" regions of the lung of current and former smokers participating in the VITAL trials.

Update

Since the delay of the VITAL trials, we still utilized the same cell types as described above for our pilot studies as presented last year.

In the last report, we indicated that the frequency of ongoing genetic instability events of the various bronchial epithelial cell lines appeared to be low in normal bronchial epithelial cells, slightly elevated in immortalized HccBE1 cells, and significantly increased in the large T-antigen-immortalized Beas2B as well as its derivative, more progressed cell lines (1799, 1198, and tumorigenic 1170I cells). This increased genetic instability appeared to be associated with dysregulated cell cycle proliferation since the frequency of abnormal genetic events (i.e., chromosome instability as evidenced by chromosome bridges and lagging chromosomes at anaphase) seemed to be increased in cells that proliferated away from the basement membrane (Figure 6-left and 6-right). Moreover, the chromosome regions that were physically involved in the chromosome instability events (e.g., lagging chromosome fragments; chromosome bridges) appeared to preferentially involve late replicating regions of the cellular genome.



More recently, we have compared the genetic instability levels in the three HccBE cell lines that had been derived from three different individuals who had a long history of chronic smoking exposure. Of interest, the three cell lines exhibited different levels of chromosome instability in three dimensional cultures as evidenced by the presence of chromosome bridges, lagging chromosomes, and multipolar mitoses. HccBE1 cells showed the highest level of chromosome instability with 23.5% of the anaphases showing lagging chromosomes. Hcc-BE2 cells showed 2.7% and 2.7% of the anaphases with lagging chromosomes or chromosome bridges, respectively. HccBE3 cells showed lower instability levels, closer to that found in normal

bronchial epithelial cells. Interestingly, as found previously, the frequency of chromosomal instability events was increased in cells that proliferated away from the basal layer.

To better understand the molecular mechanisms driving genetic instability, we examined the cell populations growing in the three dimensional, organotypic cultures. We first employed an antibody that recognizes phosphorylated Histone H2AX. Recent studies have indicated that histone H2AX gets phosphorylated and localizes to the sites of DNA double strand breaks. An antibody to phosphorylated H2AX has been used to visualize the location of DNA double strand breaks and their repair foci in cells. More recently, it has been suggested that this antibody can also recognize phosphorylated H2AX in other molecular entities in the cell such as blocked DNA replication forks. We therefore stained organotypic cultures of our various cell lines with this antibody to phosphorylated Histone H2AX and quantified the frequency and spatial localization of labeling. Qualitatively speaking, the frequency of NHBE cells decorated with this antibody was quite low in these organotypic cultures. However, if we irradiated these cells with ionizing radiation just prior to harvesting the cultures, nearly all the cells exhibited nuclear foci with profound positive staining (Figure 7). This suggested that normal bronchial epithelial cells are capable of phosphorylating Histone H2AX when stressed with ionizing radiation; however, they do not show significant Histone H2AX phosphorylation in organotypic culture growth. In striking contrast, tumorigenic 1170 I cells showed a high frequency of cells exhibiting phosphorylated Histone H2AX, even in the unperturbed state of organotypic culture (Figure 8). Two types of staining patterns were detected. Apoptotic cells showed a high uniform nuclear staining pattern, likely associated with DNA fragmentation associated with the apoptotic process. The second pattern of staining observed was the presence of nuclear focal staining, similar to that seen in cells early after exposure to ionizing radiation. Interestingly, the frequency of cells positive for Histone H2AX phosphorylation was markedly increased in cells away from the basal layer.

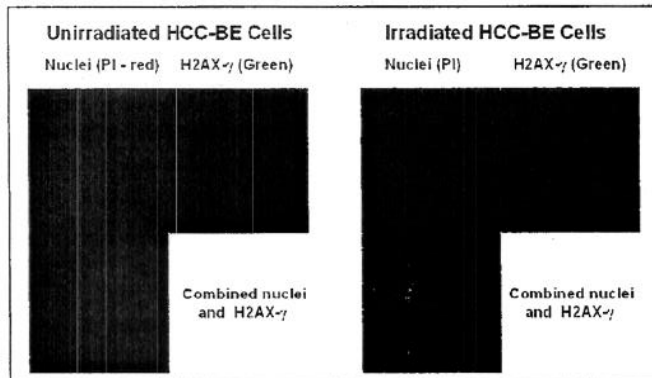


Figure 7. Induction of phosphorylated H2AX foci in organotypic cultures of Hcc-BE cells by ionizing radiation. Hcc-BE cells were grown in organotypic cultures and treated with ionizing radiation 2 hr prior to fixation. Nuclear foci showing phosphorylated H2AX were detected by immunostaining (green) and nuclear counterstaining with PI.

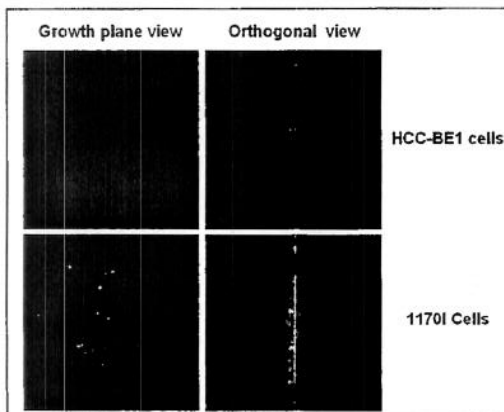


Figure 8. Differential patterns of H2AX γ staining in immortalized Hcc-BE1 cells and in 1170I lung tumor cells. Note the infrequent positive cell in Hcc-BE1 cells and the frequent H2AX γ -positive cells in the 1170I organotypic cultures, especially in cells away from the basal layer.

To determine whether the frequency of cells exhibiting phosphorylated H2AX staining was associated with the degree of chromosome instability, we compared the three HccBE cell lines for their frequencies and spatial location patterns of H2AX phosphorylation staining. Interestingly, HccBE1 cells, the population showing the highest levels of chromosome instability, showed the highest level of phosphorylated H2AX staining when compared to HccBE2 and HccBE3 cells. But as found with other cell lines, the frequencies of cells showing phosphorylated Histone H2AX was highest in cells away from the basal layer. At present, we cannot distinguish whether histone H2AX gets phosphorylated following genetic instability events at mitosis or whether the phosphorylation event precedes the mitotic event, as might be the case if the H2AX phosphorylation was a result of stalled DNA replication forks in cells dysregulated in proliferation away from the basal layer. The latter hypothesis is a distinct possibility since our earlier work indicated that chromosome instability events preferentially involve late replicating genomic regions. In addition, we have shown in other cell systems that the overexpression of cyclin D1 in cells, known to result in alteration of patterns of DNA replication, leads to chromosome instability at mitosis.

Aim 4 Characterize the impact of chemopreventive and/or chemotherapeutic agents on early lung tumorigenesis events in reconstructed bronchial epithelium and in the bronchial biopsies of subjects entered onto the VITAL trials

We proposed to determine whether treatment of these organotypic cultures with the chemopreventive agents used in the clinical trial of Project 1 would slow the aberrant properties such as clonal expansion and genetic instability *in vitro* and whether results obtained in the organotypic culture model reflected those seen in the lungs of the participants in the VITAL trials.

Update

We have not yet initiated the studies associated with Specific Aim 4. However, the new fluorescence bronchoscopy apparatus is now approved for use at M. D. Anderson Cancer Center and as our bronchial endoscopists become more familiar with the use of the instrument, we will finally be able to initiate this part of the project.

Conclusions

We have successfully completed pilot experiments that will ensure success with the bronchial biopsy and brush specimens that will be obtained from LIFE bronchoscopy of participants in the clinical trials of Project 1. We have developed and demonstrated our capability to perform gene expression microarray analyses on bronchial epithelial cells obtained from endobronchoscopic procedures. We have also developed and demonstrated our capability to carry out clonal expansion and genetic instability analyses of bronchial epithelial cell populations grown in a lung organotypic model. Our future plans will focus on utilizing bronchial specimens derived from participants of the clinical trial of Project 1. In particular, we will compare the gene expression patterns between bronchial epithelial regions that appear positive with those that appear negative on LIFE bronchoscopy. We also will inoculate bronchial epithelial cells derived from these biopsies into organotypic cultures and examine their ability of preferential take over of growth surface from other bronchial epithelial cells, examine their degree of chromosome instability in organotypic culture, and examine the effect of chemopreventive agents on preferential clonal outgrowth and genetic instability. We will also begin to seek additional funding to support expanded studies on the molecular underpinnings of preferential clonal expansion and genetic instability using this organotypic culture model.

Project 4: Modulation of Death Receptor-Mediated Apoptosis for Chemoprevention

(Project Leader and co-leader: Shi-Yong Sun, Ph.D.; Fadlo R. Khuri, M.D.)

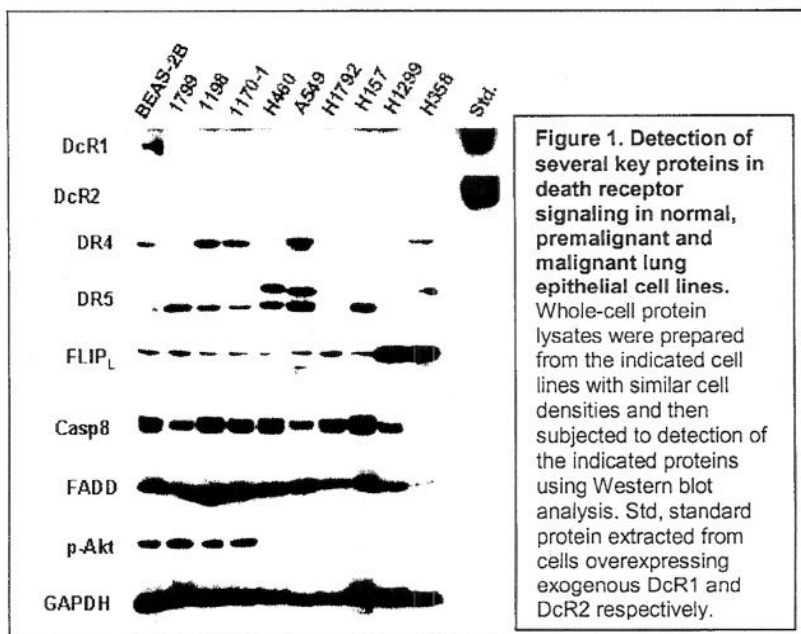
The objective is to understand the role of death receptor (DR)-mediated apoptotic pathways in lung carcinogenesis, cancer prevention, and therapy in order to develop mechanism-driven combination regimens by modulating DR-mediated apoptosis for chemoprevention and therapy of lung cancer.

Aim 1 To determine whether decoy receptor (DcR) and TRAIL expression are reduced or lost while DR remains largely expressed and whether procaspase-8 and FLIP expression and Akt activity are increased during lung carcinogenesis.

Update

As reported last year, we have optimized the IHC conditions for staining of DR4, DR5, DcR1, DcR2, phospho-Akt, TRAIL, FLIP and caspase-8.

Since the tissue specimens are not available, we instead conducted some western blotting to examine the expression of several key proteins in death receptor signaling pathways in a panel of cell lines including normal, premalignant, transformed or cancer cells. DR4 and DR5, as expected, expressed in the majority of cell lines. DcR1 expression was detected in normal BEAS-2B cells, but not in the rest of premalignant and malignant lung epithelial cell lines, whereas DcR2 was not detected in all of the cell lines. FLIP, FADD, and caspase-8 were detected in all of the tested cell lines with comparable levels except for FLIP, which was high in some lung cancer cell lines such as H1299 and H358 cells. Unexpectedly, we detected higher levels of p-Akt in normal BEAS-2B cells and its derived cell lines (1799, 1198 and 1170-1) than in many other lung cancer cell lines (Fig. 1). Our recent data from head and neck cancer cells clearly show that these proteins are indeed differentially expressed between low grade of metastatic and high grade of metastatic head and neck cancer cells. Considering the difficulty in getting premalignant lung tissues, we planned to examine the expression of these proteins in normal lung tissue, and primary and metastatic lung cancer tissues using IHC. We already purchased commercial tissue arrays that contain these tissues. We also discussed with Dr. Ignacio Wistuba the possibility of using similar tissue arrays generated in his laboratory at M. D. Anderson Cancer Center.



Aim 2 To establish TRAIL-resistant cell lines from a TRAIL-sensitive lung cancer cell line and then determine whether levels of DcRs, DRs, procaspase-8, TRAIL, FLIP, and Akt activity are altered and are associated with cell resistance to TRAIL and DR-inducing agents

Update

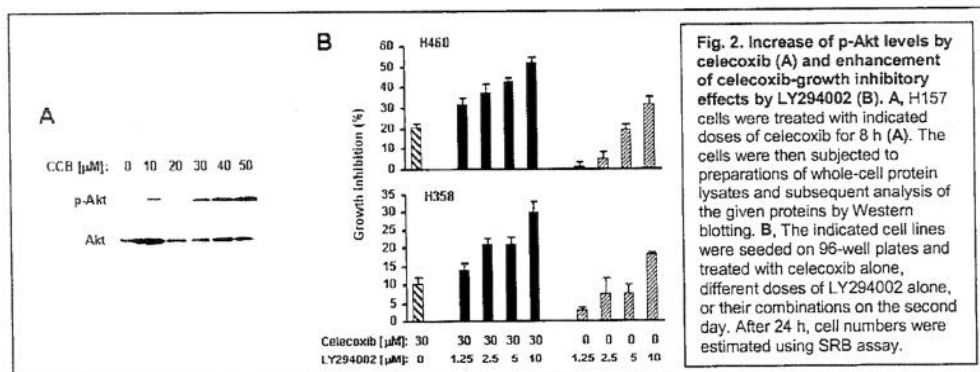
In the previous report, we showed that we established a TRAIL resistant cell line named H460-TR. By comparing the effects of various therapeutic agents including celecoxib, SCH66336, PS-341, perifosine, 4HPR, taxotere, and doxorubicin on the growth of TRAIL-sensitive cell line H460 and H460-TR cells, we found that all of these agents decreased the survival of both H460 and H460-TR cells with similar degrees, indicating that the cell line resistant to TRAIL is not cross-resistant to other therapeutic agents.

Aim 3 To determine whether suppression of PI3K/Akt activity sensitizes premalignant and/or malignant airway epithelial cells to apoptosis induced by DR-induced agents via enhancement of TRAIL/DR-mediated mechanism

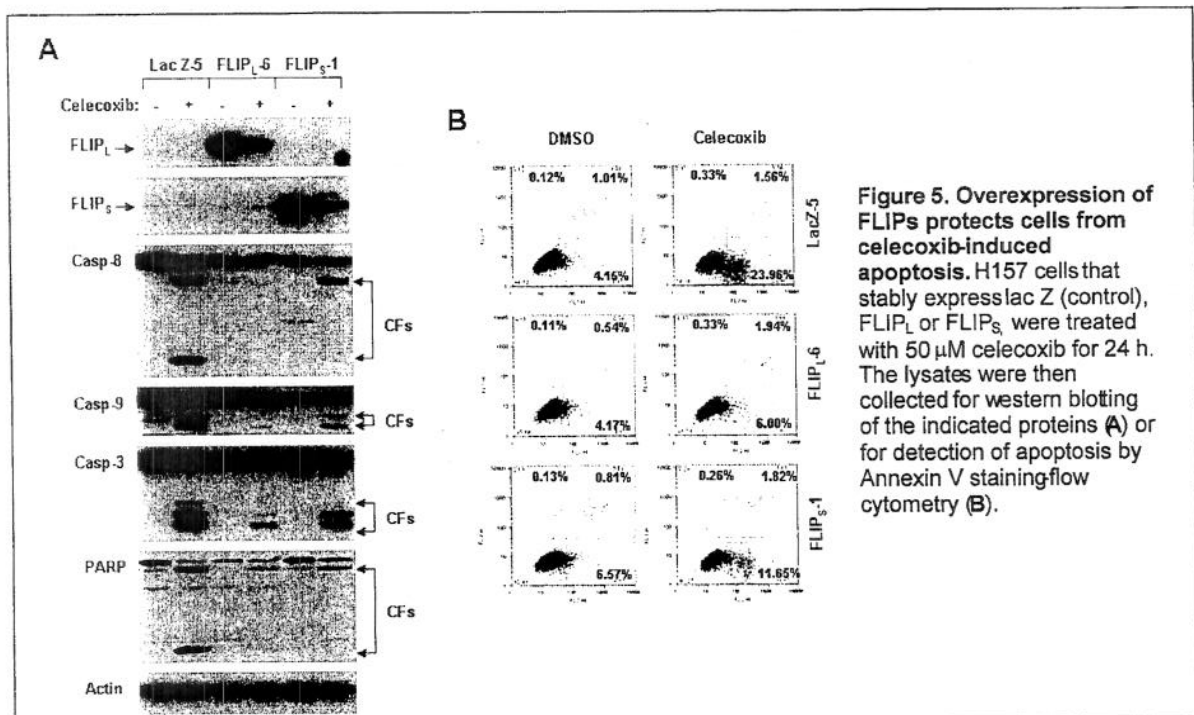
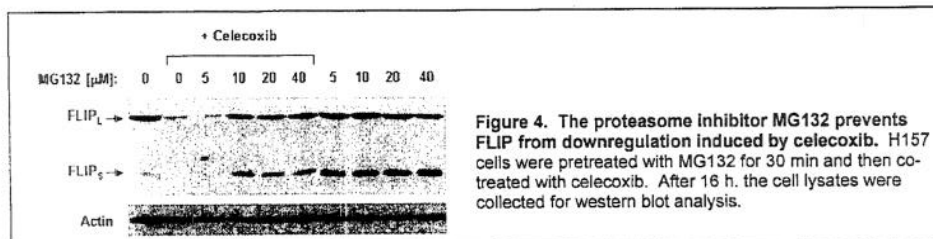
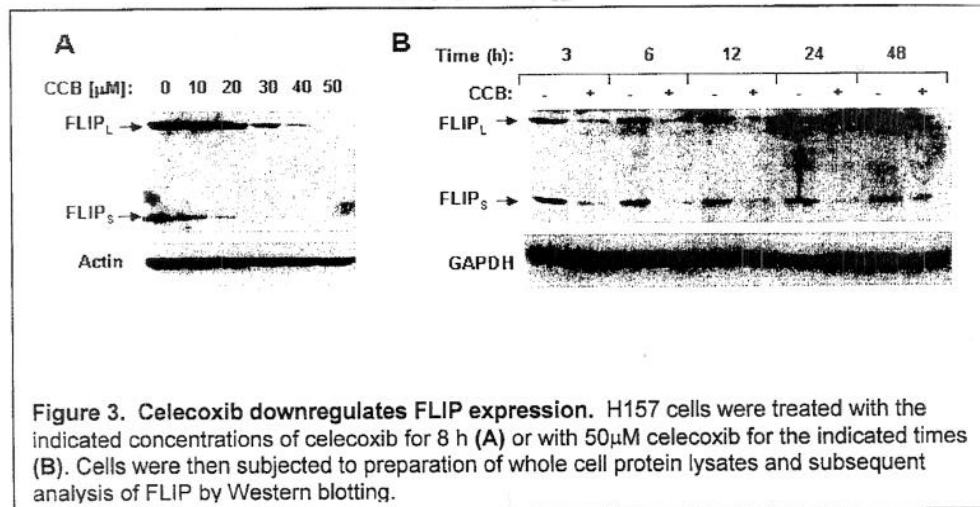
Update

As reported previously, we need first to identify the apoptosis-induced agents that can induce death receptors (DR), especially ones used in the VITAL trials such as celecoxib. We found that the celecoxib-induced and lonafarnib-induced apoptosis links to DR-mediated extrinsic apoptotic pathway in human cancer cells (Liu et al. 2004), and lonafarnib did not alter phospho-Akt expression in most human NSCLC cell lines.

Recently, our results also show that celecoxib increased p-Akt levels in some lung cancer cell lines (Figure 2A). The combination of celecoxib and LY294002 apparently inhibited the growth of human lung cancer cells in an augmented manner (Figure 2B). We also checked the effects of celecoxib combined with Iressa and found only limited enhanced growth inhibitory effects in some lung cancer cell lines.



Moreover, we found that celecoxib downregulated the expression of FLIP, a major negative regulator of the DR-mediated extrinsic apoptotic pathway, in lung cancer cells (Figure 3), further supporting that activation of the DR5-mediated death pathway plays a critical role in celecoxib-induced apoptosis. In the presence of the proteasome inhibitor MG132, celecoxib failed to reduce levels of FLIP protein (Figure 4), suggesting that celecoxib downregulates FLIP levels through promoting proteasome-mediated protein degradation. Overexpression of FLIPs, particularly FLIP_L, inhibited not only celecoxib-induced apoptosis, but also apoptosis induced by the combination of celecoxib and TRAIL (see Figure 5 as an example). These results indicate that FLIP downregulation also contributes to celecoxib-induced apoptosis and enhancement of TRAIL-induced apoptosis, which complements our previous finding that the DR5-mediated extrinsic apoptotic pathway plays a critical role in celecoxib-induced apoptosis in human lung cancer cells. Collectively, we conclude that celecoxib induces apoptosis in human lung cancer cells through activation of the extrinsic apoptotic pathway, primarily by induction of DR5 and downregulation of FLIP.



We also used the lentiviral gene delivery system to successfully establish several stable lung cancer cell lines that overexpress FLIP_L and FLIP_S respectively, including H157, A549 and H460 cells. They will be used to examine the impact of FLIP overexpression on apoptosis induced by the proposed combinations to test whether the combinations induce apoptosis through activation of the extrinsic apoptotic pathway. In addition, we conducted transient expression of FLIPs using the same lentiviral expression system.

Some of the studies can be reviewed in *Apoptosis* (Sun et al., 2006) and AACR Abstract (Liu et al., 2006). Based on these findings, we have submitted a NCI R01 and are writing a manuscript.

Aim 4 To determine whether DRs, DcRs, FLIP, and procaspase-8 serve as biomarkers for lung cancer chemoprevention and therapy.

Update

The conditions for IHC staining of these proteins have been optimized and we are ready for analysis of patient samples. We expect to receive tissue array slides generated in Dr. Wistuba's laboratory at M.D. Anderson Cancer Center, which will include the patient samples collected from the VITAL trials.

Conclusion

We have concluded that death receptors mediate a major intracellular apoptotic pathway. Defects or dysregulation in this pathway may contribute to lung carcinogenesis, whereas appropriate modulation such as upregulation of DR4 or DR5 by small molecules such as celecoxib and lonafarnib may eliminate premalignant or malignant lung epithelial cells via promoting apoptotic cell death to achieve cancer chemopreventive and therapeutic goals.

Project 5: Molecular Strategies Targeting the AKT Signaling Pathway for Lung Cancer Chemoprevention and Therapy

(PI and co-PI: Ho-Young Lee, Ph.D., Edward S. Kim, M.D.)

The purpose of the studies is to determine whether activation of Akt induces malignant transformation of HBE cells and to develop novel agents inhibiting Akt activity as a strategy of lung cancer chemoprevention.

Aim 1 Develop an adenoviral vector expressing constitutively active Akt and characterize the *in vitro* and *in vivo* effects of Akt activation on the malignant transformation of HBE cells.

Update

We have constructed adenoviral and retroviral vectors expressing constitutively active or dominant negative Akt1, 2, or 3 and confirmed their expression by sequencing and western blot analysis.

Adenoviruses were amplified using 293 cells and viral titers were determined by plaque assays and spectrophotometric analysis. Retroviruses were made by transfecting plasmid that contains the cDNA of interest into the packaging cell line PhoenixE. The supernatants from these cells were used to infect the amphotropic packaging cell line PA317. After 10 days of puromycin (3 mg/ml) selection, the supernatants from the PA317 cells were filtered and used to infect HB56B cells. After the infection, cells were selected using puromycin (750 ng/ml) for 2 weeks and then single cell subclones of constitutively active Akt-expressing HB56B cells were determined by Western blot analysis of HA.

The first part of the aim is completed.

Aim 2 Evaluate the ability of chemopreventive agents used in VITAL trials alone and in combination to inhibit Akt activity and induce apoptosis in transformed human bronchial epithelial cells (HBE) and NSCLC cell lines.

Update

Previously, we reported effects of Akt inhibitors (LY294002, Ad5-PTEN, and dominant-negative Akt (Ad5-HA-Akt-KM) on the proliferation of normal, premalignant (1799 and 1198), and malignant (1170-1) HBE cells, and also retrospectively investigated beneficial activities of 9-*cis*-RA on former smokers (Han et al., 2005).

This year, we tested agents gefitinib, erlotinib, Tarceva, SCH66336, and celecoxib on the proliferation of the same cells. We found that celecoxib did not suppress the proliferation of 1179, 1198, and 1170-1 cells at doses less than 10 μ M, a dose higher than the dose achievable *in vivo* in clinical trial. We also determined the antiproliferative effects of SCH66336, a farnesyl transferase inhibitor (FTI) that was originally designed to inhibit Ras activation and also inhibits Akt activation (Lee et al, 2004; Chun et al, 2003), comparing with those of deguelin, an Akt inhibitor (Lee et al, 2005). SCH66336 did not show specific cytotoxic effects on premalignant and malignant HBE cells, but had highly antiproliferative effects on premalignant and malignant HBE cells as well as NHBE cells (Lee et al, 2004). We found that gefitinib and erlotinib inhibited immortalized HBE cells more effectively compared to premalignant and malignant HBE cells. These findings suggest that premalignant and malignant HBE cells develop alternative survival pathways in response to blockade of the EGFR pathway.

Aim 3 Determine whether Akt is activated in bronchial specimens from enrolled patients in VITAL trials and whether treatment with chemopreventive agents suppresses Akt level or activity in these patients.

Dr. Wistuba, Pathology Core, has completed the priority distribution list and will begin to distribute the samples to VITAL individual investigators. On receipt of the samples, we will commence Aim 3.

Conclusion

Celecoxib may not be an effective antiproliferative agent. FTI SCH66336 may not be an effective chemopreventive agent due to its cytotoxicity on NHBE cells. EGFR TKIs induce alternative survival/proliferation pathways in premalignant and malignant HBE cells in response to the blockade of EGFR. Understanding the mechanism may provide better chemopreventive strategies using EGFR TKIs.

Core B: Biostatistics & Data Management Core

(Core Director: J. Jack Lee, Ph.D.)

Core Goals

1. To provide statistical design, sample size/power calculations, and integrated, comprehensive analysis for each basic science, pre-clinical, and clinical study.
2. To develop a data management system that provides tracking, quality control, and integration of clinical, pathological, and basic science data.
3. To provide statistical and data management support for genomic and imaging studies including microarray, proteomics, protein antibody array, and spiral CT.
4. To develop and adapt innovative statistical methods pertinent to biomarker-integrated translational lung cancer studies.
5. To generate statistical reports for all projects.
6. To collaborate and assist all project investigators in the publication of scientific results.

The Biostatistics and Data Management Core has continued to work actively with all the VITAL Projects in their research efforts, especially in the area of biostatistical support and consulting in the clinical trial design, implementation, and analysis of experimental results.

Update

In the first year, we provided statistical support for study preparation and submission of the Vanguard trial and started to develop a web-enabled database system to facilitate the conduct of the trial.

This year, our major effort is in the area of providing statistical/data management support for the Vanguard trial and the adjuvant celecoxib trial. Biostatistical Core was involved in the protocol design, submission and revision process. We have interacted with the study PI, IRB, and regulatory agencies to address critiques and provide revisions. We also met with investigators and research coordinators and provided assistance in designing the Case Report Forms (CRFs) for both trials.

Also, we have completed the web-enabled database system to facilitate the conduct of both trials. The database allows remote data capture from any computer with a web browser. It is secured, password protected, and is within our institutional firewall. The database also allows the research nurse to schedule patient visits and prints labels for tissue acquisition. It can track tissue distribution in both sending and receiving. The integrated reporting system provides real-time inventory reports based on the most up-to-date data. Selected screen shots are provided in Appendix 1. The database is fully functional and has captured 19 patients registered in the Vanguard trial as of November 2005.

In addition, we have reviewed statistical methods for evaluating interaction for combination therapy to determine whether the effect is synergistic, additive, or antagonistic. The current available methods require strong assumptions such as the drug interaction follows the same pattern at all doses. It is possible that the combination may produce a synergistic effect in a certain dose range, but may be additive or antagonistic in other dose ranges. We are developing two new statistical methods – one parametric generalized response surface model and one semi-parametric model that allow more general interaction patterns for the drug interaction and ease the restriction of the existing methods. The work was presented at the Spring Meeting of the International Biometric Society, Eastern North America Region in March 2005 and the Joint Statistical Meeting in August 2005. The S-PLUS codes are available for download as well. More information on the synergy research may be found in Appendix 2.

Three manuscripts have been submitted and one has gone through revision (Lee et al, 2005; Kong et al, 2005-1; Kong et al, 2005-2).

Conclusion

We continue to provide statistical support for all projects and develop related tools such as web-based databases to facilitate the interaction of clinical and basic research projects.

Core C: Pathology and Specimen Procurement Core

(Core and co-Core Director: Ignacio Wistuba, M.D. Adel K. El-Naggar, M.D.)

Aim 1 Develop and maintain a repository of tissue and other biologic specimens from patients enrolled on the clinical trials in Project 1.

Update

As reported last year, we established all procedures for sample collection, processing, banking, and distribution and were ready for conducting studies in Aim 1.

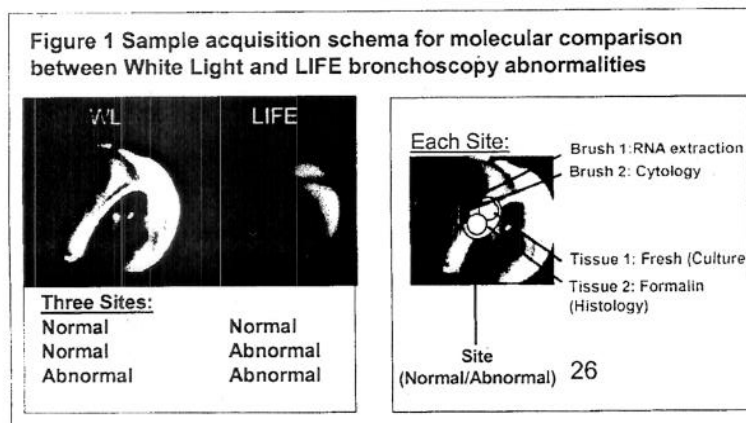
This year, the Core has been acquiring and banking the specimens obtained from bronchoscopies performed in subjects enrolled in the Vanguard Trials (Project 1). Samples from 14 baseline bronchoscopies have been obtained, processed and banked in the Core tissue bank (Table 1). We have also developed a sample processing kit that will be distributed to the three institutions that are recruiting patients for the trials. One set of bronchoscopy specimens was successfully received from Eisenhower Army Medical Center. In addition, resected specimens from lung cancer and head/neck tumors have been obtained, reviewed and banked in most cases.

Table 1. Specimens Collected and Banked in the Pathology Core (14 bronchoscopies)

Bx #	Timeline	Sputum	Buccal Brush	Bronchial Wash and BAL	Bronchial Brushes	Bronchial Tissue
1	Baseline	Yes	Yes	Yes / Yes	Yes (6)	Yes (6)
2	Baseline	Yes	Yes	Yes / Yes	Yes (6)	Yes (6)
3	Baseline	Yes	Yes	Yes / Yes	Yes (6)	Yes (6)
4	Baseline	Yes	Yes	Yes / Yes	Yes (6)	Yes (6)
5	Baseline	Yes	Yes	Yes / Yes	Yes (6)	Yes (6)
6	Baseline	No	Yes	Yes / Yes	Yes (6)	Yes (6)
7	Baseline	Yes	Yes	Yes / Yes	Yes (6)	Yes (6)
8	Baseline	Yes	Yes	Yes / Yes	Yes (6)	Yes (8)
9	Baseline	Yes	Yes	Yes / Yes	Yes (6)	Yes (10)
10	Baseline	Yes	Yes	Yes / Yes	Yes (6)	Yes (6)
11	Baseline	Yes	Yes	Yes / Yes	Yes (6)	Yes (6)
12*	Baseline	Yes	Yes	Yes / Yes	Yes (6)	Yes (5)
13	Baseline	Yes	Yes	Yes / Yes	Yes (6)	Yes (6)
14	Baseline	Yes	Yes	Yes / Yes	Yes (6)	Yes (6)
Total Samples		13	14	28	84	89

* Eisenhower Army Medical Center

A schema of specimen collection for Project 3 has been developed. Drs. Koo and Hittelman in Project 3 are interested in identifying the molecular abnormalities in the bronchial mucosa examined under the fluorescent bronchoscopy (LIFE instrument) (Figure 1). Three types of



bronchial mucosa sites will be taken from each patient including 1) normal white light (WL) and normal LIFE bronchoscopy features, 2) abnormal WL and normal LIFE, and 3) normal WL and abnormal LIFE. For each site, 2 biopsies will be taken (one for cell

culture and the other for histology assessment) and 2 brushes (one for RNA extraction and the other for cytology examination). So far, samples have been obtained from 6 patients.

Aim 2 Maintain a comprehensive database of tissue and specimen characteristics from patients enrolled in the clinical trials of Project 1, including pathologic characteristics of each specimen, inventory and distribution

Update

The Biostatistics Core has developed a web-based database (see Core B report). We have used the database to track and inventory bronchoscopy specimens, and to report

Figure 2. Database form (A) to enter histology diagnosis for bronchoscopy biopsy specimens and histological categories (B)

Figure 2 shows two parts of a database form. Part A is a screenshot of a web-based form for entering histology diagnosis. It includes fields for 'Specimen ID', 'Patient ID', 'Date', 'Location', 'Size', 'Fluorescent Abnormality Score', and 'Histology Diagnosis'. Part B is a list of histological categories with their corresponding codes. The categories include: Adenocarcinoma (A1), Squamous Cell Carcinoma (A2), Small Cell Carcinoma (A3), Bronchioloalveolar Carcinoma (A4), Bronchial Carcinoma (A5), Bronchioloalveolar Carcinoma (A6), Bronchioloalveolar Carcinoma (A7), Bronchioloalveolar Carcinoma (A8), Bronchioloalveolar Carcinoma (A9), Bronchioloalveolar Carcinoma (A10), Bronchioloalveolar Carcinoma (A11), Bronchioloalveolar Carcinoma (A12), Bronchioloalveolar Carcinoma (A13), Bronchioloalveolar Carcinoma (A14), Bronchioloalveolar Carcinoma (A15), Bronchioloalveolar Carcinoma (A16), Bronchioloalveolar Carcinoma (A17), Bronchioloalveolar Carcinoma (A18), Bronchioloalveolar Carcinoma (A19), Bronchioloalveolar Carcinoma (A20), Bronchioloalveolar Carcinoma (A21), Bronchioloalveolar Carcinoma (A22), Bronchioloalveolar Carcinoma (A23), Bronchioloalveolar Carcinoma (A24), Bronchioloalveolar Carcinoma (A25), Bronchioloalveolar Carcinoma (A26), Bronchioloalveolar Carcinoma (A27), Bronchioloalveolar Carcinoma (A28), Bronchioloalveolar Carcinoma (A29), Bronchioloalveolar Carcinoma (A30), Bronchioloalveolar Carcinoma (A31), Bronchioloalveolar Carcinoma (A32), Bronchioloalveolar Carcinoma (A33), Bronchioloalveolar Carcinoma (A34), Bronchioloalveolar Carcinoma (A35), Bronchioloalveolar Carcinoma (A36), Bronchioloalveolar Carcinoma (A37), Bronchioloalveolar Carcinoma (A38), Bronchioloalveolar Carcinoma (A39), Bronchioloalveolar Carcinoma (A40), Bronchioloalveolar Carcinoma (A41), Bronchioloalveolar Carcinoma (A42), Bronchioloalveolar Carcinoma (A43), Bronchioloalveolar Carcinoma (A44), Bronchioloalveolar Carcinoma (A45), Bronchioloalveolar Carcinoma (A46), Bronchioloalveolar Carcinoma (A47), Bronchioloalveolar Carcinoma (A48), Bronchioloalveolar Carcinoma (A49), Bronchioloalveolar Carcinoma (A50), Bronchioloalveolar Carcinoma (A51), Bronchioloalveolar Carcinoma (A52), Bronchioloalveolar Carcinoma (A53), Bronchioloalveolar Carcinoma (A54), Bronchioloalveolar Carcinoma (A55), Bronchioloalveolar Carcinoma (A56), Bronchioloalveolar Carcinoma (A57), Bronchioloalveolar Carcinoma (A58), Bronchioloalveolar Carcinoma (A59), Bronchioloalveolar Carcinoma (A60), Bronchioloalveolar Carcinoma (A61), Bronchioloalveolar Carcinoma (A62), Bronchioloalveolar Carcinoma (A63), Bronchioloalveolar Carcinoma (A64), Bronchioloalveolar Carcinoma (A65), Bronchioloalveolar Carcinoma (A66), Bronchioloalveolar Carcinoma (A67), Bronchioloalveolar Carcinoma (A68), Bronchioloalveolar Carcinoma (A69), Bronchioloalveolar Carcinoma (A70), Bronchioloalveolar Carcinoma (A71), Bronchioloalveolar Carcinoma (A72), Bronchioloalveolar Carcinoma (A73), Bronchioloalveolar Carcinoma (A74), Bronchioloalveolar Carcinoma (A75), Bronchioloalveolar Carcinoma (A76), Bronchioloalveolar Carcinoma (A77), Bronchioloalveolar Carcinoma (A78), Bronchioloalveolar Carcinoma (A79), Bronchioloalveolar Carcinoma (A80), Bronchioloalveolar Carcinoma (A81), Bronchioloalveolar Carcinoma (A82), Bronchioloalveolar Carcinoma (A83), Bronchioloalveolar Carcinoma (A84), Bronchioloalveolar Carcinoma (A85), Bronchioloalveolar Carcinoma (A86), Bronchioloalveolar Carcinoma (A87), Bronchioloalveolar Carcinoma (A88), Bronchioloalveolar Carcinoma (A89), Bronchioloalveolar Carcinoma (A90), Bronchioloalveolar Carcinoma (A91), Bronchioloalveolar Carcinoma (A92), Bronchioloalveolar Carcinoma (A93), Bronchioloalveolar Carcinoma (A94), Bronchioloalveolar Carcinoma (A95), Bronchioloalveolar Carcinoma (A96), Bronchioloalveolar Carcinoma (A97), Bronchioloalveolar Carcinoma (A98), Bronchioloalveolar Carcinoma (A99), Bronchioloalveolar Carcinoma (A100).

histopathological features of the bronchial mucosa from the bronchoscopy biopsy (Figure 2). From 14 patients, 139 cytological specimens and 89 bronchial biopsies have been tracked and inventoried using the web-site database.

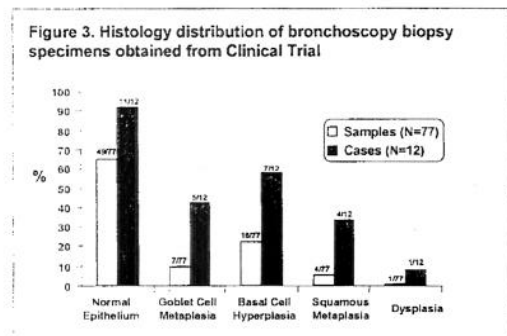
In collaboration with investigators from the Clinical Trials (Project 1), correlation between histopathological changes and white-light (WL) and LIFE bronchoscopy examination abnormalities is also being studied. LIFE bronchoscopy abnormalities, including

number of lesions, location, size and fluorescent abnormality scores, are being recorded to correlate with histopathological features. Electronic images of WL and LIFE abnormalities and histopathology are being captured and banked in the database.

Aim 3 Provide comprehensive pathologic characterization of all tissues and other biologic specimens and assist in preparation and evaluation of studies involving these tissues

Update

Using the comprehensive list of histology diagnosis for bronchoscopy biopsies prepared last year (Table 2B), we have processed and histopathologically diagnosed 77 tissue specimens from 12 baseline bronchoscopies in a timely fashion (Figure 3). Although normal bronchial



dysplastic lesions have been not detected. Tissue blocks from all these samples are available for future biomarker analysis.

Aim 4 Provide centralized immunohistochemistry and laser capture microdissection services, nucleic acid extractions and assistance with construction and evaluation of tissue arrays.

Update

As reported last year, a centralized immunohistochemistry (IHC) laboratory has been in place as part of the Pathology Core, having manual and automated immunohistochemical techniques and *in situ* tissue-based methodologies, such as FISH and laser capture microdissection available for investigators. Tissue microarray (TMA) construction is also in place, and a complete set of lung cancer specimens (N = 400) and corresponding bronchial and peripheral lung preneoplastic lesions (from 200 increased to 300) are available.

A priority sample distribution list for VITAL individual projects has been developed for IHC biomarker analysis using formalin-fixed and paraffin-embedded bronchial tissues (Table 2).

Table 2. Priority distribution list of histology sections (N=20) from bronchoscopy tissue specimens

Project	Marker	Number of Sections
Project 2 (Dr. Mao)	To validate differentially expressed proteins – Total	5
Project 3 (Drs. Hittelman/Koo)	To validate differentially expressed proteins – Total	5
Project 4 (Drs. Sun/Khuri)	DR5	1
	DR4	1
	COX-2	1
	DcR1	1
	DcR2	1
	Total	5
Project 5 (Dr. Lee)	Akt	1
	p-Akt	1
	Casp-3	1
	PARP	1
	p-mTOR	1
	Total	5

Conclusion

We have acquired and banked specimens from 14 bronchoscopy biopsies and 18 resected specimens from lung cancer and head/neck tumor patients; used the web-enabled database developed by the Biostatistics Core to track and inventory bronchoscopy specimens and report histopathological features of the bronchial mucosa from the bronchoscopy biopsy; and developed a priority sample distribution list for VITAL projects for IHC biomarker analysis using formalin-fixed and paraffin-embedded bronchial tissues.

Additional Research Activities: Molecular Pathogenesis of Lung Cancer

The main goal of the VITAL research program is to provide a better understanding of the cellular and molecular events that drive lung tumorigenesis. Thus, using a molecular pathology approach, we have attempted to understand the early molecular pathogenesis of lung cancer. We selected lung adenocarcinoma, the most frequent (~50%) histological type of lung cancer, for which there is limited knowledge early molecular pathogenesis. Recent data suggest that at least two molecular pathways (*KRAS* and *EGFR*) are involved for the development of invasive lung adenocarcinomas (alveolar adenomatous hyperplasia, AAH) in smoker and non-smoker populations, respectively. Thus, we decided to address the following questions:

- Identify the sequence of *EGFR* molecular events involved in the pathogenesis lung adenocarcinomas
- Compare the molecular events in the early pathogenesis of lung adenocarcinomas between *EGFR* and *KRAS* mutant cases

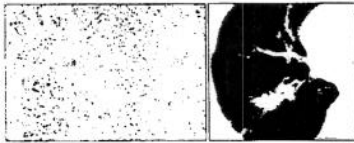
Update

- Identify the sequence of *EGFR* molecular events involved in the pathogenesis of lung adenocarcinomas.

Two cohorts of patients were analyzed. First, we evaluated 159 surgically resected NSCLC tumors for analysis of *EGFR* (exon 18-21) and *KRAS* (codon 12-13) mutations and IHC of *EGFR*, phosphorylated-*EGFR* and *HER2/Neu*, and correlated the results with clinical outcomes, patient and disease features. Of 159 patients, 14 had *EGFR* mutations and 18 had *KRAS* mutations. *EGFR* mutations were associated with several clinical and pathological features

Figure 4. Clinicopathological features of *EGFR* mutated NSCLC patients (N=159)

EGFR mutations were associated with:	
• Adenocarcinoma	$P = 0.002$
• Females	$P = 0.02$
• Never-smoking	$P < 0.0001$
• Easter Asian ethnicity	$P = 0.005$
• Air bronchograms	$P = 0.004$
• Multiple wedge resections	$P = 0.03$



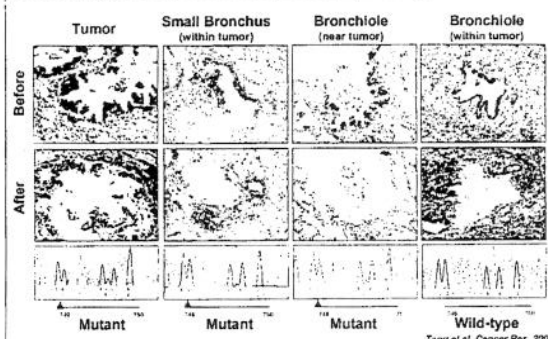
Tsao et al, JTO in press

(Figure 4). Although statistical significance was not reached, a higher incidence of synchronous primary cancers (36% versus 17%; $p=0.09$) and smaller median tumor size (11.8 cm³ versus 24.0 cm³; $p=0.24$) were seen. There was no difference in disease-free survival while median overall survival in patients with *EGFR* mutations was shorter (3.49 versus 4.29 years, $p=0.85$). *EGFR* mutation did not correlate with immunohistochemistry.

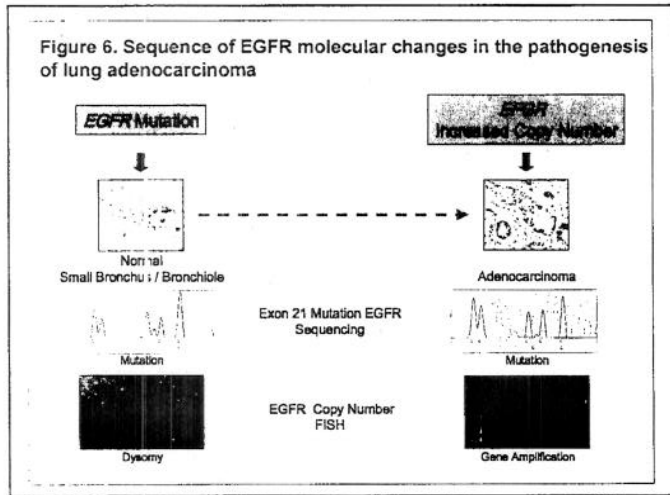
Second, we selected a cohort of Asian patients ($n=22$) and compared the *EGFR* mutation status with the birthplace and immigration to the United States. 12 of 22 (55%) Asian patients had the mutation. Of interest, there was no geographic difference in the incidence of *EGFR* mutation. Asian women with the *EGFR* mutation developed adenocarcinoma at an earlier age than other lung cancer patients. There is a distinct clinical profile for NSCLC patients with the *EGFR* mutation. However, this mutation does not alter disease-free survival and is likely due to an inherited susceptibility instead of an environmental effect (Tsao et al, in press).

To investigate in which pathogenesis stage of lung adenocarcinoma *EGFR* mutations commence, we examined the *EGFR* mutations in peripheral airway respiratory epithelia (small bronchi and bronchioles) obtained from 21 patients with lung adenocarcinoma harboring *EGFR* mutations. We compared the findings with those obtained from 16 lung cancer patients whose tumors had wild-type *EGFR*. A representative example of tumor and respiratory epithelium microdissection and *EGFR* sequencing analysis is shown in Figure 5. *EGFR* mutations were detected in the normal respiratory epithelium in 9 of 21 (43%) patients with *EGFR* mutant adenocarcinomas, but none in patients without mutation in the tumors. The finding of mutations being more frequent in normal epithelium within tumor (43%) than in adjacent sites (24%) suggests a phenomenon of localized field effect. Our findings indicate that mutation of the tyrosine kinase domain of *EGFR* is an early event in the pathogenesis of lung adenocarcinomas, and can

Figure 5. Histology, microdissection and sequencing of an *EGFR* mutant lung adenocarcinoma 15bp deletion (Exon 19)



be an early detection marker and chemoprevention target (Tang et al, 2005).



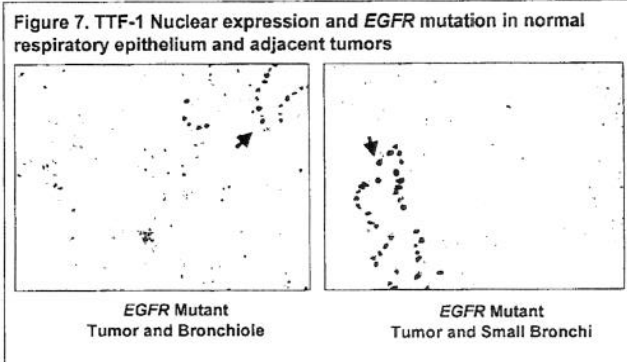
To determine the sequence of *EGFR* mutation and increased copy number, we performed a detailed mapping analysis correlating in the same tissue sites *EGFR* mutation, gene copy number and protein expression in 65 formalin-fixed tissue sites comprising normal bronchial/bronchiolar epithelium (NBE; N=22) and primary tumors (PT; N=43) from 9 surgically resected lung adenocarcinomas bearing *EGFR* mutations (exons 19 and 21). High levels of polysomy and gene amplification were considered as increased copy number. *EGFR* mutation was found in 18% (4/22)

NBE and 91% (39/43) PT sites. Low genomic gain was found in 8 NBE sites (37%), but increased copy number was not detected. Of interest, the 4 *EGFR* mutant NBE sites exhibited normal gene copy number. Our findings indicate that *EGFR* mutation precedes genomic gain in the sequential pathogenesis of lung adenocarcinoma (Figure 6).

- **Compare the molecular events in early pathogenesis of lung adenocarcinomas between *EGFR* and *KRAS* mutant cases**

Lung adenocarcinoma is usually diagnosed at advanced stages. New strategies for early diagnosis are needed. Although little is known about the histological precursors and the molecular events preceding the development of lung adenocarcinoma, at least 2 molecular pathways have been suggested: *KRAS* and *EGFR* mutation; the latter associated with non-smokers and East Asian ethnicity. Recently, we reported that *EGFR* mutations were detected in histologically normal bronchial/bronchiolar epithelium (NBE) in 43% of patients with *EGFR* mutant lung adenocarcinomas (Tang et al, 2005), indicating that this mutation represents an early "field" event in the pathogenesis of this neoplasm.

To investigate further the molecular abnormalities in the lung respiratory epithelium "field" in lung adenocarcinoma patients, we performed a detailed mapping analysis of *KRAS* and *EGFR* mutations in NBE adjacent to mutant and wild-type tumors. In NBE sites we correlated *EGFR* mutation status with immunohistochemical (IHC) expression of *EGFR* and TTF-1 (a marker for lung terminal respiratory cell differentiation) proteins (Figure 7). We selected 191 of NBE sites from 50 surgically resected lung adenocarcinomas including 12 *KRAS* mutated, 24 *EGFR* mutated (12, East Asian ethnicity), and 14 wild-type tumors. We found that 1) no *KRAS* mutation was detected in 61 NBE sites from 12 *KRAS* mutated and 11 wild-type tumors; 2) a similar frequency of *EGFR* mutation in NBE by patients (12/24, 50%) and by epithelial site (22/73, 30%) was detected in *EGFR* mutated adenocarcinomas, but *EGFR* mutations in 6 (11%) NBE sites from 3 (12%) patients



with *EGFR* wild-type tumors were found; 3) we identified 5 NBE sites from 3 East Asian patients that demonstrated different mutation patterns than their corresponding tumors different from those previously reported (the same type of *EGFR* mutation was detected in NBE and corresponding tumor); 4) No correlation among *EGFR* and p-*EGFR* expression and *EGFR* mutation was detected in NBE and interestingly, 13/21 (62%) of *EGFR* mutated NBE sites did not express TTF-1. Our findings indicate that there is a "field" defect phenomenon for lung adenocarcinoma in respiratory epithelium for *EGFR* mutation, but not for *KRAS* mutation. We have extended our findings to detect *EGFR* mutation in NBE of a small subset of East Asian patients with wild-type tumors and examined some cases with different mutation patterns by comparing NBE and corresponding tumor. We found that most *EGFR* mutated NBEs lacked TTF-1 expression suggesting that terminal respiratory epithelial cells may not be the only cell type affected by *EGFR* mutation.

DRP - 1: Enhanced Oral/Head and Neck Examination Protocol

(PI and co-PIs: Waun Ki Hong, M.D., Jack Martin, D.D.S., Captain Larry Williams)

This project has been dropped.

DRP - 2: Biomarkers for Aggressive Lung Carcinomas in African American Men

(PI: Sharon Lobert, Ph.D., University of Mississippi, Jackson, MS)

We hypothesize that 1) β class III tubulin levels are higher in NSCLCs from African American men compared to white men; 2) The expression of proteins that alter microtubule dynamics is increased in NSCLCs from African American men compared to white men. Higher levels of these proteins would reduce the effectiveness of antimitotic agents such as paclitaxel or vinorelbine used in the treatment of NSCLC that stabilize or destabilize mitotic spindles.

Update

As described in the last report, we received the funding on July 1, 2004. Over the 6 months of year 1, our efforts were to optimize methods such as extracting sufficient amounts of protein in whole cell lysates to carry out quantitative Western blotting, and optimizing quantitative Western blotting and real-time RT-PCR for comparing tubulin protein and mRNA levels.

In the grant period, we were fully capable of conducting the studies proposed in years 1 and 2.

Year 1

Goal Quantify and compare biomarker levels (β -tubulin isotypes, stathmin and MAP4) in NSCLCs from African American and white men using real-time RT-PCR.

1. Tissues (n=80) will be obtained from the NCI Cooperative Human Tissue Network (CHTN).

We have obtained 62 samples from Caucasian patients and 15 from African American patients. Recognizing that we may have difficulty reaching our goal of 40 samples from African American patients, I have consulted with the Chairman of our Department of Pathology (Dr. Steven Bigler) and two of the thoracic surgeons at the University of Mississippi Medical Center. Our institution has a large African American population and the thoracic surgeons estimate that they do about 20 lung tumor surgeries on African American patients each year. The departments of pathology and thoracic surgery are interested in being involved in basic or clinical research studies. I contacted Dr. William Grizzle (PI for the CHTN Southern Division, UAB) and he is pursuing collaboration with Dr. Bigler to have tissues submitted to CHTN from our institution. We anticipate this could be a benefit to our research, as well as for studies of many types of tumors.

2. Tissues will be processed to extract mRNA and conditions for real-time RT-PCR experiments will be optimized.

We have processed 47 tumor samples from Caucasian patients and 9 tumor samples from African American patients to obtain total RNA and samples for Western blotting. We have designed primers and made standards for all seven β -tubulin isotypes, stathmin and MAP4.

3. Real-time PCR will be conducted when sufficient numbers of samples are obtained.

We have completed qRT PCR for seven β -tubulin isotypes for 10 Caucasian patient samples and 9 African American patient samples. The results are summarized below. Tables 1 and 2 describe the 19 samples for which we have completed qRT-PCR data collection and analysis.

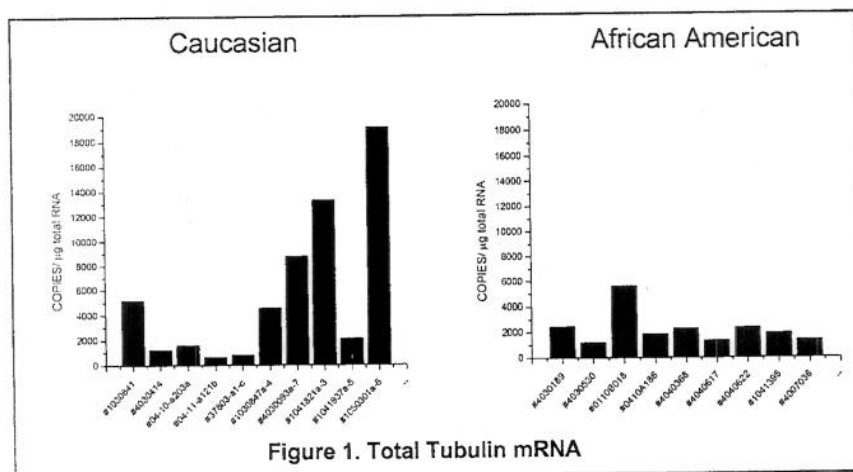
Table 1. Lung tumor samples: Caucasian patients

squamous cell carcinoma	pT2N0Mx	age 70
squamous cell carcinoma	moderately differentiated	age 62
squamous cell carcinoma	moderate to poorly differentiated	age 51
squamous cell carcinoma		age 66
large cell carcinoma	poorly differentiated with neuroendocrine features	age 60
squamous cell carcinoma	poorly differentiated, pT1N2Mx	age 47
squamous cell carcinoma	poorly differentiated	age 71
squamous cell carcinoma	poorly differentiated, grade 3, pT2N1Mx	age 66
squamous cell carcinoma	poorly differentiated, pT2N0Mx	age 66
squamous cell carcinoma	moderate to poorly differentiated, pT1N0Mx	age 63

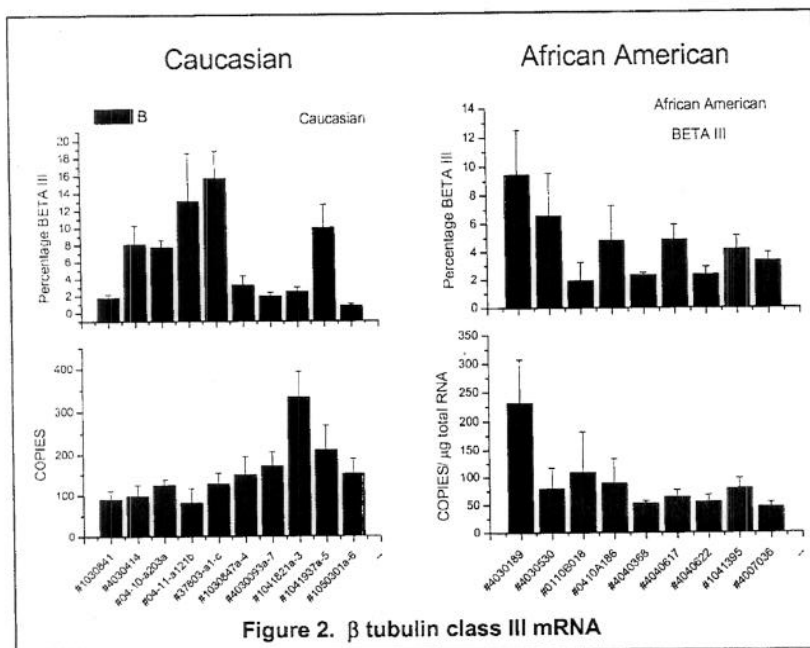
Table 2. Lung tumor samples: African American patients

large cell carcinoma	stage IB	age 51
adenocarcinoma	stage IB, poorly differentiated	age 55
adenocarcinoma	stage IA, pT1NxMx, well differentiated	age 72
adenocarcinoma	stage IIIB	age 75
large cell carcinoma	stage IB, neuroendocrine features	age 76
squamous cell carcinoma,	stage IB, poorly differentiated	age 79
squamous cell carcinoma,	pT3N1Mx, well to moderately differentiated	age 64
squamous cell carcinoma,	moderately differentiated	age 66
granular cell		age 51

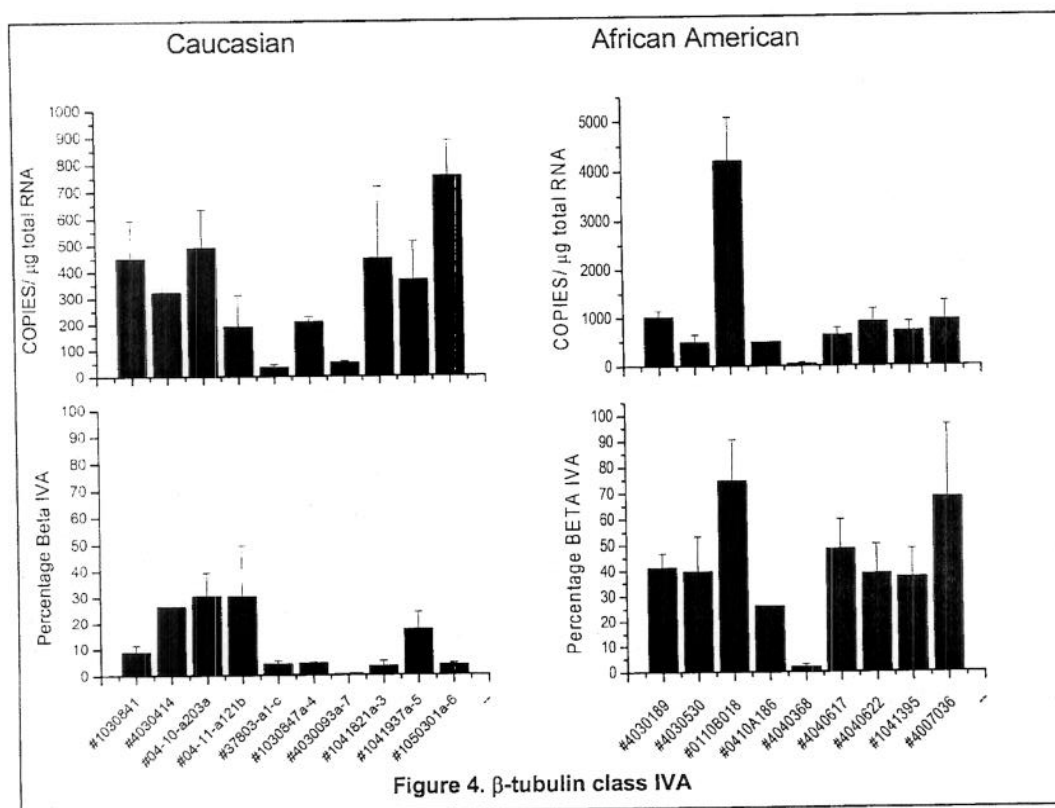
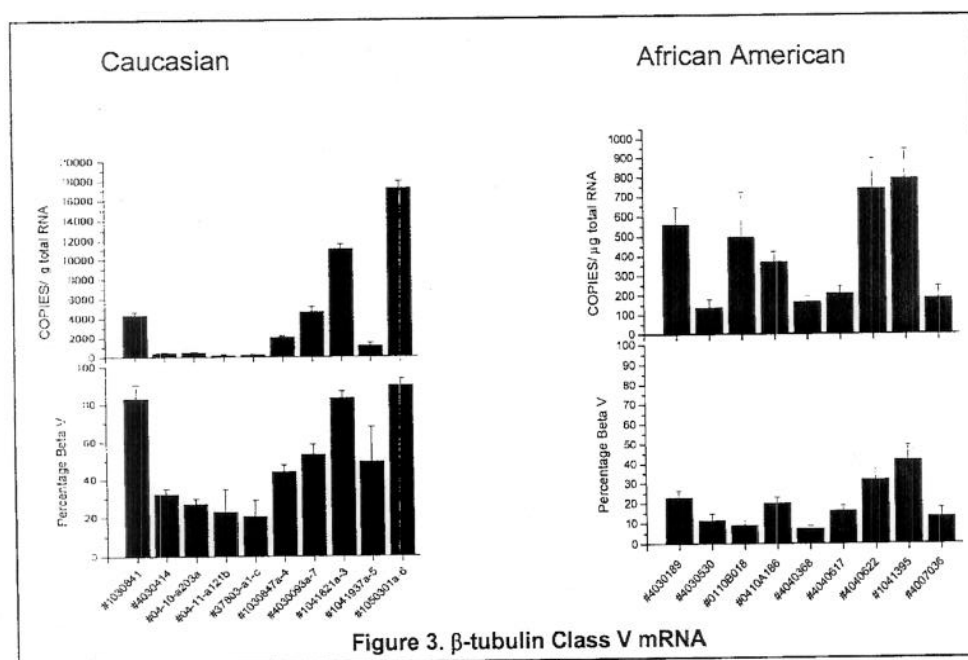
Comparison of tubulin mRNA levels among these samples shows a range of total tubulin from 1000-20000 copies/ μ g total RNA, with most samples having copy numbers between 1000 and 2500 copies/ μ g total RNA (Figure 1). Five of the samples from Caucasian patients have copy numbers greater than 4000/ μ g total RNA.



We found that β tubulin class III mRNA is in relatively low abundance in these samples (Figure 2). This is not surprising since the majority of samples are squamous cell carcinomas or low stage tumors, which is consistent with reports in the literature (Katsetos et al, 2000)



Overall, different patterns of β -tubulin isotype mRNA expression were found for tumor samples from Caucasian and African American patients. For example, β -tubulin class V mRNA was abundant in five of the Caucasian samples, but not in the African American tumor samples (Figure 3). On the other hand, β -tubulin class IVA was relatively abundant in several African American tumor samples compared to the Caucasian samples (Figure 4).



4. Tissues will also be processed for protein extraction and samples frozen for Western blotting later

Tissues were processed as described in #1.

Year 2

Goal 1 Continue to quantify and compare β -tubulin isotypes, stathmin and MAP4 levels in NSCLCs as in year 1.

1. Tissues will be processed as above for real-time RT-PCR experiments and mRNA levels will be determined and compared.

- a. Tissues have been processed for real-time RT-PCR experiments as described above. The primers and standards have been made for the stathmin and MAP4 data collection. The total RNA samples already made for the β -tubulin qRT-PCR will be used for the stathmin and MAP4 data collection.

Goal 2 Examine the protein levels of β -tubulin isotypes, stathmin and MAP4 by quantitative and semiquantitative Western blotting in samples prepared from the NSCLCs.

1. Western blotting will be done to establish the linearity of response for comparison of tissue samples.

- a. All the antibodies that will be used in the Western blotting have been tested. The procedure for quantitative Western blotting for tubulin isotypes has been developed (Hiser et al, 2006).

Conclusions

- 1) The β -tubulin class III mRNA abundance in the 19 lung tumor tissues examined thus far is low, consistent with the results obtained by immunostaining
- 2) β -tubulin class V mRNA levels are elevated in some tumor samples from Caucasian patients, corresponding to samples with significantly higher total tubulin.
- 3) β -tubulin class IVA mRNA levels are relatively higher in lung tumor samples from African American patients, a novel finding. The possibility of this tubulin isotype serving as a biomarker has not been explored previously.

KEY RESEARCH ACCOMPLISHMENTS

Project 1: Biologic Approaches for Adjuvant Treatment of Aerodigestive Tract Cancer

- Successfully opened the Vanguard trial at MDACC and Eisenhower Medical Center.
- Successfully enrolled 20 patients with specimens collected and placed in the pathology database (see Core B and C reports).
- Successfully activated the biologic adjuvant trial with celecoxib.
- Successfully secured the next biologic adjuvant trial with erlotinib with protocol under development.

Project 2: Identification of Biomarkers of Response to Chemoprevention Agents in Lung Epithelium

- The HBEC model system is a powerful new approach to assess the contribution of individual and combinations of genetic alterations to lung cancer pathogenesis.
- A combination of four genetic alterations including hTERT overexpression, bypass of p16/RB and p53 pathways, and mutant K-RAS^{V12} or mutant EGFR is still not sufficient for human bronchial epithelial cells to completely transform to cancer.
- EGFR tyrosine kinase inhibitors inhibit the growth of preneoplastic HBEC cells, suggesting their potential for chemoprevention.
- Some differentially expressed proteins were identified between NSCLC and HBEC cells.
- For the first time, a high throughput immunoblotting approach combined with an *in vitro* carcinogenesis cell model was demonstrated to be useful to identify changes in the levels of different proteins potentially associated with lung carcinogenesis.
- A novel proteomics approach was developed to detect lower abundant proteins.
- Some miRNAs differentially expressed between HBEC and lung cancer cells were identified.

Project 3: Premalignant Bronchial Epithelia - Molecular and Cellular Characterization of Lung Tumorigenesis

- Demonstrated increased expression of PSCA in bronchial epithelial cells during *in vitro* multistep lung tumorigenesis.
- Demonstrated the ability to establish organotypic, air-liquid cultures resembling bronchial epithelium from fresh bronchial biopsy specimens.
- Demonstrated that the frequency of chromosome instability increases with the multistep tumorigenesis process.
- Demonstrated that chromosome instability is associated with upregulation of phosphorylated Histone H2AX in cells grown in organotypic cultures both in terms of its frequency and spatial localization.

Project 4: Modulation of Death Receptor-Mediated Apoptosis for Chemoprevention

- Established stable lines overexpressing FLIP using several lung cancer cell lines.
- Demonstrated the downregulation of FLIP by celecoxib and the impact of down-regulated FLIP on celecoxib-induced apoptosis and enhancement of TRAIL-induced apoptosis.
- Demonstrated that TRAIL - resistant cells are not cross-resistant to various cancer therapeutic agents including DR-induced ones.

Project 5: Molecular Strategies Targeting the AKT Signaling Pathway for Lung Cancer Chemoprevention and Therapy

- Core B: Biostatistics & Data Management Core constructed retrovirus or adenovirus expressing constitutively active or dominant negative Akt.
- Celecoxib did not suppress the proliferation of premalignant and malignant HBE cells.

- Gefitinib and erlotinib inhibited immortalized cells more effectively compared to premalignant and malignant HBE cells.
- SCH66336 inhibited the proliferation of normal, premalignant, and malignant human bronchial epithelial (HBE) cells with no selectivity.
- Provided statistical/data management support for the Vanguard trial and the adjuvant celecoxib trial.
- Completed the web-enabled database system to facilitate the conduct of both trials. It is in use now.
- Developed two new statistical methods that allow more general interaction patterns for the drug interaction and ease the restriction of existing methods.

Core C: Pathology and Specimen Procurement Core

- Established a repository of tissue and other biologic specimens and banked samples of baseline bronchoscopies from 14 patients enrolled on the clinical trials in Project 1.
- Used the web-based database developed by Core B for tracking, inventory, reporting, and recording pathology-related information.
- Provide histopathological services including diagnosis, IHC staining, FISH, laser capture microdissection and tissue microarray.
- Conducted productive research activities, resulting in one article in *Cancer Research* and two in press.

DRP-2: Biomarkers for Aggressive Lung Carcinomas in African American Men

- Extracted RNA and protein samples from 47 NSCLCs of Caucasian patients and 15 of African American patients.
- Completed qRT-PCR experiments for 7 β -tubulin isotypes for 30 Caucasian and 9 African American lung tumor samples.
- Developed the procedure for quantitative Western blotting for β -tubulin isotypes.
- Primers and standard control samples have been prepared for the MAP4 and stathmin qRT-PCR experiments.

REPORTABLE OUTCOMES

Publications

1. Han J-Y, Liu DD, Lee JJ, Kurie JM, Lotan R, Hong WK, Lee H-Y. 9-*cis*-retinoic acid treatment increases serum concentrations of α -tocopherol in former smokers. *Clin Cancer Res* 11:2305-11, 2005.
2. Hiser L, Aggarwal, Young R, Spano A, Frankfurter A, Correia JJ, Lobert S. Comparison of beta-tubulin mRNA and protein levels in twelve human cancer cell lines. *Cell Motil Cytoskel* (in press), 2006.
3. Kong M, Lee JJ. A generalized response surface model with varying relative potency for assessing drug interactions. *Biometrics* (revised), 2005.
4. Kong M, Lee JJ. A semiparametric response surface model for assessing drug interaction. *Biometrics* (submitted), 2005.
5. Lee H-Y, Oh SH, Woo J-K, Price R, Cody D, Tran H, Hong WK. Chemopreventive effects of deguelin, a novel Akt inhibitor, on tobacco-induced lung tumorigenesis. *JNCI* 97: 1695-1699, 2005.
6. Lee JJ, Kong M, Ayers GD. A practical guide for determining drug interaction in combination therapy. *Statist Methods Med Res* (submitted), 2005.
7. Liu X, Yue P, Khuri FR, Sun S-Y. Decoy receptor 2 (DcR2) is a p53 target gene and regulates chemosensitivity. *Cancer Res* (Priority Reports); 65:9169-75, 2005.

8. Sato M, Vaughan MB, Girard L, Peyton M, Lee W, Shames DS, Ramirez RD, Sunaga N, Gazdar AF, Shay JW, Minna JD. Multiple oncogenic changes (K-RASV12, p53 knockdown, mutant EGFRs, p16 bypass, telomerase) are not sufficient to confer a full malignant phenotype on human bronchial epithelial cells. *Cancer Res* (in press), 2006.
9. Sun S-Y. Chemopreventive agent-induced modulation of death receptors. *Apoptosis* (in press), 2006.
10. Tang X, Shigematsu H, Bekele B N, Roth JA, Minna J D, Hong WK, Gazdar A F, Wistuba I. EGFR tyrosine kinase domain mutations are detected in histologically normal respiratory epithelium in lung cancer patients. *Cancer Res* 65:7568-7572, 2005.
11. Tsao AS, Tang X, Sabloff B, Xiao L, Shigematsu H, Roth J, Spitz M, Hong WK, Gazdar A, Wistuba I. Clinical-pathological characteristics of the EGFR gene mutation in non-small cell lung cancer. *J Thoracic Oncol* (in press), 2006.
12. Vaughan MB, Ramirez RD, Wright WE, Minna JD, Shay JW. A three-dimensional model of differentiation of immortalized human bronchial epithelial cells. *Differentiation* (in press), 2006.
13. Wistuba I and Gazdar A.F. Lung cancer preneoplasia. *Ann Rev Path. Mech Dis* 1:331-48, 2006.

Scientific Presentations

1. **Ignacio Wistuba.** EGFR tyrosine kinase domain mutations are also found in histologically normal lung epithelium of patients containing lung adenocarcinomas with EGFR mutations indicating a field effect. 96th AACR, 2005 (Platform presentation).
2. **Ignacio Wistuba.** Clinical-pathologic characteristics of the EGFR gene mutation in NSCLC. 11th World Conference on Lung Cancer, Spain 2005 (Platform presentation).

Abstracts

1. Tang X et al. Analysis of EGFR abnormalities in the sequential pathogenesis and progression of lung adenocarcinoma. *ACCR* 2006.
2. Tang X et al. "Field" defect abnormalities in lung adenocarcinoma: KRAS vs. EGFR mutant tumors. *ACCR* 2006.
3. Kong M, Lee JJ (2005). A response surface model for drug combinations. The Spring ENAR Meeting, March 2005.
4. Sato M, Girard L, Peyton M, Ramirez RD, Sunaga N, Gazdar AF, Shay JW, Minna JD. Genetic manipulation of immortalized normal human bronchial epithelial cells. *AACR*, 2005.
5. Liu X, Yue P, Khuri FR, Sun SY. FLIP downregulation and its impact on celecoxib-induced apoptosis in human lung cancer cells. *AACR* 2006.
6. Hittelman W et al. Existence of clonal and subclonal outgrowths in premalignant and stromal cells in the upper aerodigestive tract of current smokers. *AACR* 2006.

Scientific Products

1. Developed immortalized HBEC lines that are being deposited in the American Type Culture Collection (ATCC) for worldwide distribution. The HBEC lines are a valuable new tool for studying the pathogenesis of lung cancer and developing new reagents to test for chemoprevention and chemotherapeutic drugs. The isogenically manipulated HBEC system is also a powerful approach to assess the contribution of individual genetic alterations to tumorigenesis of lung cancer. (PIs: Li Mao, John Minna).

Research Grants

1. NCI R01: Molecular mechanism of celecoxib-induced apoptosis. 2005. (PI: Shi-Yong Sun)

CONCLUSION

In the second year of the grant period, the basic research projects not requiring the VITAL patient samples have been proceeding well as proposed in the Statement of Work. The comprehensive review process of the VITAL protocols and some drug issues of celecoxib delayed the opening of both Vanguard and adjuvant celecoxib trials, which affected some research projects that need the VITAL patient samples, such as Project 3. We are making a variety of efforts to speed up patient enrollment including hiring an intern fully coordinating the trials, actively contacting nearby medical institutes for referrals to the VITAL studies, and advertising via media and websites.

This year, we have 10 publications including 1 in *JNCI* and 4 in *Cancer Research*, and 3 articles in revision. We also developed immortalized HBECs deposited in ATCC for worldwide distribution. A New NCI R01 grant was submitted. Based on 2 years of work, some conclusions may be drawn for the projects.

Project 1 opened the Vanguard and adjuvant celecoxib trials. Enrollment continues and should improve with stepped-up accrual efforts. Patient samples will be distributed to individual investigators.

Project 2 developed a powerful isogenically manipulated HBEC system to assess the contribution of individual genetic alterations to tumorigenesis of lung cancer and identified effects of p53 knockdown and K-RAS^{V12} on tumorigenesis being additive; the combination of four genetic alterations, including hTERT overexpression, bypass of p16/RB and p53 pathways, and mutant K-RAS^{V12} not sufficient for human bronchial epithelial cells to completely transform to cancer; and EGFR tyrosine kinase inhibitors being useful chemopreventive drugs for lung cancer.

Project 3 completed pilot experiments that will ensure success with the bronchial biopsy and brush specimens obtained from LIFE bronchoscopy of participants in the clinical trials of Project 1. We have optimized the conditions of gene expression microarray on bronchial epithelial cells obtained from endobronchoscopic procedures and demonstrated capability to carry out clonal expansion and genetic instability analyses of bronchial epithelial cell populations grown in a lung organotypic model.

Project 4 concluded that defects or dysregulation of death receptor-mediated intracellular apoptotic pathway might contribute to lung carcinogenesis. Thus, appropriate modulation such as upregulation of DR4 or DR5 by small molecules such as celecoxib and Itonafarnib may eliminate premalignant or malignant lung epithelial cells by promoting apoptotic cell death to achieve cancer chemopreventive and therapeutic goals.

Project 5 concluded that celecoxib might not be an effective antiproliferative agent and FTI SCH66336 might not be an effective chemopreventive agent due to its cytotoxicity on NHBE cells. Also EGFR TKIs induce alternative survival/proliferation pathways in premalignant and malignant HBE cells, and therefore, understanding their mechanisms may provide better chemopreventive strategies using EGFR TKIs.

Biostatistics and Data Management Core has continued to work actively with all the VITAL Projects in their research efforts, especially in the area of biostatistical support and consulting in the clinical trial design, implementation, and analysis of experimental results. In addition, the Core developed a web-enabled database system to facilitate the conduct of the trials.

Pathology and Specimen Procurement Core has acquired and banked specimens from 14 bronchoscopy biopsies and 18 resected specimens from lung cancer and head/neck tumor patients; used the web-enabled database developed by Biostatistics Core to track and inventory bronchoscopy specimens and report histopathological features of the bronchial mucosa from the bronchoscopy biopsy; and developed a priority sample distribution list for VITAL individual projects for IHC biomarker analysis using formalin-fixed and paraffin-embedded bronchial tissues.

DRP-2 found that the β -tubulin class III mRNA abundance in the 19 lung tumor tissues examined thus far was low, consistent with the results obtained by immunostaining; the β -tubulin class V mRNA levels were elevated in some tumor samples from Caucasian patients, corresponding to samples with significantly higher total tubulin; and the β -tubulin class IVA mRNA levels were relatively higher in lung tumor samples from African American patients, a novel finding. The possibility of this tubulin isotype serving as a biomarker has not been explored previously.

REFERENCES

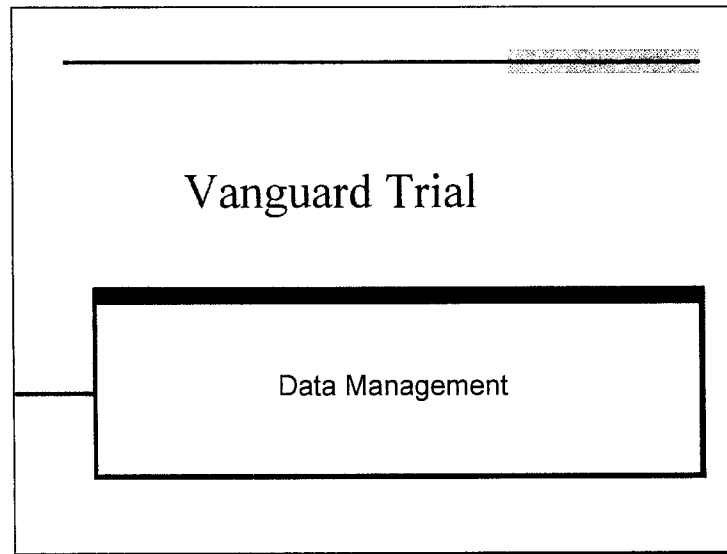
- Amara N, Palapattu GS et al. Prostate stem cell antigen is overexpressed in human transitional cell carcinoma. *Cancer Res* 61:4660-5, 2001.
- Chun K-H, Lee H-Y, Hassan K, Khuri FR, Hong WK, and Lotan R. Implication of protein kinase B/Akt and Bcl-2/Bcl-xl suppression by the farnesyl transferase inhibitor SCH66336 in apoptosis induction in squamous carcinoma cells. *Cancer Res* 63, 4796-4800, 2003.
- Gu Z.G, Thomas et al. (2000). Prostate stem cell antigen (PSCA) expression increases with high gleason score, advanced stage and bone metastasis in prostate cancer. *Oncogene* 19(10): 288-96.
- Hiser L, Aggarwal, Young R, Spano A, Frankfurter A, Correia JJ, and Lobert S. Comparison of beta-tubulin mRNA and protein levels in twelve human cancer cell lines. *Cell Motil Cytoskel* (in press) 2006.
- Katsetos CD, Kontogeorgos G, Geddes JF, Herman MM, Tsimara-Papastamatiou H, Yu Y, Sakkas LI, Tsokos M, Patchefsky AS, Ehya H, Cooper HS, Provencio J, Spano AJ, and Frankfurter A. Differential distribution of the neuron-associated class III β -tubulin in neuroendocrine lung tumors. *Arch Pathol Lab Med* 124: 535-544, 2000.
- Lam JS, Yamashiro J, et al. Prostate stem cell antigen is overexpressed in prostate cancer metastases. *Clin Cancer Res* 11: 2591-6, 2005.
- Lee H-Y, Moon HJ, Chun K-H, Chang YS, Hassan K, Ji L, Lotan R, Khuri FR, and Hong WK. Effects of insulin-like growth factor binding protein-3 and farnesyl transferase inhibitor SCH66336 on Akt expression and apoptosis in non-small cell lung cancer cells. *JNCI* 96: 1536-1548, 2004.
- Liu X, Yue P, Zhou Z, Khuri FR, Sun S-Y. Death receptor upregulation and celecoxib-induced apoptosis in human lung cancer cells. *J Natl Cancer Inst* 96:1769-1780, 2004.
- Lukyanchuk VV, Friess H et al. Detection of circulating tumor cells by cytokeratin 20 and prostate stem cell antigen RT-PCR in blood of patients with gastrointestinal cancers. *Anticancer Res* 23(3B): 2711-6.
- Ramirez RD, Sheridan S, Girard L, Sato M, Kim Y, Pollack J, Peyton M, Zou Y, Kurie JM, Dimaio JM, Milchgrub S, Smith AL, Souza RF, Gilbey L, Zhang X, Gandia K, Vaughan MB, Wright WE, Gazdar, AF, Shay JW, and Minna JD. Immortalization of human bronchial epithelial cells in the absence of viral oncoproteins. *Cancer Res* 64: 9027-9034, 2004.
- Reddel RR, Ke Y et al. Transformation of human bronchial epithelial cells by infection with SV40 or adenovirus-12 SV40 hybrid virus or transfection via strontium phosphate

coprecipitation with a plasmid containing SV40 early region genes. *Cancer Res* 48:1904-9, 1988.

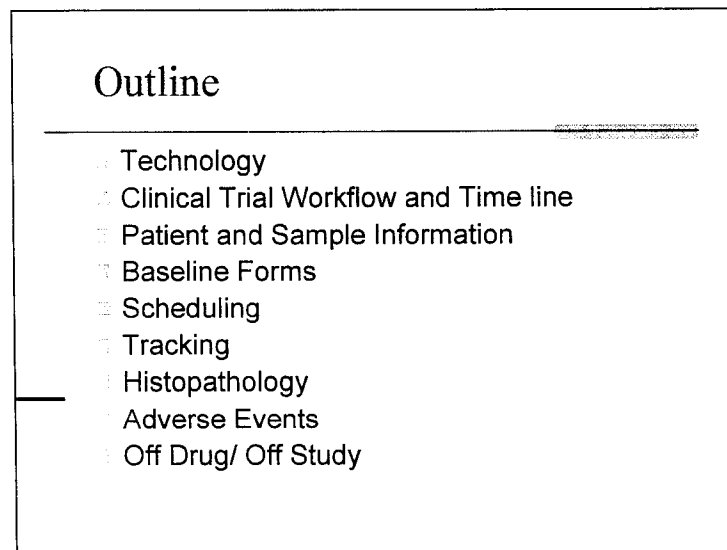
- Reiter RE, Gu Z et al. Prostate stem cell antigen: a cell surface marker overexpressed in prostate cancer. *Proc Natl Acad Sci* 95:1735-40, 1998.
- Winton T, Livingston R, Johnson D, Rigas J, Johnston M, Butts C, Cormier Y, Goss G, Inculet R, Vallieres E, Fry W, Bethune D, Ayoub J, Ding K, Seymour L, Graham B, Tsao MS, Gandara D, Kesler K, Demmy T, Shepherd F; National Cancer Institute of Canada Clinical Trials Group; National Cancer Institute of the United States Intergroup JBR 10 Trial Investigators. Vinorelbine plus cisplatin vs. observation in resected non-small-cell lung cancer. *N Engl J Med* 352: 2589-97, 2005.

APPENDIX 1
Web-Enabled Database Screen Shots

Slide 1



Slide 2



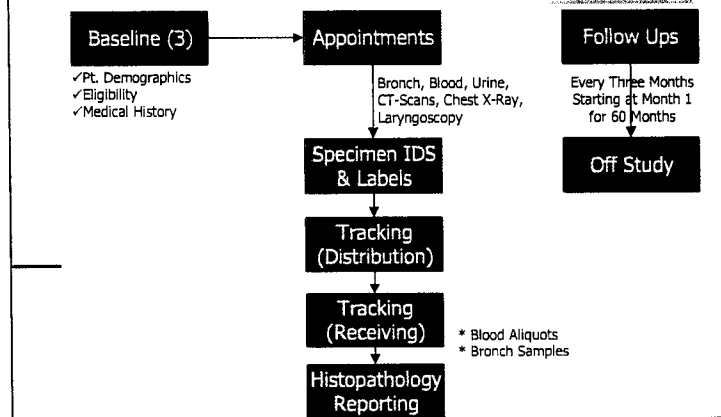
Slide 3

Technology

- ASP.Net (VB.Net)
- Web Based Software (Internet Explorer)
- SQL Server 2000 (SP3a)
- Windows 2003 Server (Operating System)
- SQL Server 2K Reporting Services
- Secure Socket Layer (SSL)

Slide 4

Clinical Trial Workflow

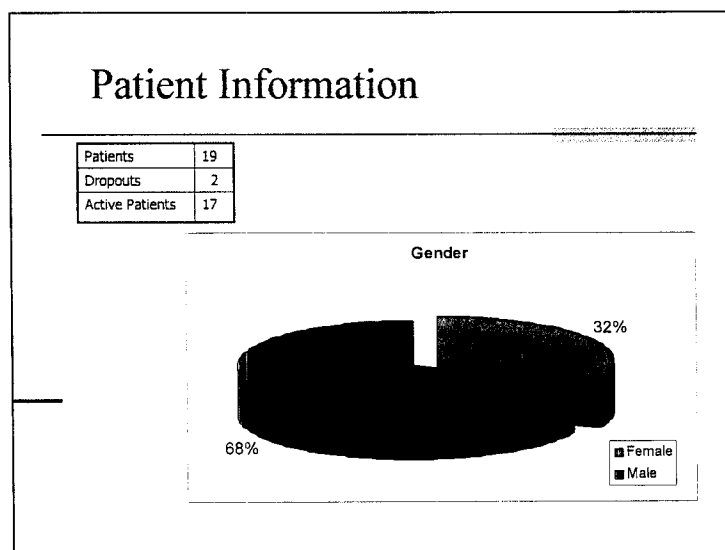


Slide 5

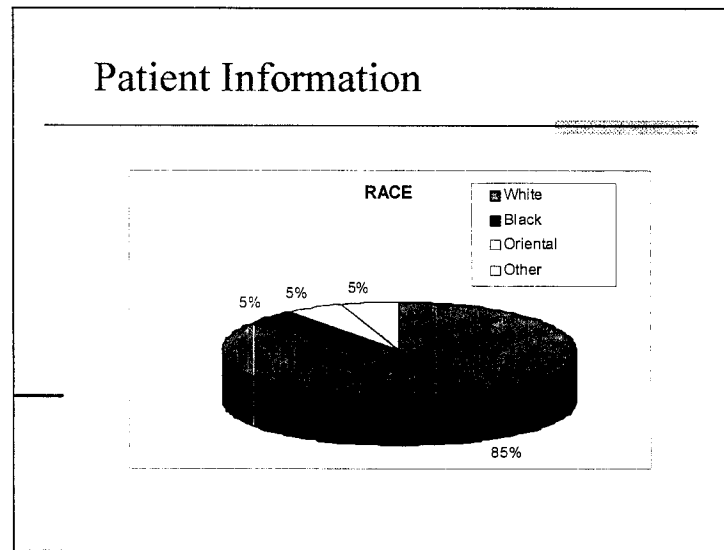
Forms Summary

A1	
A2	
B1	
Schedule	Bronchoscopy Serology Chest Xray CT Chest Laryngoscopy
Specimen Labels	
Tracking	Not Yet Delivered Delivered, Not Received Delivered and Received Future Visits All of the above
Pathology Processing	Pathology Slow/Cut Entry Histopathology Report
Monthly Safety Log	3 through 80 months
CR Down / CR Study	
IRRM Assessment	
Adverse Events	
Reporting	Complete Timeline of Events Snapshot Summary

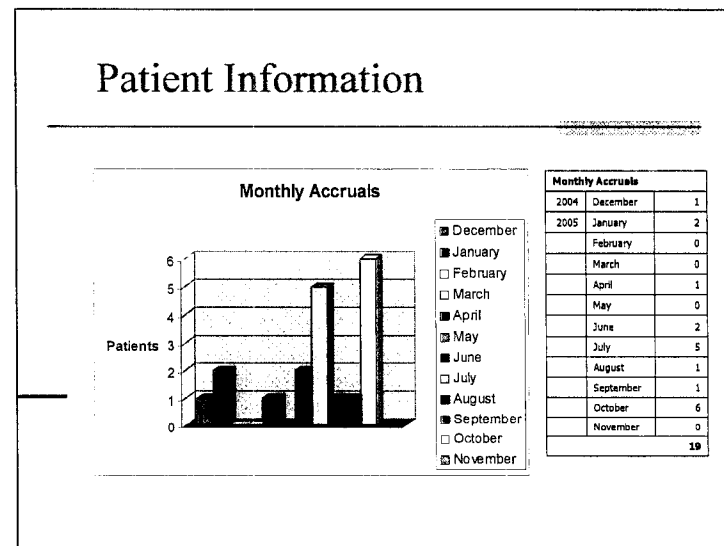
Slide 6



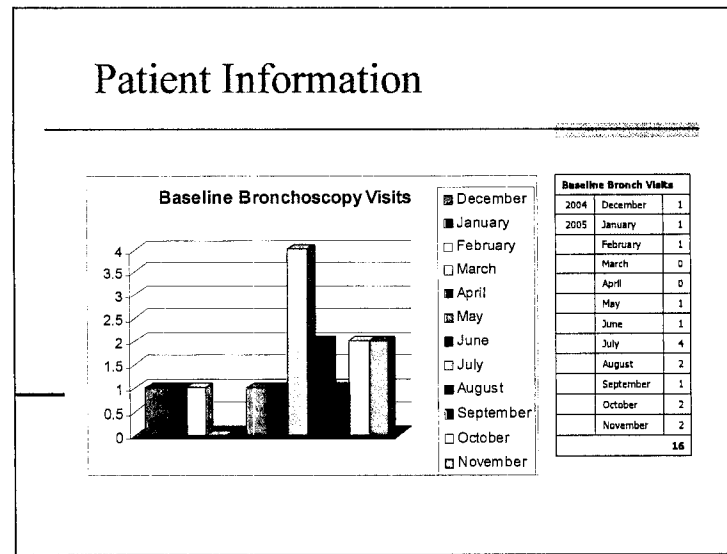
Slide 7



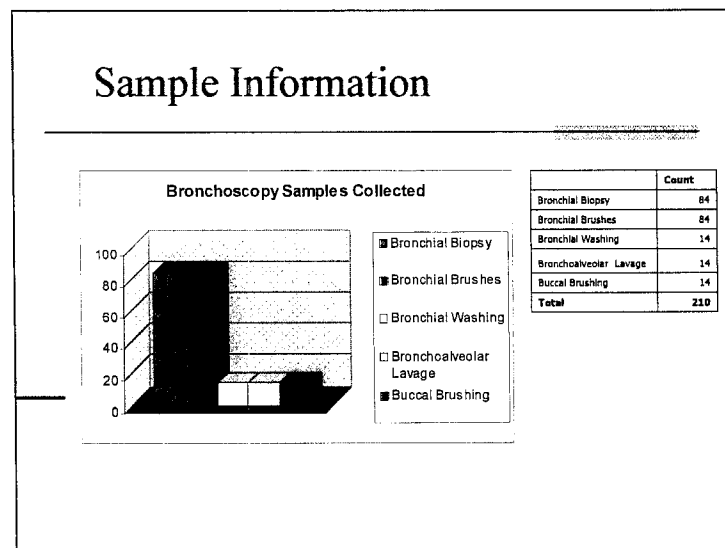
Slide 8



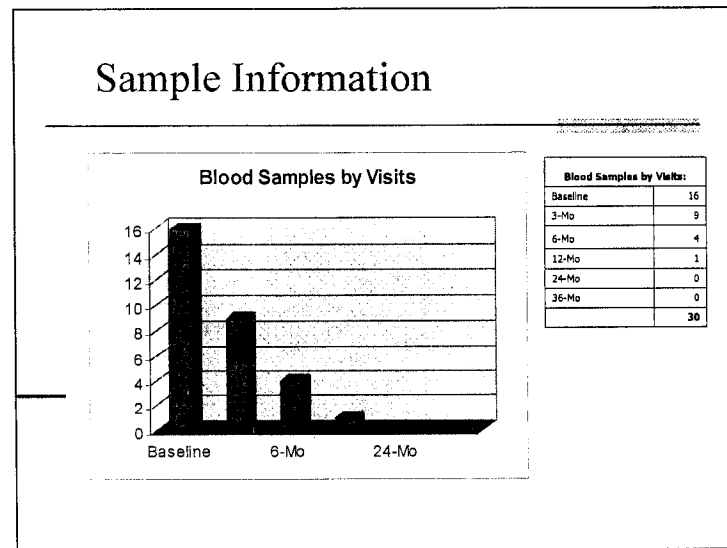
Slide 9



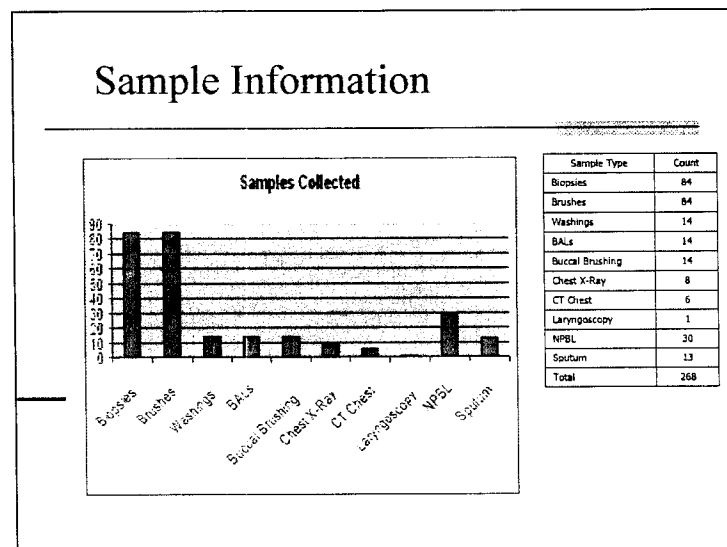
Slide 10



Slide 11



Slide 12



- Collect Patient Information
- Eligibility Criteria
- Medical History (Medications, allergies, etc)
- ETOH & Smoking Status

Slide 15

MRN, Accession

Site	Participant	MRN	Acc. #
A	Doe, John	12345	5
B	Doe, Lenny	23456	10
C	Doe, Kim	34567	7

Slide 16

Baseline Forms – A1

Form A1: Baseline Information

1.1 Are you currently smoking?

1.2 How many cigarettes per day?

1.3 Average number of cigarettes smoked per day?

1.4 If there was a quit-smoking period, total time during the smoking years.

1.5 Is this participant interested in the study?

1.6 If no, specify the reason.

1.7 Is the patient interested in future study?

General Comments

Slide 17

Baseline Form – A2 (Part 1 of 3)

Admin Projects Histo-Pathology Lab Logout

Select a participant

***1.1 Gastrointestinal problems?**

*1.1.1 Ulcers requiring medical treatment with H2 blockers (essential if 1.1 answered "Yes")

Other:

***1.2 Respiratory problem?**

Other:

***1.3 Cardiovascular problem?**

Other:

Slide 18

Baseline Form – A2 (Part 2 of 3)

***1.4 Clotting problem?**

Other:

***1.5 History of diabetes?**

***1.6 History of Systemic Lupus Erythematosus?**

***1.7 Family history of premature coronary artery disease defined as:**

1.8 Other Medical Problems

Allergies?

***2.1 Are you taking any steroids?**
If yes, describe the name and dose below.

 steroid's Name	Dose
------------------------	-------------

***2.2 Are you taking any NSAIDs?**
If yes, describe the name and dose below.

 NSAID's Name	Dose
----------------------	-------------

***2.3 Are you taking any H2 blockers?**
If yes, describe the name and dose below.

 H2 blocker's Name	Dose
---------------------------	-------------

Slide 19

Baseline Form – A2 (Part 3 of 3)

***4. Previous Surgery/Hospitalization**

Date: **Surgery/Hospitalization Type:**

***4.1 Has the patient had a surgery within the past four(4) weeks?**

***5. Any previous Cancer?**

If yes, please complete the table below for all cancers.

Cancer Type	Stage	Treatment	Diagnosis Date	Last Treatment Date	Smoking Related?
<input type="text"/>	<input type="text"/>	<input type="text"/>	<input type="text"/>	<input type="text"/>	<input type="text"/>

***5.2 Is patient free of cancer for at least six (6) months?**

***6.1 Is the participant eligible?**

Slide 20

Baseline Form – B1

Select a participant: **Status:**

Visit Date: **Device:** **Height:** **Weight:** **Performance Status:**

MDM: **Age:** **Sex:**

***4.1 Have you ever consumed alcohol?** (* If not, skip section)

***4.2 Age started consuming alcohol?**

***4.3 Are you currently consuming alcohol regularly?** Yes No

If not, date quit drinking: Age stopped drinking: Years drinking:

***4.4 Alcohol:**

Beer (12 oz)	cans	None	Daily	Weekly	Monthly	Yearly
Wine (4 oz)	glasses	None	Daily	Weekly	Monthly	Yearly
Straight Liquor	shots	None	Daily	Weekly	Monthly	Yearly
Mixed Drinks (8 oz)	glasses	None	Daily	Weekly	Monthly	Yearly

Date "Informed Consent" Signed:

Optional Procedures Consented? Yes No

Optional EPI questionnaire consented? Yes No

EPI questionnaire given? Yes No

Slide 21

Scheduling

- Database Driven:
 - Visit Types (Bronchoscope)
 - Sample Types (Biopsy)
 - Collection Time Points (Baseline, 1-Month)
 - Scheduler Matrix (Integrates above definitions)
 - Detail (Defines specimen label and collection)
- Specimens' Label Printing

Slide 22

Scheduling Form

[illegible]

Slide 23

Specimen Labels

Slide 24

Tracking

- Five display modes: All, NYD, NYR, DAR, & Future Visits
- Print Tracking Forms

Slide 25

Tracking Screen (Not Yet Delivered)

User: BioStatistics / JRevs
 Display Mode: Not Yet Delivered Laboratory: All Laboratories Date: 11/21/2005
 Filter by Year: 2005

Tracking #	Patient	Collection Date	Source/Specimen Lab	Test Type	Delivered Date	Collected	Notes
<input type="checkbox"/> 72	Doe, John	11/6/2005	Dr. Watson	bronchoscopy			
<input type="checkbox"/> 73	Smith, Jane	11/6/2005	Dr. Mao	bronchoscopy			
<input type="checkbox"/> 81	Doe, John	7/28/2005	Dr. Watson	Serology			
<input type="checkbox"/> 82	Smith, Jane	11/17/2005	Dr. Watson	bronchoscopy			
<input type="checkbox"/> 83	Doe, John	11/17/2005	Dr. Mao	bronchoscopy			
<input type="checkbox"/> 84	Smith, Jane	10/23/2005	Dr. Watson	Serology			
<input type="checkbox"/> 85	Doe, John	10/19/2005	Dr. Watson	Serology			
<input type="checkbox"/> 86	Smith, Jane	7/28/2005	Dr. Watson	Serology			
<input type="checkbox"/> 87	Doe, John	10/23/2005	Dr. Watson	Serology			
<input type="checkbox"/> 88	Smith, Jane	10/21/2005	Dr. Watson	Serology			
<input type="checkbox"/> 91	Doe, John	10/13/2005	Dr. Watson	Serology			
<input type="checkbox"/> 92	Smith, Jane	9/29/2005	Dr. Watson	Serology			
<input type="checkbox"/> 93	Doe, John	5/18/2005	Dr. Watson	Serology			
<input type="checkbox"/> 94	Smith, Jane	8/16/2005	Dr. Watson	Serology			
<input type="checkbox"/> 95	Doe, John	10/25/2005	Dr. Mao	bronchoscopy			
<input type="checkbox"/> 97	Smith, Jane	11/17/2005	Dr. Watson	bronchoscopy			
<input type="checkbox"/> 98	Doe, John	11/17/2005	Dr. Mao	bronchoscopy			

Page 1 of 1

Slide 26

Histopathology

- ☐ Track Biopsies
- ☐ Paraffin Embedding Process
- ☐ Cutting Process
- ☐ Histopathology Reporting

Slide 27

Pathology Processing

Pathology No.	Block	Scheduled Date	Time	LL	ML	UL	50%	Cut	Ship	Report
VB7-05-10070	A	8/4/2005	Baseline							
VB7-05-10070	B	8/9/2005	Baseline							

Cutting Date	11/21/2005	Number of Cuts
Cut No.	Ind. Cut	NA Not Ind
1		Comments
2		Dist. Cut
3		0100005
4		0200005

Slide 28

Histopathology Report

Cytology													
Site	WBC	NE	LY	MONO	EOS	PLAS	PLAS	PLAS	PLAS	PLAS	PLAS	PLAS	PLAS
A1 (RUL)													
A2 (RML)													
A3 (RUL)													
B4 (LLL)													
B5 (LUL)													
B6 (CAR)													

Cytology													
Site	WBC	NE	LY	MONO	EOS	PLAS	PLAS	PLAS	PLAS	PLAS	PLAS	PLAS	PLAS
A1 (RUL)													
A2 (RML)													
A3 (RUL)													
B4 (LLL)													
B5 (LUL)													
B6 (CAR)													

Site / Doc	Metaplasia	Dysplasia	Comments
Right (A)	0/6 = 0.00%		
Left (B)	0/6 = 0.00%		
Overall	0/12 = 0.00%		

Slide 29

Other Forms

- Monthly Follow Ups
- Adverse Events Form
- Off Drug/ Off Study Form

Slide 30

Monthly Follow Up

7 months: Select a participant Status: No patient selected

Follow Up Date: Check here if patient missed this follow up ☐

Pattern Changed? ☐

Start Date Since Last Visit

Quit Date Since Last Visit

Cigarettes a Day

12 Months:

Pattern Changed? ☐

Start Date Since Last Visit

Quit Date Since Last Visit

Amounts

Days (12 oz.) Lungs

Other (4 oz.) glasses

Straight Liquor (1 oz.) shots

Mixed Drinks (8 oz.) glasses

Reproductive Status (if female or childbearing potential)

14 Months:

Comments:

16 Months:

18 Months:

20 Months:

Slide 31

Adverse Events

Select Patient	Date	John Doe	Admission Event	Start Date	Recorded By	Stop Date	Recorded By	Comments
+								
/			RASH	06/10/2005	M Quillian	06/17/2005	M Quillian	Grade 1
/			FATIGUE	06/15/2005	mQUILLIAN	06/17/2005	mQUILLIAN	GRADE 1
/			PAIN	06/10/2005	m QUILLIAN	06/10/2005	mQUILLIAN	GRADE 1 JOINT PAIN
/			fatigue	06/15/2005	P Cole			baseline/g/ 1
/			PVD	06/15/2003	P Cole			baseline/g/ 2
/			CAD	06/15/1999	P Cole			baseline/g/ 2
/			HTN	06/15/1999	P Cole			baseline/g/ 2

Slide 32

Off Drug / Off Study

1.1 Select one of the reasons below:

1.1.1 If an association between select one of the following:

- Income.
- Toxicity.
- Cancer.
- Other.

1.1.2 If not patient decision select one of the following:

- Toxicity.
- Other.

Off study date: 04/2003
Subject was off the program before:

IDENTIFICATION OF REMAINS OF SON REPORTED. PT HAS
NEW
NAMES.

APPENDIX 2

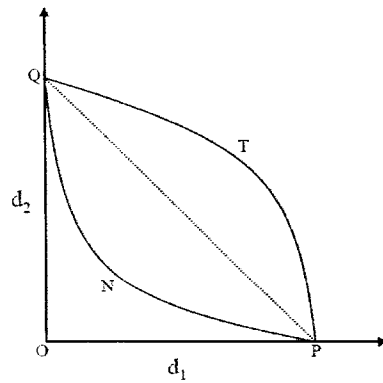
Synergy Research

Slide 1

Synergy – Loewe Additivity Model

- Additive $\frac{d_1}{D_{x,1}} + \frac{d_2}{D_{x,2}} = 1,$
- Synergistic $\frac{d_1}{D_{x,1}} + \frac{d_2}{D_{x,2}} < 1,$
- Antagonistic $\frac{d_1}{D_{x,1}} + \frac{d_2}{D_{x,2}} > 1,$

Slide 2



Slide 3

Five Methods for Drug Interaction

- Chou and Talalay (1984)

$$\log \frac{E}{1-E} = m(\log d - \log D_m).$$

$$d = D_m \left(\frac{E}{1-E} \right)^{\frac{1}{m}},$$

$$\gamma(x) = \frac{d_1}{D_{x,1}} + \frac{d_2}{D_{x,2}}.$$

Slide 4

Five Methods for Drug Interaction (cont.)

- Greco et al. (1990)

$$\frac{E-B}{E_{con}-E} = \left(\frac{d}{D_m} \right)^m.$$

$$d = D_m \left(\frac{E-B}{E_{con}-E} \right)^{\frac{1}{m}}.$$

$$1 = \frac{\frac{d_1}{D_{m,1} \left(\frac{E-B}{E_{con}-E} \right)^{\frac{1}{m_1}}}}{\frac{d_1}{D_{m,1} \left(\frac{E-B}{E_{con}-E} \right)^{\frac{1}{m_1}}} + \frac{d_2}{D_{m,2} \left(\frac{E-B}{E_{con}-E} \right)^{\frac{1}{m_2}}} + \frac{\alpha d_1 d_2}{D_{m,1} D_{m,2} \left(\frac{E-B}{E_{con}-E} \right)^{\frac{1}{2m_1}} \left(\frac{E-B}{E_{con}-E} \right)^{\frac{1}{2m_2}}}} + \frac{d_2}{D_{m,2} \left(\frac{E-B}{E_{con}-E} \right)^{\frac{1}{m_2}}} + \frac{\alpha d_1 d_2}{D_{m,1} D_{m,2} \left(\frac{E-B}{E_{con}-E} \right)^{\frac{1}{2m_1}} \left(\frac{E-B}{E_{con}-E} \right)^{\frac{1}{2m_2}}}.$$

Five Methods for Drug Interaction (cont.)

- Machado and Robinson (1994)

$$\left(\frac{d_1}{D_{x,1}}\right)^\eta + \left(\frac{d_2}{D_{x,2}}\right)^\eta = 1.$$

$$\left(\frac{d_1}{D_{m,1}\left(\frac{E}{1-E}\right)^{\frac{1}{m_1}}}\right)^\eta + \left(\frac{d_2}{D_{m,2}\left(\frac{E}{1-E}\right)^{\frac{1}{m_2}}}\right)^\eta = 1.$$

Five Methods for Drug Interaction (cont.)

- Plummer and Short (1990)

$$Y = \beta_0 - \beta_1 \log \left(d_1 + \rho \cdot d_2 + \beta_4 (d_1 \cdot \rho \cdot d_2)^{\frac{1}{2}} \right)$$

$$E = \frac{1.0}{1.0 + \exp \left(-\beta_0 - \beta_1 \log \left(d_1 + \rho \cdot d_2 + \beta_4 (d_1 \cdot \rho \cdot d_2)^{\frac{1}{2}} \right) \right)}.$$

$$\frac{d_1}{D_{x,1}} - \frac{d_2}{D_{x,2}} + \beta_4 \frac{(d_1 \cdot d_2)^{\frac{1}{2}}}{(D_{x,1} D_{x,2})^{\frac{1}{2}}} = 1.$$

Slide 7

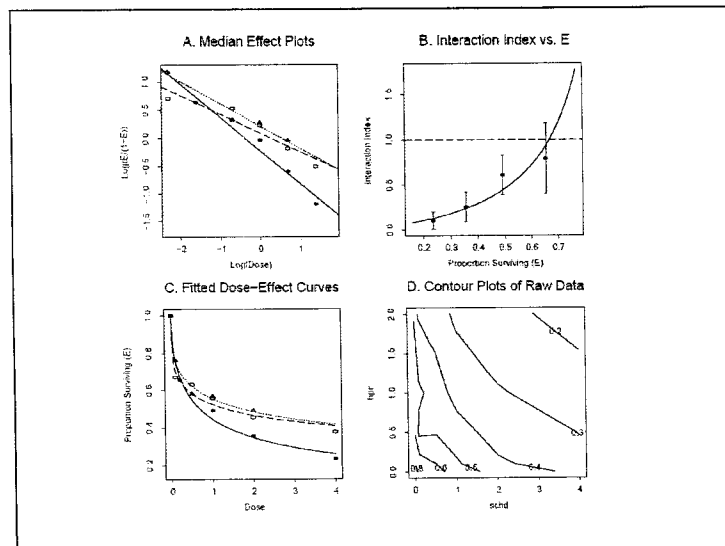
Five Methods for Drug Interaction (cont.)

- Carter et al. (1988)

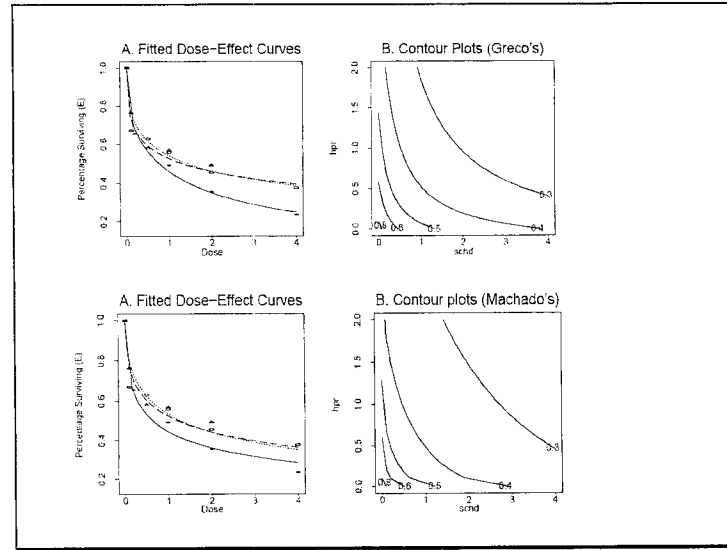
$$\text{Logit}(E) = \log\left(\frac{E}{1-E}\right) = \beta_0 + \beta_1 d_1 + \beta_2 d_2 + \beta_{12} d_1 d_2.$$

$$\begin{aligned} \frac{d_1}{D_{x,1}} + \frac{d_2}{D_{x,2}} &= \frac{\beta_1 d_1}{\log\left(\frac{E}{1-E}\right) - \beta_0} + \frac{\beta_2 d_2}{\log\left(\frac{E}{1-E}\right) - \beta_0} \\ &= 1 - \frac{\beta_{12} d_1 d_2}{\log\left(\frac{E}{1-E}\right) - \beta_0}. \end{aligned}$$

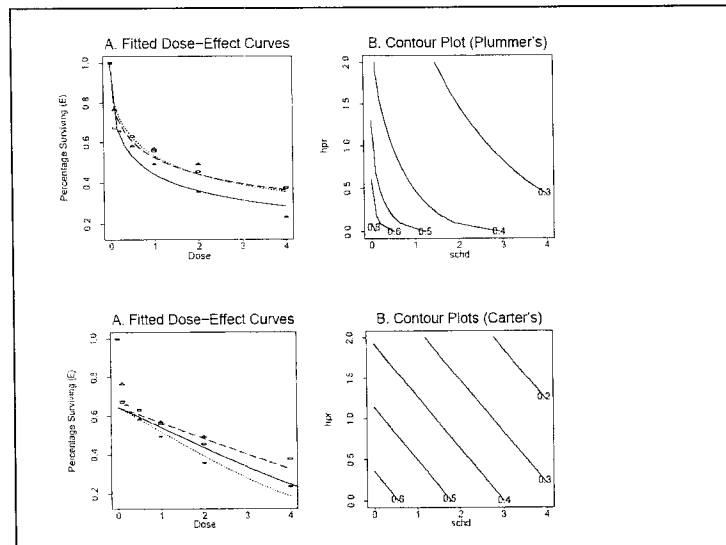
Slide 8



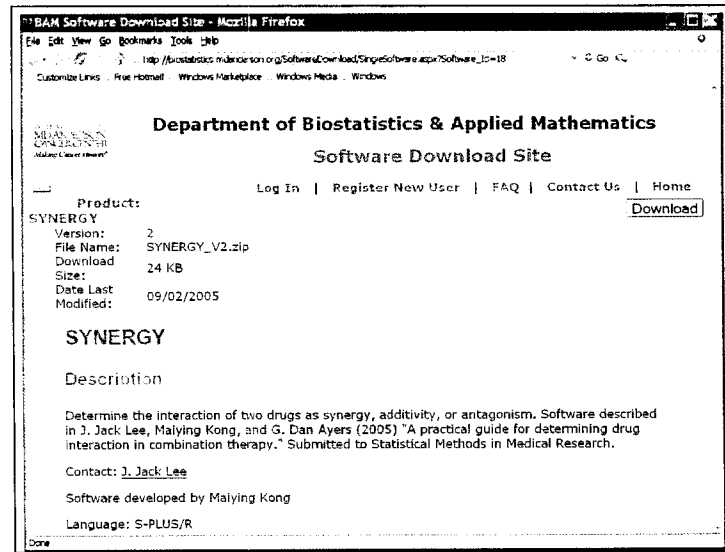
Slide 9



Slide 10



Slide 11



Slide 12

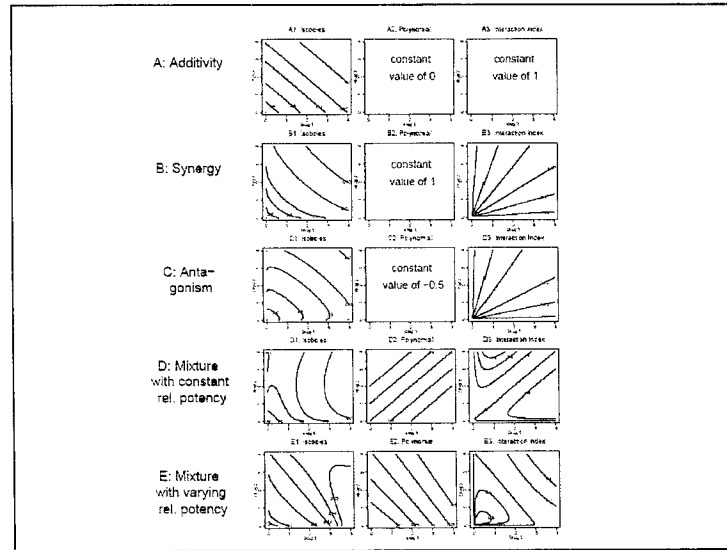
A New Method for Drug Interaction

- Kong and Lee (2005)

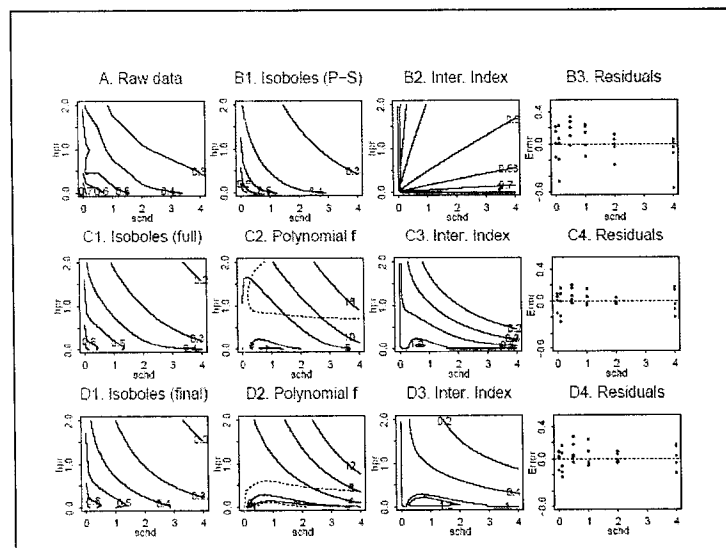
$$Y = \beta_0 + \beta_1 \log \left(d_1 + \rho d_2 + f(d_1, d_2; \gamma, \kappa) (d_1 \rho d_2)^{\frac{1}{2}} \right)$$

$$f(d_1, d_2; \gamma, \kappa) = \kappa_0 + \kappa_1 d_1^{\frac{1}{2}} + \kappa_2 (\rho d_2)^{\frac{1}{2}} + \kappa_3 d_1 + \kappa_4 \rho d_2 + \kappa_5 (d_1 \rho d_2)^{\frac{1}{2}}$$

Slide 13



Slide 14



APPENDIX 3

Publications

9-*cis*-Retinoic Acid Treatment Increases Serum Concentrations of α -Tocopherol in Former Smokers

Ji-Youn Han,¹ Diane D. Liu,² J. Jack Lee,²
Jonathan Kurie,¹ Reuben Lotan,¹ Waun K. Hong,¹
and Ho-Young Lee¹

Departments of ¹Thoracic/Head and Neck Medical Oncology and
²Biostatistics and Applied Mathematics, University of Texas M.D.
Anderson Cancer Center, Houston, Texas

ABSTRACT

Purpose: Low serum concentrations of antioxidants may be associated with an increased risk of cancer. Based on the accumulated evidence, we hypothesized that retinoids would elevate serum α -tocopherol. This study was designed to determine whether 9-*cis*-retinoic acid (9-*cis*-RA), the most common chemopreventive agent, could alter serum α -tocopherol in former smokers. Because hyperlipidemia is a known side effect of retinoids, we also evaluated the association between serum α -tocopherol and lipids in the same population.

Experimental Design: Subjects who had stopped smoking at least 12 months before the study were randomly assigned to receive oral 9-*cis*-RA or placebo daily for 3 months. Clinical information and blood samples were obtained monthly; serum α -tocopherol concentrations were measured by high-performance liquid chromatography and lipid levels by enzymatic assays before treatment and every month during the treatment.

Results: Of the 149 subjects in the study, 113 completed 3 months of treatment and provided samples for evaluation of serum α -tocopherol. Serum α -tocopherol levels in the 9-*cis*-RA group ($n = 52$) were higher after treatment ($r = 0.445$, $P < 0.01$) than before. The incidences of grade ≥ 2 hypertriglyceridemia and hypercholesterolemia were higher in the 9-*cis*-RA group than in the placebo group ($P = 0.0005$ and $P = 0.01$, respectively), but there were no serious complications related to hyperlipidemia.

Conclusions: Treatment of former smokers with 9-*cis*-RA significantly increased their serum α -tocopherol levels, and this could be a benefit. In addition, serum α -tocopherol could serve as a biomarker for 9-*cis*-RA treatment.

INTRODUCTION

Because lung cancer is the leading cause of cancer-related death worldwide (1, 2), chemoprevention has become an increasingly important priority in the effort to reduce its incidence (3). Thus far, the most often used chemopreventive agents for aerodigestive tract cancers have been retinoids (4), which bind and transactivate retinoic acid (RA) receptors (RAR) and retinoid X receptors (RXR), both of which belong to the superfamily of steroid nuclear receptors. Among the retinoids, all-*trans*-RA is selective for RARs, and 9-*cis*-RA binds both RARs and RXRs (5). In contrast, 13-*cis*-RA binds to neither receptor type but is thought to bind to the retinoid receptors after intracellular stereoisomerization to all-*trans*-RA or 9-*cis*-RA (6).

Several findings have shown the potential of retinoids as cancer chemopreventive agents (7–12). First, 9-*cis*-RA has shown antiproliferative activity against a broad range of neoplastic cells, including those from prostate cancer (7), breast cancer (8, 9), leukemia and lymphoma (10), lung cancer (11), and head and neck cancer (12). Second, 9-*cis*-RA had substantial *in vivo* anticarcinogenic activity in rat mammary glands (13, 14) and rat colons (15). Finally, in patients with a history of cancer of the head and neck region, 13-*cis*-RA treatment reduced the incidence of second primary tumors and reversed leukoplakia (i.e., premalignant oral lesions; refs. 16, 17).

Despite these promising findings, enthusiasm for the use of retinoids as chemopreventive agents for lung cancer waned after two large randomized clinical trials ended with disappointing results. The Alpha-Tocopherol, Beta Carotene Cancer Prevention Study, which tested the efficacy of the antioxidant dietary supplements α -tocopherol and β -carotene, actually showed that β -carotene significantly increased lung cancer incidence and mortality over the levels observed in participants not taking it (18). The detrimental effects of β -carotene were confirmed by the Beta-Carotene and Retinol Efficacy Trial, which revealed a 28% higher rate of lung cancer and 17% higher overall death rate in participants taking β -carotene than in those not taking the supplement (19). However, further analyses showed that the adverse effects of β -carotene were restricted to active smokers in both trials (20). In addition, there was some evidence of a benefit from retinoid treatment in nonsmokers and former smokers (21), suggesting that the response to retinoids differs in current and former smokers. Supporting these findings, 13-*cis*-RA treatment of current smokers had no effect on bronchial squamous metaplasia, a histologic abnormality associated with smoking, whereas 13-*cis*-RA treatment inhibited bronchial squamous metaplasia in former smokers (22). Wang et al. (23) reported that cigarette smoke and high doses of β -carotene induced a decrease in RA concentrations and RAR- β expression and an increase in cell proliferation and the expression of activating protein 1 family members (c-Jun and c-Fos) and cyclin D1 in the lung tissue of ferrets. Liu et al. (24) showed that the oxidative metabolites of β -carotene generated by smoke-induced production of cytochrome P450, which interferes with RA metabolism

Received 10/11/04; revised 11/24/04; accepted 12/20/04.

Grant support: NIH grants U19 CA68437 (W. Hong) and 1R01 CA100816-01A1 (H.-Y. Lee), American Cancer Society grant RSG-04-082-01-TBE (H.-Y. Lee) and Department of Defense grants DAMD17-01-1-0689 and W81XWH-04-1-0142-01-VITAL (W. Hong). The costs of publication of this article were defrayed in part by the payment of page charges. This article must therefore be hereby marked advertisement in accordance with 18 U.S.C. Section 1734 solely to indicate this fact.

Requests for reprints: Ho-Young Lee, Department of Thoracic/Head and Neck Medical Oncology, Unit 432, University of Texas M.D. Anderson Cancer Center, 1515 Holcombe Boulevard, Houston, TX 77030. Phone: 713-792-3782; Fax: 713-796-8655; E-mail: hlee@mdanderson.org.

©2005 American Association for Cancer Research.

by down-regulating RAR signaling and suppressing RAR- β expression. We recently showed in a chemopreventive trial that 9-*cis*-RA could benefit former smokers (25) by increasing RAR- β expression and decreasing metaplasia relative to the findings in the control group. These findings suggest that current and former smokers had different responses to retinoids and that retinoids, especially 9-*cis*-RA, have potential as chemopreventive agents in former smokers. Based on this notion, we sought to identify other benefits of 9-*cis*-RA for former smokers.

Antioxidants also have potential as chemopreventive agents (26–28), and low serum levels of antioxidants are associated with an increased risk of cancer (29–31). Because a correlation has been observed between serum levels of retinoids and the antioxidant α -tocopherol (32), we hypothesized that serum levels of α -tocopherol would be elevated in people who had been treated with retinoids. To test our hypothesis, we retrospectively analyzed data from a previously published three-arm, randomized, double-blinded, placebo-controlled trial comparing 9-*cis*-RA, 13-*cis*-RA plus α -tocopherol, and placebo daily for 3 months (25). Because hyperlipidemia is a common side effect of retinoid treatment (33, 34), we also evaluated possible associations between serum α -tocopherol and lipid levels in the same subjects.

MATERIALS AND METHODS

Subjects. The original trial design, the method of determining compliance with the trial protocol and the monitoring of toxic effects of the drugs have been previously described (25). That study was a three-arm, randomized, double-blinded, placebo-controlled trial comparing 9-*cis*-RA (100 mg), 13-*cis*-RA (1 mg/kg) plus α -tocopherol (1,200 IU), and placebo daily for 3 months (25). RAR- β was detected in 69.7% of all baseline biopsy samples, and metaplasia was evident in 6.9% of all baseline samples from 240 subjects enrolled between November 1995 and May 2001. RAR- β expression was restored and metaplasia was reduced after treatment in the 9-*cis*-RA group. After adjustment for years of smoking, packs per day smoked, and metaplasia, treatment with 9-*cis*-RA but not with 13-*cis*-RA plus α -tocopherol led to a statistically significant increase in RAR- β expression compared with placebo. All subjects were former smokers, defined as people with a smoking history of at least 20 pack-years who had stopped smoking at least 1 year before entering the study. To be eligible, subjects had to have adequate renal, hematologic, and hepatic function and must not have taken more than 25,000 IU of vitamin A or other retinoids per day within 3 months of study entry. Subjects with a prior smoking-related cancer were eligible if they had been tumor-free for 6 months before enrollment. Subjects were required to abstain from consuming vitamin supplements during the study. Before being randomly assigned to a treatment group, all eligible subjects provided written informed consent. This study was approved by the institutional review board at the University of Texas M.D. Anderson Cancer Center and by the U.S. Department of Health and Human Services. Subjects were seen monthly and evaluated for compliance with the trial protocol and for drug-related toxic effects. Serum cotinine levels were determined at baseline and at 3 and 6 months after treatment initiation to document compliance with smoking

abstinence during the trial. The treatment duration of 3 months was chosen on the basis of toxicity data from prior phase I trials that involved 9-*cis*-RA treatment (35, 36). In the current analysis, we did not include the group treated with 13-*cis*-RA plus α -tocopherol to avoid possible confounding effects from oral supplementary α -tocopherol.

Specimen Collection. To analyze changes in α -tocopherol levels and toxicity, blood specimens (10 mL) were drawn from each participant at the beginning of the study and then monthly during treatment. Blood was collected in heparinized tubes and transported immediately to the laboratory, where the specimens were separated and processed. Serum was collected after centrifugation of the blood at 1,500 rpm for 10 minutes at room temperature and was stored at -80°C until it was needed for testing.

High-Performance Liquid Chromatography Analysis for α -Tocopherol. Methods for extracting analytes from serum, quality control variables and the high-performance liquid chromatography (HPLC) methods for analyzing α -tocopherol in serum have been published previously (29). Briefly, a hexane extract of 0.4 mL of serum was injected onto a 3- μm C-18 Spherisorb ODS-2 HPLC column (1050 HPLC system; Hewlett-Packard, Avondale, PA) and eluted with an isocratic solvent consisting of 73% acetonitrile, 12% tetrahydrofuran, 8% methanol, 7% water, 0.025% ammonium acetate, and 0.05% diethylamine (v/v) at 1.2 mL/min. α -Tocopherol was detected at 292 nm. The HPLC system was fully automated and equipped with quaternary pumps, an electronic degasser, insulated column housing, an automatic sampler diode array detector, and software to run the system and perform data management. The coefficient of variation for the pooled quality control samples for all of the analytes was $\leq 10\%$.

Biochemical Assays. Serum levels of triglycerides and cholesterol were measured with routine enzymatic methods on a random access clinical chemistry system (Dimension, Dade Behring International, Inc., Newark, NJ).

Statistical Analyses. The Wilcoxon rank sum test and Kruskal-Wallis test were used to test the equal medians of continuous variables between two treatment groups. Either the χ^2 test or Fisher's exact test was used to test the association between two categorical variables. Because the distributions of α -tocopherol were skewed, the differences in α -tocopherol levels between treatment groups were tested with the Wilcoxon rank sum test. Changes in serum α -tocopherol levels from baseline levels were tested separately at each subsequent patient visit (i.e., at 1-, 2-, 3-, and 6-month visits) and in each group by using the Wilcoxon rank sum test. All statistical tests were two-sided, with a 5% type I error rate. Statistical analysis was done with standard statistical software, including SAS Release 8.1 (SAS Institute, Cary, NC) and S-Plus 2000 (Mathsoft, Inc., Seattle, WA).

RESULTS

Characteristics of Subjects. The characteristics of the eligible subjects have been described in detail previously (25). Two hundred forty subjects were entered into the original clinical trial, of whom 226 were eligible to be randomly assigned into one of the three treatment groups (9-*cis*-RA, 13-*cis*-RA plus α -tocopherol, or placebo); 149 of these participants

Table 1 Baseline characteristics of subjects according to treatment group

	Placebo (n = 61)	9-cis-RA (n = 52)	P*
Gender (%)			
Male	37 (60.7)	27 (51.9)	0.35
Female	24 (39.3)	25 (48.1)	
Race (%)			
White	52 (85.3)	49 (94.2)	0.35
African	6 (9.8)	2 (3.9)	
Hispanic	3 (4.9)	1 (1.9)	
Oriental	0	0	
Smoking-related cancer (%)			
No	54 (88.5)	48 (92.3)	0.54
Yes	7 (11.5)	4 (7.7)	
Age			
Mean \pm SD	58.1 \pm 8.9	55.7 \pm 9.2	0.12
Median (range)	58.8 (34.9-73.6)	54.9 (35.9-74.5)	
Body mass index			
Mean \pm SD	27.8 \pm 4.1	28.1 \pm 5.38	0.92
Median (range)	27.1 (20.6-39.4)	27.3 (19.4-44.4)	
Smoking years			
Mean \pm SD	29.1 \pm 9.8	27.3 \pm 9.5	0.39
Median (range)	30 (15-50)	26 (10-50)	
Packs per day			
Mean \pm SD	1.7 \pm 0.7	1.9 \pm 0.8	0.23
Median (range)	1.5 (1-4)	2 (0.8-4)	
Pack-years			
Mean \pm SD	50.2 \pm 27.2	52.6 \pm 30.5	0.94
Median (range)	42.5 (20-135)	42 (20-136)	
Smoking quit years			
Mean \pm SD	10.4 \pm 8.8	11.0 \pm 8.7	0.56
Median (range)	10.1 (1.1-35.2)	7.8 (1.0-38.2)	
Cholesterol			
Mean \pm SD	205.8 \pm 37.5	206.9 \pm 31.9	0.74
Median (range)	198 (141-292)	205 (151-283)	
Triglyceride			
Mean \pm SD	142.4 \pm 65.9	152.2 \pm 60.4	0.39
Median (range)	132 (43-309)	136 (58-282)	

*The Wilcoxon rank sum test was performed to test of continuous variables between two treatment groups. The χ^2 test (for sex) and Fisher's exact test (for race and smoking-related cancer) were performed to test the association between two categorical variables.

(the subjects of the current analysis) had been randomly assigned to either the placebo or the 9-cis-RA groups, and 113 of them completed 3 months of treatment. The characteristics of the evaluable subjects are summarized in Table 1. Each treatment group was well balanced for age, sex, race, history of smoking-related cancer, number of pack-years, number of years since stopping smoking, body mass index, and serum levels of cholesterol and triglycerides. Serum cotinine levels drawn at registration, at 3 and 6 months showed that >95% of the participants had serum levels in the range of nonsmokers (<1.0 ng/mL) or passive smokers (1-20 ng/mL) at all three measurement times.

Effects of 9-cis-RA Treatment on Serum α -Tocopherol Level. We investigated whether 9-cis-RA treatment affected the serum α -tocopherol level. We found that baseline serum α -tocopherol level of the placebo group was not different from that of 9-cis-RA treatment group (Table 2). Serum α -tocopherol concentrations significantly increased over time in the 9-cis-RA group but not in the placebo group, peaking 1 month after the start of treatment and maintaining this level throughout treatment. This finding indicates that 9-cis-RA can increase serum α -tocopherol concentrations in former smokers.

Table 2 α -Tocopherol level at baseline and during treatment of 9-cis-RA

	α -Tocopherol level, median (range, μ g/dl)		
	Placebo (n = 61)	9-cis-RA (n = 52)	P
Baseline	13,017 (2,241-45,620)	14,002 (6,162-33,779)	0.37*
1st month	11,818 (1,311-22,306)	16,456 (7,883-48,877)	0.005†
2nd month	11,454 (5,770-26,506)	15,847 (7,607-46,132)	0.003†
3rd month	12,354 (6,788-23,150)	15,381 (8,461-49,383)	0.01†

*P was obtained from the Wilcoxon rank sum test.

†P was obtained from repeated-measures analysis using a mixed model.

To determine whether subject characteristics may have affected their baseline serum α -tocopherol level, we evaluated possible associations between the characteristics listed in Table 1 and baseline serum α -tocopherol levels. Gender, race, body mass index, number of pack-years, number of years since stopping smoking, and levels of cholesterol were not associated with the baseline serum α -tocopherol level (Table 3). However, the baseline serum triglyceride level and age were significantly associated with higher baseline serum α -tocopherol levels. When adjusted for body mass index, the effects of both age ($P = 0.02$) and baseline serum triglyceride level ($P = 0.008$) on the baseline serum α -tocopherol concentration were found to be significant by regression analysis.

Effects of 9-cis-RA Treatment on Serum Concentrations of Triglycerides and Cholesterol. We tested the serum levels of lipids, including triglycerides and cholesterol, in all participants. During treatment, serum levels of lipids were significantly increased in 9-cis-RA group and decreased when treatment with 9-cis-RA was stopped (Fig 1). In testing the

Table 3 Association between baseline α -tocopherol level and demographic characteristics

Characteristics	α -Tocopherol level, mean \pm SD (range, ng/mL)	P*
Gender		
Male	15,090 \pm 6,967.4 (7,086-45,620)	0.96
Female	14,399 \pm 5,993.7 (2,241-33,779)	
Race		
White	15,097 \pm 6,701.4 (2,241-45,620)	0.24
African	12,796 \pm 5,252.6 (7,086-21,245)	
Hispanic	11,047 \pm 2,203.1 (8,484-13,792)	
Age (y)		
<60	13,885 \pm 6,287.0 (5,575-45,620)	0.02
≥ 60	16,380 \pm 6,758.4 (2,241-33,586)	
Body mass index		
Nonobese (<28)	14,040 \pm 5,036.2 (5,575-29,889)	0.47
Obese (≥ 28)	15,531 \pm 6,844.1 (6,162-33,779)	
Pack-years		
<40	14,357 \pm 6,742.6 (5,575-45,620)	0.47
≥ 40	15,135 \pm 6,415.0 (2,241-33,779)	
Smoking quit years		
<10	13,827 \pm 5,515.5 (2,241-30,742)	0.15
≥ 10	15,921 \pm 7,472.0 (5,575-45,620)	
Cholesterol (mg/dl)		
<200	14,060 \pm 5,560.5 (5,575-33,586)	0.32
≥ 200	15,419 \pm 6,992.6 (2,241-45,620)	
Triglyceride (mg/dl)		
≤ 135	12,562 \pm 4,550.0 (2,241-25,603)	0.008
>135	16,440 \pm 7,146.4 (7,681-45,620)	

*P was obtained from the Wilcoxon rank sum test.

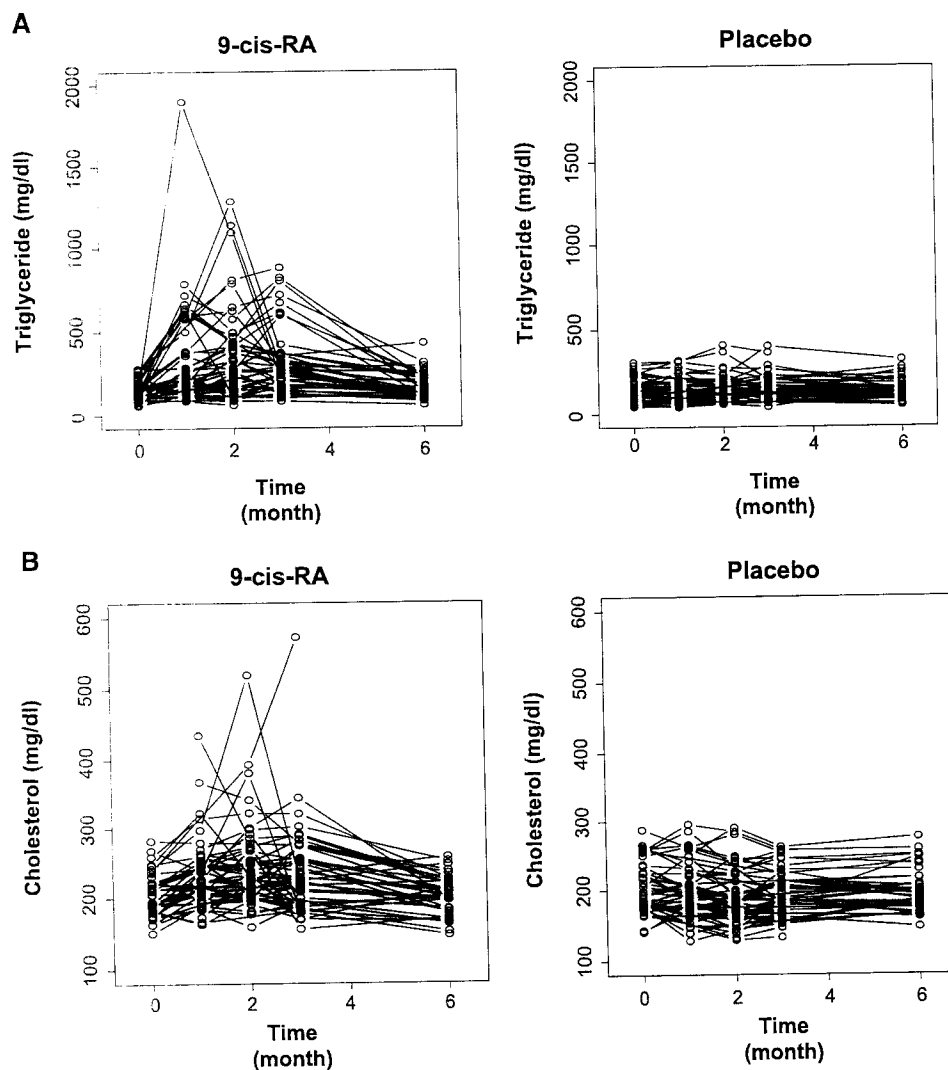


Fig. 1 Effect of 9-*cis*-RA on the serum levels of (A) triglycerides and (B) cholesterol after 3 months of treatment.

serum levels of lipids, including triglycerides and cholesterol, in all participants, we found no significant difference in the incidence of grade 1 hyperlipidemia between the 9-*cis*-RA group and the placebo group during treatment (Table 4). However, 9-*cis*-RA group showed significantly more subjects of grade ≥ 2 hypertriglyceridemia and hypercholesterolemia than the placebo group ($P < 0.0001$). Of 52 evaluable subjects in the 9-*cis*-RA group, 22 (42%, $P = 0.0001$) and 12 (23%, $P = 0.0001$) developed grade >2 hypertriglyceridemia and hypercholesterolemia, respectively. One of the participants in the 9-*cis*-RA group experienced grade 4 hypertriglyceridemia and discontinued treatment. However, no serious complications related to hypertriglyceridemia or hypercholesterolemia, such as cardiovascular events, pancreatitis, or death, were experienced in either group, and the hyperlipidemia disappeared after discontinuation of 9-*cis*-RA treatment. Finally, we evaluated whether the modulation of serum lipid levels was associated with modulation of serum α -tocopherol levels during 3 months of 9-*cis*-RA treatment. The modulation of serum α -tocopherol levels in the 9-*cis*-RA treatment group

was significantly associated with the changes in serum levels of triglyceride (Fig. 2A) and cholesterol (Fig. 2B).

DISCUSSION

To our knowledge, this is the first report showing that 9-*cis*-RA affects serum α -tocopherol levels and that serum α -tocopherol levels correlated with serum lipid levels in the setting of a chemoprevention trial. Specifically, daily doses of 9-*cis*-RA increased serum concentrations of α -tocopherol, a well-known antioxidant, in former smokers who had not smoked for at least 1 year.

It has been suggested that an imbalance between oxidants and antioxidants results in a chronic state of oxidative stress that could contribute to various human diseases, including cancer (37). In fact, reactive oxygen species are constantly generated by ionizing and UV radiation, activation of chemical carcinogens, and the presence of heavy metal carcinogens, and these reactive oxygen species can damage DNA and thus cause mutations that can lead to cancers (38). Antioxidants protect cells from DNA damage by directly removing these

Table 4 The incidence of hypertriglyceridemia or hypercholesterolemia according to treatment group

National Cancer Institute Common Toxicity Criteria	Placebo (n = 61)	9-cis-RA (n = 52)	P*
Hypertriglyceridemia			
Grade 1 ($>2.5 \times \text{ULN}$)	28	23	<0.0001
Grade 2 ($>2.5\text{--}5.0 \times \text{ULN}$)	2	15	
Grade 3 ($>5.0\text{--}10 \times \text{ULN}$)	0	6	
Grade 4 ($>10 \times \text{ULN}$)	0	1	
Hypercholesterolemia			
Grade 1 ($>\text{ULN}$ –300 mg/dl)	22	24	<0.0001
Grade 2 ($>300\text{--}400$ mg/dl)	0	8	
Grade 3 ($>400\text{--}500$ mg/dl)	0	2	
Grade 4 (>500 mg/dl)	0	2	

Abbreviation: ULN, upper limit of normal range.

*P value was obtained from the Fisher's exact test.

reactive oxygen species thus reducing DNA damage and potentially decreasing tumorigenesis. Indeed, several studies have already shown the cancer chemopreventive properties of antioxidants (39). For example, dietary supplementation with α -tocopherol has been shown to prevent exercise-induced DNA damage (40), and results from a randomized phase II chemoprevention trial showed that α -tocopherol decreased oxidative DNA damage (41). The use of α -tocopherol to prevent human cancer has been evaluated for lung cancer, oral leukoplakia, colorectal polyps, and prostate cancer (30, 39, 41, 42). In a separate study, vitamin C, vitamin E, and β -carotene supplementation also significantly reduced endogenous oxidative DNA damage in lymphocytes and increased resistance to

oxidative damage induced by hydrogen peroxide (43). Taken together, these findings suggest that 9-cis-RA can induce potential cancer chemopreventive activities in former smokers by increasing α -tocopherol levels.

We found age to be significantly associated with higher baseline serum α -tocopherol levels, an observation also found in other cohort studies (30, 44, 45). The positive association between α -tocopherol levels and age can be explained by age-related changes in the metabolism and transport of α -tocopherol; for example, the activity of lipoprotein lipase, an enzyme that releases α -tocopherol from chylomicrons and transfers it to tissues, has been shown to decrease with age (30). We also noted a positive relationship between baseline triglyceride and α -tocopherol levels. Because α -tocopherol is preferentially bound by the hepatic tocopherol binding protein, which is incorporated into both low- and high-density lipoproteins (44, 46), increases in serum triglyceride levels could be expected in association with increased serum α -tocopherol levels. Baseline serum cholesterol levels also seemed associated with baseline serum α -tocopherol levels, but this apparent relationship was not statistically significant, perhaps because baseline serum cholesterol levels were distributed over a narrow range. Because hyperlipidemia, especially hypertriglyceridemia, is a well-known effect of the clinical use of retinoids, we evaluated serum lipid concentrations and found that hypertriglyceridemia and hypercholesterolemia developed in 42% and 23% of patients, all former smokers, treated with 9-cis-RA, respectively, proportions that are consistent with previous findings (47, 48). Moreover, elevation of serum α -tocopherol concentrations was significantly

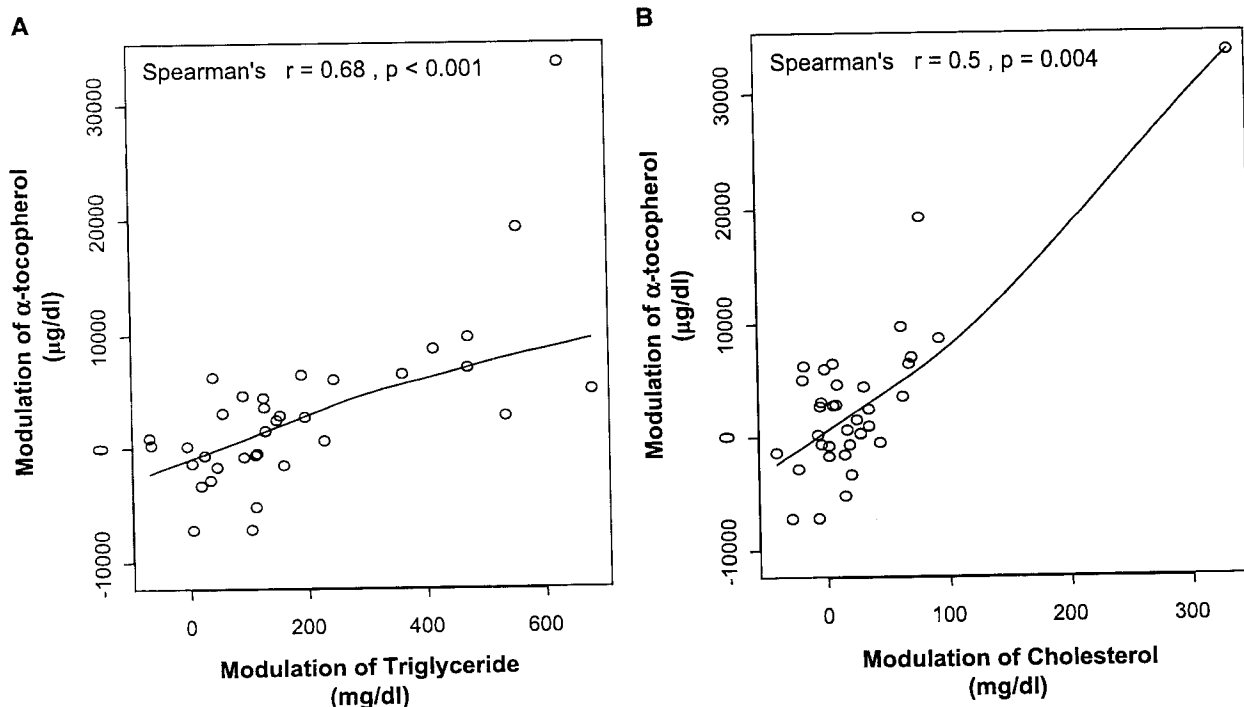


Fig. 2 The correlation between changes in serum levels of lipids and changes in serum levels of α -tocopherol level in the 9-cis-RA and placebo treatment groups. Wilcoxon rank sum test was performed to α -tocopherol level (3-month value minus baseline value) compared with the changes in the median (4) triglyceride (3-month value minus baseline value) ($r = 0.68$, $P < 0.001$) and (B) cholesterol (3-month value minus baseline value) ($r = 0.5$, $P = 0.004$) levels.

associated with elevated levels of lipids in this group. A plausible explanation for this finding is the unique binding characteristics of 9-*cis*-RA to retinoid receptors that have transcription activities. Several studies have provided evidence that retinoids induce hyperlipidemia by activating RAR, RXR, or both (49–51). In one study, the simultaneous activation of RAR and RXR by panagonists induced 2- to 3-fold higher levels of serum triglycerides than did activation of RAR alone (51). Vu-Dac et al. (52) reported that RXR activation increased the expression of apo C-III, a key player in plasma triglyceride metabolism. Furthermore, 9-*cis*-RA induces the expression of the ATP-binding cassette transporter A1, a major regulator of peripheral cholesterol efflux and plasma high-density lipoprotein metabolism and increases apo A-I-mediated cholesterol efflux, thereby increasing the cholesterol concentration in the blood (53, 54). These data indicate that RAR and RXR ligands can act synergistically to induce high serum concentrations of lipids, suggesting that hyperlipidemia may be a greater issue for 9-*cis*-RA, an RAR/RXR panagonist, than for other RAs (6).

The risk of hyperlipidemia resulting from retinoid treatment in our chemoprevention trial was not clear. More small dense low-density lipoprotein particles are present in the blood in hyperlipidemia, and these particles are more susceptible to oxidation and are associated with enhanced peroxidation products (55). A high serum level of α -tocopherol, which breaks the chain reaction of lipid peroxidation by donating a hydrogen atom to the reactive oxygen species, could result in the formation of a relatively stable α -tocopherol radical that is thought to be recycled by ascorbate and ubiquinol (56, 57), suggesting that the ability of 9-*cis*-RA to modulate serum α -tocopherol concentrations may protect cells from increased concentrations of lipid peroxidants. Indeed, no serious complications related to hypertriglyceridemia or hypercholesterolemia, such as cardiovascular problems, pancreatitis, or death, were experienced in the subjects treated with 9-*cis*-RA in our study. Only one patient with grade 4 hypertriglyceridemia stopped 9-*cis*-RA treatment, and even that patient had no hyperlipidemia-associated complications. Furthermore, measurements of serum lipid levels after treatment was discontinued showed normalization of lipid levels in all subjects. However, considering recent findings that the risk of lung cancer is higher in recent former smokers than in current smokers (58), the inclusion of subjects (albeit few) with prior cancers and recent smoking cessation might have clouded our data. Therefore, cognizance of the potential cardiovascular risk should be well advised when oral supplementation of agents that increase serum α -tocopherol levels is considered for chemoprevention trial in a group of former smokers. Close monitoring of symptoms and signs of hyperlipidemia and the use of lipid- and cholesterol-lowering agents would be recommended for subjects taking 9-*cis*-RA for long periods. In addition, further study is needed to clarify the relationship between hyperlipidemia and retinoid treatment and to define the adequate duration of retinoid treatment in a chemoprevention trial.

In summary, to our knowledge, our results show for the first time that 9-*cis*-RA treatment increased serum α -tocopherol levels in former smokers. From the perspective of directing future public health initiatives, our current findings are important because increasing serum levels of the antioxidant may inhibit

cell proliferation and angiogenesis and stimulate apoptosis and immune function (59–61). Additional work is warranted to determine whether other antioxidants, such as vitamin C, vitamin A, and β -carotene, are regulated by 9-*cis*-RA treatment in former smokers and whether the changes in α -tocopherol levels induced by 9-*cis*-RA correlate with their ability to reduce the risk of lung cancer in former smokers.

REFERENCES

1. Stewart AK, Bland KI, McGinnis LS Jr, et al. Clinical highlights from the National Cancer Data Base, 2000. *CA Cancer J Clin* 2000;50:171–83.
2. Parkin DM, Pisani P, Ferlay J. Estimates of the worldwide incidence of 25 major cancers in 1990. *Int J Cancer* 1999;80:827–41.
3. Tsao AS, Kim ES, Hong WK. Chemoprevention of cancer. *CA Cancer J Clin* 2004;54:150–80.
4. Lippman SM, Lee JJ, Karp DD, et al. Randomized phase III intergroup trial of isotretinoin to prevent second primary tumors in stage I non-small-cell lung cancer. *J Natl Cancer Inst* 2001;93:605–18.
5. Sun SY, Lotan R. Retinoids and their receptors in cancer development and chemoprevention. *Crit Rev Oncol Hematol* 2002;41:41–55.
6. Marchetti MN, Sampol E, Bun H, et al. *In vitro* metabolism of three major isomers of retinoic acid in rats. Intersex and interstrain comparison. *Drug Metab Dispos* 1997;25:637–46.
7. Blutt SE, Allegretto EA, Pike JW, et al. 1,25-Dihydroxyvitamin D3 and 9-*cis*-retinoic acid act synergistically to inhibit the growth of LNCaP prostate cells and cause accumulation of cells in G₁. *Endocrinology* 1997;138:1491–7.
8. Rubin M, Fenig E, Rosenauer A, et al. 9-*cis*-Retinoic acid inhibits growth of breast cancer cells and down-regulates estrogen receptor RNA and protein. *Cancer Res* 1994;54:6549–56.
9. Gottardis MM, Lamph WW, Shalinsky DR, et al. The efficacy of 9-*cis*-retinoic acid in experimental models of cancer. *Breast Cancer Res Treat* 1996;38:85–96.
10. Lutzky J, Vujicic M, Yamanishi DT, et al. Antiproliferative effects of all-*trans*-retinoic acid (tRA) and 9-*cis*-retinoic acid (9-*cis*RA) on human lymphoid cell lines [abstract]. *Proceedings of the American Association for Cancer Res* 1993;34:292.
11. Guzey M, Demirpence E, Criss W, et al. Effects of retinoic acid (all-*trans* and 9-*cis*) on tumor progression in small-cell lung carcinoma. *Biochem Biophys Res Commun* 1998;242:369–75.
12. Giannini F, Maestro R, Vukosavljevic T, et al. All-*trans*, 13-*cis*, and 9-*cis* retinoic acids induce a fully reversible growth inhibition in HNSCC cell lines: implications for *in vivo* retinoic acid use. *Int J Cancer* 1997;70:194–200.
13. Anzano MA, Byers SW, Smith JM, et al. Prevention of breast cancer in the rat with 9-*cis*-retinoic acid as a single agent and in combination with tamoxifen. *Cancer Res* 1994;54:4614–7.
14. Anzano MA, Peer CW, Smith JM, et al. Chemoprevention of mammary carcinogenesis in the rat: combined use of raloxifene and 9-*cis*-retinoic acid. *J Natl Cancer Inst* 1996;88:123–5.
15. Zheng Y, Kramer PM, Olson G, et al. Prevention by retinoids of azoxymethane-induced tumors and aberrant crypt foci and their modulation of cell proliferation in the colon of rats. *Carcinogenesis* 1997;18:2119–25.
16. Hong WK, Sporn MB. Recent advances in chemoprevention of cancer. *Science* 1997;278:1073–7.
17. Hong WK, Endicott J, Itri LM, et al. 13-*cis*-retinoic acid in the treatment of oral leukoplakia. *N Engl J Med* 1986;315:1501–5.
18. The Alpha-Tocopherol, Beta Carotene Cancer Prevention Study Group. The effect of vitamin E and β carotene on the incidence of lung cancer and other cancers in male smokers. *N Engl J Med* 1994;330:1029–35.
19. Omenn GS, Goodman GE, Thornquist MD, et al. Effects of a combination of β carotene and vitamin A on lung cancer and cardiovascular disease. *N Engl J Med* 1996;334:1150–5.

20. Albanes D, Heinonen OP, Taylor PR, et al. α -tocopherol and β -carotene supplements and lung cancer incidence in the Alpha-Tocopherol, Beta-Carotene Cancer Prevention Study: effects of base-line characteristics and study compliance. *J Natl Cancer Inst* 1996;88:1560-70.
21. Lippman SM, Lee JJ, Karp DD, et al. Randomized phase III intergroup trial of isotretinoin to prevent second primary tumors in stage I non-small-cell lung cancer. *J Natl Cancer Inst* 2001;93:605-18.
22. Lee JS, Lippman SM, Benner SE, et al. Randomized placebo-controlled trial of isotretinoin in chemoprevention of bronchial squamous metaplasia. *J Clin Oncol* 1994;12:937-45.
23. Wang XD, Liu C, Bronson RT, et al. Retinoid signaling and activator protein-1 expression in ferrets given β -carotene supplements and exposed to tobacco smoke. *J Natl Cancer Inst* 1999;91:60-6.
24. Liu C, Russell RM, Wang XD. Exposing ferrets to cigarette smoke and a pharmacological dose of β -carotene supplementation enhance *in vitro* retinoic acid catabolism in lungs via induction of cytochrome P450 enzymes. *J Nutr* 2003;133:173-9.
25. Kurie JM, Lotan R, Lee JJ, et al. Treatment of former smokers with 9-*cis*-retinoic acid reverses loss of retinoic acid receptor- β expression in the bronchial epithelium: results from a randomized placebo-controlled trial. *J Natl Cancer Inst* 2003;95:206-14.
26. Sawant SS, Kandarkar SV. Role of vitamins C and E as chemopreventive agents in the hamster cheek pouch treated with the oral carcinogen-DMBA. *Oral Dis* 2000;6:241-7.
27. Trickler D, Shklar G. Prevention by vitamin E of experimental oral carcinogenesis. *J Natl Cancer Inst* 1987;78:165-9.
28. Ross D, Moldeus P. Antioxidant defense system and oxidative stress. In: Vigo-Pelfrey C, editors. *Membrane lipid oxidation*. Boca Raton (FL): CRC Press; 1990. p. 151-70.
29. Goodman GE, Schaffer S, Omenn GS, Chen C, King I. The association between lung and prostate cancer risk, and serum micronutrients: results and lessons learned from β -carotene and retinol efficacy trial. *Cancer Epidemiol Biomarkers Prev* 2003;12:518-26.
30. Woodson K, Tangrea JA, Barrett MJ, Virtamo J, Taylor PR, Albanes D. Serum α -tocopherol and subsequent risk of lung cancer among male smokers. *J Natl Cancer Inst* 1999;91:1738-43.
31. Taylor PR, Qiao YL, Abnet CC. Prospective study of serum vitamin E levels and esophageal and gastric cancers. *J Natl Cancer Inst* 2003 Sep 17;95:1414-6.
32. Basile G, Gangemi S, Lo Balbo C, et al. Correlation between serum retinol and α -tocopherol levels in centenarians. *J Nutr Sci Vitaminol (Tokyo)* 2003;49:287-8.
33. Bershad S, Rubinstein A, Paterniti JR, et al. Changes in plasma lipids and lipoproteins during isotretinoin therapy for acne. *N Engl J Med* 1985;313:981-5.
34. Lowe NJ, David M. New retinoids for dermatologic diseases. Uses and toxicity. *Dermatol Clin* 1988;6:539-52.
35. Kurie JM, Lee JS, Griffin T, et al. Phase I trial of 9-*cis* retinoic acid in adults with solid tumors. *Clin Cancer Res* 1996;2:287-93.
36. Miller VA, Rigas JR, Benedetti FM, et al. Initial clinical trial of the retinoid receptor pan agonist 9-*cis* retinoic acid. *Clin Cancer Res* 1996;2:471-5.
37. Hu JJ, Chi CX, Frenkel K, et al. α -tocopherol dietary supplement decreases titers of antibody against 5-hydroxymethyl-2'-deoxyuridine (HMDU). *Cancer Epidemiol Biomarkers Prev* 1999;8:693-8.
38. Frenkel K. Role of active oxygen species in carcinogenesis. In: Bertino JR, editor. *Encyclopedia of cancer*. San Diego (CA): Academic Press; 1997. p. 233-45.
39. Benner SE, Wargovich MJ, Lippman SM, et al. Reduction in oral mucosa micronuclei frequency following α -tocopherol treatment of oral leukoplakia. *Cancer Epidemiol Biomarkers Prev* 1994;3:73-6.
40. Hartmann A, Niess AM, Grunert-Fuchs M, et al. Vitamin E prevents exercise-induced DNA damage. *Mutat Res* 1995;346:195-202.
41. McKeown-Eyssen G, Holloway C, Jazmaji V, et al. A randomized trial of vitamins C and E in the prevention of recurrence of colorectal polyps. *Cancer Res* 1988;48:4701-5.
42. Heinonen O, Albanes D, Virtamo J, et al. Prostate cancer and supplementation with α -tocopherol and β -carotene: incidence and mortality in a controlled trial. *J Natl Cancer Inst* 1998;90:440-6.
43. Duthie SJ, Ma A, Ross MA, Collins A. Antioxidant supplementation decreases oxidative DNA damage in human lymphocytes. *Cancer Res* 1996;56:1291-5.
44. White E, Kristal AR, Shikany JM, et al. Correlates of serum α - and γ -tocopherol in the Women's Health Initiative. *Ann Epidemiol* 2001;11:136-44.
45. Papas A, Stacewicz-Sapuntzakis M, Lagiou P, Bamia C, Chloutsios Y, Trichopoulos A. Plasma retinol and tocopherol levels in relation to demographic, lifestyle and nutritional factors of plant origin in Greece. *Br J Nutr* 2003;89:83-7.
46. Traber MG, Sies H. Vitamin E in humans: demand and delivery. *Annu Rev Nutr* 1996;16:321-47.
47. Bershad S, Rubinstein A, Paterniti JR, et al. Changes in plasma lipids and lipoproteins during isotretinoin therapy for acne. *N Engl J Med* 1985;313:981-5.
48. Lowe NJ, David M. New retinoids for dermatologic diseases. Uses and toxicity. *Dermatol Clin* 1988;6:539-52.
49. Standeven AM, Beard RL, Johnson AT, et al. Retinoid-induced hypertriglyceridemia in rats is mediated by retinoic acid receptors. *Fundam Appl Toxicol* 1996;33:264-71.
50. Rigas JR, Miller VA, Levine DM, et al. Lipoprotein alterations in patients treated with novel retinoids [abstract]. *Proceedings of the American Association of Cancer Research* 1995;36.
51. Standeven AM, Thacher SM, Yuan YD, et al. Retinoid X receptor agonist elevation of serum triglycerides in rats by potentiation of retinoic acid receptor agonist induction or by action as single agents. *Biochem Pharmacol* 2001;62:1501-9.
52. Vu-Dac N, Gervois P, Torra IP, et al. Retinoids increase human apo C-III expression at the transcriptional level via the retinoid X receptor: contribution to the hypertriglyceridemic action of retinoids. *J Clin Invest* 1998;102:625-32.
53. Koldamova RP, Lefterov IM, Ikonomic MD, et al. 22R-Hydroxycholesterol and 9-*cis*-retinoic acid induce ATP-binding cassette transporter A1 expression and cholesterol efflux in brain cells and decrease amyloid β secretion. *J Biol Chem* 2003;278:13244-56.
54. Mascres B, Ghyselinck NB, Watanabe M, et al. Ligand-dependent contribution of RXR β to cholesterol homeostasis in Sertoli cells. *EMBO Rep* 2004;5:285-90.
55. de Graaf J, Hak-Lemmers HL, Hectors MP, et al. Enhanced susceptibility to *in vitro* oxidation of the dense low density lipoprotein subfraction in healthy subjects. *Arterioscler Thromb* 1991;11:298-306.
56. Oostenbrug GS, Mensink RP, Al MD, et al. Maternal and neonatal plasma antioxidant levels in normal pregnancy, and the relationship with fatty acid unsaturation. *Br J Nutr* 1998;80:67-73.
57. De Vriese SR, Dhont M, Christophe AB. Oxidative stability of low density lipoproteins and vitamin E levels increase in maternal blood during normal pregnancy. *Lipids* 2001;36:361-6.
58. Ebbert JO, Yang P, Vachon CM, et al. Lung cancer risk reduction after smoking cessation: observations from a prospective cohort of women. *J Clin Oncol* 2003;21:921-6.
59. Sigounas G, Anagnostou A, Steiner M. DL- α -Tocopherol induces apoptosis in erythroleukemia, prostate, and breast cancer cells. *Nutr Cancer* 1997;28:30-5.
60. Shklar G, Schwartz JL. Vitamin E inhibits experimental carcinogenesis and tumour angiogenesis. *Eur J Cancer B Oral Oncol* 1996;32B:114-9.
61. Meydani SN, Beharka AA. Recent developments in vitamin E and immune response. *Nutr Rev* 1996;56:S49-58.

Decoy Receptor 2 (*DcR2*) Is a p53 Target Gene and Regulates Chemosensitivity

Xiangguo Liu, Ping Yue, Fadlo R. Khuri, and Shi-Yong Sun

Department of Hematology and Oncology, Winship Cancer Institute, Emory University School of Medicine, Atlanta, Georgia

Abstract

Decoy receptor 2 (*DcR2*) is one of the tumor necrosis factor-related apoptosis-inducing ligand (TRAIL) receptors and suppresses TRAIL-induced apoptosis. Its expression, like the other three TRAIL receptors (i.e., DR4, DR5, and *DcR1*), is regulated by p53. Here, we report that *DcR2* is a p53 target gene and regulates chemosensitivity. In this study, we identified a p53-binding site (p53BS) in the first intron of the *DcR2* gene. This p53BS is almost identical to the ones found in the first introns of other three TRAIL receptor genes. By a chromatin immunoprecipitation assay, we detected that the p53 protein bound to the *DcR2* p53BS in intact cells. Subcloning of the *DcR2* p53BS into a luciferase reporter vector driven by a SV40 promoter exhibited enhanced luciferase activity when transiently cotransfected with a wild-type (wt) p53 expression vector in p53-null cell lines or stimulated with DNA-damaging agents in cell lines having wt p53. Moreover, when the *DcR2* p53BS, together with its own corresponding promoter regions, was subcloned into a basic luciferase vector without a promoter element, its transcriptional activities were strikingly increased by cotransfection of the wt p53 gene. However, when this p53BS was deleted from the construct, wt p53 failed to transactivate this reporter construct. Collectively, we conclude that p53 directly regulates the *DcR2* gene expression via an intronic p53BS. In addition, overexpression of *DcR2* conferred resistance to TRAIL-mediated apoptosis and attenuated cell response to DNA-damaging agents, whereas silencing of *DcR2* expression enhanced chemotherapeutic agent-induced apoptosis. These results suggest that *DcR2* regulates chemosensitivity. (Cancer Res 2005; 65(20): 9169-75)

Introduction

p53 is the most commonly altered gene in human cancer. Thus, it plays a crucial role in protecting organisms from developing cancer (1). Compared with many normal tissues, aberrant cells with potentially malignant characteristics are highly sensitive to apoptotic signals and survive and further progress to malignancy only when they have acquired lesions, such as loss of p53, that prevent or impede cell death (2). Therefore, it is important to understand how cancer cells become resistant to apoptosis to pursue apoptosis-oriented cancer therapy. In fact, the most common antiapoptotic lesion that is detected in cancers is the inactivation of the p53 tumor suppressor pathway (2). It is well

known that activation of p53 (e.g., stress-induced stabilization) leads to either growth arrest or induction of apoptosis (3, 4). The question is how p53 contributes to the activation of cell death and what determines whether induction of p53 will trigger apoptosis.

It is generally accepted that p53 primarily acts as a transcription factor and induces apoptosis by transcriptionally modulating the expression of its proapoptotic target genes, although it also induces apoptosis in a transcription-independent fashion (2-5). It is also clear that most functional genes regulated by p53 contain classic p53-binding sites (p53BSs) in their promoter or intronic regions (6). In the last few decades, multiple proapoptotic genes that serve as p53 target genes have been identified, among which some encode death domain-containing proteins including the death receptors Fas and DR5, whereas others encode mitochondria-related proteins, such as Bax, Noxa, Puma, and p53AIP1, along with others having known or speculated roles in different steps of the apoptotic cascades such as PIGs, caspase-6, Bid, and Apaf-1 (2-7). These genes may contribute to p53-mediated cell death under certain conditions, in certain specific tissues, or in different cell types; however, no single target gene is an absolute mediator for p53-dependent apoptotic cell death (6, 7). In addition, there are increased studies showing that p53 also transactivates some target genes that are antiapoptotic, such as heparin-binding epidermal growth factor (*HB-EGF*) and *DcR1* (8-10). The roles of these antiapoptotic genes in regulating p53-dependent apoptosis are less clear, which make p53-mediated apoptosis even more complex.

The tumor necrosis factor-related apoptosis-inducing ligand (TRAIL; also called APO-2L) is a newly identified member of the tumor necrosis factor family with great therapeutic potential for cancer treatment, because it induces apoptosis in a wide variety of transformed cells but does not seem cytotoxic to normal cells *in vitro* and *in vivo* (11-13). TRAIL induces apoptosis by interacting with two death domain-containing receptors: DR4 (also called TRAIL receptor-1) and DR5 (also called TRAIL receptor 2 and Killer/DR5; refs. 11, 12). In addition, TRAIL can bind to two decoy receptors *DcR1* (also called TRAIL-R3) and *DcR2* (also called TRAIL-R4). The former does not contain a cytoplasmic death domain, whereas the latter has a truncated death domain. Therefore, both *DcR1* and *DcR2* can compete with DR4 and DR5 for TRAIL binding and negatively regulate TRAIL-induced apoptosis (11, 12). Interestingly, *DcR1* and *DcR2* as antiapoptotic genes are expressed in many normal tissues, but their expressions are frequently lost in various types of human cancer (11, 12).

It has been documented that all the four TRAIL receptors are regulated by p53 (14). Among them, DR5 is the first to be shown that its transcription is directly transactivated by p53 through an intronic sequence-specific p53BS (15, 16). Very recently, we and others have shown that p53 also directly regulates the expression of both DR4 and *DcR1* through the intronic p53BSs that are similar to the one identified in the *DR5* gene (10, 17). However, it is undetermined whether *DcR2* is also a p53 target gene.

Note: F.R. Khuri and S-Y. Sun are Georgia Cancer Coalition Distinguished Cancer Scholars.

Requests for reprints: Shi-Yong Sun, Winship Cancer Institute, Emory University School of Medicine, 1365-C Clifton Road Northeast, C3088, Atlanta, GA 30322. Phone: 404-778-2170; Fax: 404-778-5520; E-mail: shi-yong_sun@emoryhealthcare.org.
©2005 American Association for Cancer Research.
doi:10.1158/0008-5472.CAN-05-0939

It is known that the genes encoding DR4, DR5, DcR1, and DcR2 are highly homologous and map together to a tight cluster on human chromosome 8p21-22, suggesting that they arose from a common ancestral gene (6, 14). Because DR5, DR4, and DcR1 are directly regulated by p53 through similar p53BSs existing in their corresponding intronic region, we speculated that DcR2 might also be regulated by p53 through a similar intronic p53BS. In this study, we compared the sequences of first introns of these four genes and identified a similar p53BS in the first intron of the *DcR2* gene. Moreover, we have proven that it is a functional p53BS that mediates p53-dependent regulation of DcR2. In addition, we studied its roles in regulating TRAIL- and DNA-damaging agent-induced apoptosis.

Materials and Methods

Reagents. RPMI 1640 with glutamine and fetal bovine serum were obtained from Sigma Chemicals (St. Louis, MO). All restriction enzymes and T4 DNA ligase were purchased from New England Biolabs (Beverly, MA). PCR reagents were purchased from Invitrogen (Carlsbad, CA) or Eppendorf (Westbury, NY). iScript cDNA Synthesis Kit was purchased from Bio-Rad Laboratories (Hercules, CA). Etoposide (VP-16), doxorubicin, and other chemical reagents were purchased from Sigma Chemicals. Human recombinant TRAIL was purchased from PeproTech, Inc. (Rocky Hill, NJ).

Cell lines and cell culture. The human tumor cell lines H1299 (p53 null), H358 (p53 null), H460 (wild-type p53, wt p53), and MCF-7 (wt p53) were purchased from the American Type Culture Collection (Manassas, VA). HCT116 (wt p53) and HCT116 p53^{-/-} cell lines were kindly provided by Dr. B. Vogelstein (Johns Hopkins University Medical Institutions, Baltimore, MD). These cell lines were grown in monolayer culture in RPMI 1640 with glutamine or McCoy's 5A medium (HCT116) supplemented with 5% fetal bovine serum at 37°C in a humidified atmosphere consisting of 5% CO₂ and 95% air.

Western blot analysis. Preparation of whole cell protein lysates and the procedures for the Western blotting were described previously (18). Whole cell protein lysates (50 µg) were electrophoresed through 10% or 12% denaturing polyacrylamide slab gels and transferred to a PROTRAN pure nitrocellulose transfer membrane (Schleicher & Schuell BioScience, Inc., Keene, NH) by electroblotting. The blots were probed or reprobed with the antibodies and then antibody binding was detected using the SuperSignal West Pico Chemiluminescent Substrate (Pierce Biotechnology, Inc., Rockford, IL) according to the manufacturer's protocol. Mouse monoclonal anti-p53 (Ab-6) antibody and rabbit polyclonal anti-DcR2 antibody were purchased from EMD Bioscience, Inc. (La Jolla, CA) and Imgenex (San Diego, CA), respectively. Anti-V5 antibody was purchased from Invitrogen. Rabbit polyclonal anti-human glyceraldehyde-3-phosphate dehydrogenase antibody was purchased from Trevigen (Gaithersburg, MD).

Adenoviral infection. H1299 or H358 cells were infected with the adenovirus carrying wt p53 (Ad5-CMV-hp53) or empty vector (Ad-CMV) as described previously (17). Ad5-CMV-hp53 and Ad-CMV were purchased from Qbiogene, Inc. (Carlsbad, CA).

Chromatin immunoprecipitation assay. Chromatin immunoprecipitation assay was conducted using the chromatin immunoprecipitation assay kit purchased from Upstate Biotechnology (Lake Placid, NY) following the manufacturer's instruction and was described previously (17). The following specific primers for DcR1 and DcR2 were used to amplify p53BS from genomic DNA immunoprecipitated with specific p53 antibody in the chromatin immunoprecipitation assay: DcR1 sense, 5'-CTCGAGAAGTTCGTCGTCGTCATCGT-3'; DcR1 antisense, 5'-GAGCT-CACCCAGTTCTTCCCCGACT-3'; DcR2 sense, 5'-CTCGAGTTCTGTGTC-CGGTGAGTCT-3'; and DcR2 antisense, 5'-GAGCTCCCACTCTTCCCC-TGACTC-3'.

Construction of reporter plasmids. The 196- and 170-bp DNA fragments containing intronic p53BSs of DcR1 and DcR2, respectively, were amplified from H1299 genomic DNA with PCR amplification using the primers described in the above chromatin immunoprecipitation assay. These fragments were then subcloned into pGL3-Promoter luciferase vector

(pGL3-P-luc; Promega, Madison WI), which contains an SV40 promoter upstream of the luciferase gene, through *Xho*I and *Sac*I sites. The corresponding constructs were named pP-DcR1/p53BS-Luc and pP-DcR2/p53BS-Luc, respectively. In addition, a 1,443-bp DNA fragment spanning the DcR2 promoter, first exon, and partial p53BS-containing intron region and a 1,389-bp fragment spanning only the DcR2 promoter, first exon, and partial intron region without p53BS were amplified by PCR with the following primers: DcR2-BS-*Kpn*I sense, 5'-GGTACCCCTGCCATTGACCTTACTGCTT-3', DcR2-BS(+)-*Bgl*II antisense, 5'-AGATCTCACCCACTCTTCCCCT-GACTCC-3'; and DcR2-BS(-)-*Bgl*II antisense, 5'-AGATCTGCCCGCAGGC-GACCCGGGCCAAG-3'. These fragments were then cloned into a pGL3-basic vector, which has no promoter (Promega), using *Kpn*I and *Bgl*II restriction sites. These constructs were named pB-DcR2/p53BS(+)-luc and pB-DcR2/p53BS(-)-luc, respectively.

Construction of lentiviral expression vectors, virus preparation, and cell infection. DcR2 cDNA was amplified by standard reverse transcription-PCR (RT-PCR) from RNA extracted from normal human bronchial epithelia cells using the primers: sense, 5'-GACTAGTATGG-GACTTTGGGGACAAAGCGTC-3' and antisense, 5'-CGGGCCCTCTAGACTC-GAGCCCTTCAGGCAGGACGTAGCAGAGCCTG-3'. The DcR2 cDNA was then cloned into a pT-easy vector (Promega) following the manufacturer's protocol as pT-easy-DcR2. Both pLenti-DcR1 (a lentiviral vector harboring DcR1, which was constructed using the pLenti6/V5 Directional TOPO Cloning kit purchased from Invitrogen) and pT-easy-DcR2 were cut with *Spe*I and *Apa*I. The released fragment containing DcR2 cDNA was then cloned into the digested pLenti6/V5 vector and the resultant construct was named pLenti-DcR2. In this study, we used pLenti-Lac Z as a vector control, which was included in the pLenti6/V5 Directional TOPO Cloning kit.

Lentiviruses were produced using ViraPower Lentiviral Expression System (Invitrogen) according to the manufacturer's directions. The supernatants containing lentiviral particles were filtered with MILLEX-HV Syringe Driven Filter Unit (Millipore, Billerica, MA) and followed by a concentration using Amicon Ultra Centrifugal Filter Devices (Millipore). The viral titers were determined following manufacturer's manual. For infection, the viruses were added to the cells at the multiplicity of infection of 10 with 10 µg/mL polybrene. For transient expression, cells were infected and then selected in the presence of 50 µg/mL blasticidin, 24 hours after infection. After 8 days, the cells were subjected to the given experiments.

Transient transfection and reporter activity assay. The information about the plasmids used in this study, including a p53-luc reporter plasmid, a pCH110 plasmid encoding β-galactosidase, pCMV-p53, and pCMV-p53mt135 expression vectors, the purification and transfection of these plasmids, and luciferase activity assay, were described in detail previously (17).

Detection of DcR2 mRNA expression. DcR2 mRNA was detected using RT-PCR described as follows. Total cellular RNA was isolated from cells using TRIzol reagent (Invitrogen) as instructed by the manufacturer. cDNA was synthesized using iScript cDNA Synthesis Kit (Bio-Rad Laboratories) following the manufacturer's instructions. cDNA was then amplified by PCR using the following primers: DcR2 sense, 5'-CCTGTACCACGACCAGAGACAC-3'; DcR2 antisense, 5'-GAACTCGTGAAGGACATGAACG-3'; β-actin sense, 5'-GAACTACCTTCAACTCCATC-3'; and β-actin antisense, 5'-CTA-GAAGCATTTGCGGTGGACGATGGAGGGGCC-5'. The 25-µL amplification mixture contained 1 µL of cDNA, 0.5 µL of deoxynucleotide triphosphate (25 mmol/L each), 1 µL each of the sense and antisense primers (20 µmol/L each), 5 µL of TaqMaster PCR enhancer, 1 µL of Taq DNA polymerase (5 units/µL; Eppendorf), 2.5 µL 10× reaction buffer, and sterile H₂O. PCR was done for 26 cycles. After an initial step at 95°C for 3 minutes, each cycle consisted of 45 seconds of denaturation at 94°C, 45 seconds of annealing at 58°C, and 1 minute of extension at 72°C. This was followed by an additional extension step at 72°C for 7 minutes. The housekeeping gene β-actin was also amplified as an internal reference. PCR products were resolved by electrophoresis on a 1.5% agarose gel, stained, and directly visualized under UV illumination.

Silencing of DcR2 expression using small interfering RNA. Stealth DcR2 small interfering RNA (siRNA) that targets sequence of 5'-CCAA-GATCCTTAAGTTCGTCGCTT-3' and Stealth control siRNA that targets

sequence of 5'-CCTACCAGGGAATTTAAGAGTGTAT-3' were synthesized by Invitrogen. The transfection of siRNA was conducted in a 24-well plate using LipofectAMINE 2000 (Invitrogen) following the manufacturer's instructions. We transfected the same cells twice with the same siRNA with a 48-hour interval in between the two transfections as described previously (19). Twenty-four hours after the second transfection, cells were replated in fresh medium and treated on the second day with chemotherapeutic agents as indicated. The gene-silencing effect was evaluated by RT-PCR and apoptosis was measured by a Cell Death Detection ELISA^{Plus} kit as described below.

Cell survival assay. Cells were seeded in 96-well cell culture plates and treated on the second day with the indicated agents. At the end of treatment, cell number was estimated by the sulforhodamine B assay as previously described (20).

Detection of apoptosis. Apoptosis was evaluated either by Annexin V staining using Annexin V-PE apoptosis detection kit purchased from BD Bioscience (San Jose, CA), or by a Cell Death Detection ELISA^{Plus} kit purchased from Roche Molecular Biochemicals (Indianapolis, IN), following the manufacturer's instructions.

Statistical analysis. Cell survival and apoptosis (i.e., DNA fragmentation) between two groups were analyzed with two-sided unpaired Student's *t* tests by use of Graphpad InStat 3 software (GraphPad Software, Inc., San Diego, CA). In all analyses, results were considered to be statistically significant at *P* < 0.05.

Results

Overexpression of p53 increases DcR2 expression in p53-null cancer cells. Up-regulation of DcR2 expression by p53 has been shown previously by Meng et al. (21). In this study, we also examined the effect of p53 overexpression via adenoviral infection

on the expression of DcR2 in p53-null lung cancer cell lines. As shown in Fig. 1A, Ad-p53 infection resulted in increased expression of DcR2 in both H358 and H1299 cell lines evaluated by Western blot analysis. Thus, this result confirms the previous finding that DcR2 is indeed a p53-regulated gene (21).

Sequence-based identification of a putative p53BS in the first intron of the DcR2 gene. By comparing the first intron sequences of the four TRAIL receptor genes, we identified a similar p53BS (DcR2-p53BS) in the first intron of the DcR2 gene. This p53BS is almost identical to the ones reported within the first introns of DR4, DR5, and DcR1 genes (refs. 10, 16, 17; Fig. 1B). DcR2-p53BS shares 85% homology with the p53 consensus DNA-binding sequence (22). Among the p53BSs of the four TRAIL receptors, their sequences are at least 80% identical (Fig. 1B). Moreover, DcR2-p53BS and other receptor p53BSs are close to the boundary of first exon/intron and are only 107 to 109 bp away from the boundary (Fig. 1B), indicating that they are very close to their promoter regulatory regions. Considering the identical locations and similar sequences between DcR2-p53BS and other receptor p53BSs, we speculate that the DcR2-p53BS is very likely to be functional and to mediate transcriptional regulation of the DcR2 gene expression by p53.

Detection of DcR2-p53BS bound to p53 in intact cells using a chromatin immunoprecipitation assay. To determine whether p53 actually binds to DcR2-p53BS in cells on p53 activation, we did the chromatin immunoprecipitation assay to detect formation of DcR2-p53BS-binding complex with p53 in both H358 and H1299 p53-null cell lines infected with Ad-CMV-hp53. As a control, we also

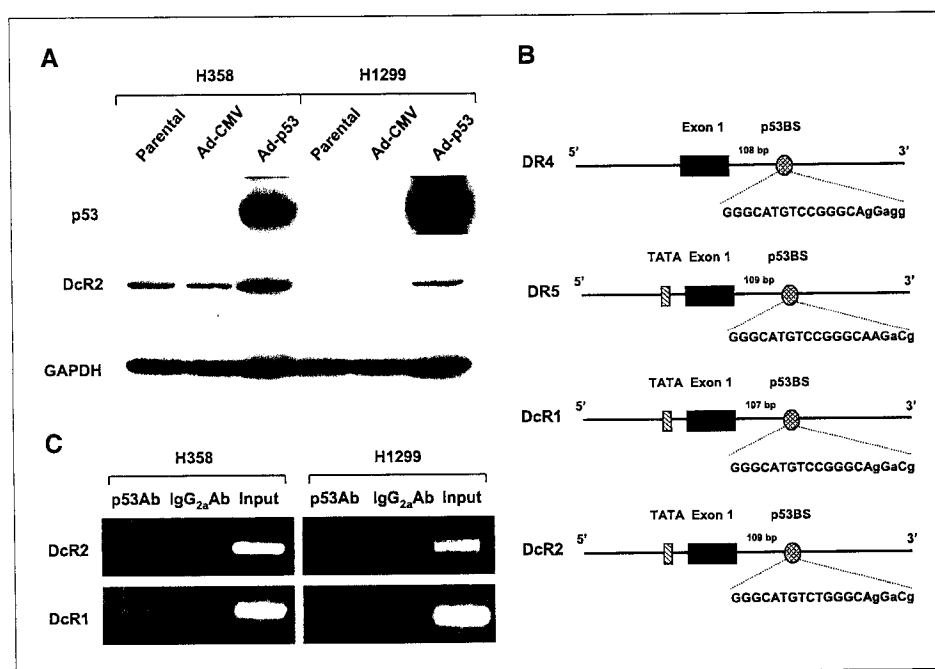


Figure 1. Up-regulation of DcR2 expression by p53 overexpression in p53-null cancer cells (A), identification of the putative DcR2-p53BS (B), and detection of DcR2-p53BS bound to p53 in intact cells upon p53 activation (C). A, H1299 or H358 cells were infected on the second day after seeding with adenovirus carrying an empty vector (Ad-CMV) or wt p53 gene (Ad-p53). After 24 hours, cells were harvested for preparation of whole cell protein lysates. Western blot analysis was done to detect the expression of p53, DcR2, and glyceraldehyde-3-phosphate dehydrogenase (GAPDH) using antibodies against them. B, DcR2-p53BS is 85% identical to the classic p53BS that is defined as two copies of the 10-bp motif 5'-PuPuPuC(A/T)(T/A)GPYPyPy-3' separated by 0 to 13 bp (22), where Pu represents purine and Py represents pyrimidine. In addition, DcR2-p53BS shares ≥90% sequence homology with the other three TRAIL receptors. C, H358 and H1299 p53-null cell lines were infected with Ad5-CMV-hp53 for 24 hours and subjected to chromatin immunoprecipitation assay as described in Materials and Methods. DcR1-p53BS here was detected as a known sequence bound to p53 when p53 is activated. The amplified DNA fragments for DcR1 and DcR2 by PCR were 196 and 170 bp, respectively. p53Ab, p53 antibody; IgG_{2a}Ab, isotype antibody.

detected DcR1-p53BS bound to p53. As shown in Fig. 1C, we detected DNA fragments containing DcR2-p53BS and DcR1-p53BS, respectively, from genomic DNA precipitated with p53-specific antibody but not from that pulled down with a control IgG2a isotype antibody in either cell line. This result clearly indicates that p53 protein binds to DcR2-p53BS as it does to DcR1-p53BS in intact cells upon p53 activation, indicating that DcR2-p53BS is a functional response element.

Reporter construct carrying DcR2-p53BS exhibits increased transcriptional activity in response to p53 overexpression or treatment with DNA-damaging agents. To examine whether DcR2-p53BS is functional in mediating p53-dependent up-regulation of the *DcR2* gene, we amplified ~170- and 196-bp intronic fragments carrying DcR2-p53BS and DcR1-p53BS, respectively, and cloned each of fragment into a pGL3-promoter luciferase vector upstream of minimal SV40 promoter (Fig. 2A). In this study, we used DcR1-p53BS, which is more related to DcR2 and known to be functional p53BS (10), as a positive control for comparison. When the individual reporter construct was transiently cotransfected with empty pCMV, pCMV-p53, or pCMV-p53mt135 vector into H1299 p53-null cells, we found that transfection of pCMV-p53 but not pCMV or pCMV-p53mt135 increased the luciferase activity of the reporter plasmid carrying either DcR2-p53BS or DcR1-p53BS (Fig. 2B). The expression of p53 and p53mt135 after transient transfection in H1299 cells has been shown in our previous study (17). Therefore, our data indicate that overexpression of p53 enhances transcriptional activity of the reporter plasmid carrying

either DcR2-p53BS or DcR1-p53BS. Similar results were also observed when we cotransfected these plasmids into H358 p53-null cells (data not shown). Moreover, we examined the effects of activation of endogenous p53 on transactivation of these reporter vectors by treating wt p53-containing cancer cells with DNA-damaging agents. In MCF-7 cells, both VP-16 and doxorubicin that are known to increase p53 levels (17) failed to increase luciferase activity of empty pGL3-P-luc lacking any p53BS. However, they increased transcriptional activities by >2-fold (VP-16) or 3-fold (doxorubicin) of the pGL3-P-luc reporter vector carrying DcR1-p53BS or DcR2-p53BS (Fig. 2C). We noted that the reporter vector carrying DcR2-p53BS exhibited a greater increase of luciferase activity than the reporter plasmid carrying DcR1-p53BS in response to activation of endogenous p53 induced by either VP-16 or doxorubicin, although the increase of luciferase activity was much greater in the reporter vector carrying DcR1-p53BS than in the reporter plasmid harboring DcR2-p53BS when stimulated with overexpression of an exogenous p53 (Fig. 2B and C). Collectively, these results suggest that DcR2-p53BS, like DcR1-p53BS, is functional to mediate p53-induced gene transactivation.

The intronic DcR2-p53BS is required for driving p53-mediated transactivation of DcR2 promoter. The aforementioned results clearly indicate that p53 protein binds to the intronic DcR2-p53BS in cells and confers p53 responsiveness when located upstream of a promoter (i.e., SV40) in a promoter-containing reporter vector (i.e., pGL3-P-luc). We next wanted to know whether DcR2-p53BS could also mediate p53-dependent transcriptional

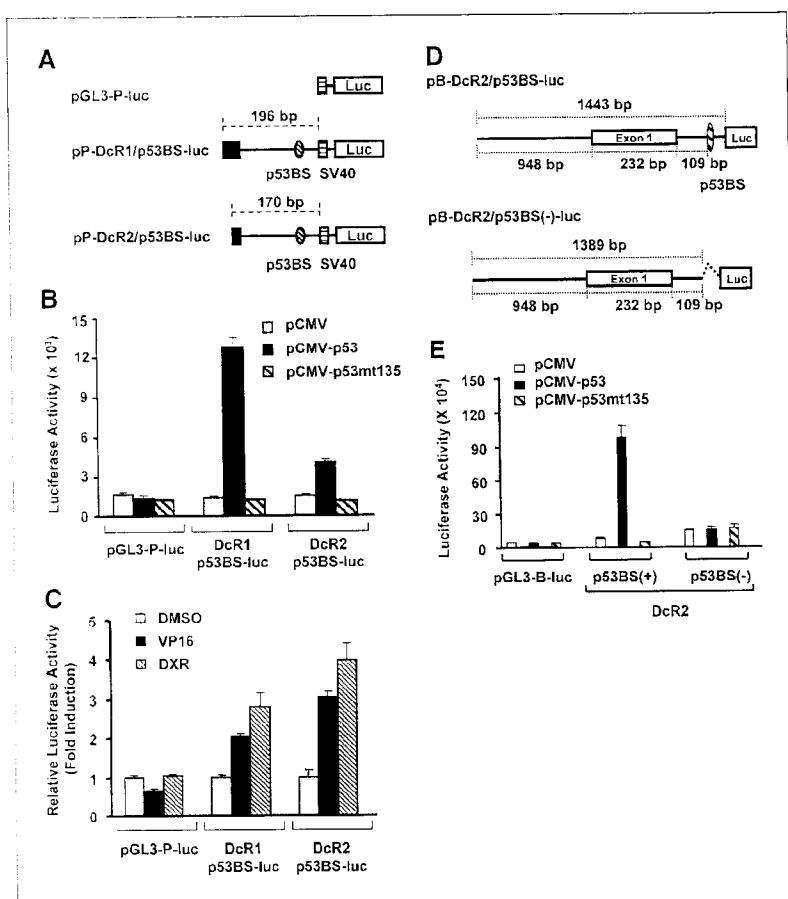
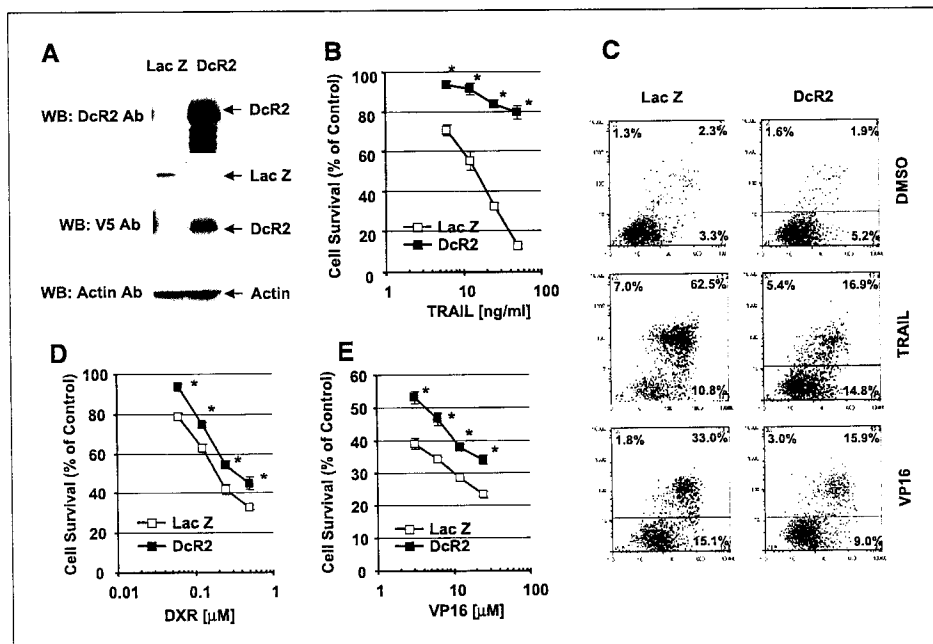


Figure 2. DcR2-p53BS is required for p53-dependent transactivation of DcR2 promoter. **A**, diagram illustrating cloning of DNA fragments containing DcR1-p53BS and DcR2-p53BS, respectively, into the pGL3-P-luc reporter vector. The DNA fragments containing DcR1-p53BS and DcR2-p53BS, respectively, were PCR amplified and cloned into pGL3-P-luc reporter vector upstream of the SV40 promoter. Black boxes, partial exon 1 sequences. **B**, comparison of the activities of the reporter constructs (**A**) in response to p53 overexpression. The indicated reporter vector together with pCMV, pCMV-p53, or pCMV-p53mt135 and pCH110 β -galactosidase expression plasmids was cotransfected into H1299 cells using the FuGene 6 transfection reagent. After 24 hours, cells were harvested and subjected to a luciferase activity assay. **C**, comparison of the activities of the reporter constructs (**A**) in response to treatment with DNA-damaging agents. MCF-7 cells transfected with the indicated reporter vector and β -galactosidase expression plasmid using the FuGene 6 transfection reagent for 16 hours were treated with 10 μ M VP-16 or 1 μ M doxorubicin (DXR). After 8 hours, the cells were harvested and subjected to the luciferase activity assay. Column, means of triplicate treatments; bars, \pm SD. **D**, diagram illustrating generation of a reporter vector that harbors a piece of natural DcR2 genomic sequence with DcR2 promoter region, exon 1, and partial intron 1 containing the DcR2-p53BS (pB-DcR2/p53BS-luc) and a corresponding construct lacking DcR2-p53BS [pB-DcR2/p53BS(-)-luc]. These DcR2 genomic fragments were PCR amplified and cloned into a pGL3 basic luciferase vector as described in Materials and Methods. **E**, comparison of the activities of the reporter constructs (**D**) in response to p53 overexpression. The indicated reporter vector together with pCMV, pCMV-p53, or pCMV-p53mt135 and pCH110 β -galactosidase expression plasmids were cotransfected into H1299 cells using the FuGene 6 transfection reagent. After 24 hours, cells were harvested and subjected to luciferase activity assay. Columns, means of triplicate treatments; bars, \pm SD.

Figure 3. Lentivirus-mediated expression of exogenous DcR2 (A) and its effects on decrease of cell survival induced by TRAIL (B), doxorubicin (DXR, D), and VP-16 (E), respectively, and on induction of apoptosis by TRAIL and VP-16, respectively (C). H460 cells were infected with 10 multiplicity of infection of lentiviruses harboring Lac Z and DcR2, respectively. Twenty-four hours later, the cells were subjected to blasticidin selection (50 μ g/mL). After 8 days, the cells were then subjected to the given experiments. The expression of DcR2 was detected by Western blot analysis using DcR2 and V5 antibody, respectively (A). Cell survival was estimated using the sulforhodamine B assay after the cells were exposed to the indicated concentrations of TRAIL (B), doxorubicin (D), and VP-16 (E), respectively, for 24 hours. Apoptosis was measured using Annexin V staining after the cells were treated with 20 ng/mL TRAIL or 25 μ M VP-16 for 24 hours (C). Points, means of four replicates; bars, \pm SD. *, $P < 0.001$, compared with each corresponding control treatment with two-sided unpaired Student's t tests.



activity of its own gene promoter when located at a natural position relative to the promoter in its genomic locus. To do this, we amplified a 1,443-bp DcR2 genomic DNA fragment consisting of the 948-bp promoter region, a 232-bp exon 1, and a 263-bp fragment of the first intron harboring the DcR2-p53BS and an identical 1,389-bp DcR2 genomic DNA fragment lacking only 54 bp with the DcR2-p53BS, respectively. By cloning these fragments into the pGL3-B-luc vector, we generated luciferase reporter constructs with and without DcR2-p53BS. These constructs were named pB-DcR2/p53BS(+)-luc and pB-DR4/p53BS(-)-luc, respectively (Fig. 2D). When each of the aforementioned reporter plasmids together with the expression vector carrying no p53, a wt p53, or a mutant p53 gene were cotransfected into H1299 cells, we found that the wt p53 but not mutant p53 increased transcriptional activity of pB-DcR2/p53BS(+) by >13-fold. In contrast, p53 completely lost its ability to increase transcriptional activity of the reporter vector with deleted DcR2-p53BS (pB-DcR2/p53BS(-)-luc; Fig. 2E). This result clearly indicates that the intronic DcR2-p53BS is essential for p53-mediated transactivation of the *DcR2* gene.

Overexpression of DcR2 confers resistance to chemotherapeutic agents. Other than its inhibitory function in negatively regulating TRAIL-induced apoptosis, the role of DcR2 in drug-induced apoptosis is largely unknown. Therefore, we examined the effect of DcR2 overexpression on apoptosis induction by chemotherapeutic agents in human cancer cells. Infection of H460 lung cancer cells with lentiviruses carrying the *DcR2* gene resulted in successful DcR2 expression evaluated by Western blot analysis using both V5 and DcR2 antibodies (Fig. 3A). Overexpression of DcR2 has been shown to inhibit TRAIL-induced apoptosis (21, 23–25). To assure the normal function of DcR2 expression in our cell system, we first determined whether cells infected with DcR2 lentiviruses were resistant to TRAIL treatment. Indeed, TRAIL effectively decreased the survival of cells infected with control lentiviruses carrying the *Lac Z* gene in a dose-dependent manner. In contrast, cells infected with lentiviruses harboring DcR2 were insensitive to TRAIL treatment. For example, TRAIL, at 50 ng/mL, rapidly

decreased cell survival by >85% in cells infected with Lac Z lentiviruses, but only by 20% in cells infected with DcR2 lentiviruses (Fig. 3B). Moreover, TRAIL treatment induced 73% cells infected with Lac Z lentiviruses undergoing apoptosis, whereas it caused only 32% cells infected with DcR2 lentiviruses to die of apoptosis when evaluated using Annexin V staining (Fig. 3C). These results indicate that DcR2 expression in our system indeed confers cell resistance to TRAIL-induced apoptosis and thereby is functionally active.

Following these experiments, we examined the effects of DcR2 overexpression on cell responses to the chemotherapeutic agents doxorubicin and VP-16. Compared with control Lac Z lentivirus-infected cells, cells expressing DcR2 were significantly less sensitive to either doxorubicin (Fig. 3D; $P < 0.001$) or VP-16 (Fig. 3E; $P < 0.001$) by measuring overall cell survival. Moreover, following VP-16 treatment, we detected about 48% apoptotic cells from cells infected with control Lac Z lentiviruses, but only about 25% apoptotic cells from cells infected with DcR2 lentiviruses (Fig. 3C). Collectively, these results indicate that the enforced DcR2 expression reduces cell sensitivity to chemotherapeutic agents and thus affects chemosensitivity.

Silencing of DcR2 expression enhances chemotherapeutic agent-induced apoptosis. To further show the relationship between DcR2 expression and chemosensitivity, we determined whether manipulation of endogenous levels of DcR2 affected cell responses to chemotherapeutic agents. Meng et al. (21) reported that the chemotherapeutic agent doxorubicin induced p53-dependent expression of DcR2 in human cancer cells. We found that both doxorubicin and VP-16 increased DcR2 expression in HCT116 (p53^{+/+}) cells but not in p53 knockout HCT116 (p53^{-/-}) cells, although they had higher basal levels of DcR2 than did HCT116 (p53^{+/+}; Fig. 4A). Thus, our results confirmed p53-dependent up-regulation of endogenous DcR2 expression by chemotherapeutic agents. Transfection of the DcR2 siRNA but not the control siRNA into HCT116 cells substantially decreased basal levels of DcR2 expression and prevented DcR2 up-regulation

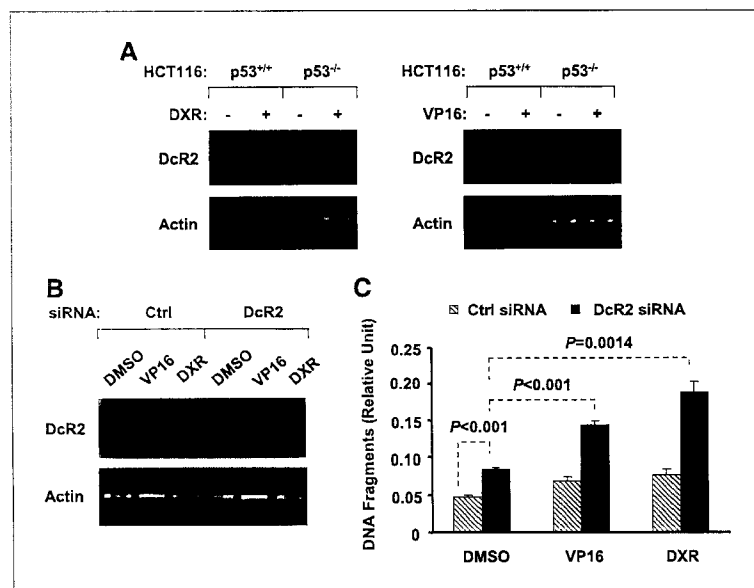


Figure 4. p53-dependent modulation of endogenous DcR2 expression by chemotherapeutic agents (A) and the effects of silencing DcR2 expression on chemotherapeutic agent-induced apoptosis (B and C). A, the indicated cell lines were treated with 50 μ M/L VP-16 or 0.5 μ M/L doxorubicin (DDXR) for 24 hours and subjected to RNA extraction. DcR2 mRNA levels were detected using RT-PCR as described in Materials and Methods. B and C, HCT116 cells were transfected twice with control (Ctrl) or DcR2 siRNA in a 48-hour interval as described in Materials and Methods. Forty hours later after the second transfection, cells were treated with 50 μ M/L VP-16 or 1 μ M/L doxorubicin (DDXR). After 24 hours, the cells were subjected to RNA extraction and subsequent detection of DcR2 expression by RT-PCR (B). In addition, the cells were subjected to estimation of DNA fragmentation using the Cell Death Detection ELISA kit (C). Columns, mean of triplicate treatments; bars, \pm SD. The statistical differences between the two treatments were analyzed by two-sided unpaired Student's *t* tests.

by chemotherapeutic agents (Fig. 4B). In the control siRNA-transfected HCT116 cells, the amounts of DNA fragments were only slightly increased upon treatment with VP-16 or doxorubicin. In contrast, in the DcR2 siRNA-transfected HCT116 cells, the basal levels of DNA fragmentation were significantly increased ($P < 0.001$). When treated with VP-16 or doxorubicin, the amounts of DNA fragments were further significantly increased ($P < 0.001$; Fig. 4C). Thus, these results indicate that prevention or blockage of endogenous DcR2 up-regulation sensitizes cells to chemotherapeutic agent-induced apoptosis, furthering the notion that DcR2 regulates chemosensitivity.

Discussion

p53-dependent up-regulation of DcR2 expression has been shown previously (21). However, the mechanism underlying p53-dependent regulation of DcR2 is unknown. In the present study, we identified a putative p53BS in the first intron of the *DcR2* gene. This p53BS is almost identical to those found in the first introns of DR5, DR4, and DcR1 in terms of their sequences and locations. p53 overexpression or treatment with DNA-damaging agents enhanced transcriptional activity of the luciferase reporter construct carrying the DcR2-p53BS upstream of the SV40 promoter, indicating that this intronic p53BS is active for p53-dependent transactivation of the *DcR2* gene. Furthermore, the reporter construct carrying the fragment consisting of the endogenous promoter region, exon 1, and partial first intron region with DcR2-p53BS exhibited increased transcriptional activity upon p53 activation. However, its corresponding construct lacking DcR2-p53BS did not show any response to the same stimulus. This result further indicates that the DcR2-p53BS is essential for p53-mediated transactivation of the *DcR2* gene. Using a chromatin immunoprecipitation assay, we were able to detect the DNA fragment containing DcR2-p53BS from DNA/protein complex precipitated only with p53-specific antibody in Ad-p53-infected p53-null cell lines, indicating that the DcR2-p53BS binds to p53 in intact cells upon p53 activation. Taken together, we conclude that p53 directly regulates transcription of the *DcR2* gene via an intronic p53BS.

It has been noted that the genes encoding DR4, DR5, DcR1, and DcR2 are highly homologous and map together to a tight cluster on human chromosome 8p21-22, suggesting that they arose from a common ancestral gene (6, 14). The current study together with others (10, 16, 17) have shown that the four TRAIL receptors are all p53 target genes and their expression is regulated by p53 through similar intronic p53BSs. By comparing the sequences and locations of these p53BSs, we found that they share high homology ($\geq 90\%$) and locate at almost the same positions that are only 107 bp (DcR1), 108 bp (DR4), or 109 bp (DR5 and DcR2) away from the exon 1 and intron 1 boundaries (Fig. 1). Thus, it seems that these p53BSs are well conserved during evolution.

It is clear that the four TRAIL receptors are critical for regulating TRAIL-induced apoptosis (11–13). Indeed, overexpression of DcR2 in our cell system protected cells from TRAIL-induced apoptosis as shown previously (21, 23–25). However, the biological significance of DcR2 as well as other TRAIL receptors as p53 target genes in regulation of p53-dependent apoptosis remains unclear. The only study dealing with this issue by Meng et al. (21) showed that overexpression of DcR2 delays p53-induced apoptosis in human colon cancer cells. In our current study, we found that overexpression of DcR2 in a human lung cancer cell line with wt p53 partially protected cells from induction of apoptosis by some chemotherapeutic agents. Although we used lentivirus to deliver DcR2 expression in our cell system, the infection or expression efficiency in this particular cell line was still $<50\%$. The brief selection using blasticidin (8 days) after infection theoretically eliminates most cells that do not express DcR2, but there might be still significant portions of surviving cells that did not express DcR2 well. Therefore, the protection of DcR2 on chemotherapeutic agent-induced apoptosis may be underestimated. Nevertheless, our current results suggest that DcR2 expression levels may affect chemosensitivity. If high levels of DcR2 expression confer cell resistance to chemotherapeutic agents, down-regulation of DcR2 expression, or prevention of DcR2 up-regulation during chemotherapy should sensitize cells to chemotherapy. In this study, we found that prevention of DcR2 up-regulation using

siRNA-mediated gene silencing indeed enhanced chemotherapeutic agent-induced apoptosis. Thus, this result further supports the notion that DcR2 regulates chemosensitivity.

In contrast to DR4 and DR5 that are expressed widely in both normal and malignant cells, DcR2 as well as DcR1 are expressed preferentially in many normal tissues (11), and their expression is often silenced or down-regulated due to promoter hypermethylation in multiple cancer types, including neuroblastoma, malignant mesothelioma, breast cancers, and lung cancers (26, 27), although they are generally considered as antiapoptotic genes (11–13). Currently, it is unknown why DcR1 and DcR2 but not DR4 and DR5 are frequently down-regulated in cancer cells. This raises a relevant question as to the normal function and importance of DcR2 as well as DcR1 in homeostasis and carcinogenesis. It seems that this needs to be further investigated in the future. Nevertheless, the down-regulation of DcR1 and DcR2 expression in cancer cells may present an opportunity for TRAIL-based cancer therapy.

In summary, this report provides compelling evidence showing that *DcR2* is a p53 target gene, which is regulated by p53 through an intronic p53BS. In addition, we also suggest that DcR2 regulates chemosensitivity. Currently, the biological significance of DcR2 in p53-regulated apoptosis and carcinogenesis has not been elucidated.

Acknowledgments

Received 3/21/2005; revised 7/14/2005; accepted 8/16/2005.

Grant support: Winship Cancer Institute faculty start-up research fund (S.-Y. Sun), Georgia Cancer Coalition Distinguished Cancer Scholar award (S.-Y. Sun), and Department of Defense VITAL grant W81XWH-04-1-0142 (S.-Y. Sun for Project 4).

The costs of publication of this article were defrayed in part by the payment of page charges. This article must therefore be hereby marked *advertisement* in accordance with 18 U.S.C. Section 1734 solely to indicate this fact.

We thank Dr. B. Vogelstein for providing us with HCT116 and HCT115 p53-null cell lines.

References

- Levine AJ. p53, the cellular gatekeeper for growth and division. *Cell* 1997;88:323–31.
- Vousden KH, Lu X. Live or let die: the cell's response to p53. *Nat Rev Cancer* 2002;2:594–604.
- Oren M. Decision making by p53: life, death and cancer. *Cell Death Differ* 2003;10:431–42.
- Vogelstein B, Lane D, Levine AJ. Surfing the p53 network. *Nature* 2000;408:307–10.
- Manfredi JJ. p53 and apoptosis: it's not just in the nucleus anymore. *Mol Cell* 2003;11:552–4.
- El-Deiry WS. Insights into cancer therapeutic design based on p53 and TRAIL receptor signaling. *Cell Death Differ* 2001;8:1066–75.
- Benchimol S. p53-dependent pathways of apoptosis. *Cell Death Differ* 2001;8:1049–51.
- Fang L, Li G, Liu G, Lee SW, Aaronson SA. p53 induction of heparin-binding EGF-like growth factor counteracts p53 growth suppression through activation of MAPK and PI3K/Akt signaling cascades. *EMBO J* 2001;20:1931–9.
- Sheikh MS, Huang Y, Fernandez-Salas EA, et al. The antiapoptotic decoy receptor TRID/TRAIL-R3 is a p53-regulated DNA damage-inducible gene that is overexpressed in primary tumors of the gastrointestinal tract. *Oncogene* 1999;18:4153–9.
- Ruiz De Almodovar C, Ruiz-Ruiz C, Rodriguez A, Ortiz-Ferron G, Redondo JM, Lopez-Rivas A. TRAIL decoy receptor TRAIL-R3 is upregulated by p53 in breast tumor cells through a mechanism involving an intronic p53 binding site. *J Biol Chem* 2004;279:4093–101.
- Ashkenazi A, Dixit VM. Death receptors: signaling and modulation. *Science* 1998;281:1305–8.
- Kelley SK, Ashkenazi A. Targeting death receptors in cancer with Apo2L/TRAIL. *Curr Opin Pharmacol* 2004;4:333–9.
- Bouralexis S, Findlay DM, Evdokiou A. Death to the bad guys: targeting cancer via Apo2L/TRAIL. *Apoptosis* 2005;10:35–51.
- Sheikh MS, Fornace AJ, Jr. Death and decoy receptors and p53-mediated apoptosis. *Leukemia* 2000;14:1509–13.
- Wu GS, Burns TF, McDonald ER III, et al. KILLER/DR5 is a DNA damage-inducible p53-regulated death receptor gene. *Nat Genet* 1997;17:141–3.
- Takimoto R, El-Deiry WS. Wild-type p53 transactivates the KILLER/DR5 gene through an intronic sequence-specific DNA-binding site. *Oncogene* 2000;19:1735–43.
- Liu X, Yue P, Khuri FR, Sun SY. p53 upregulates death receptor 4 expression through an intronic p53 binding site. *Cancer Res* 2004;64:5078–83.
- Sun SY, Yue P, Wu GS, et al. Mechanisms of apoptosis induced by the synthetic retinoid CD437 in human non-small cell lung carcinoma cells. *Oncogene* 1999;18:2357–65.
- Liu X, Yue P, Zhou Z, Khuri FR, Sun SY. Death receptor regulation and celecoxib-induced apoptosis in human lung cancer cells. *J Natl Cancer Inst* 2004;96:1769–80.
- Sun SY, Yue P, Dawson MI, et al. Differential effects of synthetic nuclear retinoid receptor-selective retinoids on the growth of human non-small cell lung carcinoma cells. *Cancer Res* 1997;57:4931–9.
- Meng RD, McDonald ER III, Sheikh MS, Fornace AJ, Jr., El-Deiry WS. The TRAIL decoy receptor TRUND (DcR2, TRAIL-R4) is induced by adenovirus-p53 overexpression and can delay TRAIL-, p53-, and KILLER/DR5-dependent colon cancer apoptosis. *Mol Ther* 2000;1:130–44.
- El-Deiry WS, Kern SE, Pietenpol JA, Kinzler KW, Vogelstein B. Definition of a consensus binding site for p53. *Nat Genet* 1992;1:45–9.
- Degli-Esposti MA, Dougall WC, Smolak PJ, Waugh JY, Smith CA, Goodwin RG. The novel receptor TRAIL-R4 induces NF- κ B and protects against TRAIL-mediated apoptosis, yet retains an incomplete death domain. *Immunity* 1997;7:813–20.
- Marsters SA, Sheridan JP, Pitti RM, et al. A novel receptor for Apo2L/TRAIL contains a truncated death domain. *Curr Biol* 1997;7:1003–6.
- Pan G, Ni J, Yu G, Wei YF, Dixit VM. TRUND, a new member of the TRAIL receptor family that antagonizes TRAIL signalling. *FEBS Lett* 1998;424:41–5.
- van Noesel MM, van Bezouw S, Salomons GS, et al. Tumor-specific down-regulation of the tumor necrosis factor-related apoptosis-inducing ligand decoy receptors DcR1 and DcR2 is associated with dense promoter hypermethylation. *Cancer Res* 2002;62:2157–61.
- Shivapurkar N, Toyooka S, Toyooka KO, et al. Aberrant methylation of trail decoy receptor genes is frequent in multiple tumor types. *Int J Cancer* 2004;109:786–92.

Multiple oncogenic changes (*K-RAS*^{V12}, p53 knockdown, *mutant EGFRs*, *p16* bypass, telomerase) are not sufficient to confer a full malignant phenotype on human bronchial epithelial cells

Mitsuo Sato¹, Melville B. Vaughan⁴, Luc Girard¹, Michael Peyton¹, Woonchang Lee¹, David S. Shames¹, Ruben D. Ramirez^{1,2,6}, Noriaki Sunaga¹, Adi F. Gazdar^{1,3}, Jerry W. Shay⁴ and John D. Minna^{1,2,5}

¹Hamon Center for Therapeutic Oncology Research and Departments of ²Internal Medicine, ³Pathology, ⁴Cell Biology, and ⁵Pharmacology, The University of Texas Southwestern Medical Center, Dallas, Texas 75390-8593, USA.

⁶Dallas Veterans Administration Medical Center, 4500 South Lancaster Road, Mail code 151, Dallas, Texas 75216, USA.

Correspondence: John D. Minna; Hamon Center for Therapeutic Oncology Research NB8.206, The University of Texas Southwestern Medical Center at Dallas, 6000 Harry Hines Blvd., Dallas, TX 75390-8593, USA.

E-mail: John.Minna@UTsouthwestern.edu

Oncogenic manipulation of immortalized bronchial epithelial cells

Tel: 214-648-4900, Fax: 214-648-4940

Running title: Oncogenic manipulation of immortalized bronchial epithelial cells

Key words: p53, K-RAS, immortalized human bronchial epithelial cell, RNA interference, tumorigenicity and, lung cancer

Abstract

We evaluated the contribution of three genetic alterations (p53 knockdown, *mutant K-RAS^{V12}*, and *mutant EGFR*) to lung tumorigenesis using human bronchial epithelial cells (HBECs) already immortalized with telomerase and cdk4 mediated p16 bypass. RNAi mediated p53 knockdown or ectopic expression of oncogenic *K-RAS^{V12}* resulted in enhanced anchorage-independent growth and increased saturation density of HBECs in confluent cultures. The combination of p53 knockdown and *K-RAS^{V12}* further enhanced the tumorigenic phenotype with increased growth in soft agar and an invasive phenotype in three-dimensional organotypic cultures but failed to cause the HBECs cells to form tumors in nude mice. Growth of HBECs was highly dependent on epidermal growth factor (EGF) and was completely inhibited by epidermal growth factor receptor (EGFR) directed tyrosine kinase inhibitors (TKIs) which induced G1 arrest. Introduction of two common types of EGFR mutations (E746-A750 del and L858R) progressed HBECs toward malignancy as measured by anchorage-independent growth, including EGF independent growth but failed to induce tumor formation. Mutant EGFRs were associated with higher levels of p-Akt, p-STAT3 (but not p-ERK1/2), and increased expression of *DUSP6/MKP-3* phosphatase (an inhibitor of p-ERK1/2), compared to introduction of wild-type EGFR. These results indicate that: 1) the HBEC model system is a powerful new approach to assess the contribution of individual and combinations of genetic alterations to lung cancer pathogenesis ; 2) a combination of four genetic alterations including hTERT overexpression, bypass of p16/RB and p53 pathways, and mutant *K-RAS^{V12}* or mutant EGFR is still not sufficient for human bronchial epithelial cells to completely transform to cancer, and ; 3) EGFR tyrosine kinase inhibitors inhibit the growth of oncogenic manipulation induced preneoplastic HBEC cells , suggesting their potential for chemoprevention.

INTRODUCTION

Human lung cancer develops as a multi-step process, usually occurring because of years of smoking related tobacco exposure which results in specific proto-oncogene and tumor suppressor gene alterations in lung epithelial cells (1). In fact, the majority of lung cancers have many such changes (1). Identifying the minimal and most crucial set of changes required for lung tumorigenesis and the impact each of these alterations has on the carcinogenic process is vital to develop the best targets for early detection and therapeutic intervention. To address this issue, an *in vitro* model system using human bronchial epithelial cells (HBECs) was recently developed to assess the contribution of specific genetic alterations to lung cancer progression (2, 3). We accomplished this by overexpressing Cdk4 to abrogate the p16/Rb cell cycle checkpoint pathway and ectopic expression of human telomerase reverse transcriptase (hTERT) to bypass replicative senescence allowing us to develop a series of immortalized human bronchial epithelial cell lines (HBECs) without using viral oncoproteins. These HBECs have epithelial morphology, express epithelial markers, are able to differentiate into mature airway cells in organotypic cultures, have minimal genetic changes and do not exhibit a transformed phenotype (2, 3). We have HBEC lines that are derived from patients with a variety of smoking histories, with and without lung cancer, which also allows us to explore inter-individual variation in the tumor formation process.

Two of the genetic alterations that occur almost universally in human lung cancer, inactivation of the p16/pRb pathway and expression of hTERT, were used for establishment of immortalized HBECs and so are already present. The pRb pathway (p16^{INK4a}-cyclinD1-CDK4-pRB pathway) is a key cell-cycle regulator at the G1/S phase transition. Absence of expression or structural abnormality of Rb protein is seen in more than 90% of small cell lung cancers

(SCLCs) and loss of p16 protein expression by several mechanisms including methylation or homozygous deletion of *p16^{INK4a}* is seen in >70% of non-small cell lung cancers (NSCLCs), both of which result in the inactivation of this pathway (1, 4, 5). Expression of high levels of telomerase is almost universal in lung cancer (1). hTERT is the key determinant of the enzymatic activity of human telomerase and its transcriptional control is a major contributor to the regulation of telomerase activity in many types of human cells (6-10). Because of the central role of the pRb pathway and telomerase expression we initially evaluated the contribution of ectopically expressing Cdk4 and hTERT on lung cancer development. However, we found that such cells, although immortal and clonable, did not show anchorage independent growth or an ability to form tumors *in vivo* (2). Other investigators and our group had also immortalized bronchial epithelial cells but these were made using viral oncoproteins such as HPV E6/E7 or SV40 large T antigen with or without hTERT (2, 11, 12). These oncoproteins are known to cause malignant transformation through their ability to inactivate Rb and/or p53, as well as provide multiple other functions, which are not characterized. These “other functions” make it difficult to estimate the importance of added genetic or epigenetic changes in bronchial epithelial cells immortalized by viral oncoproteins.

Thus, we designed the current study to determine if the HBECs were genetically tractable and to analyze the impact of additional genetic alterations frequently observed in lung cancer on tumorigenic transformation of bronchial epithelial cells. First, we introduced two well-known genetic alterations seen in lung cancer, one of which is the loss of p53 function, that is observed in 90% of SCLCs and 50% of NSCLCs (1). The other is oncogenic K-RAS, which is frequently seen in NSCLCs (~ 30%), especially in adenocarcinomas but probably never in SCLCs (1, 13, 14). Furthermore, we introduced a mutant epidermal growth factor receptor

(EGFR), which has recently been reported in NSCLCs and shown to be correlated with tumor sensitivity to the EGFR tyrosine kinase inhibitors (TKIs) (15, 16). We report here that HBECs immortalized by overexpression of Cdk4 and hTERT and subsequently manipulated to have oncogenic K-RAS, knockdown of p53, or mutant EGFR have acquired part, but not all of, the malignant phenotype by the combination of these genetic alterations. These partially progressed lung epithelial cells show that more changes are needed for the full malignant phenotype. In addition, we have found that these preneoplastic cells are exquisitely sensitive to EGFR inhibition.

Materials and Methods

Cells and culture conditions.

The HBEC3 (HBEC3-KT) immortalized normal human bronchial epithelial cell line was established by introducing mouse Cdk4 and hTERT into normal human bronchial epithelial cells obtained from a 65-year-old woman without cancer (2). NSCLC cell lines, NCI-H441, NCI-H358, NCI-H1299, and NCI-H2122 were obtained from Hamon Center collection (University of Texas Southwestern Medical Center). HBEC3 was cultured with K-SFM (Gibco, Gaithersburg, MD) media containing 50 µg/ml of Bovine Pituitary Extract (BPE) (Gibco) with or without 5 ng/ml of EGF (epidermal growth factor) (Gibco). These cells are resistant to G418 due to the neomycin resistant gene introduced with the cdk4 expression vector and to puromycin due to the puromycin resistant gene introduced with the hTERT expression vector.

Viral vector construction and viral transduction.

We used the pSUPER vector of Brummelkamp et al (OligoEngine, Seattle, WA) as the basis for generating siRNA for stable p53 knockdown (17, 18). To generate pSUPER.retro-zeocin (pSRZ), SacII and EcoRI sites were introduced into zeocin resistant gene fragment amplified from pVgRXR (a gift from Dr Preet Chaudhary) and the fragment was cloned into pSUPER.retro using SacII and EcoRI sites, resulting in the replacement of the puromycin resistant gene with a zeocin resistant gene. To generate pSRZ-p53 for p53 knockdown, EcoRI- and Hind III-digested inserts from pSUPER-p53 (18) (OligoEngine) was cloned into the same sites of pSRZ. pBabe-hyg and an oncogenic K-RAS^{V12}, pBabe-hyg-KRAS2-V12 vectors were provided by Dr Michael White (The University of Texas Southwestern Medical Center). To produce viral containing medium, 293T cells were transiently transfected with viral vector together with pVpack-VSVG and pVpack-GP vectors (Stratagene, La Jolla, CA). 48 hours after the transfection, supernatant

of the 293T cells was harvested and passed through a 0.45 µm filter, and the viral supernatant was frozen at -80 C. The supernatant was used for infection after adding 4 µg/ml of polybrene (Sigma, St. Louis, MO). 48 hours after the infection, drug selection for infected cells was started with 12.5 µg/ml of zeocin (Invitrogen, Carlsbad, CA) or 18 µg/ml of hygromycin (Clontech, Palo Alto, CA) and continued for 7 to 11 days. HBEC3 cells were infected with four different combinations of the two retroviral vectors: 1) pSRZ and pBabe-hyg (vector control); 2) pSRZ - p53 and pBabe-hyg; 3) pSRZ and pBabe-hyg-KRAS2-V12; and 4) pSRZ -p53 and pBabe-hyg-K-RAS2-V12.

To introduce wild and mutant EGFRs into HBEC3 cells we used the pLenti6/directional TOPO cloning kit. Full-length fragment of wild-type EGFR was amplified from pcDNA3.1-EGFR-wt (a gift from Dr. Joachim Herz, University of Texas Southwestern Medical Center) and cloned into pLenti6/directional TOPO vector according to manufacture instruction (pLenti-wt-EGFR). The L858R mutation was introduced into pLenti-wt-EGFR by using site-directed mutagenesis kit (Stratagene). The full length of E746-A750 del mutation was amplified from cDNA from HCC827 non-small cell lung cancer cell line (19) and cloned into pLenti6/directional TOPO vector. Correct sequences were confirmed by sequencing for all vectors. Viral transduction was performed following the manufacture instruction. Briefly, the 293FT cells were transiently transfected with viral vector together with viral power (Invitrogen). 48 hours after the transfection supernatant of the 293FT cells was harvested and passed through a 0.45 µm filter, and frozen at -80 C. The supernatant was used for infection after adding 4µg/ml of polybrene (Sigma). 48 hours after the infection drug selection for infected cells was started with 5µg/ml of Blasticidin (Invitrogen) and continued for 7 days.

Western Blot analysis.

Oncogenic manipulation of immortalized bronchial epithelial cells

Preparation of total cell lysates and Western blotting were performed as described previously (20). Primary antibodies used were mouse monoclonal anti-p53 (Santa Cruz, Santa Cruz, CA), mouse monoclonal anti-p21 (BD Transduction Laboratories, Lexington, KY), mouse monoclonal anti-K-RAS (Santa Cruz), mouse monoclonal anti-EGFR (BD transduction Laboratories), rabbit polyclonal anti-phospho-EGFR-Tyr1068 (Y1068), rabbit polyclonal anti-phospho-EGFR - Tyr845 (Y845) rabbit polyclonal anti-phospho-EGFR-Tyr992 (Y992) rabbit polyclonal anti-phospho-EGFR-Tyr1045 (Y1045) (Cell Signaling, Beverly, MA), rabbit polyclonal anti-MEK1/2 (Cell Signaling), rabbit polyclonal anti-phospho-MEK1/2 (Cell Signaling), rabbit polyclonal anti-ERK1 (Cell Signaling), rabbit polyclonal anti-phospho-ERK1 (Cell Signaling), rabbit polyclonal anti-Akt (Cell Signaling), rabbit polyclonal anti-phospho-Akt (Thr308), rabbit polyclonal anti-phospho-Akt (Ser473), mouse monoclonal anti-phospho-STAT3 (Tyr705) (Cell Signaling), PARP (Cell Signaling) ,and mouse monoclonal anti-Actin (Sigma) antibodies. Actin protein levels were used as a control for adequacy of equal protein loading. Anti-rabbit or anti-mouse antibody (1: 2000 dilution: Amersham, Piscataway, NJ) was used as the second antibody.

Immunofluorescence staining.

Cells were washed with PHEM (60 mM PIPES, 25 mM HEPES, 10 mM EGTA, 1 mM MgCl₂, pH 7.4) solution, and fixed in 3% paraformaldehyde for 10 min at 37°C in PHEM. After additional washes with PBS, the cells were permeabilized with 0.1% Triton in PBS for 10 min, blocked with 3% gelatin/3% BSA/0.2% Tween-20 for 1 h at 37°C, and incubated with mouse polyclonal anti-p63 antibody (BD Transduction) and Rhodamine phalloidin (Molecular Probe, Eugene, OR) in gelatin/BSA blocking solution for 16 h at 4°C. The cells were then incubated with the Alexa Fluor 568 anti-mouse IgG (H + L) (Molecular Probes) secondary antibody for 1 h

at 37°C. Finally, cells were stained with 0.5 µg/ml of Hoechst 33258, and examined in a fluorescence microscope.

RNA extraction and RT-PCR-RFLP analysis.

We modified previously reported RT-PCR-RFLP method designed to distinguish mutated from wild-type KRAS alleles (21). Total RNA was extracted using RNeasy mini kit (Qiagen, Valencia, CA). Four µg of total RNA were reverse transcribed with Superscript II First-Strand Synthesis using oligodeoxythymidylic acid primer system (Invitrogen). PCR amplification was carried out with 3704KRASTN sense (GAC TGA ATA TAA ACT TGT GGT AGT TGG ACC T) and 3672 KRAS-RT-R antisense (5-TCC TCT TGA CCT GCT GTG TCG-3) primers, creating BstNI restriction patterns that distinguished mutated from wild-type KRAS alleles. PCR reactions were performed in a 25 µl reaction mixture containing 1.5 mM MgCl₂, 187.5 µM of each dNTP, 10 pmol of each primer, and 1.25 unit of HotStar Taq DNA Polymerase (Qiagen). Cycling conditions were one incubation of 15 minutes at 95°C, followed by 35 cycles of a 20-second denaturation at 94°C, 60-second annealing at 58°C, and 90-second extension at 72°C, and a final elongation at 72°C for 7 minutes. PCR products were cut with BstNI, electrophoresized on 1% agarose gel with ethidium bromide, and visualized by UV. NCI-H2122 cell line containing a endogenous mutant K-RAS at codon 12 was used as a control for K-RAS^{V12} allele, and NCI-H1299 cell was used as a control for the wild-type K-RAS allele.

***In vitro* and *in vivo* cell growth assays.**

To determine growth curves, cells were cultured in triplicate wells in 12-well plates and counted every 3 days. Liquid colony formation assays were performed as previous described (22).

Briefly, 200 viable cells were plated in triplicate 100 mm plates and were cultured in K-SFM medium supplemented with 50 µg/ml of BPE with or without 5 ng/ml of EGF. To measure the

effect of gefitinib or erlotinib, 1 μ M of each drug was added to the medium and the medium was replaced every 3 days. Surviving colonies were counted 14 days later after staining with methylene blue. For soft agar-growth assays, 1,000 viable cells were suspended and plated in 0.37% Sea Kem agar (FMC, Philadelphia, PA) in K-SFM medium supplemented with 20% of fetal bovine serum (FBS) and 50 μ g/ml of BPE with or without 5 ng/ml of EGF in triplicate 12-well plates, and were layered over a 0.50% agar base in the same medium as the one used for suspending the cells. To measure the effect of gefitinib or erlotinib, 1 μ M of each drug was added to agar base layer. The number of microscopically visible colonies (>50 cells) were counted 4 weeks later. *In vivo* tumorigenicity was evaluated by injection of cells in nude mice. Male BALB/c nude (nu/nu) 3- to 6-week-old mice (Charles River Laboratories, Wilmington, DE) were irradiated on day 0 of the experiment in groups of five animals by a 5-minute exposure to 350 cGy from a cesium source. The next day, each mouse was given an injection subcutaneously on its flank $0.25-1 \times 10^7$ viable HBEC3 cells in 0.2 ml of PBS containing different combinations of ectopically introduced genes. Coinjection of Matigel (BD Bioscience, San Jose, CA) was also tested for HBEC3 cells expressing p53 RNAi and K-RAS^{V12}. Mice were monitored every 2–3 days for tumor size. All animal care was in accord with institutional guidelines and approved IACRAC protocols. The non-small cell lung cancer, NCI-H358, NCI-H441, and NCI-H1299 cell lines (5×10^6 cells) were used as positive controls.

Three-dimensional organotypic culture assay.

Cultures were established as previously described for skin equivalents (23) except that airway fibroblasts were used in place of skin cells. Briefly, type I collagen and IMR90 fibroblasts were mixed and allowed to polymerize. The collagen gels were released and incubated for a period of 4 to 10 days to allow the fibroblasts to contract the gels, creating a 'submucosa'. Cloning rings

were then placed atop the gels and HBEC cells were plated into the rings at a concentration of $2 \times 10^5/\text{cm}^2$. After allowing the cells to attach for 4 hours, the rings were removed and organotypic cultures submerged for 4 days in keratinocyte feeder layer media containing ascorbic acid, then emerged to the air-liquid interface for up to 28 days in culture, after which time the cultures were harvested, fixed, and prepared for histology. Organotypic cultures were immersed in 10% neutral buffered formalin overnight at 4°C followed by dehydration, paraffin embedding, and thin sectioning, 5 and 10µm sections were then rehydrated and stained with hematoxylin and eosin to view overall morphology (<http://www.protocol-online.org/prot/Histology/Staining/>). Stained slides were then viewed using an Axioscop-2 or Axioplan-2E microscope (Carl Zeiss, Thornwood, NY, USA; www.zeiss.com) and photographed with Hamamatsu ORCA monochrome CCD camera (Hamamatsu; Bridgewater, NJ; www.hamamatsu.com).

Cell cycle analysis.

Cells were harvested 48 h after the treatment of 1µM of gefitinib, erlotinib, or 0.1% DMSO, fixed with 70% ethanol, treated with 5 mg/ml RNase A (Roche Molecular Biochemicals), stained with 50 µg/ml propidium iodide, and analyzed by flow cytometry for DNA synthesis and cell cycle status (FACSCaliber instrument, Becton Dickinson, with FlowJo software).

Microarray analysis.

RNAs were labeled and hybridized to Affymetrix HG-U133-Plus2 GeneChips according to the manufacturer's protocol (<http://www.affymetrix.com>). This array contains 54,675 genes (29,180 unique genes). Microarray analysis was performed using Affymetrix MicroArray Suite 5.0 and in-house Visual Basic software MATRIX 1.26.

Real-time RT-PCR for DUSP6/MKP-3.

The expression of *DUSP6/MKP-3* was analyzed by quantitative real-time RT-PCR. Primers were designed to ensure a single 107 bp amplicon using the standard Taqman assay-on-demand PCR protocol with a 10 minute hot start. Products were resolved on 2% agarose (Sigma). A probe sequence was designed using PrimerExpress software (Applied Biosystems). The probe was labeled with TAMRA (quencher) and FAM (reporter) and synthesized by IDT. To establish the efficiency of this assay we used a five fold serial dilution of cDNA over 6 concentrations. These samples were run on the Gene Amp 7700 Sequence Detection System (Applied Biosystems) in triplicate. The resultant curve had a slope of -3.396 and R^2 coefficient of 0.9939. For quantitative analysis of *DUSP6/MKP-3* we used *GAPDH* (Applied Biosystems assay-on-demand) as an internal reference gene to normalize input cDNA. Quantitative real-time RT-PCR was performed in a reaction volume of 25 μ l including 1 μ l of cDNA. We used the comparative Ct method to compute relative expression values.

Statistical analyses:

For comparison of saturation density and colony formation between the different genetically manipulated cell strains we used one-way ANOVA with Bonferroni's post hoc test correction and for comparisons of the effect of EGFR on growth the Mann-Whitney U test.

Results

RNAi-mediated p53 knockdown and K-RAS^{V12} introduction in HBEC3s.

We used retroviral vector mediated-RNAi technology to generate HBEC3 clones stably knocked down for p53. HBEC3 expressing cdk4 and hTERT cells were infected with pSRZ-p53 (see

methods and legend of Figure.1), selected with zeocin, and tested for p53 and p21^{WAF1} protein expression. Western blot analysis showed clear suppression of p53 and p21^{WAF1} (Fig. 1A). Next, we introduced mutant K-RAS^{V12} into pSRZ-expressing and pSRZ-p53-expressing HBEC3 cells using pBabe-hyg-KRAS2-V12 retroviral vector followed by hygromycin selection. Western blot analysis showed that the expression levels of K-RAS in K-RAS^{V12} transfected and p53RNAi and K-RAS^{V12} transfected HBEC3 cells approximated that of vector alone transfected HBEC3 cells (Fig. 1A). Because antibodies that recognize only wild or mutant K-RAS are not available, we performed RT-PCR-RFLP analysis to distinguish between K-RAS^{V12} and wild K-RAS mRNA expression. The analysis revealed that mutant K-RAS^{V12} transcripts were the predominant form expressed in the K-RAS^{V12} transfected HBEC3 alone or with p53 RNAi cells (Fig. 1B), indicating that most of the K-RAS protein expressed in HBEC3 cells infected with pBabe-hyg-KRAS2-V12 was the mutant form. We also performed immunocytochemistry of p63 (a stem cell marker) and found that mutant K-RAS and /or p53 knockdown did not alter the p63 expression levels of HBEC3 cells (data not shown).

p53 knockdown and K-RAS^{V12} introduction into HBEC3s increases saturation density.

We assessed the effect of p53 knockdown and expression of mutant K-RAS^{V12} on cell growth and found no significant difference in growth rate in the exponential growth phase between p53RNAi expressing, K-RAS^{V12} expressing, p53RNAi and K-RAS^{V12} expressing, and vector expressing HBEC3 cells. However, p53RNAi expressing ($P < 0.01$), K-RAS^{V12} expressing ($P < 0.01$), and p53RNAi and K-RAS^{V12} expressing ($P < 0.001$) HBEC3 cells achieved significantly higher final saturation densities in confluent cultures compared to vector transfected control (in all cases here and below using one-way ANOVA with Bonferroni's post hoc test) (Fig. 1C and 1D). Also, the final density of the combined p53RNAi and K-RAS^{V12} expressing HBEC3 cells

was significantly higher than that of HBEC3 cells with either p53 knockdown ($P < 0.01$) or mutant K-RAS^{V12} ($P < 0.01$) alone (Fig. 1C and 1D). We conclude from these studies that introduction of these genetic changes produced part of the malignant phenotype, increased saturation density.

p53 knockdown and K-RAS^{V12} introduction permits anchorage-independent growth and partial bypass of EGF dependence.

HBEC3 cells are able to form colonies in liquid medium but not in soft agar (i.e. they do not display anchorage independent growth). We then tested the p53 and K-RAS^{V12} manipulated variants to see if they had acquired this ability. In addition, because HBEC3 cells express robust levels of EGFR (Fig. 4A), and EGF is in the K-SFM synthetic medium we tested the dependence of colony formation in liquid and semi-solid medium on EGF. Supplementation of EGF dramatically enhanced liquid colony formation in all HBEC3 cells (Fig. 1E). In liquid colony formation in the presence of EGF no significant difference in the number of colonies was seen between p53RNAi expressing, K-RAS^{V12} expressing, p53RNAi and K-RAS^{V12} expressing, and vector expressing HBEC3 cells. In contrast there were significant differences in the number of colonies in the absence of EGF between these four strains (Fig. 1F). In the absence of EGF, p53RNAi expressing (5.9 fold, $P < 0.001$) and p53RNAi and K-RAS^{V12} expressing (6.6 fold, < 0.001) HBEC3 cells formed a markedly increased number of colonies compared to vector control, while K-RAS^{V12} expressing HBEC3 cells formed significantly increased (3.2 fold, < 0.001) number of colonies compared to vector control (in all cases here and below using one-way ANOVA with Bonferroni's post hoc test) (Fig. 1F). In the presence of EGF, p53RNAi expressing, K-RAS^{V12} expressing, and p53RNAi and K- K-RAS^{V12} expressing HBEC3 cells formed a significantly increased number of soft agar colonies compared to vector control, 7.3 ($<$

0.001), 6.7 (< 0.001) and 16.5 fold (< 0.001) respectively, while in the absence of EGF, p53 RNAi and p53RNAi and K-RAS^{V12} expressing HBEC3 cells formed very few colonies (Fig. 4C). We conclude from these studies that introduction of these genetic changes led to anchorage-independent growth and both oncogenic KRAS or p53 knockdown led to partial bypass of dependence on EGF. However, the cells still remain dependent on EGF signaling to express this anchorage-independent growth, while an unexpected finding was the ability of p53 knockdown to partially alleviate this EGF dependence.

p53 knockdown and expression of mutant K-RAS^{V12} does not give a full malignant phenotype.

In tumorigenicity assays none of HBEC3 derivatives formed subcutaneous tumors in nude mice. Since Matrigel (BD Bioscience) accelerates tumor growth when coinjected with cells in athymic mice (24), we injected HBEC3 cells expressing p53 RNAi and K-RAS^{V12} together with Matrigel. However, even with Matrigel the HBEC3 cells expressing p53 RNAi and K-RAS^{V12} did not form tumors. In contrast, tests of 5×10^6 non-small cell lung cancer, NCI-H358, NCI-H441, and NCI-H1299 cells reproductively formed progressively growing nude mouse xenograft tumors in the 17-90 day observation period (Table 1). We conclude from these studies that even with these gain of function and loss of function manipulations a full malignant phenotype is not achieved (in vivo tumor formation).

Oncogenic manipulation leads to an invasive phenotype in a three-dimensional organotypic culture assay.

To evaluate the effect of oncogenic manipulation in HBEC3s on their ability to differentiate and to invade we performed three-dimensional organotypic culture. HBEC3 cells only expressing hTERT and Cdk4 cells formed a confluent layer of cells on the upper surface of a fibroblast and

collagen gel under layer and developed both ciliated (Fig. 2A) and mucous producing cell types. In stark contrast, the cells expressing hTERT, Cdk4, K-RAS^{V12} and p53 RNAi showed histologic change similar to metaplasia/dysplasia and they invaded into the fibroblast and collagen gel similar to cancer cells invading into the submucosal layer (Fig. 2B and Fig. 2C). We conclude from these studies that p53 knockdown and K-RAS^{V12} are additive in malignant transformation leading to the development of anchorage-independent growth and the ability to invade in a three-dimensional culture system.

Gefitinib and erlotinib inhibit proliferation and colony formation of HBEC3 cells by inducing G1 cell cycle arrest.

The dependency of HBEC3 cell on EGF signaling prompted us to investigate the effect of TKIs, gefitinib and erlotinib on cell proliferation in mass culture and colony formation of these cells. Both gefitinib and erlotinib at 1 μ M completely inhibited the mass culture proliferation of all HBEC3 cells both in the presence and the absence of EGF (data not shown). Gefitinib or erlotinib at 1 μ M also completely inhibited both anchorage-dependent and independent colony formation in all HBEC3 cells (Table 2 and Fig. 3A). Thus, while oncogenic manipulation partially relieved EGF dependence, EGF TKIs remain potent inhibitors of HBEC growth. To investigate the mechanisms of this growth inhibition by TKIs we performed apoptosis and cell cycle analyses. Western blot for PARP cleavage, an indicator of caspase-mediated apoptosis, showed that cleaved 89-Kd fragment was not detected in any of HBEC3 cells treated with TKIs but was significantly increased in HCC827 EGFR mutant cells after the treatment with TKIs for 48 hours (Fig. 3B). Cell cycle analysis also did not show sub-G1 DNA fractions indicative of apoptosis in HBEC3 cells treated with TKIs. Instead, the cell cycle analysis showed increase in the fraction of cells in G1 phase in all the HBEC3 cells treated with either of the drugs, with

reduction of S phase cell (Table 3. and Fig. 3C). These results suggest that growth inhibition for HBEC3 cells by TKIs is mainly caused by G1 cell cycle arrest and not apoptosis. Comparing the results of FACS analysis for the control cells treated with DMSO, we found that the combined HBEC3 p53 knock down and mutant K-RAS cells showed a significantly increase in G2/M phase cells compared to either manipulation alone suggesting dramatic cell cycle deregulation results from this oncogenic combination (Table 3 and Fig. 3C).

Effect of K-RAS^{V12} and EGF supplementation on expression of pEGFR, pMEK, pERK, and pAkt.

We measured the expression of phosphorylated and total EGFR, MAPKs and Akt proteins in the HBEC3 cells in the presence and the absence of EGF. Addition of EGF resulted in massive induction of phospho-EGFR, a slight induction of phospho-ERK, and a modest induction of phospho-Akt^{Thr308} in all HBEC3 cells (Fig. 4A). In the absence of EGF, two immunoreactive phospho-MEK1/2 bands were detected while the faster migrating band was not detected in the presence of EGF, representing a shift to the hyper phosphorylated form (Fig. 4A). Surprisingly, introduction of K-RAS^{V12} did not show a significant effect on phosphorylation of MAPKs in the presence or absence of EGF but led to a slight increased phospho-Akt^{Thr308} in the absence of EGF (Fig. 4A). Also surprisingly, both phospho-MEK1/2 and phospho-ERK were down-regulated in p53RNAi and K-RAS^{V12} expressing HBEC3 cells compared to the other three cell lines in the absence of EGF (Fig. 4A).

Tyrosine kinase domain mutant EGFRs enhanced anchorage-independent growth of HBEC3 cells.

EGFR with mutations in the tyrosine kinase domain have been discovered in lung cancers predominantly arising in never smokers (25). These mutant EGFRs are suspected as having

oncogenic properties. To determine if mutant EGFRs commonly found in lung cancer (E746-A750, L858R) have oncogenic ability, we evaluated the tumorigenicity of wild-type and mutant EGFR transfected HBEC3s by soft agar colony formation assays. In the absence of EGF, E746-A750 del expressing HBEC3 cells formed significantly increased number of colonies compared to wild-type expressing cells in both p53 wild-type ($p<0.001$ by Mann-Whitney U test) and p53 knocked down cells ($p<0.01$ by Mann-Whitney U test), while L858R mutant expressing HBEC3 cells increased the number of colonies only in p53 knocked down cells ($p<0.001$ by Mann-Whitney U test) (Fig. 4C). In contrast to p53 RNAi and mutant K-RAS expressing HBEC3s that formed very few number of colonies (2.7 ± 2.0 out of 1,000) in the absence of EGF, the E746-A750 del mutant transfectants formed substantial number of colonies even in the absence of EGF (Fig. 4C), suggesting that E746-A750 del mutant reduced the EGF dependence of HBEC3s in terms of anchorage-independent growth. Of interest, the L858R mutant only demonstrated this independence when p53 was removed by knockdown (Fig. 4C). Again, in these p53 knocked down HBEC3s carrying a control vector (used for EGFR introduction), the cells remained dependent on EGF for soft agar growth. These results indicate that both types of mutant EGFRs possess oncogenic properties compared to wild-type EGFR. They also provide functional differences between the deletion and missense EGFR mutants including differences in p53 interaction. We also performed nude mice injection assays for p53 knocked down HBEC3s carrying L858R mutant, which formed the most number of colonies in the absence of EGF (Fig. 4C). However, they did not form tumor in nude mice (Table 1)

Introduction of both wild and mutant EGFR into HBEC3s resulted in constitutive activation of EGFR.

Phosphorylation level of EGFR was evaluated by western blotting with four (Y845, Y992, Y1045, and Y1068) phosphorylation specific antibodies. To reduce the background for western blotting, cells were first starved in the media without BPE and EGF for 24 hrs before harvest. In the absence of exogenous EGF, we found EGFR mutants and wild-type EGFR to exhibit induced levels of phosphorylated EGFR, suggesting the existence of autocrine ligands stimulating EGFR (Fig. 4B). In p53 wild-type cells, wild-type EGFR showed phosphorylation of Y845, Y992 and Y1068 to a lesser extent than when mutant EGFRs were present (Fig. 4B). In contrast, in p53 knocked down cells, such a difference was not seen (Fig. 4B). This result suggests that the activation of wild-type EGFR might be suppressed by p53. Interestingly, the Y1045 site was highly phosphorylated in L858R transfectants, but not in E746-A750 del transfectant (Fig. 4B), indicating that Y1045 is unique in distinguishing between the two types of EGFR mutations (Fig. 4B).

AKT and STAT3 were phosphorylated at higher level in mutant EGFRs than wild-type EGFR.

The EGFR L858R mutant showed increased level of phosphorylated Akt and STAT3 in both p53 wild-type and p53 knocked down cells, while the EGFR E746-A750 del mutant showed increased level of phosphorylated Akt only in p53 knocked down cells and slightly increased level of phosphorylated STAT3 in both p53 wild-type and p53 knocked down cells (Fig. 4B). By contrast, no significant difference in phosphorylated ERK was seen between wild-type and mutant EGFRs (Fig. 4B). These results suggest that mutant EGFRs selectively transduces signals through Akt and STAT3, which is consistent with previously reported data (26).

***DUSP6/MKP-3* gene was upregulated in mutant EGFR transfected HBEC3 cells.**

Oncogenic manipulation of immortalized bronchial epithelial cells

Microarray analysis for HBEC3 cells transfected with wild-type or mutant EGFRs shows that mRNA of DUSP6/MKP-3, whose protein is a dual-specificity phosphatase that dephosphorylate the active form of ERK (27, 28), is significantly upregulated in mutant EGFR transfectants compared to wild-type and vector transfected cells (Fig. 4D). Real-time PCR analysis for DUSP6/MKP-3 also showed this result (Fig. 4D).

Discussion

We have taken human bronchial epithelial cells immortalized using overexpression of Cdk4 (to circumvent p16-mediated cell culture growth arrest) and hTERT (to prevent telomere erosion) and genetically manipulated them by stably knocking down p53, expressing oncogenic K-RAS^{V12}, and mutant EGFR, alone or in combination. The results show that these additional genetic changes, commonly found in human lung cancer, progress the HBEC3 cells part, but not all, of the way towards malignancy. The human cells exhibit higher saturation density, anchorage-independent growth, invade in an organotypic culture assay but do not form tumors in mouse xenografts. While, in general, the cells remain dependent on EGF, p53 knockdown and mutant EGFR reduce this EGF dependence. In addition, their growth and ability to form colonies in liquid and semi-solid media is dramatically reduced by EGFR-directed TKIs. These studies indicate that more than four genetic alterations are required for the full cancer transformation of human bronchial epithelial cells.

Several studies have reported that introduction of oncogenes such as KRAS or HRAS and c-myc result in malignant transformation of human bronchial epithelial cells (29-31). However, until the present study there has not been immortalized cell line with wild-type p53 function. (Prior studies were performed with viral oncoprotein immortalized cells abrogating p53 function (11, 12, 29, 30, 32).) In the present study we have shown that greater than 90% inhibition of p53 protein in immortalized human bronchial epithelial cells enhances the clonal and soft agar colony formation and results in partial loss of contact inhibition, indicating that loss of p53 function contributes importantly to the malignant progression of human bronchial epithelial cells. In addition, the combination of p53 knockdown and oncogenic K-RAS^{V12} enhanced these changes further, suggesting these two genetic alterations have additive effects on tumorigenicity. Taken

together, these results show that this model system provides a powerful new approach to assess the contribution of individual genetic alterations in human bronchial epithelial cells in the malignant process.

Ras was first identified as an oncogene by virtue of its ability to overcome cell-cell contact inhibition of proliferation and this ability has been well documented in many types of cells (33, 34). In the present study, not only oncogenic K-RAS^{V12} but also p53 knockdown resulted in partial loss of contact inhibition and the combination of them enhanced this ability. Recently, Meerson et al. reported results consistent with this finding (35). They demonstrated that p53 knockdown in WI38 human embryonic lung fibroblasts reduced density-dependent inhibition of growth by abolishing G1 phase arrest. While density-dependent inhibition of growth is a complex phenomenon and its precise mechanism is not well understood, this phenomenon is thought to be indicative of tumorigenic potential. Thus, their results and ours suggest that p53 may function as a tumor suppressor even when the cells are not under stresses such as genotoxic damage and irradiation. Recently, other studies also reported that p53 function is involved in regulating cell motility and adhesion (36, 37).

It is unclear how the mutant KRAS transfected HBECs preferentially express the mutant compared to wild type KRAS allele. These cells express mutant KRAS mRNA predominantly without changing the total KRAS protein levels, suggesting that wild type KRAS expression is suppressed at the transcriptional level in these cells. The mechanism of transcriptional regulation of KRAS has not been fully elucidated and we are unable to explain the mechanism of this observation. However, the hypothesis that oncogenic ras inhibits the transcription of wild type ras is compatible with our observations. Since the tumor suppressor function of wild-type Kras has been demonstrated in mice, one possibility is that mutant ras exerts its oncogenic ability in

part by suppressing the expression of wild-type ras. This hypothetical function of oncogenic ras seems very attractive in terms of better understanding the mechanism of oncogenic ras, and thus it will be of interest to further investigate these findings.

Previous studies have found high levels of EGFR expression in both immortalized and non-immortalized human bronchial epithelial cells (38). EGF supplementation also results in a slight increase of growth rate at normal cell density in human bronchial epithelial cells (38). Several studies have shown the existence of an EGFR autocrine loop involving EGF, TGF- α , and amphiregulin in human bronchial epithelial cells (39, 40). In addition, tobacco smoke induces proliferation of primary bronchial epithelial cell through an EGFR autocrine loop mediated by tumor necrosis factor- α converting enzyme and amphiregulin, suggesting tobacco smoke induction of the EGFR autocrine loop in lung cancer pathogenesis (41). In the present study we found that HBEC3 cells expressed high level of EGFR that was stimulated to phospho-EGFR with EGF while their colony forming ability in both liquid and soft agar was highly dependent on EGF supplementation. Signal transduction studies in HBEC3 cells suggest that this may in part be due to the upregulation of the Akt pathway. With p53 knockdown and KRAS oncogenic manipulation the EGF dependence was partially relieved, suggesting the potential for autocrine growth factor production. Thus, previous studies and our results suggest that EGF autocrine loop may play an important role in cell proliferation and tumorigenic progression of human bronchial epithelial cells

Gefitinib (Iressa[®]) and erlotinib (Tarceva[®]) are orally available TKIs that target EGFR (42-45). Gefitinib has been approved as a third-line therapy for NSCLC patients. Erlotinib has been shown to be active and well tolerated in patients with NSCLC, providing survival benefit (46). While these drugs are being developed as anticancer drugs, recent studies have shown that

gefitinib inhibits cell proliferation in immortalized normal or precancerous breast cells, supporting its role as a chemopreventive agent (47). Since we found robust expression of EGFR in HBEC3 cells and their high dependency of growth on EGF, we considered the possibility that TKIs are also effective in oncogenically manipulated HBEC3 cells. We observed that 1 μ M of gefitinib or erlotinib dramatically inhibited both anchorage-dependent and independent cell growth of HBEC3 cells. Apoptosis and cell cycle analyses showed that this inhibition was caused mainly by not apoptosis but G1 cell cycle arrest, which is consistent with previous papers reporting that gefitinib and erlotinib induce G1 cell cycle arrest in several types of cells (48-52). These results provide part of a preclinical rationale for the development of these drugs for the prevention of human lung cancer. It is important to point out that the concentrations used in the present studies are actually achieved in patients with current standard drug practices (53, 54). In addition, interestingly, we found that G2/M fraction significantly increase with the combination of p53 knock down and mutant KRAS cells compared to either oncogenic manipulation alone. We speculate that in the presence of intact p53 function, cell cycle progression induced by mutant KAS in HBEC cells is suppressed by the ability of p53 to induce G1 arrest, while in the absence of p53, mutant KAS exerts its ability to progress cell cycle from G1 to S phases, resulting in significantly increased G2/M phase fraction. Consistent with this hypothesis, one paper showed that ectopic expression of mutant N-RAS impaired the G1 and G2 cell cycle arrest only in p53-defective cells (55). In addition, it will be interesting to see whether similar types of cell cycle deregulation are also found when mutant EGFR is combined with loss of p53 function in these cells.

Introduction of tyrosine kinase domain EGFR mutants enhanced anchorage-independent growth of HBEC3s providing evidence of their oncogenic properties. In addition, signal

transduction analysis demonstrated that they stimulated Akt and STAT3 but not Erk1/Erk2 signals, consistent with previously reported results (26). Our discovery of DUSP6/MKP-3 mRNA upregulation in mutant EGFR transfectants provides an explanation for this. Since DUSP6/MKP-3 protein is a dual-specificity phosphatase that dephosphorylates the active form of ERK (27, 28), it is possible that Erk1/Erk2 phosphorylation in EGFR mutant cells is down regulated by DUSP6/MKP-3. In addition, the findings that Akt and STAT3 were not highly phosphorylated in HBECs that showed robust level of phosphorylated EGFR suggests that a negative feedback regulatory pathways may be activated for Akt and STAT3 as well, and that the mutant EGFRs bypass this regulation.

While p53 knockdown, K-RAS^{V12} and mutant EGFR progress HBEC3 cells toward malignancy, the manipulated cells are not fully malignant. What additional genetic alterations are required for full malignant transformation in HBEC3 cells? For this question there may be a clue from recent work of Hahn et al, who demonstrated that defined genetic alterations including the early region of the SV40 genome, the *hTERT* gene, and an oncogenic allele of H-ras resulted in malignant transformation in human embryonic epithelial and fibroblast cells (56). By precisely analyzing the early region of SV40 they have shown that small t antigen which is transcribed from the early region together with large T antigen may play an important role in carcinogenesis. Small t antigen has been shown to bind and to target phosphatase 2A (PP2A), which regulates the RAS/MAPK cascade. Our unpublished studies have shown no mutation but frequent loss of PP2A expression in lung cancer, raising the possibility that PP2A is involved in lung carcinogenesis. Thus, a next step would be to inactivate PP2A in HBEC3 cells in addition to p53 knockdown and K-RAS^{V12}. It will also be of interest to introduce other genetic alterations observed in lung cancer such as MYC family overexpression, FHIT inactivation, RASSF1A

inactivation, and PTEN inactivation. Although we used previously reported target sequence for p53 knockdown which has also been used in several papers (17, 18, 57), and has no other BLAST hits, we are unable to completely exclude the possibility that off-target effects might affect our phenotypic analysis.

In conclusion, we have shown that using the immortalized human bronchial epithelial cell model, p53 knockdown, K-RAS^{V12} and mutant EGFR in the presence of p16 bypass and human telomerase, contribute to lung cancer tumorigenesis but additional genetic alterations are required for full malignant transformation of human bronchial epithelial cells. In addition, we note p53 knockdown relaxes the dependence on EGF in the presence of both wild-type and mutated EGFR. However, these oncogenically manipulated HBEC cells remain highly dependent on EGFR signaling for expression of key portion of the malignant phenotype. This dependence along with activated EGFR in bronchial preneoplasia suggests the use of EGFR inhibition by TKIs as chemoprevention agents for lung cancer.

Acknowledgements

This work was supported by Lung Cancer SPORE P50CA75907, CA71618, NO1-CN-43301, DOD VITAL GRANT (W81XWH041014202PP), and the Gillson Longenbaugh Foundation.

Figure legends

Figure 1. Characterization of p53 knocked down and K-RAS^{V12} expressing HBEC3 cells. **A**, western blots showing the suppression of p53, p21^{WAF1/CIP1}, and K-RAS in p53RNAi, mutant K-RAS^{V12}, and p53RNAi and mutant K-RAS^{V12} expressing HBEC3 cells. p53 and p21^{WAF1/CIP1} are clearly knocked down in p53RNAi expressing cells, while the expression levels of K-RAS in K-RAS^{V12} transfected and p53RNAi and K-RAS^{V12} transfected HBEC3 cells approximate that of vector alone transfected HBEC3 cells **B**, Restriction fragment length polymorphism analysis of K-RAS cDNA showing mutant K-RAS^{V12} transcripts are predominantly expressed in mutant K-RAS^{V12} expressing and p53RNAi and mutant K-RAS^{V12} expressing HBEC3 cells. H2122 and H1299 are used as positive control for mutant K-RAS^{V12} and wild-type K-RAS, respectively. Brummelkamp et al reported a new vector system, named pSUPER, which generated small interfering RNAs (siRNAs) in mammalian cells to functionally inactivate p53 (18). Subsequently, they developed a retroviral version of pSUPER, named pSUPER.ret (pRS), to obtain stable knockdowns and demonstrated stable and specific knockdown of oncogenic K-RAS^{V12} (17). To see the long-term effect of p53 inactivation we used the pSUPER.ret system for p53 knockdown. Since a puromycin resistant gene in pRS was already integrated in HBEC3 in the process of introducing Cdk4, we developed pRS-zeocin vector (pSRZ) by replacing the puromycin resistant gene in pRS vector with a zeocin resistant gene. Subsequently, the published p53 target siRNA sequence was cloned into pSRZ (17, 18), yielding pSRZ-p53 vector. **C**, Increased saturation density in p53 RNAi and mutant K-RAS^{V12} expressing HBECs. 2,000 HBEC3 cells were cultured in triplicate 12-well plates and counted every 3 days. Solid circle, diamond, triangle, and square represent vector, p53RNAi, mutant- K-RAS^{V12}, and p53RNAi and mutant- K-RAS^{V12} expressing HBEC3 cells, respectively. **D**, cells were grown as described in

Fig. 1C and pictures were taken on day 12. **E**, liquid colony formation assay for vector, p53RNAi, mutant K-RAS^{V12}, and p53RNAi and mutant K-RAS^{V12} expressing HBEC3 cells in the presence or absence of EGF (5 ng/ml). A total of 200 cells were plated per dish and cultured for 2 wks before staining with methylene blue. **F**, Quantitation of the number of colonies in the absence of EGF. The data represent the mean \pm SD of three independent experiments. *, $P < 0.01$, One-way ANOVA with Bonferroni's post test.

Figure 2. Effect of p53 knock down and mutant K-RAS^{V12} on three-dimensional organotypic culture of HBEC3 cells. **A**, Stained paraffin cross-sections of organotypic cultures of HBEC3 cells demonstrated that they formed a confluent layer of cells on the upper surface of the culture with the presence of cilia-like structures. **B**, (Low magnification) and **C**, (High magnification) p53RNAi and mutant K-RAS^{V12} expressing HBEC3 cells showed a histologic change similar to metaplasia and dysplasia and they invaded into the fibroblast and collagen under layer.

Figure 3. Gefitinib and erlotinib inhibited the growth of HBEC3 cells by inducing G1 cell cycle arrest. **A**, Effect of gefitinib and erlotinib on liquid colony formation of HBEC3 cells. A total of 200 cells were treated with 1 μ M of gefitinib or erlotinib in triplicate 100mm plates in the presence or the absence of 5ng/ml of EGF and cultured for 2 wks before staining with methylene blue. **B**, PARP western blot for HBEC3 cells treated with 1 μ M of gefitinib or erlotinib or 0.1%DMSO for 48 hours. Actin is used as loading control. HCC827 cell line, which has been shown to be highly sensitive to gefitinib treatment, is used as positive control (19). Cleaved 89-kDa fragment is significantly increased in HCC827 cells but not detected in any of HBEC3 cells after the treatment. **C**, Fluorescence-activated cell-sorting profiles of vector (Control) or p53 RNAi and mutant KRAS^{V12} expressing HBEC3 cells treated with 1 μ M of gefitinib or erlotinib or 0.1%DMSO for 48 hours. Cells were harvested after the treatment, stained with propidium

iodide, and analyzed by using the flow cytometer. Horizontal and vertical axes represent DNA content and cell number, respectively. G1 fraction is significantly increased in both HBEC3 cells, with the reduction of S and G2/M fractions after the treatment of gefitinib or erlotinib. In the DMSO control G2/M fraction is significantly increased in p53 RNAi and mutant KRAS expressing HBEC3 cells compared to vector expressing HBEC3 cells. Both in control and treated cells, cell cycle distributions of p53 RNAi and mutant KRAS^{V12} alone expressing HBEC3 cells are similar to that of vector expressing HBEC3 cells.

Figure 4. Transduction analysis for oncogenically manipulated HBEC3 cells.

A, Effect of K-RAS^{V12} and EGF supplementation on expression of pEGFR, pMEK, pERK, and pAkt. HBEC3 cells were grown in the presence or absence of 5 ng/ml of EGF, and were immunoblotted to detect phospho-EGFR, EGFR, phospho-MEK1/2, MEK1/2, phospho-ERK, ERK, phospho-Akt (Thr308) and Akt. Actin was used as loading control. **B**, Effect of wild-type and mutant EGFR introduction on expression of pEGFRs, pSTAT3, pERK, and pAkt in HBEC3 cells. Wild-type or mutant EGFR introduced HBEC3 cells were grown in the absence of EGF, and were immunoblotted to detect phospho-EGFRs (Y1068, Y1045, Y992, and Y845), EGFR, phospho-STAT3, phospho-Akt (Y473), and phospho-ERK. Actin was used as loading control. **C**, soft agar colony formation assay for oncogenically manipulated HBEC3 cells. A total 1,000 of each HBEC3 cell strains were plated in agar and 4 wks later microscopically visible colonies were counted. The data represent the mean \pm SD of three independent experiments. *, $P < 0.01$, One-way ANOVA with Bonferroni's post test, #, $p < 0.01$ by Mann-Whitney test, and ##, $p < 0.001$ by Mann-Whitney test. **D**, Microarray analysis and real-time PCR validation for *DUSP6/MKP-3* gene. *Columns*, fold changes of the mRNA levels of

Oncogenic manipulation of immortalized bronchial epithelial cells

DUSP6/MKP-3 gene relative to those of *GAPDH* gene in HBEC3 cells transfected with wild-type or mutant EGFR.

Table 1. Tumorigenicity assay in nude mice for HBEC3 cells

Cell Line		# of nude mice injected	# of cells per mouse	Observation period (days)	% Tumors
NCI-H358		10	5X10 ⁶	90	100
NCI-H441		5	5X10 ⁶	61	100
NCI-H1299		40	5X10 ⁶	17-38	100
HBEC3					
HBEC3	Nontreated	5	1X10 ⁷	90	0
HBEC3	K-RAS ^{V12}	5	5X10 ⁶	90	0
HBEC3	p53RNAi	5	5X10 ⁶	90	0
HBEC3	p53RNAi and K-RAS ^{V12}	5	5X10 ⁶	90	0
HBEC3	p53RNAi and K-RAS ^{V12}	5	2.5X10 ⁶	90	0
HBEC3	with matrigel				
HBEC3	p53 RNAi and EGFR-L858R	5	2.5X10 ⁶	90	0

Table 2. Soft agar colony formation assay for HBEC3 cells treated with gefitinib or erlotinib

		HBEC3			
		Vector	p53RNAi	K-RASV12	p53RNAi and K-RASV12
EGF(+)	DMSO	1.3±0.47	11±1.6	5.7±1.2	23±2.1
	Gefitinib (1µM)	0	0	0	0
	Erlotinib (1µM)	0	0	0	0
EGF(-)	DMSO	0	0	0	1.3±0.94
	Gefitinib (1µM)	0	0	0	0
	Erlotinib (1µM)	0	0	0	0

Number of colonies after 14 days are shown as average±SD. 1,000 HBEC3 cells were plated in agar and treated with 1µM of gefitinib or erlotinib in triplicate 12-well plates for up to 2 weeks in the presence or the absence of EGF and colonies (50-100 cells) were counted.

Oncogenic manipulation of immortalized bronchial epithelial cells

Table 3. Effect of Gefitinib and Erlotinib on cell cycle progression in HBEC3 cells

	Nontreated (DMSO)			Gefitinib/Erlotinib		
	G1	S	G2/M	G1	S	G2/M
Vector	45.4±0.2	27.5±6.0	28.7±3.9	76.6±5.6**	2.6±0.5*	28.0±2.0
p53RNAi	41.4±2.9	27.6±3.7	31.0±4.5	69.5±0.2**	7.4±2.8**	27.0±3.4
KRAS ^{V12}	49.5±6.3	31.7±10.6	17.8±12.2	81.4±4.6**	7.7±2.4	16.6±2.8
p53RNAi and KRAS ^{V12}	12.9±3.2	11.8±6.2	73.7±3.8	25.6±4.8**	5.3±1.2	70.8±3.7

^aPercentages (mean±S.D.), *P<0.05; **P<0.01 in comparison with the respective control.

Averaged values of three independent experiments are shown.

Watson Pragmatic algorithm was used to calculate each cell cycle distribution.

Since the algorithm contains approximations, total of each distribution is not exactly 100%.

References

1. Sekido, Y., Fong, K. M., and Minna, J. D. Molecular genetics of lung cancer. *Annu Rev Med*, 54: 73-87, 2003.
2. Ramirez, R. D., Sheridan, S., Girard, L., Sato, M., Kim, Y., Pollack, J., Peyton, M., Zou, Y., Kurie, J. M., Dimaio, J. M., Milchgrub, S., Smith, A. L., Souza, R. F., Gilbey, L., Zhang, X., Gandia, K., Vaughan, M. B., Wright, W. E., Gazdar, A. F., Shay, J. W., and Minna, J. D. Immortalization of human bronchial epithelial cells in the absence of viral oncoproteins. *Cancer Res*, 64: 9027-9034, 2004.
3. Vaughan, M. B., Ramirez, R. D., Wright, W. E., Minna, J. D., and Shay, J. W. A Three-Dimensional Model of Differentiation of Immortalized Human Bronchial Epithelial Cells. *Differentiation*, *in press*, 2005.
4. Geradts, J. Abrogation of the RB-p16 tumor suppressor pathway in human lung cancer. *Methods Mol Med*, 74: 89-99, 2003.
5. Kaye, F. J. RB and cyclin dependent kinase pathways: defining a distinction between RB and p16 loss in lung cancer. *Oncogene*, 21: 6908-6914, 2002.
6. Horikawa, I. and Barrett, J. C. Transcriptional regulation of the telomerase hTERT gene as a target for cellular and viral oncogenic mechanisms. *Carcinogenesis*, 24: 1167-1176, 2003.
7. Meyerson, M., Counter, C. M., Eaton, E. N., Ellisen, L. W., Steiner, P., Caddle, S. D., Ziaugra, L., Beijersbergen, R. L., Davidoff, M. J., Liu, Q., Bacchetti, S., Haber, D. A., and Weinberg, R. A. hEST2, the putative human telomerase catalytic subunit gene, is up-regulated in tumor cells and during immortalization. *Cell*, 90: 785-795, 1997.
8. Nakamura, T. M., Morin, G. B., Chapman, K. B., Weinrich, S. L., Andrews, W. H., Lingner, J., Harley, C. B., and Cech, T. R. Telomerase catalytic subunit homologs from fission yeast and human. *Science*, 277: 955-959, 1997.
9. Nakayama, J., Tahara, H., Tahara, E., Saito, M., Ito, K., Nakamura, H., Nakanishi, T., Ide, T., and Ishikawa, F. Telomerase activation by hTERT in human normal fibroblasts and hepatocellular carcinomas. *Nat Genet*, 18: 65-68, 1998.
10. Kilian, A., Bowtell, D. D., Abud, H. E., Hime, G. R., Venter, D. J., Keese, P. K., Duncan, E. L., Reddel, R. R., and Jefferson, R. A. Isolation of a candidate human telomerase catalytic subunit gene, which reveals complex splicing patterns in different cell types. *Hum Mol Genet*, 6: 2011-2019, 1997.
11. Reddel, R. R., Ke, Y., Gerwin, B. I., McMenamin, M. G., Lechner, J. F., Su, R. T., Brash, D. E., Park, J. B., Rhim, J. S., and Harris, C. C. Transformation of human bronchial epithelial cells by infection with SV40 or adenovirus-12 SV40 hybrid virus, or transfection via strontium phosphate coprecipitation with a plasmid containing SV40 early region genes. *Cancer Res*, 48: 1904-1909, 1988.
12. Lundberg, A. S., Randell, S. H., Stewart, S. A., Elenbaas, B., Hartwell, K. A., Brooks, M. W., Fleming, M. D., Olsen, J. C., Miller, S. W., Weinberg, R. A., and Hahn, W. C. Immortalization and transformation of primary human airway epithelial cells by gene transfer. *Oncogene*, 21: 4577-4586, 2002.
13. Barbacid, M. ras genes. *Annu Rev Biochem*, 56: 779-827, 1987.
14. Bos, J. L. ras oncogenes in human cancer: a review. *Cancer Res*, 49: 4682-4689, 1989.

15. Paez, J. G., Janne, P. A., Lee, J. C., Tracy, S., Greulich, H., Gabriel, S., Herman, P., Kaye, F. J., Lindeman, N., Boggon, T. J., Naoki, K., Sasaki, H., Fujii, Y., Eck, M. J., Sellers, W. R., Johnson, B. E., and Meyerson, M. EGFR mutations in lung cancer: correlation with clinical response to gefitinib therapy. *Science*, 304: 1497-1500, 2004.
16. Pao, W., Miller, V., Zakowski, M., Doherty, J., Politi, K., Sarkaria, I., Singh, B., Heelan, R., Rusch, V., Fulton, L., Mardis, E., Kupfer, D., Wilson, R., Kris, M., and Varmus, H. EGF receptor gene mutations are common in lung cancers from "never smokers" and are associated with sensitivity of tumors to gefitinib and erlotinib. *Proc Natl Acad Sci U S A*, 101: 13306-13311, 2004.
17. Brummelkamp, T. R., Bernards, R., and Agami, R. Stable suppression of tumorigenicity by virus-mediated RNA interference. *Cancer Cell*, 2: 243-247, 2002.
18. Brummelkamp, T. R., Bernards, R., and Agami, R. A system for stable expression of short interfering RNAs in mammalian cells. *Science*, 296: 550-553, 2002.
19. Amann, J., Kalyankrishna, S., Massion, P. P., Ohm, J. E., Girard, L., Shigematsu, H., Peyton, M., Juroske, D., Huang, Y., Stuart Salmon, J., Kim, Y. H., Pollack, J. R., Yanagisawa, K., Gazdar, A., Minna, J. D., Kurie, J. M., and Carbone, D. P. Aberrant epidermal growth factor receptor signaling and enhanced sensitivity to EGFR inhibitors in lung cancer. *Cancer Res*, 65: 226-235, 2005.
20. Sato, M., Girard, L., Sekine, I., Sunaga, N., Ramirez, R. D., Kamibayashi, C., and Minna, J. D. Increased expression and no mutation of the Flap endonuclease (FEN1) gene in human lung cancer. *Oncogene*, 22: 7243-7246, 2003.
21. Nishikawa, T., Maemura, K., Hirata, I., Matsuse, R., Morikawa, H., Toshina, K., Murano, M., Hashimoto, K., Nakagawa, Y., Saitoh, O., Uchida, K., and Katsu, K. A simple method of detecting K-ras point mutations in stool samples for colorectal cancer screening using one-step polymerase chain reaction/restriction fragment length polymorphism analysis. *Clin Chim Acta*, 318: 107-112, 2002.
22. Burbee, D. G., Forgacs, E., Zochbauer-Muller, S., Shivakumar, L., Fong, K., Gao, B., Randle, D., Kondo, M., Virmani, A., Bader, S., Sekido, Y., Latif, F., Milchgrub, S., Toyooka, S., Gazdar, A. F., Lerman, M. I., Zbarovsky, E., White, M., and Minna, J. D. Epigenetic inactivation of RASSF1A in lung and breast cancers and malignant phenotype suppression. *J Natl Cancer Inst*, 93: 691-699, 2001.
23. Vaughan, M. B., Ramirez, R. D., Brown, S. A., Yang, J. C., Wright, W. E., and Shay, J. W. A reproducible laser-wounded skin equivalent model to study the effects of aging in vitro. *Rejuvenation Res*, 7: 99-110, 2004.
24. Fridman, R., Giaccone, G., Kanemoto, T., Martin, G. R., Gazdar, A. F., and Mulshine, J. L. Reconstituted basement membrane (matrigel) and laminin can enhance the tumorigenicity and the drug resistance of small cell lung cancer cell lines. *Proc Natl Acad Sci U S A*, 87: 6698-6702, 1990.
25. Shigematsu, H., Lin, L., Takahashi, T., Nomura, M., Suzuki, M., Wistuba, II, Fong, K. M., Lee, H., Toyooka, S., Shimizu, N., Fujisawa, T., Feng, Z., Roth, J. A., Herz, J., Minna, J. D., and Gazdar, A. F. Clinical and biological features associated with epidermal growth factor receptor gene mutations in lung cancers. *J Natl Cancer Inst*, 97: 339-346, 2005.
26. Sordella, R., Bell, D. W., Haber, D. A., and Settleman, J. Gefitinib-sensitizing EGFR mutations in lung cancer activate anti-apoptotic pathways. *Science*, 305: 1163-1167, 2004.

27. Muda, M., Boschert, U., Dickinson, R., Martinou, J. C., Martinou, I., Camps, M., Schlegel, W., and Arkinstall, S. MKP-3, a novel cytosolic protein-tyrosine phosphatase that exemplifies a new class of mitogen-activated protein kinase phosphatase. *J Biol Chem*, 271: 4319-4326, 1996.
28. Groom, L. A., Sneddon, A. A., Alessi, D. R., Dowd, S., and Keyse, S. M. Differential regulation of the MAP, SAP and RK/p38 kinases by Pyst1, a novel cytosolic dual-specificity phosphatase. *Embo J*, 15: 3621-3632, 1996.
29. Reddel, R. R., Ke, Y., Kaighn, M. E., Malan-Shibley, L., Lechner, J. F., Rhim, J. S., and Harris, C. C. Human bronchial epithelial cells neoplastically transformed by v-Ki-ras: altered response to inducers of terminal squamous differentiation. *Oncogene Res*, 3: 401-408, 1988.
30. Ura, H., Bonfil, R. D., Reich, R., Reddel, R., Pfeifer, A., Harris, C. C., and Klein-Szanto, A. J. Expression of type IV collagenase and procollagen genes and its correlation with the tumorigenic, invasive, and metastatic abilities of oncogene-transformed human bronchial epithelial cells. *Cancer Res*, 49: 4615-4621, 1989.
31. Yoakum, G. H., Lechner, J. F., Gabrielson, E. W., Korba, B. E., Malan-Shibley, L., Willey, J. C., Valerio, M. G., Shamsuddin, A. M., Trump, B. F., and Harris, C. C. Transformation of human bronchial epithelial cells transfected by Harvey ras oncogene. *Science*, 227: 1174-1179, 1985.
32. Reddel, R. R., Salghetti, S. E., Willey, J. C., Ohnuki, Y., Ke, Y., Gerwin, B. I., Lechner, J. F., and Harris, C. C. Development of tumorigenicity in simian virus 40-immortalized human bronchial epithelial cell lines. *Cancer Res*, 53: 985-991, 1993.
33. Hurlin, P. J., Fry, D. G., Maher, V. M., and McCormick, J. J. Morphological transformation, focus formation, and anchorage independence induced in diploid human fibroblasts by expression of a transfected H-ras oncogene. *Cancer Res*, 47: 5752-5757, 1987.
34. Kinch, M. S., Clark, G. J., Der, C. J., and Burridge, K. Tyrosine phosphorylation regulates the adhesions of ras-transformed breast epithelia. *J Cell Biol*, 130: 461-471, 1995.
35. Meerson, A., Milyavsky, M., and Rotter, V. p53 mediates density-dependent growth arrest. *FEBS Lett*, 559: 152-158, 2004.
36. Alexandrova, A., Ivanov, A., Chumakov, P., Kopnin, B., and Vasiliev, J. Changes in p53 expression in mouse fibroblasts can modify motility and extracellular matrix organization. *Oncogene*, 19: 5826-5830, 2000.
37. Sablina, A. A., Chumakov, P. M., and Kopnin, B. P. Tumor suppressor p53 and its homologue p73alpha affect cell migration. *J Biol Chem*, 278: 27362-27371, 2003.
38. Tsao, M. S., Zhu, H., and Viallet, J. Autocrine growth loop of the epidermal growth factor receptor in normal and immortalized human bronchial epithelial cells. *Exp Cell Res*, 223: 268-273, 1996.
39. Plowman, G. D., Green, J. M., McDonald, V. L., Neubauer, M. G., Distèche, C. M., Todaro, G. J., and Shoyab, M. The amphiregulin gene encodes a novel epidermal growth factor-related protein with tumor-inhibitory activity. *Mol Cell Biol*, 10: 1969-1981, 1990.
40. Cook, P. W., Mattox, P. A., Keeble, W. W., Pittelkow, M. R., Plowman, G. D., Shoyab, M., Adelman, J. P., and Shipley, G. D. A heparin sulfate-regulated human keratinocyte autocrine factor is similar or identical to amphiregulin. *Mol Cell Biol*, 11: 2547-2557, 1991.

41. Lemjabbar, H., Li, D., Gallup, M., Sidhu, S., Drori, E., and Basbaum, C. Tobacco smoke-induced lung cell proliferation mediated by tumor necrosis factor alpha-converting enzyme and amphiregulin. *J Biol Chem*, 278: 26202-26207, 2003.
42. Glover, K. Y., Perez-Soler, R., and Papadimitradopoulou, V. A. A review of small-molecule epidermal growth factor receptor-specific tyrosine kinase inhibitors in development for non-small cell lung cancer. *Semin Oncol*, 31: 83-92, 2004.
43. Perez-Soler, R. The role of erlotinib (Tarceva, OSI 774) in the treatment of non-small cell lung cancer. *Clin Cancer Res*, 10: 4238s-4240s, 2004.
44. Ciardiello, F., Caputo, R., Bianco, R., Damiano, V., Pomatico, G., De Placido, S., Bianco, A. R., and Tortora, G. Antitumor effect and potentiation of cytotoxic drugs activity in human cancer cells by ZD-1839 (Iressa), an epidermal growth factor receptor-selective tyrosine kinase inhibitor. *Clin Cancer Res*, 6: 2053-2063, 2000.
45. Wakeling, A. E., Guy, S. P., Woodburn, J. R., Ashton, S. E., Curry, B. J., Barker, A. J., and Gibson, K. H. ZD1839 (Iressa): an orally active inhibitor of epidermal growth factor signaling with potential for cancer therapy. *Cancer Res*, 62: 5749-5754, 2002.
46. Perez-Soler, R., Chachoua, A., Hammond, L. A., Rowinsky, E. K., Huberman, M., Karp, D., Rigas, J., Clark, G. M., Santabarbara, P., and Bonomi, P. Determinants of tumor response and survival with erlotinib in patients with non--small-cell lung cancer. *J Clin Oncol*, 22: 3238-3247, 2004.
47. Lu, C., Speers, C., Zhang, Y., Xu, X., Hill, J., Steinbis, E., Celestino, J., Shen, Q., Kim, H., Hilsenbeck, S., Mohsin, S. K., Wakeling, A., Osborne, C. K., and Brown, P. H. Effect of epidermal growth factor receptor inhibitor on development of estrogen receptor-negative mammary tumors. *J Natl Cancer Inst*, 95: 1825-1833, 2003.
48. Di Gennaro, E., Barbarino, M., Bruzzese, F., De Lorenzo, S., Caraglia, M., Abbruzzese, A., Avallone, A., Comella, P., Caponigro, F., Pepe, S., and Budillon, A. Critical role of both p27KIP1 and p21CIP1/WAF1 in the antiproliferative effect of ZD1839 ('Iressa'), an epidermal growth factor receptor tyrosine kinase inhibitor, in head and neck squamous carcinoma cells. *J Cell Physiol*, 195: 139-150, 2003.
49. Sgambato, A., Camerini, A., Faraglia, B., Ardito, R., Bianchino, G., Spada, D., Boninsegna, A., Valentini, V., and Cittadini, A. Targeted inhibition of the epidermal growth factor receptor-tyrosine kinase by ZD1839 ('Iressa') induces cell-cycle arrest and inhibits proliferation in prostate cancer cells. *J Cell Physiol*, 201: 97-105, 2004.
50. Shintani, S., Li, C., Mihara, M., Yano, J., Terakado, N., Nakashiro, K., and Hamakawa, H. Gefitinib ('Iressa', ZD1839), an epidermal growth factor receptor tyrosine kinase inhibitor, up-regulates p27KIP1 and induces G1 arrest in oral squamous cell carcinoma cell lines. *Oral Oncol*, 40: 43-51, 2004.
51. Chang, G. C., Hsu, S. L., Tsai, J. R., Liang, F. P., Lin, S. Y., Sheu, G. T., and Chen, C. Y. Molecular mechanisms of ZD1839-induced G1-cell cycle arrest and apoptosis in human lung adenocarcinoma A549 cells. *Biochem Pharmacol*, 68: 1453-1464, 2004.
52. Chinnaiyan, P., Huang, S., Vallabhaneni, G., Armstrong, E., Varambally, S., Tomlins, S. A., Chinnaiyan, A. M., and Harari, P. M. Mechanisms of enhanced radiation response following epidermal growth factor receptor signaling inhibition by erlotinib (Tarceva). *Cancer Res*, 65: 3328-3335, 2005.
53. Zhang, W., Siu, L. L., Moore, M. J., and Chen, E. X. Simultaneous determination of OSI-774 and its major metabolite OSI-420 in human plasma by using HPLC with UV detection. *J Chromatogr B Analyt Technol Biomed Life Sci*, 814: 143-147, 2005.

54. Ranson, M. and Wardell, S. Gefitinib, a novel, orally administered agent for the treatment of cancer. *J Clin Pharm Ther*, 29: 95-103, 2004.
55. Agapova, L. S., Ivanov, A. V., Sablina, A. A., Kopnin, P. B., Sokova, O. I., Chumakov, P. M., and Kopnin, B. P. P53-dependent effects of RAS oncogene on chromosome stability and cell cycle checkpoints. *Oncogene*, 18: 3135-3142, 1999.
56. Hahn, W. C., Dessain, S. K., Brooks, M. W., King, J. E., Elenbaas, B., Sabatini, D. M., DeCaprio, J. A., and Weinberg, R. A. Enumeration of the simian virus 40 early region elements necessary for human cell transformation. *Mol Cell Biol*, 22: 2111-2123, 2002.
57. Duursma, A. and Agami, R. p53-Dependent regulation of Cdc6 protein stability controls cellular proliferation. *Mol Cell Biol*, 25: 6937-6947, 2005.

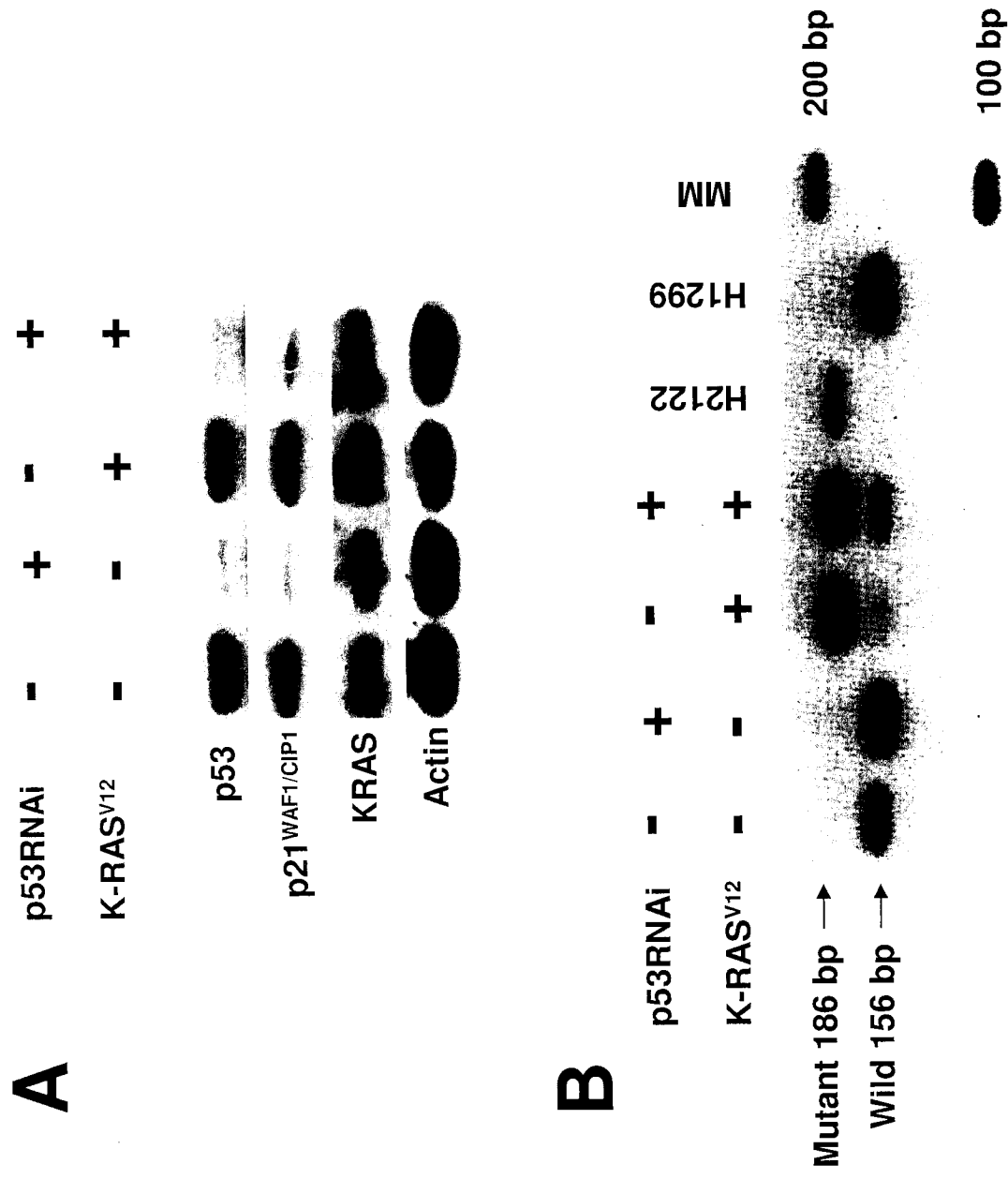


Fig.1 Sato et al.

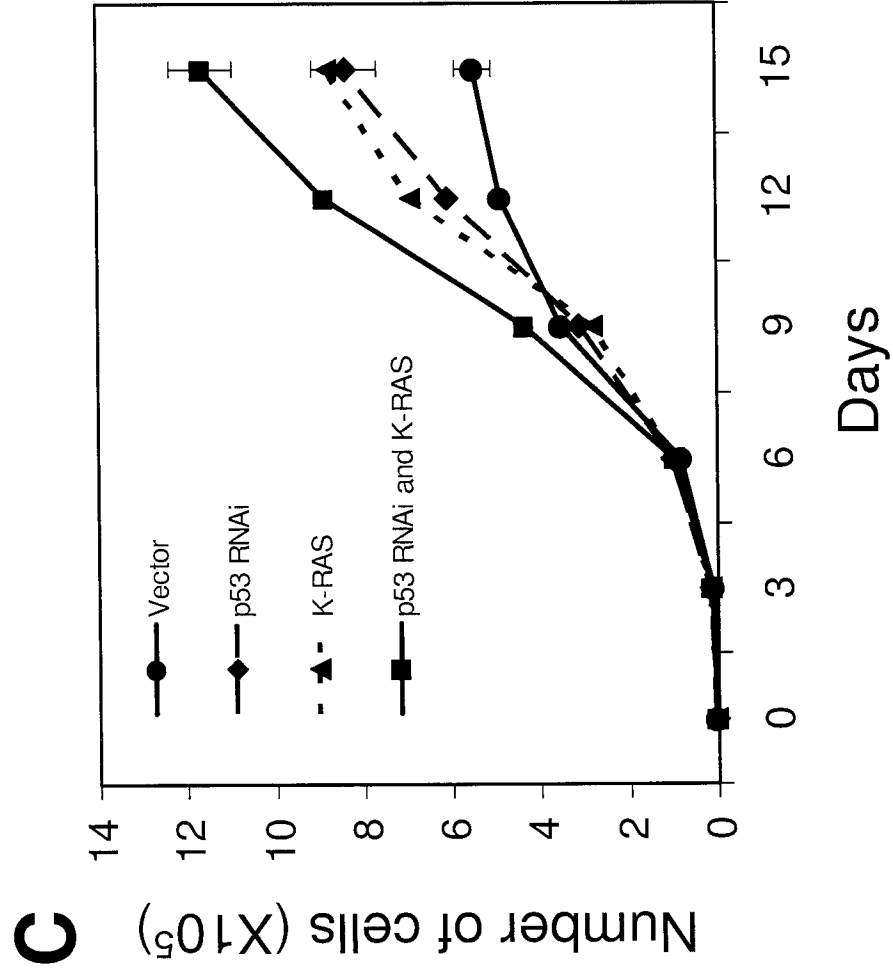


Fig.1 Sato et al.

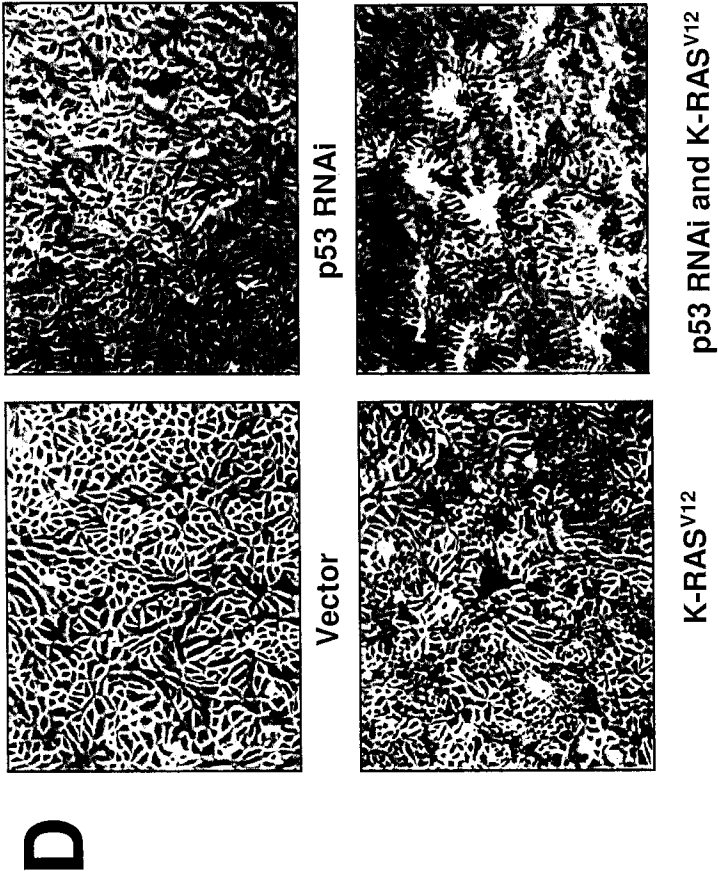


Fig.1 Sato et al.

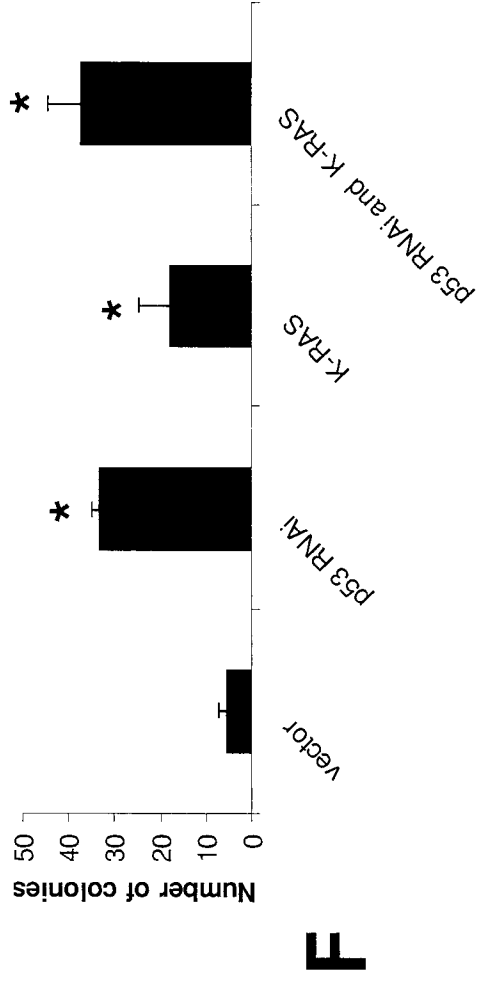
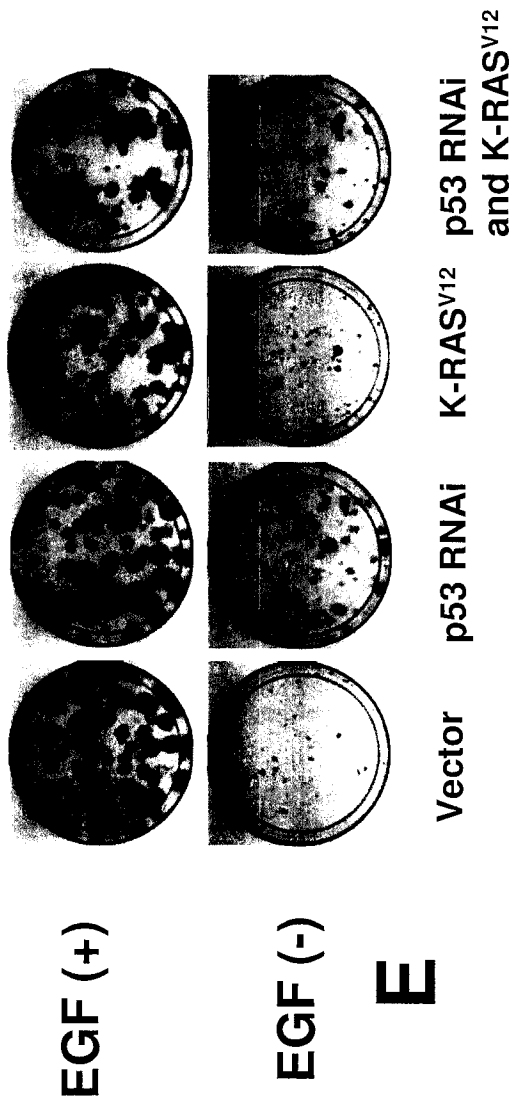


Fig.1 Sato et al.

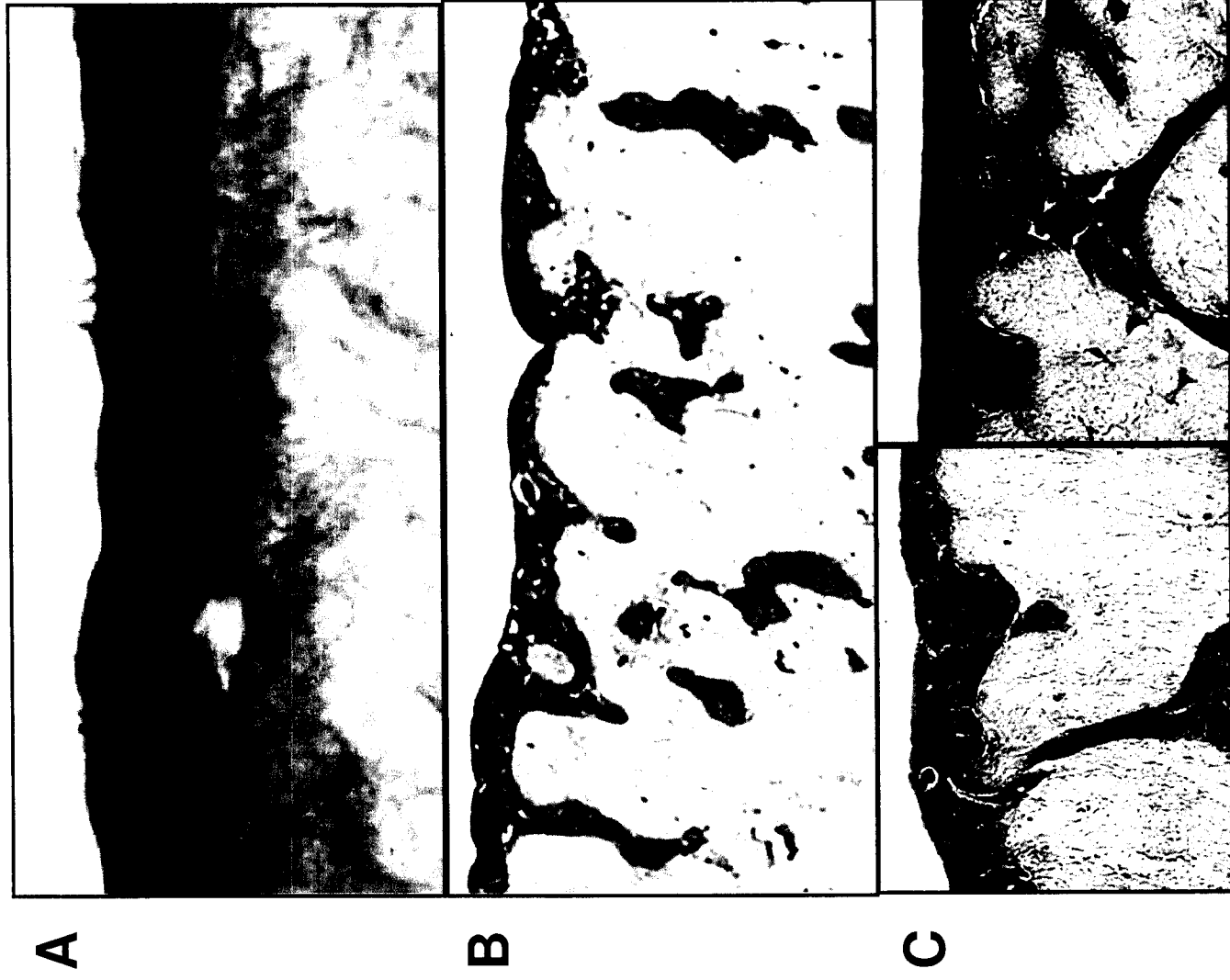


Fig.2 Sato et al.

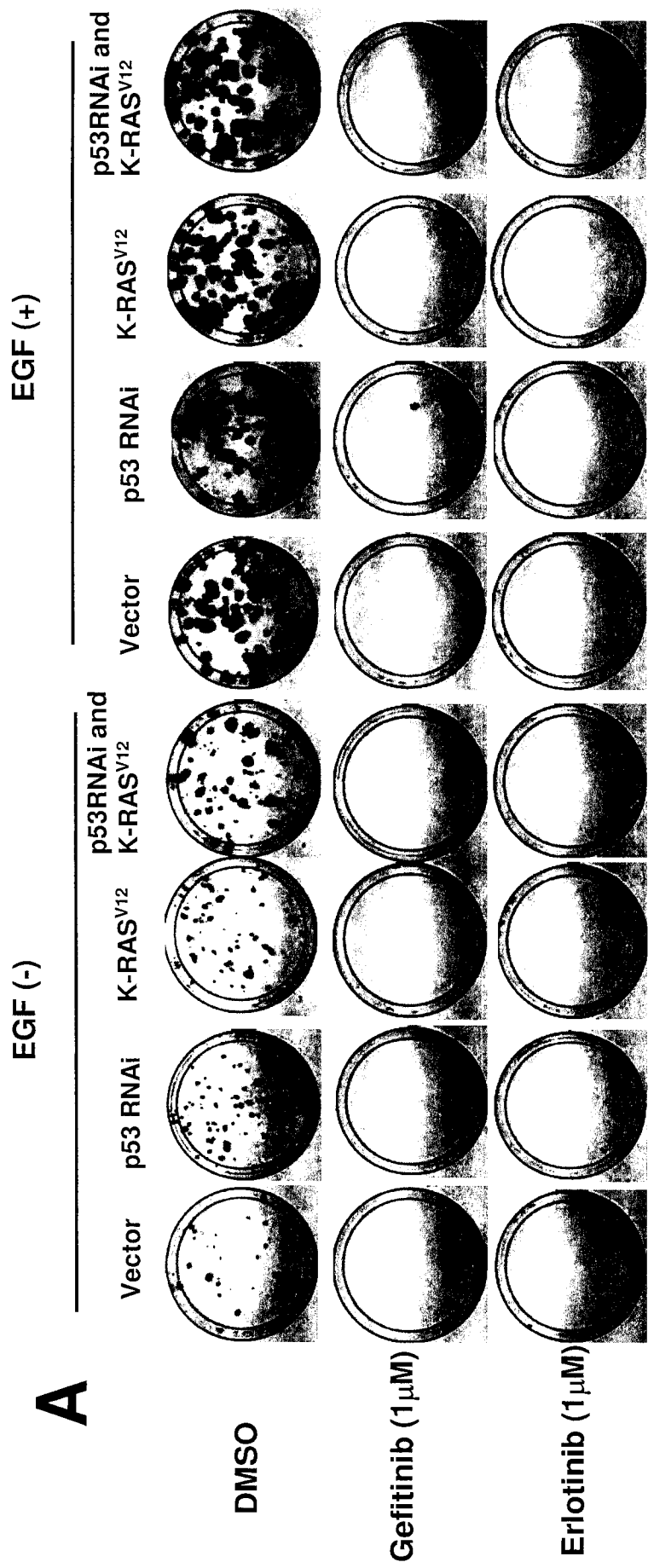


Fig.3 Sato et al.

Fig.3 Sato et al.

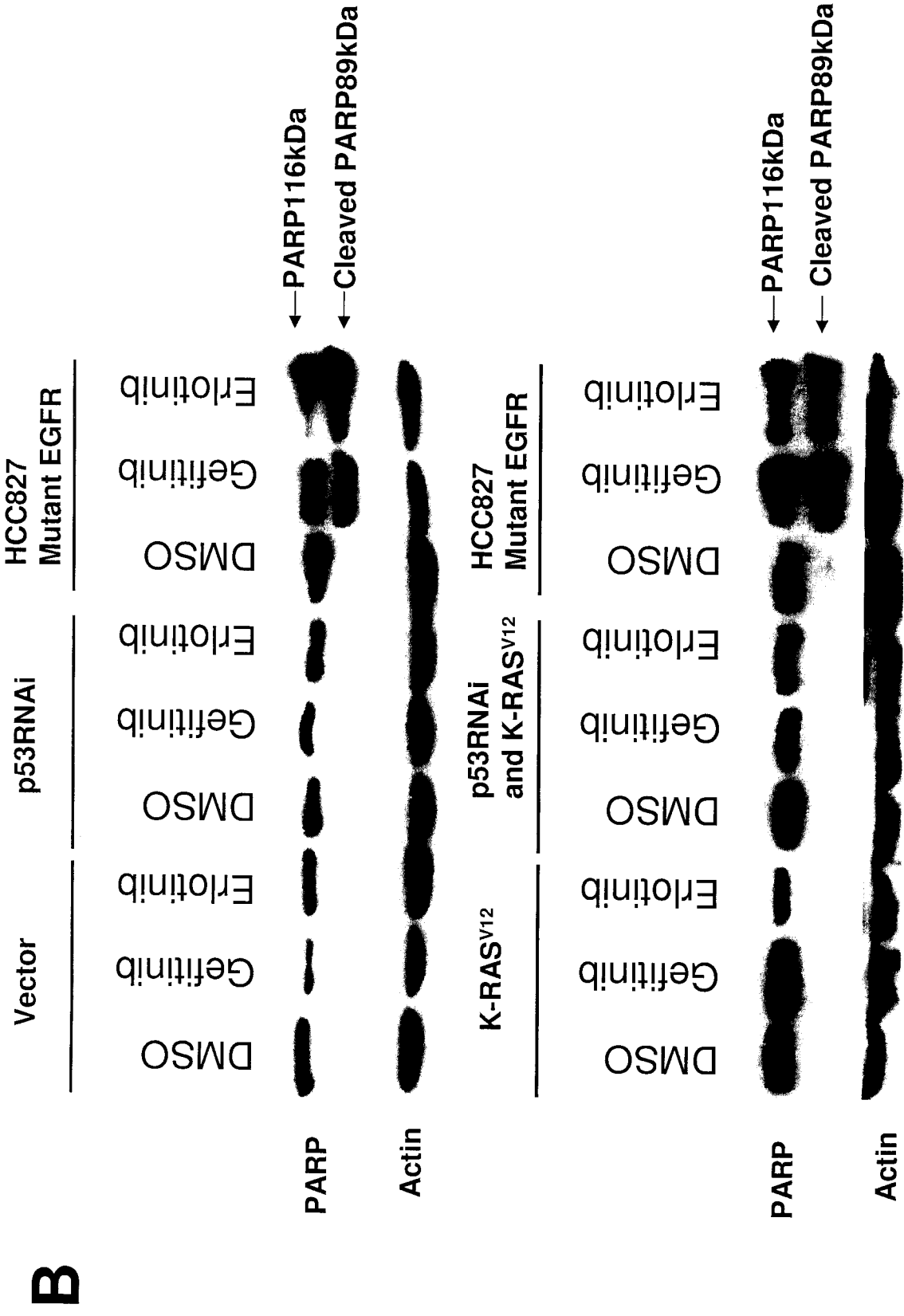
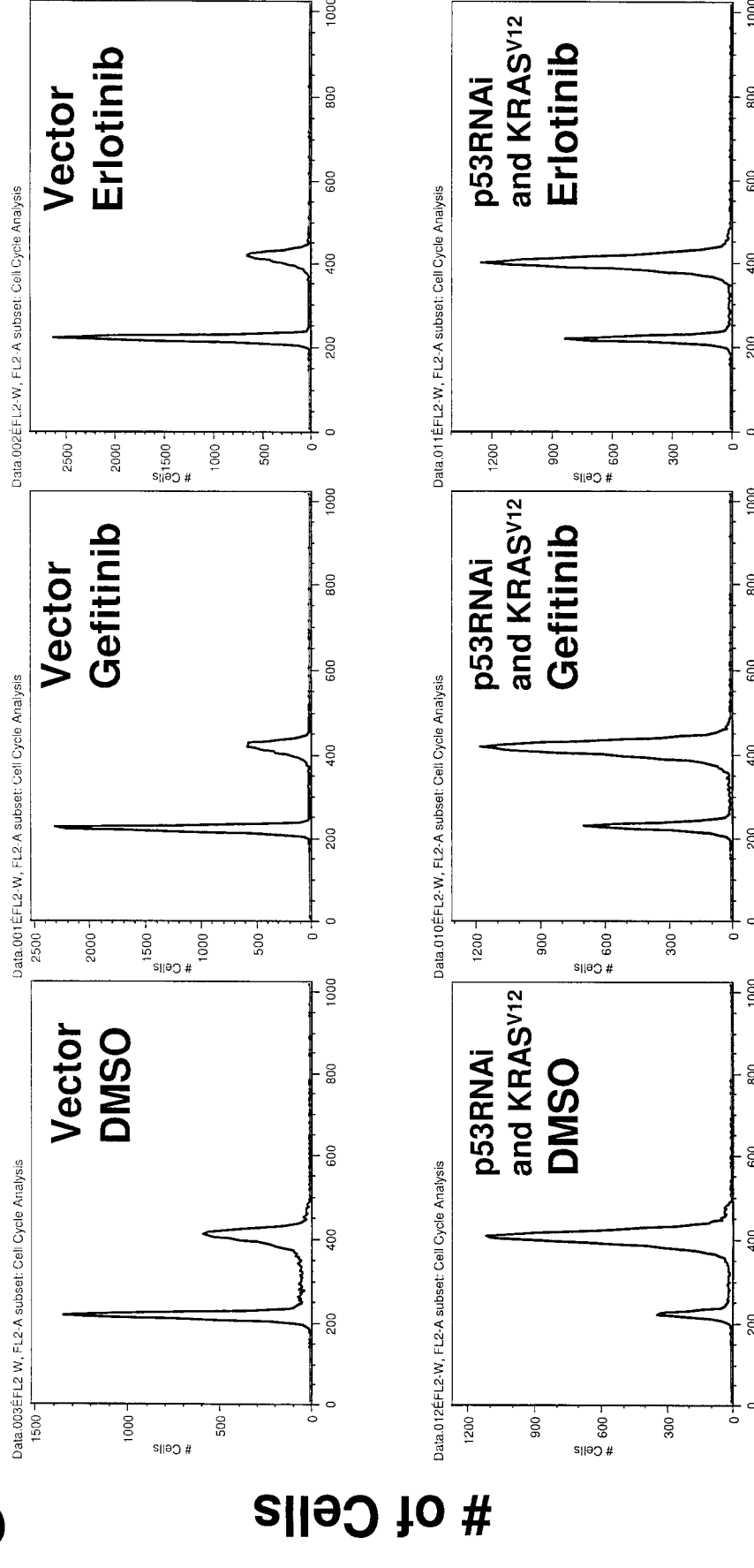


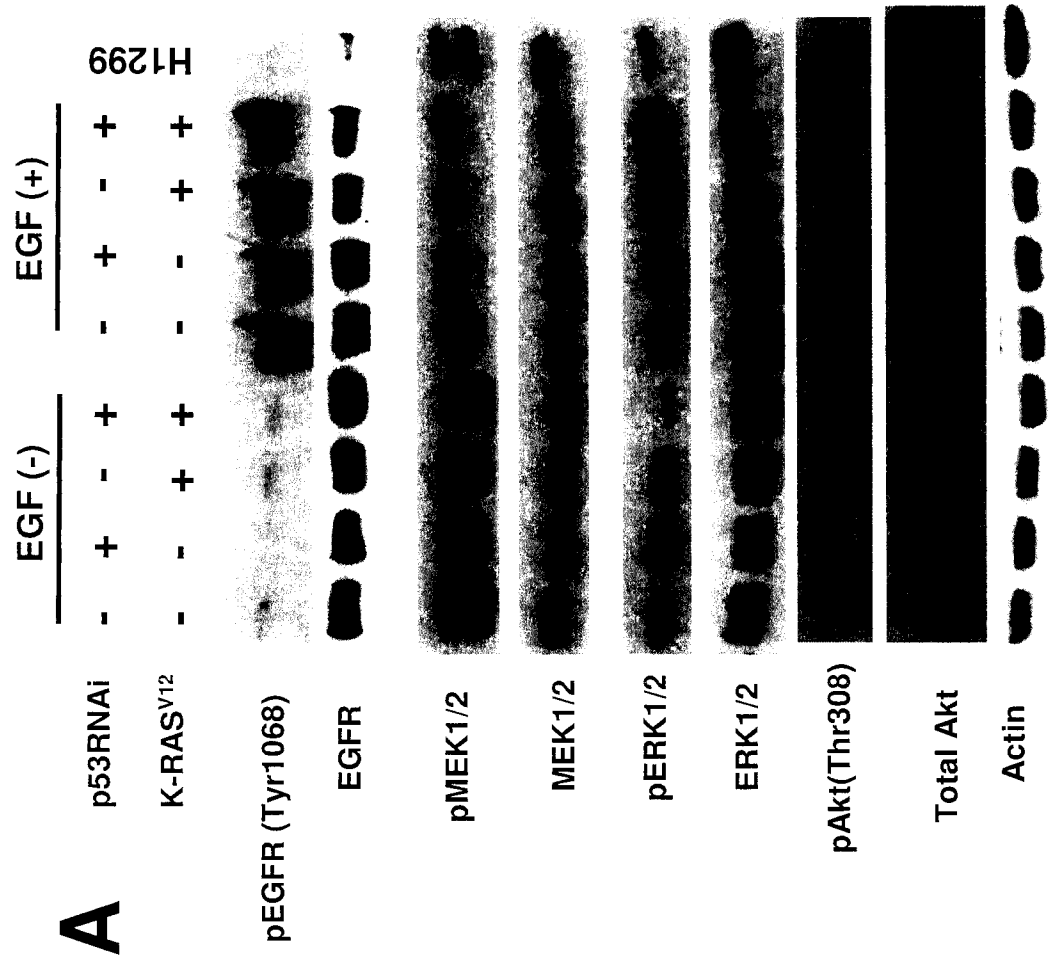
Fig.3 Sato et al.

C



DNA content

Fig.4 Sato et al.



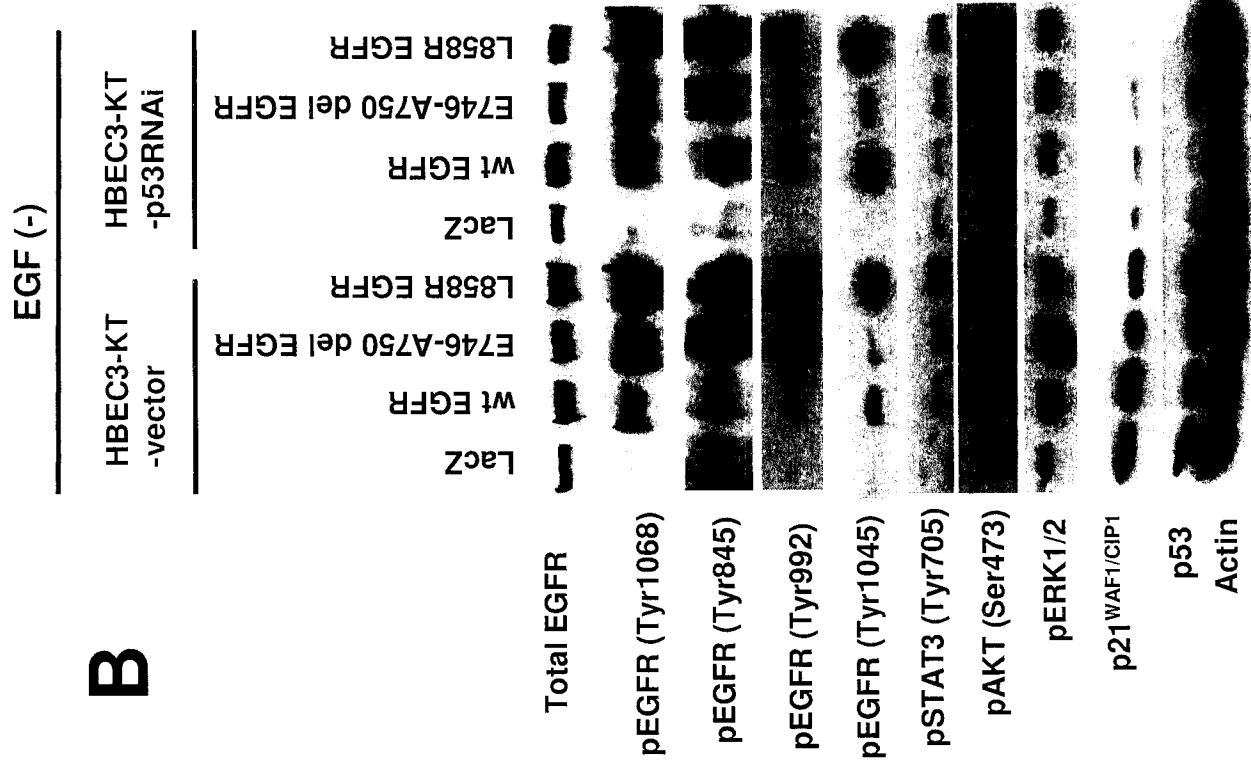


Fig.4 Sato et al.

Fig.4 Sato et al.

C

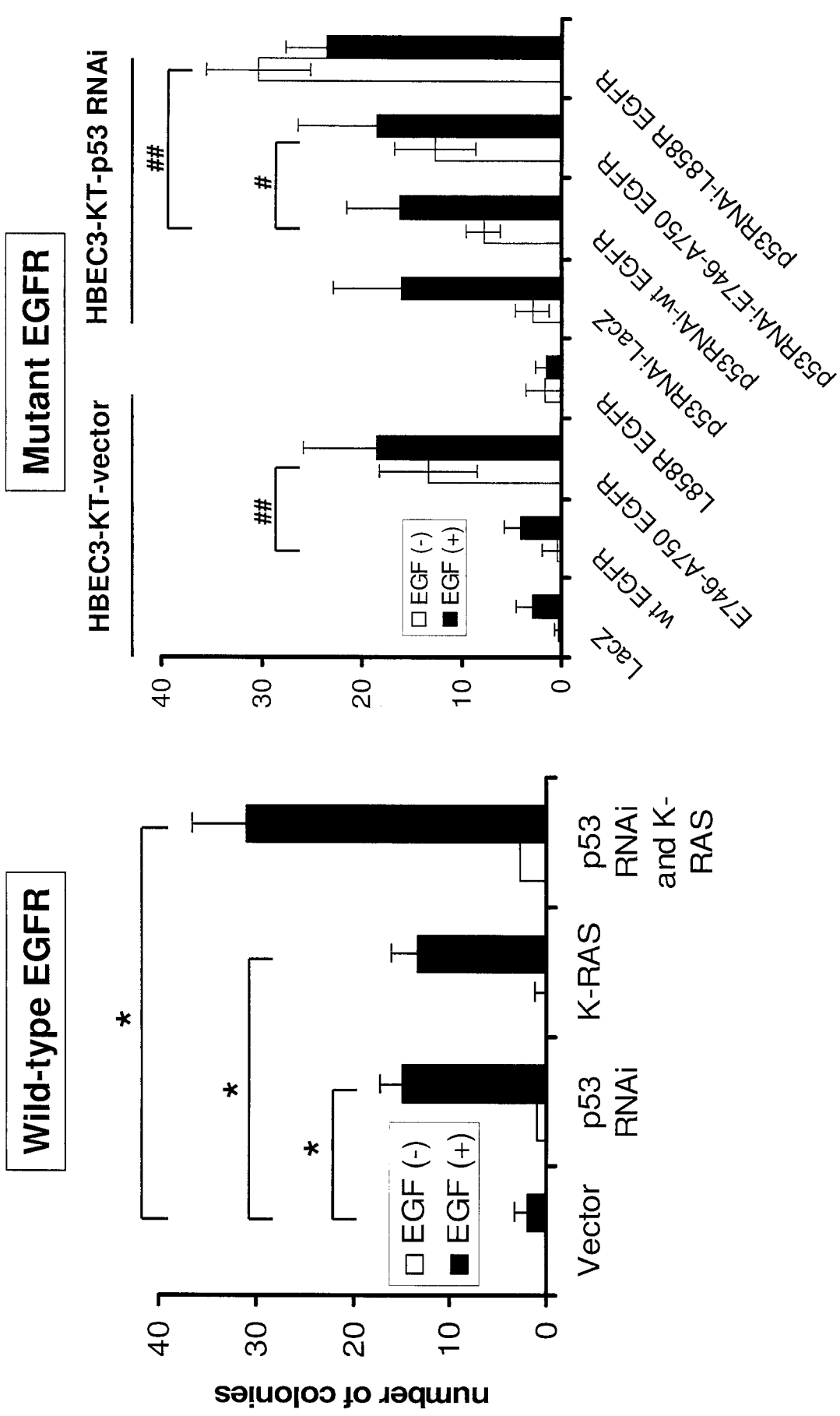
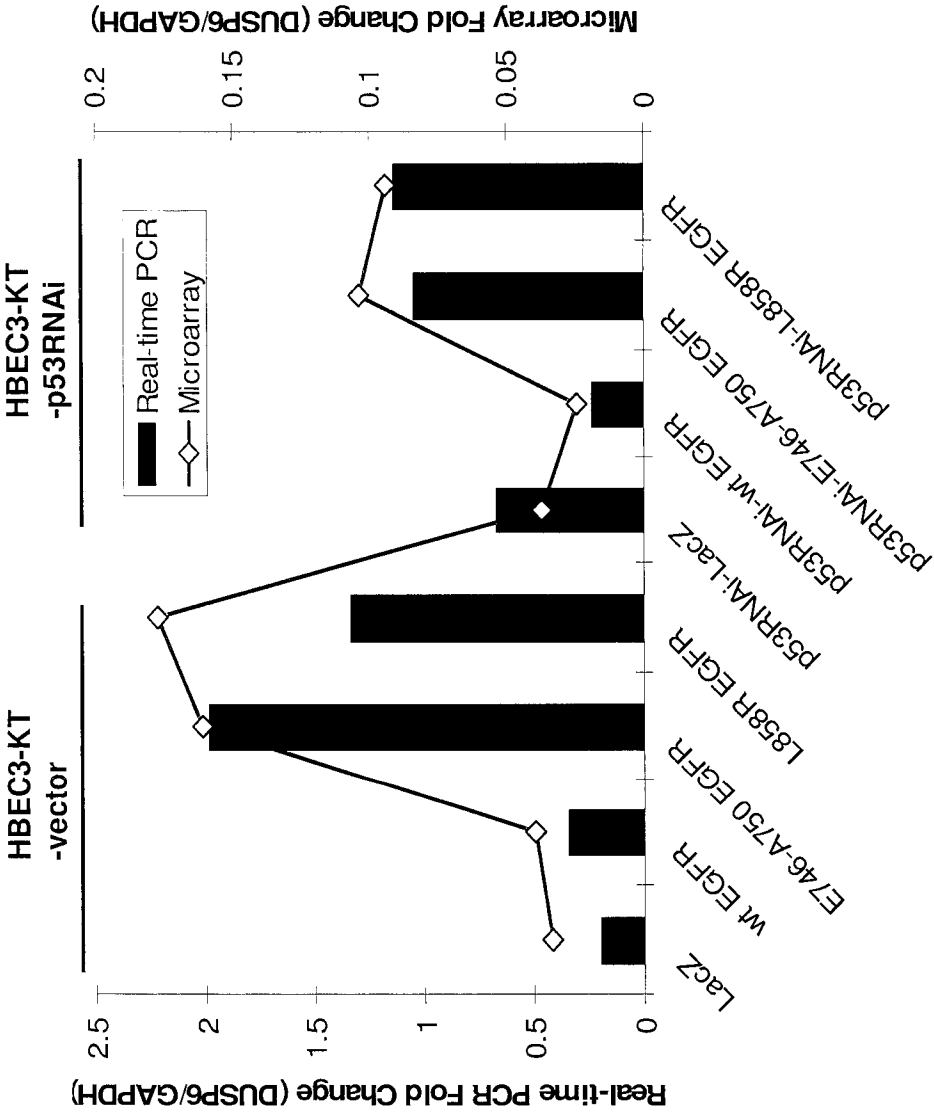


Fig.4 Sato et al.

D





Chemopreventive agent-induced modulation of death receptors

S.-Y. Sun

Department of Hematology and Oncology, Winship Cancer Institute, Emory University School of Medicine, Atlanta, Georgia USA

Published online: 3 October 2005

The goals of chemoprevention of cancer are to inhibit the initiation or suppress the promotion and progression of preneoplastic lesions to invasive cancer through the use specific natural or synthetic agents. Therefore, a more desirable and aggressive approach is to eliminate aberrant clones by inducing apoptosis rather than merely slowing down their proliferation. The increased understanding of apoptosis pathways has directed attention to components of these pathways as potential targets not only for chemotherapeutic but also for chemopreventive agents. Activation of death receptors triggers an extrinsic apoptotic pathway, which plays a critical role in tumor immunosurveillance. An increasing number of previously identified chemopreventive agents were found to induce apoptosis in a variety of premalignant and malignant cell types *in vitro* and in a few animal models *in vivo*. Some chemopreventive agents such as non-steroidal anti-inflammatory drugs, triterpenoids, and retinoids increase the expression of death receptors. Thus, understanding the modulation of death receptors by chemopreventive agents and their implications in chemoprevention may provide a rational approach for using such agents alone or in combination with other agents to enhance death receptor-mediated apoptosis as a strategy for effective chemoprevention of cancer.

Keywords: apoptosis; chemoprevention; chemopreventive agents; death receptors.

Introduction

Epithelial carcinogenesis is a multi-year (sometime decade-long) process of clonal selection and evolution of genetically damaged cells, leading to the abnormal precancer phenotype that eventually becomes invasive cancer.¹ Therefore, carcinogenesis is a chronic disease process. This nature of carcinogenesis provides a strong rationale for cancer intervention or prevention as an attractive strategy to control cancer incidence and mortality. If such a process is arrested, delayed, or reversed, cancer incidence

may be markedly reduced, eventually leading to a decline in cancer mortality rates. Such an approach is called chemoprevention, which is defined as the use of pharmacological or natural agents to inhibit the development of invasive cancer either by blocking the DNA damage that initiates carcinogenesis or by arresting or reversing the progression of premalignant cells in which such damage has already occurred.^{2,3} Several thousand agents have been reported to have chemopreventive activity.⁴ Some of the promising agents and agent combinations have been evaluated clinically for chemoprevention of major cancer types for the past few decades.² Clinical practice of chemoprevention has shown some success in reversing premalignant lesions, reducing the risk of developing second primary tumors, and decreasing cancer incidence.^{4,5} Thus, chemoprevention has emerged as an integral part of cancer control.

Apoptosis or programmed cell death is a genetically controlled mechanism essential for the maintenance of tissue homeostasis, proper development, and the elimination of unwanted cells. Thus, it represents a universal and exquisitely efficient endogenous or induced cellular suicide pathway and can be induced in many cell types via numerous physiological, biochemical and/or noxious stimuli.^{6,7} Because defects in apoptotic pathways or the inhibition of apoptosis play important roles in cancer development or carcinogenesis,⁸ targeting the induction of apoptosis in premalignant or malignant lesions may selectively eliminate aberrant precancerous clones or cancer cells while sparing normal cells. Therefore, the induction of apoptosis should be efficient not only for chemotherapy but also for chemoprevention. In comparison with other strategies that merely slow down proliferation, the induction of apoptosis appears to be a more desirable and aggressive chemopreventive approach to eliminate aberrant clones (reviewed in⁹).

Death receptors are key components in the extrinsic apoptotic pathway.¹⁰ Their activation due to ligand binding or increased expression triggers an extrinsic apoptotic signaling pathway leading to apoptosis. The expression of death receptors is inducible by many small molecules

Correspondence to: S.-Y. Sun, Winship Cancer Institute, Emory University School of Medicine, 1365-C Clifton Road, C3088, Atlanta, GA 30322, USA. Tel.: (404) 778-2170; Fax: (404) 778-5520; e-mail: shi-yong.sun@emoryhealthcare.org

including some chemopreventive agents. This review article will highlight the recent studies on the modulation of death receptors by chemopreventive agents and discuss their implications in chemoprevention.

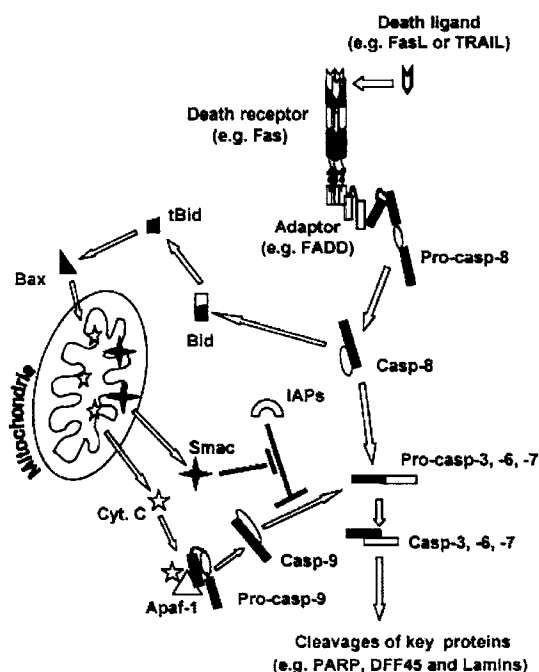
Death receptor-mediated apoptotic pathway

There are generally two major apoptotic pathways: the first involves signals transduced through death receptors; the second relies on a signal from mitochondria. Both pathways are involved in a concerted activation of a set of cysteine proteases called caspases, which in turn cleave cellular substrates and result in the characteristic morphological and biochemical changes constituting the process of apoptosis (reviewed in^{1,2}) (Figure 1).

Death receptors, including tumor necrosis factor (TNF) receptor (TNFR), Fas (CD95 or APO-1), DR3, DR4 (TRAIL-R1), DR5 (TRAIL-R2) and DR6, belong to the TNF receptor gene superfamily. They are defined by similar, cysteine-rich extracellular domains and additional cytoplasmic death domains (reviewed in³). The death domain is crucial for transmitting the death signal from the cell surface to intracellular signaling pathways. Upon ligand binding or overexpression, death receptors such as Fas are clustered to form a trimer in the cell membrane, which results in recruitment of adaptor proteins such as Fas-associated death domain (FADD) via death domain interactions. The FADD protein, containing both a death domain and an additional protein interaction domain called a death effector domain (DED), further binds via DED interactions to caspase-8, and possibly caspase-10, resulting in the recruitment and autoactivation of caspase-8. This process is referred to as the formation of the death-inducing signaling complex (DISC), an essential step in the activation of the extrinsic apoptotic pathway. The activated caspase-8 then acts to cleave and activate downstream effector caspases such as caspase-3.^{4,5} In addition to directly activating the downstream effector caspases, death receptors also indirectly activate them through Bid-mediated cytochrome C release and subsequent caspase-9 activation because Bid is a substrate of caspase-8 and can be cleaved or activated by caspase-8.^{6,7} Thus, Bid, a BH3-only protein of the bcl-2 family, provides a link and an integration between the extrinsic death receptor and intrinsic mitochondrial apoptotic pathways.

Although TNFR and Fas have been extensively studied, DR4 and DR5 recently have attracted considerable attention since their ligand TNF-related apoptosis-inducing ligand (TRAIL) has been shown to predominantly induce apoptosis of cancer cells, while sparing normal cells, showing a great potential in cancer therapy (reviewed in⁸⁻¹¹). Like Fas, both DR4 and DR5 primarily act as inducers of apoptosis, distin-

Figure 1. Schema for basic apoptotic signaling pathways. Ligation of death ligands (e.g. FasL or TRAIL) with their receptors (e.g. Fas or DR4 and DR5) results in activation of caspase-8 (Casp-8) through a death adaptor protein FADD. Certain stress signals (e.g. DNA damage) can target mitochondria and induce cytochrome C (Cyt. C) release from mitochondria into cytosol leading to caspase-9 (Casp-9) activation via binding to Apaf-1. Both caspase-8 and caspase-9 activate downstream caspase-3 (Casp-3), caspase-6 (Casp-6) and caspase-7 (Casp-7) leading to cleavages of their target proteins such as PARP, DFF45 and lamins. In addition, truncated Bid (tBid), activated by caspase-8 via cleavage, facilitates insertion of BAX into mitochondrial membrane leading to Cyt. C release. Therefore, tBid may serve as a link between death receptor- and mitochondria-mediated apoptotic pathways. Inhibitors of apoptosis proteins (IAPs) can bind to activated Casp-9 and prevent its action on effector caspases (e.g. Casp-3), whereas Smac binds to IAPs, leaving Casp-9 free to activate Casp-3.



guishing them from TNFR, which mainly activates the non-apoptotic gene-inducing functions such as NF- κ B and JNK activation.¹⁰ Currently, DR4 and DR5 are important targets for cancer therapy (reviewed in^{15,16,17}).

Death receptors, tumor immunosurveillance, and carcinogenesis

Cancer can be considered a cell clonal expansion disease. The process of clonal expansion involves genetic instability, which may result in some clones becoming predominant and tumorigenic. The growth advantage of aberrant cells or clones results from uncontrolled proliferation and

a loss of the ability to undergo differentiation and apoptosis. Very importantly, the aberrant cells or clones must build up immunosuppressive barriers to withstand or overcome host immune defense or surveillance mechanism (reviewed in ^{8,10}).

Immune surveillance against tumors is mediated by both innate and adaptive components of cellular immunity. The most crucial guardians seem to be natural killer (NK) cells (innate immunity) and cytotoxic T-cells (CTLs) (adaptive immunity). One of the mechanisms by which activated NK cells or CTLs destroy malignant (or virus-infected) cells is mediated through membrane-bound variants of the death ligands CD95L and TRAIL, which induce apoptosis in the target cells via activation of their corresponding death receptors (reviewed in ¹¹). This process can be further enhanced by interferon γ produced by activated NK- and T cells by sensitizing for death receptor-induced apoptosis and by upregulation of TRAIL.¹¹ Thus, the expression of death receptors (*e.g.*, Fas or DR4 and DR5) in premalignant and malignant cells is a prerequisite for immune cells to recognize and eliminate premalignant and malignant cells through death ligand and death receptor interaction.

Accordingly, it is understandable that one effective way for premalignant and malignant cells to escape immunosurveillance is to downregulate or inactivate death receptors on their membrane surface. Mutation analyses of the Fas gene have demonstrated that Fas mutation occurs in 0–65% of hematopoietic malignancies and 0–28% of solid tumors. Among the hematopoietic malignancies, high frequencies of Fas mutations occur in thyroid lymphoma (65.4%), cutaneous T-cell lymphoma (59%), and nasal NK/T cell lymphoma (50%). Among solid tumors, Fas mutations occurs frequently in bladder transitional cell carcinoma (28%) and burn scar-related squamous cell carcinoma (14.3%) (reviewed in ¹²). Compared to Fas, mutation analyses of DR4 and DR5 have been performed less widely in human cancers. In general, the frequencies of DR4 and DR5 mutations in detected cancers are low (0–10.6%) (reviewed in ¹³).

In addition to mutations, downregulation of death receptor expression has also been documented. Decreased expression of Fas was observed in hepatomas compared to normal hepatocytes.¹⁴ Analysis of clinical cancer tissues in normal cervical samples and different grades of cervical intraepithelial neoplasia (CIN) samples revealed that the frequency of Fas-positive staining decreased with the increasing severity of CIN.¹⁴ Analysis of small cell lung cancer (SCLC) tumors revealed reduced levels of Fas and DR4 mRNA compared to non-small cell lung cancer (NSCLC) tumors.^{15,16} The downregulation of Fas and DR4 expression was likely the consequence of methylation of their gene promoters.¹⁵ Although methylation of DR4 and DR5 are generally rare in many cancer types,¹⁷

a recent study identified a high frequency of DR4 methylation (41%) in sporadic pheochromocytomas.¹⁸

Rather than downregulate death receptors, tumor cells sometimes overexpress decoy receptors (DcRs), which lack a functional intracellular death domain and thereby compete with death receptors for death ligands to antagonize apoptosis mediated by the binding of death ligands and death receptors.¹⁰ The gene coding for DcR3, a secreted protein that binds FasL, is amplified in about 50% of lung and colon cancers.¹⁹ In addition, DcR3 is overexpressed in carcinomas of the stomach, esophagus and rectum independently of gene amplification.²⁰ Cells that overexpress DcR3 presumably have a survival advantage because of their ability to resist FasL-mediated attack by cytotoxic lymphocytes, although the role of DcR3 in tumorigenesis remains unclarified. Although DcR1 and DcR2 are generally downregulated in many types of cancer,²¹ one study showed that DcR1 expression was enhanced in primary tumors of the gastrointestinal tract.²¹ It is possible that DcR overexpressing tumors may gain a selective growth advantage by escaping from death ligand/death receptor-induced apoptosis.

Signaling through death receptors can also be negatively regulated by proteins such as FLIP that prevent interaction between FADD and caspase-8.^{11,12} High FLIP expression existing in many tumor cells has been correlated with resistance to death ligand/death receptor-induced apoptosis (reviewed in ^{2,3,5}). In addition, FLIP expression was associated with tumor escape from T-cell immunity and enhanced tumor progression in experimental studies *in vivo* (reviewed in ^{3,4}).

Modulation of death receptors by chemopreventive agents

Many studies have demonstrated that the expression of death receptors, including Fas, DR4 and DR5, is inducible by many small molecules, particularly chemotherapeutic agents. Increased evidence indicates that activation of death receptors positively impacts cancer chemotherapy (reviewed in ¹⁶). An increased number of recent studies also show that some chemopreventive agents such as non-steroidal anti-inflammatory drugs (NSAIDs), retinoids and triterpenoids, induce death receptor expression and enhance death ligand-induced apoptosis as well.

NSAIDs. Sulindac sulfide is one of the major metabolites of sulindac that is believed to mediate its antitumorigenic effects by inducing apoptosis. Sulindac sulfide specifically upregulates DR5 and activates the proximal caspase-8 in various colon and prostate cancer cell lines. Overexpression of a dominant-negative FADD (FADD-DN) suppresses sulindac sulfide-induced apoptosis and combination of sulindac sulfide with TRAIL exhibits an enhanced

apoptosis-inducing effect, suggesting the involvement of DR5 in sulindac sulfide-induced apoptosis.⁵³ Induction of DR5 by sulindac sulfide in gastric cancer cells was also reported recently. In this study, DR4 expression was also induced by sulindac sulfide.⁵⁵ Related to these findings, indomethacin and sulindac sulfide were reported to induce apoptosis of human leukemic Jurkat cells by a mechanism that requires the FADD-mediated activation of a caspase-8-dependent pathway,⁵⁷ implying the importance of a death receptor-mediated apoptotic pathway in their actions.

Celecoxib is another apoptosis-inducing NSAID with cyclooxygenase-2 (COX-2) activity and has been approved by the U.S. Food and Drug Administration (FDA) for the chemoprevention of colon cancer (*i.e.*, treatment of familial adenomatous polyposis, an inherited syndrome that predisposes individuals to colon cancer). Our recent work found that celecoxib increased the expression of DR4 and particularly DR5 at both mRNA and protein levels in human lung cancer cells. This effect appears to be independent of its COX-2 inhibitory activity and occurs at the transcriptional level. Both overexpression of FADD-DN and silencing of DR5 expression using small interfering RNA (siRNA) attenuated celecoxib-induced apoptosis. Moreover, celecoxib cooperated with TRAIL to augment the induction of apoptosis. These results indicate that the expression of death receptors, particularly DR5, contributes to celecoxib-induced apoptosis.⁵⁸

Retinoids. Retinoids refer to an entire group of natural and synthetic retinol (vitamin A) metabolites and analogues and have long been considered promising chemopreventive agents.⁵⁹ The synthetic retinoid CD437 potently induces apoptosis in a variety of human cancer cells. Our studies showed that CD437 induced Fas, DR4 and DR5 expression primarily in lung cancer cell lines with wild-type p53.^{11,40,41} The induction of these death receptors correlated with their potencies in inducing apoptosis in these cell lines.⁶⁰⁻⁶² Inactivation of p53 using HPV16 E6 abrogated CD437's ability to upregulate the expression of Fas, DR4, and DR5.⁴¹⁻⁴³ Thus, it appears that CD437 induces the expression of death receptors via a p53-dependent mechanism, at least in human lung cancer cells. Fas and DR5 are known to be p53 target genes.^{44,45} Our recent work has demonstrated that DR4 is also a p53 target gene.⁴⁶

Due to the above findings, we also determined whether CD437 induced the expression of death receptors and apoptosis in normal human lung epithelial cells, which possess wild-type p53. Significantly, CD437 did not induce the expression of Fas, DR4, and DR5, and apoptosis in both normal human bronchial epithelial (NHBE) cells and small airway epithelial cells.⁴⁷ The failure of CD437 to induce death receptor expression and apoptosis in nor-

mal lung epithelial cells may be related to its inability to increase or stabilize p53 protein in these cells.⁴⁷

Although CD437 induces a p53-dependent expression of death receptors in human lung cancer cells, our studies showed that p53 was not important for the upregulation of death receptors by CD437 in human prostate or head and neck cancer cells because CD437 induced the expression of death receptors regardless of p53 status in these cell lines.^{48,49} Thus, it appears that CD437 induces a p53-dependent and/or -independent death receptor expression depending on cell types or even cell lines. Currently, it remains unclear how CD437 upregulates the expression of death receptors through p53-independent mechanism(s) (reviewed in¹⁵).

It is generally thought that nuclear retinoid receptors mediate the major biological effects of retinoids.⁵⁹ To determine whether nuclear retinoid receptors play any role in mediating the upregulation of death receptors by CD437, we examined the effect of CD437 on the expression of death receptors in the presence of the pan RAR-specific antagonist AGN193109. We found that AGN193109 failed to block or suppress Fas, DR4, or DR5 induction by CD437, indicating that CD437 induces death receptor expression independent of nuclear retinoid receptors (¹², our unpublished data). This conclusion is further supported by the determination that other receptor-selective retinoids, except for those having similar parent structures to CD437, failed to induce the expression of death receptors (¹², our unpublished data).

N-(4-hydroxyphenyl) retinamide (4HPR; fenretinide), another synthetic retinoid that induces apoptosis in various types of cancer cells, has been evaluated in numerous clinical trials for its chemopreventive activity. A recent study has shown that 4HPR induced DR5 expression in primary meningioma cultures.⁵⁰ Another study did not find that 4HPR modulated the expression of DR4 or DR5. However, 4HPR enhanced TRAIL-mediated apoptosis in ovarian cancer cell lines but not in immortalized non-tumorigenic ovarian epithelial cells.⁵¹

Triterpenoids. Triterpenoids are another group of natural and synthetic compounds with chemopreventive potentials.⁵² The natural triterpenoids betulinic acid and boswellic acid were reported to induce DR5 expression in melanoma, glioblastoma, and leukemia cells, respectively.^{53,54} Our recent study has shown that the synthetic triterpenoid methyl-2-cyano-3,12-dioxooleana-1,9-dien-28-oate (CDDO-Me) increased the expression of DR4 and particularly DR5, and enhanced TRAIL-induced apoptosis in human lung cancer cells. Silencing of DR5 expression using siRNA inhibited both CDDO-Me-induced apoptosis and CDDO-Me-mediated enhancement of TRAIL-induced apoptosis, indicating the involvement of DR5 in both activities.⁵⁵ Induction of DR5 by betulinic acid and CDDO-Me is independent

of p53. We found that CDDO-Me rapidly activated c-Jun NH₂-terminal kinase (JNK) before DR5 up-regulation. Moreover, application of the JNK-specific inhibitor SP600125 blocked CDDO-Me-induced DR5 upregulation. These results indicate that CDDO-Me induces a JNK-dependent DR5 upregulation.⁵⁵

Polyphenols. Resveratrol, a polyphenol found in grape skin and various other food products, exhibits cancer chemopreventive activity in animal models of carcinogenesis, likely through its ability to trigger apoptosis.⁵⁶ Studies in a human colon cancer cell line show that resveratrol does not modulate the expression of Fas, DR4, and DR5 at the surface of cancer cells. However, it induces the clustering of these death receptors and their redistribution in cholesterol and sphingolipid-rich fractions (lipid rafts) of cancer cells, together with FADD and procaspase-8. These redistributions are associated with the formation of a DISC and contribute to the induction of apoptosis and sensitization of cells to death ligand- or death receptor activation-mediated apoptosis.^{57,58} (-)-Epigallocatechin-3-gallate (EGCG), a polyphenolic compound found in green tea, was reported to increase Fas protein levels in Hep G2 human liver cancer.⁵⁹ Another study reported that EGCG also bound to cell surface Fas, triggering Fas-mediated apoptosis in human monocytic leukemia U937 cells.⁶⁰

Vitamin E and its derivatives. Vitamin E (α -tocopherol) is a dietary antioxidant with chemopreventive activity. Vitamin E succinate was reported to increase not only total protein levels of Fas but also cell surface levels of Fas in human breast cancer cells.^{61,62} The upregulation of Fas is involved in vitamin E succinate-induced apoptosis⁶¹ or associated with the enhancement of Fas-induced apoptosis⁶² in these cells. Increases in cell surface Fas and enhancement of Fas-induced apoptosis by vitamin E succinate were also observed in human prostate cancer cells.⁶³ A recent study shows that the semisynthetic analogue of vitamin E, α -tocopheryl succinate, increases the expression of both DR4 and DR5 in human malignant mesothelioma cells; this increased expression is associated with its ability to enhance TRAIL-induced apoptosis.⁶⁴ Currently, it is unknown how vitamin E and its analogues upregulate the expression of death receptors.

Others. Selenium is an essential micronutrient that is currently being tested for prostate cancer chemoprevention. A recent study shows that selenium-mediated apoptosis appears to involve a DR5-dependent pathway in human prostate cancer cells. Selenium specifically induced DR5 expression, which coupled with caspase-8 activation and Bid cleavage.⁶⁵ Bovine lactoferrin, a multifunctional glycoprotein, has been shown to strongly inhibit the development of azoxymethane-induced rat colon tu-

mors. Lactoferrin was shown to enhance Fas expression in the colon mucosa during both early and late stages of carcinogenesis. The elevation of Fas expression correlates with the activation of caspase-8 and caspase-3, suggesting that apoptosis caused by elevated expression of Fas is involved in chemoprevention by lactoferrin of colon carcinogenesis.⁶⁶ Curcumin, an antioxidant with chemopreventive and apoptosis-inducing activity, was reported to increase Fas expression and induce Fas clustering in human melanoma cells, leading to the induction of apoptosis.⁶⁷ Curcumin also increased cell surface DR4 and augmented TRAIL-induced apoptosis in prostate cancer cells.⁶⁸ Interferons have been used in some chemopreventive trials. Interferon- γ was shown to induce DR5 expression in cancer cell lines independent of p53.⁵⁵ Interferon- α was also reported to increase DR5 expression in human hepatoma cells; this increased expression is associated with its ability to enhance TRAIL-induced apoptosis.⁶⁹

Implication of death receptor modulation in chemoprevention

Activation of death receptors with either ligand binding or receptor overexpression triggers the extrinsic apoptotic pathway. Apoptosis induced by the interaction between death ligand (from NK cells or T cells) and death receptors (from target cells) is the primary mechanism underlying tumor immunosurveillance (reviewed in¹⁹⁻²¹). In death ligand-expressing premalignant or malignant cells, the binding of death ligands such as Fas ligand (FasL) and TRAIL to an increased number of death receptors due to treatment with chemopreventive agents may trigger the apoptotic signal leading to the apoptotic death of these aberrant cells. Moreover, upregulation of death receptors in premalignant and malignant cells may cause these cells to become more susceptible targets for immune cells (*i.e.*, NK and T cells) that express and secrete death ligands such as TRAIL. In other words, chemopreventive agents with death receptor-inducing activity can sensitize premalignant and malignant cells to death receptor-mediated immune clearance or surveillance.

Some chemopreventive agents have been demonstrated to induce the expression of death ligands such as TRAIL. The examples of the agents are retinoic acid,^{70,71} interferons,^{71,72} and PI3 kinase inhibitors.⁷³ Therefore, it is plausible to speculate that the combination of a death receptor-inducing chemopreventive agent with a death ligand-inducing agent may enhance the killing or elimination of premalignant and malignant cells or lesions via death ligand/death receptor-mediated apoptosis. Studying the effect of this kind of combination may develop an effective and mechanism-driven combination regimen for cancer chemoprevention.

Conclusions and perspective

Chemoprevention has emerged as an essential part of cancer control. Many chemopreventive agents are thought to act as cytostatic agents. Therefore, they are traditionally suggested to be administered chronically to individuals at increased risk to develop cancer. A more desirable and aggressive approach is to use agents that can eliminate aberrant clones by inducing apoptosis rather than inhibit their proliferation. Such agents could be administered for shorter periods of time and at higher doses. Short-term treatment would allow the inclusion of agents with some reversible or moderate side effects for the prevention of premalignant lesions.

It appears that apoptosis is a useful target for the development of chemopreventive agents. Elucidation of the mechanism of chemopreventive agent-induced apoptosis in premalignant or malignant cells clearly will be helpful for developing new agents with better activity, selectivity and less toxicity. Some chemopreventive agents with apoptosis-inducing activity induce apoptosis through an intrinsic mitochondrial pathway involving the promotion of reactive oxygen species (ROS) generation (reviewed in [1]). Given that ROS-induced oxidative stress is involved in carcinogenesis, particularly in tumor promotion (reviewed in [2]), a concern is whether this kind of chemopreventive agent has a potential to promote carcinogenesis rather than prevention of cancer. From this point of view, chemopreventive agents with death receptor-inducing activity appear to have the advantage over others that induce apoptosis by promoting ROS generation. Therefore, future studies should focus on identifying and developing chemopreventive agents that, ideally, can selectively induce the expression of death receptors in preneoplastic or premalignant cells or induce the redistribution and clustering of death receptors on the membrane surface of these cells.

Acknowledgments

Works in author's laboratory were supported by Winship Cancer Institute faculty start-up research fund, the Georgia Cancer Coalition Distinguished Cancer Scholar award, and the Department of Defense VITAL grant W81XWH-04-1-0142 (for Project 4). The author is a Georgia Cancer Coalition Distinguished Cancer Scholar.

References

- Kelloff GJ, Sigman CC, Greenwald P. Cancer chemoprevention: Progress and promise. *Eur J Cancer* 1999; 35: 1755–1762.
- Hong WK, Sporn MB. Recent advances in chemoprevention of cancer. *Science* 1997; 278: 1073–1077.
- Sporn MB, Suh N. Chemoprevention: An essential approach to controlling cancer. *Nat Rev Cancer* 2002; 2: 537–543.
- Kelloff GJ, Crowell JA, Steele VE, et al. Progress in cancer chemoprevention. *Ann N Y Acad Sci* 1999; 889: 1–13.
- Tsao AS, Kim ES, Hong WK. Chemoprevention of cancer. *CA Cancer J Clin* 2004; 54: 150–180.
- Steller H. Mechanisms and genes of cellular suicide. *Science* 1995; 267: 1445–1449.
- Mercalfe A, Streuli C. Epithelial apoptosis. *BioEssays* 1997; 19: 711–720.
- Green DR, Evan GI. A matter of life and death. *Cancer Cell* 2002; 1: 19–30.
- Sun SY, Hail N Jr, Lotan R. Apoptosis as a novel target for cancer chemoprevention. *J Natl Cancer Inst* 2004; 96: 662–672.
- Ashkenazi A, Dixit VM. Death receptors: Signaling and modulation. *Science* 1998; 281: 1305–1308.
- Hengartner MO. The Biochemistry of apoptosis. *Nature* 2000; 407: 770–776.
- Green DR. Apoptotic pathways: Paper wraps stone blunts scissors. *Cell* 2000; 102: 1–4.
- Kelley SK, Ashkenazi A. Targeting death receptors in cancer with Apo2L/TRAIL. *Curr Opin Pharmacol* 2004; 4: 333–339.
- Bouralexis S, Findlay DM, Evdokiou A. Death to the bad guys: Targeting cancer via Apo2L/TRAIL. *Apoptosis* 2005; 10: 35–51.
- Yagita H, Takeda K, Hayakawa Y, Smyth MJ, Okumura K. TRAIL and its receptors as targets for cancer therapy. *Cancer Sci* 2004; 95: 777–783.
- Debatin KM, Krammer PH. Death receptors in chemotherapy and cancer. *Oncogene* 2004; 23: 2950–2966.
- Wajant H, Gerspach J, Pfizenmaier K. Tumor therapeutics by design: Targeting and activation of death receptors. *Cytokine Growth Factor Rev* 2005; 16: 55–76.
- Reed JC. Mechanisms of apoptosis avoidance in cancer. *Curr Opin Oncol* 1999; 11: 68–75.
- Smyth MJ, Hayakawa Y, Takeda K, Yagita H. New aspects of natural-killer-cell surveillance and therapy of cancer. *Nat Rev Cancer* 2002; 2: 850–861.
- Smyth MJ, Takeda K, Hayakawa Y, Peschon JJ, van den Brink MR, Yagita H. Nature's TRAIL—on a path to cancer immunotherapy. *Immunity* 2003; 18: 1–6.
- Smyth MJ, Cretney E, Kershaw MH, Hayakawa Y. Cytokines in cancer immunity and immunotherapy. *Immunol Rev* 2004; 202: 275–293.
- Lee SH, Yoo NJ, Lee JY. Death receptor mutations. In: El-Deiry WS, ed. *Cancer drug discovery and development: Death receptors in cancer biology*. New Jersey: Humana Press Inc. 2005: 149–162.
- Strand S, Hofmann WJ, Hug H, et al. Lymphocyte apoptosis induced by CD95 (APO-1/Fas) ligand-expressing tumor cells—A mechanism of immune evasion? *Nat Med* 1996; 2: 1361–1366.
- Reesink-Peters N, Hougardy BM, van den Heuvel FA, et al. Death receptors and ligands in cervical carcinogenesis: An immunohistochemical study. *Gynecol Oncol* 2005; 96: 705–713.
- Hopkins-Donaldson S, Ziegler A, Kurtz S, et al. Silencing of death receptor and caspase-8 expression in small cell lung carcinoma cell lines and tumors by DNA methylation. *Cell Death Differ* 2003; 10: 356–364.
- Shivapurkar N, Reddy J, Marra H, et al. Loss of expression of death-inducing signaling complex (DISC) components in lung cancer cell lines and the influence of MYC amplification. *Oncogene* 2002; 21: 8510–8514.

27. Shivapurkar N, Toyooka S, Toyooka KO, *et al.* Aberrant methylation of trail decoy receptor genes is frequent in multiple tumor types. *Int J Cancer* 2004; 109: 786–792.
28. Margetts CD, Astuti D, Gentle DC, *et al.* Epigenetic analysis of HIC1, CASP8, FLIP, TSP1, DCR1, DCR2, DR4, DR5, KvDMR1, H19 and preferential 11p15.5 maternal-allele loss in von Hippel-Lindau and sporadic pheochromocytomas. *Endocr Relat Cancer* 2005; 12: 161–172.
29. Pitti RM, Marsters SA, Lawrence DA, *et al.* Genomic amplification of a decoy receptor for Fas ligand in lung and colon cancer. *Nature* 1998; 396: 699–703.
30. Bai C, Connolly B, Metzker ML, *et al.* Overexpression of M68/DcR3 in human gastrointestinal tract tumors independent of gene amplification and its location in a four-gene cluster. *Proc Natl Acad Sci USA* 2000; 97: 1230–1235.
31. Sheikh MS, Huang Y, Fernandez-Salas EA, *et al.* The anti-apoptotic decoy receptor TRID/TRAIL-R3 is a p53-regulated DNA damage-inducible gene that is overexpressed in primary tumors of the gastrointestinal tract. *Oncogene* 1999; 18: 4153–4159.
32. Wajant H. Targeting the FLICE Inhibitory Protein (FLIP) in cancer therapy. *Mol Interv* 2003; 3: 124–127.
33. Roth W, Reed JC. FLIP protein and TRAIL-induced apoptosis. *Vitam Horm* 2004; 67: 189–206.
34. French LE, Tschopp J. Defective death receptor signaling as a cause of tumor immune escape. *Semin Cancer Biol* 2002; 12: 51–55.
35. Huang Y, He Q, Hillman MJ, Rong R, Sheikh MS. Sulindac sulfide-induced apoptosis involves death receptor 5 and the caspase 8-dependent pathway in human colon and prostate cancer cells. *Cancer Res* 2001; 61: 6918–6924.
36. Jang TJ, Kang HJ, Kim JR, Yang CH. Non-steroidal anti-inflammatory drug activated gene (NAG-1) expression is closely related to death receptor-4 and -5 induction, which may explain sulindac sulfide induced gastric cancer cell apoptosis. *Carcinogenesis* 2004; 25: 1853–1858.
37. Han Z, Pantazis P, Wyche JH, Kouttab N, Kidd VJ, Hendrickson EA. A Fas-associated death domain protein-dependent mechanism mediates the apoptotic action of non-steroidal anti-inflammatory drugs in the human leukemic Jurkat cell line. *J Biol Chem* 2001; 276: 38748–38754.
38. Liu X, Yue P, Zhou Z, Khuri FR, Sun SY. Death receptor regulation and celecoxib-induced apoptosis in human lung cancer cells. *J Natl Cancer Inst* 2004; 96: 1769–1780.
39. Sun SY, Lotan R. Retinoids and their receptors in cancer development and chemoprevention. *Crit Rev Oncol Hematol* 2002; 41: 41–55.
40. Sun SY, Yue P, Wu GS, *et al.* Mechanisms of apoptosis induced by the synthetic retinoid CD437 in human non-small cell lung carcinoma cells. *Oncogene* 1999; 18: 2357–2365.
41. Sun SY, Yue P, Wu GS, *et al.* Implication of p53 in growth arrest and apoptosis induced by the synthetic retinoid CD437 in human lung cancer cells. *Cancer Res* 1999; 59: 2829–2833.
42. Sun SY, Yue P, Hong WK, Lotan R. Induction of Fas expression and augmentation of Fas/FasL-mediated apoptosis by the synthetic retinoid CD437 in human lung cancer cells. *Cancer Res* 2000; 60: 6537–6543.
43. Sun SY. Regulation of death receptors by synthetic retinoids. In: El-Deiry WS, ed. *Cancer drug discovery and development: Death receptors in cancer biology*. New Jersey: Humana Press Inc. 2005: 189–200.
44. Muller M, Wilder S, Bannasch D, *et al.* p53 activates the CD95 (APO-1/Fas) gene in response to DNA damage by anticancer drugs. *J Exp Med* 1998; 188: 2033–2040.
45. Takimoto R, El-Deiry WS. Wild-type p53 transactivates the KILLER/DR5 gene through an intronic sequence-specific DNA-binding site. *Oncogene* 2000; 19: 1735–1743.
46. Liu X, Yue P, Khuri FR, Sun SY. p53 upregulates death receptor 4 expression through an intronic p53 binding site. *Cancer Res* 2004; 64: 5078–5083.
47. Sun SY, Yue P, Chen X, Hong WK, Lotan R. The synthetic retinoid CD437 selectively induces apoptosis in human lung cancer cells while sparing normal human lung epithelial cells. *Cancer Res* 2002; 62: 2430–2436.
48. Sun SY, Yue P, Mao L, *et al.* Identification of receptor-selective retinoids that are potent inhibitors of the growth of human head and neck squamous cell carcinoma cells. *Clin Cancer Res* 2000; 6: 1563–1573.
49. Sun SY, Yue P, Lotan R. Implication of multiple mechanisms in apoptosis induced by the synthetic retinoid CD437 in human prostate carcinoma cells. *Oncogene* 2000; 19: 4513–4522.
50. Puduvalli VK, Li JT, Chen L, McCutcheon IE. Induction of apoptosis in primary meningioma cultures by fenretinide. *Cancer Res* 2005; 5: 1547–1553.
51. Cuello M, Coats AO, Darko I, *et al.* N-(4-hydroxyphenyl) retinamide (4HPR) enhances TRAIL-mediated apoptosis through enhancement of a mitochondrial-dependent amplification loop in ovarian cancer cell lines. *Cell Death Differ* 2004; 1: 527–551.
52. Sporn MB, Suh N. Chemoprevention of cancer. *Carcinogenesis* 2000; 1: 525–550.
53. Meng RD, El-Deiry WS. p53-independent upregulation of KILLER/DR5 TRAIL receptor expression by glucocorticoids and interferon-gamma. *Exp Cell Res* 2001; 262: 154–169.
54. Xia L, Chen D, Han R, Fang Q, Waxman S, Jing Y. Boswellic acid acetate induces apoptosis through caspase-mediated pathways in myeloid leukemia cells. *Mol Cancer Ther* 2005; 4: 381–388.
55. Zou W, Liu X, Yue P, *et al.* c-Jun NH2-terminal kinase-mediated up-regulation of death receptor 5 contributes to induction of apoptosis by the novel synthetic triterpenoid methyl-2-cyano-3,12-dioxooleana-1, 9-dien-28-oate in human lung cancer cells. *Cancer Res* 2004; 64: 7570–7578.
56. Aggarwal BB, Bhardwaj A, Aggarwal RS, Seeram NP, Shishodia S, Takada Y. Role of resveratrol in prevention and therapy of cancer: Preclinical and clinical studies. *Anticancer Res* 2004; 24: 2783–2840.
57. Delmas D, Rebe C, Lacour S, *et al.* Resveratrol-induced apoptosis is associated with Fas redistribution in the rafts and the formation of a death-inducing signaling complex in colon cancer cells. *J Biol Chem* 2003; 278: 41482–41490.
58. Delmas D, Rebe C, Micheau O, *et al.* Redistribution of CD95, DR4 and DR5 in rafts accounts for the synergistic toxicity of resveratrol and death receptor ligands in colon carcinoma cells. *Oncogene* 2004; 23: 8979–8986.
59. Kuo PL, Lin CC. Green tea constituent (–)-epigallocatechin-3-gallate inhibits Hep G2 cell proliferation and induces apoptosis through p53-dependent and Fas-mediated pathways. *J Biomed Sci* 2003; 10: 219–227.
60. Hayakawa S, Saeki K, Sazuka M, *et al.* Apoptosis induction by epigallocatechin gallate involves its binding to Fas. *Biochem Biophys Res Commun* 2001; 285: 1102–1106.
61. Turley JM, Fu T, Ruscetti FW, Mikovits JA, Bertolette DC 3rd, Birchenall-Roberts MC. Vitamin E succinate induces Fas-mediated apoptosis in estrogen receptor-negative human breast cancer cells. *Cancer Res* 1997; 57: 881–890.
62. Yu W, Israel K, Liao QY, Aldaz CM, Sanders BG, Kline K. Vitamin E succinate (VES) induces Fas sensitivity in human

- breast cancer cells: Role for Mr 43,000 Fas in VES-triggered apoptosis. *Cancer Res* 1999; 59: 953–961.
63. Israel K, Yu W, Sanders BG, Kline K. Vitamin E succinate induces apoptosis in human prostate cancer cells: Role for Fas in vitamin E succinate-triggered apoptosis. *Nutr Cancer* 2000; 36: 90–100.
64. Tomasetti M, Rippe MR, Alleva R, *et al.* Alpha-tocopheryl succinate and TRAIL selectively synergise in induction of apoptosis in human malignant mesothelioma cells. *Br J Cancer* 2004; 90: 1644–1653.
65. He Q, Rashid A, Rong R, Hillman MJ, Huang Y, Sheikh MS. Death receptor 5 regulation during selenium-mediated apoptosis in human prostate cancer cells. *Cancer Biol Ther* 2002; 1: 287–290.
66. Fujita K, Matsuda E, Sekine K, Iigo M, Tsuda H. Lactoferrin enhances Fas expression and apoptosis in the colon mucosa of azoxymethane-treated rats. *Carcinogenesis* 2004; 25: 1961–1966.
67. Bush JA, Cheung KJ Jr, Li G. Curcumin induces apoptosis in human melanoma cells through a Fas receptor/caspase-8 pathway independent of p53. *Exp Cell Res* 2001; 271: 305–314.
68. Deeb D, Jiang H, Gao X, *et al.* Curcumin sensitizes prostate cancer cells to tumor necrosis factor-related apoptosis-inducing ligand/Apo2L by inhibiting nuclear factor-kappaB through suppression of IkappaBalpha phosphorylation. *Mol Cancer Ther* 2004; 3: 803–812.
69. Shigeno M, Nakao K, Ichikawa T, *et al.* Interferon-alpha sensitizes human hepatoma cells to TRAIL-induced apoptosis through DR5 upregulation and NF-kappa B inactivation. *Oncogene* 2003; 22: 1653–1662.
70. Altucci L, Rossin A, Raffelsberger W, Reitmaier A, Chomienne C, Gronemeyer H. Retinoic acid-induced apoptosis in leukemia cells is mediated by paracrine action of tumor-selective death ligand TRAIL. *Nat Med* 2001; 7: 680–686.
71. Clarke N, Jimenez-Lara AM, Voltz E, Gronemeyer H. Tumor suppressor IRF-1 mediates retinoid and interferon anticancer signaling to death ligand TRAIL. *EMBO J* 2004; 23: 3051–3060.
72. Wang Q, Ji Y, Wang X, Evers BM. Isolation and molecular characterization of the 5'-upstream region of the human TRAIL gene. *Biochem Biophys Res Commun* 2000; 276: 466–471.
73. Wang Q, Wang X, Hernandez A, Hellmich MR, Gatalica Z, Evers BM. Regulation of TRAIL expression by the phosphatidylinositol 3-kinase/Akt/GSK-3 pathway in human colon cancer cells. *J Biol Chem* 2002; 277: 36602–36610.
74. Klaunig JE, Xu Y, Isenberg JS, *et al.* The role of oxidative stress in chemical carcinogenesis. *Environ Health Perspect* 1998; 106: 289–295.
75. Vallyathan V, Shi X, Castranova V. Reactive oxygen species: Their relation to pneumoconiosis and carcinogenesis. *Environ Health Perspect* 1998; 106: 1151–1155.

EGFR Tyrosine Kinase Domain Mutations Are Detected in Histologically Normal Respiratory Epithelium in Lung Cancer Patients

Ximing Tang,¹ Hisayuki Shigematsu,⁵ B. Nebiyu Bekele,² Jack A. Roth,³ John D. Minna,^{5,6,7} Waun Ki Hong,¹ Adi F. Gazdar,^{5,8} and Ignacio I. Wistuba^{1,4}

Departments of ¹Thoracic/Head and Neck Medical Oncology, ²Biostatistics and Applied Mathematics, ³Thoracic Surgery, and ⁴Pathology, University of Texas M.D. Anderson Cancer Center, Houston, Texas and ⁵Hamon Center for Therapeutic Oncology Research, Departments of ⁶Internal Medicine, ⁷Pharmacology, and ⁸Pathology, University of Texas Southwestern Medical Center, Dallas, Texas

Abstract

To determine whether *EGFR* tyrosine kinase domain mutations are early events in the pathogenesis of lung adenocarcinomas, we tested for the presence of *EGFR* mutations in histologically normal bronchial and bronchiolar epithelia from lung adenocarcinomas bearing the common *EGFR* mutations. DNA was extracted from microdissected tissue obtained from 21 tumors with known *EGFR* mutations, 16 tumors without mutation, and 90 sites of normal bronchial and bronchiolar epithelium from the same surgical specimens. With the use of PCR and direct DNA sequencing, *EGFR* mutations identical to the tumors were detected in the normal respiratory epithelium in 9 of 21 (43%) patients with *EGFR* mutant adenocarcinomas but none in patients without mutation in the tumors. The finding of mutations being more frequent in normal epithelium within tumor (43%) than in adjacent sites (24%) suggests a localized field effect phenomenon. Our findings indicate that mutation of the tyrosine kinase domain of *EGFR* is an early event in the pathogenesis of lung adenocarcinomas, and suggest *EGFR* mutations as an early detection marker and chemoprevention target. (Cancer Res 2005; 65(17): 7568-72)

Introduction

Four major histologic types compose the majority of lung cancers, and adenocarcinoma histology is currently the type most frequently diagnosed (1). It has been established that adenocarcinomas usually arise from the peripheral airway; however, the specific airway structure (bronchus, bronchiole, and alveolus) and the respiratory epithelium cell type (ciliated, goblet, Clara, and type II alveolar cells) from which most adenocarcinomas develop have not been established. Recent findings indicate that clinically evident lung adenocarcinomas are the results of the accumulation of numerous genetic and epigenetic changes, including abnormalities for the inactivation of tumor suppressor genes and the activation of oncogenes (2). Despite these advances, there is extremely limited information available on the early molecular pathogenesis of lung adenocarcinomas.

Somatic mutations of *EGFR*, a tyrosine kinase of the ErbB family, recently have been reported in specific subsets of lung adenocarci-

nomas (3-9). The mutations are clinically relevant because most of them have been associated with patient tumor sensitivity to small molecule tyrosine kinase inhibitors gefitinib and erlotinib (3-5, 10). About 90% of the mutations detected in *EGFR* are composed either of in-frame deletions in exon 19 or a specific missense mutation in exon 21 (L858R; refs. 3-9). The mutations are significantly associated with adenocarcinoma histology, never or light smoker status, female gender, and East Asian ethnic origin (9). However, there is no information available on the stage of lung adenocarcinoma development when *EGFR* mutation develops. Thus, to investigate the stage of lung adenocarcinoma pathogenesis when *EGFR* mutations commence, we tested for the presence of *EGFR* mutations in peripheral airway respiratory epithelium (small bronchi and bronchioles) obtained from 21 patients with lung adenocarcinoma harboring *EGFR* mutations. We compared the findings with similar samples obtained from 16 lung cancer patients whose tumors had wild-type *EGFR*.

Materials and Methods

Case selection. Tumor tissue specimens obtained from 120 surgically resected lung adenocarcinomas, pathology stages I to IIIA, were obtained from the Lung Cancer Specialized Program of Research Excellence Tissue Bank at the M.D. Anderson Cancer Center (Houston, TX), and were examined for *EGFR* gene mutation in exons 18 to 21 (9). We selected 20 cases of adenocarcinoma and one adenosquamous carcinoma with *EGFR* mutation in exon 19 ($n = 13$) and exon 21 ($n = 8$) in which archival formalin-fixed paraffin-embedded tissues from which surgically resected lobectomy specimens were available (Table 1). Most patients were women of East Asian ethnicity and never or former smokers (Table 1). All *EGFR* mutated lung adenocarcinomas were of mixed histologic subtype (WHO classification, 2004; ref. 1). Two patients with *EGFR* mutant lung cancers were current smokers, but with only 5 and 12 pack-year exposures. None of the patients had received prior cytotoxic therapy. Patients who had smoked at least 100 cigarettes in their lifetime were defined as smokers, and smokers who quit smoking at least 12 months before lung cancer diagnosis were defined as former smokers. As a control group, 16 cases of adenocarcinoma without *EGFR* mutation, divided into 8 never and 8 former smokers, were selected. Clinical staging was based on the revised in International System for Staging Lung Cancer (11).

Respiratory epithelium foci selection. H&E-stained histology sections of archival specimens having tumor and adjacent normal lung tissues were reviewed to identify available foci of respiratory epithelium containing at least 1,000 cells. From the 21 *EGFR* mutated lung cancers, we identified noncontiguous small bronchial ($n = 26$) or bronchiolar ($n = 38$) sites suitable for microdissection. All the foci harbored histologically normal-appearing respiratory epithelium, without identifiable dysplastic or neoplastic cells (Fig. 1). No atypical adenomatous hyperplasias, putative precursors of a subset of lung adenocarcinomas, were detected. The microdissected specimens were obtained from three different locations

Requests for reprints: Ignacio I. Wistuba, Department of Pathology, Unit 85, University of Texas M.D. Anderson Cancer Center, 1515 Holcombe Boulevard, Houston, TX 77030-4009. Phone: 713-563-9184; Fax: 713-563-1848; E-mail: iiwistuba@mdanderson.org.

©2005 American Association for Cancer Research.
doi:10.1158/0008-5472.CAN-05-1705

Table 1. Clinicopathologic data of *EGFR* mutant resected lung adenocarcinomas studied

Case no.	Age	Gender	Race	Smoking status	Stage	EGFR mutation	Mutation in normal epithelium
1	55	Female	Caucasian	Never	IIB	15 bp del (746-750)	Yes
2	70	Female	Hispanic	Never	IIIA	15 bp del (746-750)	No
3	64	Male	Caucasian	Never	IA	15 bp del (746-750)	No
4	66	Female	Caucasian	Never	IB	18 bp del (746-751) and S752V	No
5	52	Female	Hispanic	Never	IIIA	L858R	Yes
6	70	Female	Caucasian	Never	IA	L858R	Yes
7	65	Female	Caucasian	Never	IA	L858R	No
8	45	Female	East Asian	Never	IA	L858R	No
9	61	Female	East Asian	Never	IIIA	L858R	No
10	49	Female	East Asian	Never	IIIA	L858R	No
11	35	Female	East Asian	Never	IA	15 bp del (746-750)	Yes
12	62	Female	East Asian	Never	IA	L858R	No
13	66	Female	Caucasian	Former	IV	15 bp del (746-750)	No
14	58	Female	Caucasian	Former	IA	15 bp del (746-750)	Yes
15	65	Male	East Asian	Former	IIB	18 bp del (746-751) and S752I	Yes
16	72	Female	Caucasian	Former	IB	15 bp del (746-750)	Yes
17	69	Male	East Asian	Former	IIIA	L858R	No
18	56	Male	East Asian	Former	IIB	18 bp del (747-752) and P753Q	Yes
19	69	Male	East Asian	Former	IB	15 bp del (747-751)	No
20	73	Male	East Asian	Current	IIB	15 bp del (746-750)	Yes
21	68	Female	Caucasian	Current	IIIA	15 bp del (746-750)	No

based on their relationship to the tumors: within the tumor (21 foci), <5 mm apart from the tumor margin (adjacent to tumor; 29 sites), and from sites located >5 mm from the tumor margin ("distant" lung; 14 sites). From the 16 non-*EGFR* mutated lung adenocarcinoma cases, we selected 26 (10 small bronchi and 16 bronchioles) sites of histologically normal respiratory epithelium (Table 2). Averages of 3.1 (range, 2-6) and 1.6 (range, 1-3) respiratory epithelium foci were examined from *EGFR* mutated and nonmutated cases, respectively. Small bronchi were identified as having well-defined smooth muscle and discontinuous cartilage layers. Bronchioles were defined as small conducting airways lacking well-defined smooth muscle wall or cartilage layers. As internal negative controls, stromal tissue obtained from bronchial walls was also selected for microdissection. As these were retrospectively collected specimens, location of the small bronchial and bronchiolar respiratory epithelium examined for mutations was assessed based on their location with respect to tumor tissue in the corresponding histology sections.

Microdissection and DNA extraction. Approximately 1,000 cells (tumor, respiratory epithelium, or stromal) were precisely microdissected from sequential 8- μ m-thick H&E-stained, formalin-fixed paraffin-embedded histology sections, using laser capture microdissection (Arcturus Engineering Laser Microdissection System, Mountain View, CA; Fig. 1). To avoid possible nonspecific binding of mutant tumor cells to the microdissection cap film, the specifically microdissected epithelial cells were redissected from the film under stereomicroscope visualization using fine needles (25G5/8). DNA was extracted using 25 μ L of Pico Pure DNA Extraction solution (Arcturus) containing proteinase K and incubated at 65°C for 24 hours. Subsequently, proteinase K inactivation was done by heating samples at 95°C for 10 minutes.

EGFR mutation analysis. Exons 19 and 21 of *EGFR* were PCR amplified using intron-based primers as previously described (10). From microdissected formalin-fixed paraffin-embedded cells, ~100 cells were used for each PCR amplification. Each amplification was done in 25 μ L volume containing 2.5 μ L DNA, 0.5 μ L each primer (20 pmol/L), 12.5 μ L HotStarTaq Master Mix (Qiagen, Valencia, CA), and 9 μ L DNase-free water. DNA was amplified for 38 cycles at 94°C for 30 seconds, 65°C for 30 seconds, and 72°C for 45 seconds, followed by 7-minute extension at 72°C. All PCR products were directly sequenced using Applied Biosystems PRISM dye terminator

cycle sequencing method (Perkin-Elmer Corp., Foster City, CA). All sequence variants were confirmed by independent PCR amplifications from at least two independent microdissections, and sequenced in both directions.

Statistical analysis. For data in which there is one record per patient, all relationships between categorical variables were assessed via the Fisher's exact test (12). For continuous outcomes, differences between cohorts were assessed via the Wilcoxon rank-sum test. Data in which there are multiple records per patient, relationships between binary variables were assessed via generalized estimating equation models.

Results

EGFR mutation in histologically normal epithelium. Mutation analysis of the microdissected tumor tissue confirmed the mutational pattern originally identified using frozen and non-microdissected formalin-fixed paraffin-embedded tissues in all 21 cases (Table 1). Of interest, *EGFR* mutations were detected in at least one sample of corresponding histologically normal small bronchial and bronchiolar epithelia in 9 of 21 (43%) *EGFR* mutant lung adenocarcinoma patients (Tables 1 and 2). By contrast, no mutations in exons 19 and 21 of the *EGFR* gene were detected in 26 respiratory epithelium foci obtained from 16 lobectomy specimens of cancers having wild-type *EGFR* ($P = 0.005$). In *EGFR* mutant lung adenocarcinomas, 16 of 64 (25%) normal respiratory epithelium foci microdissected showed *EGFR* mutations. Five of nine cases showing mutations in normal respiratory epithelium showed two or three microdissected sites with *EGFR* mutation. In all cases, the mutational patterns in the tumors and corresponding nonmalignant respiratory epithelial specimens were identical. All mutations detected were confirmed using additional microdissected samples and multiple independent sequencing experiments in both sense and antisense directions. Importantly, no mutations were detected in stromal cells microdissected from bronchial walls in five cases in which adjacent lung normal epithelium and tumor showed *EGFR* mutations.

Comparison of β -Tubulin mRNA and Protein Levels in 12 Human Cancer Cell Lines

Laree Hiser,¹ Ashish Aggarwal,² Rebekah Young,¹ Anthony Frankfurter,³
Anthony Spano,³ John J. Correia,² and Sharon Lobert^{1,2*}

¹*School of Nursing, University of Mississippi Medical Center,
Jackson, Mississippi*

²*Department of Biochemistry, University of Mississippi Medical Center,
Jackson, Mississippi*

³*Department of Biology, University of Virginia, Charlottesville, Virginia*

Antimitotic drugs are chemotherapeutic agents that bind tubulin and microtubules. Resistance to these drugs is a major clinical problem. One hypothesis is that the cellular composition of tubulin isotypes may predict the sensitivity of a tumor to antimitotics. Reliable and sensitive methods for measuring tubulin isotype levels in cells and tissues are needed to address this hypothesis. Quantitative measurements of tubulin isotypes have frequently relied upon inferring protein amounts from mRNA levels. To determine whether this approach is justified, protein and mRNA levels of β -tubulin isotypes from 12 human cancer cell lines were measured. This work focused on only β -tubulin isotypes because we had readily available monoclonal antibodies for quantitative immunoblots. The percentage of β -tubulin isotype classes I, II, III, and IVa + IVb mRNA and protein were compared. For β -tubulin class I that comprises >50% of the β -tubulin protein in 10 of the 12 cell lines, there was good agreement between mRNA and protein percentages. Agreement between mRNA and protein was also found for β -tubulin class III. For β -tubulin classes IVa + IVb, we observed higher protein levels compared to mRNA levels. β -Tubulin class II protein was found in only four cell lines and in very low abundance. We conclude that quantitative Western blotting is a reliable method for measuring tubulin isotype levels in human cancer cell lines. Inferring protein amounts from mRNA levels should be done with caution, since the correspondence is not one-to-one for all tubulin isotypes. *Cell Motil. Cytoskeleton* 2006. © 2005 Wiley-Liss, Inc.

Key words: tubulin isotypes; microtubules; tubulin; β -tubulin

INTRODUCTION

Quantitative measurement of drug target proteins is essential for developing chemotherapeutic agents and understanding mechanisms that underlie drug resistance. Quantitative (real-time) reverse transcription polymerase chain reaction (qRT-PCR) is an established method for reliably measuring mRNA levels and may be useful for describing alterations in drug targets if protein levels can be inferred from mRNA levels. However, for many proteins, this is not a valid approach [Gygi et al., 1999; Nicoletti et al., 2001]. To study changes in drug target levels that may be associated with drug resistance to anti-

Abbreviations used: MBP, maltose binding protein; MDR, multidrug resistance; NCI, National Cancer Institute.

L. Hiser and A. Aggarwal contributed equally to this manuscript.

*Correspondence to: Sharon Lobert, School of Nursing, University of Mississippi Medical Center, 2500 N. State St., Jackson, MS 39216, USA. E-mail: slobert@son.umsmed.edu

Received 17 August 2005; accepted 17 November 2005

Published online in Wiley InterScience (www.interscience.wiley.com). DOI: 10.1002/cm.20109

mitotic drugs, we wanted to determine whether mRNA levels could be used to accurately predict protein levels.

The ability of anticancer agents to destroy tumors is severely hampered by drug resistance that occurs initially or develops after prolonged or repeated exposure of cells and tissues to these drugs. In advanced-stage metastatic cancers, where treatment options are few, this problem is devastating. Important drugs used to treat solid and hematological tumors are antimitotic agents: taxanes (paclitaxel or docetaxel) and vinca alkaloids (vinblastine, vincristine, vinorelbine or vinflunine). Antimitotic drugs bind tubulin, a major protein in microtubules, and halt cell division at metaphase. Their effectiveness is thought to result from alterations of microtubule dynamics in mitotic spindles, thus preventing spindle assembly or interrupting the movement of sister chromatids toward the spindle poles [Dhamodharan et al., 1995; Yvon et al., 1999].

The drug receptor of antimitotic agents, tubulin, is a structurally heterogeneous 100,000 dalton $\alpha\beta$ heterodimer. Six or seven genes encode α -tubulin isotypes, and seven genes encode β -tubulin isotypes [Sullivan and Cleveland, 1986; Sullivan, 1988]. Antimitotics interact with β -tubulin, which consists of seven isotype classes distinguished by the last 15–20 amino acids at the carboxyl termini [reviewed in Correia and Lobert, 2001].

We present here a quantitative comparison of β -tubulin isotype mRNA and protein levels (β -tubulin classes I, II, III, and IVa + IVb) in 12 human cancer cell lines. qRT-PCR was used to measure mRNA levels of all seven classes of β -tubulin isotypes. Quantitative immunoblotting was done to measure β -tubulin isotype protein levels. β -Tubulin classes I and IVa + IVb proteins were the most abundant. The mRNA and protein levels of β -tubulin class I were found to be in good agreement. β -Tubulin classes IVa + IVb made up a larger fraction of the total protein than of the total mRNA for 11 of the 12 cell lines. β -Tubulin class III protein was found at low levels that corresponded to mRNA levels, although the relationship was not one-to-one.

MATERIALS AND METHODS

Cell Culture

Twelve cell lines were selected on the basis of their relative sensitivities to vinblastine and paclitaxel, as reported by the National Cancer Institute (NCI) Developmental Therapeutics Program Human Tumor Cell Line Screen (http://dtp.nci.nih.gov/docs/cancer/cancer_data.html). Pairs or groups of cells with reported drug sensitivities that differed significantly were selected. Only one (HCT-15) is reported to have relatively high levels of *p*-glycoprotein/MDR1, a membrane-bound pump known to extrude

drugs such as paclitaxel and vinblastine from cells [Alvarez et al., 1995; <http://dtp.nci.nih.gov/docs/compare/cellmdr.html>]. Cell lines were purchased from American Type Culture Collection (Manassas, VA), except for HOP 18, which was kindly provided by NCI-Frederick Cancer Division of Cancer Treatment and Diagnosis Tumor/Cell Line Repository (Frederick, MD). Cells were cultured according to the suppliers' recommendations, with the exception of MDA-MB-231 and Malme-3M, which were grown in RPMI-1640 rather than Leibovitz's L-15 medium.

Determination of IC₅₀ Values

We determined IC₅₀ values (concentration at which cell proliferation is reduced by 50%) for each cell line using two independent methods: cell counting and an assay for mitochondrial respiration. Duplicate 12-well plates (5000 cells/well) were set up for each cell counting experiment, and two to four independent experiments were done for each drug (vinblastine or paclitaxel) and cell line. Cells were incubated for 24 h to permit adherence and then exposed to serial dilutions (between one log unit above and below the predicted IC₅₀ value) of vinblastine or paclitaxel for 48 h, released using trypsin, and counted in a hemocytometer using trypan blue to exclude nonviable cells. For control wells, an appropriate amount of PBS or dimethyl sulfoxide for vinblastine and paclitaxel, respectively, was added. Data were plotted using Origin 7.0 (Origin-Lab, Northampton, MA) as cell number vs. drug concentration. Data were fit to first-order exponential decay, and IC₅₀ values were calculated.

The cell line sensitivities to vinblastine and paclitaxel were also determined using an assay for mitochondrial respiration. Cells were plated in 96-well microtiter plates at 8000 cells/well (10,000 cells/well for Malme-3M). Duplicate plates constituted each experiment; and two to four independent experiments were done for each drug (vinblastine or paclitaxel) and cell line. Cells were incubated for 24 h, and then the medium was replaced with fresh medium containing appropriate concentrations of drug or solvent. After 72 h, the medium was removed from the wells and 100 μ l of CellTiter 96[®] AQueous One solution (Promega, Madison, WI) diluted 1:5 with medium was added. This solution utilizes 3-(4,5-dimethylthiazol-2-yl)-5-(3-carboxymethoxyphenyl)-2-(4-sulfophenyl)-2H-tetrazolium (MTS, inner salt) in a colorimetric reaction that is a linear measure of mitochondrial respiration. The plates were incubated 2 h, and absorbance at 490 nm was read using a microplate reader. Absorbance values were corrected by subtracting baseline values obtained from wells with no cells. IC₅₀ values were determined as described for the cell counting assay.

Quantitative Reverse Transcription Polymerase Chain Reaction

Two-step qRT-PCR was used to determine the amount of mRNA present for each β -tubulin isotype (classes I, II, III, IVa, IVb, V, and VI) in all 12 cell lines. Cells were cultured as described earlier, total RNA was extracted, and qRT-PCR experiments were carried out using primers and protocols described previously [Dozier et al., 2003]. Briefly, qRT-PCR was performed on triplicate samples from at least two independent cell preps using SYBR[®] Green I (Invitrogen, Carlsbad, CA) as the detection method. The amount of β -tubulin isotype mRNA in a known amount of total RNA, determined by A_{260} measurements, was calculated using standard curves.

Quantitative Immunoblots

We developed a quantitative immunoblot assay for tubulin that is sensitive and highly reproducible. Cell lysates were prepared from 10–20 million cells by douncing on ice in 1 ml PBS with a protease inhibitor cocktail (Complete Protease Inhibitor Cocktail Tablets, Roche, Indianapolis, IN). Lysates were spun briefly in a microcentrifuge to remove membranes and mixed 1:1 with SDS sample buffer prior to electrophoresis. After electrophoresis, proteins were transferred to polyvinylidene difluoride (PVDF) membranes, incubated with primary antibody (1–2 mg/ml) at 1:2,500–1:10,000 dilutions overnight at 4°C, and developed using a horseradish peroxidase-conjugated secondary antibody. We used monoclonal antibodies that recognize individual tubulin isotypes: SAP4G5, anti- β -tubulin class I (Sigma-Aldrich, St. Louis, MO); 7B9, anti- β -tubulin class II; TUJ1, anti- β -tubulin class III; and 10A2, anti- β -tubulin classes IVa – IVb. The reactivity and specificity of SAP4G5, 7B9, and TUJ1 have been previously described [Lee et al., 1990; Lobert et al., 1995, 1998; Roach et al., 1998]. The monoclonal antibody 10A2 was raised against the carboxyl terminal peptide of β -tubulin class IVa. It was found to be specific for both β -tubulin classes IVa and IVb (Fig. 1). Blots were reacted with chemiluminescent reagents (SuperSignal[®] West Femto Maximum Sensitivity Substrate, Pierce, Rockford, IL) and exposed to X-ray film. Densities for the known and unknown sample bands on the films were obtained using a Molecular Dynamics densitometer with ImageQuant Software (Amersham, Piscataway, NJ).

Known amounts of pig brain tubulin were used as standards on all blots. Prior work demonstrated that microtubule associated protein-free phosphocellulose-purified tubulin preps from pig brain is 3% β -tubulin class I, 55% β -tubulin class II, 29% β -tubulin class III, and 13% β -tubulin class IV [Banerjee et al., 1988; Doz-

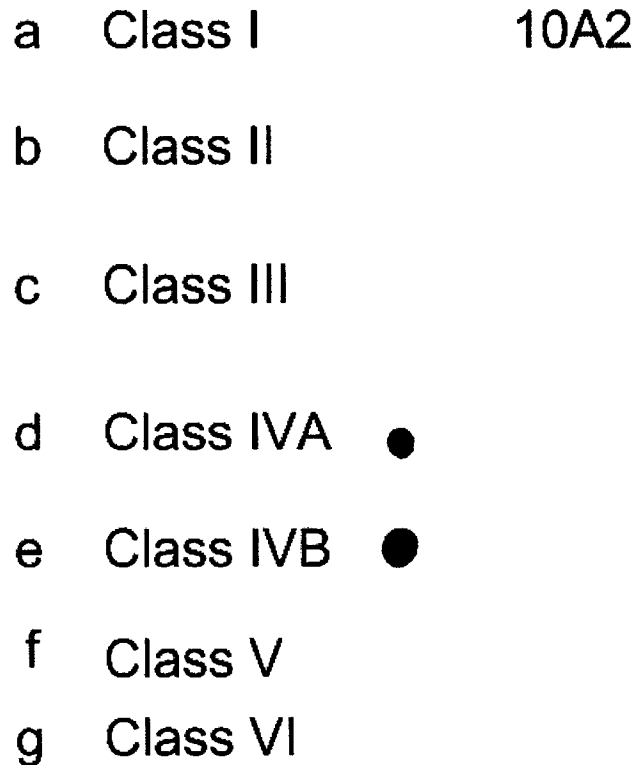


Fig. 1. Dot blots of β -tubulin isotype fusion proteins. β -Tubulin fusion proteins were transferred to PVDF filters and reacted with anti- β -tubulin class IVa + IVb monoclonal antibody 10A2. Fusion protein reactions shown are for β -tubulin class I (Panel a), class II (Panel b), class III (Panel c), class IVa (Panel d), class IVb (Panel e), class V (Panel f), and class VI (Panel g). Only β -tubulin fusion proteins constructed with class IVa or IVb carboxyl terminal peptides were found to react.

ier et al., 2003]. The quantities of tubulin isotypes in unknown samples were calculated from linear fits of standard curves from each Western blot done in triplicate and for at least two lysates prepared from independently grown cell cultures. It was critical to establish the linearity of response for each antibody and to determine that unknown samples were within the linear range. Extrapolation to values outside the standard curve can result in significant error.

Calibration of Antibody Reactivity With β -Tubulin Fusion Proteins

The tubulin protein measurements in the work presented here were done on lysates from human cell lines. Because human and pig brain tubulins may interact differentially with mouse monoclonal antibodies, we constructed fusion proteins with human β -tubulin isotype peptides to compare and calibrate the antibody reactivity. Maltose binding protein (MBP) β -tubulin fusion proteins were constructed for each of the seven human β -

TABLE I. Oligonucleotide Primers and β -Tubulin Carboxyl Terminal Sequences for β -Tubulin Fusion Proteins

Class	Forward primer sequence 5'-3'	Reverse primer sequence 5'-3'	Fragment (bp)	Cloned as	Carboxyl terminal sequences
I	aaa gaa ttc gat gcc acc gca gaa gag gag gat ttc aaa gaa ttc gag gcc acg gcc	aaa aag ctt cta ccc act acc ttc tac cat t aaa agc tta caa acg ttt atg tga ttt tag	485	EcoRI/HindIII	DATAEEEDFGEEAEEEA
II	gac gaa caa ggg aaa gaa ttc gag gcc acg gcc gag gaa gag g aaa gaa ttc gag gcc	aaa aag ctt aag ggt atc tga cag caa tag a aaa aag ctt ggg tta aag ata aat tag gg aaa tct aga atg aaa atg ctt taa tgg	325	EcoRI/HindIII	DATADEQGEFEFEFEDEEA
III	aaa gaa ttc gat gcc acc gca gaa gag gag gat ttc aaa gaa ttc gag gcc acg gcc	aaa aag ctt aag ggt atc tga cag caa tag a aaa aag ctt ggg tta aag ata aat tag gg aaa tct aga atg aaa atg ctt taa tgg	388	EcoRI/HindIII	DATAEEEGEMYEDDEEESEAQQGPK
IVa	aaa gaa ttc gat gcc acc gca gaa gag gag gat ttc aaa gaa ttc gag gcc acg gcc	aaa aag ctt aag ggt atc tga cag caa tag a aaa aag ctt ggg tta aag ata aat tag gg aaa tct aga atg aaa atg ctt taa tgg	279	EcoRI/HindIII	DATAEEGEFEFEFEFEVA
IVb	aaa gaa ttc gat gcc acc gca gaa gag gag gat ttc aaa gaa ttc gag gcc acg gcc	aaa aag ctt aag ggt atc tga cag caa tag a aaa aag ctt ggg tta aag ata aat tag gg aaa tct aga atg aaa atg ctt taa tgg	225	EcoRI/Xba I	DATAEEGEFEFEFEFEVA
V	aaa gaa ttc gat gcc acc gca gaa gag gag gat ttc aaa gaa ttc gag gcc acg gcc	aaa aag ctt aag ggt atc tga cag caa tag a aaa aag ctt ggg tta aag ata aat tag gg aaa tct aga atg aaa atg ctt taa tgg	519	EcoRI/Xba I	DATANDGEEAFEDFEFEIDG
VI	aaa gaa ttc gat gcc acc gca gaa gag gag gat ttc aaa gaa ttc gag gcc acg gcc	aaa aag ctt aag ggt atc tga cag caa tag a aaa aag ctt ggg tta aag ata aat tag gg aaa tct aga atg aaa atg ctt taa tgg	388	EcoRI/HindIII	DAKAVLEEDDEEVTEEMEPEDKKGH

tubulin isotypes (Table I). DNA fragments corresponding to the coding region of the extreme C-terminus of all seven human β -tubulin isotypes were obtained by PCR amplification from either cDNA or genomic DNA, using the primer sets indicated in Table I. The fragments were cloned in-frame (sites indicated in Table I) into a modified version of the pMBP-His-Parallel vector [Sheffield et al., 1999] (a gift from O. Karginova, Department of Biology and Z. Derewenda, Department of Physiology and Biophysics, University of Virginia), resulting in the generation of fusion proteins whose N-terminus was the MBP, and whose C-terminus was the tubulin isotype indicated, separated by a 6X His tag. Nucleotide sequences across the relevant portions of the tubulin coding regions were verified using the Big Dye method on an ABI 310 DNA sequencer. The fusion proteins were expressed in an *Escherichia coli* DH5 α background with induction by 0.5 mM isopropyl- β -D-thiogalactopyranoside, and subsequently purified by metal chelate chromatography on nickel nitrilotriacetic resin (Qiagen). Purity was assessed by SDS-PAGE.

The fusion proteins were loaded in known amounts onto SDS-PAGE along with known quantities of pig brain tubulin. The fusion protein concentrations were determined from the optical density at 278 nm, using extinction coefficients calculated from the amino acid sequence: fusion- β -tubulin class I, $\epsilon_{278} = 1.493$ l/g cm; fusion- β -tubulin class II, $\epsilon_{278} = 1.489$ l/g cm; fusion- β -tubulin class III, $\epsilon_{278} = 1.500$ l/g cm; fusion- β -tubulin class IVa, $\epsilon_{278} = 1.493$ l/g cm; fusion- β -tubulin class IVb, $\epsilon_{278} = 1.489$ l/g cm. The concentration of pig brain tubulin was also determined spectrophotometrically ($\epsilon_{278} = 1.2$ l/g cm) [Detrich III and Williams Jr., 1978]. Gels were transferred to PVDF membranes for immunoblotting and the reactivity of the fusion proteins and pig brain were compared using densitometry. Correction factors and standard errors were calculated for each antibody (Table II) from triplicate Western blots by dividing the known amount of β -tubulin fusion protein loaded on

TABLE II. Corrections for β -Tubulin Isotype Data Determined Using Pig Brain Standards

β -Tubulin class	Correction factor \pm SE ^a
I	0.64 \pm 0.12
II	0.61 \pm 0.17
III	0.27 \pm 0.047
IVa + IVb	1.31 \pm 0.31

^aThese correction factors were used to calculate the actual amount of β -tubulin in human cell lines: β -tubulin_{human} = correction factor \times β -tubulin_{pig brain}. Correction factors were calculated as the actual amount (μ g) of β -tubulin fusion protein loaded on the gel for Western blotting divided by the amount of β -tubulin predicted using pig brain tubulin for the standard curve. The standard error (SE) from triplicate blots is indicated.

TABLE III. β -Tubulin Isootype Protein and mRNA Levels

Cell line	β I	β II	β III	β IVa	β IVb	β V
<i>Percentage tubulin isotype mRNA</i>						
Colon cancer						
COLO 205	85.7	0.6	2.6	0	11.1	0
HCT-15	65.0	0.8	3.4	0	5.1	25.8
Breast cancer						
BT-549	74.9	0.1	16.0	0	2.3	6.7
T-47D	76.2	0.7	0.7	0.1	6.4	16.4
MCF-7	78.1	0.2	14.1	0.1	4.3	3.2
MDA-MB-231	78.3	0.2	2.4	0	15.8	13.2
Lung cancer						
A549	57.8	2.3	6.7	0.5	4.2	28.5
HOP 18	38.9	6.6	14.8	0	9.7	30.0
Melanoma						
Malme-3M	57.7	13.5	8.0	4.1	1.6	15.2
SK-MEL-2	51.2	1.1	3.5	0.9	3.1	40.2
Ovarian cancer						
OVCAR-3	42.6	5.2	5.2	0.7	9.4	36.8
SK-OV-3	55.9	0	1.6	0.1	4.3	38.1

Cell line	β I	β II	β III	β IVa + β IVb
<i>Percentage tubulin isotype protein</i>				
Colon cancer				
COLO 205	36.0	0	0	64.0
HCT-15	61.8	0	0.2	38.0
Breast cancer				
BT-549	65.9	0.6	6.4	27.1
T-47D	85.7	0	0	14.3
MCF-7	39.1	0	2.5	58.4
MDA-MB-231	76.1	0	0	23.9
Lung cancer				
A549	71.9	0	1.6	26.5
HOP 18	63.2	1.5	5.0	30.3
Melanoma				
Malme-3M	84.4	3.8	5.1	7.0
SK-MEL-2	73.1	1.4	1.5	24.0
Ovarian cancer				
OVCAR-3	97.0	0	0	3.1
SK-OV-3	85.6	0	0.8	13.6

the gel by the amount of β -tubulin isotype estimated from the pig brain standard curve. These factors were used to correct the data obtained using pig brain standard curves on the Western blots. The percentages of tubulin isotype proteins shown in Table III and Fig. 3b were corrected using the correction factors in Table II.

RESULTS

β -Tubulin mRNA Expression

We used qRT-PCR to measure the amounts of β -tubulin isotype mRNA classes I, II, III, IVa, IVb, V, and VI for each of the 12 cell lines (Fig. 2). The mRNA levels for each isotype, with the exception of class I, differed by more than 10-fold between the 12 cell lines; however, the total tubulin mRNA levels were found to be fairly constant, differing by less than 10-fold across

all 12 cell lines. This is consistent with the previous suggestion that total tubulin expression levels are regulated to fulfill the function of the cytoskeleton [Cabral and Barlow, 1991; Wang and Cabral, 2005].

Figure 3a and Table III present the isotype mRNA data as percentages of total β -tubulin mRNA for each cell line. As reported for other cell lines [Nicoletti et al., 2001], it is clear that β -tubulin class I mRNA comprises more than 50% of the β -tubulin mRNA for all but two of the cell lines examined. As expected, the hematopoietic-specific β -tubulin class VI mRNA was either absent or 4–6 orders of magnitude less prevalent (Fig. 2) than β -tubulin class I. The neuron-specific isotype, β -tubulin class III, was expressed at relatively high levels (>10% of total mRNA) in 3 of the 12 cell lines, including 2 of the 4 breast cancer cell lines. In fact, β -tubulin class III mRNA constituted more than 1% of the tubulin message in all of the cell lines except T-47D, a surprising result considering that β -tubulin class III is neuron specific. In addition, several cell lines expressed very low but measurable levels of the “neuron-specific” β -tubulin class IVa. Relatively high levels of β -tubulin class V mRNA (>25% of the total β -tubulin mRNA) were detected in half of the cell lines. This raises the intriguing possibility that β -tubulin class V is highly expressed in human cells, something that has not been measurable until recently due to the absence of a commercially available β -tubulin class V antibody. Overall, the mRNA levels of β -tubulin class IVb were comparable to those of β -tubulin class III, although one or the other was significantly more abundant in some cell lines. In general, β -tubulin class II mRNA was less abundant than β -tubulin classes I, III, IVb, and V messages.

Because alterations in tubulin isotype levels have been implicated in resistance to antimetabolic agents [Kavallaris et al., 1997, 1999; Ranganathan et al., 1998; Banerjee, 2002], we measured IC₅₀ levels for all 12 cell lines used in this study (Table IV). No correlations between IC₅₀ values and tubulin isotype mRNA levels were found (data not shown). However, these cell lines represent several tumor types and the contribution of tubulin isotypes to drug sensitivity could be masked by many factors.

β -Tubulin Protein Levels

Mouse monoclonal antibodies specific for β -tubulin classes I, II, III, and IVa + IVb were utilized in quantitative Western blotting of whole cell lysates from 12 human cell lines. We found that pig brain tubulin is a plentiful and reliable source of tubulin for standard curves on Western blots. However, because pig brain tubulin and human cell lysates may react differently with the monoclonal antibodies, we constructed fusion proteins with the human tubulin carboxyl terminal peptides and compared

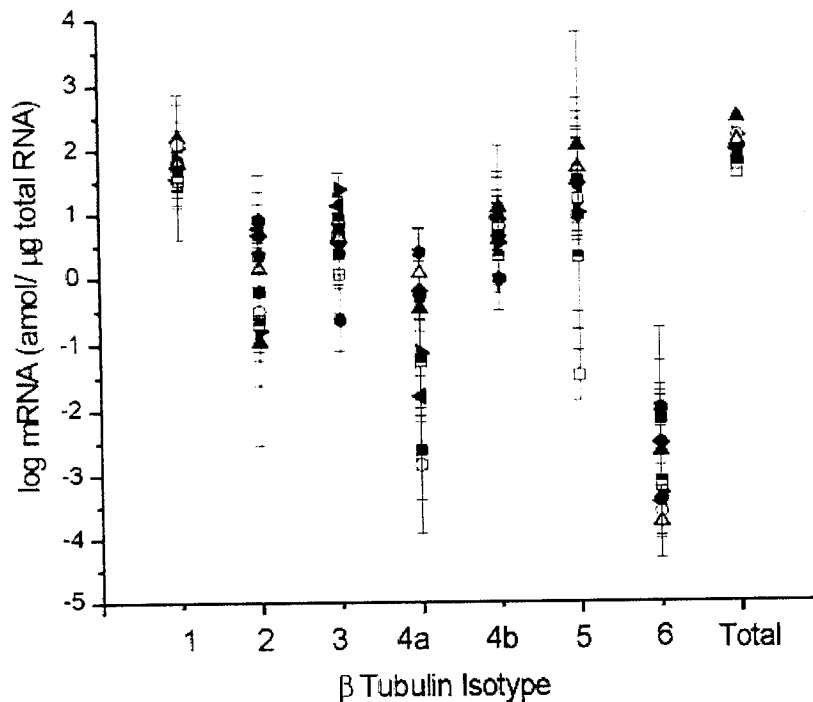


Fig. 2. β -Tubulin isotype mRNA for twelve cell lines. Mean data from qRT-PCR of two or more cell preps are shown. Data from β -tubulin isotype classes I (1), II (2), III (3), IVa (4a), IVb (4b), V (5), and VI (6) were summed to calculate the total β -tubulin mRNA in each cell line.

their reactivities on Western blots with that of pig brain tubulin. The largest difference in reactivity was found for β -tubulin class III (Table II). The reaction of TUJ1 monoclonal antibody with pig brain standard overestimates the actual amount of human β -tubulin class III fusion protein by 3.7 (± 0.6)-fold. β -Tubulin classes I and II are overestimated by about 1.6 (± 0.4)-fold using the pig brain standards, and β -tubulin classes IVa + IVb are underestimated by about 0.8 (± 0.2)-fold. We adjusted all tubulin measurements, using the correction factors in Table II, to estimate actual tubulin protein levels in human cell lines. An alternate method of standardization is to construct standard curves with the β -tubulin fusion proteins. The advantage of the quantitative immunoblot method presented here is that it can be used as a rigorous tool for studying tubulin levels in whole cell or tissue lysates without requiring fusion protein standards.

We used quantitative Western blotting of whole cell lysates to measure β -tubulin isotype protein levels for classes I, II, III, and IVa + IVb (Fig. 3b and Table III). Significant levels of β -tubulin classes I and IVa + IVb were found in all 12 cell lines, ranging from 36.0–97.0% for β -tubulin class I and from 3.1–64.0% for β -tubulin classes IVa + IVb. β -Tubulin class I comprised $>50\%$ of the total β -tubulin measured in 10 of the 12 cell lines. β -Tubulin classes IVa + IVb comprised $>50\%$ of the total β -tubulin in breast cancer (MCF-7) and colon cancer (COLO 205) cells. β -Tubulin class III comprised more than 1% of the total β -tubulin protein (1.5–6.4%) in

breast cancer cell lines, BT-549 and MCF-7; lung cancer cells, A549 and HOP 18; and melanoma cells, Malme-3M and SK-MEL-2. β -Tubulin class II was found at low but measurable levels (0.6–3.8%) in only four cell lines—breast cancer (BT-549), lung cancer (HOP 18) and melanoma (SK-MEL-2 and Malme-3M) cell lines.

Comparison of mRNA and Protein

β -Tubulin mRNA and protein levels for isotype classes I, II, III, and IVa + IVb are compared in Fig. 4. β -Tubulin classes V and VI mRNA data were not included in this analysis because we did not have corresponding protein data. Thus, the percentages of β -tubulin isotype mRNA in Fig. 4 were calculated assuming that the total tubulin was comprised of only β -tubulin isotype classes I, II, III, and IVa + IVb. β -Tubulin classes I and IVa + IVb are present in greatest abundance for both mRNA and protein. Only β -tubulin class I data suggest a near one-to-one correspondence for mRNA and protein. For β -tubulin class I, 10 of the 12 cell lines have both mRNA and protein levels $>50\%$. For β -tubulin class IVa + IVb, there is consistently more protein than mRNA in 10 of the 12 cell lines. β -Tubulin class II protein is found in only four cell lines; therefore, no general conclusions regarding the relationship between mRNA and protein levels can be made. β -Tubulin class III protein is found in eight cell lines. The mRNA and protein amounts for β -tubulin class III correspond (Fig.

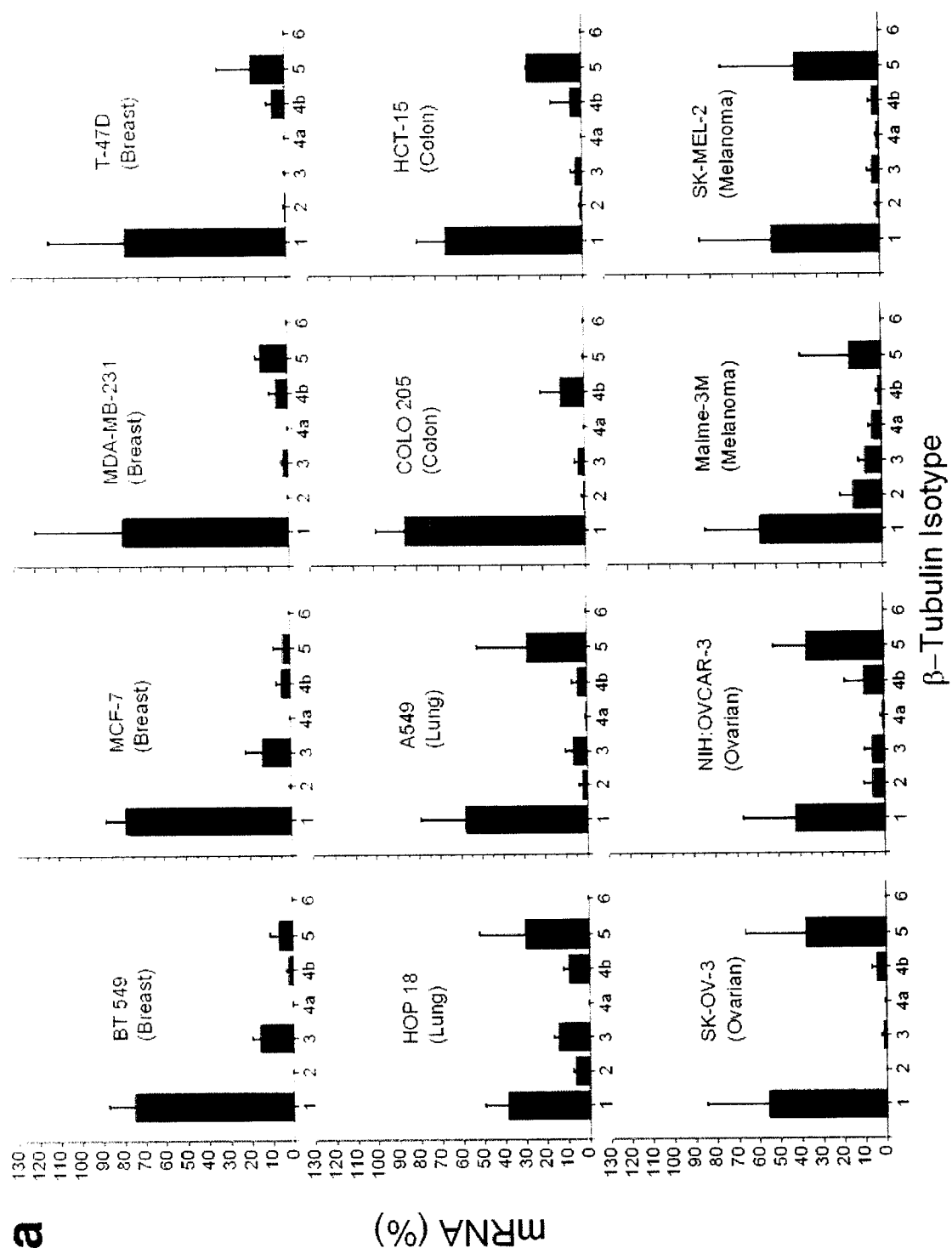


Fig. 3. β -Tubulin isotype profiles for 12 cell lines. The data in Table III are plotted as bars representing the percent contribution of each β -tubulin isotype mRNA (a) or protein (b) to the total tubulin in each cell line. The sum of the values for all six β -tubulin isotype classes was considered as the total tubulin for the mRNA percentage calculations. The sum of the β -tubulin isotype classes I, II, III, and IVa + IVb was considered to be the total tubulin for the protein analysis. Error bars represent standard deviation from multiple experiments, as described in the Materials and Methods.

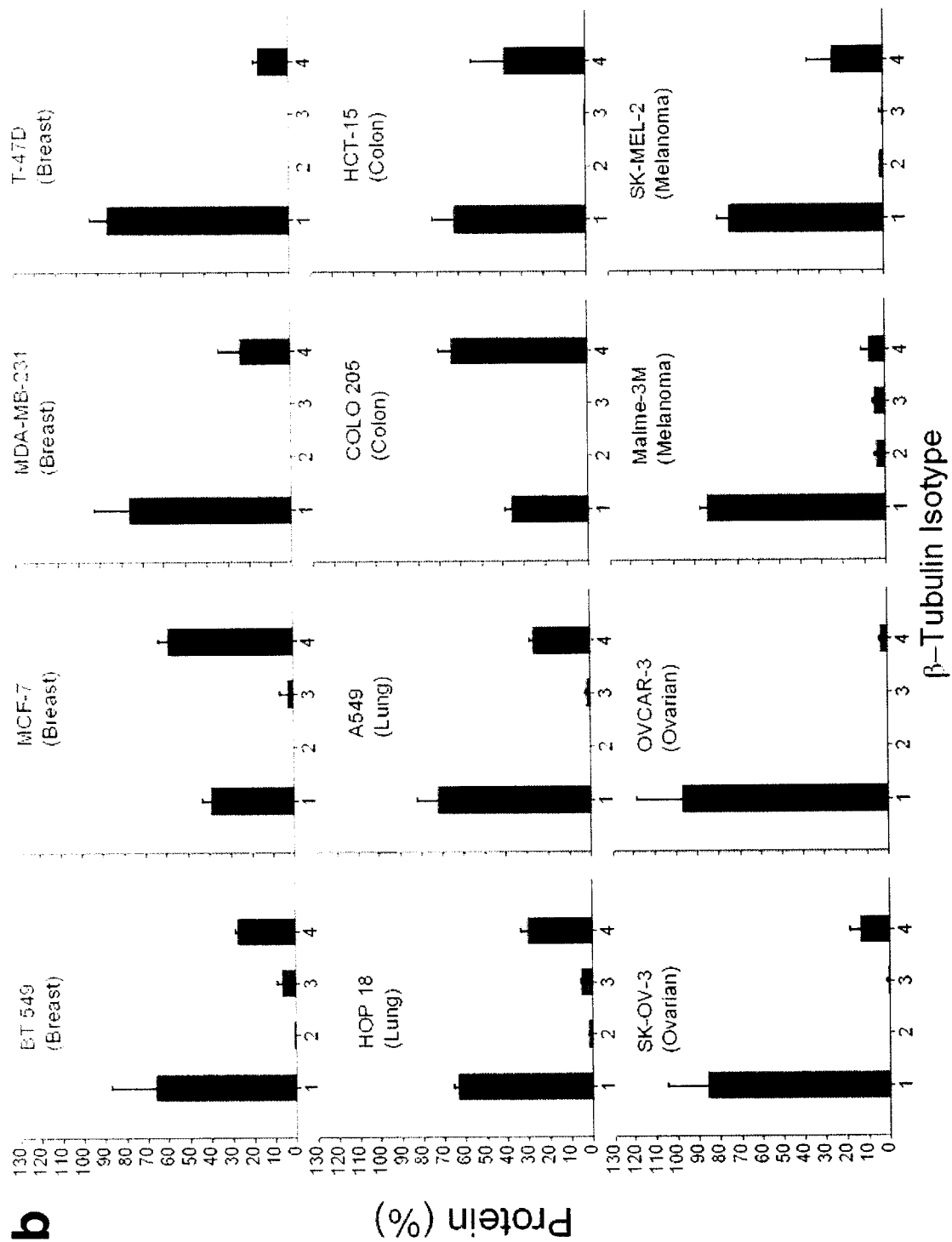


Figure 3. (Continued)

TABLE IV. Drug Sensitivities of Human Cancer Cell Lines to Paclitaxel and Vinblastine as Measured by Two Different Assays

TABLE IV. Drug Sensitivities of Human Cancer Cell Lines to Paclitaxel and Vinblastine as Measured by Two Different Assays					
Cancer cell line	Drug	IC ₅₀ (nM)		IC ₅₀ (nM) Mean	Fold difference ^b
		Cell count	MTS assay ^a		
Colon					
COLO-205	Paclitaxel	29.2	26.1	27.7	6.0
HCT-15	Paclitaxel	6.4	2.8	4.6	
COLO-205	Vinblastine	0.6	0.7	0.7	
HCT-15	Vinblastine	31.1	24.9	28.0	40
Breast					
BT-549	Paclitaxel	4.3	5.5	4.9	4.9 (MCF7), 12.3 (MDA), 3.3 (T-47D)
MCF-7	Paclitaxel	1.0	1.0	1.0	2.5 (MDA)
MDA-MB-231	Paclitaxel	0.3	0.5	0.4	
T-47D	Paclitaxel	0.8	2.3	1.5	1.5 (MCF7), 3.8 (MDA)
BT-549	Vinblastine	0.9	1.3	1.1	2.8 (MCF7)
MCF-7	Vinblastine	0.4	0.4	0.4	
MDA-MB-231	Vinblastine	2.2	0.9	1.6	1.5 (BT549), 4.0 (MCF7)
T-47D	Vinblastine	5.3	13.5	9.3	8.5 (BT549), 23.3 (MCF7), 5.8 (MDA)
Lung					
A-549	Paclitaxel	2.9	2.5	2.7	3.9
HOP-18	Paclitaxel	0.6	0.8	0.7	
A-549	Vinblastine	2.1	1.2	1.7	3.4
HOP-18	Vinblastine	0.7	0.4	0.5	
Melanoma					
Malme-3M	Paclitaxel	4.2	4.6	4.4	1.1
SK-MEL-2	Paclitaxel	3.7	4.1	3.9	
Malme-3M	Vinblastine	0.3	1.1	0.7	
SK-MEL-2	Vinblastine	0.6	1.3	0.9	1.3
Ovarian					
OVCAR-3	Paclitaxel	2.1	0.8	1.5	
SK-OV-3	Paclitaxel	2.0	4.6	3.3	2.2
OVCAR-3	Vinblastine	3.7	1.3	2.5	1.6
SK-OV-3	Vinblastine	2.3	0.9	1.6	

^aMTS is 3-(4,5-dimethylthiazol-2-yl)-5-(3-carboxymethoxyphenyl)-2-(4-sulfophenyl)-2H-tetrazolium, inner salt, a component of CellTiter 96[®] AQueous One Solution Cell Proliferation Assay.

^bDetermined by dividing the larger mean IC₅₀ by the smaller for each pair of cell lines. For the breast cancer cells, the cell line compared is given in parentheses.

4. Panel c insert), although there is consistently more mRNA than protein.

DISCUSSION

The role of β -tubulin isotype levels in determining cellular responses to antimitotic agents has been controversial for more than a decade. Most studies have relied upon measurements of intracellular tubulin mRNA levels to infer protein levels. However, mRNA and protein levels are not correlated for many human and yeast proteins, especially those that are regulated by posttranscriptional processes [Anderson and Seilhamer, 1997; Gygi et al., 1999]. Thus, it is important to establish whether there is a correlation between tubulin mRNA and protein levels so as to better understand mechanisms that may underlie drug resistance.

We present here a reliable method for quantifying β -tubulin protein levels in whole cell lysates. We demonstrated that tubulin isotype fusion proteins or pig brain

tubulin calibrated with the fusion proteins can be used to create a standard curve on Western blots. We find this to be an acceptable method for protein quantification for the following reasons: (1) The monoclonal antibodies used in this work are highly specific as demonstrated by blots with either purified tubulin isotypes or tubulin isotype fusion proteins [Lee et al., 1990; Lobert et al., 1995, 1998; Roach et al., 1998] (Fig. 1). (2) The data are highly reproducible. We present here data collected from independent cell protein extractions and at least three Western blots for each whole cell lysate. The standard error for each measurement was propagated from the biological (individual protein preparations) and technical (individual Western blots) replicates and is represented as the error bars in Fig. 3b. For the two most abundant isotypes measured, β -tubulin classes I and IVa + IVb, the average error was 14.6% and 23.3%, respectively. (3) There is good agreement between the mRNA and protein levels for β -tubulin isotype classes I and III (although for β -tubulin class III the correspondence is

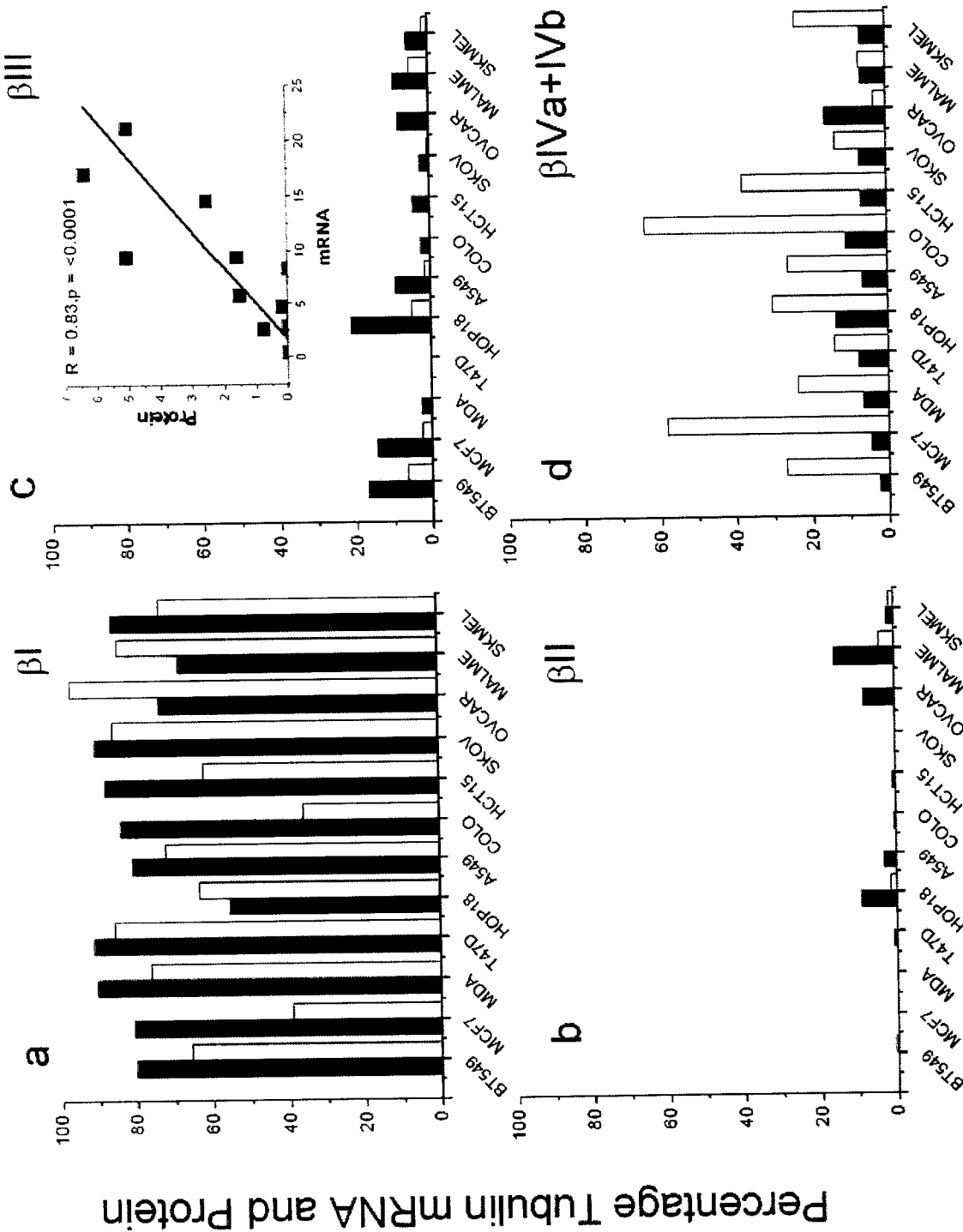


Fig. 4. Comparison of β -tubulin isotype protein levels with mRNA levels. Only β -tubulin isotype classes I (β I), II (β II), III (β III), and IV (β IVa + IVb) were considered when calculating the total mRNA and protein levels. Solid bars represent mean mRNA and open bars represent mean protein values. Panel a: β I, Panel b: β II, Panel c: β III, and Panel d: β IVa + IVb. Insert in Panel c shows a plot of mRNA vs. protein data for β -tubulin class III fit by linear regression. The straight line represents the best fit of the data. The correlation coefficient, R (Pearson's product-moment) for the fit and the P -value relative to a horizontal line (no correlation) are shown.

not one-to-one). The agreement in isotype percentages by two independent methods supports the findings and the method used for protein quantification.

The higher β -tubulin class IVa + IVb protein levels compared to mRNA levels suggest possible differential regulatory mechanisms for this isotype compared to β -tubulin classes I and III. Fine tuning of tubulin levels during the cell cycle occurs via autoregulation. This process alters mRNA stability and requires both an essential sequence on polysomal β -tubulin mRNA and an aminoterminal Met-Arg-Glu-Ile on the nascent tubulin polypeptide [Pachter et al., 1987; Cleveland, 1988; Yen et al., 1988]. Furthermore, α -tubulin mRNA levels remain high even when protein synthesis is repressed [Gonzalez-Garay and Cabral, 1996]. In fact, α -tubulin synthesis in Chinese hamster ovary (CHO) cells appears to play a role in regulating β -tubulin protein levels. This phenomenon of tubulin posttranscriptional autoregulation was demonstrated in a wide variety of vertebrate and invertebrate cell types. Intracellular tubulin levels are also transcriptionally regulated [Cleveland, 1989]. It is possible that individual isoforms may be differentially regulated while maintaining free tubulin subunits at levels necessary for different phases of the cell cycle. Our data demonstrate relatively constant amounts of total tubulin message in spite of variations in individual isotype mRNA levels (Fig. 2). Because of the relatively low levels of β -tubulin classes IVa + IVb mRNA compared to protein, our data suggest that differential methods for regulating β -tubulin classes (I or III vs. IVa + IVb) are likely. Alternatively, pairing of specific α - and β -tubulins may lead to differential stability of β -tubulins [Hoyle et al., 2001].

β -Tubulin class III has been studied extensively for its potential role in resistance to antimitotic agents. For example, paclitaxel-resistant lung cancer cells and ovarian tumors were shown to have increased levels of tubulin isoforms, particularly β -tubulin classes III and IVa mRNA levels [Kavallaris et al., 1997]. Furthermore, when paclitaxel-resistant lung cancer cells were treated with antisense oligonucleotides for β -tubulin class III, the drug resistance was partially reversed, coincident with reduced protein levels of β -tubulin class III [Kavallaris et al., 1999]. In other work, β -tubulin classes III and IVa transcripts were shown to increase in paclitaxel-resistant prostate cancer cells [Ranganathan et al., 1998]. Combined isoelectric focusing and mass spectrometry were used to measure tubulin isoforms in four cell lines [Verdier-Pinard et al., 2003]. This report demonstrated an increase in β -tubulin class III and associated this with paclitaxel resistance in lung cancer cells. In the most convincing study, when cells were transfected with β -tubulin class III, weak resistance to paclitaxel was found and this resistance was associated with decreased microtubule stability [Hari et al., 2002].

Thus, there is considerable interest in determining whether functional β -tubulin class III protein is involved in mechanisms that cause resistance to antimitotic agents. Because qRT-PCR is a commonly used reliable method for quantitation of mRNA levels, it is potentially an important method for better understanding the role of β -tubulin isoforms in drug resistance. To draw conclusions from mRNA measurements, it is essential to know whether transcript levels correlate with protein levels. In the work described here, β -tubulin class III mRNA and protein levels are correlated but do not demonstrate one-to-one correspondence. β -Tubulin class III mRNA may be useful for comparing relative amounts of this isotype across cell and tissue samples; however, quantitatively inferring β -tubulin protein levels from mRNA levels within a cell or tissue type should be done with caution.

The work of Bhattacharya and Cabral [2004] suggests a minimum threshold level for β -tubulin class V that alters mitotic spindle function. They found that modest increases in β -tubulin class V, to levels of 15% or more of the total β -tubulin, may increase microtubule dynamics and decrease microtubule polymer levels. This was shown to be associated with weak resistance to paclitaxel. We found threshold levels of β -tubulin class V mRNA (>15%) in several cell lines: colon cancer, HCT-15; breast cancer, T-47D; lung cancer, A549 and HOP-18; melanoma, Malme-3M and SK-MEL-2; ovarian, OVCAR-3 and SK-OV-3. We found no correlation between IC₅₀ values for paclitaxel or vinblastine and percentage β -tubulin class V mRNA (data not shown). While the relationship between mRNA and protein levels for this isotype remains to be determined, one difference between the work reported here and that of Bhattacharya and Cabral [2004] is that they carefully established that only one variable is altered in the β -tubulin class V overexpressing CHO cells. In our work, many variables differ among the 12 cell lines and some of them may compensate for changes in β -tubulin class V levels. Preliminary examination of one of the breast cancer cell lines, BT-549, by mass spectrometry revealed the presence of β -tubulin class V (data not shown). Therefore, we expect to find β -tubulin class V protein in some or all of the twelve cell lines. We have recently developed a monoclonal antibody to β -tubulin class V, which should permit quantitative measurement of protein levels and provide data regarding the contribution of β -tubulin class V to drug resistance.

CONCLUSIONS

From our comparison of β -tubulin isotype mRNA and protein levels on 12 human cancer cell lines, we conclude that quantitative Western blotting, utilizing human

β -tubulin fusion proteins or pig brain tubulin with appropriate correction factors, is a reliable method for quantifying β -tubulin isotypes in human cancer cell lines. We found a good correspondence between β -tubulin mRNA and protein levels for classes I and III. For β -tubulin classes IVa + IVb, the higher levels of protein compared to mRNA suggest potential differential regulatory mechanisms for β -tubulin isotypes.

REFERENCES

- Alvarez M, Paul K, Monks A, Hose A, Lee JS, Weinstein J, Grever M, Bates S, Fojo T. 1995. Generation of a drug resistance profile by quantitation of mdr-1/P-glycoprotein in the cell lines of the National Cancer Institute Anticancer Drug Screen. *J Clin Invest* 95:2205–2214.
- Anderson L, Seilhamer J. 1997. A comparison of selected mRNA and protein abundances in human liver. *Electrophoresis* 18:533–537.
- Banerjee A. 2002. Increased levels of tyrosinated α -, β (III)-, and β (IV)-tubulin isotypes in paclitaxel-resistant MCF-7 breast cancer cells. *Biochem Biophys Res Commun* 293:598–601.
- Banerjee A, Roach MC, Wall KA, Lopata MA, Cleveland DW, Luduena RF. 1988. A monoclonal antibody against the type II isotype of β -tubulin. Preparation of isotypically altered tubulin. *J Biol Chem* 263:3029–3034.
- Bhattacharya R, Cabral F. 2004. A ubiquitous β -tubulin disrupts microtubule assembly and inhibits cell proliferation. *Mol Biol Cell* 15:3123–3131.
- Cabral F, Barlow SB. 1991. Resistance to antimetabolic agents as genetic probes of microtubule structure and function. *Pharmacol Ther* 52:159–171.
- Cleveland D. 1988. Autoregulated instability of tubulin mRNAs: a novel eukaryotic regulatory mechanism. *TIBS: Trends in Biochemical Sciences* 13:339–343.
- Cleveland DW. 1989. Autoregulated control of tubulin synthesis in animal cells. *Curr Opin Cell Biol* 1(1):10–14.
- Correia JJ, Lobert S. 2001. Physicochemical aspects of tubulin-interacting antimetabolic drugs. *Curr Pharm Des* 7:1213–1228.
- Detrich HW, III, Williams RC, Jr. 1978. Reversible dissociation of the $\alpha\beta$ dimer of tubulin from bovine brain. *Biochemistry* 17:3900–3907.
- Dhamodharan R, Jordan MA, Thrower D, Wilson L, Wadsworth P. 1995. Vinblastine suppresses dynamics of individual microtubules in living interphase cells. *Mol Biol Cell* 6:1215–1229.
- Dozier JH, Hiser L, Davis JA, Thomas NS, Tucci MA, Benghuzzi HA, Frankfurter A, Correia JJ, Lobert S. 2003. β Class II tubulin predominates in normal and tumor breast tissues. *Breast Cancer Res* 5:R157–R169.
- Gonzalez-Garay ML, Cabral F. 1996. α -Tubulin limits its own synthesis: evidence for a mechanism involving translational repression. *J Cell Biol* 135:1525–1534.
- Gygi SP, Rochon Y, Franz A, Aebersold R. 1999. Correlation between protein and mRNA abundance in yeast. *Mol Cell Biol* 19:1720–1730.
- Hari M, Yang H, Canizales M, Zeng C, Cabral F. 2002. Expression of class III [β]-tubulin in CHO cells reduces microtubule stability and confers resistance to paclitaxel. *Proc Am Assoc Cancer Res* 43:LB139.
- Hoyle HD, Turner FR, Brunick L, Raff EC. 2001. Tubulin sorting during dimerization in vivo. *Mol Biol Cell* 12:2185–2194.
- Kavallaris M, Kuo DY, Burkhardt CA, Regl DL, Norris MD, Haber M, Horwitz SB. 1997. Taxol-resistant epithelial ovarian tumors are associated with altered expression of specific β -tubulin isotypes. *J Clin Invest* 100:1282–1293.
- Kavallaris M, Burkhardt CA, Horwitz SB. 1999. Antisense oligonucleotides to class III β -tubulin sensitize drug-resistant cells to Taxol. *Br J Cancer* 80:1020–1025.
- Lee MK, Tuttle JB, Rebhun LI, Cleveland DW, Frankfurter A. 1990. The expression and posttranslational modification of a neuron-specific β -tubulin isotype during chick embryogenesis. *Cell Motil Cytoskeleton* 17:118–132.
- Lobert S, Frankfurter A, Correia JJ. 1995. Binding of vinblastine to phosphocellulose-purified and $\alpha\beta$ -class III tubulin: the role of nucleotides and β -tubulin isotypes. *Biochemistry* 34:8050–8060.
- Lobert S, Frankfurter A, Correia JJ. 1998. Energetics of vinca alkaloid interactions with tubulin isotypes: implications for drug efficacy and toxicity. *Cell Motil Cytoskeleton* 39:107–121.
- Nicoletti MI, Valoti G, Giannakakou P, Zahn Z, Kim JH, Lucchini V, Landoni F, Mayo JG, Giavezzi R, Fojo T. 2001. Expression of β -tubulin isotypes in human ovarian carcinoma xenografts and in a sub-panel of human cancer cell lines from the NCI-Anticancer Drug Screen: correlation with sensitivity to microtubule active agents. *Clin Cancer Res* 7:2912–2922.
- Pachter JS, Yen TJ, Cleveland DW. 1987. Autoregulation of tubulin expression is achieved through specific degradation of polyosomal tubulin mRNAs. *Cell* 51:283–292.
- Ranganathan S, Benetatos CA, Colarusso PJ, Dexter DW, Hudes GR. 1998. Altered β -tubulin isotype expression in paclitaxel-resistant human prostate carcinoma cells. *Br J Cancer* 77:562–566.
- Roach MC, Boucher VL, Walss C, Ravdin PM, Luduena RF. 1998. Preparation of a monoclonal antibody specific for the class I isotype of β -tubulin: the β isotypes of tubulin differ in their cellular distribution within human tissues. *Cell Motil Cytoskeleton* 39:273–286.
- Sheffield P, Garrard S, Derewenda Z. 1999. Overcoming expression and purification problems of RhoGDI using a family of “parallel” expression vectors. *Protein Expr Purif* 15:34–39.
- Sullivan KF. 1988. Structure and utilization of tubulin isotypes. *Annu Rev Cell Biol* 4:687–716.
- Sullivan KF, Cleveland DW. 1986. Identification of conserved isotype-defining variable region sequences for four vertebrate β -tubulin polypeptide classes. *Proc Natl Acad Sci USA* 83:4327–4331.
- Verdier-Pinard P, Wand R, Martello L, Burd B, Orr GA, Horwitz SB. 2003. Analysis of tubulin isotypes and mutation from taxol-resistant cells by combined isoelectric focusing and mass spectrometry. *Biochemistry* 42:5349–5357.
- Wang Y, Cabral F. 2005. Paclitaxel resistance in cells with reduced β -tubulin. *Biochim Biophys Acta* 1744:245–255.
- Yen TJ, Machlin PS, Cleveland DW. 1988. Autoregulated instability of β -tubulin mRNAs by recognition of the nascent amino terminus of β -tubulin. *Nature* 334:580–585.
- Yvon AM, Wadsworth P, Jordan MA. 1999. Taxol suppresses dynamics of individual microtubules in living human tumor cells. *Mol Biol Cell* 10:947–959.

A Generalized Response Surface Model with Varying Relative Potency for Assessing Drug Interaction

Maiying Kong and J. Jack Lee *

Department of Biostatistics and Applied Mathematics, University of Texas,

M.D. Anderson Cancer Center, Unit 447, 1515 Holcombe Blvd, Houston, TX 77030

Running title: Response Surface Model for Drug Interaction

SUMMARY. When multiple drugs are administered simultaneously, investigators are often interested in assessing whether the drug combinations are synergistic, additive, or antagonistic. Based on the Loewe additivity reference model, many existing response surface models require constant relative potency and some of them use a single parameter to capture synergy, additivity, or antagonism. However, the assumption of constant relative potency is too restrictive, and these models using a single parameter to capture drug interaction are inadequate to describe the phenomenon when synergy, additivity, and antagonism are interspersed in different regions of drug combinations. We propose a generalized response surface model with a function of doses instead of one single parameter to identify and quantify departure from additivity. The proposed model can incorporate varying relative potencies among multiple drugs as well. Examples and simulations are given to demonstrate that the proposed model is effective in capturing different patterns of drug interaction.

KEY WORDS: Additivity; Antagonism; Dose-response curve; Dose-response surface; Interaction index; Loewe additivity model; Synergy.

*email: jjlee@mdanderson.org

1. Introduction

Studies of interactions among biologically active agents, such as drugs, carcinogens, or environmental pollutants, have become increasingly important in many branches of biomedical research (Suhnel, 1998). An effective and accurate evaluation of drug interaction for *in vitro* and/or *in vivo* studies can help to determine whether a combination therapy should be further investigated in clinical trials.

The literature supports the notion that Loewe additivity model can be considered as the “gold standard” to define drug interactions (Berenbaum, 1989; Greco, Bravo, and Parsons, 1995; Lee, Kong, and Ayers, 2005). Based on the Loewe additivity model, we focus on applying response surface method (RSM) to study drug interaction. The RSM, which involves an estimation of the $n - 1$ dimensional response surface in n drug combinations, can take all of the information present in the full dose-effect data set for n drugs to give a complete picture of drug interactions over all possible drug combinations. In addition, the RSM can be used to determine the optimal combination therapy. Many examples of the RSM (e.g., Finney, 1971; Greco, Park, and Rustum, 1990; and Plummer and Short, 1990) used a single parameter to capture synergy, additivity, or antagonism. These approaches are valid if only either synergy, additivity, or antagonism exists throughout the whole surface. They are inadequate to describe the presence of pockets of local synergy or local antagonism when they are interspersed in different regions of the drug combinations. White, Faessel, Slocum, Khinkis, and Greco (2004) proposed a nonlinear mixture response surface approach based on the assumption that the combination doses at each fixed ratio follow the median-effect model (Chou and Talalay, 1984), and the parameters in the median effect model are assumed to be polynomials of the ratio. The resulting models capture synergy, additivity, or antagonism exclusively based on the 50% maximal effect isoboles. However, at a fixed ratio, the combination doses of two drugs do not necessarily yield the same mode of drug interactions

as that at 50% maximal effect. For example, Savelev, Okello, Perry, Wilkins, and Perry (2003) showed that the combinations of 1,8-cineole and α -pinene at the fixed ratio 11:1 are synergistic for higher combination doses and additive for lower combination dose. To address this issue, we propose a generalized response surface (GRS) model for two drugs. Instead of using one single parameter, we construct a function of the doses of two drugs to capture synergy, additivity, and antagonism without assuming any fixed patterns of drug interactions. The model contains a rich class of dose-response relationships and allows the drug interaction patterns to be determined by the observed data.

Before we proceed, let us recall a widely used model that provides a dose-response curve for a single agent: Chou and Talalay's (1984) median effect equation,

$$E = \frac{\left(\frac{d}{D_m}\right)^m}{1 + \left(\frac{d}{D_m}\right)^m}. \quad (1)$$

Here d is the dose of a drug, D_m is the median effective dose of a drug, and m is a slope parameter depicting the shape of the dose-response curve. All these dose-response curves can be rewritten as Y , a monotone function of E , having a linear relationship with $\log d$. For example, the median effect equation has the form

$$Y = \log \frac{E}{1 - E} = m(\log d - \log D_m). \quad (2)$$

All the families described by Suhnel (1998), excluding Weibull family, can take such form by establishing a linear relationship between a monotone transformation of E and $\log d$. Tallarida (2000, Chapter 2) pointed out that, in many settings, the data point in the mid range (say between 20% and 80% of the maximum effect) typically displays a nearly linear trend between the response and the $\log d$ when responses are measured on a continuous scale. For quantal response data, Finney (1971) and Govindarajulu (2001) pointed out that the probit or logistic transformed response usually exhibits a linear relationship with $\log d$. Consequently, we assume that the

response or transformed response follows a linear function of $\log d$ for each of the two drugs when acting alone. Without loss of generality, we denote the dose-response curve as $Y = \beta_0 + \beta_1 \log d$.

Suhnel (1998) explicitly derived the combined additive effect of two drugs under the Loewe additivity model and made the assumption that the slopes β_1 are the same for both drugs. Finney (1971) proposed an additivity model for two drugs as $Y = \beta_0 + \beta_1 \log(d_1 + \rho d_2)$ for the combination dose (d_1, d_2) , where ρ is the relative potency of drug 2 versus drug 1 and is assumed to be a constant. The constant ρ again implies that the two dose-response curves have the same slope. To construct a generalized model, we would first loosen the parallel assumption by allowing a varying relative potency. Next, we propose the use of a quadratic function of two doses instead of one single parameter to depict different patterns of drug interactions. The proposed model can be considered as a generalization of Finney’s model (1971) and the model derived by Plummer and Short (1990). We will describe our proposed model in Section 2, relate this new model to isoboles and interaction indices in Section 3, state how to make inference on drug combinations in Section 4, and give simulations and examples to illustrate how the new approach performs in Section 5. The last section is devoted to discussion.

2. Derivation of the generalized response surface (GRS) model

Recall the Loewe additivity model (Loewe and Muischnek, 1926; Berenbaum, 1989; Greco *et al.*, 1995; Lee *et al.*, 2005)

$$\frac{d_1}{D_{y,1}} + \frac{d_2}{D_{y,2}} = 1, \quad (3)$$

where d_1, d_2 are doses of drug 1 and drug 2 in the mixture eliciting an effect y , and $D_{y,1}$ and $D_{y,2}$ are the respective single-agent doses of drug 1 and drug 2 that elicit the effect y . One can obtain the predicted additive effect based on the Loewe additivity model providing that the dose-effect curves for each of the two drugs are known. Suppose that the dose-effect curves are $F_1(D_1)$ for drug 1 and $F_2(D_2)$ for drug 2, then the predicted effect, say y , can be obtained by solving equation

(3) after replacing $D_{y,1}$ by $F_1^{-1}(y)$ and $D_{y,2}$ by $F_2^{-1}(y)$, where F_i^{-1} is the inverse function of F_i ($i = 1, 2$). If the observed effect at (d_1, d_2) is more than or less than the predicted effect, the combination dose (d_1, d_2) is correspondingly synergistic or antagonistic.

Note that the above additive equation (3) can be rewritten as

$$d_1 + d_2 \frac{D_{y,1}}{D_{y,2}} = D_{y,1}. \quad (4)$$

Denote $\frac{D_{y,1}}{D_{y,2}}$ as $\rho(y)$, which is the relative potency of drug 2 versus drug 1, meaning that 1 unit of drug 2 has the same effect as $\rho(y)$ units of drug 1. Grabovsky and Tallarida (2004) addressed the issue that the relative potency may vary. The nonparallel dose-effect curves introduced by Suhnel (1998) can also be interpreted as the varying relative potency. When the relative potency varies, finding a method to transform the combination dose (d_1, d_2) into the equivalent doses of drug 1 or drug 2 requires careful investigation. In the following derivation, we uphold the Loewe additivity model regardless of the shape of the dose-effect curve associated with each single drug. We expound the interpretation of the varying relative potency, its correct usage, and the relationship of various quantities in equation (4) in Appendix A. From Appendix A, it follows that the additive y -isobole is a straight line \overline{PQ} , which connects $P = (D_{y,1}, 0)$ and $Q = (0, D_{y,2})$ (Figure 1, Panel A). Each drug combination (d_1, d_2) on the y -isobole shares the same relative potency $\rho(y)$, and its equivalent amount dose is $d_1 + \rho(y)d_2$ in terms of drug 1, or $\rho(y)^{-1}d_1 + d_2$ in terms of drug 2. On the other hand, the combination doses on different additive isoboles may have different relative potencies as shown in Figure 1, Panel B.

In this paper, we construct a generalized response surface (GRS) model which incorporates the varying relative potency. We assume that the log(dose)-response curves are linear. Without loss of generality, the model derivation begins with the assumptions of a constant relative potency and a log(dose)-effect curve for drug 1:

$$Y_1 = \beta_0 + \beta_1 \log D_{Y_1,1}. \quad (5)$$

surface (GRS) model of the following form

$$Y = \beta_0 + \beta_1 \log \left(d_1 + \rho d_2 + f(d_1, d_2; \gamma, \kappa) (d_1 \rho d_2)^{\frac{1}{2}} \right) \quad (9)$$

using $f(d_1, d_2; \gamma, \kappa)$ to capture local synergy, local additivity, or local antagonism. In this paper we take

$$f(d_1, d_2; \gamma, \kappa) = \kappa_0 + \kappa_1 d_1^{\frac{1}{2}} + \kappa_2 (\rho d_2)^{\frac{1}{2}} + \kappa_3 d_1 + \kappa_4 \rho d_2 + \kappa_5 (d_1 \rho d_2)^{\frac{1}{2}}, \quad (10)$$

where f is a function of d_1 and d_2 with parameters γ 's capturing the varying relative potency ρ as described above and κ 's for the coefficients of the quadratic function.

Our main considerations for using the term $f(d_1, d_2; \gamma, \kappa) (d_1 \rho d_2)^{\frac{1}{2}}$ are: (i) the marginal dose-effect curves are easily obtained and are impacted as little as possible by this extra term, and (ii) the function f can have enough flexibility to capture the departure from the predicted additivity effect, $\beta_0 + \beta_1 \log(d_1 + \rho d_2)$. For the first consideration, we used the factor $(d_1 \rho d_2)^{\frac{1}{2}}$, and for the second consideration, we adopted the complete quadratic form of $d_1^{\frac{1}{2}}$ and $(\rho d_2)^{\frac{1}{2}}$ for $f(d_1, d_2; \gamma, \kappa)$. Extensive search and simulations show that the proposed model parametrization is reasonable and appropriate. One caveat is that the current parametrization may contain more parameters than necessary, therefore, model selection procedures need to be developed.

The following equations demonstrate how the GRS model captures different patterns of drug interaction: for each fixed effect level y , setting $d_2 = 0$ in (9), we obtain $D_{y,1} = \exp(\frac{y-\beta_0}{\beta_1})$; setting $d_1 = 0$, we obtain $D_{y,2} = \rho^{-1} \exp(\frac{y-\beta_0}{\beta_1})$; and the combination dose (d_1, d_2) satisfies $\exp(\frac{y-\beta_0}{\beta_1}) = d_1 + \rho d_2 + f(d_1, d_2; \gamma, \kappa) (d_1 \rho d_2)^{\frac{1}{2}}$. Dividing both sides by $\exp(\frac{y-\beta_0}{\beta_1})$ and rearranging the equality, the interaction index, $\frac{d_1}{D_{y,1}} + \frac{d_2}{D_{y,2}}$, could be written as

$$\begin{aligned} \text{Interaction Index} &= \frac{d_1}{D_{y,1}} + \frac{d_2}{D_{y,2}} = \frac{d_1}{\exp(\frac{y-\beta_0}{\beta_1})} + \frac{d_2}{\rho^{-1} \exp(\frac{y-\beta_0}{\beta_1})} \\ &= 1 - \frac{f(d_1, d_2; \gamma, \kappa) (d_1 \rho d_2)^{\frac{1}{2}}}{\exp(\frac{y-\beta_0}{\beta_1})} = \left[1 + \frac{f(d_1, d_2; \gamma, \kappa) (d_1 \rho d_2)^{\frac{1}{2}}}{d_1 + \rho d_2} \right]^{-1}. \end{aligned} \quad (11)$$

From (11), the polynomial function $f(d_1, d_2; \gamma, \kappa)$ being greater than, equal to, or less than zero corresponds to the interaction index being less than, equal to, or greater than 1, and consequently, this combination is synergistic, additive, or antagonistic, respectively.

3. Relating the GRS model to isoboles and interaction indices

Recall that an isobole consists of all the drug combinations which elicit the same effect y . So, each curve in the contour plot of the response surface (9) can be viewed as an isobole. To better understand the proposed GRS model, we examine the relationship between the contour plots of the response surface, the polynomial function, and the interaction index. Chou and Talalay's (1984) median effect equation (2) is used to model the dose-effect curve for each single drug. We begin by taking the simplest case that the two dose-effect curves are the same with the slope being -1 and the median effective dose being 1, which yields $\beta_0 = \gamma_1 = \gamma_2 = 0$, $\beta_1 = -1$, and $\rho = 1$. In this special case the relative potency is constant, and the model conforms to equation (6). This model can be represented in the GRS model (9) by taking $\kappa_i = 0$ ($i = 1, \dots, 5$) with different values of κ_0 in $f(d_1, d_2; \gamma, \kappa)$. Figure 2 Panels A, B, and C illustrate the cases for $\kappa_0 = 0, 1, -0.5$, respectively. In Panel A, the contour plot of the response surface shows that the isoboles are straight lines (Subpanel A1); $f(d_1, d_2; \gamma, \kappa)$ is a constant at zero (Subpanel A2); and the interaction index is a constant at 1 (Subpanel A3). All three subpanels indicate that the combination doses are additive. In Panel B, the contour plot of the response surface shows that the isoboles are concave down (Subpanel B1); $f(d_1, d_2; \gamma, \kappa)$ is a constant at 1 (Subpanel B2); and the interaction indices are less than 1 (Subpanel B3). All three subpanels indicate that the combination doses are synergistic. Similarly, Subpanel C1 shows that the isoboles are concave up, Subpanel C2 shows $f(d_1, d_2; \gamma, \kappa) = -0.5$, and Subpanel C3 shows that the interaction indices are greater than 1, indicating that the combination doses are antagonistic. These special cases of our proposed model with $\kappa_i = 0$ ($i = 1, \dots, 5$) use a single parameter κ_0 to capture synergy, additivity,

or antagonism and they reduce to Finney's model and Plummer and Short's model. Beyond these three special cases, the proposed model can be used more broadly, in particular when synergy and antagonism appear in different combination doses. We construct a case in panel D by setting $\kappa_0 = \kappa_1 = \kappa_2 = 0$, $\kappa_3 = 0.5$, $\kappa_4 = -0.5$, and $\kappa_5 = 0$, i.e., $f(d_1, d_2; \gamma, \kappa) = 0.5d_1 - 0.5d_2$. The contour plot of the response surface is shown in Subpanel D1. The contour plot of the polynomial function forms straight lines at a 45° angle (Subpanel D2). The diagonal line $0.5d_1 - 0.5d_2 = 0$ separates the space into two parts. In the area below this 45° diagonal line, the polynomial is positive and the interaction index is less than 1 (Subpanel D3), indicating that the combination doses in this area are synergistic. On the other hand, in the area above this 45° diagonal line, the polynomial is negative and the interaction index is greater than 1, indicating that the combination doses in this area are antagonistic. Furthermore, to show the varying relative potency, we set $\gamma_1 = 0.1$, $\gamma_2 = -0.4$ with $\kappa_0 = 0.9$, $\kappa_3 = -0.3$, and $\kappa_4 = -0.3$ (Panel E). The isobole with effect level 0.25 is a straight line (Subpanel E1), the corresponding polynomial is a constant at zero (Subpanel E2), and the interaction index is a constant at 1 (Subpanel E3), indicating that all the combination doses on this line are additive. The isoboles with effect levels greater than 0.25 are concave down, the corresponding polynomial is positive, and the interaction index is less than 1, indicating that the combination doses in these regions are synergistic. In contrast, the isoboles with effect levels less than 0.25 are concave up, the corresponding polynomial is negative, and the interaction index is greater than 1, indicating that the combination doses in the other areas are antagonistic.

4. Statistical consideration of the GRS model

First we may consider whether the new model (9), (10) provides a significant improvement of Plummer and Short's model by testing $H_0 : \kappa_1 = \kappa_2 = \kappa_3 = \kappa_4 = \kappa_5 = 0$ against $H_1 : \kappa_i \neq 0$ for any i ($i = 1, \dots, 5$) using the F-statistics (Gallant, 1987)

$$F = \frac{(RSS_{P-S} - RSS_{full})/q}{RSS_{full}/(n - p)} \quad (12)$$

with $q = 5$ and $n - p$ degrees of freedom. Here n is the number of observations and $p = 10$ is the number of parameters in model (9). RSS_{full} is the residual sum of squares of our GRS model, and RSS_{P-S} is the residual sum of squares of Plummer and Short's model. Rejecting H_0 suggests that Plummer and Short's model does not provide adequate fit to the data. On the other hand, failing to reject H_0 suggests that Plummer and Short's model is sufficient and there is no need to add more terms to the model. Notice that the F test requires that the responses on Y scale are normal distributed. One should check the normality assumption, e.g., applying the Q-Q plot to the residuals to examine whether the assumption is reasonable. If not, proper transformation should be sought.

The true model may include only a few terms in the GRS model (9), (10). To avoid over parametrization, we use the Akaike's information criterion (AIC) (Venables and Ripley, 2002) and a backward elimination procedure to remove the unnecessary terms and their associated parameters. Here, $AIC = -2 \times \text{maximized log-likelihood} + 2p$, which can be written as $AIC = n \log(RSS/n) + 2p + C(n)$ under the normality assumption for the response Y . For a data set, the number of observations, n , remains constant, so, comparing AIC values under different parametrization is the same as comparing the sum of the first two terms, which is referred as AIC later. To remove the unnecessary terms, we first fit the full model, calculate AIC , and then remove the parameter with the smallest absolute t-value if its p-value is greater than the level of significance α , say, $\alpha = 0.10$ (Hocking, 1976). We repeat the procedure, refit the reduced model, calculate the AIC for the reduced model, and check the t-values until either all the remaining parameters have p-values smaller than α or the AIC value is increasing.

As described in Section 3, the different patterns of drug interactions could be detected by observing the sign and magnitude of the polynomial function $f(d_1, d_2; \gamma, \kappa)$. Since these parameters γ and κ in the polynomial are estimated, their asymptotic properties follow the standard results from a nonlinear regression. For each combination dose (d_1, d_2) , the variance of the estimated

polynomial $f(d_1, d_2; \gamma, \kappa)$ can be approximated by $\widehat{Var}_f = \left(\frac{\partial f}{\partial(\gamma, \kappa)} \right)' \Sigma \left(\frac{\partial f}{\partial(\gamma, \kappa)} \right) |_{(\gamma, \kappa) = (\hat{\gamma}, \hat{\kappa})}$, where

$$\begin{aligned} \frac{\partial f}{\partial(\gamma, \kappa)} &= \left(\frac{\partial f}{\partial \gamma_1}, \frac{\partial f}{\partial \gamma_2}, \frac{\partial f}{\partial \kappa_0}, \frac{\partial f}{\partial \kappa_1}, \frac{\partial f}{\partial \kappa_2}, \frac{\partial f}{\partial \kappa_3}, \frac{\partial f}{\partial \kappa_4}, \frac{\partial f}{\partial \kappa_5} \right)' \\ &= \left(\frac{\partial f}{\partial \rho} \frac{\partial \rho}{\partial \gamma_1}, \frac{\partial f}{\partial \rho} \frac{\partial \rho}{\partial \gamma_2}, 1, d_1^{\frac{1}{2}}, (\rho d_2)^{\frac{1}{2}}, d_1, \rho d_2, (d_1 \rho d_2)^{\frac{1}{2}} \right)' \end{aligned}$$

with $\frac{\partial f}{\partial \rho} = \frac{1}{2} \kappa_2 \left(\frac{d_2}{\rho} \right)^{\frac{1}{2}} + \kappa_4 d_2 + \frac{1}{2} \kappa_5 \left(\frac{d_1 d_2}{\rho} \right)^{\frac{1}{2}}$, $\frac{\partial \rho}{\partial \gamma_1} = \frac{\rho^2 (d_2 + d_1 \rho^{-1})}{\rho (d_2 + d_1 \rho^{-1}) + \gamma_2 d_1}$, and $\frac{\partial \rho}{\partial \gamma_2} = \frac{\rho^2 (d_2 + d_1 \rho^{-1})}{\rho (d_2 + d_1 \rho^{-1}) + \gamma_2 d_1} \log(d_2 + d_1 \rho^{-1})$. Σ is the estimated covariance matrix of the parameters $(\gamma_1, \gamma_2, \kappa_0, \kappa_1, \kappa_2, \kappa_3, \kappa_4, \kappa_5)$. Thus, we may construct a $(1 - \alpha) \times 100\%$ lower and upper confidence surfaces for $f(d_1, d_2; \gamma, \kappa)$

$$f_{l,u}(d_1, d_2) = \hat{f}(d_1, d_2) \mp t_{\frac{\alpha}{2}, n-p} \sqrt{\widehat{Var}_f(d_1, d_2)},$$

where $t_{\frac{\alpha}{2}, n-p}$ is the upper $\frac{\alpha}{2}$ percentile of a t-distribution with $n - p$ degrees of freedom. The intercepts of the lower and upper confidence surfaces of $f(d_1, d_2; \gamma, \kappa)$ with the dose plane form a bound which embraces the curve $f(d_1, d_2; \gamma, \kappa) = 0$. The combination doses beyond the bound with positive polynomial values are synergistic. Conversely, the combination doses beyond the other side of the bound with negative polynomial values are antagonistic. Inside the bound, the drug combinations are considered additive because the responses are not significantly different from the predicted effect based on the additive model. When the final model is a subset of the full model, a similar approach can be used to construct the confidence bound for $f(d_1, d_2, \gamma, \kappa) = 0$ in the final model.

In the medical research and its applications, the inferences should be made considering both clinical significance and statistical significance. Although the above inferences on synergy and antagonism are primarily based on statistical significance, the importance of clinical significance, i.e., the magnitude of drug interaction to be considered clinically meaningful, should also be considered. Chou and Hayball (1996) recommended that the synergy, antagonism, and additivity at a combination dose should be made based on whether interaction index at this combination is less than 0.9, greater than 1.1, or in between. Our method provides a more rigorous way to assess

statistical significance and also provides a venue for gauging the magnitude of clinical significance.

5. Simulation and data analysis

5.1 Simulation

We performed simulation studies to examine the finite sample properties of the estimates of the proposed model. We took two sets of parameters, as shown in Figure 2, Panel D (Set 1) and Panel E (Set 2). The corresponding response surface models are:

$$\text{Set 1: } Y = \log \frac{E}{1-E} = -\log \left(d_1 + d_2 + (0.5d_1 - 0.5d_2)(d_1d_2)^{\frac{1}{2}} \right) + \epsilon$$

and

$$\text{Set 2: } Y = \log \frac{E}{1-E} = -\log \left(d_1 + \rho d_2 + (0.9 - 0.3d_1 - 0.3\rho d_2)(d_1\rho d_2)^{\frac{1}{2}} \right) + \epsilon$$

with $\rho = \exp(0.1 - 0.3 \log D_2)$, where $\epsilon \sim N(0, \sigma^2)$. For each model we generated 1000 random samples with $\sigma = 0.1$, and d_1 and d_2 taking values among (0, 0.1, 0.5, 1, 2, 4). The sample size in each simulation run was $6 \times 6 = 36$. We fitted each random sample to the full model and then the true model (i.e., only fitting the non-zero parameters), and obtained the estimated parameters and their corresponding standard errors (S.E.). For each parameter, we constructed the 95% confidence interval and observed whether the true parameter lies in the confidence interval. We report the averages of the estimated parameters, standard errors, and the coverage rate of the confidence intervals for the 1000 random samples in Table 1. We conclude that (1) the parameters are very well estimated; (2) the coverage rates are close to the nominal 95% coverage; (3) in the full model, the standard errors of β_0 , β_1 , γ_1 , and γ_2 are close to half of $\sigma (= 0.1)$, while the standard errors of κ_i ($i = 0, \dots, 5$) are two to eight folds of σ . In the true model, the standard errors for β 's, γ 's, and κ 's are all with similar magnitude, ranging from 0.020 to 0.063 with an exception of $\hat{\kappa}_0$ in Set 2 (S.E.=0.138). These facts reflect that including unnecessary parameters increases the uncertainty of estimating all parameters, especially those in the quadratic function f .

Therefore, it is important to develop an appropriate procedure to remove unnecessary parameters. A parsimonious model can increase the accuracy of the estimated parameters, hence, provides a better estimator for the dose-response relationship.

We also performed simulated case studies to examine whether the estimation and the backward elimination procedure described in Section 4 can recover the true dose response function, i.e., all the zero parameters are removed, the 95% confidence bounds for $f = 0$ have proper coverage rates, and the contours of the fitted response surfaces are similar to the underlying response surface. These simulations showed that the estimation and the backward elimination procedure work well (data not shown).

5.2 Data analysis

We analyzed data sets from cell lines in a study conducted by Dr. Reuben Lotan and his colleagues at M. D. Anderson Cancer Center. The study aimed to evaluate the efficacy of combination therapy with two novel agents, SCH66336 and 4-HPR, in a number of squamous cell carcinoma cell lines (unpublished data). Cell lines of human squamous cell carcinoma were treated with SCH66336 and 4-HPR separately and in combination. After 6 hours, the proportions of surviving cells were calculated. To illustrate, we present the result for the cell line UMSCC22B, after treating with SCH66336 at doses ranging from 0 to 4 μ M and 4-HPR at doses ranging from 0 to 2 μ M, respectively. The corresponding percentages of cells surviving at each combination dose are shown in Table 2.

Lee *et al.* (2005) analyzed the data set in detail using different methods. Based on Chou and Talalay’s model, the combination dose (0.1, 0.1) is additive, and the combination doses (0.5, 0.5), (1, 1) and (2, 2) are synergistic. The contour plot of the raw data is shown in Figure 3, Panel A. Based on Plummer and Short’s model, the combinations are synergistic ($\hat{\kappa} = 2.146$ with S.E.=1.102). The contour plot, interaction indices, and residual plot of the fitted response surface of Plummer and Short’s model are shown in Figure 3, Panel B1, B2, and B3, respectively. The

contour plot in Panel B1 differs from the raw data contour plot in Panel A. We fitted the data to our proposed full model, and found that the contour plot of the fitted response surface (Panel C1) is more similar to the raw data contour plot. The contour plot of the polynomial function $f(d_1, d_2; \gamma, \kappa)$ is shown in Panel C2, where the dotted curve is the upper boundary of the 95% confidence bound for $f(d_1, d_2; \gamma, \kappa) = 0$, and the lower boundary is below the illustrated region. The combination doses above the dotted line are synergistic. Panel C3 shows the contour plot of the interaction indices, and Panel C4 shows the residual plot of the full model. We used the aforementioned backward elimination procedure to remove γ_2 , κ_2 , κ_4 , and β_0 sequentially, and the corresponding AIC values were -106.28, -107.25, -108.23, and -108.59, respectively. The backward elimination procedure stopped when all the remaining parameters had p-values smaller than the significance level $\alpha (= 0.10)$. The results of the final model are shown in Panels D1-D4. Panel D2 shows that the combination doses above the confidence bound are synergistic, inside the bound are additive, and below the bound are antagonistic. The residual plots show that the full model (Panel C4) and the final model (Panel D4) provide better fit for the data than the Plummer and Short's model (Panel B3). The results from the final model are consistent with the results achieved by Lee *et al.* (2005).

In this example, $RSS_{P-S} = 1.238$, $RSS_{full} = 0.390$, and $n = 29$ (the model automatically assumed cell survival 1 at the combination dose $d_1 = d_2 = 0$ and this observation did not participate in the calculation). The Q-Q plots (not shown) indicated that the normality holds for the responses on Y scale, therefore, the F-test can be carried out. The F-statistics was 8.250 with degrees of freedom (5, 19), corresponding to $p < 0.003$. Hence, we rejected H_0 at $\alpha = 0.05$. The estimated parameters and their standard errors for Plummer and Short's model, the full model, and the final model are listed in Table 3. The residual standard error (RSE), which is an estimate of σ , is shown in the last column in Table 3 for each model. Figure 3 and Table 3 indicate that the final model fits the data as well as the full model, and the precisions on parameter estimation

in the final model were improved over the full model. We conclude that the proposed model and procedure work well for this data set.

6. Discussion and further extension

One important contribution of this paper is that the proposed model can incorporate varying relative potency. Although varying relative potency has been investigated by Tallarida (2000), and Grabovsky and Tallarida (2004), their interpretations resulted in inconsistent predicted additive effects for combination doses (Jonker *et al.* 2005). In Appendix A, we expound a method to correctly incorporate varying relative potency to predict the additive effect based on the Loewe additivity model. Using the proposed varying relative potency formulation, one can extend the additive response surface for k ($k \geq 2$) drug combinations as follows:

$$Y = \beta_0 + \beta_1 \log(d_1 + \rho_2 d_2 + \cdots + \rho_k d_k), \quad (13)$$

where $\rho_i = \exp(\gamma_{i0} + \gamma_{i1} \log D_1)$ ($i = 2, \dots, k$) is the relative potency of drug i versus drug 1, and D_1 is the amount of drug 1 having an equivalent effect to that of the combination (d_1, \dots, d_k) under the additive assumption. D_1 can be obtained by solving the following equation

$$d_1 + \rho_2 d_2 + \cdots + \rho_k d_k = D_1.$$

Here γ_{i0} and γ_{i1} are uniquely determined by the two dose-effect curves for drug 1 and drug i ($i = 2, \dots, k$). The additive response surface model constructed this way is consistent with the Loewe additivity model.

As shown in Section 2, the proposed model was derived to capture a variety of drug interaction patterns when synergy, additivity, and antagonism are interspersed in different regions. Under the framework of a nonlinear regression, our proposed model also can automatically take care of replications, no matter whether the numbers of replications in each combination dose are the same or not. Using our proposed model, we analyzed 10 data sets to assess the interactions between

the combination therapy SCH66336 and 4-HPR in different cell lines. By comparing the contour plot of the fitted response surface with the contour plot of the raw data, residual plots, and the results achieved by using Chou and Talalay’s method, we conclude that our proposed model can be successfully applied to fit data and capture different patterns of drug interaction.

In this paper, we assume that the effect or transformed effect has a linear relationship with the $\log d$. Although a broad class of dose-effect models satisfy this assumption, there are still some exceptions. One important exception is that the logit transform of the effect has a linear relationship with the dose, say $\log \frac{E}{1-E} = \alpha_0 + \alpha_1 d$. In that case, the relative potency for the two drugs is constant, and the additive response for the two drugs can be predicted by $\log \frac{E}{1-E} = \alpha_0 + \alpha_1 d_1 + \alpha_2 d_2$ (Carter, Gennings, Staniswalis, Cambell, and White, 1988). One can still use a quadratic function of d_1 and d_2 to detect different patterns of drug interactions by adding the product of the quadratic function and $(d_1 d_2)^{\frac{1}{2}}$ to the above model.

Sulmel (1990) used bivariate splines to fit dose response data. The determination of drug interaction was based on the visualization of whether the contours of the response surface (i.e., isoboles) were concave up or concave down. The approach did not give any summary measure on drug interaction. Kelly and Rice (1990) used a monotone spline-based procedure to fit marginal dose-response curves first, then predicted the additive effect of the combination dose based on the Loewe additivity model. Extrapolation beyond the observed dose range is dangerous in this spline-based approach and, therefore, this approach has limited usage. Tan, Fang, Tian, and Houghton (2003) proposed an optimal experimental design in the sense that it reduces the variability in modeling synergy while allocating the doses to minimize the sample size and to extract maximum information on the joint action of the compounds. The method uses a nonparametric function to detect drug interactions. Semiparametric approaches, as the format (9) or the format given by Tan *et al.* (2003), which combine parametric marginal dose-response curves with a nonparametric function to detect different patterns of drug interaction, provide logical extension to the current

model and are appropriate topics for future research.

Acknowledgment

This research was supported in part by grants from the National Cancer Institute CA16672, CA97007, CA91844, and the Department of Defense W81XWH-04-1-0142 and W81XWH-05-2-0027. The authors are thankful to the reviewers for their constructive comments, to Dr. Reuben Lotan for providing the data, and to Lee Ann Chastain for the editorial assistance.

References

- [1] Berenbaum, M. C. (1989). What is synergy? *Pharmacological Reviews* 41, 93-141.
- [2] Carter, W. H. Jr., Gennings, C., Staniswalis, J. G., Cambell, E. D., and White K. L. Jr. (1988). A statistical approach to the construction and analysis of isobolograms. *Journal of American College Toxicology* 7, 963-973.
- [3] Chou, T. C. and Hayball M. (1996). CalcuSyn for Windows: multiple-drug dose-effect analyzer and manual. Cambridge, UK: Biosoft.
- [4] Chou, T. C. and Talalay, P. (1984). Quantitative analysis of dose-effect relationships: the combined effects of multiple drugs or enzyme inhibitors. *Advances in Enzyme Regulation* 22, 27-55.
- [5] Finney D. J. (1971). *Probit Analysis*. Cambridge University Press, Cambridge.
- [6] Gallant, A. R. (1987) *Nonlinear Statistical Models*. Wiley, New York, 55-57.
- [7] Govindarajulu, Z. (2001). *Statistical Techniques in Bioassay*. Karger, Basel.

- [8] Grabovsky, Y. and Tallarida, R. J. (2004). Isobolographic analysis for combinations of a full and partial agonist: curved isoboles. *The Journal of Pharmacology and Experimental Therapeutics* 310, 981-986.
- [9] Greco, W. R., Bravo, G., and Parsons, J. C. (1995). The search of synergy: A critical review from a response surface perspective. *Pharmacological Reviews* 47(2), 331-385.
- [10] Greco, W. R., Park, H.S., and Rustum, Y. M. (1990). Application of a new approach for the quantitation of drug synergy to the combination of cis-diamminedichloroplatinum and 1- β -D-arabinofuranosylcytosine. *Cancer Research* 50, 5318-5327.
- [11] Hocking, R. R. (1976). The analysis and selection of variables in linear regression. *Biometrics* 32, 1-49.
- [12] Jonker, D. M., Visser, S. A. G., Van der Graaf, P. H., Voskuyl, R. A., and Danhof, M. (2005). Towards a mechanism-based analysis of pharmacodynamic drug-drug interactions in vivo. *Pharmacology and Therapeutics* 106, 1-18.
- [13] Kelly, C. and Rice, J. (1990). Monotone smoothing with application to dose-response curves and the assessment of synergism. *Biometrics* 46, 1071-1085.
- [14] Lee, J. J., Kong, M., and Ayers, G. D. (2005). A practical guide for determining drug interaction in combination therapy. Submitted.
- [15] Loewe, S. and Muischnek, H. (1926). Effect of combinations: mathematical basis of problem. *Archives of Experimental Pathology Pharmacology* 11, 313-326.
- [16] Plummer, J. L. and Short, T. G. (1990). Statistical modeling of the effects of drug combinations. *Journal of Pharmacological Methods* 23, 297-309.

- [17] Savelev, S., Okello, E., Perry, N. S. L., Wilkins, R. M., and Perry, E. K. (2003). Synergistic and antagonistic interactions of anticholinesterase terpenoids in salvia lavandulaefolia essential oil. *Pharmacology, Biochemistry and Behavior* 75, 661-668.
- [18] Suhnel, J. (1990). Evaluation of synergism or antagonism for the combined action of antiviral agents. *Antiviral Research* 13, 23-40.
- [19] Suhnel, J. (1998). Parallel dose-response curves in combination experiments. *Bulletin of Mathematical Biology* 60, 197-213.
- [20] Tallarida, R. J. (2000). *Drug synergy and Dose-Effect Data Analysis*. Chapman Hall/CRC Press, Boca Raton.
- [21] Tan, M., Fang, H. , Tian, G., and Houghton, P. J. (2003). Experimental design and sample size determination for testing synergism in drug combination studies based on uniform measures. *Statistics in Medicine* 22, 2091-2100.
- [22] Venables, W. N. and Ripley B. D. (2002). *Modern Applied Statistics with S*. 4th ed, Springer.
- [23] White, D. B., Faessel, H. M., Slocum, H. K., Khinkis, L., and Greco, W. R. (2004). Nonlinear response surface and mixture experiment methodologies applied to the study of synergy. *Biometrical Journal* 46, 56-71.

Appendix A: Varying relative potency and its application

Figure 1, Panel A shows that for each fixed effect y , as long as the dose-effect curves for each drug are known, $D_{y,1}$ and $D_{y,2}$ will be known and fixed, thus the relative potency defined by $\frac{D_{y,1}}{D_{y,2}}$ is fixed. Any combination dose (d_1, d_2) on the line \overline{PQ} connecting $P(= (D_{y,1}, 0))$ and $Q(= (0, D_{y,2}))$ has the same relative potency, and d_2 units of drug 2 is equivalent to $\rho(y)d_2$ units of drug 1. Therefore the combination dose (d_1, d_2) is equivalent to $d_1 + \rho(y)d_2$ units of drug 1,

which is exactly $D_{y,1}$, and the predicted effect is $F_1(d_1 + \rho(y)d_2)$, which is $F_1(D_{y,1})$. Similarly, for any combination dose (d_1, d_2) on the line \overline{PQ} , d_1 units of drug 1 is equivalent to $\rho(y)^{-1}d_1$ units of drug 2, thus the combination dose (d_1, d_2) is equivalent to $\rho(y)^{-1}d_1 + d_2$ units of drug 2, which is $D_{y,2}$. Consequently, the predicted effect is $F_2(\rho^{-1}(y)d_1 + d_2)$, i.e., $F_2(D_{y,2})$. Hence, the predicted effect either by $F_1(d_1 + \rho(y)d_2)$ or by $F_2(\rho(y)^{-1}d_1 + d_2)$ are the same.

We then pay special attention to the fact that, for a given dose d_2 of drug 2, its equivalent amount of drug 1 may be different depending on the existing amount of drug 1 due to a varying relative potency. For example, suppose from the two marginal dose-effect curves we learn that the effects of drug 1 at doses $D_{y,1}$, d_1 and $D_{y'',1}$ are the same as the effects of drug 2 at doses $D_{y,2}$, $D_{y',2}$ and d_2 , respectively. When two drugs are used, the three corresponding additive isoboles (Figure 1 Panel B) are \overline{PQ} connecting $P = (D_{y,1}, 0)$ and $Q = (0, D_{y,2})$, \overline{RS} connecting $R = (d_1, 0)$ and $S = (0, D_{y',2})$, and \overline{TU} connecting $T = (D_{y'',1}, 0)$ and $U = (0, d_2)$. All the combinations on \overline{PQ} share the relative potency $\rho(y)$, all the combinations on \overline{RS} share the relative potency $\rho(y')$, and all the combinations on \overline{TU} share the relative potency $\rho(y'')$. Thus, in terms of drug 1 the equivalent dose of d_2 in the combinations (d_1, d_2) , (d'_1, d_2) , and $(0, d_2)$ will be $\rho(y)d_2$, $\rho(y')d_2$, and $\rho(y'')d_2$, which can be illustrated by the length of \overline{RP} , \overline{VR} , and \overline{OT} , respectively. Here $y = F_1(D_{y,1}) = F_2(D_{y,2})$, $y' = F_1(d_1)$, and $y'' = F_2(d_2)$. Grabovsk and Tallarida (2004) proposed a model to incorporate the varying relative potency, but they interpret the relative potency as $\rho(y'')$ at all three combinations, namely, (d_1, d_2) , (d'_1, d_2) , and $(0, d_2)$. Consequently, the equivalent amount of drug 1 will be the dose of drug 1 plus $\rho(y'')d_2$ no matter the dose of drug 1. Their interpretation may result in two inconsistent additive effects, say $F_1(d_1 + \rho(y'')d_2)$ and $F_2(\rho(y')^{-1}d_1 + d_2)$ (Jonker *et al.* 2005), and curved additive isoboles (Grabovsk and Tallarida 2004). Therefore, their approach is questionable. On the other hand, when combinations of two drugs are additive with varying relative potency, our formulation shows straight line isoboles, which are consistent with the Loewe additivity model.

Table 1: Simulation results from fitting the full model and the true model with $\sigma = 0.1$

		Set 1						Set 2					
		$f(d_1, d_2; \gamma, \kappa) = 0.5d_1 - 0.5d_2$						$f(d_1, d_2; \gamma, \kappa) = 0.9 - 0.3d_1 - 0.3\rho d_2$					
Para- meters	True Value	Full Model			True Model			Full Model			True Model		
		Est.	S.E.	C.R.	Est.	S.E.	C.R.	Est.	S.E.	C.R.	Est.	S.E.	C.R.
β_0	0	0.002	0.044	0.950				0	0.002	0.043	0.957		
β_1	-1	-0.999	0.034	0.951	-1.000	0.020	0.954	-1.0	-0.999	0.033	0.956	-0.999	0.031
γ_1	0	0.002	0.062	0.957				0.1	0.102	0.062	0.958	0.100	0.041
γ_2	0	0.002	0.046	0.952				-0.3	-0.299	0.040	0.955	-0.299	0.038
κ_0	0	0.003	0.324	0.946				0.9	0.901	0.553	0.953	0.900	0.138
κ_1	0	-0.001	0.478	0.956				0	0.018	0.577	0.952		
κ_2	0	0.004	0.499	0.942				0	0	0.850	0.948		
κ_3	0.5	0.515	0.227	0.946	0.502	0.049	0.944	-0.3	-0.298	0.195	0.958	-0.298	0.047
κ_4	-0.5	-0.500	0.188	0.933	-0.500	0.022	0.963	-0.3	-0.293	0.366	0.958	-0.297	0.063
κ_5	0	-0.013	0.236	0.953				0	-0.017	0.312	0.950		

Note: Est.: parameter estimate, S.E.: standard error, C.R.: coverage rate.

Table 2: Percentages of cell surviving (UMSCC22B) treated by single and combination doses of SCH66336 and 4-HPR

SCH66336 Dose (μM)	4-HPR Dose (μM)				
	0	0.1	0.5	1	2
0	1	0.7666	0.5833	0.5706	0.4934
0.1	0.6701	0.6539	0.4767	0.5171	0.3923
0.5	0.6289	0.6005	0.4919	0.4625	0.3402
1	0.5577	0.5102	0.4541	0.3551	0.2851
2	0.455	0.4203	0.3441	0.3082	0.2341
4	0.3755	0.3196	0.2978	0.2502	0.1578

Table 3: The estimated parameters and their standard errors of different models for the data set shown in Table 2

		β_0	β_1	γ_1	γ_2	κ_0	κ_1	κ_2	κ_3	κ_4	κ_5	RSE
P-S model	Est.	0.099	-0.473	-0.083	0.120	2.146						0.227
	S.E.	0.093	0.062	0.292	0.259	1.102						
Full model	Est.	0.088	-0.354	-0.339	0.148	5.735	-14.104	-5.539	7.114	5.283	7.021	0.143
	S.E.	0.064	0.046	0.289	0.242	3.510	6.668	8.230	3.743	6.593	5.446	
Final model	Est.		-0.386	-0.558		3.702	-12.653		5.339		9.202	0.140
	S.E.		0.034	0.203		1.798	4.994		2.550		3.990	

Note: P-S model: the Plummer and Short's model, Est.: parameter estimate, S.E.: standard error, RSE: the residual standard error.



23

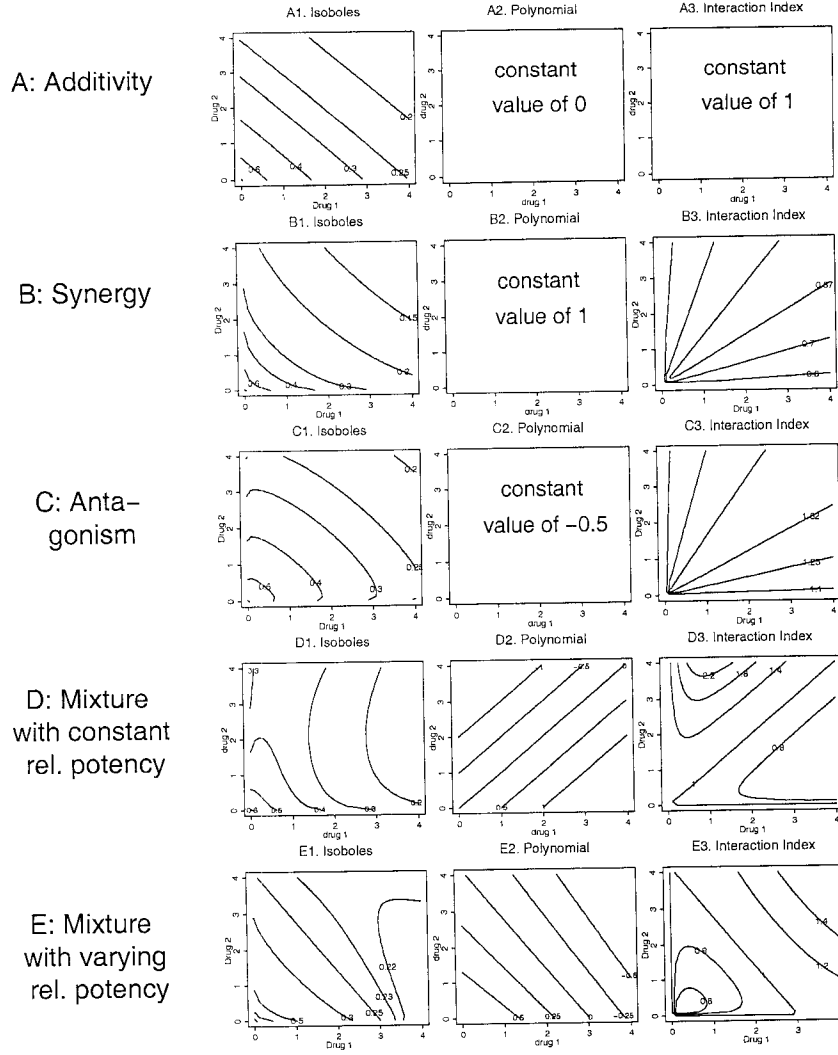


Figure 2. Contour plots of the response surfaces (i.e., isoboles), contour plots of the polynomial function $f(d_1, d_2; \gamma, \kappa)$, and contour plots of the interaction indices under different parameters. For all panels, $\beta_0 = 0$, $\beta_1 = -1$. For Panels A, B, and C, $\kappa_0 = 0, 1$, and -0.5 , respectively, while $\gamma_1 = \gamma_2 = 0$, $\kappa_i = 0$ for $i = 1, \dots, 5$. Parameters in Panel D are the same as in Panel A except $\kappa_3 = 0.5$ and $\kappa_4 = -0.5$. In panel E we set $\gamma_1 = 0.1$, $\gamma_2 = -0.4$, $\kappa_0 = 0.9$, $\kappa_3 = \kappa_4 = -0.3$, and $\kappa_1 = \kappa_2 = \kappa_5 = 0$.

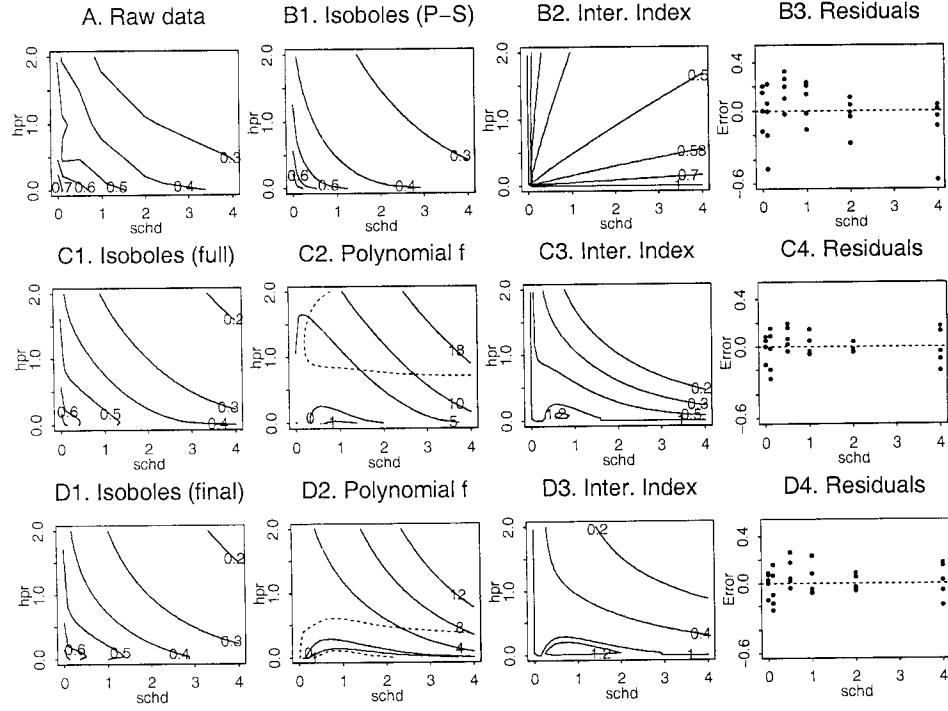


Figure 3. Results for cell line UMSCC22B: Panel A is the contour plot of the raw data; Panels B1-B3 show the results from Plummer and Short's model; Panels C1-C4 show the results from the proposed full model; Panels D1-D4 show the results from the final model. The dotted line in Panel C2 is the upper boundary of the 95% confidence bound for $f(d_1, d_2; \gamma, \kappa) = 0$, and the lower boundary is out of the dose range. The two dotted lines in Panel D2 are the two boundaries of a 95% confidence bound for $f(d_1, d_2; \gamma, \kappa) = 0$.

A Semiparametric Response Surface Model for Assessing Drug Interaction

Maiying Kong

&

J. Jack Lee

Department of Biostatistics and Applied Mathematics

University of Texas, M.D. Anderson Cancer Center, Unit 447

1515 Holcombe Blvd, Houston, TX 77030

Abstract

When multiple drugs are administered simultaneously, investigators are often interested in assessing whether the drug combinations are synergistic, additive, or antagonistic. Existing response surface models are not adequate to capture the mosaic patterns of drug interactions. We propose a two-component semi-parametric response surface model with a parametric function to describe the additive effect of a combination dose and a nonparametric function to capture the departure from the additive effect. The nonparametric function is estimated using the technique developed in thin plate splines. The proposed semiparametric model offers an effective way of formulating additive effect while allowing the flexibility of modeling the departure from the additivity. Examples and simulations are given to illustrate the proposed model provides an excellent estimation for different patterns of drug interactions of two drugs.

1. Motivation

Studies of interactions among biologically active agents, such as drugs, carcinogens, or environmental pollutants, have become increasingly important in many branches of biomedical research (Suhnel, 1998). For example, in cancer chemotherapy the therapeutic effect of many anticancer drugs is limited when they are used as a single drug (Kanzawa, Nishio, Fukuoka, Sunami, and Saijo, 1999). Combination therapies with increasing treatment

efficacy and reducing toxicity is an active and promising research area. An effective and accurate evaluation of drug interactions for *in vitro* and/or *in vivo* studies can help to determine whether a combination therapy should be further investigated in a clinical trial.

The literature supports the notion that the Loewe additivity model can be considered as the “gold standard” to define drug interactions (Berenbaum, 1989; Greco, Bravo, and Parsons, 1995; Lee, Kong, and Ayers, 2005). Based on the Loewe additivity model, approaches for assessing drug interactions can be categorized as one of three general methods: (1) the model free test method (MFT), (2) the marginal dose-response curve model method (MDRCM), or (3) the response surface method (RSM). The MFT method (Laska, Meisner, and Seigel, 1994) tests whether the combination is synergistic based on a sufficient condition for synergy at a combination dose (d_1, d_2) , that is, that the effect at (d_1, d_2) is greater than the effect of drug 1 at dose $d_1 + \rho d_2$ and the effect of drug 2 at dose $\rho^{-1}d_1 + d_2$, where ρ is the relative potency of drug 2 versus drug 1. The MDRCM (Kelly and Rice, 1990) fits a dose-response curve for each single drug, uses the fitted dose-response curves to calculate the expected additive response to a particular combination, and then compares the expected additive response to the observed response. The MFT and the MDRCM methods can only assess drug interactions at observed combinations, and do not give a complete picture of drug interactions over all possible combination doses. Although both methods are able to determine whether synergy or antagonism exists, they have limited usage in quantify the degree of drug interaction away from additivity. The RSM, which involves an estimation of the $n + 1$ dimensional response surface in n drug combinations, can take all of the information present in the full dose-effect data set for n drugs to determine the dose-effect relationship at all levels of drug combinations. In addition, the RSM can be used to quantify the amount of drug interactions and to determine the optimal combination therapy. Many examples of the RSM, such as those of Finney (1971), Carter, Gennings, Staniswalis, Cambell, and White (1988), Greco, Park, and Rustum (1990), and Plummer and Short (1990), have used a single parameter to capture synergy, additivity, or antagonism. These approaches are valid if only either synergy, additivity, or antagonism exists throughout the whole surface. These methods are inadequate to describe the presence of pockets of local synergy or local antagonism when different modes of drug interactions are interspersed in different regions of the drug combinations. Minto, Schnider, Short, Gregg, Gentilini, and Shafer (2000) and White, Faessel, Slocum, Khinkis, and Greco (2004) have proposed nonlinear mixture response surface approaches based on the assumption that the combination doses at each fixed ratio follow the median-effect model (Chou and Talalay, 1984), and the parameters in the median effect model are assumed to be polynomials of the ratio. The resulting models capture synergy, additivity, or antagonism exclusively based on the 50% maximal effect isobole. But combination doses of two drugs at a fixed ratio do not necessarily yield the same

mode of drug interactions as that at the 50% maximal effect. For example, our research group (Lee *et al.* 2005) noticed that the combinations of SCH66336 and 4-HPR are synergistic for moderate to higher combination doses and additive for lower combination dose when the cell line UMSCC22B was treated with SCH66336 and 4-HPR. Kanzawa *et al.* (1999) found that the combinations of CDDP and KRN5500 at concentrations in the ranges 0.025 to 0.25 μ g/ml and 0.005 to 0.25 μ g/ml are synergistic and otherwise additive. To address this issue, we recently developed a response surface model with a quadratic function of combination doses to capture synergy, additivity, and antagonism (Kong and Lee, 2005). Similar to many other settings, these parametric models are efficient when the model assumptions hold but not necessarily robust when the assumptions fail. Therefore, in this paper, our goal is to develop a semiparametric model combining a parametric and a nonparametric function to capture mosaic patterns of drug interactions if they do exist.

Although there is a long history using a nonparametric response surface model to describe the drug effect, a rigorous statistical consideration on these models has not yet been fully developed. Suhnel (1990) used bivariate splines to fit dose response data. The determination of drug interactions was based on the visualization of whether the contours of the response surface (i.e. isoboles) were concave up or concave down. The approach did not give any summary measure on drug interactions and did not include any statistical treatment. Prichard and Shipman (1990) proposed using the differences of the theoretical additive surface and the experimental data surface to reveal regions of synergy and antagonism. However, the theoretical additive surface was not constructed accurately, and the assessment of drug interaction was not derived from statistical point of view. Kelly and Rice (1990) used a monotone spline-based procedure to fit marginal dose-response curves first, then predicted the additive effect of a combination dose based on the Loewe additivity model. Extrapolation beyond the observed dose range is dangerous, hence, it is unclear how to estimate the drug interactions for the combination doses with effect greater than the maximal effect of each of the two single drugs.

To overcome the above limitations for the parametric and nonparametric models, we propose a semiparametric approach. We use parametric model to describe the marginal dose-effect curve for each drug used as a single agent, and then, predict the theoretical additive surface based on the fitted marginal dose-effect curves and the Loewe additivity model. Subsequently, we use a nonparametric function to describe the effect beyond the additive model. The nonparametric function is represented by thin plate splines (Green and Silverman, 1994) and estimated by the techniques developed in mixed effect model (Ruppert, Wand, and Carroll, 2003). The confidence surfaces for the nonparametric function are constructed so that the local synergy or local antagonism can be estimated from the statistical point of view. This approach can be used to analyze data from factorial design, ray design (Chou and

Talalay, 1984), and uniform design (Tan, Fang, Tian, and Houghton, 2003). In addition, this approach combines the idea used in MDRCM and has all the advantages of RSM. We will describe our model and its estimation in Sections 2 and 3, and give case studies in Section 4 and simulations in Section 5. The last section is devoted to discussion.

2. The proposed model

Recall the Loewe additivity model (Loewe and Muischnek, 1926; Berenbaum, 1989; Greco *et al.*, 1995; Lee *et al.*, 2005)

$$\frac{d_1}{D_{y,1}} + \frac{d_2}{D_{y,2}} = 1, \quad (1)$$

where d_1, d_2 are doses of drug 1 and drug 2 in the mixture, y is the theoretic additive effect at (d_1, d_2) , and $D_{y,1}$ and $D_{y,2}$ are the respective single-agent doses of drug 1 and drug 2 that elicit the effect y . The theoretic additive effect y at (d_1, d_2) can be predicted as long as the dose-response curves for each of the two drugs are known. Denote the dose-effect curves for drug 1 and drug 2 used alone as $F_1(D_1)$ and $F_2(D_2)$, respectively. Then, the predicted additive effect, say y , can be obtained by solving equation (1) after replacing $D_{y,1}$ by $F_1^{-1}(y)$ and $D_{y,2}$ by $F_2^{-1}(y)$, where F_i^{-1} is the inverse function of F_i ($i = 1, 2$). If the effect measured at (d_1, d_2) is more than or less than the predicted effect, then the combination dose (d_1, d_2) corresponds to synergy or antagonism.

Note that the above additive equation (1) can be rewritten as

$$d_1 + d_2 \frac{D_{y,1}}{D_{y,2}} = D_{y,1}. \quad (2)$$

Denote $\frac{D_{y,1}}{D_{y,2}}$ as $\rho(y)$, which is the relative potency of drug 2 versus drug 1, meaning that 1 unit of drug 2 has the same effect as $\rho(y)$ units of drug 1. Under the additive model, the combination dose (d_1, d_2) elicits the same effect as drug 1 alone at dose $D_{y,1}$ (i.e., $d_1 + \rho(y)d_2$), and drug 2 alone at dose $D_{y,2}$ (i.e., $\rho(y)^{-1}d_1 + d_2$). Thus, the predicted additive effect for the combination dose (d_1, d_2) is $F_1(d_1 + \rho(y)d_2)$. The relative potency $\rho(y)$ is determined by the two marginal dose-response curves, and equals $\frac{D_{y,1}}{D_{y,2}}$. The additive y -isobole is the straight line connecting $(D_{y,1}, 0)$ and $(0, D_{y,2})$ on the dose plane. Any combination (d_1, d_2) on the additive y -isobole shares the same relative potency (Kong and Lee, 2005). Any combination (d_1, d_2) lies on only one of the additive isoboles, so the associated relative potency is unique and $d_1 + \rho(y)d_2$ can be simplified as $d_1 + \rho d_2$, where ρ is the associated relative potency to the combination dose (d_1, d_2) . Thus, the predicted effect can be written as $F_1(d_1 + \rho d_2)$. The relative potency may be varying since the additive isoboles, the straight lines connecting equal effective doses of drug 1 and drug 2, are not always parallel.

In this report, with considering the varying relative potency, we propose a two-component model to describe the effect of combination treatment:

$$Y = F(d_1, d_2) + f(d_1, d_2) = F_1(d_1 + \rho d_2) + f(d_1, d_2). \quad (3)$$

Here $F(d_1, d_2)$, or $F_1(d_1 + d_2\rho)$ is the predicted additive effect at (d_1, d_2) , which is determined by the marginal dose-response curves and the combination dose (d_1, d_2) under the additive assumption. $f(d_1, d_2)$ is a function and to be estimated nonparametrically to capture local synergy and local antagonism, i.e., drug effect beyond the additive effect. To see this point, suppose the marginal dose-effect curves are decreasing, then $f(d_1, d_2) < 0$ implies that the effect at (d_1, d_2) is more than the predicted effect $F_1(d_1 + d_2\rho)$, thus the combination dose (d_1, d_2) is synergistic; $f(d_1, d_2) > 0$ implies that the effect at (d_1, d_2) is less than the predicted, thus the combination dose (d_1, d_2) is antagonistic. In the case that the marginal dose-effect curves are increasing, $f(d_1, d_2) > 0$ implies that the combination dose (d_1, d_2) is synergistic while $f(d_1, d_2) < 0$ implies that the combination dose (d_1, d_2) is antagonistic.

Note that a model similar to (3) was proposed by Tan *et al.* (2003) under the frame work of uniform design. However, in their work, a constant relative potency is assumed, and the function $f(d_1, d_2)$ is estimated only at the observed combination doses. In model (3), the relative potency may be constant or varying, which is determined by the marginal dose-effect curves based on the data. The function $f(d_1, d_2)$ is estimated over the region of all combination doses. Details will be given in the following section.

3. Estimation for the proposed model

From now on we assume that the observed data are (d_{1i}, d_{2i}, E_i) for $i = 1, \dots, n$. Here (d_{1i}, d_{2i}) ($i = 1, \dots, n$) is the observed combination dose, and E_i ($i = 1, \dots, n$) is the corresponding observed effect. The data should contain enough observations for each drug used alone so that the marginal dose-effect curves, and subsequently, predicted additive effects, can be estimated with small error. The choices of the dose-effect curves may be based on the biology driven mechanistic models, such as the median effect model by Chou and Talalay (1984), and with reasonable good diagnostics of the goodness of the fit. As long as we obtain an appropriate dose-effect curve for each drug, the theoretic additive effects based on the Loewe additivity model can be constructed irrespective to the function form of the dose-effect curves. In the literature, two commonly used classes of marginal dose-effect curves are reported. We will illustrate how to estimate the additive effect $F_1(d_1 + \rho d_2)$ under each class in Subsection 3.1. Then, we can obtain the difference of the observed effect and the predicted additive effect at each observed combination dose (d_{1i}, d_{2i}) ($i = 1, \dots, n$). Based on this information, we, then can estimate the function $f(d_1, d_2)$

using the technique described in Subsection 3.2.

3.1 Estimation of the marginal dose-effect curves and the theoretic additive effects

One class for commonly used dose-effect curves is that the effect or transformed effect has a linear relationship with dose or concentration. For example, a logistic model (Carter *et al.*, 1988) for the dose-effect curve has the form:

$$Y = \log \frac{E}{1-E} = \beta_0 + \beta_1 D_{y,1} \quad \text{for drug 1,} \quad (4)$$

and

$$Y = \log \frac{E}{1-E} = \beta_0 + \beta_2 D_{y,2} \quad \text{for drug 2.} \quad (5)$$

Here the intercepts are assumed to be the same since the baseline effects for the two drugs should be the same. Since the transformations from E to Y in both equations (4) and (5) are monotonic and unique, the same E in the both equations implies the same Y , vice versa. We refer Y as the transformed effect, and $Y_i = \log \frac{E_i}{1-E_i}$ ($i = 1, \dots, n$) as the observed transformed effect. Equating the right hand sides of the equations (4) and (5), we can obtain the relative potency:

$$\rho = \rho(y) = \frac{D_{y,1}}{D_{y,2}} = \frac{\beta_2}{\beta_1},$$

which is a constant. Thus, the predicted additive effect can be obtained as

$$Y = \log \frac{E}{1-E} = F_1(d_1 + \rho d_2) = \beta_0 + \beta_1(d_1 + \rho d_2) = \beta_0 + \beta_1 d_1 + \beta_2 d_2. \quad (6)$$

In application, we may first regress $\log \frac{E}{1-E}$ on dose with the observations of each drug when used alone to see whether the fit is adequate and the intercepts of the two regression lines for the two drugs are close. If the fit is adequate and the intercepts of the two regression lines for the two drugs are close, we may force the intercepts are the same by regressing $\log \frac{E}{1-E}$ on d_1 and d_2 using only the marginal data (i.e., the data with $d_1 = 0$ or $d_2 = 0$). Thus, we obtained the estimates of β_0 , β_1 , and β_2 . Plugging these estimates in equation (6), we obtain the theoretic additive effect $\hat{F}_1(d_1 + \hat{\rho}d_2)$ in the transformed scale for each combination dose (d_1, d_2) . The predicted additive effect in the original scale at (d_1, d_2) is obtained by the inverse transformation

$$\hat{E}_{d_1, d_2} = \frac{1}{1 + \exp \left(-\hat{F}_1(d_1 + \hat{\rho}d_2) \right)}. \quad (7)$$

Another class for dose-effect curves is that the effect or transformed effect has a linear relationship with $\log(\text{dose})$ or $\log(\text{concentration})$. This class is very general and includes many families. For example, the EMAX model

(Holford and Shiener, 1981),

$$E = \frac{E_{max}(\frac{d}{D_m})^m}{1 + (\frac{d}{D_m})^m}, \quad (8)$$

as well as Chou and Talalay's (1984) median effect equation (a special case with $E_{max} = 1$), and the families given by Suhnel (1998) as discussed in Kong and Lee (2005). Here d is the dose of a drug, D_m is the median effective dose of a drug, and m is a slope parameter depicting the shape of the dose-effect curve. All these dose-effect curves can be rewritten as Y , a monotone function of E , having a linear relationship with $\log d$. For example, the EMAX dose-effect curve has the form

$$Y = \log \frac{E}{E_{max} - E} = m(\log d - \log D_m). \quad (9)$$

Tallarida (2000, Chapter 2) points out that the data point in the mid range (say between 20% and 80% of the maximum effect) typically displays a nearly linear trend between the effect and $\log d$ in the case that the responses are measured on a continuous scale. Finney (1971) and Govindarajulu (2001) point out that the probit or logistic transformed effect usually has a linear relationship with $\log d$ for quantal effect data. Consequently, we assume that the effect or transformed effect follows a linear function of $\log(\text{dose})$ for each of the two drugs when acting alone:

$$Y = g(E) = \beta_0 + \beta_1 \log D_{y,1} \quad \text{for drug 1,} \quad (10)$$

$$Y = g(E) = \alpha_0 + \alpha_1 \log D_{y,2} \quad \text{for drug 2.} \quad (11)$$

Here the function g should be monotonic. Again we refer Y as the transformed effect, the same Y in both equations (10) and (11) implies the same E , and vice versa. Equating the right hand sides of the equations (10) and (11), we obtain the relative potency as

$$\rho = \rho(y) = \frac{D_{y,1}}{D_{y,2}} = \exp \left(\frac{\alpha_0 - \beta_0}{\beta_1} + \frac{\alpha_1 - \beta_1}{\beta_1} \log D_{y,2} \right), \quad (12)$$

where $D_{y,2} = \rho^{-1}d_1 + d_2$. The relative potency is constant (i.e., $\rho = \exp \left(\frac{\alpha_0 - \beta_0}{\beta_1} \right)$) if only if $\alpha_1 = \beta_1$. Otherwise, iterative methods, such as Newton-Raphson method, must be used to obtain the relative potency estimate for each combination dose (d_1, d_2) by solving

$$\rho = \exp \left(\frac{\alpha_0 - \beta_0}{\beta_1} + \frac{\alpha_1 - \beta_1}{\beta_1} \log(\rho^{-1}d_1 + d_2) \right). \quad (13)$$

Once the relative potency is obtained, the predicted additive effect,

$$Y = F_1(d_1 + \rho d_2) = \beta_0 + \beta_1 \log(d_1 + \rho d_2), \quad (14)$$

can be easily obtained for each combination dose (d_1, d_2) .

In application, we may first regress $g(E)$ on dose with the observations of each drug when used alone to see whether the fit is adequate. If the fit is adequate we may plug these estimates for β_0 , β_1 , α_0 , and α_1 in equation (13) and compute the relative potency iteratively. Then, we can obtain the theoretic additive effect $\hat{F}_1(d_1 + \hat{\rho}d_2)$ in the transformed scale for each combination dose (d_1, d_2) . The predicted additive effect in the original scale at (d_1, d_2) can be obtained by the inverse transformation

$$\hat{E}_{d_1, d_2} = g^{-1} \left(\hat{F}_1(d_1 + \hat{\rho}d_2) \right). \quad (15)$$

3.2 Estimation of $f(d_1, d_2)$

In the previous subsection, we illustrated how to estimate the additive effect for each combination dose. Particularly, we can estimate the additive effect, $\hat{F}_1(d_{1i} + \hat{\rho}d_{2i})$, for each observed combination dose (d_{1i}, d_{2i}) ($i = 1, \dots, n$). Then we can easily compute the differences of the observed effects and the predicted additive effects, $Y_i - \hat{F}_1(d_{1i} + \hat{\rho}d_{2i})$, at each observed combination dose (d_{1i}, d_{2i}) ($i = 1, \dots, n$). Note that estimating the marginal dose-response curves are based on the marginal data. Subsequently, based on the Loewe additivity model, the predicted additive effect for each combination dose (d_1, d_2) can be determined by the marginal dose-response curves and the combination dose. With this, our next step is to use $f(d_1, d_2)$ to capture the departure from the additive effect, which only exists for non-marginal combination dose, i.e., (d_1, d_2) with $d_1 \neq 0$ and $d_2 \neq 0$ because by definition, there is no interaction when a drug is used alone. Theoretically, $f(d_1, d_2)$ should be set as zero whenever $d_1 = 0$ or $d_2 = 0$. However, as far as we know, in the frame work of bivariate splines, there is no such basis functions such that the linear combination of these basis functions be zero at (d_1, d_2) with $d_1 = 0$ or $d_2 = 0$. In order to estimate $f(d_1, d_2)$ to be as close to zero as possible whenever $d_1 = 0$ or $d_2 = 0$, we force the differences of the observed and predicted effect at the marginal observations to be zero. Thus, we define

$$1_{\{d_1 \neq 0 \& d_2 \neq 0\}} = \begin{cases} 1, & \text{if } d_1 \neq 0 \& d_2 \neq 0 \\ 0, & \text{Otherwise.} \end{cases}$$

Then, we can proceed to estimate the function $f(d_1, d_2)$ based on the observed doses (d_{1i}, d_{2i}) and the modified differences $\left(Y_i - \hat{F}_1(d_{1i} + \hat{\rho}d_{2i}) \right) 1_{\{d_{1i} \neq 0 \& d_{2i} \neq 0\}}$ for $i = 1, \dots, n$.

Several available methods can be applied to estimate $f(d_1, d_2)$ in the frame work of splines including tense-product spline and thin plate splines (Green and Silverman, 1994). The bivariate tense-product splines are based on the products of two single variable splines, which generate the splines over a rectangle region, while the thin plate splines can incorporate observations from any kinds of design, such as factorial design, ray design (Chou and Talalay, 1984), and the uniform design (Tan *et al.*, 2003). Also the thin plate spline is ready to be extended to high

dimensional data (Ruppert *et al.*, 2003; Green and Silverman, 1994).

To estimate $f(d_1, d_2)$ using thin plate splines, first we need to choose knots. Here we take all the distinct values among $(d_{1i}, d_{2i})^T$ ($i = 1, \dots, n$) as the knots, say, $(\kappa_{1k}, \kappa_{2k})^T$ ($k = 1, \dots, K$). Then using the basis function given by Green and Silverman (1994) and the above knots, $f(d_1, d_2)$ can be expressed as a linear combination of the following form:

$$f(d_1, d_2) = \gamma_0 + \gamma_1 d_1 + \gamma_2 d_2 + \sum_{k=1}^K v_k \eta(\|(d_1, d_2)^T - (\kappa_{1k}, \kappa_{2k})^T\|), \quad (16)$$

where the basis function

$$\begin{aligned} \eta(r) &= \frac{1}{16\pi} r^2 \log r^2 \quad \text{for } r > 0, \\ &= 0 \quad \text{for } r = 0, \end{aligned} \quad (17)$$

and the distance between two combination doses is defined as the Euclidean distance:

$$\|(d_1, d_2)^T - (\kappa_{1k}, \kappa_{2k})^T\| = \sqrt{(d_1 - \kappa_{1k})^2 + (d_2 - \kappa_{2k})^2}.$$

The parameters γ_i ($i=0, 1, 2$) and v_k ($k = 1, \dots, K$) can be estimated by minimizing the following penalized sum of squares (PSS):

$$PSS = \sum_{i=1}^n \left((Y_i - \hat{F}_1(d_{1i} + \hat{\rho}d_{2i})) 1_{\{d_{1i} \neq 0 \text{ \& } d_{2i} \neq 0\}} - f(d_{1i}, d_{2i}) \right)^2 + \lambda J(f), \quad (18)$$

where the first term measures the goodness of fit, and the second term

$$J(f) = \int \int_{R^2} \left\{ \left(\frac{\partial^2 f}{\partial x^2} \right)^2 + 2 \left(\frac{\partial^2 f}{\partial x \partial y} \right)^2 + \left(\frac{\partial^2 f}{\partial y^2} \right)^2 \right\} dx dy$$

measures the smoothness of the function $f(d_1, d_2)$, and the smoothing parameter, λ , measures the tradeoff between the goodness of fit and the smoothness of the function f . The selection of the smoothing parameter λ is important. Following the idea of Ruppert *et al.* (2003), we develop the following procedure to estimate the parameters γ_i ($i=0, 1, 2$), v_k ($k = 1, \dots, K$), and the smoothing parameter λ .

Under the form of (16) for $f(d_1, d_2)$, Green and Silverman (1994) showed that $J(f) = v^T \Omega v$, where

$$\Omega = \left[\eta(\|(\kappa_{1k}, \kappa_{2k})^T - (\kappa_{1k'}, \kappa_{2k'})^T\|) \right]_{1 \leq k, k' \leq K}.$$

Thus (18) can be written as

$$(Y_R - X\gamma - Z_1 v)^T (Y_R - X\gamma - Z_1 v) + \lambda v^T \Omega v, \quad (19)$$

where

$$Y_R = \left[\left(Y_1 - \hat{F}_1(d_{11} + \hat{\rho}d_{21}) \right) 1_{\{d_{11} \neq 0 \text{ \& } d_{21} \neq 0\}}, \dots, \left(Y_n - \hat{F}_1(d_{1n} + \hat{\rho}d_{2n}) \right) 1_{\{d_{1n} \neq 0 \text{ \& } d_{2n} \neq 0\}} \right]^T,$$

$$X = [1, d_{1i}, d_{2i}]_{1 \leq i \leq n},$$

$$Z_1 = [\eta(|(d_{1i}, d_{2i})^T - (\kappa_{1k}, \kappa_{2k})^T|)]_{1 \leq k \leq K}]_{1 \leq i \leq n},$$

$$\gamma = (\gamma_0, \gamma_1, \gamma_2)^T, \text{ and } v = (v_1, \dots, v_K)^T.$$

Estimations of the parameters γ and v and the selection of the smoothing parameter λ can be obtained using software readily available for linear mixed effect models. To see this point, set $u = \Omega^{\frac{1}{2}}v$, where $\Omega^{\frac{1}{2}}$ is the matrix square root of Ω , which can be obtained by first finding the singular value decomposition of $\Omega = U \text{diag}(\omega) V^T$, then $\Omega^{\frac{1}{2}} = U \text{diag}(\sqrt{\omega}) V^T$. Here U and V are $K \times K$ matrices with $U^T U = V V^T = I_K$, and ω is a $K \times 1$ vector with nonnegative entries (Ruppert *et al.* 2003, p329). Thus minimizing (19) is equivalent to minimizing

$$(Y_R - X\gamma - Zu)^T (Y_R - X\gamma - Zu) + \lambda u^T u, \quad (20)$$

where $Z = Z_1 \Omega^{-\frac{1}{2}}$. The expression (20) is proportional to the negative exponential part of the joint distribution of Y_R and u under the following model assumption:

$$Y_R = X\gamma + Zu + \epsilon \quad \text{with} \quad \begin{pmatrix} u \\ \epsilon \end{pmatrix} \sim N \left(\begin{pmatrix} 0 \\ 0 \end{pmatrix}, \begin{pmatrix} \sigma_u^2 I_K & 0 \\ 0 & \sigma_\epsilon^2 I_n \end{pmatrix} \right), \quad (21)$$

where λ is replaced by $\frac{\sigma_\epsilon^2}{\sigma_u^2}$. The solution of minimizing (20) is the same as the best linear unbiased predictor (BLUP) for γ and u in the mixed model (21) and this solution can be written as

$$\begin{pmatrix} \tilde{\gamma} \\ \tilde{u} \end{pmatrix} = \text{BLUP} \begin{pmatrix} \gamma \\ u \end{pmatrix} = (C^T C + \lambda D)^{-1} C^T Y_R, \quad (22)$$

with $C = [X \ Z]$ and $D = \text{diag}(0, 0, 0, 1, \dots, 1)$, where the number of zeros in the matrix D corresponds to the number of γ_i 's ($i = 0, 1, 2$) and the number of ones corresponds to the number of u_i 's ($i = 1, \dots, K$). In Appendix A, under the model assumption (21) we proved

$$\begin{pmatrix} \tilde{\gamma} - \gamma \\ \tilde{u} - u \end{pmatrix} = -\lambda (C^T C + \lambda D)^{-1} \begin{pmatrix} 0 \\ u \end{pmatrix} + (C^T C + \lambda D)^{-1} C^T \epsilon, \quad (23)$$

and

$$\text{Cov} \begin{pmatrix} \tilde{\gamma} - \gamma \\ \tilde{u} - u \end{pmatrix} = \sigma_\epsilon^2 (C^T C + \lambda D)^{-1}. \quad (24)$$

For any combination dose (d_1, d_2) , if we denote $f(d_1, d_2) = \gamma_0 + \gamma_1 d_1 + \gamma_2 d_2 + Z_0 u$ with $Z_0 = [\eta(|(d_1, d_2)^T - (\kappa_{1k}, \kappa_{2k})^T|)]_{1 \leq k \leq K} (\Omega^{\frac{1}{2}})^{-1}$, then $\tilde{f}(d_1, d_2) = \tilde{\gamma}_0 + \tilde{\gamma}_1 d_1 + \tilde{\gamma}_2 d_2 + Z_0 \tilde{u}$ is the best linear unbiased prediction (BLUP) for $f(d_1, d_2)$. Usually σ_ϵ^2 and σ_u^2 are unknown, consequently, $\lambda = \frac{\sigma_\epsilon^2}{\sigma_u^2}$ is unknown, therefore, $\tilde{\gamma}$ and \tilde{u} are unknown.

Let $\hat{\sigma}_\epsilon^2$ and $\hat{\sigma}_u^2$ be the restricted maximum likelihood estimators (REML) of σ_ϵ^2 and σ_u^2 in the mixed model (21).

Replacing λ by $\hat{\lambda} = \frac{\hat{\sigma}_\epsilon^2}{\hat{\sigma}_u^2}$ in (22), we can obtain the estimated BLUP for γ and u , say $\hat{\gamma}$ and \hat{u} . Thus the estimated BLUP for $f(d_1, d_2)$ is $\hat{f}(d_1, d_2) = \hat{\gamma}_0 + \hat{\gamma}_1 d_1 + \hat{\gamma}_2 d_2 + Z_0 \hat{u}$. Let us denote $C_d = (1, d_1, d_2, Z_0)$ for each combination dose (d_1, d_2) , then based on (23), in general the following conditional expectation

$$E \left\{ \tilde{f}(d_1, d_2) - f(d_1, d_2) | u \right\} = C_d E \left\{ \begin{pmatrix} \tilde{\gamma} - \gamma \\ \tilde{u} - u \end{pmatrix} | u \right\} \neq 0, \quad (25)$$

while the unconditional expectation

$$E \left\{ \tilde{f}(d_1, d_2) - f(d_1, d_2) \right\} = C_d E \begin{pmatrix} \tilde{\gamma} - \gamma \\ \tilde{u} - u \end{pmatrix} = 0. \quad (26)$$

The BLUP for $f(d_1, d_2)$ is unbiased unconditionally. Therefore, the unconditional estimates are preferred. From (24) and (26), we can obtain

$$\begin{aligned} \text{Var} \left\{ \tilde{f}(d_1, d_2) - f(d_1, d_2) \right\} &= E \left\{ \tilde{f}(d_1, d_2) - f(d_1, d_2) \right\}^2 \\ &= C_d \text{Cov} \begin{pmatrix} \tilde{\gamma} - \gamma \\ \tilde{u} - u \end{pmatrix} C_d^T = \sigma_\epsilon^2 C_d (C^T C + \lambda D)^{-1} C_d^T. \end{aligned} \quad (27)$$

Since $\tilde{f}(d_1, d_2) - f(d_1, d_2) = C_d \begin{pmatrix} \tilde{\gamma} - \gamma \\ \tilde{u} - u \end{pmatrix}$, (23) and (26) imply that

$$\frac{\tilde{f}(d_1, d_2) - f(d_1, d_2)}{\sqrt{\text{Var} \left\{ \tilde{f}(d_1, d_2) - f(d_1, d_2) \right\}}} \sim N(0, 1). \quad (28)$$

This altogether with (27) suggest that

$$\widehat{\text{st.dev.}} \left\{ \tilde{f}(d_1, d_2) - f(d_1, d_2) \right\} \approx \hat{\sigma}_\epsilon \sqrt{C_d (C^T C + \hat{\lambda} D)^{-1} C_d^T}. \quad (29)$$

and

$$\frac{\hat{f}(d_1, d_2) - f(d_1, d_2)}{\widehat{\text{st.dev.}} \left\{ \hat{f}(d_1, d_2) - f(d_1, d_2) \right\}} \stackrel{\text{approx.}}{\sim} N(0, 1). \quad (30)$$

Thus, an approximate $100(1 - \alpha)\%$ confidence interval for $f(d_1, d_2)$ can be constructed as

$$\hat{f}(d_1, d_2) \pm z_{\frac{\alpha}{2}} \widehat{\text{st.dev.}} \left\{ \hat{f}(d_1, d_2) - f(d_1, d_2) \right\}, \quad (31)$$

where $z_{\frac{\alpha}{2}}$ is the upper $\frac{\alpha}{2} \times 100\%$ percentile of the standard normal distribution. $\hat{\lambda} = \frac{\hat{\sigma}_\epsilon^2}{\hat{\sigma}_u^2}$ with $\hat{\sigma}_\epsilon^2$ and $\hat{\sigma}_u^2$ being REML estimates for σ_ϵ^2 and σ_u^2 in model (21).

4. Case Studies

Example 1: We analyzed the 10 data sets derived from 10 cell lines treated with SCH66336, a farnesyl transferase inhibitor, and 4-HPR, a retinoid, alone and in combinations (data are provided by Dr. Reuben Lotan at M.D. Anderson Cancer Center). Both agents have activities in producing apoptosis or programmed cell death. The objective is to study the efficacy and quantify the drug interaction when the two agents are used in combination. To illustrate the data structure and the procedure to estimate our proposed model (3), we present the analysis on the data set derived from the cell line UMSCC22B in detail. The data set is shown in Table 1. The experiment was conducted in six trays with each tray containing 96 wells. All the wells along the margins were not used. In each of those used wells, the cells were treated either with zero dose (control group), or single drug doses, or combination doses. The fraction of cell survival in each well is recorded. The smaller fraction of cell survival indicates higher apoptosis activities, hence, higher efficacy. Aside from the control, the first group (Tray 1) in Table 1 are the fraction of cell survival resulted from treating cells with drug SCH66336 alone. The last group (Tray 6) are the cell survival resulted from treating cells with drug 4-HPR alone. The other four groups (Tray 2 to Tray 5) are the cell survival fractions resulted from the two treatments combined. In each tray there is a control group. For each dose combination in each tray, experiments were conducted with six replications. We fitted the marginal data to EMAX model (9) by taking E_{max} as the mean of the control group, and the logistic model (4). The two fitted marginal dose-effect curves for SCH66336 are shown in Figure 1, Panel A, here the solid curve is based on the model (9), and the dashed curve is based on the model (4). The two fitted marginal curves for 4-HPR are shown in Panel B. In the two panels, the observed data are shown as circles. Comparing the two fitted marginal curves with the observed data in each panel, we conclude that EMAX model fits the data better. Therefore, we choose EMAX model as the marginal dose-effect curve. Taking E_{max} as the mean of the control group, fitting the EMAX model is equivalent to fitting Chou and Talalay's median effect model with effect as the cell survival divided by the mean of the control. In the following data analysis, the effects will be taken as the observed fractions of cell survival divided by the mean of the corresponding control group in each tray (c.f., Kanzawa *et al.* (1999) for similar procedure). Based on the processed data, we can obtain the two marginal dose-effect curves: $Y = \log \frac{E}{1-E} = 0.0973 - 0.3373 \log D_{y,1}$ for SCH66336 with a residual error 0.2684 (i.e., $\hat{\sigma} = 0.2684$), and $Y = \log \frac{E}{1-E} = 0.2303 - 0.4672 \log D_{y,2}$ for 4-HPR with a residual error 0.5618. Then, we can obtain the predicted additive effect for each combination dose assuming the additive effect in E scale using the inverse transformation (7) (Panel C). The differences of observed effect and predicted effect versus the observed effect, all in logit scale, is shown in Panel D, where the "+" and

“<” correspond to the marginal data for SCH66336 dose and 4-HPR dose, respectively. The circles correspond to the non-marginal data. The differences versus SCH66336 and 4-HPR are plotted in Panel E and F, respectively. From Panels E and F, it is clear that the differences for the lower combination doses are roughly centered around zero, indicating additivity of the associated combination doses, and the differences for median to large combination doses are less than zero, indicating lack of fitting the additive model while drug combination is synergistic in the associated combination doses.

Now, we proceed to estimate $f(d_1, d_2)$. The estimated residual error $\hat{\sigma}_\epsilon = 0.217$ and the estimated smoothing parameter $\hat{\lambda} = 0.1477$. The contour plot of the estimated $f(d_1, d_2)$ were shown in Panel G. The 95% confidence surfaces for $f(d_1, d_2)$ were constructed based on (31). The 95% confidence intervals for $f(d_1, d_2) = 0$ can be formed by taking the intersection lines of the upper and lower confidence surfaces with the dose plane. The dotted line in Panel G is the intersection line of the upper confidence surface with the dose plane, and the intersection line of the lower confidence surface with the dose plane falls outside the left-lower corner of the illustrated region. From Panel G, we conclude that the combination doses above the dotted line are synergistic ($f(d_1, d_2) < 0$), and the combination doses below the dotted line are additive ($f(d_1, d_2)$ is not significantly different from zero). The residual plot (Panel H) indicates that the fit has improved compared to Panel D under the additive model although one outlier remained. This outlier came from fitting marginal dose-response curve for 4-HPR. As we reasoned, there is no drug interactions when drugs used alone, we force the differences of the observed effect and predicted effect for marginal data being zero when estimating $f(d_1, d_2)$. This is why the residual of 1.5 was not reduced in Panel H. We add $f(d_1, d_2)$ to the predicted effect surface, then, obtain the fitted effect surface on the logit scale, Panel I shows the contour plot of the fitted effect surface in the original effect scale. The contour plot of the raw data is shown in Panel J. The contour plot in Panel I is similar to the contour plot of the raw data (Panel J), which indicates the fit is reasonable. On the other hand, Panel C is quite different from Panel J suggesting that the additive model is not adequate to describe the data. We also fitted the dose-effect curve with the combination doses at fixed ratio 1:1, the curve and observed values are shown in Panel K, and the plot of the corresponding interaction indices versus the effects is shown in Panel L. Each dot in Panel L was the interaction index based on the average effect at each combination dose at the fixed ratio, the vertical bars were the corresponding confidence intervals based on the derivation in Lee *et al.* (2005) with considering the variance in the effect. From Panel L, we conclude that at fixed ratio 1:1 the lower combination doses (with higher cell survival) are additive and the moderate to higher combination doses are synergistic. The conclusions on drug interaction based on our proposed model are consistent with those based on the Chou and Talalay’s model.

Example 2. We also analyzed another data set by Kanzawa *et al.* (1999) shown in Figure 2. The data set was published in the original paper and can be found there. The two treating drugs are cisplatin (CDDP) and KRN5500, a new derivative of spicamycin having a wide range of antitumor activities. The figure layout is the same as in Figure 1 except for Panel K and L. Panel K and L are the plots of interaction indices versus the effect for the combination doses of CDDP and KRN5500 at the fixed ratio 1:1 and 10:1, respectively. Similar to Example 1, we conclude that Chou and Talalay’s median effect equation fits the marginal data better based on Figure 2, Panel A and B. The fitted marginal dose-effect curves are $Y = \log \frac{E}{1-E} = -2.1759 - 1.4491 \log D_{y,1}$ for CDDP with a residual error 0.3436, and $Y = \log \frac{E}{1-E} = -3.3736 - 1.3883 \log D_{y,2}$ for KRN5500 with a residual error 0.3088. From Panel E, it seems that the combination doses with lower CDDP are additive (i.e., the differences are centered around zero), the combination doses with median CDDP are synergistic (i.e., the differences are less than zero), and the combination doses with high CDDP are antagonistic (i.e., the differences are greater than zero). By applying the proposed semiparametric method, the residual error, $\hat{\sigma}_\epsilon = 0.152$, and the smoothing parameter was $\hat{\lambda} = 0.00188$. The well behaved residual plot (Panel H) and the similarity between the contour plot of the fitted effect surface (Panel I) and the contour plot of the raw data (Panel J) indicate that semiparametric method provides adequate fit to the data and yields much improvements over the simple additive model. In Panel G, the dotted lines (center and far left in the figure) are the intersection lines of the 95% upper confidence surface with the dose plane, while the dashed line (far right in the figure) is the intersection line of the 95% lower confidence surface with the dose plane. We conclude that the combination doses below the left most dotted line (denoted as Region I) are additive (i.e. $f(d_1, d_2)$ is not significantly different from zero), the combination doses between the left most dotted line and the middle dotted line (denoted as Region II) are synergistic ($f(d_1, d_2) < 0$), the combination doses between the middle dotted line and the dashed line (denoted as Region III) are additive (i.e. $f(d_1, d_2)$ is not significantly different from zero), and the combination doses below the dashed line (denoted as Region IV) are antagonistic ($f(d_1, d_2) > 0$). From Panel K, the combination doses with large effect at fixed ratio 1:1 (corresponding to Region I) are additive, and the combination doses with small effect at the fixed ratio 1:1 (corresponding to Region II) are synergistic. To compare the results in Panel L and Panel G, we may think of a straight line passing through (0, 0) and (2.5, 0.25) in Panel G. At the fixed ratio 10:1, the combination doses with large effect (Region I) are additive, the combination doses with moderate to small effects (Region II) are synergistic, and the combination doses with very small effect (Region III) are additive. So the conclusions from the proposed model on drug interactions are consistent with those obtained from Chou and Talalay’s model. The results in Panel G are also consistent with the findings by Kanzawa *et al.* (1999) based on isobologram and the combination index plots with $\alpha = 0$.

5. Simulation studies

In this section, we illustrate that the choice of the smoothing parameter, λ , is important. By simulations we want to see whether the estimation of the function f in our semiparametric model is accurate, and whether the semiparametric model can detect different patterns of drug interactions successfully.

As we pointed in Section 3.2, the smoothing parameter, λ , measures the tradeoff between the goodness of fit and the smoothness of the function f . As λ goes larger, the smoothness of the function f will be emphasized. Especially when λ goes to infinity, minimizing PSS in (18) will force the penalty term $J(f)$ to zero, thus, f will be a plane of the form $\gamma_0 + \gamma_1 d_1 + \gamma_2 d_2$. Contrarily, as λ goes smaller, the goodness of fit will be emphasized. Especially when λ goes to zero, f will follow the modified differences, Y_R 's, closely, and the resulting f will be wiggly. In the literature, there are two widely used methods to select the smoothing parameter. One is the so called generalized cross validation (GCV) method, which is obtained by grid search for λ in $(0, \infty)$. The other, employed in this paper, is based on the REML estimates under the frame work of linear mixed effect model. One may refer Ruppert *et al.* (2003) for details. To illustrate the importance of the choice of the smoothing parameter λ , we start with the results of Example 1. In Example 1, the smoothing parameter λ was chosen as 0.1477 based on the REML estimates. The contour plot of the corresponding estimated $f(d_1, d_2)$ is shown in Figure 1, Panel G. Let λ increase by 100 fold, the contour plot of the corresponding estimated $f(d_1, d_2)$ is shown in Figure 3, Panel A1. It appears that each contour level is close to a straight line. On the other hand, we decrease λ by 10 fold and the contour plot of the corresponding estimated $f(d_1, d_2)$ is shown in Figure 3, Panel A2. It is clear that some contour level is too wiggly. To make the comparison clear, we plotted the three estimated f versus SCH66336 dose with 4-HPR fixed at 1 in Figure 3, Panel A3. There the solid line, dotted line, and dashed line are the resulting estimated $f(d_1, d_2)$ with $\hat{\lambda}$ fixed at 0.1477, 14.77, and 0.01477, respectively. It is clear that the dotted line is close to a straight line due to f being estimated with too much smoothness, while the dashed line is too wiggly due to f being estimated locally with counting too much noise.

To examine whether the function $f(d_1, d_2)$ can be estimated accurately or not, we generate data based on the marginal dose-effect curves estimated from Example 1, and $f(d_1, d_2) = -0.2 * (d_1 d_2)^{\frac{1}{4}} (d_2 - 1.5 d_1^2 + 4.5 d_1 - 2.125)$ (Figure 3, Panel B). The construction of $f(d_1, d_2)$ mimics the scenario that there are different patterns of drug interactions within the same data and there is no drug interaction when drug used alone. We generated the marginal data by adding the white noise, $N(0, \sigma_1^2)$, to the “true” effect on the logit scale. Similarly, we generate the non-marginal data by adding the white noise, $N(0, \sigma_2^2)$, to the sum of the additive response and $f(d_1, d_2)$,

where the additive response surface is constructed based on the underlying marginal dose-effect curves. We took the same settings as in Example 1 except adding one more dose for drug 1 at $d_1 = 3$ with 6 replicates for each factorial combination dose. We took $\sigma_1 = 0.3$, which lies between the the estimated residual errors for SCH66336 and 4-HPR, and $\sigma_2 = 0.217$, which is the estimated residual error for f . We generated 20 samples, estimated $f(d_1, d_2)$, and plotted the $\hat{f}(d_1, d_2)$ at each fixed d_2 level in Figure 3, Panel C1 through Panel C5. In each Panel, the solid line is the underlying $f(d_1, d_2)$ by varying d_1 , and the dotted lines are the estimated curves for each of the 20 samples. It is evident that the fitted curves are close to the underlying true curves.

To see whether the semiparametric can detect different patterns of drug interactions, we use the same scenario as above without adding extra combination doses. We performed the simulations under three different settings on σ_1, σ_2 : $\sigma_1 = 0.3, \sigma_2 = 0.217$; $\sigma_1 = \sigma_2 = 0.1$; $\sigma_1 = \sigma_2 = 0.01$. For each setting, we generated 1000 samples. For each sample, we fitted the semiparametric model, estimated the function $f(d_1, d_2)$, and counted whether the 95% confidence interval (CI) constructed based on (31) contains zero (indicating the estimated $f(d_1, d_2)$ is not significantly different from zero, thus additive at (d_1, d_2)), or the lower limit of the CI is greater than zero (indicating the estimated $f(d_1, d_2) > 0$ significantly, thus antagonism at (d_1, d_2)), or the upper limit of the CI is less than zero (indicating the estimated $f(d_1, d_2) < 0$ significantly, thus synergy at (d_1, d_2)). The percentage of counts of the lower limit is greater than zero (denoted as pct.p), the percentage of counts of the confidence interval contains zero (denoted as pct.a), and the percentage of counts of the upper limit is less than zero (denoted as pct.n) are listed in Table 2. In Table 2, it is clear that as the standard deviation goes smaller, the precision on predicting drug interaction will be improved. Since there are 6 replicates for each combination dose, any f value lying in the interval $(-2\sigma_2/\sqrt{6}, 2\sigma_2/\sqrt{6})$ may be predicted as additive, i.e., the confidence interval (31) for the estimated f may contain zero. For example, when $\sigma_2 = 0.217$, $2\sigma_2/\sqrt{6} = 0.177$, any f value lying in the interval $(-0.177, 0.177)$ has more than 5% of chance to be predicted as additive. This explains why when the percentages of additivity counts under the fourth column are so high for smaller f values. Comparing the results under different settings, it is clear that the precision on predicting drug interactions will be improved as the standard deviations becomes smaller.

6. Discussion

We have analyzed two data sets based on *in vitro* studies (SCH66336 and 4-HPR study and Kanzawa *et al.* 1999) to assess the drug interactions. Both data sets show that the EMAX model (9) (or Chou and Talalay's median effect model with $E_{max=1}$) gives better fit than the logistic function model (4). Subsequently, we used Chou and Talalay's median effect model as the dose-effect curve for single drug. As shown in Subsection 3.1, the

relative potency in general is varying. In order to predict the additive effects for the combination doses, we have constructed an algorithm to incorporate the varying relative potency. To assess whether our method is accurate in assessing drug interactions, we fitted the data with the combination doses at a fixed ratio. Then based on the two marginal dose-effect curves and the dose-effect curve at the fixed ratio, a plot of interaction index versus effect can be obtained. The confidence interval for each interaction index can be constructed based on Lee *et al.* (2005). Based on the confidence intervals we can know the patterns of the drug interactions for combination doses at the fixed ratio. One limit of Chou and Talalay's method is that it can only detect the patterns of drug interactions for the combination doses at the fixed ratio.

In contrast, our method can give an overall picture of the patterns of drug interactions over the entire experimental dose range. The consistency on assessing drug interactions for the combination doses at several fixed ratios in the case studies in Section 4 and the simulations in Section 5 indicate the accuracy of our proposed method. In addition, we refer that the proposed semiparametric model can incorporate varying relative potency and identify different patterns of drug interactions within the same data. Because the fitted dose-effect surface $\hat{F}_\lambda(d_1 + \rho d_2) + \hat{f}(d_1, d_2)$ gives an overall picture of dose-effect relationship, it also can help us to identify the optimal combination therapy.

In the semiparametric model, we use a function f to capture the patterns of drug interactions. The estimated function \hat{f} and its 95% confidence surfaces may guide us to explore whether some parametric models are sufficient to describe the data. If the fitted function \hat{f} and its confidence surfaces indicate the modes of drug interactions for all combination doses are the same, then a parametric model with a single parameter capturing drug interaction may suffice. If the fitted function \hat{f} and its confidence surfaces indicate the modes of drug interactions for the combination doses at each fixed ratio are unique, the parametric model proposed by White *et al.* (2004) may be appropriate. We advocate our proposed semiparametric model since we typically do not know the true patterns of drug interactions. Blindly using any parametric models can be dangerous and may lead to the wrong conclusions of drug interactions. In our proposed model, we do not assume any parametric patterns for $f(d_1, d_2)$. The conclusions of drug interactions are based on the estimated \hat{f} and its confidence surfaces, which are determined by the underlying data.

The procedure for estimation of the proposed model is easy to implement in SPLUS or R. The methodology we developed here is ready to be extended to detect the patterns of drug interactions in cases with more than two drugs (say, $k > 2$ drugs). When the dose-effect curve for single drug follows model (4), the predicted additive effect

can be obtained as

$$Y = \log \frac{E}{1-E} = \gamma_0 + \gamma_1 d_1 + \cdots + \gamma_k d_k.$$

When the dose-effect curve for single drug follows model (10), one can extend the additive effect surface for k drug combinations as follows:

$$Y = \beta_0 + \beta_1 \log (d_1 + \rho_2 d_2 + \cdots + \rho_k d_k), \quad (32)$$

where $\rho_i = \exp(\gamma_{i0} + \gamma_{i1} \log D_1)$ ($i = 2, \dots, k$) is the relative potency of drug i versus drug 1, and D_1 is the amount of drug 1 having an equivalent effect to that of the combination (d_1, \dots, d_k) under the additive assumption. D_1 can be obtained by solving the following equation

$$d_1 + \rho_2 d_2 + \cdots + \rho_k d_k = D_1.$$

Here γ_{i0} and γ_{i1} are uniquely determined by the two dose-effect curves for drug 1 and drug i ($i = 2, \dots, k$). In this k -dimensional cases, the construction of $f(d_1, \dots, d_k)$ can be found in Green and Silverman (1994), and the estimation of $f(d_1, \dots, d_k)$ is parallel to Subsection 3.2.

Constructing the semiparametric method involves two steps: to estimate the marginal dose-effect curves parametrically, and to estimate the effect beyond additivity nonparametrically. Since the additive effect is estimated based on the marginal dose-effect curves, in order to estimate the additive effect with smaller error, the marginal effect curves must be estimated as accurately as possible. Thus, in the second step, the $f(d_1, d_2)$, which captures the difference of the true response surface and the additive surface, can be estimated with smaller error as well. Contrarily, when the marginal dose-response curves are estimated with large error, consequently, the predicted additive effects will be estimated with large error too. Subsequently, these errors will be passed to estimate $f(d_1, d_2)$. Thus, when we construct an 95% upper and lower confidence surfaces for $f(d_1, d_2)$ accurately, how to cooperate the errors from estimating the additive effects deserves our further investigation.

The methodology we developed can be applied to analyze data from animal studies with binary endpoints such as response or no response. In such a data set, for each dose or combination dose (d_{1i}, d_{2i}) ($i = 1, \dots, n$), the number of animals n_i assigned and the number of response r_i were recorded. We assume that r_i follow a binomial distribution with parameters n_i and E_i , where E_i is the expected probability of effect at the combination dose (d_{1i}, d_{2i}) . For such a data, the maximum likelihood estimates for parameters in the marginal dose-response curves are appropriate. However, when we estimate $f(d_1, d_2)$ in E scale, the sum $\hat{F}_1(d_1 + \rho d_2) + \hat{f}(d_1, d_2)$ may be out of the range (0,1); when we estimate $f(d_1, d_2)$ based on the transformed responses on a logit scale or a probit scale, we need to ignore the observations with the response rate being zero or one since the associated transformed

responses are infinite. By ignoring some observations, we lose information. A better estimation method using all of the information should be pursued.

Appendix A. Derivation for the variance of the BLUP for γ and u

Under the assumption of the model (21), the BLUP for γ and u can be expressed as (22). From there we have

$$\begin{aligned}
\begin{pmatrix} \tilde{\gamma} \\ \tilde{u} \end{pmatrix} - \begin{pmatrix} \gamma \\ u \end{pmatrix} &= \begin{pmatrix} \tilde{\gamma} - \gamma \\ \tilde{u} - u \end{pmatrix} = (C^T C + \lambda D)^{-1} C^T Y_R - \begin{pmatrix} \gamma \\ u \end{pmatrix} \\
&= (C^T C + \lambda D)^{-1} C^T \left(C \begin{pmatrix} \gamma \\ u \end{pmatrix} + \epsilon \right) - \begin{pmatrix} \gamma \\ u \end{pmatrix} \\
&= (C^T C + \lambda D)^{-1} C^T C \begin{pmatrix} \gamma \\ u \end{pmatrix} + (C^T C + \lambda D)^{-1} C^T \epsilon - \begin{pmatrix} \gamma \\ u \end{pmatrix} \\
&= -\lambda (C^T C + \lambda D)^{-1} D \begin{pmatrix} \gamma \\ u \end{pmatrix} + (C^T C + \lambda D)^{-1} C^T \epsilon \\
&= -\lambda (C^T C + \lambda D)^{-1} \begin{pmatrix} 0 \\ u \end{pmatrix} + (C^T C + \lambda D)^{-1} C^T \epsilon.
\end{aligned}$$

Therefore, we can obtain

$$\begin{aligned}
C_{\text{OV}} \begin{pmatrix} \tilde{\gamma} - \gamma \\ \tilde{u} - u \end{pmatrix} &= \lambda^2 (C^T C + \lambda D)^{-1} \begin{pmatrix} 0 & 0 \\ 0 & \sigma_u^2 I \end{pmatrix} (C^T C + \lambda D)^{-1} + (C^T C + \lambda D)^{-1} C^T (\sigma_\epsilon^2 I) C (C^T C + \lambda D)^{-1} \\
&= (C^T C + \lambda D)^{-1} (\lambda^2 \sigma_u^2 D + \sigma_\epsilon^2 C^T C) (C^T C + \lambda D)^{-1} \\
&= \sigma_\epsilon^2 (C^T C + \lambda D)^{-1}. \quad (\text{where } \lambda = \frac{\sigma_\epsilon^2}{\sigma_u^2})
\end{aligned}$$

Acknowledgment

This research was supported in part by grants from the National Cancer Institute CA16672, CA97007, CA91844, and the Department of Defense W81XWH-04-1-0142 and W81XWH-05-2-0027. The authors are thankful to Dr. Reuben Lotan for providing the data, to Professor Raymond Carroll for the discussion, and to Lee Ann Chastain for the editorial assistance.

References

- [1] Berenbaum, M. C. (1989). What is synergy? *Pharmacological Reviews* 41, 93-141.

- [2] Carter, W. H. Jr., Gennings, C., Staniswalis, J. G., Cambell, E. D., and White K. L. Jr. (1988). A statistical approach to the construction and analysis of isobolograms. *Journal of American College Toxicology* 7, 963-973.
- [3] Chou, T. C., and Talalay, P. (1984). Quantitative analysis of dose-effect relationships: the combined effects of multiple drugs or enzyme inhibitors. *Advances in Enzyme Regulation* 22, 27-55.
- [4] Finney D. J. (1971). *Probit Analysis*. Cambridge University Press, Cambridge.
- [5] Govindarajulu, Z. (2001). *Statistical Techniques in Bioassay*. Karger, Basel.
- [6] Greco, W. R., Bravo, G., and Parsons, J. C. (1995). The search of synergy: A critical review from a response surface perspective. *Pharmacological Reviews* 47(2), 331-385.
- [7] Greco, W. R., Park, H.S., Rustum, Y. M. (1990). Application of a new approach for the quantitation of drug synergy to the combination of cis-diamminedichloroplatinum and 1- β -D-arabinofuranosylcytosine. *Cancer Research* 50, 5318-5327.
- [8] Green, P. J., and Silverman, B. W. (1994). *Nonparametric Regression and Generalized Linear Models*. Chapman & Hall.
- [9] Holford, N. H. G. and Sheiner, L. B. (1981). Understanding the dose-effect relationship: clinical application of pharmacokinetic-pharmacodynamic models. *Clinical Pharmacokinetics* 6, 429-453.
- [10] Kanzawa, F., Nishio, K., Fukuoka, K., Sunami, T., and Saijo, N. (1999). In vitro interactions of a new derivative of spicamycin, KRN5500, and other anticancer drugs using a three-dimensional model. *Cancer Chemother. Pharmacol.* 43, 353-363.
- [11] Kong, M., Lee, J. J. (2005). A generalized response surface model with varying relative potency for assessing drug interactions. Revised to *Biometrics*.
- [12] Kelly, C. and Rice, J. (1990). Monotone smoothing with application to dose-response curves and the assessment of synergism. *Biometrics* 46, 1071-1085.
- [13] Laska, E. M., Meisner, M., and Seigel, C. (1994). Simple designs and model-free tests for synergy. *Biometrics* 50, 834-841.
- [14] Lee, J. J., Kong, M., Ayers, G. D. (2005). A practical guide for determining drug interaction in combination therapy. Submitted to *Statistics in Medicine*.

- [15] Loewe, S. and Muischnek, H. (1926). Effect of combinations: mathematical basis of problem. *Archives of Experimental Pathology Pharmacology* 11, 313-326.
- [16] Minto, C. F., Schnider, T. W., Short, T. G., Gregg, K. M., Gentilini, A., and Shafer, S. L. (2000). Response surface model for anesthetic drug interactions. *Anesthesiology* 92 (6), 1603-1616.
- [17] Prichard, M. N., and Shipman Jr. C. (1990). A three-dimensional model to analyze drug-drug interactions. *Antiviral Research* 14, 181-206.
- [18] Plummer, J. L. and Short, T. G. (1990). Statistical modeling of the effects of drug combinations. *Journal of Pharmacological Methods* 23, 297-309.
- [19] Ruppert, D., Wand, M. P., and Carroll, R. J. (2003). *Semiparametric Regression*. Cambridge University Press.
- [20] Suhnel, J. (1990). Evaluation of synergism or antagonism for the combined action of antiviral agents. *Antiviral Research* 13, 23-40.
- [21] Suhnel, J. (1998). Parallel dose-response curves in combination experiments. *Bulletin of Mathematical Biology* 60, 197-213.
- [22] Tallarida, R. J. (2000). *Drug synergy and Dose-Effect Data Analysis*. Chapman Hall/CRC Press, Boca Raton.
- [23] Tan, M., Fang, H. , Tian, G., and Houghton, P. J. (2003). Experimental design and sample size determination for testing synergism in drug combination studies based on uniform measures. *Statistics in Medicine* 22, 2091-2100.
- [24] White, D. B., Faessel, H. M., Slocum, H. K., Khinkis, L., and Greco, W. R. (2004). Nonlinear response surface and mixture experiment methodologies applied to the study of synergy. *Biometrical Journal* 46, 56-71.

Table 1: Observed fractions of cells survival from cell line UMSCC22B treated with SCH66336 and 4-HPR. The first coordinate d_1 in the combination dose (d_1, d_2) was the dose used for SCH66336 and the second coordinate d_2 was for 4-HPR.

Tray	(0, 0)		(0.1, 0)		(0.5, 0)		(1.0, 0)		(2.0, 0)		(4.0, 0)	
1	0.422	0.498	0.328	0.345	0.383	0.306	0.255	0.303	0.202	0.235	0.163	0.205
	0.473	0.453	0.335	0.336	0.282	0.329	0.297	0.228	0.258	0.229	0.213	0.196
	0.491	0.623	0.307	0.346	0.297	0.277	0.296	0.283	0.223	0.209	0.180	0.162
Tray	(0, 0)		(0.1, 0.1)		(0.5, 0.1)		(1.0, 0.1)		(2.0, 0.1)		(4.0, 0.1)	
2	0.456	0.513	0.317	0.312	0.303	0.236	0.256	0.212	0.163	0.233	0.133	0.168
	0.479	0.458	0.322	0.310	0.234	0.307	0.255	0.213	0.226	0.178	0.121	0.166
	0.456	0.429	0.255	0.309	0.262	0.334	0.252	0.236	0.202	0.171	0.149	0.155
Tray	(0, 0)		(0.1, 0.5)		(0.5, 0.5)		(1.0, 0.5)		(2.0, 0.5)		(4.0, 0.5)	
3	0.33	0.335	0.187	0.176	0.185	0.175	0.163	0.158	0.133	0.116	0.083	0.108
	0.392	0.36	0.176	0.216	0.182	0.221	0.143	0.205	0.151	0.145	0.123	0.108
	0.439	0.448	0.168	0.185	0.186	0.194	0.174	0.212	0.134	0.121	0.152	0.118
Tray	(0, 0)		(0.1, 1.0)		(0.5, 1.0)		(1.0, 1.0)		(2.0, 1.0)		(4.0, 1.0)	
4	0.358	0.382	0.215	0.215	0.176	0.186	0.145	0.176	0.148	0.108	0.130	0.093
	0.361	0.447	0.162	0.222	0.159	0.181	0.107	0.125	0.165	0.07	0.089	0.100
	0.431	0.367	0.187	0.212	0.187	0.196	0.134	0.146	0.112	0.120	0.068	0.107
Tray	(0, 0)		(0.1, 2.0)		(0.5, 2.0)		(1.0, 2.0)		(2.0, 2.0)		(4.0, 2.0)	
5	0.380	0.386	0.173	0.165	0.165	0.135	0.157	0.113	0.073	0.115	0.066	0.067
	0.417	0.409	0.157	0.153	0.140	0.133	0.116	0.114	0.087	0.103	0.051	0.071
	0.393	0.411	0.136	0.156	0.127	0.115	0.097	0.086	0.098	0.085	0.075	0.048
Tray	(0, 0)		(0, 0.1)		(0, 0.5)		(0, 1.0)		(0, 2.0)			
6	0.558	0.573	0.515	0.509	0.347	0.396	0.371	0.422	0.332	0.292		
	0.638	0.619	0.397	0.372	0.407	0.348	0.368	0.209	0.281	0.328		
	0.569	0.655	0.402	0.574	0.306	0.303	0.338	0.353	0.276	0.273		

Table 2: The percentages to be claimed to be antagonistic (pct.p), additive (pct.a), and synergistic (pct.n) at the corresponding combination dose under different settings.

(d_1, d_2)	$f(d_1, d_2)$	$\sigma_1 = 0.30$			$\sigma_1 = 0.1$			$\sigma_1 = 0.01$		
		$\sigma_2 = 0.217$			$\sigma_2 = 0.1$			$\sigma_2 = 0.01$		
		pct.p	pct.a	pct.n	pct.p	pct.a	pct.n	pct.p	pct.a	pct.n
(0.1, 0.1)	0.101	33.3	66.2	0.5	76.8	23.2	0	100	0	0
(0.1, 0.5)	0.113	36.4	63.2	0.4	86.0	14.0	0	100	0	0
(0.1, 1.0)	0.078	22.0	76.9	1.1	57.1	42.9	0	100	0	0
(0.1, 2.0)	-0.041	5.1	74.4	20.5	1.8	65.6	32.6	0	0	100
(0.5, 0.1)	0.014	8.3	86.8	4.9	11.0	85.2	3.8	95.5	4.5	0
(0.5, 0.5)	-0.035	2.2	86.4	11.4	0.7	77.3	22.0	0	0	100
(0.5, 1.0)	-0.126	0.6	56.7	42.7	0	9.7	90.3	0	0	100
(0.5, 2.0)	-0.350	0.0	3.7	96.3	0	0	100	0	0	100
(1.0, 0.1)	-0.110	0.4	69.3	30.3	0	17.1	82.9	0	0	100
(1.0, 0.5)	-0.231	0	19.0	81.0	0	0	100	0	0	100
(1.0, 1.0)	-0.375	0	0.5	99.5	0	0	100	0	0	100
(1.0, 2.0)	-0.684	0	0	100	0	0	100	0	0	100
(2.0, 0.1)	-0.130	0	62.8	37.2	0	9.6	90.4	0	0	100
(2.0, 0.5)	-0.275	0	10.5	89.5	0	0	100	0	0	100
(2.0, 1.0)	-0.446	0	0.2	99.8	0	0	100	0	0	100
(2.0, 2.0)	-0.813	0	0	100	0	0	100	0	0	100
(3.0, 0.1)	0.300	93.9	6.1	0	100	0	0	100	0	0
(3.0, 0.5)	0.360	98.5	1.5	0	100	0	0	100	0	0
(3.0, 1.0)	0.296	91.2	8.8	0	100	0	0	100	0	0
(3.0, 2.0)	0.039	18.3	76.8	4.9	27.3	71.9	0.8	100	0	0
(4.0, 0.1)	1.276	100	0	0	100	0	0	100	0	0
(4.0, 0.5)	1.814	100	0	0	100	0	0	100	0	0
(4.0, 1.0)	2.015	100	0	0	100	0	0	100	0	0
(4.0, 2.0)	2.060	100	0	0	100	0	0	100	0	0

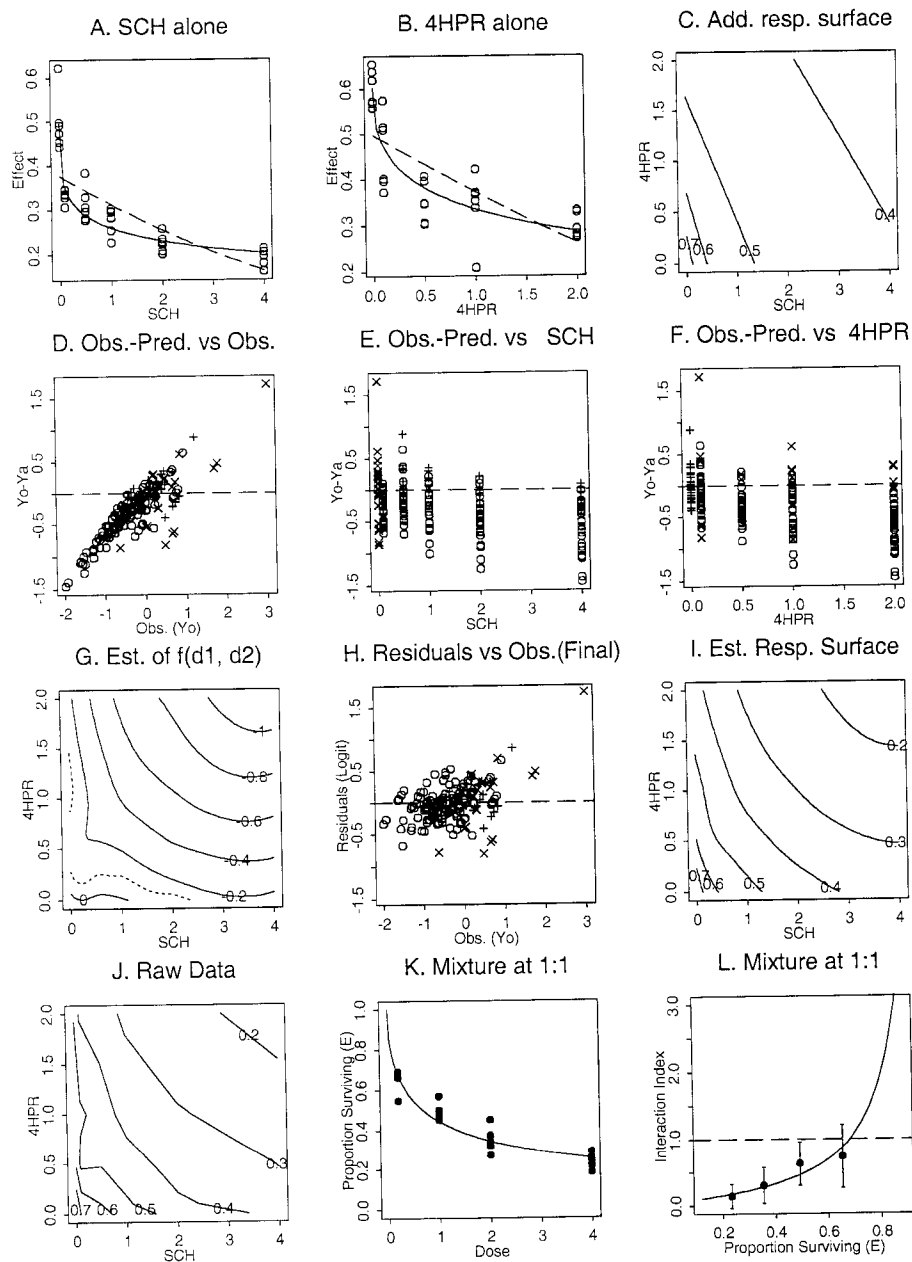


Figure 1. *The results from analyzing the data set derived from cell line UMSCC22B treated with SCH66336 and 4-HPR. Panels A and B show the fitted dose-response curves for SCH66336 and 4-HPR, respectively, and the solid lines were based on the EMAX model while the dashed lines were based on logistic model. Panel C is the contour plot of the predicted additive surface. Panels D, E, and F are the plots of the differences of the observed and the predicted effects versus the observed effects, SCH66336 doses, and 4-HPR doses, respectively. Panel G is the contour plot of the estimated $f(d_1, d_2)$ along with the intersection line of its upper 95% confidence surface with the dose plane shown in the dotted line. Panel H shows the plot of the residuals based on the final semiparametric model versus the predicted effects. Panel I is the the contour plot of the estimated response surface. Panel J is the contour plot of the raw data. Panel K shows the data and the fitted Chou and Talalay's dose-response curve with the combination doses at the fixed ratio 1:1. Panel L shows the plot of the interaction indices versus the effects for the combination doses at the fixed ratio 1:1, along with the 95% confidence intervals (vertical bars) for the interaction indices estimated at the observed combination doses at the fixed ratio 1:1.*

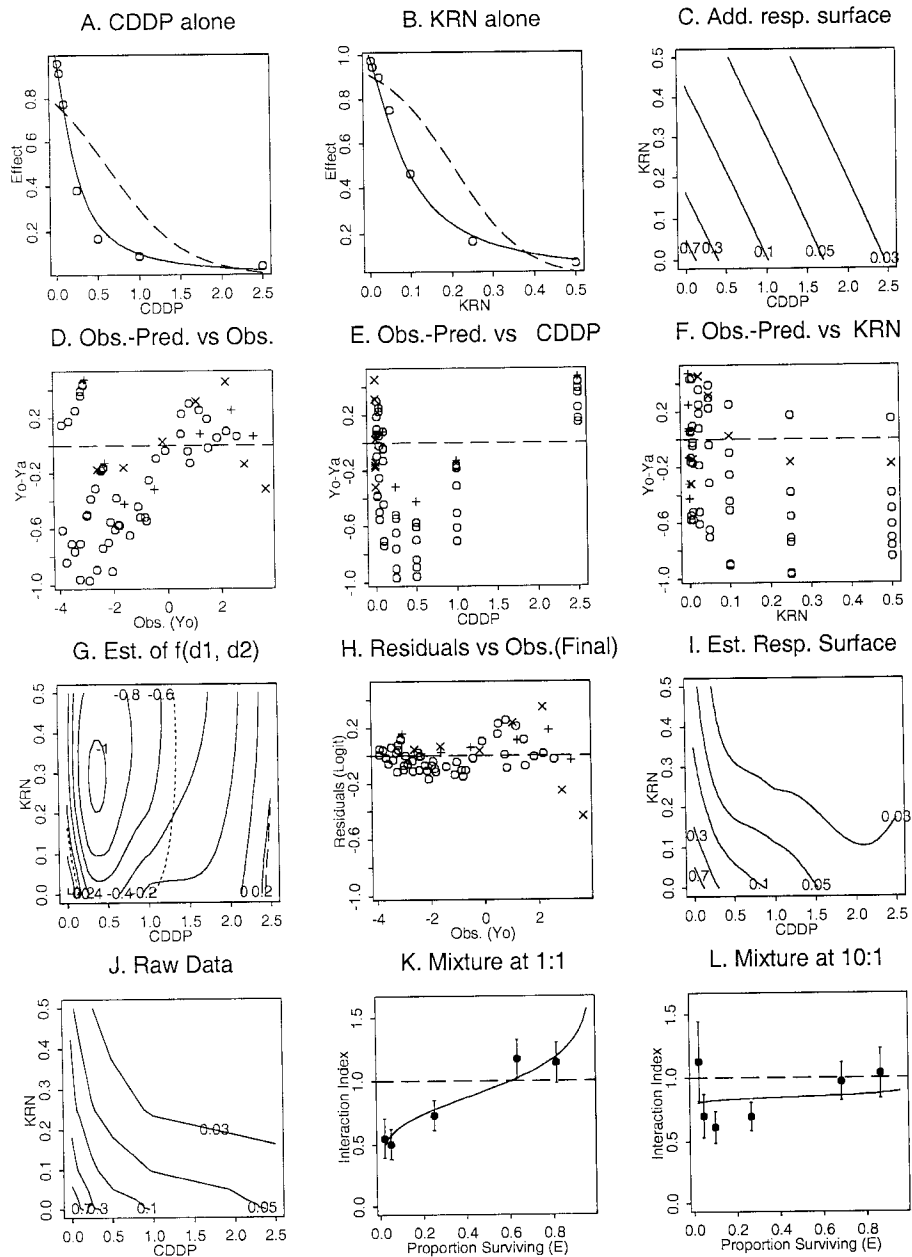


Figure 2. *The results from analyzing the data set published in Kanzawa et al. (1999). Panels A and B show the fitted dose-response curves for CDDP and KRN, respectively, and the solid lines were based on the EMAX model while the dashed lines were based on logistic model. Panel C is the contour plot of the predicted additive surface. Panels D, E, and F are the plots of the differences of the observed and the predicted effects versus the observed effects, CDDP doses, and KRN doses, respectively. Panel G is the contour plot of the estimated $f(d_1, d_2)$ along with the intersection lines of its upper and lower 95% confidence surfaces with the dose plane shown as dotted lines and dashed line, respectively. Panel H shows the plot of the final residuals versus the predicted effects. Panel I is the the contour plot of the estimated response surface. Panel J is the contour plot of the raw data. Panel K and L show the plot of the interaction indices versus the effects for the combination doses at the fixed ratio 1:1 and 10:1, respectively, along with the interaction indices and their confidence intervals estimated at the observed combination doses at each fixed ratio.*

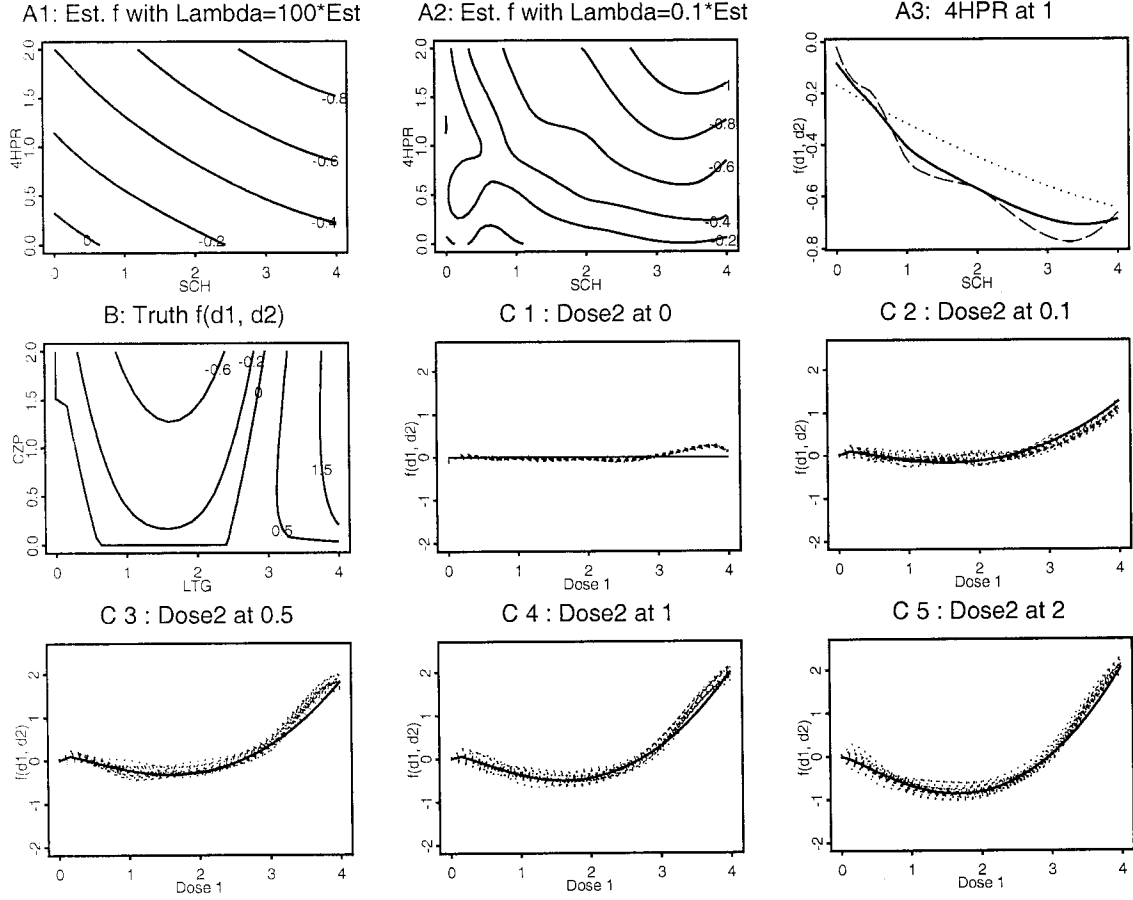


Figure 3. The results from simulation studies presented in Section 5. Panels A1 and A2 show the estimated $f(d_1, d_2)$ from Example 1 by varying the smoothing parameter λ as 14.77 and 0.01477, respectively. Panel A3 shows the plot of the estimated $f(d_1, d_2)$ versus SCH66336 with 4-HPR dose fixed at 1 under different settings for λ as 0.1477 (solid line), 14.77 (dotted line), and 0.01477 (dashed line), respectively. Panel B shows the contour plot of the underlying function $f(d_1, d_2)$. Each panel of Panels C1-C5 shows the underlying curve (solid lines) and the 20 fitted curves (dotted lines).

BRIEF COMMUNICATIONS

Chemopreventive Effects of Deguelin, a Novel Akt Inhibitor, on Tobacco-Induced Lung Tumorigenesis

Ho-Young Lee, Seung-Hyun Oh,
Jong K. Woo, Woo-Young Kim,
Carolyn S. Van Pelt, Roger E. Price,
Dianna Cody, Hai Tran, John M.
Pezzuto, Robert M. Moriarty,
Waun Ki Hong

Tobacco carcinogens induce Akt activation and lung carcinogenesis. We previously demonstrated that deguelin, a natural plant product, specifically inhibits the proliferation of premalignant and malignant human bronchial epithelial cells by blocking Akt activation. To evaluate the ability of deguelin to block tobacco carcinogen-induced lung tumorigenesis, we evaluated the *in vivo* effects of deguelin on Akt activation and lung tumorigenesis in transgenic mice in which Akt expression was induced by tamoxifen and in 4-(methylnitrosoamino)-1-(3-pyridyl)-1-butanone (NNK)/benzo(a)pyrene (BaP)-treated A/J mice. Deguelin suppressed Akt activation *in vivo*, as measured by immunohistochemistry and immunoblotting, and statistically significantly reduced NNK/BaP-induced lung tumor multiplicity, volume, and load in A/J mice, as monitored by microcomputed tomography image analysis, with no detectable toxicity. These results indicate that deguelin warrants consideration as a chemopreventive agent for early-stage lung carcinogenesis in a clinical lung cancer chemoprevention trial. [J Natl Cancer Inst 2005;97:1695-9]

In the United States and western Europe, lung cancer leads all other cancers in both incidence and mortality rate (1), underscoring the need for effective lung

cancer chemopreventive agents. Because tobacco smoking confers the greatest risk of developing lung cancer (2), molecules that target pathways involved in tobacco-mediated lung carcinogenesis could be effective lung cancer chemopreventive agents. The PI3K/Akt pathway could be such a target because Akt is activated in premalignant and malignant human bronchial epithelial cells, as well as non-small-cell lung cancer cells, through the activating mutation of ras, overexpression of the epidermal growth factor receptor and subunits of PI3K, inactivation of tumor suppressor genes such as PTEN, or exposure to tobacco carcinogens, all of which are frequent events in lung cancer (3-9). Akt is activated by phosphorylation at two key regulatory sites, Thr³⁰⁸ and Ser⁴⁷³ (10). Akt promotes cell survival by phosphorylating proapoptotic and antiapoptotic proteins, including the Bcl-2 family member BAD, caspase-9, cAMP response element-binding protein, inhibitor of kappaB kinase complex α , and forkhead transcription factor-1 (11-19).

We and others have shown that pharmacologic and genetic approaches targeting Akt suppress the proliferation of premalignant and malignant human bronchial epithelial cells and reverse characteristics of transformed human bronchial epithelial cells (20,21), indicating that inhibitors of Akt could be effective lung cancer chemopreventive agents. We have previously found that deguelin, isolated from several plant species, including *Mundulea sericea* (Leguminosae), inhibits the PI3K/Akt pathway and decreases the expression of cyclooxygenase-2, which participates in xenobiotic metabolism, angiogenesis, and inhibition of immune surveillance and apoptosis during tumorigenesis (22). Importantly, deguelin induces apoptosis in premalignant and malignant human bronchial epithelial cells, with minimal effects on normal human bronchial epithelial cells *in vitro* at dosages attainable *in vivo* (23). Deguelin has been shown to have cancer chemopreventive activities in the two-stage skin carcinogenesis model (24) and in the N-nitroso-N-methylurea-induced rat mammary carcinogenesis model (25). It also exhibits therapeutic activities in colon cancer, melanoma, and lung cancer (22,26,27). These findings led us to hypothesize that deguelin could be an effective lung cancer chemopreventive agent by blocking

Akt activation. In the present study, we attempted to test our hypothesis in Akt-inducible transgenic mice, in which Akt is activated by tamoxifen (tmaAkt/Z;CAG::Cre) (28), and in A/J mice, in which lung tumors are induced by 4-(methylnitrosoamino)-1-(3-pyridyl)-1-butanone (NNK) and benzo(a)pyrene (BaP) (20,29).

To test the effects of deguelin on Akt activation in tmaAkt/Z;CAG::Cre mice, we performed immunohistochemical (Fig. 1, A) and immunoblot (Fig. 1, B) analyses with phosphorylated (p)Akt (at Ser473) on lung tissues from tmaAkt/Z;CAG::Cre mice treated with 4 mg/kg of deguelin for 3 days. pAkt staining was homogeneous in the bronchial epithelium of the control and deguelin-treated mice; however, levels of pAkt in the lung tissues of control mice were higher than in that of deguelin-treated mice. Western blot analysis also showed decreased expression of pAkt in the lungs of deguelin-treated mice, indicating that deguelin affects Akt activation *in vivo*.

To evaluate the chemopreventive effects of deguelin in the A/J mice, we first evaluated the serum and tissue distribution of deguelin in A/J mice. Fig. 2, A, shows the concentration-time curve of deguelin in serum and various organs after oral gavage administration of 4 mg/kg deguelin, the maximum tolerated dose in rats (25). The total body clearance of deguelin was 0.33 L/kg/hour, the apparent volume of distribution was 1.86 L/kg, and the half-life was 3.98 hours. One hour after the treatment, concentrations of deguelin in

Affiliations of authors: Departments of Thoracic/Head and Neck Medical Oncology (H-YL, S-HO, JKW, W-YK, HT, WKH), Imaging Physics (REP, DC), and Veterinary Medicine and Surgery (CSVP), The University of Texas M. D. Anderson Cancer Center, Houston, TX; Pharmacy Nursing Health Science, Purdue University, West Lafayette, IN (JMP); Department of Medicinal Chemistry and Pharmacognosy, University of Illinois at Chicago, Chicago, IL (RMM).

Correspondence to: Ho-Young Lee, PhD, Department of Thoracic/Head and Neck Medical Oncology, Unit 432, The University of Texas M. D. Anderson Cancer Center, 1515 Holcombe Boulevard, Houston, TX 77030 (e-mail: hlee@mdanderson.org).

See "Notes" following "References."

DOI: 10.1093/jnci/dji377

© The Author 2005. Published by Oxford University Press. All rights reserved. For Permissions, please e-mail: journals.permissions@oxfordjournals.org.

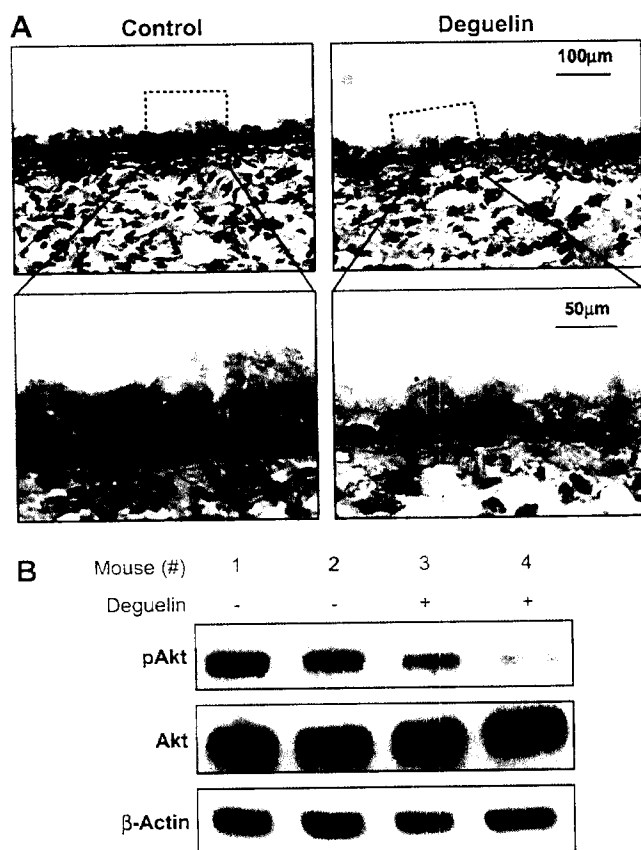


Fig. 1. Effects of deguelin on Akt activation in the transgenic mice expressing tamoxifen-inducible Akt. The mouse line expressing tamoxifen-inducible Akt (tmaAkt/Z;CAG::Cre) was generated by crossing the "master" line (CAG::loxP::CAT::loxP::tmaAkt::IRESLacZ) (provided by Thomas N. Sato, Weill Medical College of Cornell University, New York, NY) to CMV:Cre (distributed by the Mouse Resource Facility at M. D. Anderson Cancer Center, Houston, TX), which led to the expression of inactive (not phosphorylated) Akt by excising the floxed CAT. Six-week-old tmaAkt/Z;CAG::Cre mice were orally treated with deguelin (4 mg/kg) during feeding twice a day for 3 days (five mice/group) and then were injected intraperitoneally with 5 mg of tamoxifen (Sigma, St. Louis, MO). The next day, the mice were killed by CO₂ asphyxiation. Lungs were surgically removed, and **A**) half of each lung was fixed with 10% formaldehyde, embedded in paraffin, sectioned (5-µm thick), and processed for immunohistochemical analysis. The sections were deparaffinized, immersed in methanol containing 0.3% hydrogen peroxide to block endogenous peroxidase activity, and then incubated in blocking serum (Vector Laboratories, Burlingame, CA) to reduce nonspecific antibody binding. The sections were incubated overnight at 4 °C with rabbit polyclonal anti-Akt (diluted 1:100 in 2.5% blocking serum) or rabbit polyclonal anti-phosphorylated Akt (pAkt, Ser473) (diluted 1:200) (Cell Signaling Technology, Beverly, MA) and were then processed using standard avidin-biotin immunohistochemical techniques according to the manufacturer's recommendations (Vector Laboratories, Burlingame, CA). Diaminobenzidine was used as a chromogen, and commercial hematoxylin was used as a counterstain. **B**) The other half of each lung was lysed in 150 mM NaCl, 20 mM Tris-HCl, pH 7.5, 1% Triton X-100, 1 mM phenylmethylsulfonyl fluoride, 10 mM EDTA, 0.1 mM vanadate, and 1 µg/mL aprotinin by mechanical homogenization. Equivalent amounts of protein were resolved on sodium dodecyl sulfate-polyacrylamide gels (10%) and electrophoretically transferred to nitrocellulose membranes. After membranes were blocked in Tris-buffered saline (TBS) containing 0.05% Tween-20 (TBST) and 5% (w/v) nonfat powdered milk, they were incubated with primary antibodies against pAkt (Ser473) (1:1000) and unphosphorylated Akt (1:1000) (Cell Signaling Technology, Beverly, MA) or with a goat polyclonal anti-β-Actin (1:4000) (Santa Cruz Biotechnology, Inc., Santa Cruz, CA) in TBS-5% nonfat milk at 4 °C for 16 hours. The membranes were then washed three times with TBST and incubated with secondary antibody for 1 hour at room temperature. The goat anti-rabbit immunoglobulin G (IgG) or bovine anti-goat IgG horseradish peroxidase-conjugated complexes were detected using the enhanced chemiluminescence kit (Amersham, Arlington Heights, IL) according to the manufacturer's recommended protocol.

various organs ranged from less than 1 ng/mL in the brain tissue to 57.1 ng/mL in the kidneys. The peak concentration in these organs occurred between 1 hour (lung, heart, and kidney) and 6 hours (liver) after administration. These stud-

ies indicate that oral deguelin administration can achieve effective absorption and distribution in several organs, including the lung.

We next tested the chemopreventive effects of deguelin in the A/J mice, in

which lung carcinogenesis was induced by NNK and BaP, as previously described (30). Cancer chemopreventive agents are classified as either blocking or suppressing agents (31). Blocking agents, which prevent the metabolic activation of carcinogens and reduce DNA damage, are tested by administering them before or simultaneously with the carcinogen. Suppressing agents, which inhibit the neoplastic progression of premalignant cells, are usually tested by administering them after the carcinogen (32). Hence, deguelin (4 mg/kg twice a day) was administered either 1 week after the first dose of NNK/BaP (entire period, group 3) or after completion of carcinogen administration (postcarcinogen, group 4) (Fig. 2, B). A/J mice untreated (group 1) or treated with NNK plus BaP (group 2) received only the vehicle (corn oil) during this period. Sixteen and/or 20 weeks after the first dose of NNK and BaP, representative A/J mice from groups 1, 2, and 3 were analyzed by microcomputed tomography to monitor changes in the number and size of lung tumor nodules. The lung structure in a control mouse (Fig. 2, C, 1) and tumor nodules (Fig. 2, C, 2) less than 1 mm in diameter in a NNK/BaP-treated mouse (10) were easily detected and were consistent with the block-faced image (Fig. 2, C, 3) at 16 weeks. A second NNK/BaP-treated mouse (33) had two tumor nodules (0.4 mm and 0.55 mm) at 16 weeks (Fig. 2, C, 4) that became larger (0.4 mm to 0.6 mm and 0.55 mm to 1 mm) at 20 weeks (Fig. 2, C, 5), when a new tumor nodule (0.8 mm) was observed. In contrast, a tumor nodule (1.1 mm) detected at 16 weeks (Fig. 2, C, 6) in the deguelin-treated mouse was not detectable at 20 weeks (Fig. 2, C, 7). All mice were killed at 20 weeks. Gross evaluation revealed no tumors in the lungs of control mice (group 1) and 100% lung tumor formation in NNK/BaP-treated mice (group 2) (Supplementary Fig. 1 and Supplementary Table 1 available at <http://jncicancerspectrum.oxfordjournals.org/jnci/content/vol97/issue22>). Deguelin-treated mice had fewer lung tumors (Supplementary Fig. 1 and Supplementary Table 1 available at <http://jncicancerspectrum.oxfordjournals.org/jnci/content/vol97/issue22>); mice in groups 3 and 4 had fewer lung tumor nodules than NNK/BaP-treated mice in group 2 (mean = 4.57 versus mean = 11.0, difference = 6.43, 95% confidence intervals

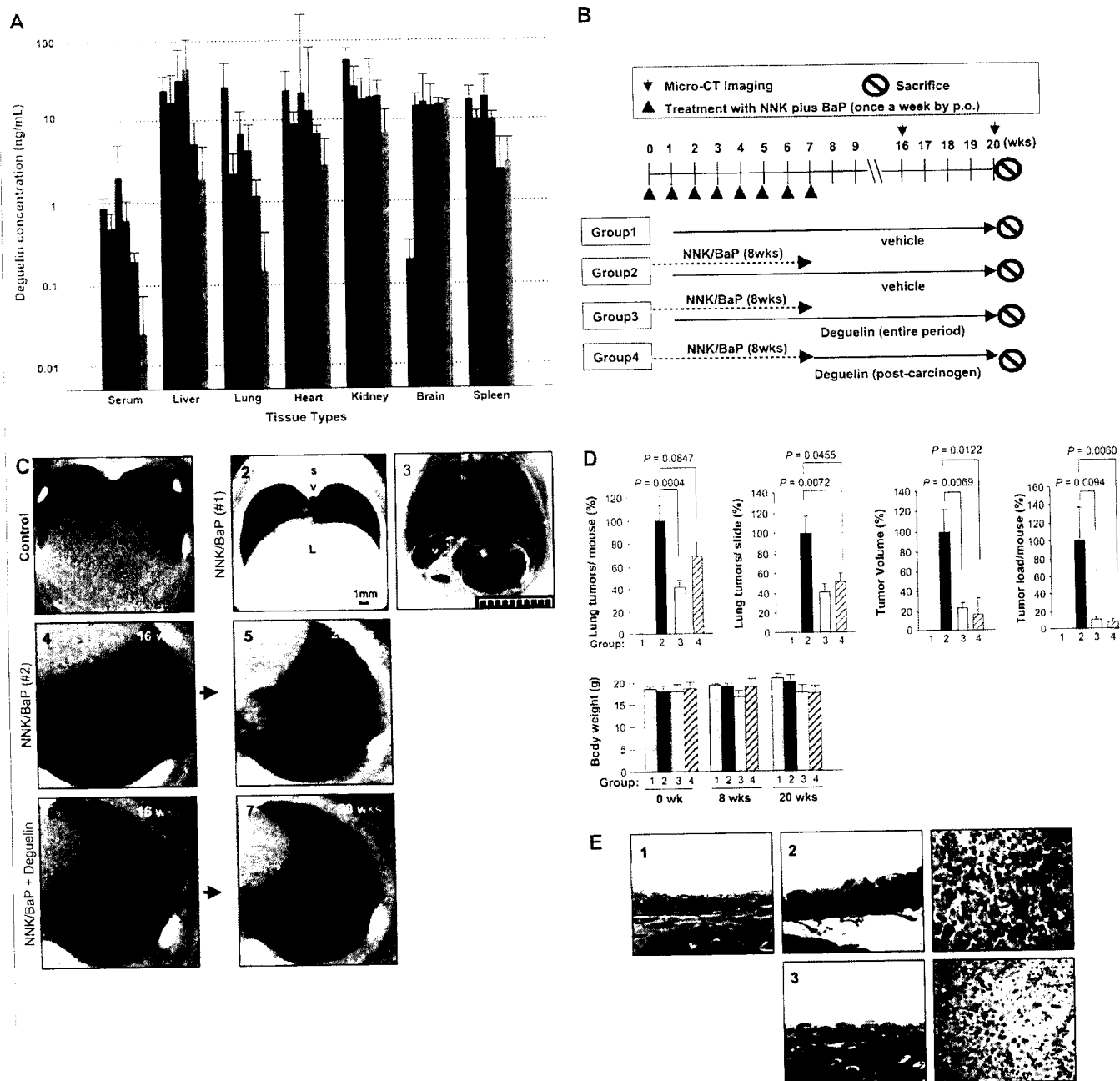


Fig. 2. Evaluation of the chemopreventive effects of deguelin in the A/J mice. **A)** Six-week-old A/J mice were given 4 mg/kg deguelin orally. The serum and indicated organ samples were collected at 0 (baseline), 1 (purple), 2 (turquoise), 4 (blue), 6 (green), 12 (brown), or 24 (orange) hours after deguelin administration. Blood samples were immediately placed on ice and centrifuged at 2000g at 4 °C for 15 minutes, and the serum was stored at -70 °C until analysis. The mice were killed prior to organ sample collection. Each organ sample was suspended in acetonitrile, sonicated, and then centrifuged at 1500g for 3 minutes at 4 °C. The liquid-tissue extraction process was repeated three times, and each time, 100 μ L of supernatant was collected. To the final 300- μ L sample, 2700 μ L of 0.1 M ammonium acetate, pH 5.5, was added. Deguelin was isolated from both serum and organ (liquid-extracted) samples by solid-phase chromatography (tC18 solid-phase extraction [SPE] cartridge, 100 mg, Waters Corp, Millford, MA). After the SPE cartridge was conditioned with 2 mL of methanol and 2 mL of high-performance liquid chromatography-grade water, either 100 μ L of serum or 3 mL (a volume of 1 mL pulled through the column each time) of liquid-extracted sample was placed into the SPE cartridge. Deguelin was eluted with 1 mL of methanol, dried, and then reconstituted with a 100- μ L mixture of methanol and 0.1% formic acid (50:50, v/v). Thirty microliters of the reconstituted sample was then injected onto a high-performance liquid chromatography

mass spectrometer (LC/MS-ES⁺, MicroMass, Beverly, MA). Standard calibration curves for deguelin ranged from 5 to 1000 ng/mL. The lower limit of quantitation was 0.01 ng/mL. Pharmacokinetic modeling was completed using a noncompartment method (WinNonlin version 3.1, Pharsight Corporation, Mountain View, CA). The results are expressed as means and 95% confidence intervals (CIs), four mice/group. **B-E)** Six-week-old male A/J mice (Jackson Laboratories, Bar Harbor, ME) were randomized into three groups of 12–14 mice (groups 2–4). We included five untreated A/J mice (group 1) as a negative control. Except for group 1, all mice were treated with 4-(methylnitrosoamino)-1-(3-pyridyl)-1-butanone (NNK)/benzo(a)pyrene (BaP) (3 μ mol each in 0.1 mL cottonseed oil) once per week for 8 weeks by oral gavage. Vehicle (groups 1 and 2) or deguelin (groups 3 and 4) was administered by oral gavage (4 mg/kg twice a day) beginning 1 week after the first dose of NNK/BaP (entire period) (group 3) or after the last dose of NNK/BaP treatment (postcarcinogen) (group 4) until the end of the experiment. The experimental design is summarized in (B). During the experiments, drinking water was available ad libitum, and the body weights of the mice were measured at 0, 8, and 20 weeks. Arrows indicate the time points at which microcomputed tomography (CT) image analysis was performed. **C)** Registered axial respiratory-gated micro-CT image and block-faced image analyses were performed in one of the A/J mice at 16 and 20 weeks

[CIs] on the difference = 3.25 to 9.60, $P = <.001$ for group 3; mean = 7.60 versus mean = 11.0, difference = 3.4, 95% CIs on the difference = -0.39 to 7.19, $P = .085$, Fig. 2, D). Microscopic evaluation of the lungs revealed a statistically significant decrease in tumor multiplicity, the number of tumors inside the lung (group 3: 59.4%; mean = 1.70 tumors/slide, difference = 2.48, 95% CIs on the difference = 0.97 to 4.0, $P = .007$; and group 4: 48.8%; mean = 2.14 tumors/slide, difference = 2.04, 95% CIs on the difference = 0.52 to 3.56, $P = .046$), volume (group 3: 76.1%; mean = 0.016 mm³, difference = 0.051, 95% CIs on the difference = 0.021 to 0.082, $P = .007$; and group 4: 83.58%; mean = 0.011 mm³, difference = 0.056, 95% CIs on the difference = 0.019 to 0.093, $P = .012$), and load (group 3: 89.3%; mean = 0.032 mm³, difference = 0.27, 95% CIs on the difference = 0.051 to 0.48, $P = .009$; and group 4: 92.3%; mean = 0.023 mm³, difference = 0.27, 95% CIs on the difference = 0.06 to 0.49, $P = .006$) in the deguelin-treated mice compared with the NNK/BaP-treated mice in group 2 (tumor multiplicity, mean = 4.182 tumors/slide; volume, mean = 0.067 mm³; load, mean = 0.298 mm³). Mice in groups 3 and 4 showed a statistically non-significant decrease in body weight compared with mice in groups 1 and 2.

Immunohistochemical analysis revealed stronger cytoplasmic and nuclear pAkt staining in airway epithelial cells (Fig. 2, E, 2) in mice in group 2 compared with those in group 1 (Fig. 2, E, 1) and group 3 (Fig. 2, E, 3). The tumors in group 2 (Fig. 2, E, 4) also showed stronger pAkt staining compared with those in group 3 (Fig. 2, E, 5).

In spite of its potential as a cancer chemopreventive/therapeutic agent, there is concern about possible side effects of deguelin treatment. Deguelin is derived from rotenone, which can inhibit NADH: ubiquinone oxidoreductase, an enzyme complex involved in mitochondrial oxidative phosphorylation (34), and induce cardiotoxicity, respiratory depression, and nerve conduction blockade at high doses (a dose that is lethal to 50% of those exposed = 10–100 g in humans). However, we did not observe major toxicity or substantial loss of body weight in the deguelin-treated A/J mice at the dose used in this study. Deguelin is also safer in terms of its mechanism of action, which differs from that of rotenone, which inhibits tubulin polymerization. Additionally, deguelin rapidly decomposes in light and air. All of these results suggest that deguelin would be harmless when orally administered. Moreover, in contrast to some natural products presently used in cancer chemoprevention and therapy, deguelin could be easily synthesized using commercially available rotenone as a starting material; therefore, its clinical use as a lung cancer chemopreventive agent is feasible. These collective findings provide a strong rationale for testing deguelin in a phase I clinical trial of lung cancer chemoprevention after its complete toxicity profile in humans is known.

REFERENCES

- (1) Greenlee RT, Hill-Harmon MB, Murray T, Thun M. Cancer statistics, 2001. *CA Cancer J Clin* 2001;51:15–36.
- (2) van Zandwijk N, Hirsch FR. Chemoprevention strategies for non-small cell lung cancer. *Curr Opin Oncol* 2002;14:185–90.
- (3) Richardson CM, Sharma RA, Cox G, O'Byrne KJ. Epidermal growth factor recep-

tors and cyclooxygenase-2 in the pathogenesis of non-small cell lung cancer: potential targets for chemoprevention and systemic therapy. *Lung Cancer* 2003;39:1–13.

- (4) Rusch V, Klimstra D, Venkatraman E, Pisters PW, Langenfeld J, Dmitrovsky E. Overexpression of the epidermal growth factor receptor and its ligand transforming growth factor alpha is frequent in resectable non-small cell lung cancer but does not predict tumor progression. *Clin Cancer Res* 1997;3:515–22.
- (5) Fontanini G, De Laurentiis M, Vignati S, Chine S, Lucchi M, Silvestri V, et al. Evaluation of epidermal growth factor-related growth factors and receptors and of neoplasia in completely resected stage I-IIIa non-small-cell lung cancer: amphiregulin and microvessel count are independent prognostic indicators of survival. *Clin Cancer Res* 1998;4:241–9.
- (6) Lin X, Bohle AS, Dohrmann P, Leuschner I, Schulz A, Kremer B, et al. Overexpression of phosphatidylinositol 3-kinase in human lung cancer. *Langenbecks Arch Surg* 2001;386:293–301.
- (7) Mitsudomi T, Steinberg SM, Oie HK, Mulshine JL, Phelps R, Viallet J, et al. ras gene mutations in non-small cell lung cancers are associated with shortened survival irrespective of treatment intent. *Cancer Res* 1991;51:4999–5002.
- (8) Mills NE, Fishman CL, Rom WN, Dubin N, Jacobson DR. Increased prevalence of K-ras oncogene mutations in lung adenocarcinoma. *Cancer Res* 1995;55:1444–7.
- (9) Soria JC, Lee HY, Lee JI, Wang L, Issa JP, Kemp BL, et al. Lack of PTEN expression in non-small cell lung cancer could be related to promoter methylation. *Clin Cancer Res* 2002;8:1178–84.
- (10) Alessi DR, James SR, Downes CP, Holmes AB, Gaffney PR, Reese CB, et al. Characterization of a 3-phosphoinositide-dependent protein kinase which phosphorylates and activates protein kinase Balpha. *Curr Biol* 1997;7:261–9.
- (11) Cross DA, Alessi DR, Cohen P, Andjelkovich M, Hemmings BA. Inhibition of glycogen synthase kinase-3 by insulin mediated by protein kinase B. *Nature* 1995;378:785–9.

using a model RS-9 tabletop CT scanner (General Electric Medical Systems, London, Ontario) as previously described (35,36). The technique used was 80 kVp and 450 μ A, with 720 views obtained at 0.5-degree increments at 400 msec per view. The radiation dose delivered during this scan was approximately 0.26 Gy. Labview software (National Instruments, Austin, TX) provided an interface for selecting the mouse respiratory parameters. The Feldkamp reconstruction method was used to normalize the raw images and to correct for nonuniformities in the detector (35). Images were formed with isotropic 91-mm voxels. NNK/BaP-treated mice sections (10) were fast-frozen immediately after their micro-CT scan session to confirm their position in the images relative to block-faced pathologic sections. A representative micro-CT (1, 2, 4–7) or block-faced (3) image analysis of the lungs from a control mouse (1) or mice treated with NNK/BaP alone (2–5) or with NNK/BaP plus deguelin (group 3) at 16 (4, 6) and 20 (5, 7) weeks is shown. l = lung; e = esophagus; v = thoracic vertebra; L = liver; s = spinal cord. D) Postmortem examinations were performed on the lungs of the A/J mice after mice were killed at 20 weeks. The lung tissues were fixed in Bouin's solution, and the gross tumor nodules (lung tumors/slide) were counted. Microscopic evaluation of lung tissues was also performed to measure mean tumor number (N), volume (V), and total tumor load (N \times V) in a blinded fashion. The

tumor volume was calculated by the formula of $V \text{ (mm}^3\text{)} = (\text{long diameter} \times \text{short diameter}^2)/2$. The number and size of tumors in five sections distributed uniformly through each lung were calculated. Body weight of the mice was measured at 0 (baseline), 8, and 20 weeks (wks). Effects of deguelin on lung tumorigenesis were expressed by means and 95% CIs of tumor nodules/mouse, tumor nodules/slide (multiplicity), volume, and load from 12 (group 2) or 14 (groups 3 and 4) samples. The data were analyzed in comparison with that from the mice treated with NNK/BaP (group 2). We set values from group 2 at 100% and then calculated the others as a percentage of that. Differences between groups were compared using the *t* test or Mann-Whitney statistical test. Differences were considered statistically significant if $P < .05$. Histopathologic evidence of pulmonary toxicity, i.e., edema or inflammation of the bronchial epithelium and alveoli and inflammation and injury in other organs were evaluated by a veterinary pathologist. These animal studies were approved by M. D. Anderson Cancer Center's Institutional Animal Care and Use Committee. E) After the evaluation of tumor nodules, lung tissues were surgically removed and paraffin embedded. Bronchial epithelium (1, 2, 3) and lung adenoma (4, 5) lesions in the A/J mice that were untreated (1) or treated with NNK/BaP alone (2, 4) or NNK/BaP plus deguelin (3, 5) were processed for immunohistochemical analysis with anti-pAkt (Ser473) as described in Fig. 1.

- (12) Brunet A, Bonni A, Zigmond MJ, Lin MZ, Juo P, Hu LS, et al. Akt promotes cell survival by phosphorylating and inhibiting a Forkhead transcription factor. *Cell* 1999;96:857-68.
- (13) Cardone MH, Roy N, Stennicke HR, Salvesen GS, Franke TF, Stanbridge E, et al. Regulation of cell death protease caspase-9 by phosphorylation. *Science* 1998;282:1318-21.
- (14) Datta SR, Dudek H, Tao X, Masters S, Fu H, Gotoh Y, et al. Akt phosphorylation of BAD couples survival signals to the cell-intrinsic death machinery. *Cell* 1997;91:231-41.
- (15) del Peso L, Gonzalez-Garcia M, Page C, Herrera R, Nunez G. Interleukin-3-induced phosphorylation of BAD through the protein kinase Akt. *Science* 1997;278:687-9.
- (16) Krasilnikov MA. Phosphatidylinositol-3 kinase dependent pathways: the role in control of cell growth, survival, and malignant transformation. *Biochemistry (Mosc)* 2000;65:59-67.
- (17) Brognard J, Clark AS, Ni Y, Dennis PA. Akt/protein kinase B is constitutively active in non-small cell lung cancer cells and promotes cellular survival and resistance to chemotherapy and radiation. *Cancer Res* 2001;61:3986-97.
- (18) Kennedy SG, Kandel ES, Cross TK, Hay N. Akt/protein kinase B inhibits cell death by preventing the release of cytochrome c from mitochondria. *Mol Cell Biol* 1999;19:5800-10.
- (19) Chen RH, Su YH, Chuang RL, Chang TY. Suppression of transforming growth factor-beta-induced apoptosis through a phosphatidylinositol 3-kinase/Akt-dependent pathway. *Oncogene* 1998;17:1959-68.
- (20) West KA, Linnoila IR, Belinsky SA, Harris CC, Dennis PA. Tobacco carcinogen-induced cellular transformation increases activation of the phosphatidylinositol 3'-kinase/Akt pathway in vitro and in vivo. *Cancer Res* 2004;64:446-51.
- (21) Lee HY. Molecular mechanisms of deguelin-induced apoptosis in transformed human bronchial epithelial cells. *Biochem Pharmacol* 2004;68:1119-24.
- (22) Lee HY, Suh YA, Kosmeder JW, Pezzuto JM, Hong WK, Kurie JM. Deguelin-induced inhibition of cyclooxygenase-2 expression in human bronchial epithelial cells. *Clin Cancer Res* 2004;10:1074-9.
- (23) Chun KH, Kosmeder JW 2nd, Sun S, Pezzuto JM, Lotan R, Hong WK, et al. Effects of deguelin on the phosphatidylinositol 3-kinase/Akt pathway and apoptosis in premalignant human bronchial epithelial cells. *J Natl Cancer Inst* 2003;95:291-302.
- (24) Gerhauser C, Lee SK, Kosmeder JW, Moriarty RM, Hamel E, Mehta RG, et al. Regulation of ornithine decarboxylase induction by deguelin, a natural product cancer chemopreventive agent. *Cancer Res* 1997;57:3429-35.
- (25) Udeani GO, Zhao GM, Shin YG, Kosmeder JW 2nd, Beecher CW, Kinghorn AD, et al. Pharmacokinetics of deguelin, a cancer chemopreventive agent in rats. *Cancer Chemother Pharmacol* 2001;47:263-8.
- (26) Murillo G, Kosmeder JW 2nd, Pezzuto JM, Mehta RG. Deguelin suppresses the formation of carcinogen-induced aberrant crypt foci in the colon of CF-1 mice. *Int J Cancer* 2003;104:7-11.
- (27) Mehta RG, Pezzuto JM. Discovery of cancer preventive agents from natural products: from plants to prevention. *Curr Oncol Rep* 2002;4:478-86.
- (28) Kroll J, Cobo P, Sato TN. Versatile inducible activation system of Akt/PKB signaling pathway in mice. *Genesis* 2003;35:160-3.
- (29) Hecht SS, Isaacs S, Trushin N. Lung tumor induction in A/J mice by the tobacco smoke carcinogens 4-(methylnitrosamino)-1-(3-pyridyl)-1-butanone and benzo[a]pyrene: a potentially useful model for evaluation of chemopreventive agents. *Carcinogenesis* 1994;15:2721-5.
- (30) Hoffmann D, Hecht SS. Advances in tobacco carcinogenesis. 1990;94:63-102.
- (31) Wattenberg LW. Chemoprevention of cancer. *Cancer Res* 1985;45:1-8.
- (32) Hecht SS, Upadhyaya P, Wang M, Bliss RL, McIntee EJ, Kenney PM. Inhibition of lung tumorigenesis in A/J mice by N-acetyl-S-(N-2-phenethylthiocarbamoyl)-L-cysteine and myo-inositol, individually and in combination. *Carcinogenesis* 2002;23:1455-61.
- (33) Beckett WS. Epidemiology and etiology of lung cancer. *Clin Chest Med* 1993;14:1-15.
- (34) Fang N, Casida JE. Anticancer action of cube insecticide: correlation for rotenoid constituents between inhibition of NADH:ubiquinone oxidoreductase and induced ornithine decarboxylase activities. *Proc Natl Acad Sci U S A* 1998;95:3380-4.
- (35) Cavanaugh D, Johnson E, Price RE, Kurie J, Travis EL, Cody DD. In vivo respiratory-gated micro-CT imaging in small animal oncology models. *Mol Imaging* 2004;3:55-62.
- (36) Rivera B, Miller S, Brown E, Price R. A novel method for endotracheal intubation of mice and rats used in imaging studies. *Contemp Top Lab Anim Sci* 2005;44:52-5.

NOTES

Supported by National Institutes of Health grants R01 CA100816-01 and CA109520-01 (to H.-Y. Lee) and American Cancer Society grant RSG-04-082-01-TBE 01 (to H.-Y. Lee) and partly by Department of Defense grant W81XWH-04-1-0142-01-VITAL (to W. K. Hong) and National Institutes of Health Cancer core grant CA16672. We thank the staff of the Small Animal Cancer Research Imaging Facility for their diligence and devotion. WKH is an American Cancer Society clinical research professor.

Manuscript received March 29, 2005; revised August 23, 2005; accepted September 7, 2005.

A Practical Guide for Determining Drug Interaction in Combination Therapy

J. Jack Lee ^{*}†, Maiying Kong and G. Dan Ayers

Department of Biostatistics and Applied Mathematics,

University of Texas M. D. Anderson Cancer Center,

Houston, Texas, USA

Short title: Determining Drug Interaction

SUMMARY: Studying the joint effect of combined treatments is important in pharmacology and in the development of combination therapies. We review the primary candidates for reference models of additivity and conclude that the Loewe additivity is the best general reference model for evaluating drug interactions. Synergy occurs when the combined effects of two or more drugs is greater than predicted under Loewe additivity, while antagonism occurs when the combined effects are less than predicted from this model. We review the most popular method for analyzing drug interactions in the literature, proposed by Chou and Talalay, and four response surface models based on Loewe additivity using a single parameter to determine drug interactions. We describe the relationships between the various methods and discuss their advantages and disadvantages. We also provide S-PLUS/R code for each approach to facilitate the implementation of these five commonly used methods.

KEY WORDS: antagonism; drug interaction; Loewe additivity model; response surface model; synergy

^{*}Correspondence to: J. Jack Lee, Department of Biostatistics and Applied Mathematics, University of Texas M. D. Anderson Cancer Center, 1515 Holcombe Blvd. Houston, Texas 77030, USA.

[†]Email: jlee@mdanderson.org; Tel: 713-794-4158; Fax: 713-563-4242.

Grant sponsor: National Cancer Institute; grant numbers: CA16672, CA97007, CA91844.

Grant sponsor: Department of Defense; grant numbers: W81XWH-04-1-0142, W81XWH-05-2-0027.

1. Introduction

Studying the combined effects of multiple treatments has been of long-standing interest to basic scientists, clinicians, and statisticians with a goal of developing better treatment regimens by increasing efficacy while reducing toxicity. Many such successful studies can be found in the literature including, for example, a study of the cocktail approach to control AIDS with nucleoside reverse transcriptase inhibitors, non-nucleoside reverse transcriptase inhibitors, and protease inhibitors [1]; studies of platinum-based doublets that include a taxane, vinorelbine, or gemcitabine [2] or the use of chemoradiation therapy [3] for non-small-cell lung cancer. Recent advancements in molecular target-based treatments for cancer has rekindled an interest in studying combinations of targeted agents and chemotherapy, or combinations of different classes of targeted agents [4]. In addition, examining the adverse effect following the simultaneous administration of multiple drugs is important in toxicology studies to ensure that combination therapy can be given safely.

To examine the efficacy and toxicity of a combination therapy, the dispositional data from *in vitro* and *in vivo* assays is useful for screening out those regimens that should not be placed into more expensive and labor-intensive animal experiments or brought to a clinical trial while bringing in promising ones for further development. Although it is generally recognized that *in vitro* data cannot directly be extrapolated to *in vivo* or clinic settings, there are many successful examples in which the *in vitro* data predict the *in vivo* drug interactions [5]. Failure of accurate predictions may be caused by the methodology used, inappropriate model selection, and errant scale-up factors, etc. In this paper, we intend to examine the current use of response surface models on drug interactions in pre-clinical assays, outline their advantages and disadvantages, and give a practical guidance and a future research direction. Review and discussions are provided for models pertinent to both *in vitro* and *in vivo* studies.

A drug-induced effect may be expressed on a continuous scale or on a binary scale [6]. For example, in cell line study, percent cell survival or percent cell killed is commonly applied to measure the drug effect. In animal study, when a binary response status is recorded, the response rate, i.e., the number of responses to the total number assigned to a dose, can be constructed as a measurement of treatment effect [7, 8, 9]. To characterize drug interaction, we first need to define an appropriate reference model for additive effects of drug combinations. When the effects of drugs in combination are greater (less) than that predicted by the additivity model, the effect is synergistic (antagonistic). Historically, three additivity reference models: 1) effect addition, 2) Bliss

independence, and 3) Loewe additivity, are commonly used [10, 11, 12]. There is a debate over which is the best reference model for defining interaction. The effect addition model [12, 13] $E(d_1, d_2) = E(d_1) + E(d_2)$ has been used as a reference model, where $E(d_1, d_2)$ is the effect at (d_1, d_2) , and $E(d_i)$ is the effect of drug i alone at dose d_i with $i = 1, 2$. However, this model is not correct in general. For example, when $E(d_1) = E(d_2) = 70\%$, clearly $E(d_1, d_2)$ can not be 140% when the effect measure is percentage killed.

Bliss independence has some mechanistic and probabilistic support [7, 12, 14]. The Bliss independence model for percentage survival is $E(d_1, d_2) = E(d_1)E(d_2)$ or for percentage killed, $E(d_1, d_2) = E(d_1) + E(d_2) - E(d_1)E(d_2)$. Observed effects less than predicted by the model are synergistic, and conversely, antagonistic.

The Loewe additivity model [15] is:

$$\frac{d_1}{D_{x,1}} + \frac{d_2}{D_{x,2}} = 1, \quad (1)$$

where d_1, d_2 are doses of drug 1 and drug 2 in the mixture that elicit an effect x , and $D_{x,1}, D_{x,2}$ are the doses of the drugs that result in the effect x for each respective drug given alone. When the Loewe additivity model (1) holds, the combination dose (d_1, d_2) is considered additive. The left hand side in equation (1) is also called the *interaction index*, and when

$$\frac{d_1}{D_{x,1}} + \frac{d_2}{D_{x,2}} < 1, \quad (2)$$

we say that the combination dose (d_1, d_2) is synergistic, whereas when

$$\frac{d_1}{D_{x,1}} + \frac{d_2}{D_{x,2}} > 1, \quad (3)$$

we say the combination dose (d_1, d_2) is antagonistic. Note that the mode and magnitude of drug interactions depend on the choices of the measurement of drug effect, doses of drugs, and their scales. In general, the results are not scale invariant. Thus, proper choices of the measurements and their scales are essential for a meaningful assessment of drug interactions. From (1) the Loewe additivity is invariant under the simple multiplicative transformation of each dose, but is not invariant under other transformations, such as the logarithmic transformation. In addition, the Loewe additivity is invariant under any monotone transformation for effect as long as the same transformation applied to all measurements of the drug effects.

We describe a thought experiment against Bliss independence as a general reference model for no interaction. Consider a simple function $E = \frac{1}{1 + d^2}$ describing the effect of a single drug on percentage survival. Here the median effect dose $d = D_{50} = 1$ elicits 50% effect. When $d = 0.5$ the predicted effect for the drug is 0.8. Suppose

the drug is given in combination with itself at $d_1 = d_2 = 0.5$ in a sham experiment [10, 11]. By definition, the effects of same drug given with itself are additive. Under Bliss independence, the expected effect for the sham experiment is $E(d_1)E(d_2) = 0.8^2 = 0.64$. But in fact at $d = d_1 + d_2 = 1$, the dose yields a 50% survival given the above model. Therefore Bliss independence infers synergy for a fundamentally additive scenario. Contrarily, with 50% survival at the combination $d_1 = d_2 = 0.5$ and at the respective dose $D_{50,1} = D_{50,2} = 1$, equation (1) holds and the Loewe additivity model predicts the additivity correctly. Bliss independence is also extensively criticized for its dependence on mechanistic considerations which may only apply in simple systems. Since the state of knowledge about the mechanisms may change, the formulation and the expected value for a given experiment may change accordingly. Consequently, the same data could be considered synergism in one setting but antagonism at another [10, 12]. On the other hand, the Loewe additivity model depends only on observed data and is “mechanism free”. We agree with the prevailing view in the literature that the Loewe additivity model stands alone as a general and valid reference model for studying drug interactions [10, 11, 12, 16, 17].

Berenbaum [11] extended the Loewe additivity model (1) to the general case with n drugs present together,

$$\frac{d_1}{D_{x,1}} + \dots + \frac{d_n}{D_{x,n}} = 1. \quad (4)$$

Again here d_1, \dots, d_n are doses of each drug in the mixture of the n drugs that yield an effect x , and $D_{x,1}, \dots, D_{x,n}$ are the doses of drugs that result in the effect x for each respective drug given alone. When the left hand side of equation (4) is less than 1, equal to 1, or greater than 1, this combination (d_1, \dots, d_n) is synergistic, additive, or antagonistic, respectively.

In this paper we focus on the response surface approach since response surface represents a natural and effective mean of using all data, with single agents and combinations, to model the relationship between observed outcomes and dose levels. Greco *et al.* [12] provided an extensive and excellent review on this subject. We focus on the parametric response surface methodology based on the Loewe additivity model (1) and extend the review to include some other commonly used methods, such as the one proposed by Machado and Robinson [18] and the one by Plummer and Short [19]. Since the median-effect method proposed by Chou and Talalay [20, 21] is the most influential method for assessing drug interactions [12], we include this method to compare with the other response surface approaches proposed by Greco *et al.* [22], Machado and Robinson [18], Plummer and Short [19], and Carter *et al.* [23]. In Section 2 we give different dose-effect models for a single drug. In Section 3 we expound on the meaning of the interaction index from the pharmacological point of view and from the

geometric point of view. In Section 4 we review the approach by Chou *et al.* [20, 21] and four other response surface approaches [22, 18, 19, 23] based on the Loewe additivity model (1) and the dose-effect models (5) to (7), to be described later. Those approaches can be used both *in vitro* and *in vivo* studies [6, 7, 12]. We give an example of the combination of two agents to elicit cell death in a cancer cell line study in Section 5. The results of analyses from these methods are given in Section 6 to illustrate the properties of various methods. In addition, we supply S-PLUS/R code to provide investigators useful tools in studying drug interactions. In Section 7, we discuss our findings and make suggestions on future research areas.

2. Statistical Modeling of a Single Drug

Before discussing the interaction of two drugs, a brief description of the analysis of a single drug is appropriate. Although historically a probit model [8] has been used, the empirical model

$$E = \frac{(E_{con} - B)(\frac{d}{D_m})^m}{1 + (\frac{d}{D_m})^m} + B \quad (5)$$

and its other forms such as (6) and (7) are shown to be more general and are extensively used [12, 20, 21, 22]. Here d is the dose of drug, E_{con} is the control effect (i.e. the effect when no drug is applied), B is the background effect observed at the infinite drug concentration with $E_{con} > B$, D_m is the median effective dose of a drug, and m is a slope parameter. In an opposite setting when $E_{con} < B$, one may reverse the roles of E_{con} and B in equation (5). When m is negative, the curve described by equation (5) falls with increasing drug concentration; when m positive, the curve rises with increasing drug concentration.

When B is zero, then E_{con} is equivalent to E_{max} , which is the full range of responses that can be elicited by the drug, and model (5) becomes the so-called EMAX model [24]:

$$E = \frac{E_{max}(\frac{d}{D_m})^m}{1 + (\frac{d}{D_m})^m}. \quad (6)$$

When $E_{max} = 1$, model (6) becomes the median effect equation

$$E = \frac{(\frac{d}{D_m})^m}{1 + (\frac{d}{D_m})^m}, \quad (7)$$

derived by Chou and Talalay based on mechanistic considerations that have physiochemical and biochemical validity in simple systems [20].

Notice that (7) can be rewritten as

$$\frac{E}{1-E} = \left(\frac{d}{D_m} \right)^m, \quad (8)$$

and taking the logarithm of both sides, we have

$$\log \frac{E}{1-E} = m(\log d - \log D_m). \quad (9)$$

A high correlation coefficient value ($r > 0.9$), well behaved residual diagnostics such as residuals are randomly scattered around 0 without outliers and with small variation, and the linearity of the plot of $\log \frac{E}{1-E}$ with respect to $\log d$ altogether provide a way to check whether the data follows the median effect equation. If so, the median effect plot provides a general and simple method for determining the pharmacological median effective dose D_m and the slope m . Here m is a Hill-type coefficient typically used to describe the sigmoidicity of the dose-effect curve, and $m = 1$ corresponds to hyperbolic systems [20].

Note that although no stochastic error terms are explicitly given in the above models, they are implicitly specified. For example, when the effect E is measured on a continuous scale, e.g. percent cell survival, model (7) assume that the error is linear in E while model (9) assume that the error is linear in $\log \frac{E}{1-E}$. The parameters then can be solved by the least squares method or by the maximum likelihood method with additional assumption on the error distribution. When the effect E is measured as the response rate with responses from a binomial distribution, model (9) conforms to the standard logistic regression setting and the parameters can be estimated from the standard maximum likelihood method.

3. Interaction Index, Isoboles and the Terminology for Drug Interactions

Suppose that the combination (d_1, d_2) elicits the same effect x as drug 1 alone at dose level $D_{x,1}$, and drug 2 alone at dose $D_{x,2}$, then $\frac{d_1}{D_{x,1}} + \frac{d_2}{D_{x,2}}$, the interaction index at dose (d_1, d_2) , is used to measure additivity, synergy, or antagonism according to the relations (1), (2), and (3), respectively. Given the dose-effect curve for each single drug, the interaction index is determined by the combination dose (d_1, d_2) and its corresponding effect x . For example, if the effect at the combination dose (d_1, d_2) is x , and the dose-effect curve is $f_1(D_1)$ for drug 1, and $f_2(D_2)$ for drug 2, then $D_{x,1} = f_1^{-1}(x)$, and $D_{x,2} = f_2^{-1}(x)$, where f_i^{-1} ($i = 1, 2$) is the inverse function of f_i . Thus we can estimate the value of the interaction index without specifying a joint model, $f(d_1, d_2)$, for the combination effect of d_1 and d_2 .

Geometrically, the drug interaction can be illustrated by constructing an isobole. An isobole corresponding to an effect x consists of all the combination doses (d_1, d_2) that elicit the effect x . When the two drugs act additively, the isobole will be a straight line \overline{PQ} (Figure 1), where P is the point $(D_{x,1}, 0)$, and Q is the point $(0, D_{x,2})$. In this case each of the combinations of (d_1, d_2) on the line \overline{PQ} satisfies equation (1). When the two drugs act synergistically, the isobole will be a concave up curve[10] similar to the solid curve \widehat{PNQ} and each of the combinations (d_1, d_2) on this curve will satisfy equation (2); that is, the interaction index will be less than 1 for each combination of (d_1, d_2) on the curve, except at P and Q. The interaction index for different combinations may be different. For example, the interaction index will be less than but close to 1 when the combination is close to points P and Q, and the interaction index possibly has a minimum at point N. Similarly, when the two drugs act antagonistically, the isobole will be a concave down curve [10] like the solid curve \widehat{PTQ} , and each combination of (d_1, d_2) on the curve \widehat{PTQ} will satisfy equation (3), except at the points P and Q.

Suppose that the combination dose (d_1, d_2) is synergistic with an effect x , and drug 1 alone at dose $D_{x,1}$ and drug 2 alone at dose $D_{x,2}$ give the respective effect x . Then (d_1, d_2) , denoted as N' in Figure 2, must lie beneath the straight line \overline{PQ} and satisfy the following equation

$$\frac{d_1}{D_{x,1}} + \frac{d_2}{D_{x,2}} = \gamma \quad (10)$$

with $\gamma < 1$.

What does the interaction index γ mean? We provide several interpretations in the following derivation. The synergy equation (10) can be rewritten as

$$\frac{d_1 + d_2 \frac{D_{x,1}}{D_{x,2}}}{\gamma} = D_{x,1}. \quad (11)$$

Suppose $\rho(x) = \frac{D_{x,1}}{D_{x,2}}$, the relative potency [9] is a constant ρ at any level of effect, then

$$\frac{d_1 + d_2 \rho}{\gamma} = D_{x,1}. \quad (12)$$

That is, the combination (d_1, d_2) acts just like drug 1 alone with dose $\frac{d_1 + d_2 \rho}{\gamma}$. The numerator represents the equivalent amount of drug 1 given in combination assuming the additive drug effect after converting the dose of drug 2 to a comparable dose of drug 1 based on the relative potency. The denominator γ , namely the interaction index, is a scaler reflecting the mode and magnitude of drug interaction in reference to the additive effect.

We can explore γ in another point of view. If two drugs work additively, then there exists a level of effect y that is less effective than x such that $\frac{d_1}{D_{y,1}} + \frac{d_2}{D_{y,2}} = 1$. Here drug 1 alone at dose $D_{y,1}$ and drug 2 alone at dose $D_{y,2}$ elicit the effect y , and $D_{y,1}$ and $D_{y,2}$ can be represented by the length of \overline{OR} and \overline{OS} in Figure 2, respectively. Then, we will have $d_1 + d_2 \frac{D_{y,1}}{D_{y,2}} = D_{y,1}$, i.e. $d_1 + d_2 \rho = D_{y,1}$. In other words, the combination (d_1, d_2) acts like drug 1 alone at dose $d_1 + \rho d_2$ under the assumption that the combination dose (d_1, d_2) is additive. Thus, it follows that [25]

$$D_{x,1} = \frac{D_{y,1}}{\gamma}, \quad \text{i.e.,} \quad \gamma = \frac{D_{y,1}}{D_{x,1}}. \quad (13)$$

From (13), γ could be viewed as the ratio of the equally effective dose of drug 1 under the assumption of additivity to the equally effective dose of drug 1 under the assumption of synergism. The more synergistic the combination dose (d_1, d_2) is, the smaller is γ . Hence, The interaction index is therefore a quantitative measure capturing the mode and magnitude of drug interactions [26].

If the relative potency $\rho(x)$ varies at different levels of effect x , the relation in (13) does not hold, but the relation between $D_{x,1}$ and γ can then be expressed as

$$d_1 + d_2 \rho(x) = \gamma D_{x,1}.$$

Whether the relative potency $\rho(x)$ is constant or varies, if we rescale the isobole by dividing d_1 by $D_{x,1}$, and d_2 by $D_{x,2}$, then the rescaled isobole will pass by (1,0) and (0,1), and (d_1, d_2) is rescaled to $(\frac{d_1}{D_{x,1}}, \frac{d_2}{D_{x,2}})$, represented by point N' in Figure 3. Thus the interaction index $\gamma_{N'} (= \frac{d_1}{D_{x,1}} + \frac{d_2}{D_{x,2}})$ at N' is the length of \overline{OS} , which is the same as the length of \overline{OR} . In Figure 3, \overline{RS} is parallel to \overline{PQ} , therefore $\gamma_{N'}$ also can be viewed as the length of the line from the origin to the combination $(\frac{d_1}{D_{x,1}}, \frac{d_2}{D_{x,2}})$ divided by the length of the line from the origin, passing through the combination, to the theoretical additive isobole, i.e., $\gamma_{N'} = \frac{\text{length}(\overline{ON'})}{\text{length}(\overline{OM'})}$ in Figure 3. Note that an isobole is defined as all the drug pairs (d_1, d_2) that elicit the same level of effect x , and the joint action ratio, defined as $\frac{\text{length}(\overline{OM})}{\text{length}(\overline{ON})}$ by Hewlett [27], should be $\frac{1}{\min \gamma}$ (Figure 3), where γ represents all the interaction indices over the isobole for a fixed level of effect x , and N is the point on the scaled synergistic isobole farthest from the scaled additive isobole.

4. Comparison of Five Approaches to Detect Drug Interactions

There are many published methods for assessing drug interactions. We compare the following five commonly used models which are based on the Loewe additivity model.

4.1 Median-effect method of Chou and Talalay

According to Greco *et al.* [12], the median-effect method of Chou and Talalay [20] is the most influential method to assess drug interactions introduced since 1970. Chou and Talalay [20] derived the equation (7), which is independent of the drug's mechanisms of action and does not require knowledge of conventional kinetic constants.

When the effect E is on continuous scale and the dose-effect relationships follow the median-effect equation (7), the plot of $\log \frac{E}{1-E}$ versus $\log d$ should approximately follow a straight line with a slope m and x -intercept $\log D_m$. Particularly when we regress $y = \log \frac{E}{1-E}$ on $x = \log d$ to obtain $\log \frac{E}{1-E} = \beta_0 + m \log d$, D_m can be obtained by $\exp(-\frac{\beta_0}{m})$. Once we have m and D_m , we can obtain the dose d for any effect level E by

$$d = D_m \left(\frac{E}{1-E} \right)^{\frac{1}{m}}, \quad (14)$$

which is another equivalent form of (8).

The analysis of the combined effects of two drugs involves the following five steps [21]:

- Step 1: Graph the data with the median-effect plot for drug 1 alone, drug 2 alone, and a mixture of the two drugs having a fixed ratio, then estimate the parameters m_1 , D_{m1} , r_1 , m_2 , D_{m2} , r_2 , m_{12} , D_{m12} , and r_{12} using linear regression. The slope gives the m value, $D_m = \exp(-\frac{\beta_0}{m})$, where β_0 is the constant, y-intercept term in the linear regression, and r is the correlation coefficient. Chou and Talalay suggested that the correlation coefficient should be greater than 0.9 to recommend the median effect model.
- Step 2: Calculate the dose $D_{x,1}$, $D_{x,2}$, and $D_{x,12}$ at each given level of effect x using equation (14) and replacing E by x , D_m by D_{m1} , D_{m2} , and D_{m12} respectively, and d by $D_{x,1}$, $D_{x,2}$, and $D_{x,12}$ respectively. $D_{x,1}$, $D_{x,2}$, and $D_{x,12}$ are doses of drug 1, drug 2, and their mixture which are required to elicit a given effect level x .
- Step 3: Calculate the contributions of d_1 and d_2 in the mixture $D_{x,12}$ from the known dose ratio of the two drugs. For example, if $\frac{d_1}{d_2} = \frac{P}{Q}$, then $d_1 = D_{x,12} \cdot \frac{P}{P+Q}$, and $d_2 = D_{x,12} \cdot \frac{Q}{P+Q}$, where $D_{x,12} = d_1 + d_2$.
- Step 4: Calculate the interaction index at the level of effect x with the mixture of drugs at the fixed ratio:

$$\gamma(x) = \frac{d_1}{D_{x,1}} + \frac{d_2}{D_{x,2}}. \quad (15)$$

- Step 5: Repeat steps 2 to 4 many times with different levels of effect x at each time, and plot the interaction index versus the level of effect x .

Plotting the interaction index versus the level of effect x provides estimates of the interaction index over a large range of doses for a fixed ratio of two drugs. By examining several ratios, synergism and antagonism may be detected in a large range, and inconsistent drug interactions, i.e., some combinations showing synergy, and some showing additivity or antagonism, may also be detected.

Remark 1: Chou and Talalay [20] explicitly derived the relationship between the effect E and drug combination (d_1, d_2) when $m_1 = m_2$. If $m_1 = m_2 = m_{12}$, then the effects of drug 1 and drug 2 are mutually exclusive. They defined the combination index, which is the same as the interaction index in this case, to identify drug interactions. If $m_1 = m_2 \neq m_{12}$ and the median effect plot of the mixture has a tendency to intersect the plot of the more potent of the two drugs, then their effects are mutually nonexclusive. In this case, the combination index is defined as $\frac{d_1}{D_{x,1}} + \frac{d_2}{D_{x,2}} + \frac{d_1 d_2}{D_{x,1} D_{x,2}}$, which has one more term than the interaction index. Chou and Talalay did not provide a test-based approach for defining exclusivity. Instead, they recommend reporting the combination indices for both mutually exclusive and mutually non-exclusive assumptions. This approach can result in inconsistent conclusions for drug interactions and has been criticized [10, 12]. When we adopt Chou's approach we use the interaction index, $\frac{d_1}{D_{x,1}} + \frac{d_2}{D_{x,2}}$, to identify drug interactions instead of the combination index.

Remark 2: Once we obtain the two dose-effect curves for the two single drugs, we can calculate the interaction index and its corresponding confidence interval for any observation. Suppose we have an observation (d_1, d_2) with effect x . We can calculate $D_{x,1}$ and $D_{x,2}$ using (14) by replacing D_m with $\exp(-\frac{\beta_{0,i}}{m_i})$ and E with x , resulting

$$D_{x,i} = \exp(-\frac{\beta_{0,i}}{m_i}) \left(\frac{x}{1-x} \right)^{\frac{1}{m_i}}. \quad (16)$$

where $\beta_{0,i}$ is the constant y-intercept term of the linear regression in Step 1 for drug i ($i=1,2$). Notice that the two parameters $\beta_{0,i}$ and m_i and their variances and covariance are estimated already. Based on equation (16), an estimate of the variance of $D_{x,i}$ with $i = 1, 2$ can be approximated by using the delta method [28], which is

$$\text{Var}(D_{x,i}) \approx D_{x,i}^2 \left(\delta^2 \text{Var}(m_i) - 2\delta \frac{1}{m_i} \text{Cov}(\beta_{0,i}, m_i) + \frac{1}{m_i^2} \text{Var}(\beta_{0,i}) \right) \quad (17)$$

with $\delta = \frac{\beta_{0,i}}{m_i^2} - \frac{1}{m_i^2} \log \frac{x}{1-x}$. The subjects treated with drug 1 alone and the subjects treated with drug 2 alone are independent. Using the delta method again on the interaction index, we can calculate the variance of the

interaction index (II), which is given by

$$\text{Var}(II) \approx \frac{d_1^2}{D_{x,1}^4} \text{Var}(D_{x,1}) + \frac{d_2^2}{D_{x,2}^4} \text{Var}(D_{x,2}). \quad (18)$$

Remark 3: If the effect E measures the response rate with responses from a binomial distribution, Step 1 can be modified using the logistic regression instead of the linear regression.

4.2 Model of Greco *et al.*

The first response surface model we discuss was proposed by Greco *et al.* [22] using a single parameter to identify and quantify drug synergism. This approach is mathematically consistent with the traditional isobologram approach but is more objective and has been successfully applied to many applications for detecting drug interactions [29].

Greco *et al.* adopted (5) as the dose-response relationship for each single drug. From (5) we have

$$\frac{E - B}{E_{con} - E} = \left(\frac{d}{D_m}\right)^m. \quad (19)$$

So if the dose-relationship follows model (5), the dose to elicit an effect E is

$$d = D_m \left(\frac{E - B}{E_{con} - E}\right)^{\frac{1}{m}}. \quad (20)$$

The model proposed by Greco *et al.* [22] has the following form:

$$\begin{aligned} 1 = & \frac{d_1}{D_{m,1} \left(\frac{E - B}{E_{con} - E}\right)^{\frac{1}{m_1}}} + \frac{d_2}{D_{m,2} \left(\frac{E - B}{E_{con} - E}\right)^{\frac{1}{m_2}}} \\ & + \frac{\alpha d_1 d_2}{D_{m,1} D_{m,2} \left(\frac{E - B}{E_{con} - E}\right)^{\frac{1}{2m_1}} \left(\frac{E - B}{E_{con} - E}\right)^{\frac{1}{2m_2}}}. \end{aligned} \quad (21)$$

Here, m_1 , m_2 are the slopes of the dose-response relationships (5) for drug 1 and drug 2, respectively, and $D_{m,1}$ and $D_{m,2}$ are the median effect doses for drug 1 and drug 2 respectively, while E_{con} and B have the same meaning as defined previously, and α is the parameter to detect synergism, additivity, or antagonism.

The dose level for each single drug can be expressed as the right-hand side of equation (20), i.e., $D_{x,1} = D_{m,1} \left(\frac{E - B}{E_{con} - E}\right)^{\frac{1}{m_1}}$ and $D_{x,2} = D_{m,2} \left(\frac{E - B}{E_{con} - E}\right)^{\frac{1}{m_2}}$. The first two terms on the right-hand side of equation (21) are exactly the interaction index written as $\frac{d_1}{D_{x,1}} + \frac{d_2}{D_{x,2}}$. So we can rewrite (21) as

$$\frac{d_1}{D_{x,1}} + \frac{d_2}{D_{x,2}} = 1 - \frac{\alpha d_1 d_2}{D_{m,1}^{\frac{1}{2}} D_{m,2}^{\frac{1}{2}} D_{x,1}^{\frac{1}{2}} D_{x,2}^{\frac{1}{2}}}.$$

When $\alpha > 0$, the interaction index is less than one, and synergism is detected; when $\alpha < 0$, antagonism is detected; and when $\alpha = 0$, the combination of the two drugs works additively. When α is estimated from the data, the inference should be made in the statistical point of view. For example, we claim $\alpha > 0$ only when the lower limit of the confidence interval for α is positive.

We may estimate all seven parameters ($m_1, m_2, D_{m,1}, D_{m,2}, B, E_{con}, \alpha$) by the least-squares method or the maximum likelihood method according to the distribution of error, whenever appropriate. We obtain the effect E by the bisecting root finder in each iteration. If the data set follows the median effect principle, one may use the median effect equation (7) as the dose-response curve for each single drug, and then fit the following model with five parameters ($m_1, m_2, D_{m,1}, D_{m,2}, \alpha$):

$$1 = \frac{d_1}{D_{m,1} \left(\frac{E}{1-E} \right)^{\frac{1}{m_1}}} + \frac{d_2}{D_{m,2} \left(\frac{E}{1-E} \right)^{\frac{1}{m_2}}} + \frac{\alpha d_1 d_2}{D_{m,1} D_{m,2} \left(\frac{E}{1-E} \right)^{\frac{1}{2m_1}} \left(\frac{E}{1-E} \right)^{\frac{1}{2m_2}}}. \quad (22)$$

4.3 Model of Machado and Robinson

Of the several models investigated, Machado and Robinson [18] recommended the following model which was originally derived by Plackett and Hewlett [30]:

$$\left(\frac{d_1}{D_{x,1}} \right)^\eta + \left(\frac{d_2}{D_{x,2}} \right)^\eta = 1. \quad (23)$$

Similar to the α in the model of Greco *et al.*, when $0 < \eta < 1$, the combinations of the two drugs are synergistic; when $\eta = 1$, the combinations are additive; and when $1 < \eta < \infty$, the combinations are antagonistic. Again we should view these equalities or inequalities from the statistical point of view when the drug interaction parameter is estimated from the data.

To use the approach proposed by Machado and Robinson, we need to choose an appropriate dose-effect curve for each single drug. We will follow the stream of literature using either (5), (6), or (7) according to the data structure. If we adopt the general model (5) as the dose-effect curve for a single drug, then Machado and Robinson's model has the following form:

$$\left(\frac{d_1}{D_{m,1} \left(\frac{E-B}{E_{con}-E} \right)^{\frac{1}{m_1}}} \right)^\eta + \left(\frac{d_2}{D_{m,2} \left(\frac{E-B}{E_{con}-E} \right)^{\frac{1}{m_2}}} \right)^\eta = 1, \quad (24)$$

which includes seven parameters ($m_1, m_2, D_{m,1}, D_{m,2}, E_{con}, B, \eta$). Again, these seven parameters can be estimated by appropriate methods.

If one adopts the median effect equation (7) as dose-effect curve for each drug, then Machado and Robinson's model of the following form can be constructed with five parameters $(m_1, m_2, D_{m,1}, D_{m,2}, \eta)$:

$$\left(\frac{d_1}{D_{m,1} \left(\frac{E}{1-E} \right)^{\frac{1}{m_1}}} \right)^\eta + \left(\frac{d_2}{D_{m,2} \left(\frac{E}{1-E} \right)^{\frac{1}{m_2}}} \right)^\eta = 1. \quad (25)$$

Remark 4: Note that for each fixed η , when rescaled to pass through $(1, 0)$ and $(0, 1)$, all isoboles from a response surface are identical. Therefore, this model is very restrictive.

4.4 Model of Plummer and Short

Plummer and Short [19] proposed a model of the form

$$Y = \beta_0 + \beta_1 \log \left(d_1 + \rho \cdot d_2 + \beta_4 (d_1 \cdot \rho \cdot d_2)^{\frac{1}{2}} \right) \quad (26)$$

to identify and quantify departures from additivity. This model was originally proposed by Finney [8] with a fixed relative potency ρ , and was generalized by Plummer and Short to allow relative potency ρ to vary. Here, Y is the transformed effect, d_1 is the amount of drug 1 and d_2 is the amount of drug 2 in a combination, and ρ is a relative potency of drug 1 versus drug 2 given by $\log(\rho) = \beta_2 + \beta_3 \log D_2$, in which D_2 is the solution to $D_2 - d_2 - \frac{d_1}{\rho} = 0$. To use this model, the plots of Y versus the $\log(\text{dose})$ for both drugs should be linear but need not be parallel. If the data for each single drug follow equation (5), (6), or (7), then Y as $\log \frac{E-B}{E_{con}-E}$, $\log \frac{E}{E_{max}-E}$, or $\log \frac{E}{1-E}$ will have a linear relationship with the $\log(\text{dose})$, so model (26) is applicable. When we take $Y = \log \frac{E-B}{E_{con}-E}$, the model becomes

$$E = \frac{B + E_{con} \exp \left(\beta_0 + \beta_1 \log \left(d_1 + \rho \cdot d_2 + \beta_4 (d_1 \cdot \rho \cdot d_2)^{\frac{1}{2}} \right) \right)}{1.0 + \exp \left(\beta_0 + \beta_1 \log \left(d_1 + \rho \cdot d_2 + \beta_4 (d_1 \cdot \rho \cdot d_2)^{\frac{1}{2}} \right) \right)}, \quad (27)$$

which contains seven parameters $(\beta_0, \beta_1, \beta_2, \beta_3, \beta_4, E_{con}, B)$. If we adopt the median effect equation (7) as the dose-effect relationship for each single drug, we may take $Y = \log \frac{E}{1-E}$, and then Plummer and Short's model will have the following form:

$$E = \frac{1.0}{1.0 + \exp \left(-\beta_0 - \beta_1 \log \left(d_1 + \rho \cdot d_2 + \beta_4 (d_1 \cdot \rho \cdot d_2)^{\frac{1}{2}} \right) \right)}. \quad (28)$$

With the appropriate methods, the five parameters $(\beta_0, \beta_1, \beta_2, \beta_3, \beta_4)$ can be estimated accordingly. The parameter β_4 captures synergism ($\beta_4 > 0$), additivity ($\beta_4 = 0$), or antagonism ($\beta_4 < 0$). Again we make inferences about these relations from the statistical point of view.

Let us look at why β_4 can capture synergism and antagonism. If we set $d_2 = 0$ for Plummer and Short's

model (26), we will get

$$D_{x,1} = \exp\left(\frac{Y - \beta_0}{\beta_1}\right),$$

which is the dose of drug 1 eliciting the effect Y . If we set $d_1 = 0$ we will get

$$D_{x,2} = \frac{\exp\left(\frac{Y - \beta_0}{\beta_1}\right)}{\rho},$$

which is the dose of drug 2 eliciting the effect of Y . From model (26) we can get

$$\frac{d_1}{\exp\left(\frac{Y - \beta_0}{\beta_1}\right)} + \frac{d_2 \cdot \rho}{\exp\left(\frac{Y - \beta_0}{\beta_1}\right)} + \beta_4 \frac{(d_1 \cdot \rho \cdot d_2)^{\frac{1}{2}}}{\exp\left(\frac{Y - \beta_0}{\beta_1}\right)} = 1,$$

that is,

$$\frac{d_1}{D_{x,1}} + \frac{d_2}{D_{x,2}} + \beta_4 \frac{(d_1 \cdot d_2)^{\frac{1}{2}}}{(D_{x,1} D_{x,2})^{\frac{1}{2}}} = 1. \quad (29)$$

Therefore β_4 captures synergism, additivity, or antagonism, coincident with the Loewe additivity model (1). Note that (29) is one of the models mentioned by Machado and Robinson [18] and has the shortcoming we pointed out in Remark 4.

4.5 Model of Carter *et al.*

The model proposed by Carter *et al.* [23] implies that the dose-effect for a single drug follows a logistic model. The model has the following form,

$$\text{Logit}(E) = \log\left(\frac{E}{1-E}\right) = \beta_0 + \beta_1 d_1 + \beta_2 d_2 + \beta_{12} d_1 d_2. \quad (30)$$

By setting $d_2 = 0$ we can estimate the dose of drug 1 eliciting a fixed effect E

$$D_{x,1} = \frac{\log\left(\frac{E}{1-E}\right) - \beta_0}{\beta_1}.$$

By setting $d_1 = 0$ we can estimate the dose of drug 2 eliciting the fixed effect E

$$D_{x,2} = \frac{\log\left(\frac{E}{1-E}\right) - \beta_0}{\beta_2}.$$

From Carter's model (30) we can obtain the interaction index

$$\begin{aligned} \frac{d_1}{D_{x,1}} + \frac{d_2}{D_{x,2}} &= \frac{\beta_1 d_1}{\log\left(\frac{E}{1-E}\right) - \beta_0} + \frac{\beta_2 d_2}{\log\left(\frac{E}{1-E}\right) - \beta_0} \\ &= 1 - \frac{\beta_{12} d_1 d_2}{\log\left(\frac{E}{1-E}\right) - \beta_0}. \end{aligned} \quad (31)$$

If $\log\left(\frac{E}{1-E}\right) - \beta_0 > 0$, then the combination doses are synergistic with $\beta_{12} > 0$, additive with $\beta_{12} = 0$, or antagonism with $\beta_{12} < 0$. If $\log\left(\frac{E}{1-E}\right) - \beta_0 < 0$, then the combination doses are synergistic with $\beta_{12} < 0$ or antagonistic with $\beta_{12} > 0$.

5. Data Set

A principal focus of chemoprevention research at M.D. Anderson Cancer Center is to identify efficient combinations of chemotherapeutic and biologic agents that eliminate precancerous cells or slow the carcinogenic processes in patients at high-risk for the development of cancer. Combinations of drugs acting synergistically have the primary benefits of improving therapeutic activity with lower toxicity. This is particularly important in the prevention setting because preventive regimen must elicit low toxicity profiles before they can be administered to relatively healthy subjects. Dr. Reuben Lotan and colleagues at M.D. Anderson Cancer Center evaluated the efficacy of two such novel agents, SCH66336 and 4-HPR, in squamous cell carcinoma cell lines (unpublished data). SCH66336, a tricyclic peptidomimetic compound, has extensive activity in preclinical studies in head and neck squamous cell carcinoma and in non-small-cell lung cancer cell lines. 4-HPR is a potent retinoid that induces apoptosis (cell death) in malignant cells.

Cell lines of human squamous cell carcinoma were treated with SCH66336 and 4-HPR separately and in combination. After 6 hours, the proportions of surviving cells at each single dose and combination dose levels were calculated. In order to illustrate the methods we described in Section 4, we used a human squamous cell carcinoma cell line (UMSCC22B) with the treating doses, or, in this case, concentrations ranged from 0 to 4 μM and 0 to 2 μM for SCH66336 and 4-HPR, respectively. The corresponding percentages of cells surviving at each combination of dose levels are shown in Table 1.

6. Data Analysis

We illustrate the methods described above to identify synergism, additivity, or antagonism by analyzing a data set in which the percentages of surviving cells were measured on the cell line UMSCC22B in response to different combination treatments with SCH66336 and 4-HPR (see Table 1). Cell survival ranged from 67% at 0.1 μM to only 38% at 4 μM by treating with SCH66336 alone. 4-HPR was slightly less effective as a single agent eliciting 77% cell survival at 0.1 μM and 49% cell survival at 2 μM . Equidose concentrations of the combination of the two agents ranged from 65% at 0.1 μM (total dose= $d_1 + d_2=0.2 \mu\text{M}$) to 23% at 2 μM (total dose=4 μM). The data suggest some supra-additive effects by the combination. For example, a total dose of 1 μM of the combination elicited 49% cell survival whereas the single agent effect at this dose was 56% and 57% for SCH66336 and 4-HPR, respectively. We treat the effect, i.e., percent cell survival as a continuous variable and

assume the stochastic error is linear in $\log \frac{E}{1-E}$. The least squares method was applied in solving the parameters for all methods described below.

The median effect plot can be obtained by a linear regression of $\log \frac{E}{1-E}$ on $\log d$ based on the data in Table 1. Recall that $\log \frac{E}{1-E} = m(\log d - \log D_m) = \beta_0 + m \log d$. The estimates of β_0 , m , D_m , r for drug 1, drug 2, and the mixture of the drugs with equal concentrations are summarized in Table 2.

The transformed data $\log \frac{E}{1-E}$ versus $\log d$ are shown in Figure 4A. Open circles identify the transformed observations for drug 1 alone, the triangles for drug 2 alone, and the filled circles refer to the mixture of the two drugs with the fixed ratio of 1:1. The median effect plot for drug 1 (SCH66336) is shown in a dashed line, the median effect plot for drug 2 (4-HPR) as a dotted line, and the median effect plot for the mixture of the two drugs with the fixed ratio is shown as a solid line in Figure 4A. Figure 4C shows the corresponding observed data and the fitted dose-effect curves for drug 1, drug 2, and the mixture of the two drugs. The median effect equation constrains the effect to be 1 at dose zero for $m < 0$. In fact only five observations were used to calculate the median effect model for drug 1 alone, four observations for drug 2 alone, and four observations for the mixture. The remaining 16 data points at other dose combinations were not used. The median effect plots in Figure 4A and r values in Table 2 indicate that the data follow the median effect equation (7) reasonably well. We followed the procedure described in Section 4.1 to plot the interaction index versus the effect E , which is shown in Figure 4B. The figure shows that when $E \leq 0.68$, the interaction index is less than 1 and the corresponding combination dose is synergistic. We calculated four interaction indices and their confidence intervals at the four observed data points (d_1, d_2) being $(0.1, 0.1)$, $(0.5, 0.5)$, $(1, 1)$ and $(2, 2)$. The four interaction indices were 0.791, 0.609, 0.256, and 0.103, and their corresponding 95% confidence intervals were $[0.405, 1.177]$, $[0.388, 0.831]$, $[0.092, 0.421]$, and $[0.002, 0.203]$, respectively. The four pairs of interaction index versus the effect along with their 95% confidence intervals are shown in Figure 4B. From these four interaction indices and their confidence intervals, it is reasonable to conclude that the combination doses at the fixed ratio of 1:1 are synergistic for doses ≥ 0.5 μM for each single drug. The 95% confidence interval of the interaction index at the drug combination $(0.1, 0.1)$ contains 1, therefore the combination dose $(0.1, 0.1)$ is declared additive. The above analyses do not adjust for multiple comparisons. Table 3 provides summaries of the estimated synergism-antagonism parameter, its 95% confidence interval, and the conclusion using each of the five models described.

In order to compare the results obtained from each model with those obtained from Chou and Talalay's

model, we chose to use the median effect equation as a dose-effect curve for the use of the single drugs on the models described in Section 4.2 to 4.4. Thus the parameters estimated in the median effect plot could be used as the initial values for parameter estimation. We fitted each of the models mentioned in Section 4.2 to Section 4.5, and plotted the observed values and the fitted dose-effect curves for drug 1, drug 2, and the mixture of the drugs at the fixed ratio of 1:1 (Figure 5A, 6A, 7A, and 8A), where the fitted dose-response curves were obtained from the corresponding response surface models. Selected contours of each fitted response surface are shown in Figures 5B, 6B, 7B, and 8B. Comparing these plots with the raw data and comparing the contour plot of each fitted response surface with the contour plot of the raw data (Figure 4D) provide a crude visual assessment of whether the fit is good or not. The residual sum of squares (RSS) is another useful measure of the goodness of fit.

For Greco's model, the initial values for m_1, m_2, D_{m1}, D_{m2} are given in Table 2, and the initial value for α is set as 0. The two-component plot is shown in Figure 5 and $RSS=0.618$. The fitted parameters are $m_1 = -0.383$, $m_2 = -0.449$, $D_{m1} = 1.316$, $D_{m2} = 1.430$, and the estimated synergism and antagonism parameter $\alpha = 5.622$ with standard error 3.105. The 95% confidence interval for α is $[-0.464, 11.708]$. The confidence interval, which includes 0, precludes a statement of statistical significance for α being different from 0, and thus synergy. However, the confidence interval of α expands mostly in positive range, suggesting the combinations of the two drugs may have some synergistic effect instead of pure additive effect. Table 3 may aid in interpreting this result. The confidence interval for the interaction index at the lowest dose combination $d_1 = d_2 = 0.1\mu M$ was not significantly different from 1. However, the interaction indices at the other three higher dose combinations ($d_1 = d_2 = 0.5\mu M, 1\mu M, 2\mu M$) all showed synergistic effect. Greco's α provides an overall estimation of synergy across all dose levels, and appears to weigh in a less than synergistic effect at the low-dose combinations of the two agents.

For Machado and Robinson's model, the initial values for m_1, m_2, D_{m1}, D_{m2} were taken from Table 2 with $\eta = 0.7$. The two plots are shown in Figure 6 and $RSS=1.232$. The fitted parameters are $m_1 = -0.471$, $m_2 = -0.538$, $D_{m1} = 1.220$, $D_{m2} = 1.282$, and the estimated synergism and antagonism parameter $\eta = 0.507$ with standard error 0.092, so the 95% confidence interval for η is $[0.327, 0.687]$, which does not contain 1 and indicates synergy for the effect of the two drugs.

For Plummer and Short's model, the initial values for β_0, β_1 could be taken as $\beta_{0,1}$ and slope m_1 in Table 2.

The initial value for β_2 could be $\frac{\beta_{0,2} - \beta_{0,1}}{m_1}$, and the initial value for β_3 could be $\frac{m_2 - m_1}{m_1}$. We used Newton-Raphson method to solve D_2 in Plummer and Short's model. The convergence of the algorithm is sensitive to the initial value of β_4 , therefore, one may try different initial values for β_4 to see whether the solutions are obtainable and converge to the same value. In this example, we took 2.5 as the initial value for β_4 . The corresponding two-component plot is shown in Figure 7 and $RSS=1.238$. The fitted parameters are $\beta_0 = 0.099$, $\beta_1 = -0.473$, $\beta_2 = -0.083$, $\beta_3 = 0.120$, and the estimated synergism and antagonism parameter $\beta_4 = 2.146$ with standard error 1.102, so the 95% confidence interval for β_4 is $[-0.014, 4.305]$. The conclusion is that these two drugs are additive with respect to cell survival.

For Carter's model (30), the initial values can be obtained using logistic regression for each single drug. The two-component plot is shown in Figure 8. The fitted parameters were $\beta_0 = 0.590$, $\beta_1 = -0.331$, $\beta_2 = -0.516$. The estimated synergy-antagonism parameter $\beta_{12} = -0.003$ with standard error 0.043, thus the 95% confidence interval for β_{12} , $[-0.087, 0.081]$, contains zero, we cannot claim that synergy exists using this model. From the plots in Figure 8, we can see that the fit is not good either for a single drug or for the mixture of the two drugs, and the contour plot of the fitted surface is far away from the contour of the raw data. These figures show that Carter's model does not provide a good fit for our data. Table 3 also shows that Carter's model yields the largest RSS ($RSS=1.399$).

In conclusion, we have fitted five models to the data in Table 1 with summary statistics shown in Table 3. We compared the fitted dose-effect curves with raw data given in Figure 4C and panel A of Figures 5-8. In addition, the fitted contour plots in panel B of Figures 5-8 were compared to the raw data contour plot in Figure 4D. The correlation coefficients in Table 2 and standard regression diagnostics indicated that Chou and Talalay model fit the data well. The RSSs of the fitted models of Greco, Machado and Robinson, and Plummer and Short showed these models fit the data reasonably well. The only exception was Carter's model which did not fit the data adequately. Machado and Robinson's model gave a conclusion that the combinations of the two drugs are synergistic on this cell line UMSCC22B (Table 3). Chou and Talalay's model gave synergistic effects at moderate to high dose combinations but additive effect at low dose combinations. The coexistence of synergism and additivity of the two agents probably explains why the confidence interval for Greco's α and Plummer and Short's β_4 barely include zero but tend to be positive. Overall, we recommend using Chou and Talalay's model with interaction index as the measure of drug interaction. Greco's model has the least RSS

among the four parametric response surface models for this data set. However, all the four methods are not sufficient to describe the data set where synergy, additivity, or antagonism are interspersed. New method should be developed to capture different patterns of drug interactions.

We developed S-PLUS/R programs to provide estimates for each of the five methods described. The S-PLUS/R code and the data example are available in *synergy* which can be downloaded from <http://odin.mdacc.tmc.edu/anonftp/>.

7. Discussion and Future Research

Some investigators advocate using the Bliss independence model, since Bliss independence implies that the two agents do not physically, chemically, or biologically cooperate, which has an intuitive appeal and a theoretical basis [31, 32, 33, 34]. However, we agree with many authors that the “mechanistic free” Loewe additivity model should be the standard reference model for defining drug interactions as synergistic, additive, or antagonistic [10, 11, 12, 16, 17, 22, 18, 23].

Chou and Talalay [20, 21] proposed the plot of the interaction index versus the effect E for the drug combination with a fixed ratio, and by examining at several ratios, the synergy and antagonism can be identified across a range of doses even when the modes of drug interactions are inconsistent, i.e., synergy at certain dose combinations but antagonism at others. Not every data set follows the median effect equation well. Therefore, if one can find a better approach to fit the dose-effect curves for a single drug and drug combinations at a fixed ratio, following Step 2 to Step 5 described in Section 4.1, a more accurate model to detect synergy and antagonism may be developed. Kelly and Rice [35] proposed a spline method to fit the dose-effect curve, which could be combined with Chou and Talalay’s idea to detect synergy and antagonism.

Greco’s model (21) implies that E_{con} and B are the same for drug 1, drug 2 and the mixture of drugs, which may not be true. Approaches assuming that E_{con} and B are polynomials of the drug ratio were developed by White *et al.* [29], and the assessment of drug interactions of this approach is based on the 50% isobole. Further examination is needed in order to specify these polynomials precisely.

For our data set, we had only a single observation, i.e., the proportion of surviving cells, for each drug combination. We used the least-squares method to estimate the parameters in the models as mentioned above. The results will be the same as the maximum likelihood estimate for Gaussian distributed errors. If we have multiple observations for each drug combination, we can detect whether the variance is constant, and, if not,

The frequency of mutations in the histologically normal respiratory epithelium was higher in samples microdissected within the tumor (9 of 21, 43%) than samples obtained from tissue adjacent to tumor (distance of <5 mm from the tumor margin; 7 of 29, 24%; $P = 0.013$; Table 2). No mutation was detected in 14 distant bronchial and bronchiolar samples. Although not statistically significant, a higher incidence of mutation was detected in small bronchial (9 of 26, 35%) compared with bronchiolar structures (7 of 38, 18%; $P = 0.093$). More frequent mutations affecting normal epithelium were found in *EGFR* exon 19 (14 of 16, 54%) compared with exon 21 (2 of 28, 7%; $P = 0.02$). There was no correlation noted between mutations in the normal epithelium and age, gender, ethnic background, former or never smoker status, or lung cancer clinical stage in our patients.

Discussion

This is the first report of the presence of *EGFR* mutations in histologically normal bronchial and bronchiolar epithelium in patients with lung adenocarcinomas. Our findings of identical *EGFR* mutations in normal-appearing respiratory epithelium in 9 of 21 (43%) patients with mutant tumors suggest that the mutations occur as early events in the pathogenesis of a subset of lung adenocarcinomas, commencing in histologically normal peripheral airways. These findings impact our understanding of

the early pathogenesis of *EGFR* mutant lung adenocarcinomas, and may lead to clinical applications, such as targeted early detection and chemoprevention strategies.

It has been proposed that lung cancer cells with mutant *EGFR* might become physiologically dependent on the continued activity of the gene for the maintenance of their malignant phenotype (13). Mutant *EGFR* selectively transduces survival signals, specifically Akt, and signal transduction and activator of transcription signaling pathways, on which lung cancer tumor cells become dependent (14). Our finding of identical *EGFR* mutations (15 or 18 bp in-frame deletion and L858R mutation) in lung adenocarcinoma cells and in 25% of the corresponding adjacent histologically normal epithelial sites examined indicates that *EGFR* tyrosine kinase mutations also may play an important role in the initiation of the malignant phenotype. This notion is further supported by the absence of *EGFR* mutations in normal-appearing epithelium from 16 lung adenocarcinomas with wild-type *EGFR* from never and former smokers.

Clinically and pathologically (1), most adenocarcinomas of the lung are considered to arise from the peripheral lung airway compartment (small bronchi/bronchioles and alveoli; ref. 15), which arise by division of the tertiary bronchi (16). Whereas bronchi are lined by pseudostratified ciliated epithelium with occasional mucin-producing cells, bronchioles contain ciliated cells and secretory Clara cells (16). The latter are believed to be

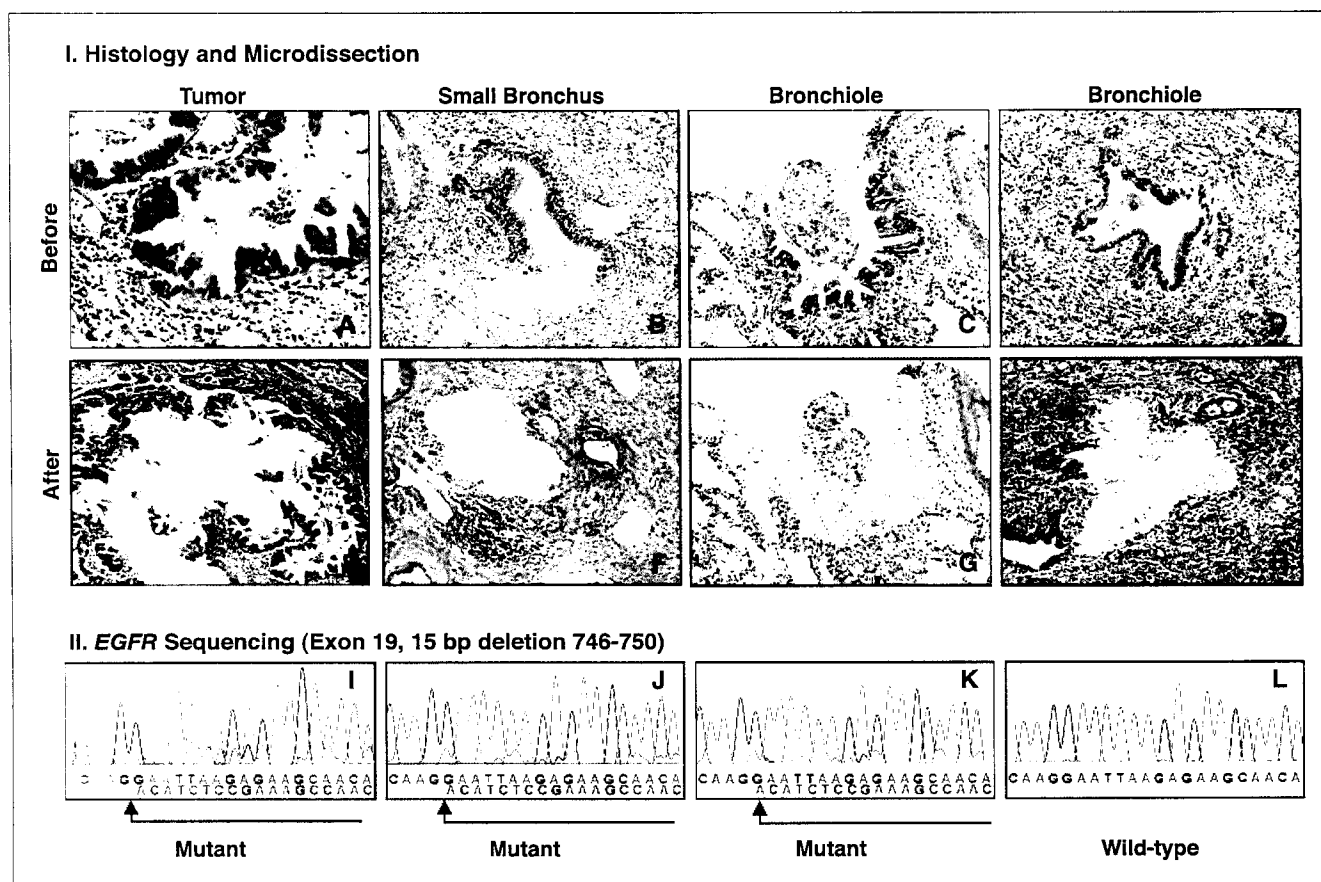


Figure 1. I, examples of tumor and histologically normal airway structures harboring the mutations are illustrated before (A-D) and after microdissection (E-H). II, sequencing chromatograms showing the presence of wild-type and mutant forms in the tumor (I), a small bronchus (J), and bronchiole (K), whereas only wild-type form is present in another bronchiole (L). Arrow, in-frame deletion mutation sequence.

Table 2. Frequency of *EGFR* tyrosine kinase domain mutations in microdissected histologically normal bronchial and bronchiolar epithelium in lung adenocarcinoma patients

Cases/samples	Mutated tumors			Wild-type tumors
	Exon 19 deletion	Exon 21 mutation	Total mutated	
Patients by smoking status (<i>n</i> = 30)				
Never	2 of 5	2 of 7	4 of 12	0 of 8
Former	4 of 6	0 of 1	4 of 7	0 of 8
Current	1 of 2	—	1 of 2	—
Total patients	7 of 13 (54%)	2 of 8 (25%)	9 of 21 (43%)*	0 of 16*
Foci by location compared with tumor (<i>n</i> = 90)				
Within	8 of 14 (57%)	1 of 7 (14%)	9 of 21 (43%) [†]	0 of 8
Near (<5 mm)	6 of 13 (46%)	1 of 16 (6%)	7 of 29 (24%) [†]	0 of 13
Distant	0 of 9	0 of 5	0 of 14 [†]	0 of 5
Foci by respiratory structure (<i>n</i> = 90)				
Small bronchus	8 of 17 (47%)	1 of 9 (11%)	9 of 26 (35%)	0 of 10
Bronchiole	6 of 19 (32%)	1 of 19 (5%)	7 of 38 (18%)	0 of 16
Total foci	14 of 36 (39%) [‡]	2 of 28 (7%) [‡]	16 of 64 (25%)	0 of 26

**P* value of comparison: 0.0046.[†]*P* value of comparison: 0.013.[‡]*P* value of comparison: 0.021.

the progenitor cells of the bronchiolar epithelium. Respiratory bronchioles terminate in alveolar ducts and alveolar sacs, which are lined by type I and II pneumocytes (16). Our finding of *EGFR* mutations in microdissected histologically normal epithelial cells obtained from small bronchi and bronchioles supports the concept of adenocarcinomas arising from the peripheral lung airway compartment. The tendency of higher frequency of *EGFR* mutations in normal epithelium obtained from small bronchi (35%) compared with bronchioles (18%) may correlate with different cell types populating those epithelia, which could represent the site of the cell of origin for *EGFR* mutant adenocarcinomas. However, the possibility that common stem or progenitor cells for both bronchial and bronchiolar epithelia are the cell type bearing *EGFR* mutation cannot be excluded.

The finding of *EGFR* mutations in small bronchial and bronchiolar epithelium obtained from sites within (43%) and adjacent (24%) to tumors, but none in the distant peripheral lung sites, suggests that a localized type of field effect phenomenon may exist for *EGFR* mutations in the lung respiratory epithelium. A widespread field effect phenomenon with several molecular

changes affecting histologically normal and abnormal bronchial and bronchiolar epithelium has been previously shown by us (17, 18) and others (19) in the smoking-damaged respiratory epithelium from lung cancer patients and from smokers without lung cancer. Therefore, our findings extend the field theory from centrally arising squamous carcinomas to peripheral occurring adenocarcinomas arising both in smokers and never smokers.

Our findings of *EGFR* mutations present in histologically normal epithelium of patients with lung adenocarcinomas bearing identical mutations open new avenues of investigation in the early pathogenesis of lung adenocarcinoma, including the identification of specific epithelial cell types hit by crucial genetic abnormalities involved in lung tumorigenesis.

Acknowledgments

Received 5/18/2005; revised 6/14/2005; accepted 6/22/2005.

Grant support: Specialized Program of Research Excellence in Lung Cancer grant P50CA70907, National Cancer Institute (Bethesda, MD), and Department of Defense grant W81XWH-04-1-0142.

The costs of publication of this article were defrayed in part by the payment of page charges. This article must therefore be hereby marked *advertisement* in accordance with 18 U.S.C. Section 1734 solely to indicate this fact.

References

- Travis WD, Brambilla E, Muller-Hermelink HK, Harris CC, editors. World Health Organization classification of tumours, pathology and genetics: tumours of the lung, pleura, thymus and heart. Lyon: IARC Press; 2004. p. 9–124.
- Minna JD, Gazdar A. Focus on lung cancer. *Cancer Cell* 2002;1:49–52.
- Paez JG, Janne PA, Lee JC, et al. *EGFR* mutations in lung cancer: correlation with clinical response to gefitinib therapy. *Science* 2004;304:1497–500.
- Lynch TJ, Bell DW, Sordella R, et al. Activating mutations in the epidermal growth factor receptor underlying responsiveness of non-small-cell lung cancer to gefitinib. *N Engl J Med* 2004;350:2129–39.
- Pao W, Miller V, Zakowski M, et al. *EGF* receptor gene mutations are common in lung cancers from “never smokers” and are associated with sensitivity of tumors to gefitinib and erlotinib. *Proc Natl Acad Sci U S A* 2004;101:13306–11.
- Huang SF, Liu HP, Li LH, et al. High frequency of epidermal growth factor receptor mutations with complex patterns in non-small cell lung cancers related to gefitinib responsiveness in Taiwan. *Clin Cancer Res* 2004;10:8195–203.
- Kosaka T, Yatabe Y, Endoh H, Kuwano H, Takahashi T, Mitsudomi T. Mutations of the epidermal growth factor receptor gene in lung cancer: biological and clinical implications. *Cancer Res* 2004;64:8919–23.
- Tokumo M, Toyooka S, Kiura K, et al. The relationship between epidermal growth factor receptor mutations and clinicopathologic features in non-small cell lung cancers. *Clin Cancer Res* 2005;11:1167–73.
- Shigematsu H, Lin L, Takahashi T, et al. Clinical and biological features associated with epidermal growth factor receptor gene mutations in lung cancers. *J Natl Cancer Inst* 2005;97:339–46.
- Amann J, Kalyankrishna S, Massion PP, et al.

- Aberrant epidermal growth factor receptor signaling and enhanced sensitivity to EGFR inhibitors in lung cancer. *Cancer Res* 2005;65:226-35.
11. Mountain CF. Revisions in the International System for Staging Lung Cancer. *Chest* 1997;111:1710-7.
 12. Snedecor GW, Cochran WG. Statistical method. 7th ed. Ames: Iowa State University Press; 1980.
 13. Gazdar AF, Shigematsu H, Herz J, Minna JD. Mutations and addiction to EGFR: the Achilles "heel" of lung cancers? *Trends Mol Med* 2004;10:481-6.
 14. Sordella R, Bell DW, Haber DA, Settleman J. Gefitinib-sensitizing EGFR mutations in lung cancer activate anti-apoptotic pathways. *Science* 2004;305:1163-7.
 15. Yatabe Y, Mitsudomi T, Takahashi T. TTF-1 expression in pulmonary adenocarcinomas. *Am J Surg Pathol* 2002;26:767-73.
 16. Gartner LP, Hiatt JL. Respiratory system. In: Gartner LP, Hiatt JL, editors. *Color textbook of histology*. Philadelphia: W.B. Saunders Company; 2001. p. 343-64.
 17. Wistuba II, Lam S, Behrens C, et al. Molecular damage in the bronchial epithelium of current and former smokers. *J Natl Cancer Inst* 1997;89:1366-73.
 18. Wistuba II, Behrens C, Virmani AK, et al. High resolution chromosome 3p allelotyping of human lung cancer and preneoplastic/preinvasive bronchial epithelium reveals multiple, discontinuous sites of 3p allele loss and three regions of frequent breakpoints. *Cancer Res* 2000;60:1949-60.
 19. Mao L, Lee JS, Kurie JM, et al. Clonal genetic alterations in the lungs of current and former smokers. *J Natl Cancer Inst* 1997;89:857-62.

Clinical-Pathological Characteristics of the *EGFR* Gene Mutation in Non-Small Cell Lung Cancer

Anne S. Tsao¹, Xi Ming Tang¹, Bradley Sabloff², Lianchun Xiao³, Hisayuki Shigematsu⁸, Jack Roth⁴, Margaret Spitz⁵, Waun Ki Hong¹, Adi Gazdar^{7,8}, Ignacio Wistuba^{1,6}

Departments of Thoracic/Head & Neck Medical Oncology¹, Diagnostic Radiology², Biostatistic and Applied Mathematics³, Thoracic and Cardiovascular Surgery⁴, Epidemiology⁵, and Pathology⁶, University of Texas M.D. Anderson Cancer Center, Houston, Texas 77030, USA; Hamon Center for Therapeutic Oncology Research⁷ and Department of Pathology⁸, University of Texas Southwestern Medical Center, Dallas, Texas 75390, USA.

Running Title: Characterizing the EGFR gene mutation in NSCLC

Correspondence:

Ignacio I. Wistuba
Department of Pathology, Unit 85
University of Texas M. D. Anderson Cancer Center
1515 Holcombe Blvd.
Houston, TX 77030-4009
Tel: (713) 563-9184
Fax: (713) 563-1848
Email: iiwistuba@mdanderson.org

Supported by Department of Defense grant W81XWH-04-1-0142 and by grant 5U01CA8497102 from the Specialized Program of Research Excellence (SPORE) in Lung Cancer P50CA70907, National Cancer Institute. We thank Natalie Ozburn and Xiaoquin (Rachel) Bi for their technical assistance.

ABSTRACT

Background: We sought to define clinical-pathologic features associated with mutations of the *EGFR* gene in non-small cell lung cancer (NSCLC). **Methods:** We evaluated surgically resected NSCLC tumors for *EGFR* (exon 18-21) and *KRAS* (codon 12-13) mutations, immunohistochemistry (EGFR, phosphorylated-EGFR, and HER2/Neu), and correlated results with clinical outcome, patient and disease features. After our analysis on 159 patients was completed, we selected a second cohort of Asian patients (n=22) and compared *EGFR* mutation results to place of birth and immigration to the United States. **Results:** Of 159 patients, 14 had *EGFR* mutations, and 18 had *KRAS* mutations. *EGFR* mutations were associated with adenocarcinoma (p=0.002), females (p=0.02), never-smoking (p<0.0001), Asian ethnicity (p=0.005), air bronchograms (p=0.004), and multiple wedge resections (p=0.03). Although statistical significance was not reached, a higher incidence of synchronous primary cancers (36% versus 17%; p=0.09) and smaller median tumor size (11.8 cm³ versus 24.0 cm³; p=0.24) were seen. There was no difference in disease-free survival, however median overall survival in patients with *EGFR* mutations was shorter (3.49 versus 4.29 years, p=0.85). *EGFR* mutation did not correlate with immunohistochemistry. In the second cohort of 22 Asian patients, 12 (55%) patients had the mutation. Of interest, there was no geographic difference in incidence of *EGFR* mutation. Asian women with the *EGFR* mutation developed adenocarcinoma at an earlier age than other lung cancer patients. **Conclusions:** There is a distinct clinical profile for NSCLC patients with the *EGFR* mutation. However, this mutation does not alter disease-free survival and is likely due to an inherited susceptibility instead of an environmental effect.

INTRODUCTION

The epidermal growth factor receptor (EGFR) has been the recent subject of great interest in lung cancer treatment. EGFR is overexpressed in 40-80% of non-small cell lung cancer (NSCLC) patients and regulates cell proliferation, cell survival, angiogenesis, and tumor metastasis.(1) Recently, critical mutations in the adenosine triphosphate (ATP) pocket of the tyrosine kinase binding region were reported in patients with NSCLC.(2, 3) These mutations are suspected to cause constitutive activation of the receptor and confer susceptibility to EGFR tyrosine kinase inhibitors.(2) *EGFR* exons 18 through 21 encode for structures around the ATP binding cleft within the tyrosine kinase domain.(2-5) This is the binding area for the EGFR tyrosine kinase small molecule inhibitors gefitinib and erlotinib.

Based on the prior studies (IDEAL) using EGFR tyrosine kinase inhibitors, approximately 9-12% of European patients and 18-19% of Asian patients with NSCLC experienced a tumor response to these agents.(6, 7) Subpopulation analyses revealed that responders were more likely to be female, non-smokers, and have adenocarcinoma with bronchioloalveolar features.(8) However, more specific predictors of response were unknown as immunohistochemical studies of EGFR were not reliable in predicting response to therapy.(9) The discovery of *EGFR* mutations in the tyrosine kinase domain provides some insight into why only a small proportion of patients benefit from EGFR targeted therapy. We sought to further define the clinical, pathologic and biologic features associated with the *EGFR* mutation in lung cancer to determine the most likely population to benefit from screening for the mutation.

MATERIAL AND METHODS

Methodology and Case Selection

We evaluated *EGFR* and *KRAS* gene mutations in archived frozen and paraffin-embedded NSCLC tumor specimens obtained from patients who underwent resection at the University of Texas M. D. Anderson Cancer Center. This retrospective study was approved by our Institutional Review Board. One hundred fifty-nine tumor specimens were selected from the University of Texas M. D. Anderson Cancer Center Lung SPORE Tissue Bank based on equal numbers of squamous cell and adenocarcinoma histologies. Patients with medical histories of never- and long-term former smoking were also selected to increase the likelihood of locating tumors with the *EGFR* mutation. The *EGFR* and *KRAS* mutation data from this first cohort of 159 patients have been previously published as part of a larger series.(4)

We determined the association between the mutation analysis results with immunohistochemical expression of EGFR, phosphorylated EGFR (p-EGFR, Y1086), and HER2/Neu. In addition, all laboratory results were compared to detailed clinical and-pathologic disease features and outcome. After the analysis on the first 159 patients was completed, we selected a second group of patients (n=22) from our archived Lung SPORE tissue bank based on Asian ethnicity to conduct the *EGFR* mutation analysis. In this Asian cohort, we determined the association between mutation status and focused clinical information regarding smoking history, place of birth, and time lived in the United States or Asian country.

Clinical Information Collection

Patient charts were reviewed and demographic data were collected, including age, gender, and ethnicity. We also collected patients' past medical history, including an extensive history of previous cancers and cancer therapies. A breakdown of aerodigestive tract cancers compared to

hematologic and other solid tumors was done. Extensive family medical histories, including immediate family member cancer histories, were obtained. We also collected data on disease characteristics including pathologic confirmation of primary tumor sites, areas of clinical metastasis, histologic pattern (including extensiveness of the bronchioloalveolar component), level of aggressiveness (lymphatic or vascular invasion, extra-capsular invasion, microscopic lymph node metastasis, and pleural invasion), and tumor size. Bronchioloalveolar carcinoma (BAC) was defined using the 2004 WHO classification for lung cancer(10) and characterized by the growth of neoplastic cells along pre-existing alveolar structures without evidence of stromal, pleural, or vascular invasion and in the absence of metastasis. Both clinical and pathologic TNM staging data were obtained. Radiographic clinical information prior to surgery was collected, including chest computer tomography (CT) location of tumor, presence of air bronchograms, quality of tumor margins (smooth or ill-defined), extension to pleura, amount of solid component to the tumor, presence of pseudocavitation, amount of pleural thickening, and degree of tumor spiculation. Data on induction therapies used and response were tabulated as were type of surgical resection, adjuvant therapy, and response to adjuvant therapy. Information on post-operative complications was also collected, and categorized into cardiovascular, pulmonary, gastrointestinal, neurologic, hematologic, or wound infection. Both disease-free and overall survival duration from the time of diagnosis were evaluated.

EGFR and KRAS Mutation Analysis

For the gene mutation analyses, genomic DNA was obtained from frozen normal and primary lung tumor specimens by overnight digestion with sodium dodecyl sulfate and proteinase K digestion (Life Technologies, Inc., Rockville, MD) at 37°C, followed by standard phenol-chloroform (1:1) extraction and ethanol precipitation. *EGFR* mutation analysis of four tyrosine

kinase domain exons (18 to 21), that are frequently mutated in lung cancer was performed using an intron-based polymerase chain reaction (PCR) as previously reported.(4) All PCRs were carried out in 25µl of solution containing 100 ng of genomic DNA using HotStarTaq DNA polymerase (QIAGEN Inc., Valencia, CA). DNA was amplified for 33 cycles at 95°C for 30 seconds, 65°C for 30 seconds, and 72°C for 45 seconds, followed by 7 minutes' extension at 72°C. The intron-based PCR primer sequences for exon 2 of KRAS were as previously published.(4) For the *KRAS* mutation analysis, DNA was amplified for 33 cycles at 95°C for 30 seconds, 55°C for 30 seconds, and 72°C for 30 seconds, followed by 7 minutes' extension at 72°C. All PCR products were incubated using exonuclease I and shrimp alkaline phosphatase (Amersham Biosciences, Inc., Piscataway, NJ) and sequenced directly using Applied Biosystems PRISM dye terminator cycle sequencing method (Perkin-Elmer Corp., Foster City, CA). All sequence variants were confirmed by independent PCR amplifications and sequenced in both directions.

Immunohistochemical Analysis

Immunohistochemical analyses were performed on formalin-fixed, paraffin-embedded specimens from surgically resected primary lung NSCLC. Tissue microarrays (TMAs) were prepared using 1 mm core sections in triplicate. Four-microns-thick histology sections from TMAs were prepared for immunohistochemical analysis. Antibodies against the EGFR clone 31G7 (Zymed, catalog #36-9700), Her2/Neu (Dako catalog#A0485), and p-EGFR (Tyr 1086, Zymed catalog #36-9700) were used as the primary antibodies. Tissue slides were baked at 67°C for 30 minutes, deparaffinized in xylene, followed by graded alcohol and DI H₂O washes, and rehydrated in TBS-t buffer. Slides were placed in 10% DAKO Target Retrieval Solution 10X and then steamed for 30 minutes in a 10 mM Na Citrate bath (pH 6.0) at 95°C. The bath and

slides were removed from the steamer and cooled for 30 minutes until the temperature reached 50°C. Endogenous peroxidase activity was then blocked by incubating the slides for 15 minutes in a 3% H₂O₂ solution and 50 µl of Tween-20. Nonspecific protein-protein interaction was blocked with the addition of 200 µl of 10% fetal bovine serum/protein block solution to each slide for 35 minutes. The primary antibody was then added (200 µl of 1:100 dilution with 10% fetal bovine serum/protein block solution), and slides were incubated at room temperature for 90 minutes. Slides were washed and placed in a TBS-t bath. DAKO Envision plus Dual-link labeled polymer was added directly to the slides, which were then incubated for 30 minutes. After the slides were washed, 200 µl of DAKO substrate buffer/DAB plus chromogen substrate was added to the slides, and the slides were incubated for 5 minutes at room temperature. Slides were immersed in H₂O to stop the reaction, counterstained in 1:3 diluted hematoxylin (Dako #S3301) for 6 minutes, and rinsed in H₂O. Scott's Bluing reagent was applied for 1 minute, followed by graded alcohol washes and then xylene incubation for 4 minutes. Immunostaining of the cell membrane and cytoplasm for EGFR, p-EGFR, and Her2/Neu was evaluated by light microscopy using a 20X magnification objective. A semi-quantitative approach was used to generate a score for each tissue core, as previously described.⁽¹¹⁾ The percentage of positive tumor and epithelial cells per foci (0% to 100%) was multiplied by the dominant intensity pattern of staining (1, negative or trace; 2, weak; 3, moderate; and 4, intense); therefore, the overall score ranged from 0 to 400. Antibody specificity was confirmed using blocking peptide and phosphatase incubation experiments. For controls, we used formalin-fixed and paraffin-embedded pellets from lung cancer cell lines with p-EGFR overexpression confirmed by Western blot analysis.

Statistical Analysis

Fisher's exact test or the chi-square test was used to evaluate the association between *EGFR* mutations and clinical, pathologic, and demographic features. Kaplan-Meier survival curves were estimated, and the log-rank test was applied to assess the differences in survival distributions by *EGFR* mutations, clinical and pathologic variables. The Cox proportional hazards model was modeled to estimate the effect of *EGFR* mutation, *KRAS* mutation, and other covariates on survival.

RESULTS

Clinical-pathological Associations

Of our first cohort of 159 patients, 14 had *EGFR* mutations, and 18 had *KRAS* mutations. Patient and disease characteristics are summarized in Table 1. Eight *EGFR* mutations occurred in exon 19 (15 to 18-bp in-frame deletions), one occurred in exon 20 (exon 20 insertion), and five occurred in exon 21 (L858R point mutation). Table 2 provides details on the 14 patients with *EGFR* mutations. Fifteen *KRAS* mutations occurred in exon 12, and three occurred in exon 13. None of the patients had both *EGFR* and *KRAS* mutations. *EGFR* mutations were associated with adenocarcinoma histology ($p=0.002$), female gender ($p=0.02$), never-smoker status ($p<0.0001$), and Asian ethnicity ($p=0.005$). Four out of ten adenocarcinomas with bronchioloalveolar component demonstrated *EGFR* mutations (range 20% to 50%, Figure 1, Table 2), but none of the patients with pure bronchioloalveolar histology ($n=7$) had an *EGFR* mutation. All *EGFR* mutated lung adenocarcinomas were mixed histological subtype (World Health Organization Classification, 2004), with acinar predominant component in 11, papillary in 1 and solid in 2.

Patients with *EGFR* mutations were more likely to have undergone multiple wedge resections than non-carriers were (28.5% versus 7.5%, $p=0.03$). No differences in any other type of surgical resection were found. This was supported by a trend towards having synchronous primary disease or lung metastases in patients with *EGFR* mutations (36% compared to 17% of those without the mutation; $p=0.09$). Air bronchograms were the only significant radiographic findings associated with the *EGFR* mutations (22% versus 2%; $p=0.004$) as depicted in Figure 2.

There were no differences between patients with *EGFR* mutations and those without in tumor location, tumor margin characteristics, amount of extension to pleura, pseudocavitation, amount of solid tumor component within the tumors, presence of spiculation, or amount of pleural thickening. Although statistically not significant, the median pathologic tumor size was smaller in patients with *EGFR* mutations (11.8 cm^3 versus 24.0 cm^3 ; $p=0.24$). There was no association between *EGFR* mutation and age, clinical or pathological TNM stage, complications of surgery, location of the primary tumor, pathological features of tumor aggressiveness, or response to adjuvant or neoadjuvant therapy. *EGFR* mutations were not associated with family history of cancer, number of immediate family members with cancer, or personal history of cancer. Four of the patients with *EGFR* mutations had prior cancers: one breast ductal carcinoma in situ, one follicular lymphoma, one lung cancer, and one basal cell carcinoma of the skin.

We conducted a limited multivariate logistic regression analysis to determine the independent predictors for the *EGFR* mutation. This analysis determined that Asian ethnicity ($p=0.0004$), never-smoking ($p=0.0001$), and multiple wedges ($p=0.004$) were the only features that predicted for the *EGFR* mutation. However, this reduced model was handicapped by the small number of patients analyzed.

Survival Analysis

The median overall survival duration in patients with *EGFR* mutations was shorter than that in patients without the mutation (3.49 years versus 4.29 years). However, this difference was not statistically significant ($p = 0.85$) and did not account for the effect of stage (Figure 3). After adjustment for stage, the presence of the *EGFR* mutations did not appear to affect survival duration although the number of events was small (figures not shown). A Cox proportional hazard model showed that pathologic stage independently determined outcome in our population: a higher stage conferred a hazards ratio of 3.54 ($p < 0.0001$).

Selected Asian Population Analysis

As we found an association between the *EGFR* mutations and Asian ethnicity in our first patient cohort, we selected tissue samples from an additional second cohort of 22 Asian patients from the tissue bank for *EGFR* analysis. Twelve patients (55%) had the mutation (Table 3). Detailed information on patient ethnicity, place of birth, and length of time they had lived in the United States was known for 20 patients. Eleven of 12 patients with *EGFR* mutations were born in Far East Asian nations (three from China, four from Vietnam, one from the Philippines, and three from Korea). The one patient born in the United States was of Greek and Filipino descent. Six of these patients with the *EGFR* mutation had lived in the United States for more than 28 years, and the other six patients had lived most of their lives in Asian countries. Of the patients who did not have *EGFR* mutations, all were born in Far East Asian countries, and more than 50% had lived in the United States for more than twenty years (range 21 to 44 years). Two patients had never lived in the United States. Data on length of time lived in the United States and Asia was missing for two patients. In patients who had lived in the United States for more than 20 years (range 21-46 years; $n = 12$), and in patients who had lived in their home countries

most of their lives (n=8), the incidence of *EGFR* mutation was similar, 6/12 (50%) and 6/8 (67%), respectively.

The median age at lung cancer diagnosis was 64 years (range, 36-84 years) for the entire Asian cohort, with equal numbers of men and women. The median age at diagnosis of patients with *EGFR* mutations was a slightly lower than those who did not have the mutation (58.6 vs. 64 years). A subset analysis of patient age and gender (Table 4) showed that the median age of diagnosis of Asian women with *EGFR* mutations was lower than that of Asian men who have the mutations and Asian patients without mutations. However, this did not reach statistical significance due to the small number of patients involved in this study (p=0.4).

Immunohistochemistry Analysis

Tumors with *EGFR* mutations did not overexpress cytoplasmic or membranous EGFR or p-EGFR (Y1086). Patients who had *EGFR* mutations were more likely to have low immunohistochemical expression of EGFR when compared to patients who did not have *EGFR* mutation (77% versus 35%, p=0.02). However, there was no difference between the two groups in level of phosphorylated EGFR expression in both the cytoplasm and membrane. There was also no association between *EGFR* mutations and the presence or level of HER2/Neu expression.

DISCUSSION

Prior clinical studies on *EGFR* mutations in NSCLC report a higher frequency in women with adenocarcinoma, Asian patients, and non-smokers.(2-5, 8, 12) Although our retrospective analysis was limited by small sample sizes and availability of patient medical records, we were able to confirm the clinical findings of earlier studies and also expand the clinical profile of patients likely to harbor *EGFR* mutations. In our study, tumors with these mutations were more likely to be associated with air bronchograms but no other distinguishing radiographic features.

This finding should be considered with caution as there are so few patients evaluated. Although the differences were not statistically significant, tumors with the *EGFR* mutation were smaller in volume and were more likely to metastasize to the lung or present as synchronous tumors. Patients with *EGFR* mutations did not have more previous malignancies, indicating that these mutations arise de novo in the majority of cases. Also, the lack of family history of cancer suggests that a germ-line predisposition to acquiring these mutations is not present.

Our second cohort of Asian patients was limited in number (n=22) and by the nature of a retrospective analysis. However, two important observations are seen from this study. First, our analysis showed a similar incidence of *EGFR* mutations in Asian patients who had lived in the United States for more than 20 years (50%) as compared to patients living in Asian countries most of their lives (67%). This finding suggests that the development of a mutation in the *EGFR* gene is not related to the environment but is instead dependent on a strong genetic predisposition. This concept is supported by the differences in the length of the *EGFR* intron 1 polymorphic CA dinucleotide repeat (CA-SSR 1) between Japanese and Chinese and Caucasian and African American populations.(13) In Asian patients, the repeat lengths are considerably longer than are those found in Caucasian and African American patients. It is of interest that the length of repeat sequences influences *EGFR* gene expression, with longer lengths leading to less gene transcription.(14) The effect that these and other genetic polymorphisms have on the rate of mutation in the *EGFR* gene is unknown and provides a strong rationale for conducting further molecular epidemiological studies.

Secondly, we report a younger median age of developing lung cancer in the Asian women with the *EGFR* mutation (Table 4). This result should be viewed with caution due to the very small sample size and the lack of statistical significance. However, this observation is

important as it suggests that the estrogen pathway (patients were in the pre-menopausal age group) may play a critical role in the early onset of carcinogenesis in Asian patients with *EGFR* gene mutations. We did not see this wide age difference between the genders in our first cohort of predominantly Caucasian patients, but it is interesting that the one Asian female in that first cohort was 45 years old. There may also be some variation in the effect of gender among the Asian ethnicities. A previous report by a Japanese group(15) noted no difference in age between the women with *EGFR* mutations and other male patients. Our cohort did not include any Japanese female patients, but instead consisted of women of Chinese, Vietnamese, Filipino, and Korean ethnicities. A recent report by a group from Taiwan evaluated 39 Chinese patients with *EGFR* mutations(16) and found the median age in women was 62 years compared with 68 years in men.

Although our findings of Asian women with the *EGFR* mutation developing NSCLC at an earlier age are preliminary, there is compelling evidence to consider the role of estrogen as a carcinogenic promoter in these patients. First, it is well known that female gender is an independent risk factor for the development of NSCLC and that premenopausal women present with more aggressive disease.(17-21) Secondly, estrogens may act as tumor promoters or direct carcinogens with DNA adduct formation(23, 25-29). Thirdly, Stabile et al. report a functional interaction between the estrogen receptor and the EGFR pathways in NSCLC.(25, 30) This study also finds synergistic anti-tumor effects with fulvestrant (estrogen receptor antagonist) and gefitinib (EGFR tyrosine kinase inhibitor) in murine xenografts and NSCLC cell lines. Although this analysis did include a cell line with a *EGFR* mutation (273T heterozygous point mutation at exon 18 nucleotide 2180), conclusions on the effect of estrogen cannot be drawn as it is not one

of the typical mutations found in patients with NSCLC. The role of gender on *EGFR* mutation is unclear at this time but should be explored further.

In our laboratory analysis, we found low immunohistochemical expression of both EGFR and phosphorylated EGFR at site Y1086 in tumors of patients with *EGFR* mutations. This apparently conflicts with the premise that the mutations in the EGFR tyrosine kinase domain are activating mutations (L747-P753insS, L858R) with higher phosphorylation capability.(2) Our study is not the first to report this difference. Pao et al.(5) conducted functional studies on receptor mutations in exon 19 (del L747-S752, del E746-A750) and reported low kinase activity. This was seen with both low autophosphorylation Y1092 (p-EGFR) and low tyrosine-phosphorylated proteins when compared to wild-type EGFR assays. It is therefore possible that the mechanism of EGFR tyrosine kinase inhibitor sensitivity does not occur via intrinsic enhanced receptor tyrosine kinase activity but may be due to altered receptor-substrate binding capability. It is also plausible that de novo mutations in the *EGFR* gene may lead to variable protein expression with some dominant activating mutations and others that affect substrate binding. In support of this premise, there are at least seven different phosphorylation sites for EGFR, and the distinct mutations appear to have preferential phosphorylation patterns. The L858R mutation is associated with phosphorylation at sites Y845 and Y1092; whereas phosphorylation of sites Y992 and Y1068 are associated with both the L858R mutation and deletion of exon 19.(2, 5, 31) Phosphorylation at sites Y1173 and Y1045 do not appear to be associated with either mutation.(31) The lack of association found in our study between p-EGFR and *EGFR* mutation could be explained by the fact that our analysis focused solely on the Y1086 phosphorylation site. We plan to further document the preferential phosphorylation patterns of the distinct *EGFR* mutations. Further molecular studies to clarify the biology of these mutations

is necessary to understand the efficacy of tyrosine kinase inhibitor treatment and development of tumor resistance.

CONCLUSION

In conclusion, our analysis reports the following characteristics to be associated with the *EGFR* mutation: female gender, Asian ethnicity, adenocarcinoma histology, never-smoker status, presence of multiple lung lesions, and air bronchograms on imaging. In our Asian cohort, the results suggest an inherent and non-environmental susceptibility to development of *EGFR* mutations. There is also some speculation that Asian women with the *EGFR* mutations may develop adenocarcinoma at an earlier age than other patients. Further studies on the interaction of estrogen with *EGFR* pathway are warranted and continued efforts to define the mechanism of tyrosine kinase inhibitor sensitivity are needed to optimize cancer therapy.

REFERENCES

1. Mendelsohn J, Baselga J. The EGF receptor family as targets for cancer therapy. *Oncogene* 2000;19(56):6550-65.
2. Lynch TJ, Bell DW, Sordella R, et al. Activating mutations in the epidermal growth factor receptor underlying responsiveness of non-small-cell lung cancer to gefitinib. *N Engl J Med* 2004;350(21):2129-39.
3. Paez JG, Janne PA, Lee JC, et al. EGFR mutations in lung cancer: correlation with clinical response to gefitinib therapy. *Science* 2004;304(5676):1497-500.
4. Shigematsu H, Lin L, Takahashi M, et al. Clinical and Biological Features of Epidermal Growth Factor Receptor Mutations in Lung Cancers. *Journal of the National Cancer Institute* 2005;97(5):339-46.
5. Pao W, Miller V, Zakowski M, et al. EGF receptor gene mutations are common in lung cancers from "never smokers" and are associated with sensitivity of tumors to gefitinib and erlotinib. *Proc Natl Acad Sci U S A* 2004;101(36):13306-11.
6. Fukuoka M, Yano S, Giaccone G, et al. Multi-institutional randomized phase II trial of gefitinib for previously treated patients with advanced non-small-cell lung cancer (The IDEAL 1 Trial) [corrected]. *J Clin Oncol* 2003;21(12):2237-46.
7. Kris MG, Natale RB, Herbst RS, et al. Efficacy of gefitinib, an inhibitor of the epidermal growth factor receptor tyrosine kinase, in symptomatic patients with non-small cell lung cancer: a randomized trial. *Jama* 2003;290(16):2149-58.
8. Miller VA, Kris MG, Shah N, et al. Bronchioloalveolar pathologic subtype and smoking history predict sensitivity to gefitinib in advanced non-small-cell lung cancer. *J Clin Oncol* 2004;22(6):1103-9.
9. Bailey R, Kris MG, Wolf MK, et al. Gefitinib ('Iressa', ZD1839) monotherapy for pretreated advanced non-small cell lung cancer in IDEAL 1 and 2: tumor response is not clinically relevantly predictable from tumor EGFR membrane staining alone. In: *Lung Cancer*; 2003:S71.
10. Travis W, Brambilla E, Muller-Hermelink H, et al. Tumours of the lung. [World Health Organization Classification of Tumours]. Lyon: IARC Press; 2004.
11. Hirsch FR, Varella-Garcia M, Bunn PA, Jr., et al. Epidermal growth factor receptor in non-small-cell lung carcinomas: correlation between gene copy number and protein expression and impact on prognosis. *J Clin Oncol* 2003;21(20):3798-807.
12. Kris MG, Sandler A, Miller VA, et al. EGFR and Kras mutations in patients with bronchioloalveolar carcinoma treated with erlotinib in a phase II multicenter study [abstract]. In: *American Society of Clinical Oncology*; 2005; 2005.
13. Tidow N, Boecker A, Schmidt H, et al. Distinct amplification of an untranslated regulatory sequence in the egfr gene contributes to early steps in breast cancer development. *Cancer Res* 2003;63(6):1172-8.
14. Gebhardt F, Zanker KS, Brandt B. Modulation of epidermal growth factor receptor gene transcription by a polymorphic dinucleotide repeat in intron 1. *J Biol Chem* 1999;274(19):13176-80.
15. Kosaka T, Yatabe Y, Endoh H, Kuwano H, Takahashi T, Mitsudomi T. Mutations of the epidermal growth factor receptor gene in lung cancer: biological and clinical implications. *Cancer Res* 2004;64(24):8919-23.

16. Huang SF, Liu HP, Li LH, et al. High frequency of epidermal growth factor receptor mutations with complex patterns in non-small cell lung cancers related to gefitinib responsiveness in Taiwan. *Clin Cancer Res* 2004;10(24):8195-203.
17. Zang EA, Wynder EL. Differences in lung cancer risk between men and women: examination of the evidence. *J Natl Cancer Inst* 1996;88(3-4):183-92.
18. Gasperino J, Rom WN. Gender and lung cancer. *Clin Lung Cancer* 2004;5(6):353-9.
19. Patel JD, Bach PB, Kris MG. Lung cancer in US women: a contemporary epidemic. *Jama* 2004;291(14):1763-8.
20. Taioli E, Wynder EL. Re: Endocrine factors and adenocarcinoma of the lung in women. *J Natl Cancer Inst* 1994;86(11):869-70.
21. Moore KA, Mery CM, Jaklitsch MT, et al. Menopausal effects on presentation, treatment, and survival of women with non-small cell lung cancer. *Ann Thorac Surg* 2003;76(6):1789-95.
22. Wei Q, Cheng L, Amos CI, et al. Repair of tobacco carcinogen-induced DNA adducts and lung cancer risk: a molecular epidemiologic study. *J Natl Cancer Inst* 2000;92(21):1764-72.
23. Toyooka S, Tsuda T, Gazdar AF. The TP53 gene, tobacco exposure, and lung cancer. *Hum Mutat* 2003;21(3):229-39.
24. Nelson HH, Christiani DC, Mark EJ, Wiencke JK, Wain JC, Kelsey KT. Implications and prognostic value of K-ras mutation for early-stage lung cancer in women. *J Natl Cancer Inst* 1999;91(23):2032-8.
25. Siegfried JM. Women and lung cancer: does oestrogen play a role? *Lancet Oncol* 2001;2(8):506-13.
26. Cheng YW, Hsieh LL, Lin PP, et al. Gender difference in DNA adduct levels among nonsmoking lung cancer patients. *Environ Mol Mutagen* 2001;37(4):304-10.
27. Shriver SP, Bourdeau HA, Gubish CT, et al. Sex-specific expression of gastrin-releasing peptide receptor: relationship to smoking history and risk of lung cancer. *J Natl Cancer Inst* 2000;92(1):24-33.
28. Omoto Y, Kobayashi Y, Nishida K, et al. Expression, function, and clinical implications of the estrogen receptor beta in human lung cancers. *Biochem Biophys Res Commun* 2001;285(2):340-7.
29. Stabile LP, Davis AL, Gubish CT, et al. Human non-small cell lung tumors and cells derived from normal lung express both estrogen receptor alpha and beta and show biological responses to estrogen. *Cancer Res* 2002;62(7):2141-50.
30. Stabile LP, Lyker JS, Gubish CT, Zhang W, Grandis JR, Siegfried JM. Combined targeting of the estrogen receptor and the epidermal growth factor receptor in non-small cell lung cancer shows enhanced antiproliferative effects. *Cancer Res* 2005;65(4):1459-70.
31. Sordella R, Bell DW, Haber DA, Settleman J. Gefitinib-sensitizing EGFR mutations in lung cancer activate anti-apoptotic pathways. *Science* 2004;305(5687):1163-7.

FIGURE LEGENDS

Figure 1. Microphotographies of two representative lung adenocarcinomas with *EGFR* mutations (hematoxylin and eosin stained). Pictures *a* (100x) and *b* (200x) are from a lung adenocarcinoma with a point mutation L858R (T to G) in exon 21 (*c*) and with invasive acinar and solid patterns (*a* and *b*), and without any bronchioloalveolar component in the periphery. Pictures *d* (100x) and *e* (200x) were obtained from a lung adenocarcinoma having a 15bp (746-750) in-frame deletion mutation in exon 19 (*f*), and with a predominant invasive acinar component (*e*) and some areas of bronchioloalveolar-like pattern (~20%) in the periphery (*d*).

Figure 2. Two lung tumors cases with *EGFR* mutations showing invasive adenocarcinoma histology features (mostly acinar pattern, *a* and *c*) and corresponding chest computer tomography images (*b* and *d*). Computed tomography radiographs (*b* and *d*) show 2 cases of non-small cell lung cancer, (*b*) right upper lobe, (*d*) right lower lobe, manifesting as ill-defined nodules. Note air bronchograms, which correlate with *EGFR* mutation status, (black arrows).

Figure 3. Survival by presence of *EGFR* and *KRAS* mutations

Table 1. Patient and tumor characteristics by *EGFR* mutation status

Characteristics	Patients with <i>EGFR</i> Mutations (n=14)	Patients without <i>EGFR</i> mutations (n=145)	
Age (years)			
Mean	64	66	
Median	66	68	
Range	45-77	40 -90	
Gender			
Female	11	63	p=0.02
Male	3	82	
Ethnicity			
African-American	0	8	
Asian	3	1	p=0.005
Caucasian	10	129	
Hispanic	1	7	
Prior Cancer History			
Yes	5	44	
No	9	101	
Smoking Status			
Never	8	15	p<0.0001
Current	0	49	
Former	6	81	
Histology			
Adenocarcinoma*	14	75	p=0.002
Bronchioloalveolar	0	7	
Squamous Cell	0	63	
Pathologic Stage			
I	11	80	
II	0	28	
III	3	30	
IV	0	7	
Synchronous Primary or Lung Metastasis			
Present	6	25	
Absent	8	120	
Tumor Size (cm ³)			
Median	11.8	24	
Range	5.1 – 1080	0.36 – 2178	
Overall Survival (years)			
Median	3.49	4.29	

*Includes 10 adenocarcinomas with bronchioloalveolar features, 4 with and 6 without the *EGFR* mutation.

Table 2. Clinical-Pathologic features of patients with lung adenocarcinoma *EGFR* mutants from the first cohort

Patient Age and Gender	Ethnicity	Smoking History	Pack years	Prior Cancer	Stage	Site** of Tumor	BAC (%)	Air*** Bronchogram	Multiple Lesions	Surgical resection	Type of <i>EGFR</i> Mutation
72 F	Caucasian	Former	25	No	1B	LUL	50	INEV	No	Lobectomy	Exon 19 / 15 bp del (746-750)
66 F	Caucasian	Former	20	No	4	RLL	30	Yes	Yes	Lobectomy, Multiple wedges	Exon 19 / 15 bp del (746-750)
68 F	Caucasian	Current	80	No	4	RUL	20	INEV	Yes	Multiple wedges	Exon 19 / 15 bp del (746-750)
58 F	Caucasian	Current	37.5	No	1A	LLL	20	No	Yes	Lobectomy	Exon 19 / 15 bp del (746-750)
66 F	Caucasian	Never	0	No	1B	RUL	0	INEV	No	Lobectomy	Exon 19 / 18 bp del (746-751) & S752V
64 M	Caucasian	Never	0	No	1A	RLL	0	Yes	Yes	Lobectomy, Multiple wedges	Exon 19 / 15 bp del (746-750)
65 M	Asian	Former	0.8	Yes	2B	RML, RLL	0	No	Yes	Bilobectomy	Exon 19 / 18 bp del (746-751)&S752I
70 F	Caucasian	Never	0	Yes	3A	LLL	0	Yes	No	Lobectomy	Exon 19 / 15 bp del (746-750)
55 F	Caucasian	Never	0	No	2B	RML	0	INEV	No	Lobectomy	Exon 20
70 F	Caucasian	Never	0	Yes	1A	LUL	0	INEV	No	Lobectomy	Exon 21 / L858R
69 M	Asian	Former	42	No	3A	RUL	0	INEV	No	Lobectomy	Exon 21 / L858R
52 F	Hispanic	Never	0	No	4	RUL	0	No	No	Lobectomy, Multiple wedges	Exon 21 / L858R
65 F	Caucasian	Never	0	Yes	1A	RUL	0	Yes	Yes	Lobectomy	Exon 21 / L858R
45 F	Asian	Never	0	No	1A	LUL	0	INEV	No	Lobectomy	Exon 21 / L858R

**Site of primary lung tumor location: RUL – right upper lobe, RML – right middle lobe, RLL – right lower lobe, LUL – left upper lobe, LLL – left lower lobe

***Presence of air bronchograms on radiographic imaging: Yes – present, No- not present, INEV – inevaluable due to lack of adequate radiographic imaging

Table 3. Patient Demographics of the Asian cohort

Patient Age and Gender	Ethnicity	Place of Birth	Number of years lived in the USA	Smoking Status	Type of <i>EGFR</i> Mutation
63 F	Filipino	Philippines	32	Never	None
43 F	Filipino	Philippines	35	Never	None
65 M	Filipino	Philippines	35	Current	None
64 M	Filipino	Philippines	>32	Current	None
70 F	Japanese	Japan	44	Former	None
84 M	Chinese	China	21	Former	None
57 M	Chinese	China	28	Former	Exon 19 / 18bp Del (747-752)+ P753Q
68 M	Chinese	China	31	Former	Exon 19 / 15 bp Del (747-751)
36 F	Vietnamese	Vietnam	30	Never	Exon 19 / 15 bp Del (746-750)
52 M	Vietnamese	Vietnam	33	Former	Exon 19 / 15 bp Del (746-750)
65 M	Korean	Korea	39	Former	Exon 19 / 18 bp Del (746-751)
46 F	Filipino/Greek	USA	46	Never	Exon 21 / L858R
64 M	Filipino	Philippines	Unknown	Current	None
63 M	Taiwan	Taiwan	Unknown	Unknown	None
68 F	Korean	Korea	0	Never	None
62 F	Korean	Korea	0	Never	None
66 F	Vietnamese	Vietnam	0	Unknown	Exon 19 / 15 bp Del (746-750)
74 M	Vietnamese	Vietnam	Lived mostly in Vietnam	Current	Exon 19 / 15 bp Del (746-750)
72 F	Chinese	China	Lived mostly in China	Never	Exon 21 / L858R
49 F	Korean	Korea	0	Never	Exon 21 / L858R
49 F	Korean	Korea	0	Never	Exon 21 / L858R
69 M	Filipino	Philippines	0	Former	Exon 21 / L858R

Table 4. Age analysis of the Asian cohort of patients with and without *EGFR* mutations

Gender / Age	Positive <i>EGFR</i> mutation	Negative <i>EGFR</i> mutation
Female Age	(n = 6)[*]	(n=5)
Median	49	63
Mean	53	61
Range	36-72	43-70
Male Age	(n=6)	(n=5)
Median	66.5	64
Mean	64	68
Range	52-74	63-84

^{*} p-value =0.4

Figure 1

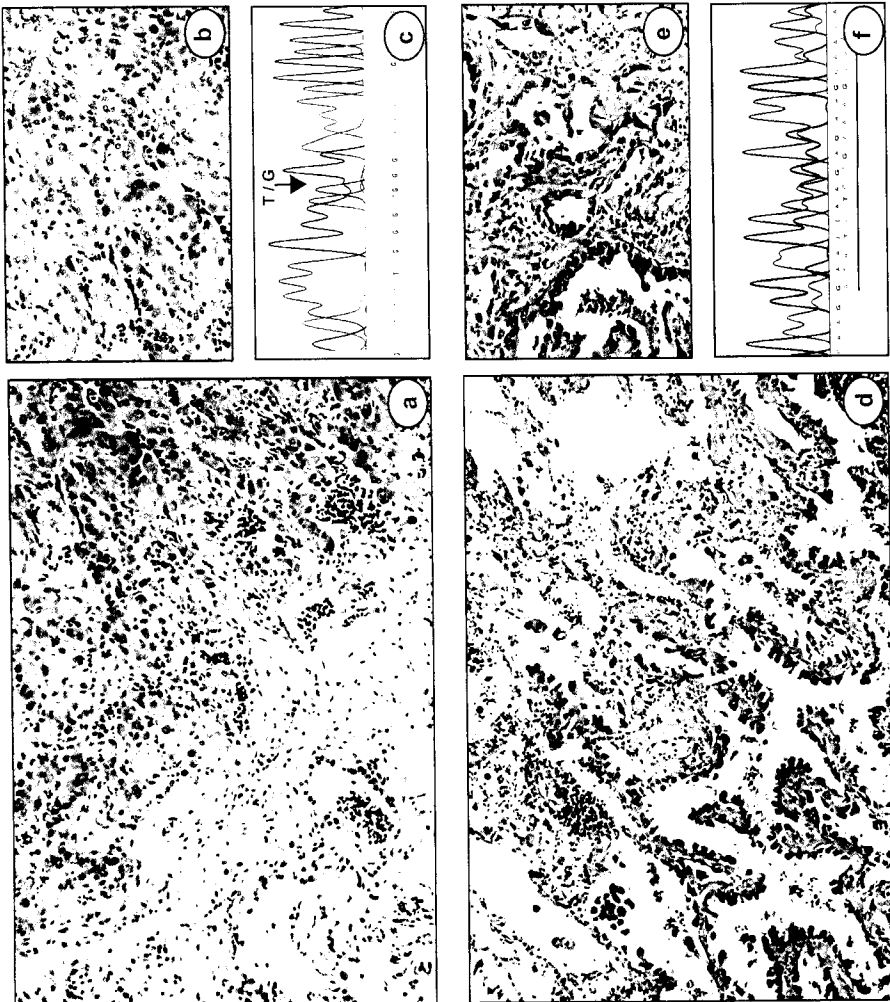


Figure 2

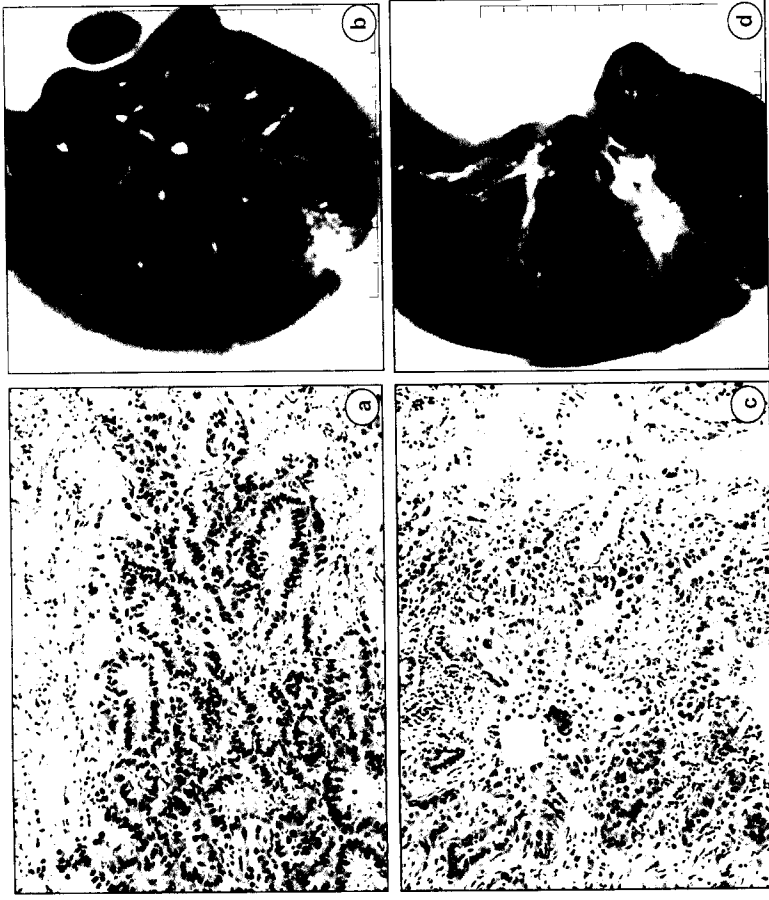
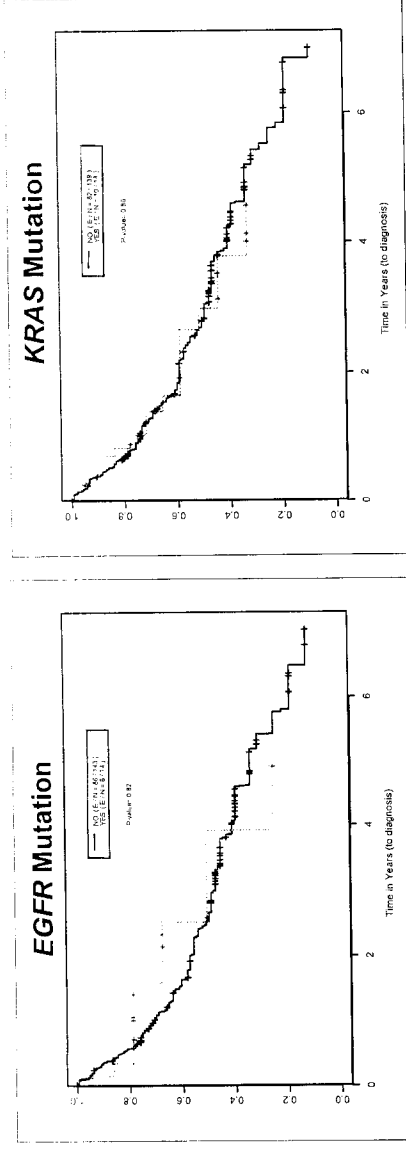


Figure 3



A Three-Dimensional Model of Differentiation of Immortalized Human Bronchial Epithelial Cells

Melville B. Vaughan, Ruben D. Ramirez, Woodring E. Wright, John D. Minna,
and Jerry W. Shay

Woodring E. Wright, Jerry W. Shay (corresponding author): Department of Cell Biology, The University of Texas Southwestern Medical Center, Dallas, TX 75390-9039, USA.

Email: Jerry.Shay@UTSouthwestern.edu Tel: 214-648-3282, Fax: 214-648-8694

John D. Minna: The Hamon Center for Therapeutic Oncology Research, Department of Internal Medicine and Pharmacology, The University of Texas Southwestern Medical Center, Dallas, TX, USA

Ruben D. Ramirez: Dallas Veterans Affairs Medical Center, 4500 South Lancaster Road, Mail Code 151, Dallas, TX, USA

Melville B. Vaughan: Department of Biology, University of Central Oklahoma, Edmond, OK, USA

Running Title: Differentiation of Human Bronchial Epithelial Cells

Abstract:

A therapeutic approach being investigated for a variety of pathologies is tissue regeneration using a patient's own cells. Such studies have been hampered due to the difficulty in growing epithelial cells for prolonged periods in culture. Replicative senescence due to short telomeres and p16 induced by culture stress work together to inhibit cell growth. Forced expression of telomerase (hTERT) can prevent replicative senescence, and expression of the cell cycle protein cdk4 can sequester p16, thereby immortalizing epithelial cells in culture. In the present study we used this method to immortalize human bronchial epithelial cells (HBECs) to determine whether immortalized HBECs retain the ability to differentiate normally. HBECs were plated atop contracted collagen gels containing lung fibroblasts. This three-dimensional (3D) tissue model was cultured initially submerged, then raised to the air/liquid interface for up to 28 days. Normal differentiation was assessed by the presence of ciliated cells, goblet (mucin-producing) cells, and basal epithelial cells. Scanning electron microscopic observations revealed both ciliated and non ciliated cells in these 3D tissues. Histological examination revealed the presence of mucin-producing cells, and immunohistochemistry using antibodies against p63 and keratin 14 showed the presence of basal cells. These results demonstrate that immortalized HBECs retain the capacity to differentiate into each of three cell types: basal, mucin-producing, and columnar ciliated epithelial cells. Such cells will be useful cellular reagents for research in aging, cancer progression, as well as normal bronchial epithelial differentiation and will help progress the use of engineered cells to enhance tissue regeneration.

Key Words: Telomerase, immortalization, ciliogenesis, mucin, human bronchial epithelial cells; organotypic culture, basal cell, stem cell.

Introduction:

Tissue engineering offers great promise for the generation of therapeutic materials for the replacement of damaged organs. There has been significant success in producing artificial skin by combining dermal fibroblasts in contracted collagen gels with human keratinocytes (Vaughan et al., 2004; Auger et al., 1998), and in creating three dimensional cultures reproducing some of the characteristics of a cornea by combining keratocytes with corneal epithelial cells (Reichl et al. 2004; Taliana et al., 2001). Both of these systems exhibit a stratified squamous epithelium. There has only been very limited success in producing artificial tissues using other types of epithelium such as bronchial epithelium (Choe et al., 2003; Paquette et al., 2003). A major problem in the development of such tissues is the availability of normal human cells capable of reproducing the diversity of cell types seen *in vivo*. Lack of sufficient cell numbers is especially evident when cells are harvested from older individuals (Harley, 2002). The limited lifespan of human cells and the variability encountered when using primary cultures from human biopsies further complicates the difficulties.

Replicative senescence is a phenomenon associated with progressive telomere shortening. With every cell division a cell's telomeres shorten until some of the telomeres reach a critically short length where the cells are signaled to stop dividing. This occurs in fibroblasts (Harley et al., 1990; 1992) and in epithelial cells that have minimized the effects of p16 in culture (Ramirez et al., 2003). Overexpression of the catalytic subunit of the telomerase enzyme, hTERT, stabilizes telomere length and allows greatly extended or unlimited proliferation potential of cells in culture without causing oncogenic transformation (Harley, 2002; Herbert et al., 2002; Harada et al., 2003; Lee et al., 2003; Morales et al., 2003; Alvero et al., 2004; Ramirez et al., 2004).

Previous studies have shown that hTERT alone, or hTERT in the absence of p16 effects, not only immortalizes cells in culture but also allows the cells to retain their normal differentiation and/or function (Dickson et al., 2000; Harley 2002, Forsyth et al., 2003; Wootton et al., 2003; Abdallah et al., 2005). We have previously shown that immortalized keratinocytes retain the ability to differentiate and function normally within the context of an organotypic construct (Ramirez et al., 2003). This important step implied that immortalized cells might be useful in tissue regeneration. More recently we have shown that human bronchial epithelial cells can be immortalized by overexpression of cdk4 (to bypass the inhibitory effects of p16 of cells growing in plastic culture dishes in normal atmospheric oxygen levels) and hTERT. Since patients with respiratory diseases such as cystic fibrosis and lung cancer could potentially benefit from tissue engineering or regeneration therapy, the purpose of this study was to determine whether immortalized HBECs can retain normal differentiation potential and promote the establishment of bronchial epithelial tissue in a simplified three-dimensional organotypic environment.

Methods

Cell cultures: Bronchial epithelial cells were isolated and cultured as previously described (Ramirez et al., 2004). In brief, cells were grown from explant cultures of non-involved areas of lung tissue removed during cancer surgery. Subsequent cultures were grown on collagen-coated dishes in serum-free media (KSFM; GIBCO) containing $50 \mu\text{g mL}^{-1}$ gentamicin sulfate. Cells were retrovirally-infected, first to overexpress the cell-cycle protein cdk4 followed by overexpression of the catalytic component of telomerase (hTERT) (Ramirez et al., 2003). Each culture was passaged beyond 100 population doublings to determine *in vitro* immortality. Immortal bronchial epithelial cells from four patients were used in this study and designated HBEC 1, 2, 3, and 4. HBEC cells were also plated at very low density to allow clonal expansion. 4 clones from each of the 3 HBEC populations were isolated to use in subsequent experiments. Human embryonic lung fibroblasts (IMR90) (ATCC, CCL-186) were maintained in four parts Dulbecco's modified Eagle's medium to one part Medium 199 supplemented with 10% Cosmic calf serum (HyClone) and $50 \mu\text{g mL}^{-1}$ gentamicin sulfate. All cell cultures were kept in log phase growth until ready to use.

Organotypic culture: (figure 1): Cultures were established as previously described for skin equivalents (Vaughan et al., 2004) except that airway cells were used in place of skin cells. Briefly, type I collagen and IMR90 fibroblasts were mixed and allowed to polymerize (figure 1B, top). The collagen gels were released and incubated for a period of 4 to 10 days to allow the fibroblasts to contract the gels (figure 1B, bottom), creating a 'mucosa'. Cloning rings were then placed atop the gels and HBEC cells were plated into the rings at a concentration of $2 \times 10^5/\text{cm}^2$.

After allowing the cells to attach for 4 hours, the rings were removed and organotypic cultures submerged for 4 days in keratinocyte feeder layer media containing ascorbic acid, then emerged to the air-liquid interface (figure 1C) for up to 28 days in culture, after which time the cultures were harvested, fixed, and prepared for histology and Immunohistochemistry.

Histology and immunohistochemistry: Certain organotypic cultures were immersed in 10% neutral buffered formalin overnight at 4°C followed by dehydration and paraffin embedding, while others were preserved in 4% paraformaldehyde and subsequently embedded in OCT compound and frozen (Halliday and Tomasek, 1995). 5 and 10µm sections were then rehydrated and stained with hematoxylin and eosin to view overall morphology using a technique available online (<http://www.protocol-online.org/prot/Histology/Staining/>). Rehydrated unstained tissues were incubated in the presence of antibodies against p63 (clone 63p02), keratin 14 (clone LL002), Ki67 (clone SP6), and mucin (clone MUC5AC) (Neomarkers; LabVision Corp). Paraffin sections incubated with primary antibodies were stained using a kit (Vecta-Stain, Vector Labs) followed by a DAB kit (Vector Labs) and subsequently mounted. Keratin 14-incubated frozen sections were followed by a fluorescent secondary antibody (rhodamine red; Molecular Probes, Eugene, OR) and subsequently mounted in an aqueous media with the nuclear-staining DAPI (Vectashield with DAPI; Vector Labs). Stained slides were then viewed using an Axioscop-2 or Axioplan-2E microscope (Carl Zeiss, Thornwood, NY, USA; www.zeiss.com) and photographed with an Axiocam MRC color digital camera (Zeiss) or Hamamatsu ORCA monochrome CCD camera (Hamamatsu; Bridgewater, NJ; www.hamamatsu.com).

Ultrastructure: Specimens for scanning electron microscopy (SEM) were fixed in 2% glutaraldehyde in 0.01mol/L sodium cacodylate buffer and subsequently stained with 2% osmium tetroxide. The tissues were then dehydrated in ethyl alcohol and critical point dried using liquid carbon dioxide. The dried specimens were mounted on aluminum stubs and coated with gold–palladium prior to SEM study. SEM images were obtained using a JEOL model JSM-840A microscope operated at an accelerating voltage of 10 kV and a probe current of 6×10^{-11} . Digital images were captured using OpenLab software (Improvision; Lexington, MA; www.improvision.com/).

Results:**Human bronchial epithelial cells (HBEC) form a layer of epithelial cells on the surface of the organotypic culture**

Normal human bronchial epithelium is composed of pseudostratified columnar epithelium containing ciliated cells, goblet cells, and basal cells (figure 1A). H&E-stained paraffin sections using HBECs from various donors and placed in 3-D organotypic culture (figure 1B and C) demonstrate a confluent layer of cells on the upper surface of the culture. The cells' morphology ranged from squamous to high cuboidal, often appearing to be multi-layered or pseudostratified (figure 2A). Since bronchial epithelium is known to contain both goblet secretory cells and ciliated cells, we immunostained sections with an antibody against the secretory product mucin to observe mucous-producing cells (Groneberg et al., 2002), which appeared to be scattered throughout the surface (figure 2B). Cilia-like structures were also observed in some of the cells (figure 2A, 2B). In contrast to normal epithelium, metaplastic human bronchial epithelium changes to a stratified squamous epithelium (figure 2C). In some organotypic cultures, especially those using HBEC1 derived from a long-time smoker, stratified squamous epithelium similar to metaplasia was observed (figure 2D). Upon cytogenetic examination, HBEC1 was determined to have several alterations not present in the other cell lines (data not shown).

Basal and stem cell markers detected in the epithelial compartment of organotypic culture

Basal-like cells of the bronchus function as stem cells (Inayama et al., 1988; 1989; Hong et al., 2004) and express the stem cell markers p63 (Wang et al., 2002; Reis-Filho et al., 2003;

Danieli et al., 2004) and keratin 14 (Broers et al., 1989; Wetzels et al., 1992; Nakajima et al., 1998; Reis-Filho et al., 2003). To determine the presence of these markers we immunostained 3D organotypic tissue sections. Using frozen sections we observed the presence of keratin 14 in basal-like cells of the organotypic constructs (figure 3A), while using paraffin sections we detected the presence of p63 in the basal cells (figure 3B). We also immunostained organotypic constructs to determine whether the proliferation antigen Ki67 was present. Paraffin sections demonstrated only the sporadic presence of Ki67 in the organotypic constructs and these did not co-localize to the p63 expressing cells (figure 3C).

Apical surface differentiated phenotype developed in organotypic cultures of immortalized HBECs

We next prepared organotypic cultures for ultrastructural analysis of the apical surface. Scanning electron micrographs of organotypic cultures revealed the presence of cilia at various stages of differentiation (figure 4). In addition, cells with large blebs on the surface were observed and these may be goblet cells. Often multiple cell types were present in the same field. Large areas of ciliated cells were not present prior to 28 days at the air/liquid interface, although cells with small, cilia-like projections similar to those seen in the lower-right image of figure 4 were observed in every sample taken. Interestingly, ciliated cells of the organotypic tissue as a whole were not evenly distributed; rather, small areas of the tissue, frequently near the edge close to the membrane, contained the majority of cells with long cilia, while other areas, especially at the high point near the middle of the tissue, contained cells with short cilia.

HBEC clones function as multipotent stem cells

Stem cells of the bronchus have been shown to produce three cell types: ciliated, mucus-producing, and basal cells (Inayama et al., 1989; Engelhardt et al., 1995; Hong et al., 2004). To determine whether immortalized HBECs could act as restricted-lineage stem cells, we isolated single cells and picked individual clones from HBECs 3 and 4 for use in organotypic cultures using conditions similar to the above studies. Results using HBEC3 and HBEC4 showed ciliogenesis, cell morphologically resembling goblet cells (mucin⁺), and protein expression levels similar to the mixed populations (data not shown). Thus, the immortalized HBECs are multipotential.

Discussion:

The ability to extend the lifespan or reversibly immortalize cells without altering their phenotype would allow expansion of a patient's biopsied cells *ex vivo* and permit the construction of simplified tissues, with the long-term goal of returning these tissues to the patient. Previous studies have shown that overexpression of the telomere-stabilizing enzyme telomerase is sufficient to immortalize fibroblasts (Bodnar et al., 1998; Vaziri and Benchimol, 1998). Epithelial cells have been more difficult to immortalize *in vitro*, probably because appropriate culture conditions that do not stress the cells are lacking (Ramirez et al., 2001; Wright and Shay, 2002). For these cells it has been necessary to inactivate/bypass the stress- and senescence-related p16^{INK4a} protein (by overexpressing cDNAs such as cdk4 or expression of viral oncoproteins such as HPV16 E7), (Kiyono et al., 1998; Rheinwald et al., 2002; Sviderskaya et al., 2003) or by preventing the culture-induced stress activation in the first place (e.g culturing the cells on feeder-layers). Bronchial epithelial cells have been immortalized using various methods (see table 1), each of which can give rise to either ciliated or mucus cells, or both. However, each method employs the use of viral oncoproteins, which can lead to genomic instability. In one study (Zabner et al., 2003), the ciliated phenotype was inhibited with culture time, possibly due to the use of viral oncoproteins. We have shown previously that skin epithelial keratinocytes (Ramirez et al., 2003) can be immortalized *in vitro* by overexpression of hTERT and the cell cycle protein cdk4 without affecting their differentiation profile. Inadequate culture conditions induce the cells to express p16, which probably binds to the overexpressed cdk4, thereby sequestering p16 and allowing further proliferation in the presence of culture stress. We have recently shown that bronchial epithelial cells will also immortalize by overexpression of hTERT and cdk4 (Ramirez et al., 2004). Herein we show that these cells will also differentiate

and produce bronchial epithelial-like tissue in a three dimensional simplified organotypic culture environment.

Normal bronchial epithelium contains ciliated epithelial cells, mucin-producing cells, and basal cells that can proliferate and differentiate into each of the 3 major cell types (Inayama et al., 1989; Otto, 2002; Hong et al., 2004). In our studies immortalized bronchial epithelial cells from 3 different patients were able to produce ciliated, mucin, and basal cells based on characteristic protein expression and morphological observations. In addition, isolated clones from 2 patients were able to produce 3 major cell types present in bronchial epithelium. In this regard, the clones function as multipotent cells. While it is possible that the multipotent cells that immortalized might be true stem cells, it is also possible that they might be dedifferentiated epithelial cells (Blau et al., 2001) or non-stem cell basal cells. Nevertheless, this demonstrates the presence *in vivo* of bronchial cells that, if necessary, can be harvested and manipulated in order to produce bronchial cells with the ability to regenerate normal tissue as needed. Such tissues can be useful both for basic research or to rebuild tissue damaged by trauma or cancerous lesions. These tissues can be important tools to study effects of toxins, to study cancer progression, and may complement animal models often employed in respiratory system research. In addition, this 3D organotypic model can be used to test new chemopreventive drugs and study their effects on “normal” or “preneoplastic” epithelia, providing valuable information regarding chemopreventive agents as well as potential side effects. Before attempting to use such tissues in human grafting, it will likely be necessary to use xenografts onto nude mice to understand long-term effects, since it is difficult to maintain organotypic tissues *in vitro* for longer than 2 months. Xenografts of bronchial tissue and organotypic constructs have been successfully performed as

subcutaneous implants in mouse skin, so the feasibility of this approach has already been tested (Engelhardt et al., 1992; Inayama et al., 1989; Yankaskas et al., 1993).

An interesting observation is that none of the clones gave rise to only ciliated epithelium or mucin-producing cells. This implies that more-committed cells either do not immortalize or clone well, or that more-committed cells de-differentiate into a stem cell during the culturing process. The latter idea has been postulated elsewhere (Blau et al., 2001). While it is beneficial to provide all three cell types, it would be interesting to have the ability to provide each as needed, especially to study the differentiation pathway.

We observed what appeared to be multilayering in some constructs and occasional hyperproliferation at discrete areas of the constructs. Multilayering has been shown in other studies using normal bronchial epithelium (Paquette et al., 2003) and could be attributed to the culture media that are formulated to promote proliferation and inhibit differentiation. Some have suggested that retinoic acid may inhibit the skin-like morphology of bronchial epithelium (Jetten, 1989; Sachs et al., 2003) and might be necessary for ciliary and mucous cell development (Gray et al., 1996; Koo et al., 1999). While we were successful in obtaining ciliogenesis using the current medium formulation, future modifications of the medium such as switching to a more basal media at late time points, or performing xenograft studies may result in different outcomes. In addition, tissues *in vivo* are under tension; tension affects fibroblast phenotype (Grinnell, 2000; 2003). Tension may also affect the bronchial epithelial phenotype as well (Choe et al., 2003). The organotypic construct as described here is not under tension, which may be a reason for the appearance of multilayering seen here and elsewhere; current studies are underway to address the effects of tension on bronchial epithelium.

Immortalizing cells in culture and returning them to an individual may in the future be helpful as a short-term solution to tissue regeneration. However, it is possible that long-term effects may be harmful. An alternate solution would be to briefly immortalize only during the regeneration process. We have used an excisable system to briefly express hTERT in fibroblasts (Steinert et al., 2000). A similar system could be used to express hTERT and cdk4 to allow expansion in culture. These cells could then be returned to the patient, perhaps in the context of an organotypic construct, to promote normal function of the respiratory system without the increased risk of subsequent carcinogenesis.

Two most challenging problems facing cell biologists are growing difficult cell types in culture, and immortalizing cells using the fewest possible changes in protein expression. As techniques become more sophisticated, these challenges are being surmounted, and now many cell types have been successfully grown in culture and immortalized (Harley, 2002). Future studies using organotypic constructs or xenograft studies will help to determine when tissue regeneration *in vivo* will be a possible therapy for replacement of damaged or diseased organs.

Acknowledgements: This work was support by Lung SPORE CA70907, NASA NSCOR NNJ05HD36G, and the Nash Foundation. The authors would like to thank Jimmy C. Yang and Jason Nagati for technical assistance; Barbara Harris for histology; George Lawton and Tom Januszewski for electron microscopy preparation; and James Tomasek for helpful discussions.

References:

Abdallah, B.M., Haack-Sorensen, M., Burns, J.S., Elsnab, B., Jakob, F., Hokland, P., and Kassem, M. (2005) Maintenance of differentiation potential of human bone marrow mesenchymal stem cells immortalized by human telomerase reverse transcriptase gene despite of extensive proliferation. *Biochem Biophys Res Commun* 326:527-538.

Auger, F.A., Rouabhia, M., Goulet, F., Berthod, F., Moulin, V., and Germain, L. (1998) Tissue-engineered human skin substitutes developed from collagen-populated hydrated gels: clinical and fundamental applications. *Med Biol Eng Comput.* 36:801-812.

Alvero, A.B., Fishman, D.A., Qumsiyeh, M.B., Garg, M., Kacinski, B.M., and Sapi, E. (2004) Telomerase prolongs the lifespan of normal human ovarian surface epithelial cells without inducing neoplastic phenotype. *J Soc Gynecol Investig* 11:553-561.

Blau, H.M., Brazelton, T.R., and Weimann, J.M. (2001) The evolving concept of a stem cell: entity or function? *Cell* 105:829-841.

Bodnar, A.G., Ouellette, M., Frolkis, M., Holt, S.E., Chui, C.-P., Morin, G.B., Harley, C.B., Shay, J.W., Lichsteiner, S., and Wright, W.E. (1998) Extension of life-span by introduction of telomerase into normal human cells. *Science* 279:349–352.

Broers, J.L., de Leij, L., Rot, M.K., ter Haar, A., Lane, E.B., Leigh, I.M., Wagenaar, S.S., Vooijs, G.P., and Ramaekers, F.C. (1989) Expression of intermediate filament proteins in fetal and adult human lung tissues. *Differentiation* 40:119-128.

Choe, M.M., Sporn, P.H., and Swartz, M.A. (2003) An *in vitro* airway wall model of remodeling. *Am J Physiol Lung Cell Mol Physiol* 285:L427-433.

Cozens, A.L., Yezzi, M.J., Kunzelmann, K., Ohrui, T., Chin, L., Eng, K., Finkbeiner, W.E., Widdicombe, J.H., and Gruenert, D.C. (1994) CFTR expression and chloride secretion in polarized immortal human bronchial epithelial cells. *Am J Respir Cell Mol Biol.* 10:38-47.

Danieli, Y., Liao, G., Dixon, D., Linnoila, R.I., Lori, A., Randell, S.H., Oren, M., and Jetten, A.M. (2004) Critical role of p63 in the development of a normal esophageal and tracheobronchial epithelium. *Am J Physiol Cell Physiol* 287:C171-181.

Dickson, M.A., Hahn, W.C., Ino, Y., Ronfard, V., Wu, J.Y., Weinberg, R.A., Louis, D.N., Li, F.P., and Rheinwald, J.G. (2000) Human keratinocytes that express hTERT and also bypass a p16(INK4a)-enforced mechanism that limits life span become immortal yet retain normal growth and differentiation characteristics. *Mol Cell Biol* 20:1436-1447.

Engelhardt, J.F., Schlossberg, H., Yankaskas, J.R., and Dudus, L. (1995) Progenitor cells of the adult human airway involved in submucosal gland development. *Development* 121:2031-2046.

Forsyth, N.R., Wright, W.E., and Shay, J.W. (2002) Telomerase and differentiation in multicellular organisms: turn it off, turn it on, and turn it off again. *Differentiation* 69:188-197.

Gray, T.E., Guzman, K., Davis, C.W., Abdullah, L.H., and Nettesheim, P. (1996) Mucociliary differentiation of serially passaged normal human tracheobronchial epithelial cells. *Am J Respir Cell Mol Biol* 14:104-112.

Grinnell, F. (2000) Fibroblast-collagen-matrix contraction: growth-factor signalling and mechanical loading. *Trends Cell Biol* 10:362-365.

Grinnell, F. (2003) Fibroblast biology in three-dimensional collagen matrices. *Trends Cell Biol* 13:264-269.

Groneberg, D.A., Eynott, P.R., Oates, T., Lim, S., Wu, R., Carlstedt, I., Nicholson, A.G., and Chung, K.F. (2002) Expression of MUC5AC and MUC5B mucins in normal and cystic fibrosis lung. *Respir Med* 96:81-86.

Halliday, N.L. and Tomasek, J.J. (1995) Mechanical properties of the extracellular matrix influence fibronectin fibril assembly *in vitro*. *Exp Cell Res* 217:109-117.

Harada, H., Nakagawa, H., Oyama, K., Takaoka, M., Andl, C.D., Jacobmeier, B., von Werder, A., Enders, G.H., Opitz, O.G., and Rustgi, A.K. (2003) Telomerase induces immortalization of human esophageal keratinocytes without p16INK4a inactivation. *Mol Cancer Res* 1:729-738.

Harley, C.B. (2002) Telomerase is not an oncogene. *Oncogene* 21:494-502.

Harley, C.B., Futcher, A.B., and Greider, C.W. (1990) Telomeres shorten during ageing of human fibroblasts. *Nature* 345:458-460.

Harley, C.B., Vaziri, H., Counter, C.M. and Allsopp, R.C. (1992) The telomere hypothesis of cellular aging. *Exp Gerontol* 27:375–382.

Herbert, B.S., Wright, W.E., and Shay, J.W. (2002) p16(INK4a) inactivation is not required to immortalize human mammary epithelial cells. *Oncogene* 21:7897-7900.

Hong, K.U., Reynolds, S.D., Watkins, S., Fuchs, E., and Stripp, B.R. (2004) Basal cells are a multipotent progenitor capable of renewing the bronchial epithelium. *Am J Path* 164:577-588.

Inayama, Y., Hook, G.E., Brody, A.R., Cameron, G.S., Jetten, A.M., Gilmore, L.B., Gray, T., and Nettesheim, P. (1988) The differentiation potential of tracheal basal cells. *Lab Invest* 58:706-717.

Inayama, Y., Hook, G.E., Brody, A.R., Jetten, A.M., Gray, T., Mahler, J., and Nettesheim, P. (1989) *In vitro* and *in vivo* growth and differentiation of clones of tracheal basal cells. *Am J Path* 134:539-549.

Jetten, A.M. (1989) Multistep process of squamous differentiation in tracheobronchial epithelial cells *in vitro*: analogy with epidermal differentiation. *Environ Health Perspect* 80:149-160.

Kaartinen, L., Nettesheim, P., Adler, K.B., and Randell, S.H. (1993) Rat tracheal epithelial cell differentiation *in vitro*. *In Vitro Cell Dev Biol-Animal* 29A:481-492.

Kiyono, T., Foster, S.A., Koop, J.I., McDougall, J.K., Galloway, D.A., and Klingelutz, A.J. (1998) Both Rb/p16INK4a inactivation and telomerase activity are required to immortalize human epithelial cells. *Nature* 396:84-88.

Koo, J.S., Jetten, A.M., Belloni, P., Yoon, J.H., Kim, Y.D. and Nettesheim, P. (1999) Role of retinoid receptors in the regulation of mucin gene expression by retinoic acid in human tracheobronchial epithelial cells. *Biochem J* 338: 351-357.

Lee, K.M., Nguyen, C., Ulrich, A.B., Pour, P.M., and Ouellette, M.M. (2003) immortalization with telomerase of the Nestin-positive cells of the human pancreas. *Biochem Biophys Res Commun* 301:1038-1044.

Lundberg, A.S., Randell, S.H., Stewart, S.A., Elenbaas, B., Hartwell, K.A., Brooks, M.W., Fleming, M.D., Olsen, J.C., Miller, S.W., Weinberg, R.A., and Hahn, W.C. (2002) immortalization and transformation of primary human airway epithelial cells by gene transfer. *Oncogene* 21:4577-4586.

Morales, C.P., Gandia, K.G., Ramirez, R.D., Wright, W.E., Shay, J.W., and Spechler, S.J. (2003) Characterisation of telomerase immortalised normal human oesophageal squamous cells. *Gut* 52:327-333.

Nakajima, M., Kawanami, O., Jin, E., Ghazizadeh, M., Honda, M., Asano, G., Horiba, K., and Ferrans, V.J. (1998) Immunohistochemical and ultrastructural studies of basal cells, Clara cells and bronchiolar cuboidal cells in normal human airways. *Pathol Int* 48:944-953.

Otto, W.R. (2002) Lung epithelial stem cells. *J Pathol* 197:527-535.

Paquette, J.S., Tremblay, P., Bernier, V., Auger, F.A., Laviolette, M., Germain, L., Boutet, M., Boulet, L.P., and Goulet, F. (2003) Production of tissue-engineered three-dimensional human bronchial models. *In Vitro Cell Dev Biol-Animal* 39:213-220.

Ramirez, R.D., Herbert, B.S., Vaughan, M.B., Zou, Y., Gandia, K., Morales, C.P., Wright, W.E., and Shay, J.W. (2003) Bypass of telomere-dependent replicative senescence (M1) upon overexpression of Cdk4 in normal human epithelial cells. *Oncogene* 22:433-444.

Ramirez, R.D., Morales, C.P., Herbert, B.S., Rohde, J.M., Passons, C., Shay, J.W., and Wright, W.E. (2001) Putative telomere-independent mechanisms of replicative aging reflect inadequate growth conditions. *Genes Dev* 15:398-403.

Ramirez, R.D., Sheridan, S., Girard, L., Sato, M., Kim, Y., Pollack, J., Peyton, M., Zou, Y., Kurie, J.M., Dimaio, J.M., Milchgrub, S., Smith, A.L., Souza, R.F., Gilbey, L., Zhang, X., Gandia, K., Vaughan, M.B., Wright, W.E., Gazdar, A.F., Shay, J.W., and Minna, J.D. (2004) Immortalization of human bronchial epithelial cells in the absence of viral oncoproteins. *Cancer Res* 64:9027-9034.

Reichl, S., Bednarz, J., and Muller-Goymann, C.C. (2004) Human corneal equivalent as cell culture model for *in vitro* drug permeation studies. *Br J Ophthalmol* 88:560-565.

Reis-Filho, J.S., Simpson, P.T., Martins, A., Preto, A., Gartner, F., and Schmitt, F.C. (2003) Distribution of p63, cytokeratins 5/6 and cytokeratin 14 in 51 normal and 400 neoplastic human tissue samples using TARP-4 multi-tumor tissue microarray. *Virchows Arch* 443:122-132.

Rheinwald, J.G., and Green, H. (1975) Serial cultivation of strains of human epidermal keratinocytes: the formation of keratinizing colonies from single cells. *Cell* 6:331-343.

Rheinwald, J.G., Hahn, W.C., Ramsey, M.R., Wu, J.Y., Guo, Z., Tsao, H., De Luca, M., Catricala, C., and O'Toole, K.M. (2002) A two-stage, p16 (INK4A)- and p53-dependent keratinocyte senescence mechanism that limits replicative potential independent of telomere status. *Mol Cell Biol* 22:5157–5172.

Sachs, L.A., Finkbeiner, W.E., and Widdicombe, J.H. (2003) Effects of media on differentiation of cultured human tracheal epithelium. *In Vitro Cell Dev Biol Anim* 39:56-62.

Shay, J.W., and Wright, W.E. (2004) Senescence and immortalization: role of telomeres and telomerase. *Carcinogenesis* 25:1-8.

Steinert, S., Shay, J.W., and Wright, W.E. (2000) Transient expression of human telomerase extends the life span of normal human fibroblasts. *Biochem Biophys Res Commun* 273:1095-1098.

Sviderskaya, E.V., Gray-Schopfer, V.C., Hill, S.P., Smit, N.P., Evans-Whipp, T.J., Bond, J., Hill, L., Bataille, V., Peters, G., Kipling, D., Wynford-Thomas, D., and Bennett, D.C. (2003) p16/cyclin-dependent kinase inhibitor 2A deficiency in human melanocyte senescence, apoptosis, and immortalization: possible implications for melanoma progression. *J Natl Cancer Inst* 95:723-732.

Taliana, L., Evans, M.D., Dimitrijevic, S.D., and Steele, J.G. (2001) The influence of stromal contraction in a wound model system on corneal epithelial stratification. *Invest Ophthalmol Vis Sci* 42:81-89.

Vaziri, H., and Benchimol, S. (1998) Reconstitution of telomerase activity in normal human cells leads to elongation of telomeres and extended replicative life span. *Curr Biol* 8: 279–282.

Vaughan, M.B., Ramirez, R.D., Brown, S.A., Yang, J.C., Wright, W.E., and Shay, J.W. (2004) A reproducible laser-wounded skin equivalent model to study the effects of aging *in vitro*. *Rejuvenation Res* 7:99-110.

Wang, B.Y., Gil, J., Kaufman, D., Gan, L., Kohtz, D.S., and Burstein, D.E. (2002) p63 in pulmonary epithelium, pulmonary squamous neoplasms, and other pulmonary tumors. *Hum Pathol* 33:921-926.

Wetzels, R.H., Schaafsma, H.E., Leigh, I.M., Lane, E.B., Troyanovsky, S.M., Wagenaar, S.S., Vooijs, G.P., and Ramaekers, F.C. (1992) Laminin and type VII collagen distribution in different types of human lung carcinoma: correlation with expression of keratins 14, 16, 17 and 18. *Histopathology* 20:295-303.

Wootton, M., Steeghs, K., Watt, D., Munro, J., Gordon, K., Ireland, H., Morrison, V., Behan, W., and Parkinson, E.K. (2003) Telomerase alone extends the replicative life span of human skeletal muscle cells without compromising genomic stability. *Hum Gene Ther* 14:1473-1487.

Wright, W.E., and Shay, J.W. (2002) Historical claims and current interpretations of replicative aging. *Nat Biotechnol* 20:682-688.

Yankaskas, J.R., Haizlip, J.E., Conrad, M., Koval, D., Lazarowski, E., Paradiso, A.M., Rinehart, C.A. Jr., Sarkadi, B., Schlegel, R., and Boucher, R.C. (1993) Papilloma virus immortalized tracheal epithelial cells retain a well-differentiated phenotype. *Am J Physiol* 264:C1219-1230.

Zabner, J., Karp, P., Seiler, M., Phillips, S.L., Mitchell, C.J., Saavedra, M., Welsh, M., and Klingelutz, A.J. (2003) Development of cystic fibrosis and noncystic fibrosis airway cell lines. *Am J Physiol Lung Cell Mol Physiol* 284:L844-854.

Figure Legends:

Figure 1. Development of the organotypic culture. Normal human bronchial epithelium contains ciliated columnar cells, mucous-producing goblet cells, and basal cells (A). To produce a bronchial 'submucosa' *in vitro*, fibroblasts were combined with type I collagen, allowed to gel (B, top), then the gel was released from the dish and allowed to contract over a period of 4 to 7 days (B, bottom). Bronchial epithelial cells were then seeded onto the top of the gels and allowed to attach for 4 hours to create the organotypic culture. Cultures were submerged for 4 days, then placed into a 6-well insert which was fed from beneath by media placed into well below the insert (C), thereby leaving the upper surface of the tissue emerged from the media. Triplicate cultures were placed into each insert. Cultures were fed every other day, and harvested at various time points in culture.

Figure 2. Morphology of immortalized HBECs cultured on organotypic cultures. Stained paraffin cross-sections of organotypic cultures demonstrated the presence of squamous to cuboidal epithelial cells with the presence of cilia-like structures (A). Mucin staining (brown) demonstrated the presence of goblet cells interspersed among ciliated cells (B). In pathologies such as bronchial metaplasia, stratified epithelium can be observed (C). Some of the organotypic cultures, especially those using HBEC1 cells, produced similar stratification (D). 630x magnification.

Figure 3. Appearance of basal or stem cell markers in HBECs on organotypic cultures. Stained paraffin sections showed the presence of basal cell cytokeratin 14 (A) and p63 (B), as well as proliferation marker Ki67 (C). 400x magnification.

Figure 4. Apical surface modifications in HBEC-populated organotypic cultures. Cultures were prepared for scanning electron microscopy. Ciliated cells in various stages of differentiation were present, as were goblet-like cells. Picture in the upper right shows an undifferentiated cell at top, a goblet cell at center, and a ciliated cell at bottom. Magnification varies in this perspective.

Table 1. Differentiation Characteristics of Human Bronchial Epithelial Cells

Immortalization method	Differentiation culture conditions	Cell age when tested	Phenotype	Reference
cdk4, hTERT	IMR90 fibroblast-contracted collagen gel, keratinocyte feeder layer medium, air/liquid interface	PD >100	Basal, ciliated, mucus cells present	This study
HPV-16 E6/E7, hTERT	Collagen-coated membrane, defined medium, air/liquid interface	> passage 30	Ciliated and mucus	Zabner et al., 2003
SV40ER, hTERT	Nude mouse subcutaneous injection	>10 PD beyond crisis	Histology similar to normal airway	Lundberg et al., 2002
SV40 large T antigen	Vitrogen-coated membrane, serum-containing medium, air/liquid interface	Post-crisis	Ciliated	Cozens et al., 1994
HPV-18 E6/E7	Devitalized tracheal substrate xenografted subcutaneously	passage 14	Ciliated and secretory cells	Yankaskas et al., 1993

Figure 1

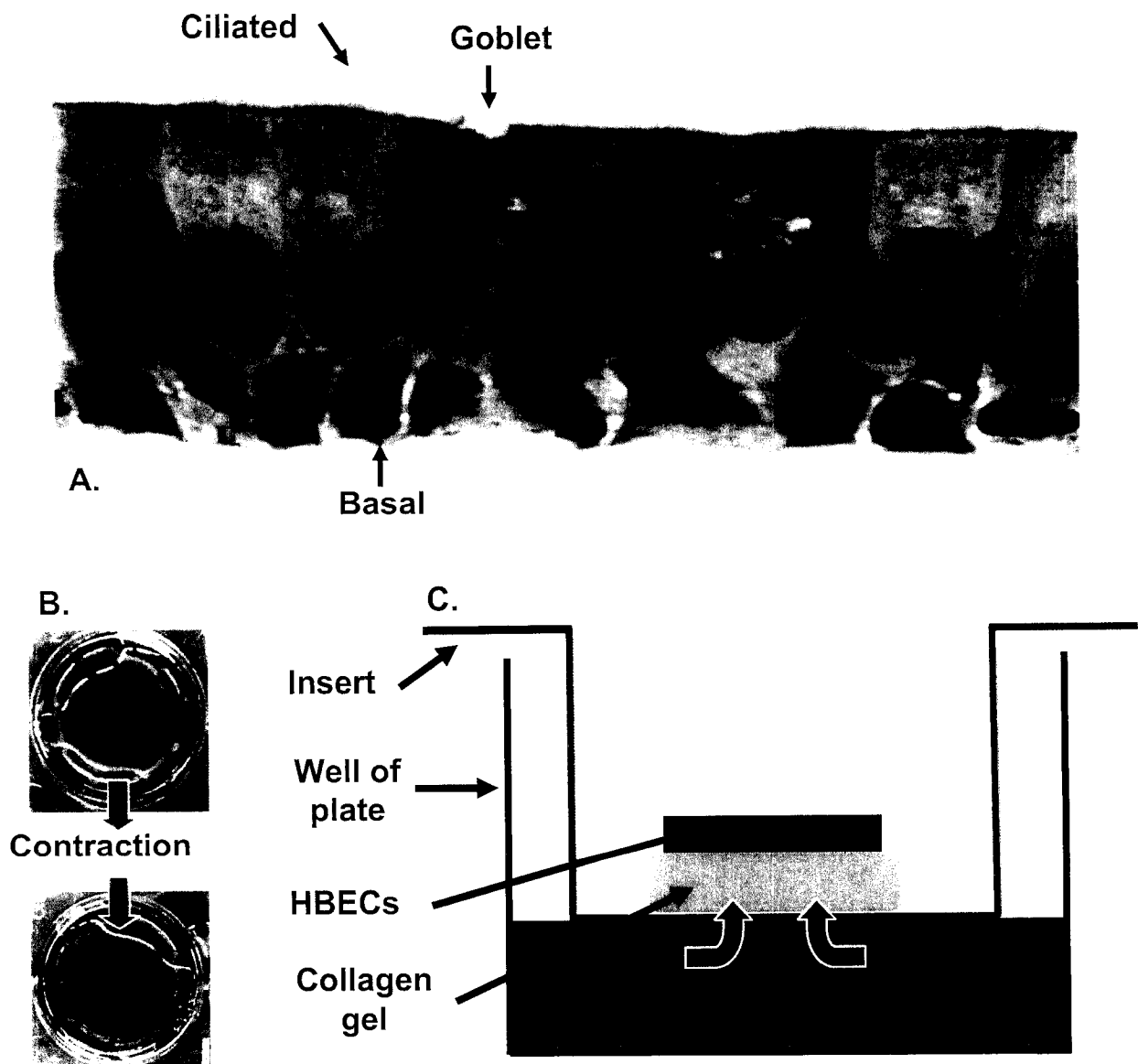


Figure 2

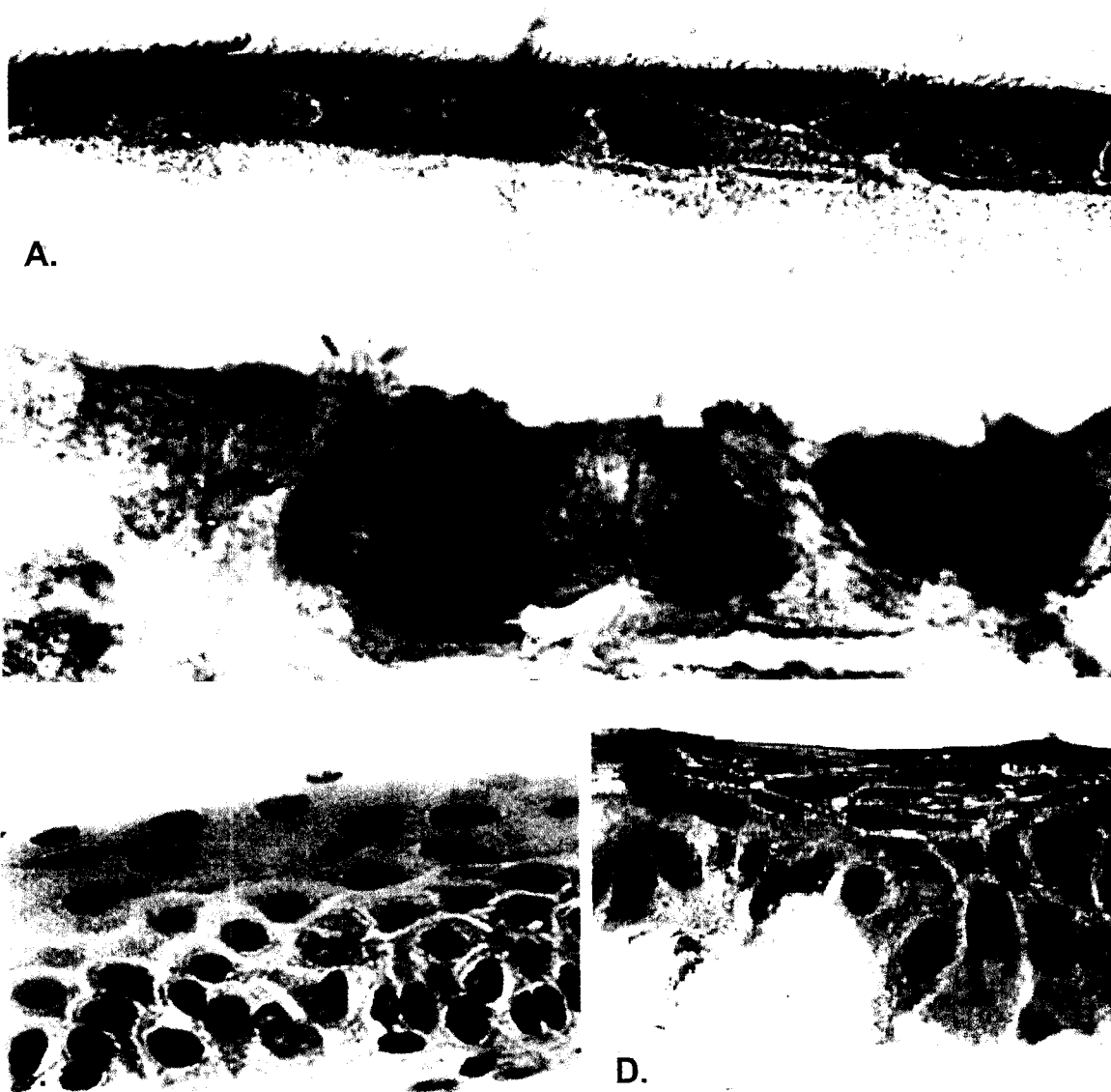


Figure 3

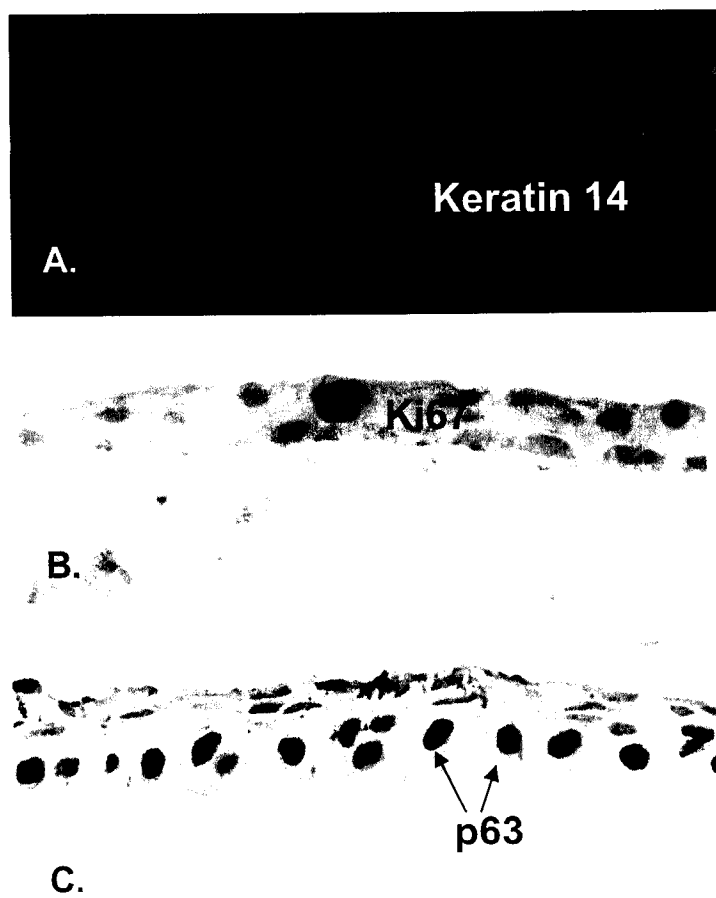
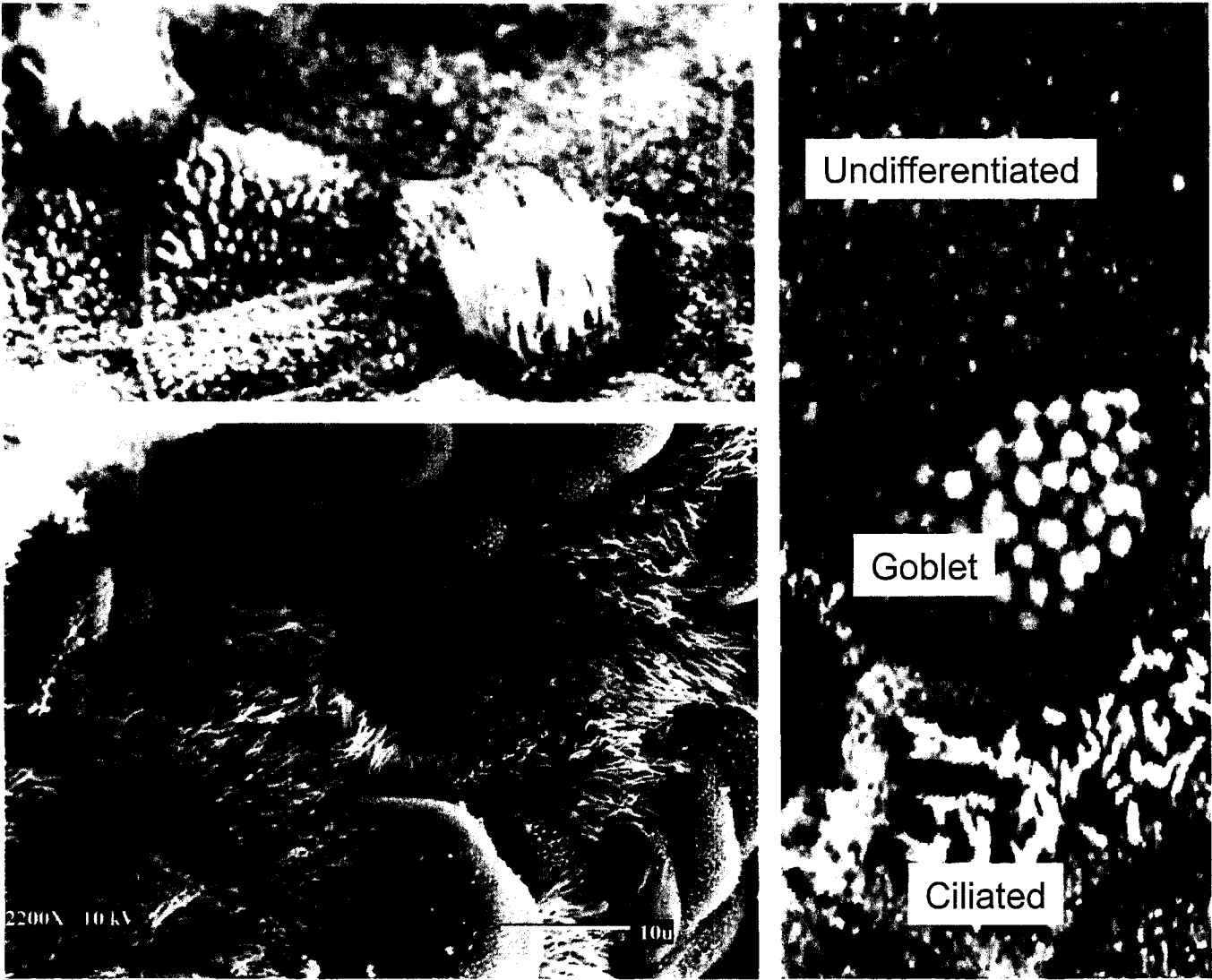


Figure 4





Lung Cancer Preneoplasia

Ignacio I. Wistuba¹ and Adi F. Gazdar²

¹Department of Pathology, Thoracic/Head and Neck Medical Oncology, M.D. Anderson Cancer Center, University of Texas, Houston, Texas 77030; email: iiwistuba@mdanderson.org

²Department of Pathology, Hamon Center for Therapeutic Oncology Research, University of Texas Southwestern Medical Center, Dallas, Texas 75390; email: adi.gazdar@utsouthwestern.edu

Annu. Rev. Pathol. Mech. Dis.
2006. 1:331–48

The *Annual Review of
Pathology: Mechanisms of
Disease* is online at
pathmechdis.annualreviews.org

doi: 10.1146/
annurev.pathol.1.110304.100103

Copyright © 2006 by
Annual Reviews. All rights
reserved

1553-4006/06/0114-
0331\$20.00

Key Words

smoking, bronchial dysplasia, atypical adenomatous hyperplasia, EGFR mutations

Abstract

From histological and biological perspectives, lung cancer is a complex neoplasm. Although the sequential preneoplastic changes have been defined for centrally arising squamous carcinomas of the lung, they have been poorly documented for the other major forms of lung cancers, including small cell lung carcinoma and adenocarcinomas. There are three main morphologic forms of preneoplastic lesions recognized in the lung: squamous dysplasias, atypical adenomatous hyperplasia, and diffuse idiopathic pulmonary neuroendocrine cell hyperplasia. However, these lesions account for the development of only a subset of lung cancers. Several studies have provided information regarding the molecular characterization of lung preneoplastic changes, especially for squamous cell carcinoma. These molecular changes have been detected in the histologically normal and abnormal respiratory epithelium of smokers. Two different molecular pathways have been detected in lung adenocarcinoma pathogenesis: smoking-associated activation of KRAS signaling, and nonsmoking-associated activation of EGFR signaling; the latter is detected in histologically normal respiratory epithelium.

small cell
lung carcinoma
non-small
cell lung carcinoma
carcinoma in
situ
atypical
adenomatous
hyperplasia

INTRODUCTION

Lung cancer is the leading cause of cancer deaths in the United States and worldwide (1). The high mortality rate of this disease is due primarily to the fact that the majority of lung cancers are diagnosed at advanced stages when the options for treatment are mostly palliative. Experience with other epithelial tumors, such as uterine, cervical, esophageal, and colon carcinomas, has shown that if neoplastic lesions can be detected and treated at their intraepithelial stage the chances for survival can be improved significantly. Thus, to reduce the mortality rate of lung cancer, new techniques and approaches must be developed to diagnose and treat pre-invasive lesions. However, the early diagnosis of lung cancer represents an enormous challenge. From histopathological and biological perspectives, lung cancer is a highly complex neoplasm (2), probably having multiple preneoplastic pathways.

Lung cancer consists of several histological types, including small cell lung carcinoma (SCLC) and non-small cell lung carcinoma (NSCLC) types of squamous cell carcinoma, adenocarcinoma (including the noninvasive type of bronchioloalveolar carcinoma), and large cell carcinoma (3). Lung cancers may arise from the major bronchi (central tumors) or small bronchi, bronchioles, or alveoli (peripheral tumors) of the distant airway of the lung. Squamous cell carcinomas and SCLCs usually arise centrally, whereas adenocarcinomas and large cell carcinomas usually arise peripherally. However, the specific respiratory epithelial cell type from which each lung cancer type develops has not been established. As with other epithelial malignancies, researchers believe lung cancers arise after a series of progressive pathological changes, known as preneoplastic or premalignant lesions (4). Although the sequential preneoplastic changes have been defined for centrally arising squamous carcinomas of the lung, they have been poorly doc-

umented for the other major forms of lung cancers (4).

Although many molecular abnormalities have been described in clinically evident lung cancers (2), relatively little is known about the molecular events preceding the development of lung carcinomas and the underlying genetic basis of lung carcinogenesis. In the past decade, several studies have provided information regarding the molecular characterization of the preneoplastic changes involved in the pathogenesis of lung cancer, especially squamous cell carcinoma and adenocarcinoma (5, 6). Many of these molecular changes have been detected in the histologically normal respiratory mucosa of smokers (5).

The high-risk population targeted for early detection efforts are heavy smokers and patients who have survived a cancer of the upper aerodigestive tract. However, conventional morphologic methods for the identification of premalignant cell populations in the lung airways have important limitations. This has led to research in biological properties, including molecular and genetic changes, of the respiratory epithelium and its corresponding preneoplastic cells and lesions. Further research in this area may provide new methods for assessing the likelihood of developing invasive lung cancer in smokers and allow for early detection and monitoring of their response to chemopreventive regimens.

In this review we will describe the recognized preneoplastic lesions for major types of lung cancers, such as bronchial squamous dysplasia and carcinoma in situ (CIS) for squamous cell carcinoma (7); atypical adenomatous hyperplasia (AAH), a putative preneoplastic lesion, for a subset of adenocarcinomas (6); and neuroendocrine cell hyperplasia for neuroendocrine lung carcinomas (7). In addition, we will review the current concepts of early pathogenesis and the progression of lung cancer.

OVERVIEW OF LUNG CANCER MOLECULAR PATHOLOGY

Several molecular and genetic studies have revealed that multiple genetic and epigenetic changes are found in clinically evident lung cancers, involving known and putative recessive oncogenes (tumor suppressor genes, TSG) as well as several dominant oncogenes (8). Most of the molecular and genetic studies of lung cancers have been performed on the major types of lung cancer (2). Many growth factors or regulatory peptides and their receptors are overexpressed by cancer cells and adjacent normal-appearing cells in the lung, and thus provide a series of autocrine and paracrine growth stimulatory loops in this neoplasm (9). The list of recessive oncogenes involved in lung cancer is likely to include as many as 10 to 15 known and putative genes (2), and possibly many more. Oncogenes that contribute to the pathogenesis of lung cancer include *CMYC*, mutated *KRAS* (10% to 20%, predominantly adenocarcinomas), overexpression of *Cyclin D1* and *BCL2*, and mutations in *ERBB* family genes such as *EGFR* (epidermal growth factor receptor) (10–12) and *HER2/neu* (12, 13). The latter two oncogenes occur almost exclusively in adenocarcinomas, patients of East Asian ethnic groups, and non- or light smokers (12). Several TSGs, such as *TP53* (17p13), *RB* (13q14), *p16^{INK4a}* (9p21), and new candidate TSGs at several chromosomal regions, including the short arm of chromosomes 3 (3p12, *DUTTI* gene; 3p14.2, *FHIT* gene; 3p21, *RASFF1A* and *FUS-1* gene; 3p22–24, *BAP-1* gene), show frequent abnormalities in lung cancer (2). Recessive oncogenes are believed to be inactivated via a two-step process involving both alleles. Knudson has proposed that the first hit is frequently a point mutation, whereas the second allele is subsequently inactivated via a chromosomal deletion, translocation, or other event such as methylation of gene promoter regions (14). In addition to those specific genetic changes, other evidence indicates that genetic instability is concurrent with lung cancer. This

evidence includes changes in the number of short-tandem DNA repeats (also known as microsatellites), which are frequently present in a wide variety of cancer types, including lung. Overall, an average of 35% (range 0%–76%) of SCLCs and 22% (range 2%–49%) of NSCLCs show some evidence of genetic instability at individual loci (8).

Studies of many lung cancers have demonstrated different patterns of molecular alterations between the two major groups of lung carcinomas (SCLC and NSCLC) (15, 16) and among the two major histologic types of NSCLC (squamous cell carcinomas and adenocarcinomas) (17–20). Allelic loss analyses at different chromosomal regions and the methylation status of multiple genes have provided clear evidence, on a genome-wide scale, that SCLC and NSCLC differ significantly in the TSGs that are inactivated during their pathogenesis (21–24). In addition, a variety of studies on gene expression profiles have sought to identify specific profiles and new molecular markers for histologically different lung cancers, including adenocarcinomas (25, 26). Specifically, we have found different patterns of allelic loss involving the two major histologic types of NSCLC, with higher incidences of deletions at 17p13 (*TP53*), 13q14 (*RB*), 9p21 (*p16^{INK4a}*), 8p21–23, and several 3p regions in squamous cell carcinomas (17, 27, 28). Recently, differences in *p16^{INK4a}*, *APC*, and *H-cadherin* gene methylation frequencies have been detected between squamous cell and adenocarcinoma, suggesting that different gene methylation patterns characterize the two major histologic types of NSCLC (24). Recent findings indicate that mutations in three genes, *KRAS*, *EGFR*, and *Her2/neu*, occur almost exclusively in lung cancers of adenocarcinoma histology (12, 29). In lung adenocarcinoma, *KRAS* and *EGFR* mutations are mutually exclusive, which indicates two distinct pathways for lung adenocarcinoma development (12, 30). Whereas in smokers tobacco-related carcinogens favor *KRAS* mutations, in nonsmokers unidentified carcinogens induce *EGFR* mutations (30).

TSG: tumor suppressor gene

EGFR: epidermal growth factor receptor

We refer to nonsmokers as people who have never smoked.

LUNG CANCER PRENEOPLASTIC LESIONS

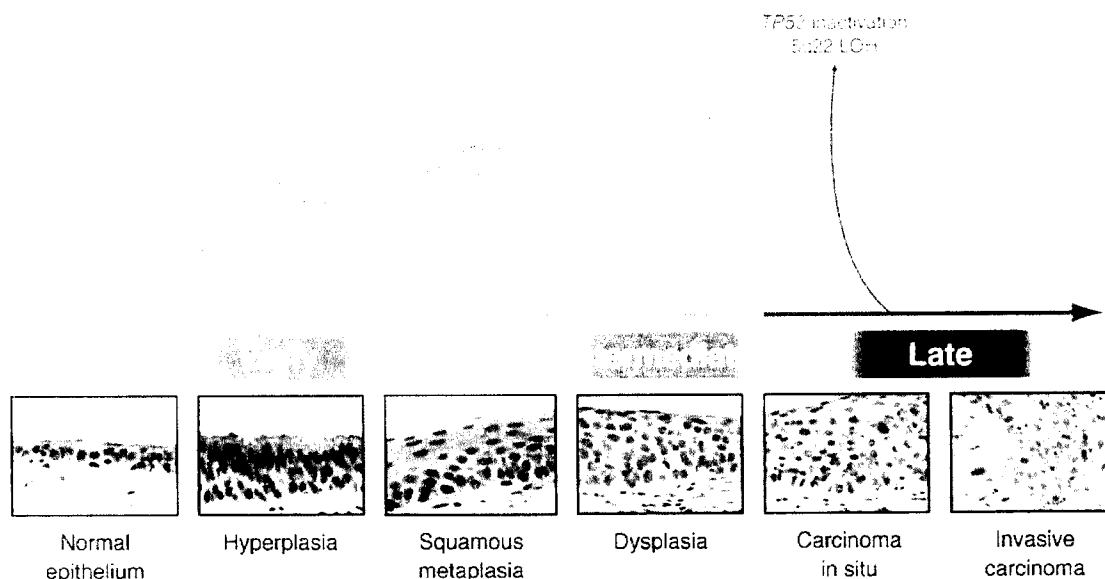
Lung cancers are believed to arise after a series of progressive pathological changes (preneoplastic or precursor lesions) in the respiratory mucosa. Although the sequential preneoplastic changes have been defined for centrally arising squamous carcinomas, they have been poorly documented for large cell carcinomas, adenocarcinomas, and SCLCs (4, 7). Mucosal changes in the large airways that may precede invasive squamous cell carcinoma include squamous dysplasia and CIS (4, 7). Adenocarcinomas may be preceded by morphological changes including AAH (4, 6) in peripheral airway cells. For SCLC, no specific preneoplastic changes have been described in the respiratory epithelium. Current information suggests that preneoplastic lesions are frequently extensive and multifocal throughout the lung, indicating a field effect (field cancerization) by which much of the respiratory epithelium has been mutagenized, presumably from exposure to tobacco-related carcinogens (5).

The recent histological classification of pre-invasive lung lesions by the World Health Organization (WHO) lists three main morphologic forms of preneoplastic lesions (3): (a) squamous dysplasia and CIS, (b) AAH, and (c) diffuse idiopathic pulmonary neuroendocrine cell hyperplasia (DIPNECH). However, as we will explain in this review, these lesions account for the development of only a subset of lung cancers.

Squamous Cell Carcinoma Preneoplastic Lesions

Mucosal changes in the large airways that may precede or accompany invasive squamous cell carcinoma include hyperplasia, squamous metaplasia, squamous dysplasia, and CIS (Figure 1) (4, 7). Two types of bronchial ep-

ithelial hyperplasia that are thought to be reactive lesions, goblet cell hyperplasia and basal cell (reserve cell) hyperplasia, may occur. Dysplastic squamous lesions are considered true preneoplastic lesions and may vary in degree (i.e., mild, moderate, or severe); however, these lesions represent a continuum of cytologic and histologic atypical changes that may show some overlapping features between categories. Whereas mild squamous dysplasia is characterized by minimal architectural and cytological disturbance, moderate dysplasia exhibits more cytological irregularity, which is even higher in severe dysplasia and is accompanied by considerable cellular polymorphism. In a subset of squamous dysplastic changes, the basal membrane thickens and there is vascular budding in the subepithelial tissues that results in papillary protrusions of the epithelium, lesions that have been termed angiogenic squamous dysplasia (31). CIS demonstrates extreme cytological aberrations with almost complete architectural disarray, but with an intact basement membrane and absence of stromal invasion. Foci of CIS usually arise near bifurcations in the segmental bronchi, subsequently extending proximally into the adjacent lobar bronchus and distally into subsegmental branches. These lesions are often not detected by conventional white-light bronchoscopy or gross examination. However, the utilization of fluorescent bronchoscopy, such as lung-imaging fluorescent endoscopy (LIFE), greatly increases the sensitivity for detection of squamous dysplastic and CIS lesions (32–34). Little is known about the rate and risks of progression from squamous dysplasia to CIS and ultimately to invasive squamous cell carcinoma. Recently, a longitudinal study addressing the natural histopathologic course of squamous preneoplastic lesions in bronchial epithelium using white-light and fluorescent bronchoscopy examinations was reported (35). In this study, the progression rate to CIS and invasive carcinoma was significantly higher in lesions with severe dysplasia (32%) compared with squamous metaplasias (4%) and low-grade



Histopathological and molecular changes during the pathogenesis of squamous cell carcinoma of the lung with molecular changes commencing at early stages, and a histologically normal respiratory epithelium. There is stepwise molecular and histopathological sequence of events leading to dysplastic and invasive carcinoma stages. LOH, loss of heterozygosity.

dysplasias (9%). Somewhat striking, at the individual level, the rates of progression to squamous carcinoma were not significantly higher in individuals harboring high-grade dysplastic lesions (39%) compared with individuals having only lower-grade lesions (26%). In addition, the study detected the progression from squamous metaplasia and low-grade dysplasias (mild and moderate) to CIS and invasive carcinoma, suggesting that a stepwise histopathologic multistage development of lung squamous cell carcinoma does not always occur, or it is not always detected because of rapid progression. These findings suggest that the current histologic classification of preneoplastic squamous lesions of the bronchial epithelia may not be a reliable guide for risk assessment of lung cancer. Other types of biomarkers, including molecular and genetic markers, are needed.

There are no squamous cells in the normal airways. The progenitor or stem cells for the squamous metaplastic epithelium of the prox-

imal airway is not known, but it is presumed that the basal cells represent a relatively quiescent zone that is the precursor of preneoplastic epithelium. In fact, squamous metaplasia usually precedes and accompanies basal cell hyperplasia. Interestingly, these cells express significant levels of Egfr protein and increased proliferative activity measured by Ki-67 staining (36, 37).

The current working model of the sequential molecular abnormalities in the pathogenesis of squamous cell lung carcinoma (**Figure 1**) indicates the following: (a) Genetic abnormalities commence in histologically normal epithelium and grow with increasing severity of histologic changes (27). (b) Mutations follow a sequence, with progressive allelic losses at multiple 3p (3p21, 3p14, 3p22-24, and 3p12) chromosome sites and 9p21 (*p16^{INK4a}*) as the earliest detectable changes. Later changes occur at 8p21-23, 13q14 (*RB*), and 17p13 (*TP53*) (17, 27, 28). *p16^{INK4a}* methylation has also been detected at an early

bronchioloalveolar carcinoma

stage of squamous pre-invasive lesions with a frequency that increases during histopathologic progression (by 24% in squamous metaplasia and 50% in CIS) (38). (c) Molecular changes in the respiratory epithelium are extensive and multifocal throughout the bronchial tree of smokers and lung cancer patients, indicating a field cancerization effect by which much of the respiratory epithelium has been mutagenized, presumably from exposure to tobacco-related carcinogens (27, 28, 39, 40). (d) Multiple small patches of histologically normal and hyperplastic epithelium with clonal and subclonal molecular abnormalities, not much larger in size than the average bronchial biopsy obtained by fluorescent bronchoscopy and estimated to be approximately 40,000 to 360,000 cells, such as allelic loss (chromosome 3p and 9p21 regions) and genetic instability, can be detected in the normal and slightly abnormal bronchial epithelium of patients with lung cancer (41). These findings are consistent with evidence of numerous small monosomic and trisomic clonal and subclonal patches present in smoking-damaged upper aerodigestive epithelium as determined by fluorescent in situ hybridization (FISH) analyses (42).

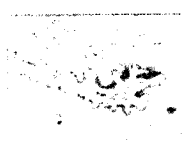
Adenocarcinoma Precursor Lesions

In alveoli, type I pneumocytes are involved in respiratory gas exchange whereas type II cells produce surfactant proteins, essential for preventing alveoli from collapsing (43). In bronchioles, short, stubby ciliated cells and the secretory Clara cells are present. The Clara cells and the type II pneumocytes are believed to be the progenitor cells of the peripheral airways, and peripherally arising adenocarcinomas often express markers of these cell types (44, 45). Researchers suggest that adenocarcinomas may be preceded by AAH in peripheral airway cells (4, 6); however, the respiratory structures and the specific epithelial cell types involved in the origin of most lung adenocarcinomas are unknown. Although there is only one sequence of morphologic change identi-

fied so far for the development of invasive lung adenocarcinomas (AAH and bronchioloalveolar carcinoma, BAC), recent data indicate that at least two molecular pathways are involved, the *KRAS* and *EGFR* pathways in smoker and nonsmoker populations, respectively (Figure 2).

Atypical adenomatous hyperplasia. AAH is considered a putative precursor of adenocarcinoma (4, 6). AAH is a discrete parenchymal lesion arising in alveoli near terminal and respiratory bronchioles (Figure 2) and may be single or multiple lesions. These lesions maintain an alveolar structure lined by rounded, cuboidal, or low columnar cells. The alveolar walls may be slightly thickened by collagen, occasional fibroblasts, and lymphocytes. Cellularity and cytological atypia vary from minimal to high grade. The postulated progression of AAH to adenocarcinoma with BAC features, which is characterized by the growth of neoplastic cells along pre-existing alveolar structures without evidences of stromal, pleural, or vascular invasion and without metastasis, is supported by morphometric, cytofluorometric, and molecular studies (6, 7). Distinction between highly atypical AAH and BAC is sometimes difficult. Somewhat arbitrarily, BAC are considered generally >10 mm in diameter, with more pleomorphism, mild stratification, packed cells, and abrupt transitions to adjacent alveolar lining cells. However, the distinction may, on occasion, be difficult. The differentiation phenotype derived from immunohistochemical and ultrastructural features indicates that AAHs originate from the progenitor cells of the peripheral airways (46, 47). Surfactant apoprotein and Clara cell-specific 10-kDd protein are expressed in almost all AAHs (46). As many as 25% of the cells show ultrastructural features of Clara cells and type II pneumocytes (47). Recent results from a study (48) performed in mice and lung cancer mouse models suggest that peripheral bronchioalveolar cells expressing Clara cell-specific protein and surfactant protein-C, and having in vitro stem

Peripheral airway epithelium



Normal
small bronchus



Normal
bronchiole



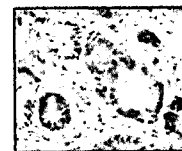
Normal
alveoli



AAH



BAC



Invasive
adenocarcinoma

Nonsmoker
Egfr
signaling pathway

Smoker
Ras
signaling pathway

Two molecular pathways involved in the development of lung cancer have been recognized. AAH, atypical adenomatous hyperplasia; BAC, bronchioloalveolar carcinoma.

cell properties (termed bronchioalveolar stem cell, BASC), are the stem cell population that maintains the bronchiolar Clara cells and alveolar cells of the distal respiratory epithelium. In vitro studies performed in the same study indicated that the BASC-transformed counterpart gives rise to adenocarcinoma of the lung. BASCs expanded in response to oncogenic *KRAS* in culture and in precursors of mouse lung tumors in vivo (48).

An increasing body of evidence supports the concept of AAH as the precursor of at least a subset of adenocarcinomas. AAH is most frequently detected in lungs of patients bearing lung cancers (9%–20%), especially adenocarcinomas (as many as 40%), compared with squamous cell carcinomas (11%) (7, 49–

52). In contrast, autopsy studies have reported AAH in ~3% of noncancer patients (53). Because inflation of the lungs prior to sectioning (a practice not common in the United States) aids identification, their true incidence may be higher than indicated. Some patients display a large number of AAH lesions (>40) in conjunction with multiple synchronous peripheral lung adenocarcinomas or BACs (51). However, it is extremely difficult to know the progression rate of AAH to lung adenocarcinoma, and it is also currently almost impossible to determine if AAHs may regress. Because they are air-filled structures, they may appear as ground glass opacities on computed tomography scans. However, AAH location, size, and relative invisibility to most imaging

methods make longitudinal studies even more difficult than centrally located squamous preneoplastic lesions.

Several molecular changes frequently present in lung adenocarcinomas are also present in AAH lesions, and they are further evidence that AAH may represent true preneoplastic lesions (46). The most important finding is the presence of *KRAS* (codon 12) mutations in as many as 39% of AAHs, which are also a relatively frequent alteration in lung adenocarcinomas (6, 54). Other molecular alterations detected in AAH are overexpression of Cyclin D1 (~70%), p53 (ranging from 10% to 58%), survivin (48%), and HER2/neu (7%) proteins (6, 55, 56). Some AAH lesions have demonstrated loss of heterozygosity (LOH) in chromosomes 3p (18%), 9p (*p16^{INK4a}*, 13%), 9q (53%), 17q, and 17p (*TP53*, 6%), changes that are frequently detected in lung adenocarcinomas (57, 58). A study on lung adenocarcinoma with synchronous multiple AAHs showed frequent LOH of tuberous sclerosis complex (TSC)-associated regions (*TSC1* at 9q, 53%, and *TSC2* at 16p, 6%), suggesting that these are candidate loci for TSG in a subset of adenocarcinomas of the lung (58). Some cases of AAH have been monoclonal, suggesting that it may be a true preneoplastic lesion (59). Activation of telomerase, required for the perpetuation of cancer cells and expressed by human telomerase RNA component and telomerase reverse transcriptase mRNA, has been detected in 27% to 78% of AAH lesions, depending on their atypia level (60). Recently, it was shown that loss of *LKB1*, a serine/threonine kinase that functions as a TSG, is frequent in lung adenocarcinomas (25%) and AAH (21%) with severe cytological atypia, whereas it is rare in mild atypical AAH lesions (5%), suggesting that *LKB1* inactivation may play a role in the AAH progression to malignancy (61).

Bronchial and bronchiolar epithelium as precursors of adenocarcinomas. Despite evidence that AAH is a precursor lesion for peripheral lung adenocarcinomas, there is

general consensus that the pathogenesis of many adenocarcinomas, especially those of central origin, is still unknown. The presence of *KRAS* mutations in bronchiolar epithelium with atypical changes raised the possibility that non-AAH lesions could also be the origin of lung adenocarcinomas (62). The recent findings of several distinct genetic changes specifically associated to lung adenocarcinoma, such as *EGFR* (10–12), *Her2/neu* (29), and *BRAF* (63) genes mutations, represent a unique opportunity to study further the pathogenesis of adenocarcinomas of the lung.

Somatic mutations of *EGFR*, a tyrosine kinase (TK) of the *ERBB* family, have been reported recently in a subset of lung adenocarcinomas (10–12, 64–67) (Figure 3). Those mutations are clinically relevant because most of them have been associated with sensitivity of lung adenocarcinoma to small molecule TK inhibitors (gefitinib and erlotinib) (10, 11, 64, 68). The mutations are associated significantly with adenocarcinoma histology, non- or light-smoker status, females, and East Asian ethnic groups (12). Data analysis from 13 (10, 12, 45, 65–67, 69–75) recently published studies on *EGFR* mutations in surgically resected specimens in more than 1600 lung cancers indicates that the incidence of mutations in adenocarcinomas is at least fourfold higher in East Asian populations (China, Japan, Korea, and Taiwan) compared with Western populations (Australia, Italy, and the United States) (Figure 3a). Analysis of 721 *EGFR* mutations reported from surgically resected (12, 65–67, 69–71, 73–75) and small-biopsy lung cancer specimens (10, 11, 71, 76–82) demonstrated that more than 90% of the mutations detected in *EGFR* are in-frame deletions in exon 19, and there was a single missense mutation in exon 21 (L858R) (10–12, 64–67) (Figure 3b). Researchers propose that lung cancer cells with mutant *EGFR* may become physiologically dependent on the continued activity of the gene for the maintenance of their malignant phenotype, which leads to accelerated development of lung adenocarcinoma (30). Recent studies indicate that

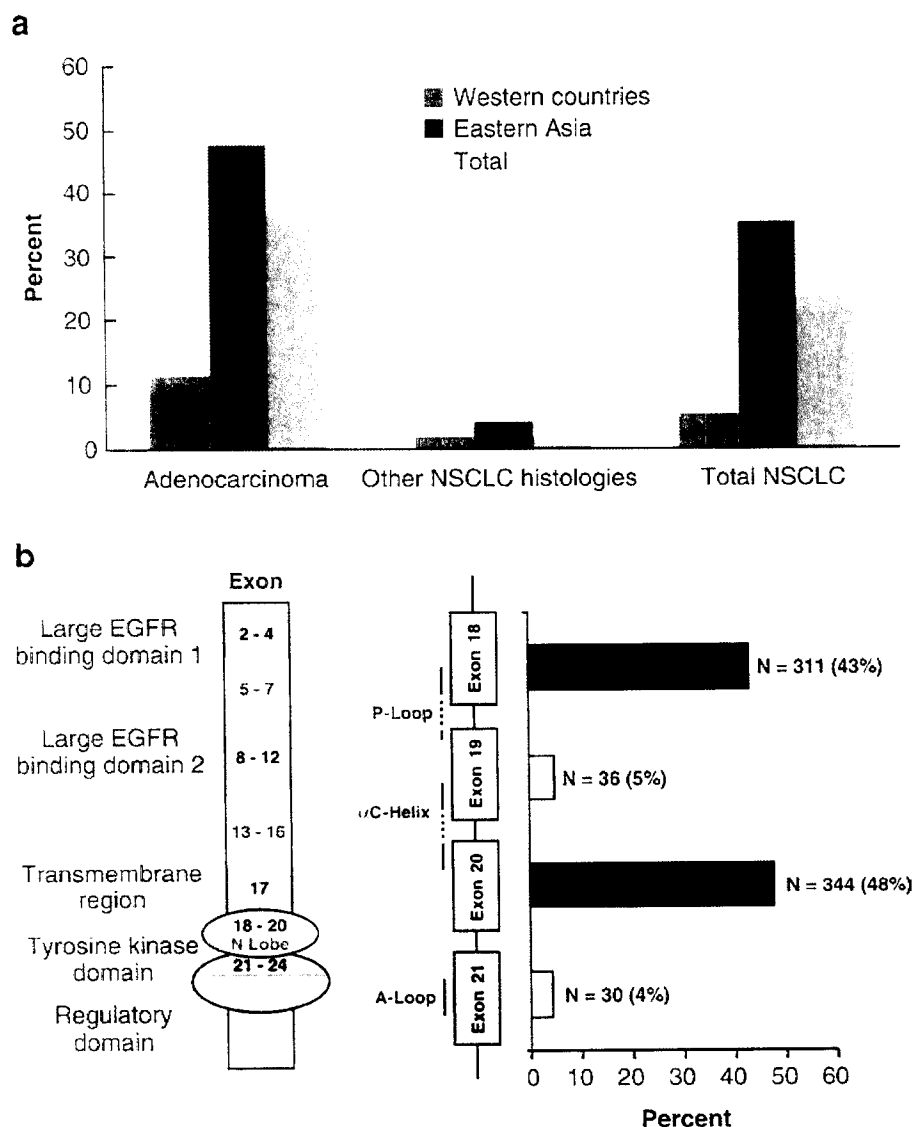


Figure 3

(a) Summary of epidermal growth factor receptor (*EGFR*) gene mutation frequency in lung cancer by histology and country of origin. Data analysis from 13 (10, 12, 45, 65–67, 69–75) recently published studies examining more than 1600 lung cancers have been summarized.

(b) Summary of exon distribution of 721 *EGFR* mutations reported from surgically resected (12, 65–67, 69–71, 73–75) and small-biopsy (10, 11, 71, 76–82) lung cancer specimens.

tumor cell high *EGFR* copy number, identified by FISH technique, and *Egfr* immunohistochemical expression may also be effective predictors for *EGFR* TK inhibitors (76, 79, 83).

Some studies have investigated *Egfr* expression in centrally located bronchial preneoplastic lesions of the lung (36, 84), which are considered markers for squamous metaplasia (84). In lung adenocarcinoma, recent

studies indicate that the recently identified TK domain of *EGFR* mutations is an early development in the pathogenesis of lung cancer, being identified in histologically normal epithelium of small bronchi and bronchioles adjacent to *EGFR* mutant adenocarcinomas (85). We have detected *EGFR* mutations in normal-appearing peripheral respiratory epithelium in 9 out of 21 (43%) adenocarcinoma patients (85), but not in patients without

diffuse idiopathic pulmonary neuroendocrine cell hyperplasia

mutation in the tumor (85). Our finding of more frequent *EGFR* mutations in normal epithelium within the tumor (43%) than in adjacent sites (24%) suggests a localized field effect phenomenon for this abnormality in the respiratory epithelium of the lung. A higher frequency of mutations in cells obtained from small bronchi (35%) compared with bronchioles (18%) was detected. This finding may correlate with different cell types populating those epithelia, which could represent the site of the cell of origin for *EGFR* mutant adenocarcinomas of the lung. Although the cell type having those mutations is unknown, we hypothesize that stem or progenitor cells of the bronchial and bronchiolar epithelium bear such mutations. The finding of relatively infrequent *EGFR* mutations in AAH lesions (3 out of 40 examined) (45, 86) and the finding of no mutation (12) or relatively low frequency of mutation in true BACs of the lung (86) support the concept that genetic abnormalities of *EGFR* are not relevant in the pathogenesis of alveolar-type lung neoplasia.

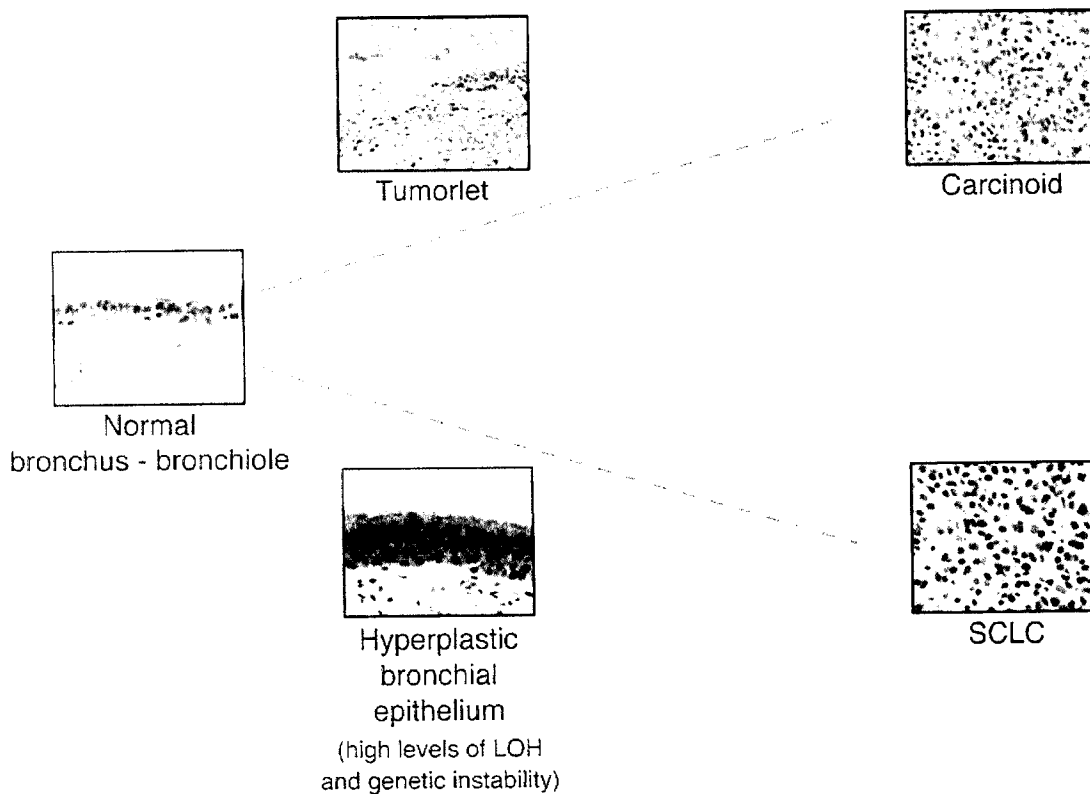
The low frequency of molecular abnormalities detected in the centrally located bronchial respiratory epithelium in patients with peripheral lung adenocarcinomas, compared with specimens from patients with squamous cell carcinomas and SCLC (87), suggests the presence of two compartments in the lung with different degrees of smoking-related genetic damage. Thus, smokers who develop squamous cell carcinoma and SCLC have more smoking-related genetic damage in the respiratory epithelium of the central airway, whereas patients who develop adenocarcinoma have damage mainly in the peripheral airways (small bronchus, bronchioles, and alveoli).

Precursor Lesions of Neuroendocrine Tumors

As stated above, the precursor lesions for the most common type of neuroendocrine carcinoma of the lung, the SCLC, are unknown (4, 7). However, a rare lesion termed dif-

fuse idiopathic pulmonary neuroendocrine cell hyperplasia (DIPNECH) has been associated with the development of other neuroendocrine tumors of the lung, typical and atypical carcinoids (4, 88, 89) (**Figure 4**). DIPNECH consists of a generalized proliferation of scattered single cells, small nodules, or linear proliferations of neuroendocrine cells present in the bronchial and bronchiolar epithelium. These lesions include local extraluminal proliferations in the form of tumorlets.

Small cell lung carcinoma precursors. As the development of epithelial cancers requires the stepwise accumulation of multiple mutations, which may represent a mutator phenotype, it is possible that those epithelial cell clones that have accumulated multiple mutations are at higher risk for developing malignant transformation (90). As stated before, no phenotypically identifiable epithelial lesion has been identified as a precursor for SCLC. We performed a study comparing the molecular changes (LOH at several chromosomal sites and microsatellite instability) occurring in histologically normal and mildly abnormal (hyperplastic), centrally located bronchial epithelium accompanying SCLCs and NSCLCs (squamous cell carcinomas and adenocarcinoma) (87). Normal and hyperplastic bronchial epithelium accompanying SCLC demonstrated a significantly higher incidence of genetic abnormalities than those adjacent to NSCLC tumor types (19). These findings indicate that more widespread and more extensive genetic damage is present in bronchial epithelium in patients with SCLC (**Figure 4**). The finding that some specimens of normal or mildly abnormal epithelia accompanying SCLCs have a high incidence of genetic changes (19) suggests that SCLC may arise directly from histologically normal or mildly abnormal epithelium, without passing through a more complex histologic sequence (parallel theory of cancer development).



Although the molecular information is limited, available data suggest that tumorlet is the potential precursor for lung carcinoids, and small cell lung carcinoma (SCLC) may arise from molecularly altered, histologically normal, or hyperplastic bronchial epithelium. LOH, loss of heterozygosity.

SMOKING-DAMAGED BRONCHIAL EPITHELIUM

After smoking cessation, the risk of developing lung cancer decreases, but never reaches baseline levels of nonsmokers (91). Advanced lung preneoplastic changes occur more frequently in smokers than nonsmokers, and they increase in frequency with the amount of smoke exposure, adjusted by age (92). Risk factors that identify normal and premalignant bronchial tissue for malignant progression need to be better defined. However, only scant information is available regarding molecular changes in the respiratory epithelium of smokers without cancer. Two independent studies show that the genetic changes

(loss of heterozygosity and microsatellite instability) found in invasive cancers and preneoplasia can also be identified in morphologically normal-appearing bronchial epithelium from current or former smokers, and they may persist for many years after smoking cessation (39, 40). In general, such genetic changes are not found in the bronchial epithelium from true nonsmokers. As has been observed in epithelial foci accompanying invasive lung carcinoma (27), allelic losses on chromosomes 3p and 9p are often present. These findings support the hypothesis that identifying genetic abnormalities, such as allelic losses, in biopsies may provide new methods for assessing the risk of smokers developing invasive

lung cancer and monitoring their response to chemoprevention.

We have demonstrated that molecular changes (allelic loss and genomic instability) in the bronchial epithelium may persist long after smoking cessation (39, 40). Of interest, Lee and colleagues (37) reported that smoking appears to elicit a dose-related proliferative response in the bronchial epithelia of active smokers measured by the Ki-67 proliferation index. Although the proliferative response decreased gradually in former smokers, a subset of individuals had detectable proliferation for many years after quitting smoking (37).

Recent results on methylation analysis of several genes, including *RAR β -2*, *H-cadherin*, *APC*, *p16^{INK4a}*, and *RASFF1A*, indicate that abnormal gene methylation is a relatively

frequent occurrence in oropharyngeal and bronchial epithelial cells in heavy smokers with evidence of sputum atypia (93). Methylation in one or more of three genes tested (*p16^{INK4a}*, *GSTP1*, and *DAPK*) has been demonstrated in bronchial brush specimens in approximately one third of smoker subjects (94). Aberrant promoter methylation of *p16^{INK4a}* was seen in at least one bronchial epithelial site from 44% of lung cancer patients and cancer-free smokers. No promoter methylation of these genes was detected in bronchial epithelium from nonsmokers. These results indicate that aberrant promoter hypermethylation of the *p16^{INK4a}* gene, and to a lesser extent, *DAPK*, occurs frequently in the bronchial epithelium of lung cancer patients and cancer-free smokers and persists after smoking cessation (95).

1. Lung cancer results from the accumulation of multiple genetic and epigenetic changes. Different patterns of molecular alterations have been detected among the major lung cancer histology types.
2. Recent findings indicate that mutation of *KRAS*, *EGFR*, and *Her2/neu* genes occur almost exclusively in lung cancer of adenocarcinoma histology.
3. There are three main morphologic forms of preneoplastic lesions recognized in the lung: squamous dysplasias, atypical adenomatous hyperplasia, and diffuse idiopathic pulmonary neuroendocrine cell hyperplasia. However, these lesions account for the development of only a subset of lung cancers.
4. For squamous cell carcinoma of the lung, the current working model indicates a stepwise sequence of molecular and histopathological changes, with the molecular abnormalities starting in histologically normal and mildly abnormal epithelia.
5. AAH is considered a putative precursor of a subset of lung adenocarcinoma, and they demonstrate similar molecular changes than invasive tumors.
6. Two different molecular pathways have been detected in lung adenocarcinoma pathogenesis: smoking-related pathways associated with *KRAS* mutations and nonsmoking-related pathways associated with *EGFR* mutations; the latter are detected in histologically normal respiratory epithelium.
7. Molecular changes detected in lung tumors and associated preneoplastic lesions have been detected in smoking-damaged epithelium of smokers, including histologically normal bronchial epithelium.

8. Molecular changes in the respiratory epithelium are extensive and multifocal throughout the bronchial tree of smokers and lung cancer patients, indicating a field effect (i.e., field cancerization).

ACKNOWLEDGMENTS

The authors were supported by grant 5U01CA8497102, Specialized Program of Research Excellence (SPORE) in Lung Cancer grant P50CA70907 from the National Cancer Institute, Bethesda, MD (I.L.W. and A.E.G.), and the Department of Defense grant W81XWH-04-1-0142 (I.L.W.).

LITERATURE CITED

1. Jemal A, Murray T, Ward E, Samuels A, Tiwari RC, et al. 2005. Cancer statistics, 2005. *CA Cancer J. Clin.* 55:10–30
2. Minna JD, Gazdar A. 2002. Focus on lung cancer. *Cancer Cell* 1:49–52
3. Travis WD, Brambilla E, Muller-Hermelink HK, Harris CC. 2004. Tumours of the lung. In *Pathology and Genetics: Tumours of the Lung, Pleura, Thymus and Heart*, ed. WD Travis, E Brambilla, HK Muller-Hermelink, CC Harris, pp. 9–124. Lyon: IARC
4. Colby TV, Wistuba II, Gazdar A. 1998. Precursors to pulmonary neoplasia. *Adv. Anat. Pathol.* 5:205–15
5. Wistuba II, Mao L, Gazdar AF. 2002. Smoking molecular damage in bronchial epithelium. *Oncogene* 21:7298–306
6. Westra WH. 2000. Early glandular neoplasia of the lung. *Respir. Med.* 1:163–69
7. Kerr KM. 2001. Pulmonary preinvasive neoplasia. *J. Clin. Pathol.* 54:257–71
8. Zochbauer-Muller S, Minna JD. 2000. The biology of lung cancer including potential clinical applications. *Chest Surg. Clin. N. Am.* 10:691–708
9. Viallet J, Sausville EA. 1996. Involvement of signal transduction pathways in lung cancer biology. *J. Cell Biochem. Suppl.* 24:228–36
10. Paez JG, Janne PA, Lee JC, Tracy S, Greulich H, et al. 2004. EGFR mutations in lung cancer: correlation with clinical response to gefitinib therapy. *Science* 304:1497–500
11. Lynch TJ, Bell DW, Sordella R, Gurubhagavatula S, Okimoto RA, et al. 2004. Activating mutations in the epidermal growth factor receptor underlying responsiveness of non-small-cell lung cancer to gefitinib. *N. Engl. J. Med.* 350:2129–39
12. Shigematsu H, Lin L, Takahashi T, Nomura M, Suzuki M, et al. 2005. Clinical and biological features associated with epidermal growth factor receptor gene mutations in lung cancers. *J. Natl. Cancer Inst.* 97:339–46
13. Stephens P, Hunter C, Bignell G, Edkins S, Davies H, et al. 2004. Lung cancer: intragenic ERBB2 kinase mutations in tumours. *Nature* 431:525–26
14. Knudson AG. 1989. Hereditary cancers disclose a class of cancer genes. *Cancer* 63:1888–91
15. Virmani AK, Fong KM, Kodagoda D, McIntire D, Hung J, et al. 1998. Allelotyping demonstrates common and distinct patterns of chromosomal loss in human lung cancer types. *Genes Chromosomes Cancer* 21:308–19
16. Girard L, Zochbauer-Muller S, Virmani AK, Gazdar AF, Minna JD. 2000. Genome-wide allelotyping of lung cancer identifies new regions of allelic loss, differences between small cell lung cancer and non-small cell lung cancer, and loci clustering. *Cancer Res.* 60:4894–906

17. Wistuba II, Behrens C, Virmani AK, Milchgrub S, Syed S, et al. 1999. Allelic losses at chromosome 8p21-23 are early and frequent events in the pathogenesis of lung cancer. *Cancer Res.* 59:1973-79
18. Shivapurkar N, Virmani AK, Wistuba II, Milchgrub S, Mackay B, et al. 1999. Deletions of chromosome 4 at multiple sites are frequent in malignant mesothelioma and small cell lung carcinoma. *Clin. Cancer Res.* 5:17-23
19. Wistuba II, Berry J, Behrens C, Maitra A, Shivapurkar N, et al. 2000. Molecular changes in the bronchial epithelium of patients with small cell lung cancer. *Clin. Cancer Res.* 6:2604-10
20. Wistuba II, Behrens C, Virmani AK, Mele G, Milchgrub S, et al. 2000. High resolution chromosome 3p allelotyping of human lung cancer and preneoplastic/preinvasive bronchial epithelium reveals multiple, discontinuous sites of 3p allele loss and three regions of frequent breakpoints. *Cancer Res.* 60:1949-60
21. Zochbauer-Muller S, Fong KM, Virmani AK, Geradts J, Gazdar AF, Minna JD. 2001. Aberrant promoter methylation of multiple genes in non-small cell lung cancers. *Cancer Res.* 61:249-55
22. Virmani AK, Rahti A, Zöchbauer-Muller S, Sacchi N, Fukuyama Y, et al. 2000. Promoter methylation and silencing of the retinoic acid receptor beta gene in lung carcinomas. *J. Natl. Cancer Inst.* 92:1303-7
23. Burbee DG, Forgacs E, Zochbauer-Muller S, Shivakumar L, Fong K, et al. 2001. Epigenetic inactivation of RASSF1A in lung and breast cancers and malignant phenotype suppression. *J. Natl. Cancer Inst.* 93:691-99
24. Toyooka S, Maruyama R, Toyooka KO, McLerran D, Feng Z, et al. 2003. Smoke exposure, histologic type and geography-related differences in the methylation profiles of non-small cell lung cancer. *Int. J. Cancer* 103:153-60
25. Bhattacharjee A, Richards WG, Staunton J, Li C, Monti S, et al. 2001. Classification of human lung carcinomas by mRNA expression profiling reveals distinct adenocarcinoma subclasses. *Proc. Natl. Acad. Sci. USA* 98:13790-95
26. Beer DG, Kardia SL, Huang CC, Giordano TJ, Levin AM, et al. 2002. Gene-expression profiles predict survival of patients with lung adenocarcinoma. *Nat. Med.* 8:816-24
27. Wistuba II, Behrens C, Milchgrub S, Bryant D, Hung J, et al. 1999. Sequential molecular abnormalities are involved in the multistage development of squamous cell lung carcinoma. *Oncogene* 18:643-50
28. Wistuba II, Behrens C, Virmani AK, Mele G, Milchgrub S, et al. 2000. High resolution chromosome 3p allelotyping of human lung cancer and preneoplastic/preinvasive bronchial epithelium reveals multiple, discontinuous sites of 3p allele loss and three regions of frequent breakpoints. *Cancer Res.* 60:1949-60
29. Shigematsu H, Takahashi T, Nomura M, Majmudar K, Suzuki M, et al. 2005. Somatic mutations of the HER2 kinase domain in lung adenocarcinomas. *Cancer Res.* 65:1642-46
30. Gazdar AF, Shigematsu H, Herz J, Minna JD. 2004. Mutations and addiction to EGFR: the Achilles 'heel' of lung cancers? *Trends Mol. Med.* 10:481-86
31. Keith RL, Miller YE, Gemmill RM, Drabkin HA, Dempsey EC, et al. 2000. Angiogenic squamous dysplasia in bronchi of individuals at high risk for lung cancer. *Clin. Cancer Res.* 6:1616-25
32. Lam S, Kennedy T, Unger M, Miller YE, Gelmont D, et al. 1998. Localization of bronchial intraepithelial neoplastic lesions by fluorescence bronchoscopy. *Chest* 113:696-702
33. Kennedy TC, Lam S, Hirsch FR. 2001. Review of recent advances in fluorescence bronchoscopy in early localization of central airway lung cancer. *Oncologist* 6:257-62

34. Hirsch FR, Prindiville SA, Miller YE, Franklin WA, Dempsey EC, et al. 2001. Fluorescence versus white-light bronchoscopy for detection of preneoplastic lesions: a randomized study. *J. Natl. Cancer Inst.* 93:1385–91
35. Breuer RH, Pasic A, Smit EF, van Vliet E, Vonk Noordegraaf A, et al. 2005. The natural course of preneoplastic lesions in bronchial epithelium. *Clin. Cancer Res.* 11:537–43
36. Hirsch FR, Franklin WA, Gazdar AF, Bunn PA Jr. 2001. Early detection of lung cancer: clinical perspectives of recent advances in biology and radiology. *Clin. Cancer Res.* 7:5–22
37. Lee JJ, Liu D, Lee JS, Kurie JM, Khuri FR, et al. 2001. Long-term impact of smoking on lung epithelial proliferation in current and former smokers. *J. Natl. Cancer Inst.* 93:1081–88
38. Belinsky SA, Nikula KJ, Palmisano WA, Michels R, Saccomanno G, et al. 1998. Aberrant methylation of p16(INK4a) is an early event in lung cancer and a potential biomarker for early diagnosis. *Proc. Natl. Acad. Sci. USA* 95:11891–96
39. Wistuba II, Lam S, Behrens C, Virmani AK, Fong KM, et al. 1997. Molecular damage in the bronchial epithelium of current and former smokers. *J. Natl. Cancer Inst.* 89:1366–73
40. Mao L, Lee JS, Kurie JM, Fan YH, Lippman SM, et al. 1997. Clonal genetic alterations in the lungs of current and former smokers. *J. Natl. Cancer Inst.* 89:857–62
41. Park IW, Wistuba II, Maitra A, Milchgrub S, Virmani AK, et al. 1999. Multiple clonal abnormalities in the bronchial epithelium of patients with lung cancer. *J. Natl. Cancer Inst.* 91:1863–68
42. Hittelman WN. 1999. Molecular cytogenetic evidence for multistep tumorigenesis: implications for risk assessment and early detection. In *Molecular Pathology of Early Cancer*, ed. S Srivastava, AF Gazdar, DE Henson, pp. 385–404. Van Demanstratt, Netherlands: IOS
43. Gartner LP, Hiatt JL. 2001. Respiratory system. In *Color Textbook of Histology*, ed. LP Gartner, JL Hiatt, pp. 343–64. Philadelphia: Saunders
44. Yatabe Y, Mitsudomi T, Takahashi T. 2002. TTF-1 expression in pulmonary adenocarcinomas. *Am. J. Surg. Pathol.* 26:767–73
45. Yatabe Y, Kosaka T, Takahashi T, Mitsudomi T. 2005. EGFR mutation is specific for terminal respiratory unit type adenocarcinoma. *Am. J. Surg. Pathol.* 29:633–39
46. Kitamura H, Kameda Y, Ito T, Hayashi H. 1999. Atypical adenomatous hyperplasia of the lung. Implications for the pathogenesis of peripheral lung adenocarcinoma. *Am. J. Clin. Pathol.* 111:610–22
47. Osanai M, Igarashi T, Yoshida Y. 2001. Unique cellular features in atypical adenomatous hyperplasia of the lung: ultrastructural evidence of its cytodifferentiation. *Ultrastruct. Pathol.* 25:367–73
48. Kim CF, Jackson EL, Woolfenden AE, Lawrence S, Babar I, et al. 2005. Identification of bronchioalveolar stem cells in normal lung and lung cancer. *Cell* 121:823–35
49. Weng SY, Tsuchiya E, Kasuga T, Sugano H. 1992. Incidence of atypical bronchioalveolar cell hyperplasia of the lung: relation to histological subtypes of lung cancer. *Virchows Arch. A* 420:463–71
50. Nakanishi K. 1990. Alveolar epithelial hyperplasia and adenocarcinoma of the lung. *Arch. Pathol. Lab. Med.* 114:363–68
51. Chapman AD, Kerr KM. 2000. The association between atypical adenomatous hyperplasia and primary lung cancer. *Br. J. Cancer* 83:632–36
52. Koga T, Hashimoto S, Sugio K, Yonemitsu Y, Nakashima Y, et al. 2002. Lung adenocarcinoma with bronchioalveolar carcinoma component is frequently associated with foci of high-grade atypical adenomatous hyperplasia. *Am. J. Clin. Pathol.* 117:464–70

53. Yokose T, Doi M, Tanno K, Yamazaki K, Ochiai A. 2001. Atypical adenomatous hyperplasia of the lung in autopsy cases. *Lung Cancer* 33:155–61
54. Westra WH, Baas IO, Hruban RH, Askin FB, Wilson K, et al. 1996. K-ras oncogene activation in atypical alveolar hyperplasias of the human lung. *Cancer Res.* 56:2224–28
55. Tominaga M, Sueoka N, Irie K, Iwanaga K, Tokunaga O, et al. 2003. Detection and discrimination of preneoplastic and early stages of lung adenocarcinoma using hmRNP B1, combined with the cell cycle-related markers p16, cyclin D1, and Ki-67. *Lung Cancer* 40:45–53
56. Nakanishi K, Kawai T, Kumaki F, Hiroi S, Mukai M, Ikeda E. 2003. Survivin expression in atypical adenomatous hyperplasia of the lung. *Am. J. Clin. Pathol.* 120:712–19
57. Kitaguchi S, Takeshima Y, Nishisaka T, Inai K. 1998. Proliferative activity, p53 expression and loss of heterozygosity on 3p, 9 and 17p in atypical adenomatous hyperplasia of the lung. *Hiroshima J. Med. Sci.* 47:17–25
58. Takamochi K, Ogura T, Suzuki K, Kawasaki H, Kurashima Y, et al. 2001. Loss of heterozygosity on chromosome 9q and 16p in atypical adenomatous hyperplasia concomitant with adenocarcinoma of the lung. *Am. J. Pathol.* 159:1941–48
59. Niho S, Yokose T, Suzuki K, Kodama T, Nishiwaki Y, Mukai K. 1999. Monoclonality of atypical adenomatous hyperplasia of the lung. *Am. J. Pathol.* 154:249–54
60. Nakanishi K, Kawai T, Kumaki F, Hiroi S, Mukai M, Ikeda E. 2002. Expression of human telomerase RNA component and telomerase reverse transcriptase mRNA in atypical adenomatous hyperplasia of the lung. *Hum. Pathol.* 33:697–702
61. Ghaffar H, Sahin F, Sanchez-Cespedes M, Su GH, Zahurak M, Sidransky D, et al. 2003. LKB1 protein expression in the evolution of glandular neoplasia of the lung. *Clin. Cancer Res.* 9:2998–3003
62. Sugio K, Kishimoto Y, Virmani A, Hung JY, Gazdar AF. 1994. K-ras mutations are a relatively late event in the pathogenesis of lung carcinomas. *Cancer Res.* 54:5811–15
63. Brose MS, Volpe P, Feldman M, Kumar M, Rishi I, et al. 2002. BRAF and RAS mutations in human lung cancer and melanoma. *Cancer Res.* 62:6997–7000
64. Pao W, Miller V, Zakowski M, Doherty J, Politi K, et al. 2004. EGF receptor gene mutations are common in lung cancers from “never smokers” and are associated with sensitivity of tumors to gefitinib and erlotinib. *Proc. Natl. Acad. Sci. USA* 101:13306–11
65. Huang SF, Liu HP, Li LH, Ku YC, Fu YN, et al. 2004. High frequency of epidermal growth factor receptor mutations with complex patterns in non-small cell lung cancers related to gefitinib responsiveness in Taiwan. *Clin. Cancer Res.* 10:8195–203
66. Kosaka T, Yatabe Y, Endoh H, Kuwano H, Takahashi T, Mitsudomi T. 2004. Mutations of the epidermal growth factor receptor gene in lung cancer: biological and clinical implications. *Cancer Res.* 64:8919–23
67. Tokumo M, Toyooka S, Kiura K, Shigematsu H, Tomii K, et al. 2005. The relationship between epidermal growth factor receptor mutations and clinicopathologic features in non-small cell lung cancers. *Clin. Cancer Res.* 11:1167–73
68. Amann J, Kalyankrishna S, Massion PP, Ohm JE, Girard L, et al. 2005. Aberrant epidermal growth factor receptor signaling and enhanced sensitivity to EGFR inhibitors in lung cancer. *Cancer Res.* 65:226–35
69. Sonobe M, Manabe T, Wada H, Tanaka F. 2005. Mutations in the epidermal growth factor receptor gene are linked to smoking-independent, lung adenocarcinoma. *Br. J. Cancer* 93:355–63
70. Sasaki H, Shimizu S, Endo K, Takada M, Kawahara M, et al. 2005. EGFR and erbB2 mutation status in Japanese lung cancer patients. *Int. J. Cancer.* In press

71. Mu XL, Li LY, Zhang XT, Wang MZ, Feng RE, et al. 2005. Gefitinib-sensitive mutations of the epidermal growth factor receptor tyrosine kinase domain in chinese patients with non-small cell lung cancer. *Clin. Cancer Res.* 11:4289–94
72. Soung YH, Lee JW, Kim SY, Seo SH, Park WS, et al. 2005. Mutational analysis of EGFR and K-RAS genes in lung adenocarcinomas. *Virchows Arch.* 446:483–88
73. Yang SH, Mechanic LE, Yang P, Landi MT, Bowman ED, et al. 2005. Mutations in the tyrosine kinase domain of the epidermal growth factor receptor in non-small cell lung cancer. *Clin. Cancer Res.* 11:2106–10
74. Qin L, Tamasi J, Raggatt L, Li X, Feyen JH, et al. 2005. Amphiregulin is a novel growth factor involved in normal bone development and in the cellular response to parathyroid hormone stimulation. *J. Biol. Chem.* 280:3974–81
75. Marchetti A, Martella C, Felicioni L, Barassi F, Salvatore S, et al. 2005. EGFR mutations in non-small-cell lung cancer: analysis of a large series of cases and development of a rapid and sensitive method for diagnostic screening with potential implications on pharmacologic treatment. *J. Clin. Oncol.* 23:857–65
76. Tsao MS, Sakurada A, Cutz JC, Zhu CQ, Kamel-Reid S, et al. 2005. Erlotinib in lung cancer-molecular and clinical predictors of outcome. *N. Engl. J. Med.* 353:133–44
77. Zhang XT, Li LY, Mu XL, Cui QC, Chang XY, et al. 2005. The EGFR mutation and its correlation with response of gefitinib in previously treated Chinese patients with advanced non-small-cell lung cancer. *Ann. Oncol.* 16:1334–42
78. Chou TY, Chiu CH, Li LH, Hsiao CY, Tzen CY, et al. 2005. Mutation in the tyrosine kinase domain of epidermal growth factor receptor is a predictive and prognostic factor for gefitinib treatment in patients with non-small cell lung cancer. *Clin. Cancer Res.* 11:3750–57
79. Cappuzzo F, Hirsch FR, Rossi E, Bartolini S, Ceresoli GL, et al. 2005. Epidermal growth factor receptor gene and protein and gefitinib sensitivity in non-small-cell lung cancer. *J. Natl. Cancer Inst.* 97:643–55
80. Kim KS, Jeong JY, Kim YC, Na KJ, Kim YH, et al. 2005. Predictors of the response to gefitinib in refractory non-small cell lung cancer. *Clin. Cancer Res.* 11:2244–51
81. Mitsudomi T, Kosaka T, Endoh H, Horio Y, Hida T, et al. 2005. Mutations of the epidermal growth factor receptor gene predict prolonged survival after gefitinib treatment in patients with non-small-cell lung cancer with postoperative recurrence. *J. Clin. Oncol.* 23:2513–20
82. Han SW, Kim TY, Hwang PG, Jeong S, Kim J, et al. 2005. Predictive and prognostic impact of epidermal growth factor receptor mutation in non-small-cell lung cancer patients treated with gefitinib. *J. Clin. Oncol.* 23:2493–501
83. Hirsch FR, Varella-Garcia M, McCoy J, West H, Xavier AC, et al. 2005. Increased epidermal growth factor receptor gene copy number detected by fluorescence in situ hybridization associates with increased sensitivity to gefitinib in patients with bronchioloalveolar carcinoma subtypes: A Southwest Oncology Group Study. *J. Clin. Oncol.* 23:6838–45
84. Kurie JM, Shin HJ, Lee JS, Morice RC, Ro JY, et al. 1996. Increased epidermal growth factor receptor expression in metaplastic bronchial epithelium. *Clin. Cancer Res.* 2:1787–93
85. Tang X, Shigematsu H, Bekele BN, Roth JA, Minna JD, et al. 2005. EGFR tyrosine kinase domain mutations are detected in histologically normal respiratory epithelium in lung cancer patients. *Cancer Res.* 65:7568–72
86. Yoshida Y, Shibata T, Kokubu A, Tsuta K, Matsuno Y, et al. 2005. Mutations of the epidermal growth factor receptor gene in atypical adenomatous hyperplasia and bronchioloalveolar carcinoma of the lung. *Lung Cancer.* 50:1–8

87. Wistuba II, Berry J, Behrens C, Maitra A, Shivapurkar N, et al. 2000. Molecular changes in the bronchial epithelium of patients with small cell lung cancer. *Clin. Cancer Res.* 6:2604–10
88. Aguayo SM, Miller YE, Waldron JA Jr, Bogin RM, Sunday ME, et al. 1992. Brief report: idiopathic diffuse hyperplasia of pulmonary neuroendocrine cells and airways disease. *N. Engl. J. Med.* 327:1285–88
89. Armas OA, White DA, Erlanson RA, Rosai J. 1995. Diffuse idiopathic pulmonary neuroendocrine cell proliferation presenting as interstitial lung disease. *Am. J. Surg. Pathol.* 19:963–70
90. Loeb LA. 1991. Mutator phenotype may be required for multistage carcinogenesis. *Cancer Res.* 51:3075–79
91. Peto R, Darby S, Deo H, Silcocks P, Whitley E, Doll R. 2000. Smoking, smoking cessation, and lung cancer in the UK since 1950: combination of national statistics with two case-control studies. *Br. Med. J.* 321:323–29
92. Lam S, leRiche JC, Zheng Y, Coldman A, MacAulay C, et al. 1999. Sex-related differences in bronchial epithelial changes associated with tobacco smoking. *J. Natl. Cancer Inst.* 91:691–96
93. Zochbauer-Muller S, Lam S, Toyooka S, Virmani AK, Toyooka KO, et al. 2003. Aberrant methylation of multiple genes in the upper aerodigestive tract epithelium of heavy smokers. *Int. J. Cancer* 107:612–16
94. Soria JC, Rodriguez M, Liu DD, Lee JJ, Hong WK, Mao L. 2002. Aberrant promoter methylation of multiple genes in bronchial brush samples from former cigarette smokers. *Cancer Res.* 62:351–55
95. Belinsky SA, Palmisano WA, Gilliland FD, Crooks LA, Divine KK, et al. 2002. Aberrant promoter methylation in bronchial epithelium and sputum from current and former smokers. *Cancer Res.* 62:2370–77

(Abstract submitted to the ENAR meeting, March 2005)

A response surface model for drug combinations

Maiying Kong and J. Jack Lee
Department of Biostatistics and Applied Mathematics
University of Texas M.D. Anderson Cancer Center

When drugs having like effect are given in combinations, investigators often want to assess whether the joint effect is additive, synergistic, or antagonistic. Several response surface models (Machado and Robinson 1994; Greco *et al* 1990; Carter *et al.* 1988; Plummer and Short 1990) have been proposed in the literature by using a single parameter to capture synergism or antagonism. Limitation of these models exists when combinations at certain doses are synergistic while at other doses of the exact same drugs are antagonistic.

We propose a response surface model, where a function of doses in a combination Instead of a single parameter will be used to identify and quantify departures from additivity for different combinations. The proposed model can be considered as a generalized form of Plummer and Short's model (1990), and could capture all forms of synergism, antagonism, and additivity at different combinations of the two drugs. Examples will be given to illustrate the advantages of using the proposed method.

Genetic manipulation of immortalized normal human bronchial epithelial cells
Mitsuo Sato, Luc Girard, Michael Peyton, Ruben D. Ramirez, Noriaki Sunaga, Adi F. Gazdar, Jerry W. Shay, John D. Minna. UTsouthwestern Medical Center, Dallas, TX

Purpose: To evaluate the oncogenic impact of p53 knockdown, mutant K-RAS^{V12}, mutant EGFR alone and their combination on tumorigenicity of a newly developed immortalized human bronchial epithelial cell line.

Background: Molecular analysis of lung cancer has revealed several genetic and epigenetic alterations in the multistep pathogenesis of lung cancer. However, little is known about the relative importance of each individual alteration on the tumorigenic process. One approach is to use a model system in which the contribution of each genetic alteration to lung tumorigenesis can be assessed individually and combinatorially. We have developed an *in vitro* model system using normal human bronchial epithelial cells that overexpress Cyclin-dependent kinase 4 and human telomerase. Ectopic expression of these two genes enables the cells to bypass the growth inhibitory signals of the p16/Rb pathway and also replicative senescence induced by shortened telomeres. We manipulated this cell line (HBEC3), by stably knocking down p53 using RNA interference, by introducing a mutant form of K-RAS^{V12}, and by introducing a mutant epidermal growth factor receptor (EGFR), alone and in combination.

Methods: pSuper.retro vector was used for p53 knockdown and a mutant K-RAS^{V12} and mutant EGFRs (EGFR^{del746-750} and EGFR^{L858R}) were introduced using viral expression vectors. To test the genetically manipulated lines for changes in their malignant potential, growth in liquid culture, colony formation ability, growth factor dependence, and growth as xenografts in immuno-compromised mice were performed. To determine the effect of tyrosine kinase inhibitors (TKIs) (gefitinib and erlotinib) on manipulated HBEC3 cells and to assess their potential as chemopreventive agents, the cells were evaluated both in the presence or absence of these drugs for colony forming ability.


Results: Stable knockdown of p53 and overexpression of mutant EGFR were confirmed by immunoblotting in manipulated cells. K-RAS^{V12} expression was confirmed by RFLP analysis. p53 knockdown and K-RAS^{V12} alone caused cells to be less sensitive to contact inhibition and to be capable of partial anchorage-independent growth. The combination of p53 knockdown and K-RAS^{V12} further enhanced the tumorigenic phenotype by growth in soft agar but failed to cause cells to form tumors in nude mice. In addition, the ability of both anchorage-dependent and-independent cell growth of HBEC3 cells was highly dependent on epidermal growth factor (EGF) and this ability was completely inhibited with TKIs. Both types of mutant EGFRs enhanced the tumorigenic phenotype by growth in soft agar. Importantly, introduction of mutant EGFR^{L858R} into the HBEC3-p53 knockdown cells abrogated EGF dependence as measured by anchorage-independent colony formation ability. These results demonstrate that this isogenic *in vitro* model system is a powerful approach for studying lung cancer development.

FLIP downregulation and its impact on celecoxib-induced apoptosis in human lung cancer cells. Xiangguo Liu, Ping Yue, Fadlo R. Khuri, Shi-Yong Sun. *Winship Cancer Institute, Emory University School of Medicine, Atlanta, GA.*

The cyclooxygenase-2 (COX-2) inhibitor celecoxib is an approved drug in the clinic for colon cancer chemoprevention and has been tested for its chemopreventive and therapeutic efficacy in various clinical trials. Celecoxib induces apoptosis in a variety of human cancer cells including lung cancer cells. Our previous work has demonstrated that celecoxib induces DR5 expression, resulting in induction of apoptosis and enhancement of tumor necrosis factor-related apoptosis-inducing ligand (TRAIL)-induced apoptosis in human lung cancer cells (Liu et al, JNCI, 2004). In the current study, we found for the first time that celecoxib downregulated the expression of FLIPs (i.e., FLIP_L and FLIP_S), major negative regulators of the death receptor-mediated extrinsic apoptotic pathway, in human lung cancer cells. Overexpression of FLIPs, particularly FLIP_L, inhibited not only celecoxib-induced apoptosis, but also apoptosis induced by the combination of celecoxib and TRAIL. These results thus indicate that FLIP downregulation also contributes to celecoxib-induced apoptosis and enhancement of TRAIL-induced apoptosis, which compliment our previous finding that the DR5-mediated extrinsic apoptotic pathway plays a critical role in celecoxib-induced apoptosis in human lung cancer cells. Collectively, we conclude that celecoxib induces apoptosis in human lung cancer cells through activation of the extrinsic apoptotic pathway, primarily by induction of DR5 and downregulation of FLIP. (Supported in part by WCI faculty start-up research fund, GCC Distinguished Cancer Scholar award and DOD VITAL grant W81XWH-04-1-0142).

97th Annual Meeting 2006

ABSTRACT SUBMITTER

 [Print this Page for Your Records](#)

[Close Window](#)

Control/Tracking Number: 06-AB-6978-AACR

Activity: Abstract Submission

Current Date/Time: 11/14/2005 7:20:24 PM

Existence of clonal and subclonal outgrowths in the bronchial epithelium and stroma of current smokers

Short Title:

Clonal outgrowth in smokers

Author Block: *Tao Lu, Ignacio I. Wistuba, Walter N. Hittelman.* UT MD Anderson Cancer Center, Houston, TX

The identification of individuals at high risk for lung cancer is critical for individualized clinical management and is important for the identification of suitable subjects for chemoprevention trials. Using chromosome in situ hybridization (CISH) technology, we previously demonstrated the presence of chromosomal instability and multifocal clonal/subclonal outgrowths in the bronchial epithelium of current and former smokers. We also verified the presence of these clonal/subclonal outgrowths in normal-appearing bronchial epithelium in lung cancer resections using fluorescence inter-simple sequence repeat PCR (FISSR-PCR) analysis, a DNA fingerprinting methodology. To evaluate and compare FISSR-PCR and CISH technologies for accessing genetic instability and clonal/subclonal outgrowth, we subjected frozen bronchial biopsies obtained prior to entry onto a chemoprevention trial to FISSR-PCR analysis from sixteen (16) current smokers without lung cancer. The group of biopsies from these same individuals have previously been analyzed by CISH and exhibited a wide range of chromosomal changes. Multiple regions (i.e., 1-4 areas each) of bronchial epithelium and stroma were microdissected, and purified genomic DNA was analyzed by FISSR-PCR using three sets of primers ((CA)₈RG, (CA)₈RY, and (AGC)₄Y), providing a maximum of 350 informative DNA bands of varying lengths. Overall, we detected from 0 to 55 total band changes per microdissected epithelial region (median = 1.6 per 100 DNA bands). Different regions within the same bronchial biopsies showed both common and distinct DNA band changes, suggesting subclonal variations even within a single biopsy. We also detected from 0-20 total band changes per microdissected stromal region (median = 1.0 per 100 DNA bands), suggesting the presence of clonal outgrowths even in the stroma. Interestingly, bronchial biopsies with high clonal frequencies showed increased clonal

change in the associated stroma ($p=0.04$, two-tailed chi square). Importantly, bronchial biopsies from individuals showing high clonal changes by FISSR-PCR also showed evidence of high clonal change by CISH ($R^2 = 0.3$). These results confirm the existence of clonal/subclonal outgrowths in both the bronchial epithelium and stroma of smokers. With future improvements in microdissection, automated genomic DNA extraction, and DNA sequencing, FISSR-PCR has potential to be a sensitive method with high dynamic range to detect clonal/subclonal outgrowths in lung tissue. Such a methodology may be of use in identifying individuals at high risk for developing lung cancer. Supported in part by DAMD17-02-1-0706, NIH/NCI CA-91844, and EDNRN NCI CA-86390.

Author Disclosure Block: T. Lu, None; I.I. Wistuba, None; W.N. Hittelman, None.

Additional Disclosures (Complete):

The presenter of this abstract will discuss commercial products, devices, or technology in this presentation, as outlined below. : No - [Type "none" in the first box below]

1. Generic Name: : None

I anticipate discussing an OFF-LABEL use of a commercial product/device in this educational activity. : No - [Type "none" in the box below]

If you selected "Yes" above, you must indicate the product/device and describe its intended use in the box below. If you selected "No" above, you must type "none" in the box below: : None

Investigational Use (Not approved by the FDA for any purpose):

I anticipate discussing an INVESTIGATIONAL use of a commercial product/device in this educational activity. : No - [Type "none" in the box below]

If you selected "Yes" above, you must indicate the product/device and describe its intended use in the box below. If you selected "No" above, you must type "none" in the box below: : None

I agree with the declaration statement above. : True

Name: : Tao Lu

Date [mm/dd/yyyy]: : 11/14/2005

Category and Subclass (Complete): EP02-01 Biomarkers of human exposure to carcinogens and DNA damaging agents

Keywords/ Indexing (Complete): Genomic instability ; Smoking ; bronchial ; FISSR-PCR

Sponsor (Complete):

2006 Travel Awards (Complete):

Payment (Complete): Your credit card order has been processed on Monday 14 November 2005 at 7:19 PM.

Status: Complete